Development of a combined creep-fatigue model for engineering purposes

A thesis submitted for the degree of
Doctor of Philosophy in
Mechanical Engineering
University of Canterbury

Author:

DAN LIU

Supervisors:

DR. DIRK PONS

DR. SID BECKER

31 October 2017

Abstract

Short Abstract

Creep-fatigue damage reflects the combined effect of fatigue and creep. The existing creep-fatigue models are difficult to apply to engineering design. This situation is improved by the development of a formulation that integrates fatigue, creep, and creep-fatigue into one single mathematical representation. This combination is termed the unified creep-fatigue equation proposed in the present work. *Unified* in this context refers to the combination of the multiple creep/fatigue load regimes, integration of multiple load characteristics of temperature and cyclic time, and applicability of the general formulation to multiple metallic materials. The work makes multiple original contributions. The first is the development of validated unified creep-fatigue models covering both the strain and stress based situations. This was based on the concept of 'fatigue capacity', and was achieved by including an element of physical justification. The second is the inclusion of grain-size, which is important as it provides a means to include heat-treatment effect into the formulations. The third contribution is the partial extension to non-zero mean-stress conditions, and an identification of potential issues with stress-strain compatibility under this loading regime. A fourth contribution is the development of proposed underlying physical mechanisms for creep-fatigue at the microstructural level. Application of the method to engineering design has been demonstrated. This indicates that the application of the unified model gives a high-quality fatigue-life prediction, and reduces the complexity of finite element analysis under the creep-fatigue condition. Benefits of the unified model are its coverage of the full range from pure fatigue to pure creep, its ability to be applied in multiple situations of temperature and cyclic time, its applicability to multiple metallic materials, its ability to accommodate grain size (hence heat treatment condition), and its economy regarding requisite test data. Furthermore, it is conceptual underpinned by the physical mechanisms at the microstructural level.

Long Abstract

Creep-fatigue damage is caused by reversed loading at elevated temperature, which presents the interaction of fatigue and creep. This behaviour normally spans a wide range of industries,

such as aerospace, nuclear and automotive industries. In general, the creep-fatigue evaluation may be conducted by performing the creep-fatigue test under the running conditions, but this is uneconomical. Typical practice is to apply numerical models to pre-evaluate creep-fatigue behaviour at the initial stage of design. However, these models cannot effectively and efficiently be applied to engineering design because of a poor balance between accuracy and economy. Consequently, there is value in developing a new creep-fatigue model to improve the limitations presented by the existing models.

The present work developed strain-based and stress-based unified creep-fatigue equations. This started from an investigation of the underlying physical justification of fatigue and creep. We introduced the concept of fatigue capacity to represent the combined damage of creep and fatigue. The relationships between relevant variables were extracted from the conventional models, and were then applied to constitute the numerical representation of creep fatigue based on the concept of fatigue capacity. Furthermore, the heat-treatment effect was included into the unified model by introducing the parameter of grain size. Then a method of extracting the coefficients was proposed. Specifically a moderating factor was introduced to transfer the creep damage under constant loading into an equivalent situation with cyclic loading, and the compatibility was included to give a better description of the pure-fatigue condition.

The unified creep-fatigue equations were validated on multiple materials, including 63Sn37Pb solder, 96.5Sn3.5Ag solder, 2024T3 aluminium alloy, stainless steel 316, stainless steel 304, Inconel 718 and GP91 casting steel, where the empirical data of creep rupture and creep fatigue were extracted from existing literature. The validation verified the numerical structure of the unified creep-fatigue models, and demonstrated that the unified formulations can be applied in multiple situations for multiple materials to describe creep-fatigue behaviour with high quality of fitting to empirical data.

The unified creep-fatigue equations have significant advantages compared to existing creep-fatigue models, when applied to engineering design. Specifically, the unified models can be applied in multiple situations for multiple materials, can cover the full range of conditions from pure fatigue to pure creep, and can provide an economical method for fatigue-life prediction. Application of the unified method to engineering design was demonstrated via application to a gas turbine blisk. Combining the unified model with finite element analysis (FEA) reduced the complexity of creep-fatigue simulation.

Further refinements of the unified model were made to develop a simplified strain-based creep-fatigue formulation, the benefit of which is less reliance on empirical data collection, hence greater economy. A grain-size modified Manson-Haferd parameter was likewise introduced.

Another development of the theory was towards more complex mean stress conditions. The unified creep-fatigue equations were originally developed for the situation with zero mean stress. The model was extended to non-zero mean-stress situation. This was based on the simplifying assumption that the strain-stress relations under the situations with/without mean-stress effect share the same characteristic.

A physical explanation was developed for the terms in the unified creep-fatigue formulation. The unified models may be explained by the underlying physical mechanisms. This was

achieved by reference to the physical phenomena of diffusion creep and crack growth at the microstructural level. A graphical representation of the crack growth process was proposed. This conceptual model illustrates the whole process of damage accumulation from crack initiation to crack propagation, then to structural failure.

Overall, the strain-based and stress-based unified creep-fatigue equations provide an improved formulation for creep fatigue, where the improvements are evident in greater accuracy, improved economy of empirical testing, coverage of the three conditions (pure fatigue, pure creep, and creep fatigue), inclusion of grain size, and applicability to engineering design. The benefits are a more effective and efficient method for creep-fatigue life prediction.

Acknowledgements

It is an exciting journey which started three years ago, and it is also an impossible exploration without those people in my life. First and foremost, I would like to thank my supervisor, Dr. Dirk Pons, who has given me the most powerful support and guide on my research (also my English study). Especially, he accepted me and gave me confidence and encouragement at the most difficult period when my initial supervisor suddenly left the university. I also would like to thank my co-supervisor, Dr. Sid Becker, who supported me not only on academic issues but also for the study process. Especially, he helped me to solve troublesome issues when I first enrolled and helped me to find a new supervisor when my initial supervisor resigned.

I would like to thank Annie Homewood, particularly, as she tried her best to help me to complete my first enrolment (a complex and hopeless situation) when my visa was close to expiring. In addition, I would like to thank Jessica Ritchie (learning advisor in academic skill centre) for the help in English study (writing and speaking). Furthermore, I would like to thank my colleague, Abbas Tamadon, for his help on understanding fracture mechanics.

I also thank the department of mechanical engineering, who provided me with a departmental scholarship to support my tuition fees. This funding gives me enough time and energy to throw myself into my research.

Thanks to my parents, who have given me the biggest spiritual support. I also need to apologize to them since I could not take care of them during the period of my PhD study in New Zealand (I am the only child in my family).

Thanks to my colleagues who gave me some new ideas on my project, and also my friends who bring me a different life after study.

Finally, I would like to appreciate my initial supervisor, Dr. Ee-hua Wong, who brought me through the door and helped me to build the foundation for this research.

From the bottom of my heart, I thank everyone who helped me during the period of my PhD study. I believe I am lucky just because I met you. A new journey is opening for me, and I will start another adventure with your blessing.

Preface

This thesis is submitted for the degree of Doctor of Philosophy in Mechanical Engineering at the University of Canterbury. The research described in this thesis is based on the perspective of mechanical engineering rather than material science per se, and was conducted under the primary supervision of Dr. Dirk Pons. Publications that have arisen from this work are [1-7]:

The results shown in this thesis have been presented at the following international conference:

(1) Liu, D., D.J. Pons, and E.H. Wong, Proposal for a unified creep-fatigue equation, in International Conference on Innovative Design and Manufacturing (ICIDM). 24-26 January 2016: Auckland, New Zealand.

Publications:

(2) Liu, D., D.J. Pons, and E.H. Wong, The Unified Creep-Fatigue Equation for Stainless Steel 316. Metals, 2016. 6(9): p. 219.
http://dx.doi.org/10.3390/met6090219

(3) Liu, D., D.J. Pons, and E.H. Wong, Creep-integrated fatigue equation for metals. International Journal of Fatigue, 2017. 98: p. 167-175.
http://dx.doi.org/10.1016/j.ijfatigue.2016.11.030

(4) Liu, D. and D.J. Pons, Development of a unified creep - fatigue equation including heat treatment. Fatigue & Fracture of Engineering Materials & Structures, 2018. 41(1): p. 170-182.
http://dx.doi.org/10.1111/ffe.12670

(5) Liu, D. and D.J. Pons, A unified creep-fatigue equation with application to engineering design, in Creep, T. Tomasz, S. Marek, and A. Zieliński, Editors. 2018, InTechOpen: Rijeka, Croatia.
http://dx.doi.org/10.5772/intechopen.70877

(6) Liu, D. and D.J. Pons, Development of a stress-based creep-fatigue equation: Accommodating pure-fatigue to pure-creep for the high-cycle loading regime. International Journal of Damage Mechanics, 2017: p. 1-19.
https://dx.doi.org/10.1177/1056789517735678

(7) Liu, D. and D.J. Pons, Physical-Mechanism Exploration of the Low-Cycle Unified Creep-Fatigue Formulation. Metals, 2017. 7(9): p. 379.
http://dx.doi.org/10.3390/met7090379

In submission:

(8) Liu, D. and D.J. Pons, Conceptual model of crack growth for creep fatigue, Engineering Fracture Mechanics, 2017. (Submitted)

The published and accepted papers are attached in Appendix A.

The present work aims to develop a unified creep-fatigue model. *Unified* in this context refers to the combination of the multiple creep/fatigue load regimes, integration of multiple load characteristics of temperature and cyclic time, and applicability of the general formulation to multiple metallic materials. In this thesis, the work is described in thirteen chapters. Chapter 1 gives a general description of the present work. In particular, we indicate that the unified creep-fatigue model was developed for engineering application. Chapter 2 reviews the existing models, including the pure-fatigue models, pure-creep models and creep-fatigue models. In particular, the existing creep-fatigue models were evaluated, and then the gaps in the body of knowledge were identified.

The methodology is described in Chapter 3.

Ideally, the attempted model should be totally based on the observation at the microstructural level, but it is difficult to quantitatively relate the coefficients with the microstructure. The problem is one of multiscale modelling, whereby the phenomena of creep-fatigue emerges at the engineering scale from effects at the grain level. It would be valuable to build a bridge between the grain and engineering scales, whereby the description at the microstructural level is upgraded to the macroscopic level. However, it is unclear how this may be done. While qualitative explanations and quantitative formulations exist for some of the processes at the individual levels, there is no existing theory that cover this whole scale.

In this case, the unified creep-fatigue model was developed by the combination of empirical-based and constitutive-based methods with a deliberate attempt throughout that was based on the underlying physical mechanisms. Specifically, the development of the unified creep-fatigue model started from the identification of relevant variables (temperature, cyclic time, applied loading and grain size) and physical phenomena of fatigue and creep. The relationships between different variables were then extracted from the conventional models. Finally, the unified model was constructed based on these identified relationships and the proposed concept of fatigue capacity. Initially, we proposed that the strain-based model was developed through the empirical-based method, and the stress-based model was developed through the combined method shown above. However, afterwards we realized that both the strain-based and stress-based models could be developed by the combined method. In this case, both models have an element of physical justification.

Although the relationships between different variables in the new model are derived from the conventional models, the present work integrated them holistically to present fatigue and creep effects. This is a complex process, wherein the concept of fatigue capacity, the stress moderating functions, the well-known time-temperature parameters, and the reference condition are introduced; and a numerical simplification is applied.

The results of the present work are discussed in Chapters 4 to 11.

Chapter 4 presents the development and validation of the strain-based unified creep-fatigue equation. The method described in Chapter 3 was applied. The relationships between different variables were extracted from the conventional models, including the Arrhenius equation, the

Coffin-Manson equation and the Manson-Haferd parameter. The strain-based model was then constructed by these relationships and the concept of fatigue capacity. In particular, we did not apply the linear relation between time and loading, but accepted the exponential relation between temperature and strain from the Arrhenius equation. This is because the creep-deformation stage has a strong dependency on time, but not temperature. In addition, we assumed that time and temperature were not convoluted with each other, and thus the overall effect caused by temperature and time were additive. After this, we showed that this assumption gives sufficiently accurate outcomes. This model was then validated on multiple materials. The accuracy of the fatigue-life prediction was evaluated by a prediction ratio and reference-condition transformation. Specifically, the ratios of predicted life to experimental life need to be within a reasonable range which is defined between 0.75 and 1.25. When the creep-fatigue data are transformed to the reference condition, all data points need to be collected into one power-law curve with good quality and the coefficients of this trendline need to be close to the pure-fatigue-related coefficients given by the unified model.

The equation developed in Chapter 4 was then further modified to show creep-fatigue behaviour with a heat-treatment effect through introducing the parameter of grain size. This is presented in Chapter 5. The results of first attempts of the strain-based unified creep-fatigue equation were published in [1, 6, 7]. Subsequently, we added more data and optimized the unified model, hence the coefficients in the thesis are slightly different. The strain-based model is critiqued in Chapter 6, where the advantages of this model (including the unified characteristic, the integrated characteristic and good economy) were identified. This is desirable for engineering application. Particularly, a simplified formulation of the strain-based unified model was proposed by introducing the parameter of ductility. This simplified form provides a more economical method for the fatigue-life prediction because there is no need for the creep-fatigue data tests.

The strain-based models are normally applied in the low-cycle regime. In order to construct a whole map of loading-cycle regime, a stress-based unified model was developed in Chapter 7, but its importance is lower than the strain-based model since the loading condition in the low-cycle regime is more common in service. The method described in Chapter 3 was applied. The relationships between different variables were extracted from the conventional models, including the equation of steady-state creep rate, the Hall-Patch equation and the Basquin equation. Then, the stress-based model was constructed by these relationships and the concept of fatigue capacity. In particular, contrary to the strain-based model, the linear relationship between time and loading was accepted since it is reasonable to assume failure occurs at the steady (second) stage of creep deformation for the high-cycle fatigue behaviour. We could have applied the same numerical structure as the strain-based model, but introducing the relationships extracted from the conventional models into this structure created an apparently needless complexity. A key problem was encountered with the temperature-time relationship. Hence, we attempted a product relationship instead, and this gave satisfactory results. The stress-based unified creep-fatigue model was then validated on multiple materials, and the quality of this model to describe creep-fatigue behaviour was evaluated by a prediction ratio

and reference-condition transformation. In particular, the concept of compatibility was introduced to derive the coefficients, which gave a better description for the pure-fatigue condition.

All the work up to this point had assumed zero mean stress. The unified models were then extended to the situation with non-zero mean stress in Chapter 8. This transformation was conducted by the well-accepted premise of compatibility between the strain-life relation and the stress-life relation. However our results suggest that this premise may not be universally correct. This implies that once non-zero mean stress is included, the complexity is presented by an ongoing tension-compression stress loading and method to include this behaviour in the formulation. This raised the further discussion of the tension-compression process.

The physical aspect of tension-compression process is described in Chapter 9 in terms of crack-growth behaviour. In this chapter, we offer a qualitative description of crack growth at the grain level. This conceptual model accommodates the three stages of crack growth and includes different mechanisms of failure for tension and compression. Then, based on the mechanisms of failure, the physical explanation of the unified models are discussed in Chapter 10. In this chapter the effects of temperature, cyclic time and grain size on creep fatigue were investigated, and the unified models were linked to proposed underlying physical mechanisms.

Chapter 11 explains how the unified creep-fatigue model is applicable to engineering design. In this chapter, a general guide is given to show the process of applying the unified model, and then a case study of turbine blisk is presented. Particularly, the case study indicated that combining the unified model with finite element analysis (FEA) can significantly reduce the complexity of creep-fatigue simulation.

The overall results of the present work are presented in Chapter 12 and Chapter 13. Specifically, Chapter 12 presents the outcomes, limitations and research opportunities. In particular, a four-level maturity model was proposed to provide an overall evaluation of the creep-fatigue equations. In addition, Chapter 13 lists the original contributions.

Three appendixes are attached to this thesis. Specifically, Appendix A presents all the published and accepted papers. Appendix B and Appendix C show a general description of the XFEM (extended finite element method)-based method and CZM (cohesive zone modelling)-based method respectively. These were applied to simulate crack-growth behaviour through grains (fatigue behaviour) and along grain boundaries (creep behaviour). Examples for these two methods are also given.

Contents

Glossary

Creep damage: Creep damage occurs when materials are exposed to high levels of stress for a long term at elevated temperature, and it is manifested by the formation and growth of creep voids or cavities within the microstructure of the material.

Creep-fatigue damage:

Creep-fatigue damage is subject to the interaction between fatigue damage and creep damage, which is generally affected by temperature, frequency/strain rate/cyclic time, grain size and applied loading.

Elastic strain: Elastic strain is the proportional deformation of a dimension of physical geometry that returns after removal of the deforming force.

Fatigue damage: Fatigue damage occurs when materials experience cyclic loading. It is always physically performed by crack-growth behaviour, and numerically presented by the Basquin equation or the Coffin-Manson equation.

Plastic strain: Plastic strain is the proportional deformation of a dimension of physical geometry that is left after removal of the deforming force.

Strain: Strain is the proportional change in length, which represents the displacement relative to a reference length.

Stress: Stress is pressure or tension exerted on a material object.

Unified: This refers to the combination of the multiple creep/fatigue load regimes, integration of multiple load characteristics of temperature and cyclic time, and applicability of the general formulation to multiple metallic materials.

Nomenclature

α = Nozzle angle

α_1, α_2 = the scaling factors

β = the energy exponent

β_0 = the fatigue ductility exponent at the pure-fatigue condition

δ = the rupture ductility

γ = the surface energy

δ_0 = the ductility obtained under a sufficiently high strain rate

δ_t = the total error

δ_a = the average error

$\dot{\varepsilon}$ = the strain rate

$\Delta\varepsilon_{mech}$ = the mechanical strain range

$\Delta\varepsilon_p$ = the plastic strain amplitude

ε_f' = the fatigue ductility coefficient

ε_a = the total strain range

$\dot{\varepsilon}_{in}$ = the inelastic strain rate

$\Delta\varepsilon_{pp}$ = the completely reversed plastic strain

$\Delta\varepsilon_{pc}$ = the tensile plastic strain reversed by compressive creep

$\Delta\varepsilon_{cp}$ = the tensile creep strain reversed by compressive plasticity

$\Delta\varepsilon_{cc}$ = the completely reversed creep strain

ε_p = the residual fatigue capacity

ε_{pm} = the mean plastic strain

ε_m^p = the macroscopic strain

ε_{ar} = the equivalent plastic strain amplitude

ε_t = the total strain

$\varepsilon_{p,ref}$ = the full fatigue capacity

η_1 = the dynamic resistance effect of dashpot

θ = the angle in the polar coordinates

μ = the shear modulus

ρ = the density

σ = the applied stress

$\Delta\sigma$ = the stress amplitude

σ_f' = the fatigue strength coefficient

σ_{ar} = the equivalent stress amplitude

σ_a = the stress amplitude

σ_m = the mean stress

σ_y = the yield stress

σ_u = the ultimate stress

σ_{ij} = the stress distribution at polar coordinates

$\bar{\sigma}$ = the effective stress

σ_H = the hydrostatic stress

σ_0 = the fatigue strength coefficient reflects the full fatigue capacity

σ_s = the fatigue strength

τ_e = the shear stress

Φ_c = the phasing factor for the creep damage

Φ_{ox} = the phasing factor for the oxidation damage

φ = the concentration of vacancies

Ω = the atomic volume

ω = the rotational velocity in rad/s

A, A_2 = the constants dependent on the material and the particular creep mechanism

a_1, a_2 = the constants obtained from creep-rupture tests

b = the fatigue strength exponent

b_0 = the constant reflects the full fatigue capacity

C_0 = the fatigue ductility coefficient at the pure-fatigue condition

c = the fatigue ductility exponent

D = the ductility

D_t = the accumulated total fatigue damage

D_f = the pure fatigue damage

D_c = the pure creep damage

D_{ox} = the damage caused by oxidation

D_v = the amount of substance following through a unit area

D_t = the amount of substance following during a unit time

d = the grain size

d_c = the creep damage for one cycle

d_f = the fatigue damage for one cycle

d_{ref} = the reference grain size

E = the Young's modulus

ΔE_f = the change in internal energy due to formation of a vacancy

F_c = the centrifugal force

F_t = the tangential force

F_a = the axial force

f = the frequency

f_{ref} = the reference frequency

f_m = the moderating factor for stress

ΔG = the total change in free energy

ΔG_f = the Gibbs free energy for formation of a vacancy

H_{ij} = the prediction ratio

h_{cr} = the critical crack length when crack starts to rapidly grow before failure

J = the diffusion flux

ΔJ_{eff} = the effective range of J-integral

ΔK = the difference between the maximum and minimum stress intensity factors

K_{eff} = the effective stress intensity factors for one cycle

K_{max} = maximum stress intensity factors for one cycle

K_{min} = minimum stress intensity factors for one cycle

K_p^{eff} = the constant of effective oxidation

K, K', K'' = the strength coefficient

k = the number of block loading

k_a = the surface condition modification factor

k_b = the size modification factor, k_c is the load modification factor

k_d = the temperature modification factor

k_e = the reliability factor

k_f = the miscellaneous-effects modification factor

L_p = the pile-up length

$\dot{M}$ = the Mass flow rate

N_f = the number of cycles

N_{pp} = the fatigue life under the strain of $\Delta\varepsilon_{pp}$

N_{cc} = the fatigue life under the strain of $\Delta\varepsilon_{cc}$

N_{cp} = the fatigue life under the strain of $\Delta\varepsilon_{cp}$

N_{pc} = the fatigue life under the strain of $\Delta\varepsilon_{pc}$

N_i = the number of cycles to fatigue failure under the ith strain/stress range

$N_{pre,ij}$ = the predicted creep-fatigue life at the conditions of $\varepsilon_{p,j}$, T_i and $t_{c,i}$

$N_{exp,ij}$ = the experimental creep-fatigue life at the conditions of $\varepsilon_{p,j}$, T_i and $t_{c,i}$

$N_{f-\sigma}{}^*$ = the stress-based equivalent fatigue life

$N_{f-\varepsilon}{}^*$ = the strain-based equivalent fatigue life

N_{f0} = the fatigue life under the pure-fatigue condition

N_{total} = the total life

N_{Inc} = the number of cycles to incubate a crack at t micro-notch

N_{MSC} = the number of cycles required for propagation of a microstructurally small crack with the crack length

N_{PSC} = the number of cycles required for propagation of a physically small crack

N_{LC} = the number of cycles required for long crack propagation

n_i = the number of constant amplitude cycles under the ith strain/stress range

n_p = the number of dislocations

n_v = the number of vacancies are formed during the process of diffusion

n, n', n'' = the strain hardening exponent

P_{SD} = the Sherby-Dorn Parameter

P_{LM} = the Larson-Miller Parameter

P_{MH} = the Manson-Haferd Parameter

P = the pressure

Q = the activation energy of the creep mechanism

R = the Boltzmann's constant

R_1 = the distance from center to tip of the blade

R_2 = the distance from center to root of the blade

r = the distance in the polar coordinates

r_y = the radius of the plastic zone

$\overline{r_y}$ = the equivalent radius of the plastic zone

ΔS_c = the configurational entropy

S_1, S_2 = the elastic modules for springs

S_e = the endurance limit at the critical location of a machine part in the geometry and condition of use

S'_e = the rotary-beam test specimen endurance limit

ΔS_f = the entropy for formation of a vacancy

T = the absolute temperature

T_{ref} = the reference temperature

T_m = the melting temperature

T_0 = the room temperature

$\bar{T}$ = the mean temperature

t_i = the duration of creep under the applied stress σ_i at temperature T_i

$t_{R(i)}$ = the creep-rupture time under the applied stress σ_i at temperature T_i

t_c = the cyclic time

t_R = the rupture time

t_h = the time of hold period

t_{ref} = the reference cyclic time

ΔV_f = the volume of a vacancy

W = the ways that n_v vacancies can be located among the n sites

ΔW_P = the plastic energy per cycle

W'_f = the energy coefficient

ΔW_t = the total energy density

W''_f = the constants in the energy-life relation

ΔW_e^+ = the tensile elastic energy density

ΔW_p = the plastic energy density

ΔW_{lim} = the elastic energy density at fatigue limit

$\Delta W_{thermal}$ = the energy density consumed in the form of thermal contribution

$\Delta W_{f-damage}$ = the energies (per cycle) which cause fatigue damage

$\Delta W_{c-damage}$ = the energies (per cycle) which cause creep damage

$\Delta W_{f-deformation}$ = the energies (per cycle) which cause fatigue deformation

$\Delta W_{c-deformation}$ = the energies (per cycle) which cause creep deformation

W^{open} = the opening energy

x = the position

$a_1(T_0)$ = the fatigue strength coefficient at the temperatures of T_0

$a_1(0)$ = the fatigue strength coefficient at the temperatures of 0K

$a'(d)$ = the grain-size modifying function for creep component in strain-based model

$\frac{da}{dN}$ = the total crack growth per cycle

$\left(\frac{da}{dN}\right)_f$ = the crack growth per cycle due to cyclic load changes

$\left(\frac{da}{dN}\right)_c$ = the crack growth per cycle due to hold time

$\left(\frac{da}{dN}\right)_{cf}$ = the crack growth caused by the interaction effect between fatigue and creep

$B(d)$ = the grain-size moderating function for pure fatigue in stress-based model

$b_1(T_0)$ = the fatigue strength exponent at T_0

$b'(d)$ = the grain-size modifying function for pure fatigue in strain-based model

$C(T, t, \sigma, d)$ = the creep moderating function in stress-based model

$c(\sigma, T, t_c)$, $c(\sigma, T, t_c, d)$ = the creep moderating function in strain-based model

$c_1'(\sigma, T)$ = the thermal-related effect on the full fatigue capacity

$c_2'(\sigma, t_c)$ = the time-related effect on the full fatigue capacity

$c_1(\sigma)$, $c_2(\sigma)$ = the stress functions related to creep

$K(T, t_c)$ = the strength coefficient

$n(T, t_c)$ = the strain hardening exponent

($log\ t_a$, T_a) = the point of convergence of the $log\ t$-T lines

Chapter 1

1. Introduction

This chapter gives an introduction to the present work, including the industrial needs, research aims and general description of the present work.

Creep-fatigue damage is defined as the damage caused by reversed loading at elevated temperatures, which presents a combined effect of fatigue and creep. This is a complex process since fatigue and creep behaviours present significantly opposite mechanisms at the microstructural level. Specifically, fatigue effect occurs via cracks through the grains, while creep effect involves the grain boundary cracking [8]. Creep-fatigue phenomenon spans a wide range of industries, thus is a non-ignorable issue for engineering design. The exploration of a numerical representation of creep-fatigue behaviour has been frequently investigated. However, previous research in this area shows some significant limitations. In this case, to improve these limitations, a new creep-fatigue formulation was developed in the present work.

1.1 Industrial context

Fatigue is an effect whereby damage happens when the material is subjected to cyclic loading, and creep is an effect whereby damage happens when the material is exposed to high levels of stress for a long time. Creep-fatigue damage can be regarded as the interacted damage caused by fatigue and creep, which is influenced by temperature, frequency/time and applied loading.

The creep-fatigue phenomenon spans a wide range of industries, such as aerospace, naval, nuclear and automotive industries [9]. For example, in the aerospace industry (Fig.1.1), turbine blades in aircraft engines normally work under cyclic loading and elevated temperature (the condition of creep fatigue). During the running process, microscopically, a crack initially starts from the root of the blade, then it propagates with increasing cycles, then structural failure

happens when the crack achieves a critical value. Generally, creep-fatigue damage for one component can be evaluated by conducting experiments under the running condition, which presents a reliable result but provides a non-economical method (since the creep-fatigue test is time-consuming and expensive) for fatigue-life evaluation.

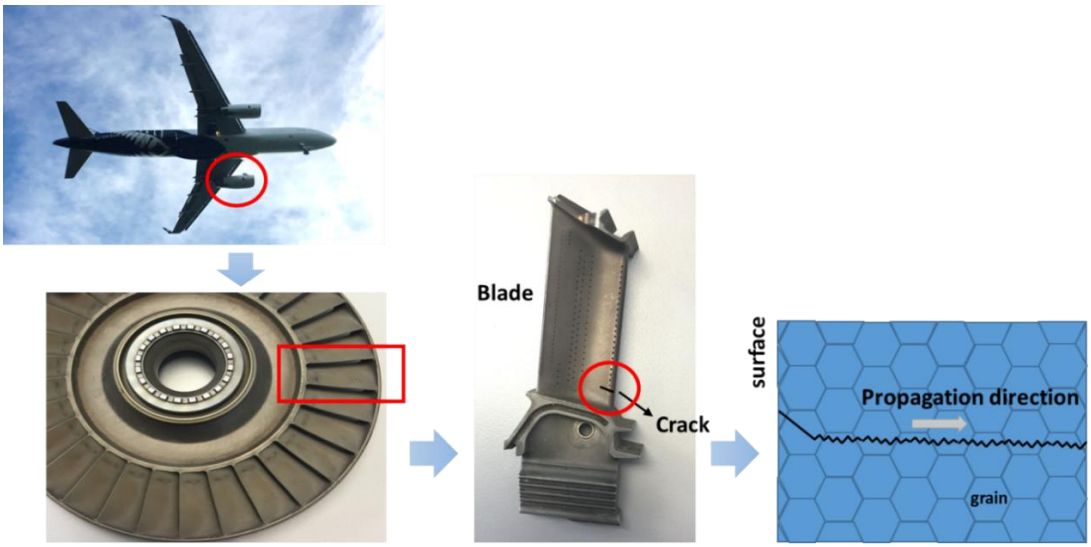

Figure 1.1 Creep-fatigue behaviour in the aerospace industry

For engineering design, a pre-evaluation of fatigue life (or damage) is normally applied at the initial stage of design to make a material selection or structural optimization. Normally, in creep-fatigue situation, the total damage is numerically evaluated through the theory of damage accumulation and conventional-fatigue-based formulations. Specifically, the creep-fatigue evaluation based on damage accumulation is normally conducted by the linear damage rule or crack growth law [8], wherein fatigue damage and creep damage are evaluated separately and then are numerically added.

Engineering designers typically use the simple Marin equation (Eq.1.1) [10] to determine the acceptable fatigue stress in a part. This modified endurance limit is based on the ultimate tensile strength, and several multiplicative factors for surface condition, part size, type of load, operating temperature, etc. The only mechanical property included here is the ultimate tensile strength – no other properties are required. The benefits of this approach are ease of use, since the tensile strength is readily known, or easily measured. The detriments of this approach are that it only applied to pure fatigue, and even then is merely an approximation.

$$S_e = k_a k_b k_c k_d k_e k_f S'_e \tag{1.1}$$

where S_e is the endurance limit at the critical location of a machine part in the geometry and condition of use, S'_e is the rotary-beam test specimen endurance limit, k_a is the surface condition modification factor, k_b is the size modification factor, k_c is the load modification factor, k_d is the temperature modification factor, k_e is the reliability factor, k_f is the miscellaneous-effects modification factor.

In addition, the conventional fatigue models have been frequently extended to the creep-fatigue condition by integrating creep effect, and then the creep-fatigue models are applied to calculate fatigue capacity under one specific situation directly.

In the present work, a new creep-fatigue model was developed to satisfy the requirements of engineering applications, wherein a good balance between accuracy and economy is crucial. In general, the derivation of a new creep-fatigue model is a complex task. This is because the creep-fatigue damage appears to be a complicated issue for numerical representation of creep fatigue, wherein the physical principles of fatigue and creep mechanisms are remarkably different, and the interaction effect of fatigue and creep is unknown.

1.2 Aims of the present work

The present work attempts to develop a new creep-fatigue model for engineering applications. In this case, the new numerical representation should:

(1) have the ability to be applied in multiple situations for multiple materials;

(2) have the ability to cover the full range of conditions from the pure-fatigue condition to the pure-creep condition;

(3) provide an economical method for fatigue-life prediction;

(4) be consistent with the underlying physical mechanisms of fatigue and creep.

We identify that the last item shown above (consistency with physical mechanisms) is the basis for the other characteristics. Therefore, a physical-based explanation of the unified creep-fatigue equation should be investigated at a microstructural level.

It is important that the unified creep-fatigue model should be applicable to engineering design. In this case, a case study of a practical situation should be given to show the applicability of this new formulation. In particular, introducing a unified approach should provide an easier method for fatigue-life prediction for the creep-fatigue situation.

1.3 Brief description of present work

The existing creep-fatigue models present significant limitations in the areas of unifying, integration, economy and physical explanations, which imply non-applicability of engineering design. In this case, a new creep-fatigue formulation should be developed to have the ability to be applied in multiple situations for multiple materials, to cover the full range of conditions from the pure-fatigue condition to the pure-creep condition, and to provide an economical method for fatigue-life prediction. These characteristics were fundamentally achieved due to including an element of physical justification, which was then proven through linking the unified model with the underlying physical mechanisms. Sepcifically, the development of the

unified model started from the identification of the relavent variables (temperature, frequency/time, grain size and applied loading) and the investigation of the physical phenomena. Then, the relationships between these variables were extracted from the conventional fatigue and creep models. Finally, based on the concept of fatigue capacity, the unified model was numerically constructed by these relationships. In particular, the parameter of grain size was introduced into the unified formulations to describe creep-fatigue behaviour at a microstructural level. Then, the method to derive the coefficients was proposed, where the empirical data and numerical optimization are combined. In addition, a moderating factor was introduced to transfer the creep damage at constant loading into an equivalent value for the cyclic-loading situation, and the compatibility was applied to present a better description of the pure-fatigue condition.

The unified creep-fatigue equations were validated in multiple situations for multiple materials, and the high quality of fitting to empirical data was given. Then, through comparing with other existing creep-fatigue models, the new creep-fatigue models present significant advantages of the unified characteristic, integrated feature and economy. This implies better applicability to engineering design. In addition, the fundamental principle of derivation implies that the unified creep-fatigue equations may be explained by the underlying physical mechanisms of fatigue and creep. This was demonstrated through investigating the influences of relevant variables on creep-fatigue behaviour and the relationships between these variables at a microstructural level. This characteristc is significantly superior to other empirical-based creep-fatigue models.

Based on the discussion of fatigue and creep mechanisms, a conceptual graphical-based model was initially proposed and presented through investigating the crack-growth behaviour. We believe that this model could be further modified as a deeper investigation of the physical mechanisms of fatigue and creep. Finally, a guide for applying the unified creep-fatigue equation to engineering design was described, then a case study on gas turbine blisk was presented. In particular, this case study implies that the combination of the unified formulation and FEA-based method has the ability to effectively reduce the complexity of creep-fatigue simulation.

Consequently, the present work presents an applicable method of creep-fatigue evaluation for engineering applications. This is a significant research area of fatigue, and thus it is worthwhile to be conducted.

1.4 Organization of thesis

The present work is described in the following thirteen chapters to show the derivation, validation, critique, physical explanation and application of the unified creep-fatigue equations (general structure of the present work is illustrated in Fig.1.2).

Chapter 1 gives an introduction to the present work, including the industrial needs, research aims and general description of the present work.

Chapter 2 starts with a review of the existing creep-fatigue models, including the damage-accumulated-based method, strain-based method, stress-based method and energy-based method. Then, the overall evaluation of these existing models gives the gaps in the body of knowledge, which implies the problems that should be solved in the present work.

Chapter 3 gives the description of methodology, wherein the research question is emphasized, and the method for deriving the new creep-fatigue model is proposed. In addition, the complexity of the present work is identified.

Chapters 4 to 10 are the results, and Chapter 11 provides an application to turbine blade design.

Chapter 4 describes the development of the strain-based unified creep-fatigue equation (without grain-size dependence). In this chapter, the strain-based model is constructed through including an element of physical justification and applying the concept of fatigue capacity, then the method to extract coefficients is given. Finally, this strain-based model is validated on multiple materials (63Sn37Pb solder, 96.5Sn3.5Ag solder, 2024T3 aluminium alloy, stainless steel 304 and stainless steel 316), which shows the high quality of fitting to empirical data.

Chapter 5 gives an extension of the model proposed in Chapter 4, where the grain-size dependence is introduced to describe creep-fatigue behaviour at a microstructural level. Then, the method to extract the coefficients is presented, and this formulation is validated on the materials of Inconel 718 and GP91 casting steel.

Chapter 6 critiques the strain-based creep-fatigue approach. In this chapter, the Matlab-based and Excel-based numerical optimizations are compared, which indicates that both methods present the same quality on a solution, but the Excel-based method gives an easier method for engineering. Then, through comparing with other existing creep-fatigue models proposed in Chapter 2, the new formulation presents significant advantages in the areas of unifying, integration, and economy. A grain-size-modified Manson-Haferd parameter and a simplified strain-based formulation are proposed. In addition, the introductions of the moderating factor and grain-size dependence are also discussed in this chapter.

Chapter 7 gives a stress-based unified creep-fatigue equation, which is normally applied to the high-cycle regime. In this chapter, the derivation of this new formulation is presented, and the extraction of the coefficients is given. Then, the stress-based approach is validated on the materials of Inconel 718 and GP91 casting steel. Introducing the compatibility gives a better description of the pure-fatigue condition; in addition, comparing with the existing stress-based models indicates that this new formulation can well present the unified and integrated characteristics.

Chapter 8 extends the formulations presented in Chapters 5 and 7 into the situation with mean-stress effect. This extension is based on an assumption that the stress-strain relations under the situations with/without the mean-stress effect share the same characteristic, but this assumption may be ineffective (the discussion is presented).

Chapter 9 initially gives a conceptual graphical-based model, which illustrates the whole process of damage accumulation from crack initiation to crack propagation then to structural failure.

Chapter 10 links the unified models to the underlying physical mechanisms, which is identified as the fundamental principle to make the unified creep-fatigue models superior to the existing models. In this chapter, the influences of temperature, cyclic time and grain size on creep-fatigue behaviour are discussed. Especially, the grain size effect is further proven by finite element analysis. Then, the consistency between the unified models and the microstructural phenomena is investigated. This strongly proves that the unified creep-fatigue model can present a better physical explanation.

Chapter 11 demonstrates the applicability of the unified creep-fatigue approach. It provides a guide to application from the perspective of an engineering designer, and is illustrated with a case study on a gas turbine blisk. It is shown that the combination of the unified approach and finite element analysis can significantly reduce the complexity of creep-fatigue simulation.

Chapter 12 evaluates the results given by the present work. In this chapter, the outcomes are collected. Then an overall evaluation of the usefulness of the unified creep-fatigue models is conducted through applying a four-level maturity model. Finally, the limitations of the present work are identified, and the future directions of research are proposed.

Chapter 13 concludes the original contributions made by the present work.

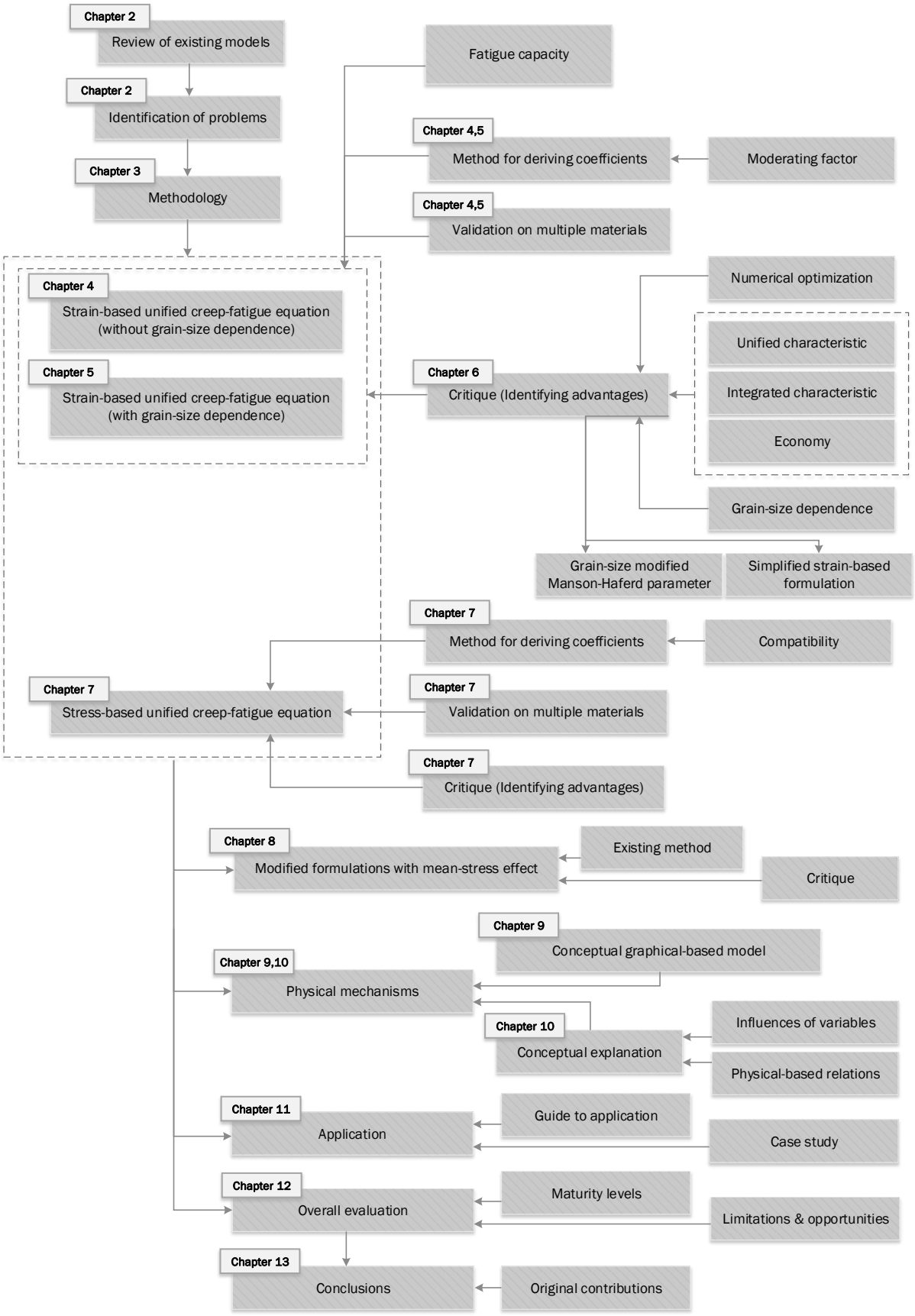

Fig.1.2 General structure of the present work

Chapter 2

2. Literature review

This chapter starts with a review of the existing creep-fatigue models, including the damage-accumulated-based method, strain-based method, stress-based method and energy-based method. Then the overall evaluation of these existing models gives the gaps in the body of knowledge, which implies the problems that should be solved in the present work.

2.1 Historical development of fatigue and creep field

Fatigue life for creep fatigue is always related to the plastic strain, not the elastic strain. This is because the externally applied deformation energy at the macroscopic level is consumed in many small plastic strains at the microstructure level. This plastic strain then breaks molecular bonds and contributes to micro cracks, hence the failure of the material. In addition, applied stress is also related to fatigue life to describe creep-fatigue behaviour. This is because the stress above yield value results in unrecoverable deformation; then the accumulated damage leads to structural failure. Normally, frequency and temperature are regarded as the two main effects on the creep-fatigue process, and a large number of experiments have been conducted to explore the relationship between them and creep-fatigue life.

It is noticeable that cyclic creep (ratcheting) is not the creep mentioned in this thesis because cyclic creep (ratcheting) is caused by non-zero mean stress while creep is caused by environmental factors [8], such as temperature and frequency. In this case, the cyclic creep-fatigue equation (ratcheting situation) is always developed through the stress-based equation, like the Basquin equation.

2.1.1 Development of fatigue models

Fatigue damage occurs when a material is subjected to cyclic loading. Although the term 'fatigue' first appeared in 1854, the history of fatigue can be traced as far back as 1837, when the first fatigue test results were published by Albert [11]. The period of almost two hundred years has witnessed many significant milestones in fatigue theory.

In the present work, the fatigue damage, which only results from alternating applied loading, is called *pure fatigue*, where the creep effect is dormant. Generally, there are multiple forms of loading in pure fatigue:

2.1.1.1 Alternating applied loading with zero mean stress

The simplest form comprises an alternating applied stress (cyclic stress) with zero mean stress. This is the type of loading applied to obtain the common S-N curves (stress-life) in empirical testing, where the fatigue life is normally above 10^4 cycles (high-cycle regime) [8]. In this case, a relatively small amount of plastic deformation is accumulated at each cycle, and thus a large number of cycles is needed until final fracture. This is frequently represented by the Basquin equation (Eq.2.1) [12, 13]:

$$\frac{\Delta\sigma}{2} = \sigma_f'(2N_f)^b \tag{2.1}$$

where $\Delta\sigma$ is the stress amplitude, σ_f' is the fatigue strength coefficient, b is the fatigue strength exponent and N_f is the number of cycles. However, when failure occurs within a relatively small number of cycles, namely below 10^4 cycles (low-cycle regime) [8], fatigue behaviour is referred to as low cycle fatigue, where the plastic strain is commonly used as the independent variable and is normally related to the fatigue life by the Coffin-Manson equation (Eq.2.2) [14, 15]:

$$\frac{\Delta\varepsilon_p}{2} = \varepsilon_f'(2N_f)^c \tag{2.2}$$

where $\Delta\varepsilon_p$ is the plastic strain amplitude, ε_f' is the fatigue ductility coefficient and c is the fatigue ductility exponent. Both of these loading regimes, including the low-cycle regime and high-cycle regime, are discussed in the present work. Across these two loading regimes, an energy-based equation (Eq.2.3) [16] was then developed by Morrow:

$$\Delta W_P = W_f'(2N_f)^\beta \tag{2.3}$$

where ΔW_P is the plastic energy per cycle, W_f' is the energy coefficient and β is the energy exponent.

The common concepts across these three models is that the relationship is the number of cycles (N_f) to the power of a coefficient. However, these models are different in the way they attribute this to stress, strain and energy. Power-law curves can be transferred into straight lines at log-

log scales, which provides an easy and clear way to illustrate the stress/strain/energy-fatigue life relation. At log-log scales, the coefficients of these models represent the intercept, and this quantifies the stress/plastic strain/energy when $2N_f = 1$. The exponent of these models shows the slopes of the straight lines, which presents the change rate of fatigue life to stress/plastic strain/energy. This power-law relation is consistent with empirical data, but the underlying reason why the relationship should be a power law was not mentioned when these models were developed. However, some effects were conducted on fatigue damage which could be used to explain the reasonability of the power-law relation. For example, the reasonability of the power-law relation could be explained through crack growth behaviour. To be specific, firstly, the number of cycles to nucleate plays an important role for fatigue damage. Research [17-19] shows that 10% of fatigue life in the low cycle regime contributes to nucleate the first micro-cracks while this percentage is 60% in the high cycle regime. This means that in the low cycle regime the small change of applied loading amplitude leads to a drastic change of fatigue life, but a slight change in the high cycle regime. Secondly, because the density of surface micro-cracks in the low cycle regime is larger than in the high cycle regime, a big change rate of fatigue life to applied loading is presented in the low cycle regime while a small change rate is shown in the high cycle regime. It is reasonable that these phenomena can be described by a power-law relation, and this power-law relation provides us a good starting to develop a unified creep-fatigue equation.

2.1.1.2 Alternating applied loading with non-zero mean stress

A more complex loading form is for an alternating stress with non-zero mean stress, and the equivalent stress is normally represented by the Soderberg relation (Eq.2.4) [20], the Morrow relation (Eq.2.5) [21, 22], the Goodman relation (Eq. 2.6) [23] and the Gerber relation (Eq. 2.7) [24]:

$$\sigma_{ar} = \frac{\sigma_a}{1 - \frac{\sigma_m}{\sigma_y}} \tag{2.4}$$

$$\sigma_{ar} = \frac{\sigma_a}{1 - \frac{\sigma_m}{\sigma_f'}} \tag{2.5}$$

$$\sigma_{ar} = \frac{\sigma_a}{1 - \frac{\sigma_m}{\sigma_u}} \tag{2.6}$$

$$\sigma_{ar} = \frac{\sigma_a}{1 - \left(\frac{\sigma_m}{\sigma_u}\right)^2} \tag{2.7}$$

where σ_{ar} is the equivalent stress amplitude, σ_a is the stress amplitude, σ_m is the mean stress, σ_y is the yield stress, σ_u is the ultimate stress and σ_f' is the fatigue strength coefficient. In the case where plastic flow occurs, controlled stress amplitude arises cycle-dependent creep (ratcheting), while controlled strain amplitude results in cycle-dependent relaxation. Normally, the fatigue behaviour with mean-stress effect is described from the perspective of applied stress,

where controlled stress is imposed. Therefore, the numerical fatigue formulation (Eq.2.8) [25, 26] with mean-stress effect was developed from the stress-life relation by Manson and Halford through introducing the concept of 'equivalent fatigue life' and the Morrow relation (Eq.2.5).

$$\varepsilon_a = \frac{\sigma_f'}{E}\left(1 - \frac{\sigma_m}{\sigma_f'}\right)\left(2N_f\right)^b + \varepsilon_f'\left(1 - \frac{\sigma_m}{\sigma_f'}\right)^{c/b}\left(2N_f\right)^c \tag{2.8}$$

where ε_a is the total strain range; the first term shows the elastic strain and the second term gives the plastic strain.

2.1.1.3 Random loading

Still more complex loading arises when the load has a high degree of random variability. This is an important consideration in vehicle suspensions and similar design problems. This form of fatigue is accommodated by the Palmgren-Miner relationship (Eq.2.9) (linear damage rule), which was first proposed by Plamgren in 1924 [27], and then was further developed by Miner in 1945 [28]. This rule shows that the damage caused by partial loading are accumulated in a linear manner and the engineering structure failure when total damage (*D*) equals to 1.

$$D = \sum_{i=1}^{k} \frac{n_i}{N_i} \tag{2.9}$$

where *D* is the accumulated total fatigue damage, *k* is the number of block loading, n_i is the number of constant amplitude cycles under the i^{th} strain/stress range, and N_i is the number of cycles to fatigue failure under the i^{th} strain/stress range.

With the same concept of accumulated damage, the theory of crack growth was proposed. This theory states that the fatigue life is the number of loading cycles required to achieve the critical crack size, and this process is divided into three stages: initiation, propagation and fracture. The total crack size can be presented as the linear addition of initial crack size and propagative crack size. Specifically, the initial crack reflects the pre-existing damage, and the propagative crack (produced in the second stage) denotes the major damage. Normally, the initial crack is identified as the real crack size in the structures before loading and the propagative crack can be obtained through Paris's model (Eq.2.10) [29]:

$$\frac{da}{dN} = C\left(\Delta J_{eff}\right)^l \tag{2.10}$$

where $\frac{da}{dN}$ is the total crack growth per cycle, ΔJ_{eff} is the effective range of J-integral, and *C* and *l* are material constants obtained from experiments.

2.1.2 Development of creep models

Creep damage occurs when a material is exposed to high levels of stress for a long term at elevated temperature, and this is named as *pure creep* in the present work. Generally, creep is divided into three stages (Fig.2.1) [8]: primary creep, where the creep strain rate is relatively

high but decreases with increasing time; secondary creep, where the creep strain rate arrives at a minimum value and stays constant; and the tertiary stage, where the creep strain rate increases with increasing time, and the structure fails at the end of this stage.

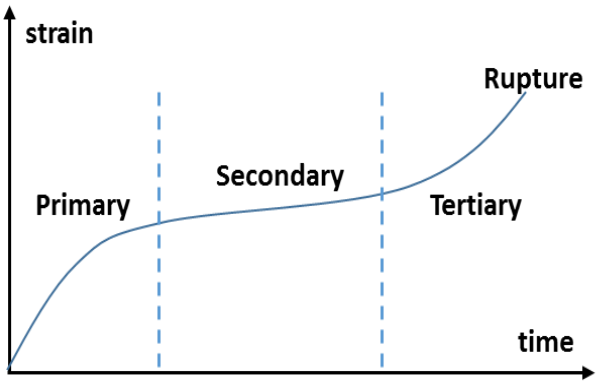

Figure 2.1 Creep stages

As the most steady state in the process of creep, secondary creep has been described by multiple creep models. Early work mainly focused on the effect of temperature on creep, whereby the Arrhenius equation (Eq.2.11) [30, 31] was proposed by Svante in 1889 to describe the relationship between strain rate and temperature. Then, combined with the effects of stress and grain size, a general equation (Eq.2.12) [8] was produced.

$$\dot{\varepsilon} = Ae^{\frac{-Q}{RT}} \tag{2.11}$$

$$\dot{\varepsilon} = \frac{A_2\sigma^m}{d^qT}e^{\frac{-Q}{RT}} \tag{2.12}$$

where $\dot{\varepsilon}$ is the strain rate, A and A_2 are constants dependent on the material and the particular creep mechanism, Q is the activation energy of the creep mechanism, σ is the applied stress, T is the absolute temperature, m and q are the exponents dependent on the creep mechanism, d is the grain size of the material, and R is the Boltzmann's constant.

Normally, the creep rupture test cannot persist for a long time, such as more than one year, due to test-time limitation. Therefore, an accelerated test which employs a higher temperature is conducted to build the time-temperature relation, such as the Sherby-Dorn Parameter (Eq.2.13) [32], the Larson-Miller Parameter (Eq.12.14) [33] and the Manson-Haferd Parameter (Eq.2.15) [34].

$$P_{SD} = te^{-Q/RT} \tag{2.13}$$

$$P_{LM} = T(\log t + C) \tag{2.14}$$

$$P_{MH} = \frac{T - T_a}{\log t - \log t_a} \tag{2.15}$$

where P_{SD} is the Sherby-Dorn Parameter, P_{LM} is the Larson-Miller Parameter, P_{MH} is the Manson-Haferd Parameter, Q is the activation energy of the creep mechanism, R is the

Boltzmann's constant, *t* is the rupture time, *T* is the absolute temperature, *C* is a constant and $(\log t_a, T_a)$ is the point of convergence of the $\log t$-*T* lines. The temperature-time relation shown by the Sherby-Dorn Parameter at different stresses is presented as the slope of several parallel curves of *1/T* vs. *logt*. The temperature-time relation presented by the Larson-Miller Parameter shows that the curves of *1/T* vs. *logt* at different stresses can converge to one point *(0, -C)*, wherein *C* is a material constant usually approximated as 20. The same extrapolation procedure is used to develop the Manson-Haferd Parameter, which shows that all $log\ t$-*T* lines at different stresses can converge into one point $(\log t_a, T_a)$. Generally, the Sherby-Dorn Parameter and the Larson-Miller Parameter have a good physical base since they are developed from the Arrhenius equation, while the Manson-Haferd Parameter shows poor performance in this area because this parameter was extracted from empirical data. However, the Manson-Haferd Parameter presents a better numerical description of creep-rupture behaviour than the other two parameters, which has been well proven on multiple materials [35].

Normally, the data of creep rupture tests at different stresses are plotted as time-temperature curves (*1/T-logt* curves for both the Sherby-Dorn Parameter and the Larson-Miller Parameter, and *T-logt* curves for the Manson-Haferd Parameter), and then the creep parameters are given. Meanwhile, the relationship between stress and the time-temperature parameter can be derived through curve fitting. Consequently, a rupture time-stress-temperature relation is built, and thus one of these three parameters (rupture time, applied stress and temperature) can be predicted when the others are defined.

2.1.3 Models based on physical cracks or voids

The conventional fatigue models (shown in Section 2.1.1) were developed from empirical data by curving fatigue. This method provides the simplest process to construct a numerical model, and thus is well-accepted in the field of mechanical engineering. However, from the perspective of material science, the fatigue models should be constructed through observing the physical phenomena (such as the micro-crack growth and void growth), whereby some physical-based models were developed. For example:

(1) Micromechanical cyclic void growth model (Kiran's model Eq. 2.16 [36])

$$D = \sum_{T_\sigma^+} \int a_1 |T_\sigma|^{b_1} d\varepsilon_m^p - \sum_{T_\sigma^-} \int a_2 |T_\sigma|^{b_2} d\varepsilon_m^p \tag{2.16}$$

where D is the total damage, $\sum_{T_\sigma^+} \int a_1 |T_\sigma|^{b_1} d\varepsilon_m^p$ and $\sum_{T_\sigma^-} \int a_2 |T_\sigma|^{b_2} d\varepsilon_m^p$ stand for the damages caused by positive cycles and negative cycles respectively, ε_m^p is the macroscopic strain, T_σ is the magnitude of stress, and a_1, a_2, b_1 and b_2 are constants which are obtained from the micromechanical analyses.

(2) Fatigue model based on a partition of energy and micro-crack growth (Maurel's model Eq. 2.17 [37])

$$\frac{da}{dN} = \lambda \left[\left(\beta_e \frac{W_e^{open}}{\gamma_e} a \right)^{m_e} + \left(\beta_p \frac{W_p^{open}}{\gamma_p} a \right)^{m_p} \right] \tag{2.17}$$

where subscripts of 'e' and 'p' stand for the elastic component and plastic component respectively, W^{open} is the opening energy, a is the crack growth in one cycle, γ is the surface energy, β is the constant to account for crack geometry effects, and m is the exponent for non-linear crack growth.

(3) Microstructure-based multistage fatigue model (Xue's model Eq.2.18 [38])

$$N_{total} = N_{Inc} + N_{MSC/PSC} + N_{LC} \tag{2.18}$$

with

$$C_{Inc} N_{Inc}^{\alpha} = \beta = \frac{\Delta \gamma_{max}^{p}}{2}$$

$$\left(\frac{da}{dN}\right)_{MSC} = \chi(\Delta CTD - \Delta CTD_{th}) \tag{2.19}$$

$$\left(\frac{da}{dN}\right)_{LC} = A\left[\left(\Delta K_{eff}\right)^{m} - \left(\Delta K_{eff,th}\right)^{m}\right]$$

where N_{total} is the total life, N_{Inc} is the number of cycles to incubate a crack at t micro-notch, N_{MSC} is the number of cycles required for propagation of a microstructurally small crack with the crack length, N_{PSC} is the number of cycles required for propagation of a physically small crack, N_{LC} is the number of cycles required for long crack propagation, β is the non-local maximum plastic shear strain amplitude around the inclusion calculated using an average of maximum plastic shear strain over an area approximately one percent of the inclusion area, C_{Inc} and α are the linear and exponential coefficients in the modified Coffin-Manson model at the micro-notch, ΔCTD is the crack tip displacement, ΔK_{eff} is the effective stress intensity factor range, and χ, A and m are constants.

Limitations of the models

Superficially these models are attractive because they relate physically measureable microstructural properties (e.g. crack growth in one cycle, void-growth, and crack length) to life or total damage. However they suffer from multiple serious limitations from the perspective of an engineering designer:

- They do not always directly relate to life, and this is a particular limitation of the damage models.
- They require the measurement of microstructural parameters of damage. This information is not readily available to design engineers, certainly not at the onset of design.
- They require sacrifice of the machine part – they require destructive testing.
- They have complex mathematical formulations that are not easily to conceptualise and apply to design.

- They have multiple coefficients, and each equation has coefficients that can only be determined empirically by fitting. They also have power law formulations.
- They provide no connection to mechanical properties that design engineers are familiar with, such as tensile strength. Consequently knowledge of mechanical properties is insufficient to be able to even estimate the coefficients of the equations.

Microstructural damage is fundamentally not the issue for design engineers. Instead such engineers assume that the material is in the intact condition. They accept that damage occurs to a machine element during its life, and in some specialised cases they may be interested in determining the residual life given knowledge of existing crack size. This is the case in the aviation industry, where airframes may be flown with known cracks, providing these are limited in size and location. In these cases the cracks are observable, and the material tends to be thin plate. Even so, the observations are not at the microstructural level – it is merely the gross features of the crack that are observed, e.g. through dye penetrant and other non-destructive methods. Engineering designers have a lower tolerance where cracks would be difficult to observe, e.g. in thicker components and in locations where inspection is difficult.

2.2 Review of creep-fatigue models

Creep-fatigue damage occurs when materials experiment cyclic loading under elevated temperature, where the creep effect is active. Therefore, creep-fatigue behaviour is defined as the combination of fatigue effect and creep effect. The review of the existing creep-fatigue models mainly focus on the empirical-based models, and some constitutive-based models are somewhat presented. This is because the empirical-based models normally present clearer/simpler numerical representations for engineering application than the constitutive-based models. This characteristic shown by the empirical-based models is very important for engineers who need to obtain the fatigue life through simpler physical parameters, such as applied loading, temperature and cyclic time. This is typically consistent with the attempt at developing a new creep-fatigue model for engineering application. In addition, a relatively short fatigue life is presented at the creep-fatigue condition due to the negative influence of creep, and thus most of the existing creep-fatigue models are based on the strain-life relation.

2.2.1 Accumulated-damage-based creep-fatigue models

The idea of accumulated damage in the creep-fatigue condition indicates that the total damage can be linearly accumulated by the damage caused by fatigue and creep. Generally, this is presented through the linear damage rule and the crack growth law.

2.2.1.1 Linear accumulation of damage

The conventional linear damage rule (Eq.2.9) was extended into the creep-fatigue situation through integrating the creep component, whereby the total damage (Eq.2.20) [8, 39] is defined

as the linear summation of the pure-fatigue damage (Eq.2.21) [27, 28] and the pure-creep damage (Eq.2.22) [40], and the final fracture appears when the total damage equals 1.

$$D = D_f + D_c \tag{2.20}$$

with

$$D_f = \sum_i \frac{n_i}{N_i} \tag{2.21}$$

$$D_c = \sum_i \frac{t_i}{t_{R(i)}} \tag{2.22}$$

where D is the total creep-fatigue damage, D_f is the pure fatigue damage, D_c is the pure creep damage, t_i is the duration of creep under the applied stress σ_i at temperature T_i, and $t_{R(i)}$ is the creep-rupture time under the applied stress σ_i at temperature T_i. Significantly, the linear damage rule can be applied to the condition with irregular loading, and the damage at each loading section are linearly accumulated to give the total damage.

For the situation with cyclic loading, based on the idea of linear damage rule where failure occurs when total damage reaches unity, the creep-fatigue life (N_f) can be evaluated by Eq.2.23:

$$N_f = \frac{1}{d_c + d_f} \tag{2.23}$$

where d_c is the creep damage for one cycle and d_f is the fatigue damage for one cycle. Normally, the fatigue damage for one cycle (Eq.2.24) is defined as the reciprocal of the fatigue life under the pure-fatigue condition (N_{f0}):

$$d_f = \frac{1}{N_{f0}} \tag{2.24}$$

The creep damage for one cycle can be given by Eq.2.25:

$$d_c = \int_0^{t_c} \frac{dt}{t_R(\sigma, T)} \tag{2.25}$$

where t_c is the cyclic time, and t_R is the rupture time presented as a function of applied stress and temperature.

When a hold period is introduced, the creep damage becomes more significant, and can be evaluated through the ductility exhaustion method, where the creep damage for one cycle is presented as [41, 42]:

$$d_c = \int_0^{t_h} \frac{\dot{\varepsilon}_{in}}{\delta(\dot{\varepsilon}_{in}, T)} dt \tag{2.26}$$

where t_h is the time of hold period, $\dot{\varepsilon}_{in}$ is the inelastic strain rate and δ is the rupture ductility (strain limit). This method indicates that inelastic strain plays an important role in creep damage,

and reflects that failure occurs when the accumulated strain over multiple cycles achieves the strain limit (δ). Considering the high-strain-rate effect at the early stage during the hold period, where less creep damage is produced than the latter portion, a modified ductility exhaustion model was then proposed (Eq.2.27) [41, 42]:

$$d_c = \int_0^{t_h} \left[\frac{1}{\delta(\dot{\varepsilon}_{in}, T)} - \frac{1}{\delta_0(T)}\right] \dot{\varepsilon}_{in} dt \tag{2.27}$$

where δ_0 is the ductility obtained under a sufficiently high strain rate.

To further improve the accuracy of fatigue-life prediction by the linear accumulation of damage, the total damage is divided into more components. For example, Manson et al. [43] proposed a constitutive material model, the strain range partitioning model. This model implies that the inelastic strain (plastic strain and creep strain) in a cyclic stress-strain loop is divided into four components: completely reversed plastic strain ($\Delta\varepsilon_{pp}$), tensile plastic strain reversed by compressive creep ($\Delta\varepsilon_{pc}$), tensile creep strain reversed by compressive plasticity ($\Delta\varepsilon_{cp}$), and completely reversed creep strain ($\Delta\varepsilon_{cc}$). Then, the damage caused by these four components are linearly accumulated to give the total damage (Eq.2.28), and structural failure occurs when total damage (D) reaches 1.

$$D = \frac{N_f}{N_{pp}} + \frac{N_f}{N_{cc}} + \frac{N_f}{N_{cp}} \; or \frac{N_f}{N_{pc}} \tag{2.28}$$

where N_{pp}, N_{cc}, N_{cp} and N_{pc} are the fatigue life under the strain of $\Delta\varepsilon_{pp}$, $\Delta\varepsilon_{cc}$, $\Delta\varepsilon_{cp}$ and $\Delta\varepsilon_{pc}$ respectively, and they obey the Coffin-Manson equation.

In addition, another constitutive material model (Eq.2.29) was developed by Sehitoglu [44], wherein the total damage is divided into three sub-damage categories caused by fatigue, oxidation and creep.

$$D = D_f + D_c + D_{ox} \tag{2.29}$$

where D_{ox} reflects the damage caused by oxidation. In this model, the fatigue damage (D_f), creep damage (D_c) and oxidation damage (D_{ox}) can be evaluated by Eq.2.21, Eq.2.30 and Eq.2.31 respectively.

$$D_c = \Phi_c \int_0^{t_c} A e^{(-\Delta H/RT)} \left(\frac{\alpha_1 \bar{\sigma} + \alpha_2 \sigma_H}{K}\right)^m dt \tag{2.30}$$

$$D_{ox} = \left(\frac{h_{cr}\delta_o}{B\Phi_{ox}K_p^{eff}}\right)^{-1/\beta} \frac{2(\Delta\varepsilon_{mech})^{(2/\beta)+1}}{\dot{\varepsilon}^{1-(a/\beta)}} \tag{2.31}$$

where Φ_c and Φ_{ox} are the phasing factors, $\bar{\sigma}$ is the effective stess, σ_H is the hydrostatic stress, K is the drag stress, α_1 and α_2 are scaling factors which reflect the damage produced in the periods of tensile loading and compressional loading respectively, t_c is the cyclic time, A and m are constants, h_{cr} reflects the critical crack length when crack starts to rapidly grow before

failure, K_p^{eff} is the constant of effective oxidation, $\Delta\varepsilon_{mech}$ is the mechanical strain range, $\dot{\varepsilon}$ is the strain rate, and δ_o, B, β and a are constants.

2.2.1.2 Crack-growth method

The conventional crack-growth law (Eq.2.10) was extended into the creep-fatigue condition through introducing the creep component. By this means, the total crack growth (Eq.2.32) [45] is calculated through the summation of fatigue crack growth (Eq.2.33) [29] and creep crack growth (Eq.2.34) [45], and failure occurs when the total crack achieves the critical size of the crack.

$$\frac{da}{dN} = \left(\frac{da}{dN}\right)_f + \left(\frac{da}{dN}\right)_c \tag{2.32}$$

with

$$\left(\frac{da}{dN}\right)_f = C\left(\Delta J_{eff}\right)^l \tag{2.33}$$

$$\left(\frac{da}{dN}\right)_c = \int_0^{t_h} AC^{*q} dt \tag{2.34}$$

where $\frac{da}{dN}$ is the total crack growth per cycle, $\left(\frac{da}{dN}\right)_f$ is the crack growth per cycle due to cyclic load changes (fatigue component), $\left(\frac{da}{dN}\right)_c$ is the crack growth per cycle due to hold time (creep component), t_h is the hold time, C^* is the time-dependent fracture parameter, and A and q are material constants obtained from experiments.

2.2.1.3 Overall evaluation for the damage-accumulated-based models

The damage-accumulated-based models show that fatigue damage and creep damage are calculated separately, and then linearly accumulated. However, the fatigue and creep effects do not produce damage in a fully separate way but partly interweave. In this case, the linear summation of fatigue damage and creep damage ignores the interaction between fatigue and creep [46, 47].

For the linear damage rule shown in section 2.2.1.1, failures are frequently observed to occur when $D_f + D_c < 1$ [47, 48]. This indicates that the additional damage caused by the interaction between fatigue and creep (D_{cf}) should be included, and failure occurs when:

$$D_f + D_c + D_{cf} = 1 \tag{2.35}$$

However, the mathematical expression for D_{cf} is unknown, thus Eq.2.35 still cannot be used to predict fatigue life.

In addition, the ignorance of interaction between fatigue and creep also appears in the crack growth law shown in section 2.2.1.2. Therefore, through involving the interactive effect [49, 50], the total crack growth should be represented as:

$$\frac{da}{dN} = \left(\frac{da}{dN}\right)_f + \left(\frac{da}{dN}\right)_c + \left(\frac{da}{dN}\right)_{cf} \tag{2.36}$$

where $\left(\frac{da}{dN}\right)_{cf}$ reflects the crack growth caused by the interactive effect of fatigue and creep. However, Eq.2.36 still cannot be used for fatigue-life prediction due to the unknown mathematical expression for $\left(\frac{da}{dN}\right)_{cf}$.

It seems that the strain range partitioning model (shown in section 2.2.1.1) peels off interactive effect from total damage, and the interactive component is shown by $\frac{N_f}{N_{cp}}$ or $\frac{N_f}{N_{pc}}$. However, this method is generally based on the transformation and decomposition of the hysteresis loop, and thus does not describe the interaction between fatigue and creep effects. In addition, the strain range partitioning model may present good ability of fatigue-life prediction in the situation of cyclic loading with hold time, but it is near impossible to segregate the $\Delta\varepsilon_{pp}$, $\Delta\varepsilon_{cc}$, $\Delta\varepsilon_{cp}$ (or $\Delta\varepsilon_{pc}$) components in a real-life cyclic stress-strain hysteresis loop under cyclic loading without hold time. Therefore, the accuracy and applicability of the strain range partitioning model are ineffective and inconvenient for engineering design.

Normally, we believe that the constitutive material models have better ability to describe creep-fatigue damage since they are derived from the fundamental theories of fatigue and creep, and some material properties are included. This is typically represented by Sehitoglu's model (shown in section 2.2.1.1). However, the interactive effect between fatigue and creep is still ignored. In addition, the constitutive models always present a complex structure, and thus are not convenient to be used by engineers. In this case, the empirical-based method might provide more favourable numerical representations for engineering application (The discussion of constitutive-based method and empirical-based method will be further discussed in Chapter 3). Although it is believed that the empirical-based models have better ability to be applied in engineering design because of their clearer/simpler structure, some disadvantages still cannot be ignored, and thus they are discussed in terms of the strain-based and stress-based models.

2.2.2 Coffin-Manson-based creep-fatigue models

The Coffin-Manson-based formulations describe creep-fatigue behaviour from the perspective of strain and show an extension of the conventional strain-life relation (the Coffin-Manson equation). These models are normally applied in the low-cycle regime, and the creep effect is presented through introducing frequency or/and temperature dependencies. In addition, these models were derived through an empirical-based method, and thus provide a more convenient approach to predict fatigue life for engineering application.

2.2.2.1 Coffin's equation

The first attempt for the extension of the Coffin-Manson equation was made by Coffin, who proposed the frequency-modified Coffin-Manson equation (Eq.2.37) [51]:

$$\varepsilon_p = C\left(N_f f^{k-1}\right)^{-\beta_0} \tag{2.37}$$

where f is the frequency and k is a constant obtained from experiments. In this equation, the fatigue life is modified by the frequency-related component and is named as frequency-modified fatigue life. In addition, the temperature effect is indirectly integrated into the coefficient of k, which is given by different values for different temperatures for one specific material.

Then, the frequency-modified Coffin-Manson equation (Eq.2.37) was further modified through directly incorporating the temperature dependence, such as Solomon's equation and Shi's equation.

2.2.2.2 Solomon's equation

Based on the frequency-modified Coffin-Manson equation (Eq.2.37) and creep-fatigue data for the material of Sn40Pb solder, a new creep-fatigue model (Eq.2.39) [52] was proposed by Solomon through introducing temperature dependence.

$$\varepsilon_p = C_1(T)\left(N_f f^{k-1}\right)^{-\beta_0} \tag{2.38}$$

with

$$C_1(T) = 1.338 - 2\times10^{-4}T - 1\times10^{-5}T^2 - 2\times10^{-7}T^3 \tag{2.39}$$

where T is the temperature in °C, β_o=0.5, and k is the constant and related to the frequency: k=-0.42 for $6\text{x}10^{-5}\text{Hz} \le f \le 3\text{x}10^{-4}\text{Hz}$ and k=-0.84 for $3\text{x}10^{-4}\text{Hz} \le f \le 0.3\text{Hz}$.

2.2.2.3 Shi's equation

Another modification of the frequency-modified Coffin-Manson equation (Eq.2.37) was conducted by Shi et al., and a creep-fatigue formulation (Eq.2.40) [53] was given based on the experimental data of 63Sn37Pb solder. The same as Solomon's equation, Shi's equation also shows the influences of both frequency and temperature on creep-fatigue behaviour.

$$\varepsilon_p = C_2(T)\left[N_f f^{k(T)-1}\right]^{-\beta_0(T)} \tag{2.40}$$

with

$$
\begin{aligned}
C_2(T) &= 2.122 - 3.57 \times 10^{-3}T + 1.329 \times 10^{-5}T^2 - 2.502 \times 10^{-7}T^3 \\
\beta_0(T) &= 0.731 - 1.63 \times 10^{-4}T + 1.392 \times 10^{-6}T^2 - 1.151 \times 10^{-8}T^3 \\
k_1(T) &= 0.919 - 1.765 \times 10^{-4}T - 8.634 \times 10^{-7}T^2 \\
k_2(T) &= 0.437 - 3.753 \times 10^{-4}T - 8.04 \times 10^{-7}T^2
\end{aligned}
\tag{2.41}
$$

where T is the temperature in °C, and $k_1(T)$ and $k_2(T)$ are the frequency-exponent functions for 10^{-3}Hz $< f <$1Hz and 10^{-4}Hz $< f < 10^{-3}$Hz, respectively.

However, not all strain-based creep-fatigue models follow the pattern of frequency-modified Coffin-Manson equation (Eq.2.31), such as Jing's equation, Engelmaier's equation and the Wong & Mai equation (discussed in the next sections), but they are all Coffin-Manson-type formulations.

2.2.2.4 Jing's equation

In contrast to Coffin's equation (Eq.2.38), Jing [54] proposed a temperature-modified Coffin-Manson equation (Eq.2.42) based on the empirical data of 80Au/20Sn, where the influence of the time-related parameter on creep fatigue is ignored, but temperature dependence is directly introduced.

$$
\frac{\Delta\varepsilon_p}{2} = C_3(T)\left(2N_f\right)^{\beta(T)} \tag{2.42}
$$

with

$$
\begin{aligned}
C_3(T) &= 68.79 - 0.34T + 250.56/\sqrt{T} \\
\beta(T) &= 1.29 - 0.0053T + 2.5/\sqrt{T}
\end{aligned}
\tag{2.43}
$$

where T is the temperature in °C. Jing's equation shows that the coefficient and exponent of the Coffin-Manson equation are modified to the functions of temperature.

2.2.2.5 Engelmaier's equation

Through incorporating the time-related parameter (frequency) with temperature, Engelmaier [55] proposed a new Coffin-Manson-type creep-fatigue equation (Eq.2.44):

$$
\varepsilon_p = C_4 {N_f}^{-\beta_0(\bar{T},f)} \tag{2.44}
$$

with

$$
\beta_0(\bar{T},f) = 0.442 + 6 \times 10^{-4}\bar{T} - 1.74 \times 10^{-2}\ln(1 + 43200f) \tag{2.45}
$$

where $\bar{T}$ is the mean temperature in °C and f is the cyclic frequency ($1 \le f \le 1000$ cycles/day). Engelimaier's equation represents a linear relation between fatigue ductility exponent and

temperature, and a logarithmic relation between the fatigue ductility exponent and frequency, which were derived from experimental data of 63Sn37Pb solder.

2.2.2.6 Wong & Mai's equation

To build a bridge between the pure-fatigue condition and the creep-fatigue condition, Wong & Mai [56] proposed a unified creep-fatigue equation (Eq.2.46) based on the empirical data of 63Sn37Pb solder. This equation accommodates the parameters of temperature, frequency and applied loading, and these parameters are identified to have a remarkable influence on creep effect.

$$\varepsilon_p = C_0 s(\sigma) c(T,f) N_f^{-\beta_0 b(T,f)} \tag{2.46}$$

with

$$\begin{aligned} s(\sigma) &= \begin{cases} 1 & when\ creep\ is\ dormant \\ exp\left[-\left(\sigma_{yield}\varepsilon_p^{n'}\right)/A\right] & when\ creep\ is\ active \end{cases} \\ c(T,f) &= 1 - c_1\left(T - T_{ref}\right) - c_2 \log\left(f/f_{ref}\right) \\ b(T,f) &= 1 - b_1\left(T - T_{ref}\right) - b_2 \log\left(f/f_{ref}\right) \end{aligned} \tag{2.47}$$

where *n'* is cyclic hardening index; *A*, c_1, c_2, b_1 and b_2 are positive constants; σ_{yield} is the yield stress, T_{ref} is the reference temperature (in Kelvin) below which creep becomes dormant and f_{ref} is the reference frequency above which creep becomes dormant. In particular, the Wong & Mai equation introduces the concept of 'the reference condition', which presents a threshold between pure fatigue and creep fatigue.

2.2.2.7 Overall evaluation for the strain-based models

Generally, the strain-based models started from the Coffin-Manson equation, and then the creep-related parameters, including temperature, frequency/time and applied loading, were incorporated through fitting empirical data. The goodness of these Coffin-Manson-based creep-fatigue equations shown in section 2.2.2 is discussed in terms of the unified characteristic and the integrated characteristic.

(1) Unified characteristic

In the present work, the unified characteristic is defined as the ability to cover multiple materials and multiple situations (the external factors, including temperature, frequency/time and applied loading).

On the one hand, the ideal creep-fatigue formulation should be applied for multiple materials, but the existing models may not entirely satisfy this requirement. Specifically, the relationships between different variables in the equations of Coffin, Solomon, Shi, Jing and Englemaier were

totally derived from empirical data of one specific material through curve fitting. This implies that these creep-fatigue models may only be effectively applied to the material where they were derived from, but may not be extended to other materials. In general, this is because the influences of temperature and/or frequency on creep fatigue for different materials may be different; for example, solder and stainless steel have quite different material properties. In this case, the relationships between the parameters obtained through curving fitting for one specific material may be different from the relationships given by the empirical data for other materials. However, the ability to cover multiple materials may be potentially accommodated into these creep-fatigue equations through recalculating the coefficients for each material. This is built on the assumption that the influences of temperature and/or frequency follow the same pattern for different materials. Although this modification gives these equations a potential opportunity to be equipped with the unified characteristic, poor economy is given since more empirical data are needed to get a better quality of fitting. In addition, the unified characteristic obtained through the numerical method is not a real sense of the unified characteristic because of no link to physical mechanisms.

On the other hand, an ideally unified creep-fatigue formulation should also be applied to multiple temperatures, frequencies/times and loadings. In this case, the model should accommodate all these parameters. However, the existing creep-fatigue model shown in section 2.2.2 (except Wong & Mai's equation) cannot fully satisfy this characteristic, where not all these related parameters are included. This situation is shown in Table 2.1.

Table 2.1 Goodness of unified characteristic for the existing creep-fatigue models

No.	Models	Materials	Variables		
			Temperature	Frequency	Loading
1	Coffin's equation (Eq.2.37)	SS 304	X	√	X
2	Solomon's equation (Eq.2.38)	60Sn40Pb	√	√	X
3	Shi's equation (Eq.2.40)	63Sn37Pb	√	√	X
4	Jing's equation (Eq.2.42)	80Au/20Sn	√	X	X
5	Engelmaier's equation (Eq.2.44)	63Sn37Pb	√	√	X
6	Wong & Mai's equation (Eq.2.46)	63Sn37Pb	√	√	√

Creep behaviour is generally influenced by temperature, time and applied loading. Briefly, elevated temperature accelerates the diffusion process, a longer time gives more time for creep promotion, and higher applied loading makes bonds between atoms more vulnerable. In this case, none of these three factors can be ignored to build a unified creep-fatigue formulation. As shown in Table 2.1, only time (frequency) dependence is accommodated in Coffin's

equation, only temperature dependence is included in Jing's equation, and for both the influence of temperature and time (frequency) are introduced into the equations of Solomon, Shi and Engelmaier, but all these three variables are involved in Wong & Mai's equation.

Overall, the equations of Coffin, Solomon, Shi, Jing and Englemaier do not present well the ability to cover multiple materials, and the ability to include relevant variables. However, Wong & Mai's equation may well present the unified characteristic. To be specific, Wong & Mai's equation, on the one hand, has the ability to cover multiple environmental factors (temperature, frequency/time and applied loading) since more relevant variables are accommodated into this equation. On the other hand, although this equation was built only based on the empirical data of 63Sn37Pb solder through curve fitting, it may still have the potential to be extended to other materials. This is because Wong & Mai's equation has seven independent parameters, which implies this equation may mathematically provide a good fit for the situations with multiple materials at different temperatures, frequencies and applied loadings. However, the more parameters that are included, the more empirical data are needed, and then a better quality of fitting can be obtained. This implies that Wong & Mai's equation has poor economy for engineering design; the economy will be discussed in Section 6.2.3.

The unified characteristic will be further discussed in Section 6.2.1, where the accuracy of fatigue-life prediction for multiple materials by using different models will be presented.

(2) Integrated characteristic

In the present work, the integrated characteristic is defined as the ability to cover the full range of conditions from the pure-fatigue condition to the pure-creep condition. In this case, the existing strain-based creep-fatigue equations cannot satisfy this requirement (see Table 2.2).

Table 2.2 Integrated characteristic for existing strain-based creep-fatigue models

No.	Models	Pure-fatigue condition	Creep-fatigue condition	Pure-creep condition
1	Coffin's equation (Eq.2.37)	X	√	X
2	Solomon's equation (Eq.2.38)	X	√	X
3	Shi's equation (Eq.2.40)	X	√	X
4	Jing's equation (Eq.2.42)	X	√	X
5	Engelmaier's equation (Eq.2.44)	√	√	X
6	Wong & Mai's equation (Eq.2.46)	√√	√√	X

√√: This equation can well describe the phenomena of this condition
√: This equation may describe the phenomena of this condition
X: This equation cannot describe the phenomena of this condition

Specifically, the existing models cannot be transformed to describe the pure-fatigue and the pure-creep behaviours. This is because that the creep-activation temperatures derived from these models are not consistent with our general understanding of creep activation (creep is activated when the temperature is higher than 35% of melting temperature for metals [57]). The detailed discussion on the integrated characteristic will be presented in Section 6.2.2.

In addition, between the pure-fatigue condition and the pure-creep condition, the goodness of creep-fatigue description can be represented by the unified characteristic. In this case, the equations of Coffin, Solomon, Shi, Jing and Engelmaier cannot represent a good fatigue-life prediction in multiple situations for multiple materials, because they were derived from empirical data of one specific material through curve fitting and do not accommodate relevant variables. In contrast, the Wong & Mai equation may well predict fatigue life since it can numerically fit multiple situations and multiple materials through incorporating amounts of empirical data. The unified characteristic will be further discussed in Section 6.2.1.

2.2.3 Basquin-based creep-fatigue models

The Basquin-based creep-fatigue equations describe creep fatigue in terms of stress, and represent an extension of the conventional stress-life relation (the Basquin equation). These models are normally derived from empirical data and applied in the high-cycle regime.

2.2.3.1 Kohout's equation

The existing literature shows that a number of empirical experiments have been conducted to explore the fatigue behaviour at elevated temperature in the high-cycle regime, where the fatigue strength has a strong dependency on temperature. However, the results obtained from these experiments have not been formulated as an equation to predict the fatigue life at the creep-fatigue condition. This problem has been somewhat addressed by Kohout [58], who proposed a temperature-modified Basquin equation (Eq.2.48):

$$\frac{\Delta\sigma}{2} = a\left(2N_f\right)^{-b} T^c \tag{2.48}$$

where *a*, *b* and *c* are constants obtained from experiments. This equation represents the product of the fatigue-related component ($a\left(2N_f\right)^{-b}$) and the creep-related component (T^c), and the temperature dependence is introduced in a power-law relation.

2.2.3.2 Mivehchi's equation

It is clear that fatigue effect and creep effect are separately represented in Kohout's equation (Eq.2.42), and the interactive effect between them is not numerically performed. This weakness was improved by Mivehchi [59], who proposed another formulation (Eq.2.49) to represent

creep-fatigue behaviour, where both the coefficient and exponent of the Basquin equation are modified as the functions of temperature.

$$\frac{\Delta\sigma}{2} = a_1(T)\left(2N_f\right)^{-b_1(T)} \tag{2.49}$$

with

$$a_1(T) = a_1(T_0)\left[1 - \frac{\frac{a_1(0)}{a_1(T_0)} - 1}{\ln\left(1 - \frac{T_0}{T_m}\right)} \ln\frac{1 - \frac{T}{T_m}}{1 - \frac{T_0}{T_m}}\right]$$
$$b_1(T) = b_1(T_0)\frac{\ln\left(1 - \frac{T}{T_m}\right)}{\ln\left(1 - \frac{T_0}{T_m}\right)} \tag{2.50}$$

where T_m is the melting temperature, T_0 is the room temperature, $a_1(T_0)$ and $a_1(0)$ are the fatigue strength coefficients at the temperatures of T_0 and 0K respectively, and $b_1(T_0)$ is the fatigue strength exponent at T_0.

2.2.3.3 Overall evaluation for the Basquin-based models

Amounts of stress-based creep-fatigue experiments were conducted to investigate the stress-life relation under the creep-fatigue condition, but most of them did not fit to any numerical formulation. This provides a capacious space for developing a stress-based creep-fatigue equation.

Kohout's equation and Mivehchi's equation shown in section 2.2.3 cannot well represent both the unified characteristic and the integrated characteristic. Firstly, Kohout's equation was derived from the observation of experimental data for different materials under various temperatures, which implies that this equation may have the ability to cover multiple materials. While Mivehchi's equation was developed from one specific material, thus it may not be extended to predict fatigue life for other materials. Both of these two equations cannot effectively predict fatigue life under multiple external conditions because the influences of frequency/time and applied loading on creep-fatigue behaviour are not included. As a result, the unified characteristic is not entirely accommodated into Kohout's equation and Mivehchi's equation.

In addition, Kohout's equation and Mivehchi's equation have the opportunity to represent the pure-fatigue condition. Specifically, both of them can be restored to the Basquin equation through letting the temperature component (T^c) equal 1 for Kohout's equation and substituting the temperature with room temperature (a reference temperature where creep is dormant) for Mivehchi's equation. However, Kohout's equation and Mivehchi's equation may not well represent creep-fatigue behaviour since only temperature dependence is included, and also cannot be transformed to the pure-creep condition because letting $\Delta\sigma = 0$ cannot give any numerical formulation for creep behaviour. Consequently, the integrated characteristic is not entirely represented by Kohout's equation and Mivehchi's equation.

2.2.4 Energy-based creep-fatigue models

2.2.4.1 Theoretical basis of the model

The power-law relation shown by the conventional energy-based fatigue model (Eq.2.51) [16, 60] can also be explained to present the relationship between total energy density and the number of cycles. This model ideally can be applied at both fatigue and creep-fatigue conditions.

$$\Delta W_t = W_f''(2N_f)^{\beta'} \tag{2.51}$$

where ΔW_t is the total energy density, and W_f'' and β' are constants which describe the energy absorption of a material.

2.2.4.2 Partition of energy

The existing research mainly focuses on finding a more accurate method to determine the total energy, since this is a critical part of the model. For example, Zhu et al. [61] proposed a unified criterion for creep-fatigue life prediction, where the total energy is represented as Eq.2.52:

$$\Delta W_t = \Delta W_p + \Delta W_e^+ - \Delta W_{lim} \tag{2.52}$$

where ΔW_e^+ is the tensile elastic energy density, ΔW_p is the plastic energy density, and ΔW_{lim} is the elastic energy density at fatigue limit which reflects the portion of the tensile elastic energy where no damage is caused. In addition, Jalaj et al. [62] indicated that the total input energy is partially consumed by the form of thermal energy, and the residual energy is totally stored to produce damage (for example, micro-cracks) and deformation (for example, dislocations). Thus the total energy is written as:

$$\Delta W_t = \Delta W_{thermal} + \Delta W_{f-damage} + \Delta W_{c-damage} + \Delta W_{f-deformation} + \Delta W_{c-deformation} \tag{2.53}$$

where $\Delta W_{thermal}$ is the energy density consumed in the form of thermal contribution, $\Delta W_{f-damage}$ and $\Delta W_{c-damage}$ are the energies (per cycle) which cause fatigue damage and creep damage respectively, and $\Delta W_{f-deformation}$ and $\Delta W_{c-deformation}$ are the energies (per cycle) which cause fatigue deformation and creep deformation respectively.

2.2.4.3 Overall evaluation for the energy-based models

The effort to improve the accuracy of the energy-based models has been attempted through decomposing the total energy into different components, such as plastic and elastic components in Zhu's equation, and fatigue and creep components in Kumar's equation. Although the accuracy may be improved, the complexity is enhanced. It is clear that the more components decomposed from the total energy given, the more complexity arises from evaluating the total energy presented. This is not desirable for engineering application; it is not easy for a design engineer to obtain the input energy or accurately determine the partition into the various

components. An inaccurate partition could significantly affect the accuracy of the outcome. The methods are mathematically complex in that they are not straight-forward to solve and do not present as neatly as say the Marin equation (Eq.1.1) with which design engineers are familiar. Of itself this is not a problem as computational power is no longer a significant barrier. Nonetheless the complexity of the formulations is potentially unattractive to design engineers, especially when coupled with the ambiguity about how the sub-components should be constituted in their specific situation. Design engineers generally prefer simpler conservative methods rather than complex ones in which they are not confident about the veracity of the outcomes.

Thus in our evaluation the energy-based models do not provide a viable path towards a creep-fatigue model that is intended specifically for design engineers as the users. Hence further improvements of the energy-based models is not included in the present work. The present work aims to find a creep-fatigue formulation which could be effectively and efficiently applied to engineering design.

Overall, the existing creep-fatigue equations shown in sections 2.2.1, 2.2.2, 2.2.3 and 2.2.4 have their own limitations on the prediction of creep-fatigue life. Specifically, the damage-accumulated-based models ignore the interactive effect between fatigue and creep; the strain-based and stress-based creep-fatigue equations are weak in representing the unifying, integration and economy; and the energy-based equations represent a more complex method for fatigue-life prediction. Consequently, the existing creep-fatigue models are inapplicable for engineering design, and thus provide an opportunity to develop a new creep-fatigue formulation for engineering application.

2.3 Empirical work

Creep fatigue occurs at an elevated temperature, and reflects the superposition of creep effect and fatigue effect. Some industries, such as nuclear, aerospace and microelectronic industries, are suffering from the influence of creep-fatigue damage because some components (such as, process reactor in unclear industry [63], fasteners and turbine blade in aerospace industry [64, 65], and solder joints in microelectronic industry [66]) in these industries are working at reversed loading and elevated temperature. Therefore, the creep-fatigue models are frequently used to describe damage behaviour and predict fatigue life in these industries.

Taking the nuclear industry as an example, creep-fatigue damage occurs on some components, such as blades, piping and tanks which are working at elevated temperature. Normally, the linear damage rule (Eq.2.20) and the crack growth law (Eq.2.32) are two main creep-fatigue evaluation and design methods in this area [8]. These two damage-accumulated-based rules show that the total damage is divided into a fatigue portion and a creep portion, and these two portions are calculated respectively and then linearly summated. This process implies that fatigue damage and creep damage occur separately, and no interactive effect between them is

included. Then over-estimation of creep-fatigue life may be represented, and thus a factor needs to be introduced to modify the result.

In addition, the creep-fatigue damage also happens in the microelectronic industry [67, 68], such as solder joints, where a mismatch of thermal expansion between the PCB (printed circuit board) component and the IC (integrated circuit) component is represented when power is turned on and off. Creep-fatigue behaviour has been studied on different solder materials, and then some models (which have been described in section 2.2.2) were developed, such as Shi's model and Jing's model. These models were derived from amounts of creep-fatigue experiments through curve fitting.

The creep-fatigue test normally is the major method to explore creep-fatigue behaviour, and the fatigue life is evaluated through conducting creep-fatigue tests under service conditions. In addition, some existing creep-fatigue models (such as the strain-based and stress-based models shown in sections 2.2.2 and 2.2.3) were also obtained through performing a large number of creep-fatigue tests. Although this method is expensive and time-consuming for industries, it is a relatively reliable way to predict fatigue life for one specific condition and develop a creep-fatigue model. Generally, a creep-fatigue test is conducted under elevated temperatures and cyclic loading (stress or strain). The combination of creep effect (caused by elevated temperature) and fatigue effect (caused by cyclic loading) enhances damage and then results in failure. Finally, the data of fatigue life vs. applied loading are recorded and then plotted to develop a stress/strain-life relation through curve fitting.

The creep damage is normally explored through performing a creep-rupture test. Generally, this test is conducted under elevated temperature and constant stress, and then progressive deformation leads to failure [8]. Finally, the empirical data of temperature vs. rupture time at multiple stresses are recorded and then plotted to extract the temperature-time relation. This relation is normally represented in the forms of the Sherby-Dorn parameter (Eq.2.13), the Larson-Miller parameter (Eq.2.14) or the Manson-Haferd parameter (Eq.2.15).

2.4 Gaps in the body of knowledge

The evaluation shown in section 2.2.5 indicates that the damage-accumulated-based models ignore the interaction between fatigue effect and creep effect. However, it is a complex problem to explore a numerical formulation to describe the interactive effect from the underlying mechanism, because it is nearly impossible to extract this component from the creep-fatigue process. In addition, the energy-based creep-fatigue models frequently tend to disassemble the total energy into different components for improving accuracy. However, this results in a more complicated method of fatigue-life prediction, which is not desired for engineering design. In this case, it is difficult to balance the accuracy and applicability for practical engineering cases. Consequently, the new creep-fatigue formulation could take the forms of the strain-life relation or/and the stress-life relation. Then the limitations shown by the existing creep-fatigue models may be partly, or even totally improved. In the present work, the gaps between the weaknesses

shown by the existing strain-based and stress-based creep-fatigue formulations and our attempted aims are identified as: (1) non-unifying; (2) non-integration; (3) poor economy; and (4) poor explanation.

2.4.1 Non-unifying

Generally, the relationships between different variables obtained from one specific material under specific temperature or/and frequency cannot be applied to predict fatigue life for other situations (including temperature or/and frequency) and other materials. This is a problem of poor external construct validity. This problem occurs because the model arises from curve fitting and insufficient experiments in multiple situations and multiple materials. For example, Shi's equation may only be applied to the material of solder, and Jing's model may not be used at other frequencies. Although some models potentially have the opportunity to be extended to other materials, this numerical-based modification cannot represent the real sense of the unified characteristic because there is no significant link to the underlying physical mechanisms of fatigue and creep.

Therefore, the present work is to build a new creep-fatigue equation the formulation of which could cover as many materials as possible and could be applied to fatigue-life prediction under multiple temperatures and frequencies.

2.4.2 Non-integration

The evaluation of the strain-based and stress-based creep-fatigue equations shown in sections 2.2.4.2 and 2.2.4.3 respectively, indicates that the existing models cannot be extended to the pure-fatigue condition or/and the pure-creep condition. For example, Shi's equation cannot be applied in the pure-fatigue condition where an impossibly infinite temperature is imposed, and Solomon's equation cannot be extended to the pure-creep condition because an unreasonable value of the creep activation temperature which is close to the melting point is given. In this case, the existing models cannot act as a bridge between the pure-fatigue condition and the pure-creep condition. This problem arises because these models were derived from empirical data through the method of curve fitting.

Therefore, the present work is to build a creep-fatigue formulation which can cover the full range of conditions from the pure-fatigue condition to the pure-creep condition.

2.4.3 Poor test economy

The existing strain-based and stress-based creep-fatigue models are based on amounts of creep-fatigue tests. This process is time-consuming and expensive, and thus shows a poor economy for engineering design. In this case, accuracy requires time and cost. For example, although Wong & Mai's equation may have the ability to represent the unified characteristic, this plausible advantage is obtained by sacrificing economy. This is because the Wong & Mai equation has seven independent coefficients, which implies that the quality of fitting is strongly sensitive to the amount of empirical data, and more data are required to purchase high accuracy.

Shi's model gives a high accuracy of fitting to empirical data, but at the expense of requiring a complex expression of coefficient and exponent that must be precisely determined using amounts of empirical data.

In addition, the models with poor economy tend to result in sparse data and this causes poor accuracy. This is because the multiple coefficients in these models are determined by curve fitting, and the accuracy thereof is highly dependent on the number of empirical data points.

This problem arises because the authors of these models desired close curve-fitting results for a specific situation, rather than understanding of creep-fatigue phenomena.

Therefore, the present work is to develop a creep-fatigue model whose coefficients can be obtained through a more cost-efficient solution. In addition, this new creep-fatigue formulation could accommodate relevant variables and have weak sensitivity.

2.4.4 Poor explanation

As the existing strain-based and stress-based creep-fatigue models were derived from curve fitting, the effect of fatigue and creep on life can only be explained numerically not physically. Note also the diverse range of mathematical formulations on offer. These models are based on curve-fitting convenience rather than physical phenomena of failure, as apparent in the general lack of physical motivation. Among these existing creep-fatigue models, although the negative influence of temperature and frequency on creep-fatigue life has been verified by a large number of creep-fatigue tests, this influence can only be represented mathematically and it has not been explained through microscopic deformation or dislocation.

Hence it is not possible to see microstructural attributes fully incorporated into models of creep and fatigue. This is a problem for all models in the literature.

At a fundamental level the failure of the part is caused by the progressive deterioration of the microstructure. There is a process whereby microstructure as supplied is subject to changes from the fabrication process. The microstructure further evolves in response to the applied loading in service. Eventually the damage results in gross failure of the part or machine element, and this corresponds to the end of its useful life. Hence there is a complex evolution of the microstructure over the life of the part. The general process is shown in Fig.2.2. In attempting to solve this problem, there are two broad classes of approach taken in the literature, and neither is fully successful.

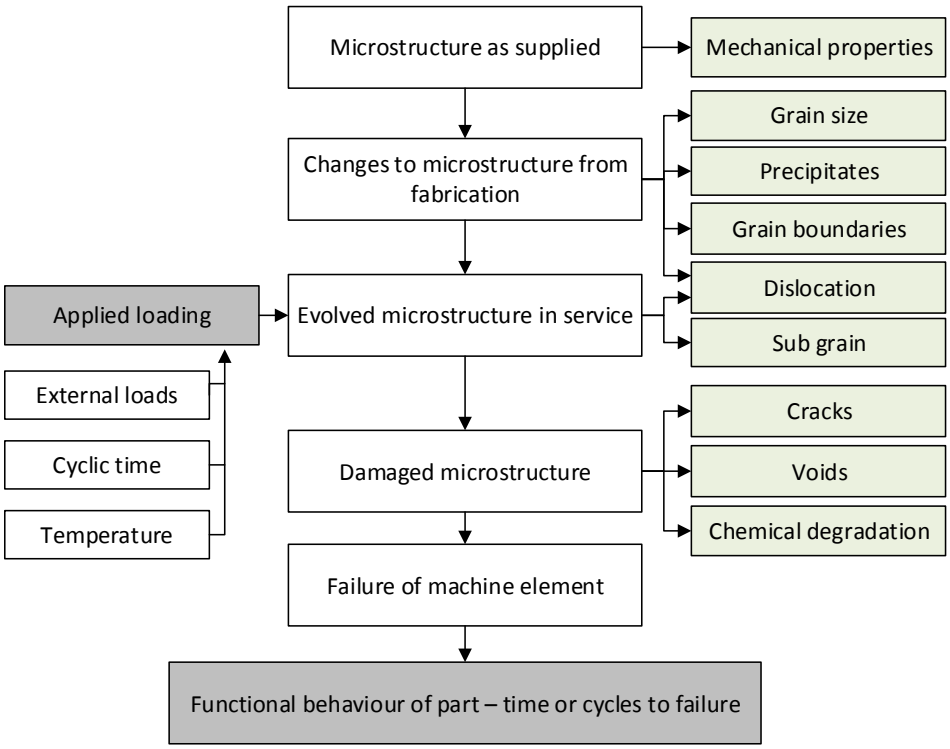

Figure 2.2 The general process of microstructural-based failure

In the first case are the methods based on physical observation of the microstructure, such as the damage and crack type models. These have the benefit of being based on observables. Even so they have parameters that must be fitted to empirical data. These models align well with a metallurgist point of view whereby macroscopic properties arise from the microstructure. There ought to be a causal relationship from the small to the large scale. However the reality is that this is still unknown. This class of models have the disadvantage that they do not relate to stress-strain variables and the full interaction of creep and fatigue as encountered by engineering designers. Furthermore, at least for the damage type models, they are not useful at the initial design stages where the material is in the virgin condition.

The second group are models that represent the functional output of the machine element, i.e. the time or cycle to failure for various input loading conditions (temperature, stress, frequency, etc.).

These have the benefit of being based on useful variables that design engineers can control (such as loading). They also relate directly to the functional purpose of the machine element, which is its life. They have parameters that must be fitted to empirical data. With good quality data the accuracy of the fit can be outstanding, hence giving design engineers confidence in using the material. These models align well with a design engineer point of view whereby the longevity and functional properties of the material are the reason why the material exists on the market. The disadvantage of these models is that that (a) their accuracy is critically dependent on the quality of the input test data, and this data is time consuming to obtain, (b) data is needed for each material in each condition (e.g., heat treatment) as the models are highly specific (poor external validity), (c) the models do not cover the full range of interactions between creep and fatigue in a single formulation. Disadvantages of a philosophical nature are

that (d) the models suffer from degeneracy (poor parameter identification), and (e) the coefficients have little or no physical meaning. In practice (d) and (e) are of no consequence in practical applications where the objective is only to predict life.

An ideal future state would be to find a creep-fatigue model that included the mechanical materials properties (such as elastic modulus, yield stress, hardness, etc.). No existing model does this satisfactorily. Why is this? We propose the reason is that the mechanical properties are dependent on the microstructure at the time the part is put into service, i.e. the virgin properties plus the effect of the production processes. However, and this is key, it is possible that the damage caused by thermal (creep) and cyclic (fatigue) loading is a complex emergent property, i.e. arises progressively and is high dependent on the immediate prior state of the microstructure in a chaotic manner. In which case it is to be expected that the relationship would be that *virgin mechanical properties* represent the *initial microstructural condition*, the *applied loading* affects the *evolution of microstructural damage*, which in turn results in life (time/cycles to failure). Consequently it is possible that the lifetime of the part does not have a simple or direct relationship with the mechanical properties.

In summary there may be intrinsic limitations in the ability of all existing models to describe the relationships between microstructure, mechanical properties, and part life.

2.4.5 Overly complex formulations for design purposes

In the present context *complexity* has multiple components. Possibly the least significant component is the *computational complexity*. This refers to the computational effort requires to solve the equations. This is a consequence of the mathematical formulation of the equations. With modern computational power this is not an issue on its own. Equations that require numerical simulation are not intrinsically a problem any longer.

The other form of complexity is the *ambiguity* of key variables. The issue here is that formulations have been offered in the literature that have either many coefficients, or variables that are difficult to determine from the perspective of a design engineer.

Those formulations that use multiple coefficients, such as Shi's equation (Eq.2.40), tend to have high *precision*: they can fit a curve to the empirical data very closely, hence small residuals. However this comes at the cost of high *specificity*: the coefficients only apply to that particular case, and cannot be extended. They also have a second problem of *model non-identifiability* or *degeneracy*: a different set of numerical coefficients might also solve the problem. Many of the existing equations in the literature have the risk of being structurally non-identifiable, and the more the tuneable parameters the greater the risk. It is rare to see any of the models evaluated in these terms. Consequently the trueness or *veracity* of the models is difficult to determine.

Even if the parameters do not suffer from degeneracy, there is a further problem if they are difficult to determine. In some case they require destructive testing – this is particularly the case with models that include microstructural damage. This is problematic for the design engineer, as the information is either not able to be practicably obtained, or is simply non-

existent (when the material is new). In all cases the parameters require multiple testing, which goes back to the issue of test economy (see above).

In none of the models except the simplest is there any connection between the coefficients in the model and the mechanical properties familiar to design engineers. Consequently knowledge of mechanical properties is insufficient for estimating the coefficients of the equations. This means that new materials, for which only the mechanical properties are known, cannot be used in the formulations.

If there is a new material in a specific microstructural condition, e.g. a new grade of alloy for use in gas turbine blades, then the design engineer has a major problem. Even if the mechanical properties are all quantified, and images exist for the microstructure, the design engineer has no method to consider this material for a creep-fatigue situation, until the creep-fatigue tests have been completed using reversed loading at multiple different temperatures and various cycling times. No bridge exists between the microstructural and macroscopic levels for design engineers. There is no predictive model in the literature. In all cases it is necessary to go through the tedious process of conducting the creep-fatigue tests. Even then, the best of the existing methods uses curve-fitting to determine coefficients – there is no connection to mechanical properties.

2.5 Summary

Creep-fatigue damage occurs when a material is exposed to reversed loading at elevated temperature, and thus is defined as the combination of fatigue effect and creep effect.

The behaviours of fatigue, creep fatigue, and creep are numerically presented by multiple formulations. In summary, the relationships between pure-fatigue models, creep-fatigue models and pure-creep models are shown in Fig.2.3:

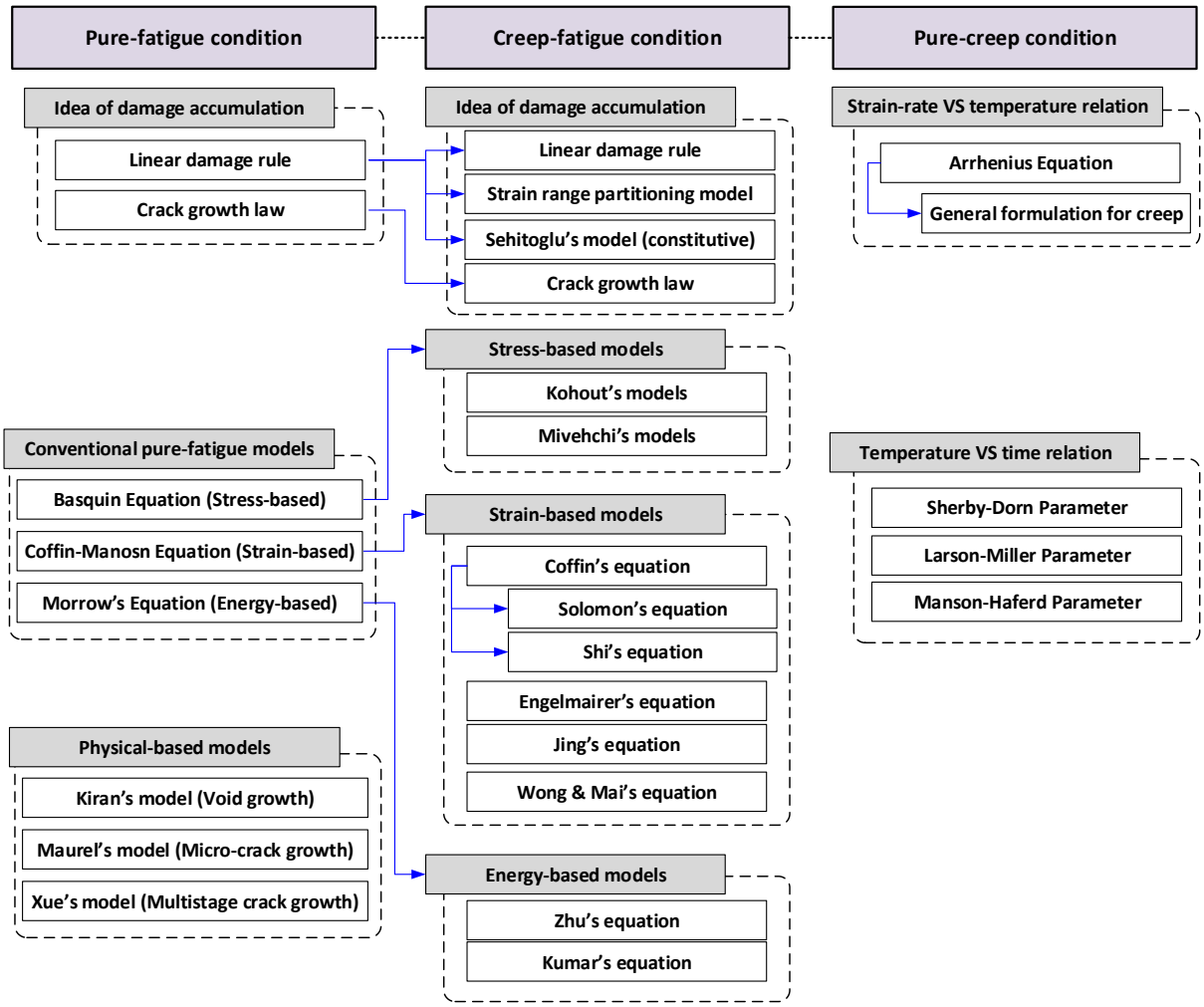

Figure 2.3 Relationships between models

Theoretically, fatigue effect and creep effect are not absolutely separate but partially interwoven; thus the total creep-fatigue damage is caused by the fatigue effect, the creep effect and the interactive effect between them. However, this interactive effect is ignored by the damage-accumulated-based models, including the methods (Eqs.2.20, 2.23, 2.28 and 2.29) extended from the conventional linear damage rule (Eq.2.9) and the method (Eq.2.32) extended from the conventional crack growth law (Eq.2.10). It is a complex problem to use a numerical formulation to describe the interactive effect from the underlying mechanisms; thus it is not included in the present work.

In addition, the effort to improve the accuracy of the energy-based models (Eq.2.52 and Eq.2.53) is mainly conducted to disassemble the total energy into different components. However, the more components which are disassembled, the more complexity is obtained. This is significantly not desirable for engineering application, and thus further improvements of the energy-based formulation is not included in the present work.

In addition, based on amounts of creep-fatigue experiments, some creep-fatigue models were developed through curve fitting, such as Coffin's equation (Eq.2.37), Solomon's equation (Eq.2.38), Shi's equation (Eq.2.40), Jing's equation (Eq.2.42), Engelmaier's equation (Eq.2.44), Wong & Mai's equation (Eq.2.46), Kohout's equation (Eq.2.48) and Mivehchi's

equation (Eq.2.43). These existing strain-based and stress-based models represent an extension of conventional fatigue models (the Basquin equation (Eq.2.1) and the Coffin-Manson equation (Eq.2.2)). However, they were derived from the specific situation and specific material through the high quality of curve fitting. Thus they cannot be extended to be applied in other situations for other materials; they cannot show the integration among pure fatigue, creep fatigue and pure creep; they cannot provide an economical method of fatigue-life prediction for engineering application and they cannot be linked to the underlying physical mechanisms. In this case, the gaps between existing creep-fatigue models and our attempted aims are identified as non-unifying, non-integration, poor economy and poor explanation.

Chapter 3

3. Methodology

This chapter gives a description of the methodology, wherein the research question is emphasized, and the method for deriving the new creep-fatigue model is proposed. In addition, the complexity of the present work is identified.

The existing strain-based and stress-based creep-fatigue models cannot cover multiple situations and materials, cannot integrate the full range of conditions from the pure-fatigue condition to the pure-creep condition, cannot provide an economical method for engineering design, and cannot reflect the physical phenomena. This provides an opportunity to develop a new creep-fatigue model which could represent the unified characteristic, integrated feature, economical method of fatigue-life prediction and consistency with physical mechanisms. Generally, this new model was developed through including an element of physical justification, whereby the creep effect was incorporated with fatigue effect. This new creep-fatigue formulation was validated with multiple situations and materials, and the advantages were then discussed.

Unified in this context refers to the combination of the multiple creep/fatigue load regimes, integration of multiple load characteristics of temperature and cyclic time, and applicability of the general formulation to multiple metallic materials.

3.1 Research question

Creep-fatigue behaviour is frequently described by the strain-life relation in the low-cycle regime only because such a loading condition is encountered in service. In this case, it is practical for the present work to develop the new creep-fatigue model taking the form of the strain-life relation for engineering application, which is highly recommended. Therefore, the

present work mainly focuses on the strain-based formulation. However, as the most classic method, the stress-life relation for the high-cycle regime may not be ignored since the combination of the strain-based model and the stress-based model construct a whole map for the loading condition. Although the stress-based creep-fatigue model is less practical than the strain-based model for the creep-fatigue condition, experimental-based research was still conducted to explore the stress-life relation. Therefore, a new stress-based creep-fatigue model is presented here but its importance is secondary to the strain-based creep-fatigue model.

According to the evaluations of the existing strain-based and stress-based models, there is a need for a new creep-fatigue formulation with the following attributes:

(1) This new creep-fatigue formulation needs to accommodate relevant variables, including temperature, frequency/cyclic time and applied loading, and to be applied to multiple materials.

(2) This new creep-fatigue formulation has the ability to cover the full range of conditions from the pure-fatigue condition to the pure-creep condition.

(3) The coefficients of this new formulation should ideally be obtained with minimum experimental effect, and have low sensitivity. This is important for industrial applicability.

(4) The relationships between different variables shown in this new formulation should be explained by the underlying physical mechanisms.

The present work seeks to develop a new creep-fatigue model that meets the above needs. We can evaluate this formulation through model validation parameters:

- *Does this model accurately represent the empirical data for multiple situations and multiple materials?*
- *Does this model have the ability to cover the pure-fatigue condition, the creep-fatigue condition and the pure-creep condition?*
- *Is this model practicable and useful for engineering design?*
- *Is this model consistent with the underlying physical mechanisms?*

In this present work, these questions will be answered by the new creep-fatigue formulation.

In addition, the new model aims to be applied for engineering design. In this case, it is desirable that this new model should have a clear structure that is understood by engineering practitioners, include the general variables at the engineering scale (such as temperature, time and loading), and be easily mathematically solved. In the present work, these requirements also will be satisfied by the new creep-fatigue formulation.

3.2 Approach

The approach was to identify the existing creep-fatigue models in the literature and evaluate them for advantages and disadvantages. Then a new creep-fatigue formulation was developed

through including an element of physical justification. This model was validated against empirical data for solder, stainless steel and other materials. Then based on the validation, the advantages of this model were discussed, and a case study was presented. Finally, the unified model was linked to the underlying physical mechanisms of fatigue and creep. Significantly, the new numerical representation is named as a 'unified' equation, and by 'unified' we mean that this refers to the combination of the multiple creep/fatigue load regimes, integration of multiple load characteristics of temperature and cyclic time, and applicability of the general formulation to multiple metallic materials.

The unified models developed in the presented work would be applied to describe creep-fatigue behaviour when temperature is higher than 35% of melting temperature and frequency is in the general range of engineering cases (where the combined effect of internal thermal and reversed loading is ignored).

The specific methodologies used, and their sequence, are shown as follows.

3.2.1 Foundational developments

Based on reading the literature, the existing creep-fatigue models were identified. These models are generally divided into four categories: the damage-accumulated-based models, the strain-based models, the stress-based models and the energy-based models. Then, the gaps between existing models and the attempted aims were found through discussing the advantages and disadvantages.

We identified that the damage-accumulated-based models ignore the interactive effect between fatigue and creep, but improving on this weakness is a complex problem due to the nearly impossibly numerical formulation derived from the underlying physical mechanisms. In addition, the energy-based models represent a complicated method to obtain more accurate fatigue-life prediction, but this is not desirable for engineering design. In this case, a complex problem to balance the accuracy and applicability for practical engineering cases is presented. However, the disadvantages presented by the strain-based and stress-based models, including non-unifying, non-integrated, poor economy and poor explanation, provide a possible opportunity to develop a new creep-fatigue formulation. These significant weaknesses were improved in the present work.

3.2.2 Fatigue capacity

The unified creep-fatigue model is based on the concept of 'fatigue capacity' which further explained and numerically applied in the present work. Briefly, this concept reflects that the full fatigue capacity is gradually consumed by the creep effect until the residual fatigue capacity is totally consumed, thus linking the full range of conditions from the pure-fatigue condition to the pure-creep condition. Significantly, the introduction of fatigue capacity accommodates the integrated characteristic and imposes the physical justification into the new creep-fatigue formulation.

The negative influence of the creep effect on the full fatigue capacity can be numerically represented in the form of '1-x', where x reflects the creep-related damage, and the full fatigue capacity is shown by unit damage. This expression gives the major structure of the unified creep-fatigue formulation and provides a reasonably numerical explanation of creep effect on fatigue (the negative effect of creep on fatigue capacity).

3.2.3 Method for developing the unified creep-fatigue model

3.2.3.1 The general methods to construct a numerical formulation

The existing creep-fatigue models are normally developed through two different methods, the constitutive-based method and the empirical-based method.

The constitutive-based method is typically conducted by exploring the physical phenomena of fatigue and creep, and including parameters representing the properties of the material. As mentioned in Chapter 2, some constitutive models were extended from the conventional idea of continuum damage, including the linear damage rule and the crack growth law. Examples of such models are presented in sections 2.2.1.1 and 2.2.1.2. The constitutive models based on continuum damage are successful in evaluating creep and fatigue separately, but do not address the interaction of fatigue and creep, hence weakening the applicability. The deeper issue is that the interactive effect between fatigue and creep is complex and the numerical formulism is unknown. Thus, it is difficult to further improve the continuum-damage-based models by introducing an interactive effect. Some constitutive models try to avoid the need to evaluate the interactive component, by treating the total damage or the fatigue ability as a single component. Examples are the model [69, 70] extended from the Chaboche model [71], the models [72, 73] that describe the crack-tip behaviour, and the model [74, 75] that evaluated dissipated energy. Although these models represent a comprehensive numerical representation of creep fatigue, they provide mathematically complex structures. Therefore, these models are not convenient to be used by engineers who need to obtain fatigue life through simpler physical parameters such as applied loading, temperature and cyclic time.

The empirical-based method is typically conducted by fitting a mathematical formula to the empirical data, with the emphasis on high quality of fit. By the empirical-based method, creep-fatigue behaviour is numerically represented; this is achieved by incorporating the creep-related parameters into one of the conventional fatigue models, such as the Coffin-Manson equation and the Basquin equation. Examples of such models are presented in sections 2.2.2 and 2.2.3. Generally, the models derived from the empirical-based method are more favourable for engineering application since these models provide simpler and clearer numerical representations, and thus are convenient to be used by engineers. However, these models cannot be linked to the underlying physical mechanisms, and thus cannot represent the unified characteristic, integrated feature and good economy (these disadvantages have been discussed in Chapter 2).

3.2.3.2 Ideal model linked to underlying physical mechanisms

Normally, the plastic strain-life relation is applied to describe fatigue behaviour in the low-cycle regime, while the fatigue behaviour in the high-cycle regime is represented by the stress-life relation. Therefore, to build a whole picture for the applied regime, the unified creep-fatigue model is represented as a strain-based formulation and a stress-based formulation, but the importance of the strain-based model is higher than the stress-based model since the loading condition in the low-cycle regime is more common in service. Ideally, the attempted creep-fatigue model is totally based on observation at the microstructural level. This implies that both the relationships between different variables and the coefficients in this model could be determined by the microstructural characteristics. However, this is a complex and difficult problem, especially to predict the coefficients without any empirical effort. In this case, the unified creep-fatigue model may be developed through a method that combines the constitutive-based method and the empirical-based method. Specifically, the relationships between different variables may be extracted from the conventional fatigue and creep models (but the material properties may not be included in this new model), and the coefficients of this new creep-fatigue model may be extracted from empirical data. This method was with a deliberate attempt throughout that the development of the unified model was based on the underlying physical mechanisms. This assumption was then proven through linking this new model to the underlying physical mechanisms.

We have been aware of the desirability of being able to quantitatively (not qualitatively) link the coefficients in a creep-fatigue model to factors at the microstructural level, such as grain size, misorientation angles of grain boundaries and crystal structure. By this means, the coefficients can be predicted through observing microstructure, and the creep-fatigue tests can be eliminated. However, this remains a difficult problem that has not been solved in the literature. The complexity arises because there is no known way to mathematically determine the impact intensity of macro-variables (such as temperature and time) on creep-fatigue behaviour at the fundamental level (micro-structural level).

In addition, although the coefficients in the existing creep-fatigue models are obtained by reasonably good curve fitting, this does not mean that the coefficients show a true representation of the underlying processes. The difficulty of quantitatively relating the coefficients with microstructure also could be presented through the concept of multiscale modelling (Fig.3.1) which shows a gradient process in terms of time and size scales. Specifically, an ideal numerical formulation (a computational modelling) should start from the first principle, then upgrade to the atomic scale, and then to grain scale. The most important stage is to build a bridge between grain scale and engineering scale, whereby the description in a microstructural level is upgraded to macroscopic level. However, this is a complex process. This is because the evolution in microstructural level has still not been fully researched, thus current research on computational modelling is only limited among the initial three stages. In addition, the link between microstructural scale and engineering scale can be identified as a dramatical leap since they do not stand at the same scales in time and size, and the distance between them is still unknown (it may involve more steps between them). Therefore, determining the coefficients in a creep-fatigue model upwards from the microstructural

characteristics has not been achieved before, and it is unclear how this may be done. While qualitative explanations and quantitative formulations exist for some of the processes at the individual levels, there is no existing theory that cover this whole scale.

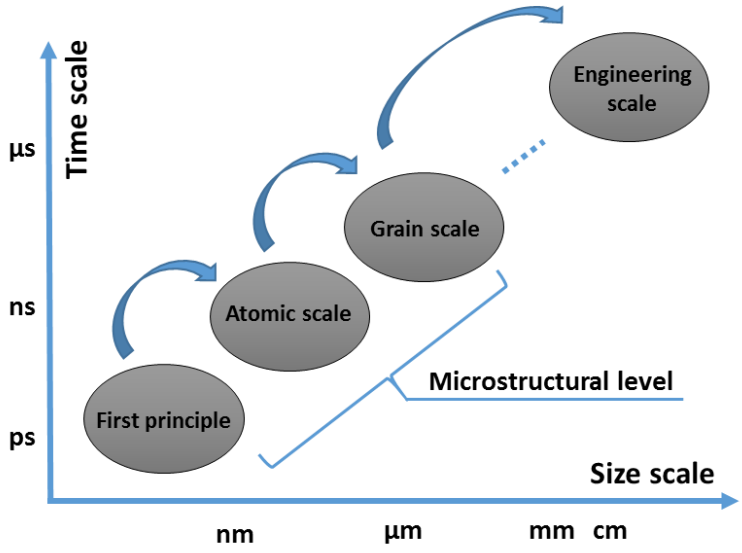

Figure 3.1 Presentation of multi-scale modelling

Consequently, attempting to determine the coefficients of a macroscopic model of creep fatigue from the fundamental microstructural characteristics is a seriously difficult problem. It is the long-term goal of the whole research field, and its accomplishment is an ideal future vision.

Nonetheless, what can be attempted within the present project is to develop a formalism for creep fatigue based on the combination of empirical data obtained from creep-fatigue tests and creep tests, and the deductive reasoning applied to microstructural characteristics and failure mechanisms.

Generally, the relationships between the macro-variables may be derived from the conventional models, while the coefficients may be extracted from empirical data and be partially related to the conventional models.

3.2.3.3 Critique of numerical solutions and curve fitting

A number of criticisms may be raised regarding the reliance on curve fitting to empirical data to construct the new creep-fatigue model.

First, this does not provide any difference in approach compared to existing models.

The existing models rely on numerical optimisation to some extent. There is no known formulation based on first principles that links microstructure, mechanical properties, and creep-fatigue life. It is possible that no explicit formulation exists, that instead the failure is an emergent phenomenon, see Section 12.3. The ideal model should be constructed by building a bridge between the grain and engineering scales, whereby the description at the microstructural

level is upgraded to the macroscopic level. However, this process has not been achieved before, and it is unclear how this may be done (see Section 3.2.3.2). Consequently for the foreseeable future it is necessary to apply numerical methods to represent the life.

Second, curve fitting results in models that are empirical, hence makes it difficult to improve on previous models that have shortcomings in their inability account for physical processes at the microstructural level.

Numerical representation of empirical data, and curve fitting, is needed for all models in the literature, including the energy-based methods. They all have coefficients that must be determined empirically. Other extant models, such as those based on power series, have an even greater reliance on numerical methods. Where the current model differs is that it is built on a physically plausible framework. In a way the unified model is similar to the energy based models in that it is based on physical principles (though not at such a deep level of physics) and is sparse in is use of coefficients (unlike the models that use extensive power series). Specifically, the relationships between different variables are extracted from the conventional models, whereby the physical events are indirectly incorporated. The unified model presented in Chapter 6 only has two independent coefficients (C_0 and β_0) which are determined by numerical optimization.

In contrast, the existing Coffin-Manson and Basquin-based models are purely empirical-based models, and thus no physical meaning is involved. Hence those models cannot present a broader set of conditions than the data on which they were built. In addition, those models are normally take the polynomial form, and the accuracy of curve fitting strongly depends on the number of power series. Thus, large amounts of empirical data are involved, and the test economy is poor. These issues are improved by the unified model (see Sections 6.2.1 and 6.2.3), even though the curve fitting is still required.

Third, the relationships between different variables are extracted from the conventional models. These conventional models were also developed from empirical data by curve fitting. This makes the new model again empirical. Hence it may be unclear how the present work improves on previous limitations.

The relationships between different variables in the new model are derived from the conventional models. However those conventional models are individual and separate – they each only represent one or a limited range of phenomenon. The key difference is that the present work integrated them holistically to present fatigue and creep effects. Specifically, this process is not simply completed by linearly summating different factors and giving different coefficients to each factor. Instead, the unified models were developed by organizing different parameters in a defensible manner, wherein the concept of fatigue capacity, the stress moderating functions, the well-known time-temperature parameters, and the reference condition are introduced; and a numerical simplification was applied (see Section 5.1). In this way, the link between this new model and the microstructural phenomena is partially built, and some of the limitations of the existing models are overcome.

Fourthly, numerical solutions risks causing model degeneracy, where multiple different sets of numerical values can have equivalent overall accuracy of fit.

The existing empirical-based models are constructed by multiple power series in the pursuit for high fitting-accuracy, and thus multiple independent coefficients are included. In this case, they may suffer from the problem of parameter non-identifiability or degeneracy: a different set of numerical coefficients might also solve the problem. However, this risk is avoided by the new model (See Section 6.2.4). This is mainly because that the new model has less independent coefficients which are determined by numerical optimization.

The advantages of the unified model (compared with the existing models) are discussed in Section 6.2, and the link between the unified models and the microstructural phenomena is discussed in Chapter 10.

3.2.3.4 Process of developing the new model

The development of the unified creep-fatigue model took a bottom-up method (Fig.3.2), where the development of a numerical formulation was started from a general understanding of the physical mechanisms. Specifically, an intended bottom-up process is normally conducted through the following nine steps:

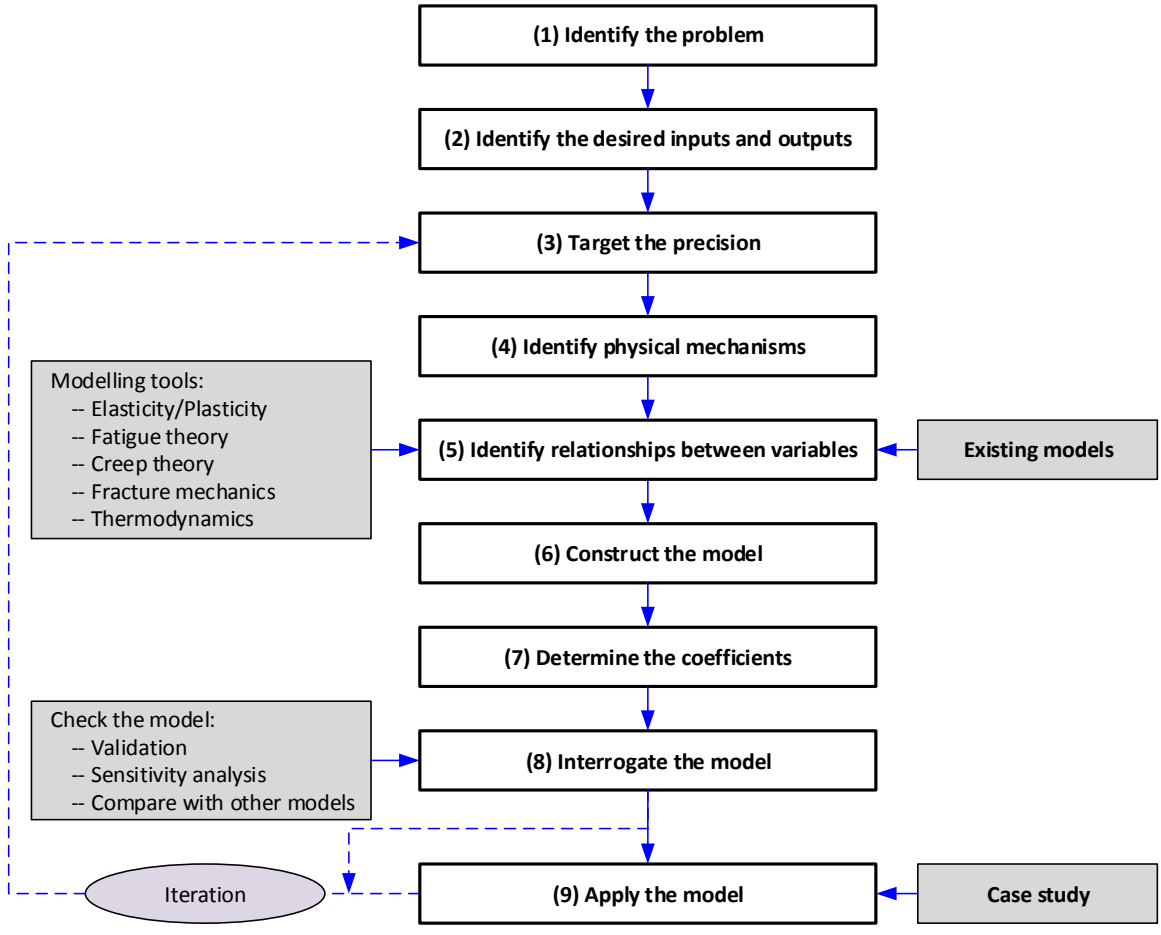

Figure 3.2 Process of bottom-up approach to the research

(1) The problems are identified through discussing the advantages and disadvantages of the existing creep-fatigue models. Briefly, the existing formulations show the weaknesses in

applying in multiple situations for multiple materials, covering the full range of conditions from pure fatigue to pure creep, providing an economical method for engineering design and giving a physical explanation.

(2) Relevant variables, including temperature, frequency/cyclic time and applied loading, are identified based on the literature review. In addition, creep-fatigue behaviour is attempted to be formulated as a plastic strain-life relation for the low-cycle regime and a stress-life relation for the high-cycle regime.

(3) The present work aims to improve the problems identified through evaluating the existing creep-fatigue models. The accuracy of fatigue-life prediction is evaluated by comparing the results calculated from the new formulation with the empirical data.

(4) The various behaviours that cause plastic deformation at the microstructural level are identified, such as diffusion behaviour for creep and crack growth for fatigue. This provides the opportunities to explore the relationships between the creep-fatigue-related variables.

(5) The relationships between different variables were extracted from the conventional models. These desirable relationships are reliable since the conventional models have been well validated in multiple situations for multiple materials. The consistency between the new model and physical mechanisms is then discussed in the chapter on 'physical explanation'.

(6) Based on the concept of fatigue capacity, a new creep-fatigue model was constructed by the relationships extracted from the conventional fatigue and creep models. Specifically, introducing the concept of fatigue capacity gives a major structure to the new creep-fatigue formulation. Then, this general formulation was further expanded through integrating with the relationships between different variables. This theoretical model may suffer from degeneracy, in that there may be too many coefficients to permit a unique calibration (different sets of numerical values for the coefficients may give equally good results). Consequently, a further state of reduction may be necessary. This did not appear in the present work. In addition, this theoretical model may be reduced to a simpler form through applying mathematical simplification or observing empirical data.

(7) The method for extracting the coefficients of the new creep-fatigue formulation was determined. Briefly, this method shows that both creep-rupture data and creep-fatigue data are needed, and minimizing the difference between empirical data and predicted data yields to the magnitude of coefficients. Particularly, the well-known time-temperature parameters, such as the Manson-Haferd Parameter and the Sherby-Dorn Parameter, are included. This significantly builds a link between the creep-fatigue situation and the pure-creep situation. The coefficients were determined by numerical optimisation using MS Excel ® and Matlab ®, as detailed in Section 6.1.

(8) The new creep-fatigue formulation needs to be interrogated through different aspects. Firstly, this new formulation should be validated on different materials under multiple temperatures and frequencies/cyclic times. The empirical data for multiple materials, including solder, stainless steel, superalloys and other materials, were extracted from the literature. During this process, the coefficients of this new model for different materials were given. In

addition, to emphasize the advantages of the new creep-fatigue formulation, it was compared with the existing creep-fatigue models and then was evaluated in the areas of the unified characteristic, the integrated feature, the economy and the physical explanation. Particularly, the sensitivity to the quality and quantity of raw data was analysed. In this case, we attempt to construct a formulation with relatively low sensitivity (good economy) and high accuracy, which is important for engineering design.

(9) Finally, this new creep-fatigue formulation should be practically applied in engineering design. In this case, a guide for engineering application was given, which generally represents the process of extracting the coefficients for one specific material and the application of this new formulation in practical situations. In addition, a case study was represented to further demonstrate the applicability of the new formulation for engineering design. The components, such as turbine blade and process reactor, which are working under elevated temperatures and cyclic loading, ideally can be selected to perform the case study. The structure and working environment can be extracted from the literature, and the results may be compared with the results obtained from finite element analysis.

If the interrogation of the unified model, and the practical application for engineering design cannot represent reasonable results, then a further modification of this new creep-fatigue formulation would be needed where the process of building the model is repeated.

3.2.4 Development of the strain-based unified creep-fatigue model

The strain-based unified creep-fatigue equation was developed by following the bottom-up method shown in section 3.2.3. Specifically, creep-fatigue behaviour is influenced by temperature, frequency/cyclic time and applied loading, and thus they were introduced to develop the strain-based approach. The relationships between different variables in the strain-based formulation were directly extracted from the conventional fatigue and creep models. For example, a natural exponential relation between plastic deformation and temperature is shown by the Arrhenius equation, the logarithmic relation between temperature and time is presented by the Manson-Haferd parameter, and the power-law relation between plastic strain and fatigue life is represented in the Coffin-Manson equation. Based on the concept of fatigue capacity, these relationships were then applied to construct the strain-based creep-fatigue model through numerically incorporating. There may be a need for simplification for engineering purposes.

Then an efficient method for extracting the coefficients of the strain-based equation was given. Specifically, the creep-related coefficients were derived from the empirical data of creep-rupture tests through the method of curve fitting, where the conventional creep models were introduced. Then other coefficients were obtained through minimizing the difference between the predicted life calculated by the unified formulation and the empirical data of creep-fatigue tests. This numerical optimization can be conducted by Excel or Matlab; ideally, Excel provides an easier method for engineering application.

The strain-based creep-fatigue equation was validated on materials with a low melting point (63Sn37Pb solder and 96.5Sn3.5Ag solder), a moderate melting point (AL2024-T3 aluminium alloy), and a high melting point (stainless steel 316 and stainless steel 304). The empirical data

of creep rupture and creep fatigue were extracted from literature, and the coefficients for different materials were given. An accurate prediction of fatigue life by using the unified model should result in a small error between predicted values and empirical data. In addition, according to the concept of fatigue capacity, the unified model should be capable of collapsing the dispersed strain-life data obtained at diverse temperatures and cyclic times into a cohesive strain-life formulaic representation (the reference condition).

However, there is a potential limitation. For the materials whose fatigue behaviour is strongly influenced by heat treatment, the coefficients obtained from one specific material condition cannot be extended to predict the fatigue life of the same material with other material conditions. Consequently, a modified formulation was proposed, where the parameter of grain size was introduced.

3.2.5 Inclusion of heat treatment via grain size

Normally, heat treating has significant influences on the mechanical properties, such as elasticity, ductility, strength, and hardness. This process can be evaluated through different variables, such as lattice structure, grain size, and the formation of precipitation, martensite, ferrite, cementite, and pearlite. However, most of them are unmeasurable as a parameter, thus are impractical to be introduced into a numerical formulation for engineering application. In this case, as a measurable parameter, the grain size was selected and then introduced to further modify the strain-based unified creep-fatigue equation.

The same method mentioned in section 3.2.4 was applied. Specifically, both the Arrhenius equation and the Hall-Petch equation give a power-law relation between grain size and fatigue capacity, and this relation was incorporated into the strain-based formulation. A simplification was applied to reduce the number of coefficients, which is based on the understanding of physical mechanisms and the observation of empirical data. Then, this modified formulation was validated on the materials of Inconel 718 and GP91 casting steel. The effective performance of the fatigue-life prediction provides a small error for fitting with the empirical data and transforms all raw data into the reference condition.

3.2.6 Development of the stress-based unified creep-fatigue equation

The strain-based formulation is normally used in the low-cycle regime, while the stress-based formulation describes creep-fatigue behaviour in the high-cycle regime. According to the development, the strain-based formulation, the variables of temperature, cyclic time, applied loading and grain size should also be accommodated into the stress-based creep-fatigue equation. The same method applied to develop the strain-based model was accepted to derive the stress-based model. Specifically, the relationships between different variables were directly extracted from the conventional fatigue and creep models. For example, the general creep-deformation equation gives the power-law relationship of grain size vs. applied loading and the natural exponential relationship of temperature vs. time, the Basquin equation shows the power-law relationship of applied loading vs. life, and the Hall-Petch equation represents the

power-law relationship of applied loading vs. grain size. Since these conventional models have been well verified through much empirical data in multiple situations for multiple materials, it is believed that these relationships are reliable and can be directly applied to construct the stress-based creep-fatigue equation. During the process of derivation, a simplification was needed to reduce the number of coefficients and recognize the numerical structure. This simplification is significantly important for engineering application.

Similar to the strain-based creep-fatigue formulation, the creep-related coefficients in the stress-based equation were extracted from creep-rupture data through curve fitting, where the conventional creep models were introduced. Then, other coefficients were obtained through minimizing the difference between the predicted life calculated by a stress-based formulation and the empirical data of creep fatigue.

The stress-based unified creep-fatigue equation was validated on Inconel 718 and GP91 casting steel. The creep-rupture data and creep-fatigue data were extracted from the literature, and then the coefficients for different materials were given. A good fit against empirical data gives a small error and transforms all raw creep-fatigue data under multiple situations into a cohesive situation where the reference condition is presented.

3.2.7 Advantages of the unified creep-fatigue equations

Creep-fatigue behaviour is frequently represented as the numerical formulation of strain-life relation which is more practical for engineering situation. Therefore, discussion of the advantages mainly focuses on the strain-based unified creep-fatigue equation through comparing with other existing creep-fatigue models (including Coffin's equation, Solomon's equation, Shi's equation, Engelmaier's equation, Jing's equation and Wong & Mai's equation). The advantages were shown in the following four aspects: the unified characteristic, the integrated characteristic, the good economy and the good physical explanation.

The unified characteristic is defined as the ability to be applied in multiple situations for multiple materials. This feature was evaluated by comparing the accuracy of fatigue-life prediction among different creep-fatigue models, and the empirical data were extracted from literature. In addition, the integrated characteristic refers to the ability to cover the full range of conditions from pure fatigue to pure creep. The creep-fatigue models were re-organized to represent the behaviour at the pure-fatigue condition or the pure-creep condition, and the consistency between the revised equations and the general understanding of fatigue or creep phenomena was then investigated. The good consistency demonstrates the ability to cover this loading condition. Furthermore, economy is important for engineering design, where a low cost and a highly accurate method for fatigue-life prediction is required. Since the creep-fatigue test is time-consuming and expensive (high cost), reducing the number of creep-fatigue tests can significantly improve the economy. In this case, the accuracies of fatigue-life prediction using the coefficients obtained under a different amount of raw data were investigated. We define the numerical model which could present a slight reduction in accuracy with the significantly decreased amount of empirical data gives good economy. Finally, the relationships between different variables should be consistent with the underlying physical mechanisms. This is

strongly related to the method of deriving the formulation. Specifically, the method of curve fitting cannot impose the underlying physical mechanisms onto the numerical representation, while the method including an element of physical justification can provide a good physical explanation for the creep-fatigue formulation.

In addition, the stress-based creep-fatigue model was also evaluated in the areas of unified and integrated characteristics through comparing with the existing stress-based models (Kohout's equation and Mivehchi's equation). The stress-based model also presents good consistency with the underlying physical mechanisms. In particular, the introduction of compatibility was discussed, which provides a more accurate description for the pure-fatigue condition.

3.2.8 Application of the unified creep-fatigue formulation

The unified approach should be effectively applied to engineering design. The strain-based unified formulation was selected to present the process of application only since such loading condition is frequently encountered in service. Firstly, a guide to apply this formulation was presented, which collects the requirements of experiments, the method of extracting the coefficients and the application to the specific situation. Then a case study was given to further demonstrate the applicability for engineering design. In this case study, the gas turbine blisk which works under elevated temperature and cyclic loading was selected, and the structure and service conditions were extracted from the literature. The theory of highly accelerated life test, which is normally used at the initial stage of design to improve the reliability of the product was accepted to determine the material of the turbine blisk. During the process, the fatigue damage and creep damage were evaluated separately, and the results obtained from the numerical calculation and finite element analysis (FEA) were compared. In particular, in the process of simulation, the fatigue-related coefficients obtained from the unified equation were imported into FEA as the engineering data, and this results in a significant reduction in the complexity of creep-fatigue simulation.

3.2.9 Physical explanation

Fatigue and creep behaviours show different underlying principles at the microstructural level. Specifically, the fatigue effect occurs via cracks through the grains while the creep effect involves the grain boundary cracking. In the present work, a crack-growth-based model was illustrated to show the extension of the crack at the grain level, where the situations of the crack tip within the grain, crack tip at the grain boundary and crack tip across the grain boundary were considered.

Creep-fatigue behaviour is normally influenced by temperature, frequency/cyclic time, applied loading and grain size. Briefly, elevated temperature accelerates creep diffusion, prolonged cyclic time gives more time for creep deformation, increased loading intensifies plastic deformation, and small grain size is beneficial to fatigue but negative to creep. The influences of these factors were described based on the fatigue and creep mechanisms at the microstructural level. In particular, the influence of grain size on fatigue and creep were further represented by simulating the process of crack growth in FEA. Specifically, a XFEM-based

simulation technique was applied to perform the crack-growth behaviour for fatigue, and a CZM-based method was used to conduct crack-growth simulation for creep. Then, the unified formulation was linked to the underlying physical mechanisms of fatigue and creep. This was achieved through explaining the relationships between defferent variables by investivating physical phenomena. In particular, the physical explanation proved that the deliberate attempt of the derivation is accurate.

3.3 Complexity

According to the description of the research method in section 3.2, the present work is regarded as a complex undertaking. This is because:

(1) The new creep-fatigue has multiple parameters, including the number of loading cycles, applied loading, temperature, frequency/cyclic time and grain size. The interlaced relationships between them are not understood at a fundamental level, and multiple conflicting formulations exist with no clear way of identifying their merits.

(2) Organizing the parameters is another challenge because this creep-fatigue model should be well constructed through representing the multiple parameters in a reasonable order to represent the fatigue and creep effect. The existing creep-fatigue models were derived from curve fitting; they provide multiple numerical formulations, thus they cannot give any general instructions for the development of a new formulation with an element of physical justification.

(3) This new creep-fatigue formulation has multiple coefficients, which are attempted to be obtained through minimum empirical effort. This is not simply accomplished through reducing the number of coefficients because there does need to be a balance between cost and accuracy. This is important for engineering design, which needs a low cost and high accuracy method for fatigue-life prediction. However, the existing creep-fatigue models cannot show the situation of low cost with high accuracy because the coefficients strongly rely on the quality and quantity of empirical data, and thus there is no instructional way of reducing the sensitivity of the creep-fatigue formulation.

3.4 Brief introduction to results

In the present work, the strain-based and stress-based unified creep-fatigue equations were developed through including an element of physical justification, and then the method for extracting the coefficients was proposed. The unified formulations were validated on the materials of solder, stainless steel, superalloys and others. Then comparing this new approach with the existing creep-fatigue models gives the following advantages:

(1) Ability to be applied in multiple situations for multiple materials;

(2) Ability to cover the full range of conditions from the pure-fatigue condition to the pure-creep condition;

(3) Economical method for fatigue-life prediction since minimum experimental effort is involved;

(4) Good consistency with the underlying physical mechanisms of fatigue and creep.

A case study on gas turbine blisk demonstrated the applicability of this unified formulation to engineering design. Finally, the unified formulation was explained at the microstructural level, and a crack-growth-based model (a graphical-based model) was proposed.

3.5 Summary

The numerical representations of creep-fatigue behaviour are presented as a strain-based formulation for the low-cycle regime and the stress-based formulation for the high-cycle regime. The new creep-fatigue model should: be applied in multiple situations for multiple materials; cover the full range of loading conditions; present an economical method for fatigue-life prediction; and give a reasonable physical explanation. The general process of developing the new formulation is shown in Fig.3.1. Specifically, the new creep-fatigue formulation started from the identification of the relevant variables and the physical phenomena, and it showed an extension of the conventional models based on the concept of 'fatigue capacity'. Then the method of extracting the coefficients was given, and this new model was validated on multiple materials. The empirical data were derived from the literature. The advantages of this new formulation were evaluated through comparing with the existing creep-fatigue models, where the unified characteristic, integrated feature, economy and physical explanation were investigated. Then the application of the unified creep-fatigue model was described, and a case study on gas turbine blisk was given. Finally, the physical explanation was presented through describing the influence of temperature, time and grain size on creep or/and fatigue behaviours at a microstructural level. Meanwhile, a conceptual graphical-based model was proposed based on crack-growth behaviour. The whole process is a complex work since the existing models do not provide any instructional method of determining the interlacing relationships between different variables, organizing the parameters in a reasonable order and obtaining the coefficients by minimum experimental effort.

Chapters 4 to 10 are the results of applying the methodology to develop, validate and evaluate the unified models, and Chapter 11 provides an application to turbine blisk design.

Chapter 4

4. Strain-based unified creep-fatigue equation

This results chapter describes the development of the strain-based unified creep-fatigue equation (without grain-size dependence). In this chapter, the strain-based model is constructed through including an element of physical justification and applying the concept of fatigue capacity, then the method to extract coefficients is given. Finally, this strain-based model is validated on multiple materials (63Sn37Pb solder, 96.5Sn3.5Ag solder, 2024T3 aluminium alloy, stainless steel 304 and stainless steel 316), which shows the high quality of fit to empirical data.

Publications relevant to this chapter are as follows (see Appendix A for details):

(1) Liu, D., D.J. Pons, and E.H. Wong, Proposal for a unified creep-fatigue equation, in International Conference on Innovative Design and Manufacturing (ICIDM). 24-26 Jan, 2016: Auckland, New Zealand.

(2) Liu, D., D.J. Pons, and E.H. Wong, The Unified Creep-Fatigue Equation for Stainless Steel 316. Metals, 2016. 6(9): p. 219.

(3) Liu, D., D.J. Pons, and E.H. Wong, Creep-integrated fatigue equation for metals. International Journal of Fatigue, 2017. 98: p. 167-175.

The strain-life relation is frequently applied to describe creep-fatigue behaviour in the low-cycle regime which is encountered in service, and thus the strain-based unified creep-fatigue equation is highly recommended in the present work. In this case, the strain-based formulation was developed to be applied in the low-cycle regime, and to present the relationship between the plastic strain and the number of loading cycles. The development of this new formulation started from the investigation of the physical phenomena, and then the pure-fatigue effect was numerically incorporated with the creep effect based on the concept of ‘fatigue capacity’. By

this means, the strain-based approach shows an extension of the Coffin-Manson equation; meanwhile, the Manson-Haferd parameter is introduced to show the creep effect.

4.1 Applying the concept of fatigue capacity

In the present work, the term 'fatigue capacity' is introduced to develop the unified model. This concept could be explained from two different perspectives:

- **Fatigue capacity represents the number of cycles which a material can carry under one specific cyclic loading (strain or stress).**

This gives the most conventional understanding of fatigue, where the creep-fatigue life is evaluated under one specific applied loading.

- **Fatigue capacity also can be defined to show the total accumulated damage which a material can resist under a specific number of cycles to failure.**

This explanation is based on the idea of damage accumulation, which indicates that failure occurs when the total damage is accumulated to a critical value. In this case, fatigue capacity gives this critical value of strain (or stress) for a specific creep-fatigue life.

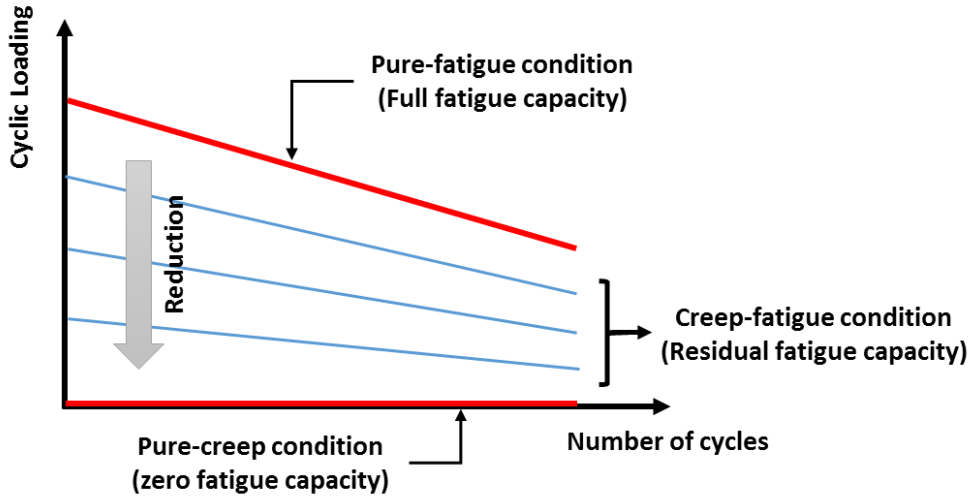

Figure 4.1 Description of 'fatigue capacity'

In the present work, we apply the term 'fatigue capacity' to describe the full range of conditions from pure fatigue to pure creep (Fig.4.1).

In Fig.4.1, the topmost curve shows the situation where creep is dormant. This is defined as the pure-fatigue condition and is presented as the full fatigue capacity. Then, the full fatigue capacity is gradually reduced because of the increasing influence of creep, where the residual fatigue capacity is given. This situation is named as creep-fatigue condition and is illustrated as a group of curves between the pure-fatigue curve and the x-axis in Fig.4.1. Finally, when the full fatigue capacity is totally consumed by the creep effect, the pure-creep condition is

presented. This is illustrated as a horizontal line which coincides with x-axis in Fig.4.1 and shows that the applied loading contributing to fatigue damage is zero.

In addition, fatigue capacity is more than definitions of fatigue life and damage accumulation in the following areas:

- The fatigue capacity shows a process where the full *fatigue* capacity is gradually consumed by the *creep* effect. We propose that the fatigue capacity is the basic capacity and at a physical level represents the crack growth phenomenon (e.g. through the grains). The creep effect imposes additional damage mechanisms at the microstructural level (see Chapter 9), which reduce the overall capacity. This leads to the premise that the mathematical representation of the failure process would take the form of '1-x', which is the basis of the unified creep-fatigue model. The first term implies the full fatigue capacity, and the second term reflects the creep-related damage. In this way, the introduction of fatigue capacity gives a numerical explanation of the negative effect on creep fatigue, and the physical phenomenon of creep activation is numerically included.
- The description of fatigue capacity also integrates three loading conditions into one common causal mechanism: pure-fatigue condition, creep-fatigue condition, and pure-creep condition. In this case, the established characteristics and mathematical representations of these various failure may be imported and adapted for inclusion in this new formulation.

Overall, the fatigue capacity shows a process where the full fatigue capacity is gradually consumed by the creep effect and links three loading conditions into one chain. In this case, the fatigue capacity gives the fundamental idea of developing the unified creep-fatigue equation and imports the integrated characteristic into this new formulation.

4.2 Development of the strain-based unified creep-fatigue equation

The discussion in Chapter 2 indicates that the existing creep-fatigue models have significant limitations. These disadvantages are fundamentally raised from the curve-fitting-based derivation method since the limitation of this approach is that accuracy does not necessarily translate into a robust description of the underlying physical mechanisms. Therefore, a new creep-fatigue model needs to be proposed by linking to the physical phenomena, whereby the weaknesses shown by the existing creep-fatigue models can be improved.

Generally, the development of the new creep-fatigue model started from the identification of relevant variables of creep-fatigue behaviour. Then, the relationships between different variables were extracted from the conventional models of fatigue and creep. This is based on the following definition:

The relationships between relevant variables shown in the conventional models are reliable. This is because these models have been well proven in multiple situations for multiple materials.

Then, we integrated these extant relationships holistically to reflect fatigue and creep effects. In this process, we included the concept of fatigue capacity, the reference condition, the stress moderating functions and the time-temperature parameter; and applied a numerical-based simplification to provide better applicability for engineering design.

4.2.1 Identification of creep-fatigue-related variables

In general, the creep-fatigue damage is caused by reversed loading at elevated temperature, thus it is recognized to have temperature, frequency/cyclic time and loading dependencies. In this case, these three parameters should be considered to develop the new creep-fatigue formulation.

Temperature is the main factor to activate creep behaviour [8, 76]. The threshold between pure fatigue and creep fatigue is normally defined as 35% of the melting temperature [57], and increasing temperature results in reduced fatigue capacity due to the intensified creep effect. The influence of temperature on creep fatigue has been frequently researched, whereby the temperature dependence was introduced to develop different numerical formulations for creep-fatigue behaviour, such as Shi's equation (Eq.2.34) and Engelmaier's equation (Eq.2.38). As a result, temperature dependence, which presents a remarkable effect on creep as well as creep fatigue, should be included to build the strain-based creep-fatigue equation. The influence of temperature on creep-fatigue behaviour will be further discussed in Section 10.1.1.

Frequency or cyclic time is identified as another main factor to influence creep-fatigue behaviour [76]. This fundamentally results from a general understanding of the creep mechanism which is normally defined as a time-dependent deformation. This definition implies that the longer the time (smaller frequency) leads to more accumulation of creep damage and then to more damage of creep fatigue. Significantly, this process is numerically described by a time-related formulation, such as the Arrhenius equation, where time dependence is presented in the form of rate and time-temperature parameters (including the Sherby-Dorn parameter, the Lason-Miler parameter and the Manson-Hafer parameter) where time is extracted at the stage of rupture. Consequently, it is necessary to introduce a time-related parameter into the strain-based creep-fatigue model. It is notable that the conventional frequency/cyclic time in the general range of engineering cases does not affect fatigue behaviour at the pure-fatigue condition, and the time-related effect only works when creep is active (the temperature is higher than 35% of the melting temperature) [76]. However, at the high-frequency (low-cyclic-time) situation (such as 1000Hz/0.001s) which is normally out of the general range of engineering cases, creep deformation is produced due to the heat generated by energy dissipation [77, 78], even though the environmental temperature is lower than the 35% of the melting temperature. This implies that a frequency-related threshold exists, above which the total damage is caused by the combined effect of internal thermal and reversed loading at the pure-fatigue situation (external temperature is lower than the 35% of the melting temperature). This situation is not

considered in the present work. The time-related influence on creep fatigue will be further described in Chapter 10.

General understanding of fatigue and creep shows that the damage is always intensified when applied loading is increased. This could be explained through the fact that the loading is the driving force of damage not only for fatigue but also for creep. Specifically, increased applied loading accelerates crack growth and damage accumulation for fatigue, which is numerically presented by Pair's law and conventional fatigue models (such as the Basquin equation and the Coffin-Manson equation). In addition, increased applied loading also accelerates diffusion process for creep, where a power-law relation between stress and accumulated damage is always presented in conventional creep models, such as the Arrhenius equation and its modified forms. Microstructurally, the loading effect is attributed to the condition of bonds between atoms, that is, increasing loading results in more vulnerable atomic bonds, which then leads to a more favourable situation for dislocation or diffusion.

Overall, the creep-fatigue damage has a significant dependency on temperature, time and loading, and thus their influences on creep fatigue should be considered to develop the new creep-fatigue formulation. The relationships between these variables could be extracted from the conventional fatigue and creep models. By this means, the weakness caused by the curve-fitting method (discussed in Chapter 2) could be somewhat improved, and a better engineering design theory could be provided.

4.2.2 Relationships between relevant variables

The relationships between the relevant variables (temperature, cyclic time and applied loading) recognized in section 4.2.1 can be extracted from the conventional models. Since these conventional models have been well demonstrated in multiple situations for multiple materials, it is reasonable to assume that these numerical representations are consistent with the physical phenomena. In this case, we can logically imagine that the relationships between different variables shown in the conventional models can describe fatigue and creep behaviours from a microstructural level. Therefore, these relationships can be ideally accepted, extracted and then applied to determine the sound relationships in the new creep-fatigue model. In this case, the new model is potentially linked to the underlying physical mechanisms, and this was proven in Chapter 10.

The determination of all possible relationships, including the relationships of temperature vs. strain, temperature vs. cyclic time and applied loading vs. fatigue capacity, are shown in the next sections.

Note that the relationship between time and creep-related strain was not identified. This is because this relationship has a significant dependency on the stages of creep behaviour, which results in a complex situation. Specifically, structural failure may occur either in the initial stage or the steady stage of creep deformation under the low-cycle fatigue, where two different time-strain relationships are proposed. However, it is difficult to determine the stage of final fracture.

4.2.2.1 Relationship between temperature and strain

Generally, a higher temperature gives more creep damage, and thus a directly proportional relationship between them is presented. In the present work, we believe that temperature only does work when it is higher than 35% of the melting temperature due to the activated creep effect, and the fatigue behaviour is independent of temperature when the creep is dormant (temperature is below 35% of the melting temperature) [76]. Therefore, the temperature dependence is directly related to creep damage (creep strain), and the relationship between temperature and creep strain should be investigated. As mentioned in Chapter 2, creep behaviour is normally divided into three stages, in which the second stage shows the most steady state of creep deformation and occupies the most time of the creep process. The observation of creep behaviour in this steady stage gives the Arrhenius equation (Eq.4.1):

$$\dot{\varepsilon} = Ae^{\frac{-Q}{RT}} \tag{4.1}$$

where $\dot{\varepsilon}$ is the strain rate, Q is the activation energy of the creep mechanism, T is the absolute temperature, R is the Boltzmann's constant and A is constant. Significantly, this equation numerically presents the fact that higher temperature results in more creep strain, and a natural exponential relationship (Eq.4.2) between them is given:

$$\varepsilon \propto e^{-1/T} \tag{4.2}$$

Although this relation was derived from the steady stage of creep, we believe that it still could be extended to other stages since temperature dependence is physically related to diffusion behaviour which is temperature-motivated behaviour and independent of creep stage (this will be discussed in Chapter 10). However, the linear relationship between time and creep-related strain shown by the Arrhenius equation (Eq.4.1) is not considered to develop the strain-based formulation. This is because time has a strong dependency on the creep stage, and it is unreasonable to assume that creep-fatigue failure occurs at the steady stage of creep behaviour in the low-cycle fatigue regime (but this assumption will be applied to developing the stress-based model as the total failure time is long enough in the high-cycle fatigue regime).

As a result, a natural exponent relationship between temperature and creep-related strain could be introduced into the new creep-fatigue model. This relationship is physically consistent with creep behaviour and is reasonably extended to the creep-fatigue situation.

4.2.2.2 Relationship between temperature and time

It is well-known that increased temperature or prolonged time results in more accumulation of creep damage. In this case, we propose that for a first approximation they are independent of each other rather than convoluted with each other, hence the overall effect is additive (this approximation will be applied to construct the unified formulation in section 4.2.3). However, this statement is only one aspect of describing the temperature-time relation, which is based on the situation with unspecified creep damage. When the creep damage is specified, the temperature can be related to time to show an inversely proportional relation. For example, for one specific creep damage, the effect caused by increasing temperature could be compensated

for by decreasing the time. This behaviour is represented by the Arrhenius equation, which implies that higher temperature accelerates creep-strain accumulation, then one specific creep damage is achieved within a shorter time period. In this case, the Arrhenius equation numerically and physically gives a natural exponential relation (Eq.4.3) between temperature and time:

$$t \propto e^{1/T} \tag{4.3}$$

Also, the conventional time-temperature parameters also numerically indicate the inverse proportional relationship of time vs. temperature, wherein time is addressed as rupture time. Specifically, both the Sherby-Dorn parameter and the Larson-Miller parameter were derived from the Arrhenius equation, but different assumptions were applied. As a result, a natural exponential relationship (Eq.4.3) between temperature and time is given by the Sherby-Dorn parameter, while the Larson-Miller parameter represents a logarithmical relationship between them (Eq.4.4). Both of these two time-temperature parameters have sound physical fundamental, and thus it is reasonable to believe that the time-temperature relations (natural exponential relation and logarithmical relationship) shown by them are consistent with creep mechanism. Note that Eq.4.4 was extracted from an additive relation in the Larson-Miller parameter, and thus we address that Eq.4.4 cannot be directly included in the new equation taking the form of $T \cdot \log(1/t)$. This is strongly consistent with the preceding statement, which indicates that the temperature effect and the time effect can be additive, and shows an inversely proportional relation between them. Both of these two pieces of information could be accepted and applied to develop the new creep-fatigue formulation.

$$T \propto \log(1/t) \tag{4.4}$$

Another time-temperature parameter, the Manson-Haferd parameter, was extracted from empirical data, and a logarithmical relationship (Eq.4.4) between time and temperature is also indicated. Although this parameter does not have a physical basis [8], it has been well validated in multiple situations for multiple materials with high accuracy for describing the creep-rupture characteristic [35]. Compared with other Arrhenius-equation-based parameters, the Manson-Haferd parameter has been found to be the most successful method for describing the creep-rupture behaviour of engineering metals [35]. In this case, we conclude that the Manson-Haferd parameter has a better ability to present the physical phenomenon of creep, and the logarithmical relation shown in this parameter is reliable and acceptable.

This logarithmical relation was extracted from the creep-rupture behaviour, and thus this time dependence (shown in Eq.4.4) is identified as rupture time. In the present work, this time dependence can be re-defined as the cyclic time in the creep-fatigue condition. This is because:

The pure-creep condition could be ideally regarded as the creep-fatigue situation with extremely prolonged cyclic time, and thus it is reasonable to replace the creep-deformation time in the pure-creep condition into cyclic time in the creep-fatigue condition.

This operation may also give the unified model a possible chance to present creep behaviour according to the pure-creep condition.

Consequently, a logarithmical relation is extracted from the Manson-Haferd parameter to show the relationship between temperature and cyclic time. This provides a good numerical description of creep behaviour, and thus acceptably is included to develop the new creep-fatigue formulation.

4.2.2.3 Relationship between loading and life

Fatigue behaviour presents a process of gradual accumulation of damage, which is macroscopically presented as the crack-growth behaviour. Normally, this process is divided into three phases: crack initiation, crack propagation and structural fracture. Primarily, the second stage presents a relatively steady state and consumes most of lifetime to structural failure. A numerical representation (Eq.4.5) of this stage is proposed by Paris [29] based on the observation of crack-growth behaviour, where a power-law relation between the stress-related parameter and crack growth rate is presented:

$$\frac{da}{dn} = C(\Delta K)^m \tag{4.5}$$

where $\frac{da}{dn}$ is the crack growth rate which reflects the length of the crack growing during the period of one cycle, ΔK is the range of stress intensity factor, and C and m are constants. This equation remarkably shows that the damage is accumulated in a power-law form with applied loading.

Also, the direct exploration of loading-life relation based on a number of experiments gives the conventional fatigue models, including the Basquin equation and the Coffin-Manson equation, where a power-law relation between applied loading and fatigue life is presented. These conventional fatigue models can also be understood from the perspective of damage accumulation. To be specific, the irreversible damage (strain or stress) is gradually stored in the structure with an increased number of cycles, and then the structural failure occurs when the total damage achieves a critical value.

Consequently, the crack-growth behaviour expresses a power-law relationship between life and the loading-related parameter. This is numerically represented by Paris' equation and pure-fatigue models, which are significantly consistent with physical phenomena. In this case, this power-law relationship can be introduced to relate fatigue capacity with fatigue life.

Overall, the possible relationships between different variables were directly extracted from the conventional fatigue and creep models. These relationships are collected in Table 4.1 and could be applied to develop the new creep-fatigue formulation.

Table 4.1 Possible relationships between relevant variables

No.	Variables	Relationships
1	Temperature vs. strain	Natural exponential relation
2	Temperature vs. cyclic time	Logarithmical relation

3	Loading vs. life	Power-law relation

4.2.3 Constructing creep-fatigue formulation

Based on the relationships between different variables identified in section 4.2.2, the creep-fatigue formulation can be numerically constructed based on the concept of fatigue capacity (shown in section 4.1), which indicates that the presence of creep reduces the full fatigue capacity ($\varepsilon_{p,ref}$).

Since fatigue capacity for the creep-fatigue condition is influenced by temperature, cyclic time and applied loading, the reduced fatigue capacity is postulated as given by Eq.4.6:

$$\varepsilon_p = c(\sigma, T, t_c)\varepsilon_{p,ref} \tag{4.6}$$

where ε_p presents residual fatigue capacity due to the creep effect, and the function $c(\sigma, T, t_c)$ reflects the fatigue moderating behaviour and is named as the creep-damage function to numerically represent the creep effect. Then, based on the concept of fatigue capacity, function $c(\sigma, T, t_c)$ is further expanded as the form of '1-x', and Eq.4.6 is given:

$$\varepsilon_p = \varepsilon_{p,ref}[1 - c'(\sigma, T, t_c)] \tag{4.7}$$

where the produce of $\varepsilon_{p,ref}$ and $c'(\sigma, T, t_c)$ reflects creep-related strain. We assume that time and temperature were not convoluted with each other, and thus the overall effect caused by temperature and time are additive. We show after, this assumption gives sufficiently accurate outcomes. Then the function $c'(\sigma, T, t_c)$ is split into a thermal component and a time component:

$$\varepsilon_p = \varepsilon_{p,ref}[1 - c_1'(\sigma, T) - c_2'(\sigma, t_c)] \tag{4.8}$$

where functions $c_1'(\sigma, T)$ and $c_2'(\sigma, t_c)$ represent thermal-related and time-related effects on the full fatigue capacity respectively, which implies that the full fatigue capacity is gradually consumed at elevated temperature and prolonged cyclic time.

As shown in section 4.2.2, two relationships should be included. They are:

(1) A natural exponential relationship of temperature vs. creep-related strain;

(2) A logarithmical relationship of temperature vs. cyclic time.

In addition, three important trends should be considered. They are:

(1) The direct proportion between temperature and creep-related damage, which implies that increasing temperature results in decreased fatigue capacity;

(2) The direct proportion between cyclic time and creep-related damage, which implies that prolonged time leads to decreased fatigue capacity;

(3) The inverse proportion between cyclic time and temperature, which implies for one specific creep damage, the decreased fatigue capacity caused by increasing temperature can be compensated for by reducing time.

These relations then are introduced into Eq.4.8, and Eq.4.8 is regenerated as:

$$\varepsilon_p = \varepsilon_{p,ref}\left[1 - c_1(\sigma)e^{-1/T} - c_2(\sigma)e^{\log t_c}\right] \tag{4.9}$$

Significantly, the expressions of $exp(-1/T)$ and $exp(\log t_c)$ are not simple formulas, thus Eq.4.9 is not appropriate for engineering application. In this case, a numerical simplification should be applied to produce a simpler formulation. Specifically, the expression of $exp(-1/T)$ can be simplified as a linear dependence when the temperature is high enough and within the application range (normally the range of experimental investigation). For example, at the temperature range from 650K to 1000K, a linear relation between temperature and $exp(-1/T)$ is illustrated (Fig.4.2), wherein a small error (R^2=0.985) of linear fitting is given.

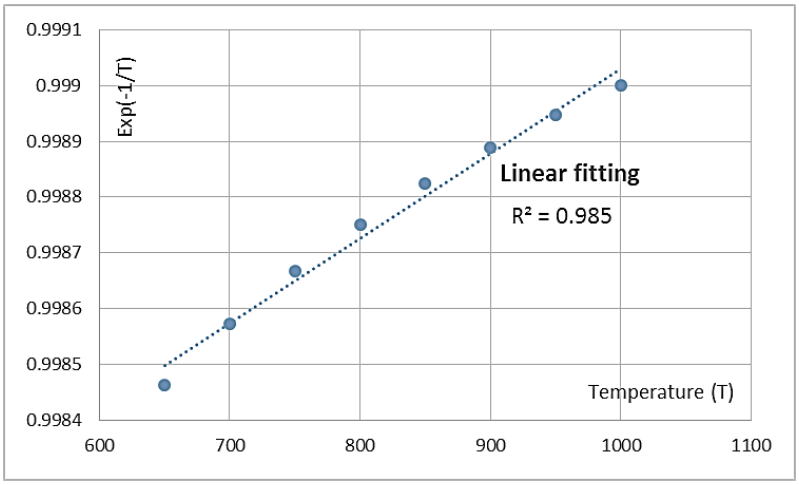

Figure 4.2 A linear relation between temperature (T) and $exp(-1/T)$

As a result, this numerical simplification gives a linear relation between temperature and creep-related strain:

$$\varepsilon \propto T \tag{4.10}$$

It is notable that this simplification retains the trend of temperature effect, where higher temperature results in more creep damage and reduces fatigue capacity. Then this simplified relationship (Eq.4.10) is incorporated into Eq.4.8, and the residual fatigue capacity is further modified as:

$$\varepsilon_p = \varepsilon_{p,ref}[1 - c_1(\sigma)T - c_2(\sigma)\log t_c] \tag{4.11}$$

Eq.4.11 remarkably provides a simpler formulation to represent the thermal effect and time effect, and shows the direct proportion of temperature vs. creep-related damage, cyclic time vs. creep-related damage, and the inverse proportion of temperature vs. cyclic time. Since $\varepsilon_{p,ref}$ describes fatigue capacity for the pure-fatigue condition, it can be formulated as the Coffin-

Manson equation. By this means, the power-law relationship between applied loading and life is introduced. Then, Eq.4.11 is given the form of:

$$\varepsilon_p = C_0[1 - c_1(\sigma)T - c_2(\sigma)\log t_c]N_f{}^{-\beta_0} \tag{4.12}$$

where C_0 and β_0 reflect fatigue behaviour at the pure-fatigue condition.

Note that C_0 and β_0 are empirically determined properties, which may be determined from data produced by conventional pure-fatigue tests. As such the coefficients do not explicitly include material properties such as tensile strength as in the simpler formulations. These parameters scale with tensile strength but not in an explicit formulation.

The loading-related (stress) dependence is incorporated into the functions $c_1(\sigma)$ and $c_2(\sigma)$ as the correction coefficients for thermal component and time component. The general equation of steady creep state shows the relationship of temperature vs. stress ($\sigma \propto Te^{1/T}$), time vs. stress ($\sigma \propto t^m$), and these relationships may introduce into Eq.4.12 to further expand the functions $c_1(\sigma)$ and $c_2(\sigma)$. However, we cannot assume creep-fatigue failure occurs at the steady stage of creep in the low-cycle regime. Thus it is not reasonable for these two relationships to be included. Even though this assumption is applied, introducing these two relationships is still a difficult and complex process due to the incongruous presentations of temperature dependence between Eq.4.12 (a linear temperature dependence) and the general creep formulation (the numerical expression of $Te^{1/T}$). In addition, this may also cause more coefficients to be introduced, which results in numerical complexity and implies that more experiments are needed to extract these coefficients. This is undesirable for engineering design because of poor economy. In this case, functions $c_1(\sigma)$ and $c_2(\sigma)$ are not further expanded, and are directly extracted from empirical data. This is main reason for defining the new creep-fatigue formulation as an incompletely constitutive model, wherein the stress-related component should be derived through empirical data.

We show after (see Section 4.3), although the functions $c_1(\sigma)$ and $c_2(\sigma)$ are not further expanded, they are not meaningless and are not a pure product of curve fitting. Specifically, these two functions can be linked to the creep-rupture process, wherein they are numerically solved by introducing the Manson-Haferd parameter. Through linking the stress moderating functions to the creep-rupture behaviour, the number of the independent coefficients which are needed to be determined by numerical optimization is significantly reduced. Thus, the risk of model non-identifiability or degeneracy is avoided.

Also, Chapter 3 shows that a desirable creep-fatigue formulation should cover the full range from the pure-fatigue condition to the pure-creep condition. In this case, a threshold reflecting the activation of the creep effect should be introduced, which is defined as the reference condition. Specifically, below the reference condition, creep is dormant, and thus the thermal effect and time effect do not work and are numerically given as zero value. In this case, introducing the reference temperature (T_{ref}) and the reference cyclic time (t_{ref}) into Eq.4.12 gives:

$$\varepsilon_p = C_0\left[1 - c_1(\sigma)\left(T - T_{ref}\right) - c_2(\sigma)\log\left(t_c/t_{ref}\right)\right]{N_f}^{-\beta_0} \tag{4.13}$$

The reference temperature is identified as 35% of the melting temperature, where the creep is activated. In the present work, the cyclic time is limited within the general range of engineering cases, and thus the damage caused by the internal energy dissipation is not considered. In this case, the reference cyclic time is suggested as a small value, below which we assume that the change of cyclic time does not have significant influence on the total creep-fatigue damage (this situation may not appear since we select a small value as the reference time and the high-frequency effect is not common for general engineering cases). The proposal of the reference condition provides a baseline (the full fatigue capacity) to evaluate creep-fatigue behaviour. Significantly, at the reference condition (T=T_{ref} and t_c=t_{ref}), the creep-fatigue equation is restored into the Coffin-Manson equation to present the pure-fatigue behaviour, wherein the creep effect is removed through imposing a zero thermal component and time component. When the full fatigue capacity is totally consumed by the creep effect, the pure-creep condition is achieved. In this situation, ε_p=0, then a Manson-Haferd-type parameter is given as:

$$\frac{c_2(\sigma)}{c_1(\sigma)} = \frac{T - T_{ref}}{\log\left(t_c/t_{ref}\right)} \tag{4.14}$$

where t_c could be defined as the creep rupture time. In this case, the expression of $c_2(\sigma)/c_1(\sigma)$ could be defined as the Manson-Haferd parameter, and Eq.4.14 implies that the new creep-fatigue equation has the ability to present the pure-creep condition. This also provides an effective method to extract the functions $c_1(\sigma)$ and $c_2(\sigma)$ through investigating the creep-rupture behaviour. As a result, the integrated characteristic is accommodated into the new creep-fatigue formulation.

Overall, the strain-based unified creep-fatigue equation integrates the relationships and trends mentioned above and then is constituted as:

$$\varepsilon_p = C_0 c(\sigma, T, t_c){N_f}^{-\beta_0} \tag{4.15}$$

with

$$\begin{gathered} c(\sigma, T, t_c) = 1 - c_1(\sigma)\left(T - T_{ref}\right) - c_2(\sigma)\log\left(t_c/t_{ref}\right) \\ T - T_{ref} = \begin{cases} T - T_{ref} & for \;\; T > T_{ref} \\ 0 & for \;\; T \le T_{ref} \end{cases} \\ t_c/t_{ref} = \begin{cases} t_c/t_{ref} & for \;\; t_c > t_{ref} \; and \; T > T_{ref} \\ 1 & for \;\; t_c \le t_{ref} \; or \; T \le T_{ref} \end{cases} \end{gathered} \tag{4.16}$$

where ε_p is the plastic strain which reflects fatigue capacity, N_f is the creep-fatigue life, C_0 and β_0 are fatigue ductility coefficient and fatigue ductility exponent respectively, which are related to fatigue capacity at the pure-fatigue condition, T is the temperature, t_c is the cyclic time which is the reciprocal of loading frequency, T_{ref} is the reference temperature which is defined as 35% of the melting temperature, t_{ref} is the reference cyclic time which is suggested as a

small value, and σ reflects the applied loading which can be related to plastic strain through the cyclic strain-stress relation.

Significantly, the reference condition is introduced to build a bridge between the pure-fatigue condition and the creep-fatigue condition, where the unified equation can be restored to the Coffin-Manson equation at the pure-fatigue condition. In addition, this unified formulation can be reorganized as the Manson-Haferd parameter at the pure-creep condition. In this case, the integrated characteristic is presented (this characteristic will be further discussed in Chapter 6).

4.3 Method of extracting the coefficients

The strain-based unified creep-fatigue equation is based on the concept of fatigue capacity, whereby the ability to cover the full range of conditions from the pure-fatigue condition to the pure-creep condition is theoretically accommodated into this new model. Therefore, some or all of the coefficients can be extracted from empirical data of pure fatigue and pure creep.

4.3.1 Derivation of creep-related coefficients

At the pure-creep condition, fatigue capacity is totally consumed by creep effect, thus ε_p=0. Then, the unified formulation can be presented as:

$$c(\sigma, T, t_c) = c(\sigma, T, t_R) = 1 - c_1(\sigma)\left(T - T_{ref}\right) - c_2(\sigma)\log\left(t_R/t_{ref}\right) = 0 \tag{4.17}$$

where t_R is the rupture time under the stress of σ and the temperature of T. According to the Manson-Haferd parameter, creep effect is illustratively activated at the convergent point (T_a, $\log t_a$) of all *T-log* t_R curves under different stress. Therefore, at this point, T=T_a=T_{ref} and t_R=t_a, then Eq.4.17 is shown as:

$$c_2 = \frac{1}{\log\left(t_a/t_{ref}\right)} \tag{4.18}$$

Significantly, function $c_2(\sigma)$ is independent of applied loading, and is a constant which is related to the creep-rupture behaviour. In addition, when creep rupture occurs at the reference cyclic time where t_R=t_{ref}, Eq.4.17 is presented as:

$$c_1(\sigma) = \frac{1}{T - T_{ref}} \tag{4.19}$$

Invoking the Manson-Haferd parameter and Eq.4.18, Eq.4.19 can be further represented as:

$$c_1(\sigma) = -\frac{c_2}{P_{MH}(\sigma)} \tag{4.20}$$

Then, function $c(\sigma, T, t_c)$ is defined as:

$$c(\sigma, T, t_c) = 1 + \frac{1}{P_{MH}(\sigma) \cdot \log(t_a/t_{ref})}(T - T_{ref}) - \frac{1}{\log(t_a/t_{ref})}\log(t/t_{ref}) \qquad (4.21)$$

In this case, the coefficients of function $c(\sigma, T, t_c)$ can be completely extracted from the creep-rupture tests. Specifically, the data of temperature vs. rupture time under multiple stresses are collected by performing creep-rupture tests. Then plotting curves of *T vs. log* t_R under multiple stresses gives the convergent point $(T_a, \log t_a)$ and the Manson-Haferd parameters under different stresses. The convergent point can be directly introduced into Eq.4.18 for calculating constant c_2. The data of the Manson-Haferd parameters vs. stress can be fitted to function $P_{MH}(\sigma)$, then the combination of c_2 and $P_{MH}(\sigma)$ gives function $c_1(\sigma)$.

Function $c_1(\sigma)$ is significantly evaluated under constant loading, but this may enlarge the creep effect because creep-fatigue damage occurs under reversed loading. This is demonstrated by the research conducted by Gary [79], which shows that the curves of stress vs. creep-rupture time under cyclic loading lie above those curves under constant loading. This implies that, compared to the creep-rupture situation with a constant loading, a higher cyclic loading is required to obtain the same rupture time. Therefore, it is reasonable to introduce a moderating factor (f_m) to transfer a cyclic-stress effect to an equivalently constant-stress effect, whereby the creep effect obtained through constant loading is compressed. This moderating factor is related to the shape of the loading wave, and reflects the average level of the cyclic loading. Illustratively, the area below the contour of the cyclic loading along the time dimension should be equal to the area below the contour of the equivalent constant loading $(f_m \cdot \sigma_{max})$ over the same time period. Generally, for a cyclic loading given by a function, $f(t)$, the moderating factor is represented as Eq.4.22:

$$f_m = \frac{2\int_0^{t_c/2} f(t)dt}{t_c \cdot \sigma_{max}} \qquad (4.22)$$

where σ_{max} is the maximum value of the cyclic loading. In particular, this moderating factor is defined as 0.6366 for the sinusoidal wave and 0.5 for a triangular wave. Eq.4.22 is built on the assumption that:

The creep effect in the tensile portion is the same as in the compressive portion, thus the moderating factor (f_m) is evaluated based on half-cycle loading.

Although this assumption may be not appropriate for some materials [80, 81], it could simplify the method of extracting the moderating factor, which is essential for engineering design. Through including this moderating factor, the function $c_1(\sigma)$ is converted to $c_1(f_m \cdot \sigma)$. Then, stress is transformed to plastic strain through cyclic strain-stress relation for the reasons of expressing creep damage from the strain perspective and keeping consistent with the Coffin-Manson equation. These transformations give Eq.4.23:

$$c_1(\sigma) = -\frac{c_2}{P_{MH}(\sigma)} = -\frac{c_2}{P_{MH}[f_m \cdot K(T, t_c) \cdot {\varepsilon_P}^{n(T,t_c)}]} \qquad (4.23)$$

where $K(T, t_c)$ and $n(T, t_c)$ are the strength coefficient and strain hardening exponent under cyclic loading respectively, and they are functions of temperature and cyclic time. It may also

be said that the influence of temperature and cyclic time on material properties is presented through the functions $K(T, t_c)$ and $n(T, t_c)$.

Overall, the derivation of the functions $c_1(\sigma)$ and constant c_2 is based on the experimental data of creep-rupture tests and cyclic deformation tests.

4.3.2 Derivation of fatigue-related coefficients

For the pure-fatigue condition, the unified formulation is restored to the Coffin-Manson equation, where the magnitudes of $C_0$and β_0 can be ideally derived from the pure-fatigue data. However, this may result in reduced quality of creep-fatigue fitting. Specifically, the strain-based unified creep-fatigue equation is based on the concept of fatigue capacity. An assumption arises, that is:

The slopes of plastic strain vs. fatigue life curves at multiple temperatures and/or cyclic times remain the same at the log-log coordinate.

However, this assumption is inconsistent with the empirical data of creep fatigue, but this inconsistency is not remarkable, because the slope is slightly influenced by temperature and cyclic time. In this case, for the reason of simplification, C_0 and β_0 can be directly extracted form pure-fatigue tests. While for the purpose of obtaining a higher quality of describing creep-fatigue behaviour, the pure-fatigue-related coefficients (C_0 and β_0) may not be directly extracted from the empirical data of pure-fatigue test, but the numerical optimization based on the creep-fatigue data may give a better solution for these two coefficients. Specifically, C_0 and β_0 can be numerically obtained through minimizing the difference (δ_t) (Eq.4.24) between the predicted creep-fatigue life ($N_{pre,ij}$) and the experimental creep-fatigue life ($N_{exp,ij}$) for the conditions of $\varepsilon_{p,j}$, T_i and $t_{c,i}$:

$$\delta_t = \sum \left(\log N_{pre,ij} - \log N_{exp,ij}\right)^2 \tag{4.24}$$

with

$$N_{pre,ij} = \left[\frac{\varepsilon_{p,j}}{C_0 c\left(\varepsilon_{p,j}, T_i,\ t_{c,i}\right)}\right]^{-1/\beta_0} \tag{4.25}$$

and the average error (δ_a) is defined by dividing the total error (Eq.4.24) by the number of data points (n_{data}):

$$\delta_a = \sum \left(\log N_{pre,ij} - \log N_{exp,ij}\right)^2 / n_{data} \tag{4.26}$$

In the present work, it is notable that we use the logarithmical form to evaluate the error (Eq.4.24) since this operation can numerically shrink the magnitude of fatigue life. This is significantly beneficial for the optimization calculation using Excel, where the object (maximum value or minimum value) could be effectively and easily returned. The adoption of Excel will be discussed in Chapter 6.

4.4 Evaluation of the unified formulation

The quality/error of fatigue-life prediction through using the strain-based unified creep-fatigue equation can reflect the goodness of this new formulation on describing the creep-fatigue behaviour. Generally, this can be evaluated through the prediction ratio and reference-condition transformation.

4.4.1 Evaluation through prediction ratio

The prediction ratio (H_{ij}) (Eq.4.27) is defined as the ratio of predicted creep-fatigue life ($N_{pre,ij}$) to experimental creep-fatigue life ($N_{exp,ij}$). Any prediction ratio which is greater than 1 implies an unconservative fatigue-life prediction, where a longer life (calculated from the unified equation) is given than empirical data. On the contrary, a prediction ratio lower than 1 means a conservative prediction.

$$H_{ij} = \frac{N_{pre,ij}}{N_{exp,ij}} \tag{4.27}$$

In the present work, we define that:

An acceptable prediction ratio should be between 0.75 and 1.25.

This also can be illustratively presented (Fig.4.3). Specifically, the data points of $N_{pre,ij}$ vs. $N_{exp,ij}$ under multiple temperatures and cyclic times should be within 25% above and below the ideal correlation (H=1). This is further explained by Figure 4.3, where all data points fall between the upper bound (+25%) and the lower bound (-25%).

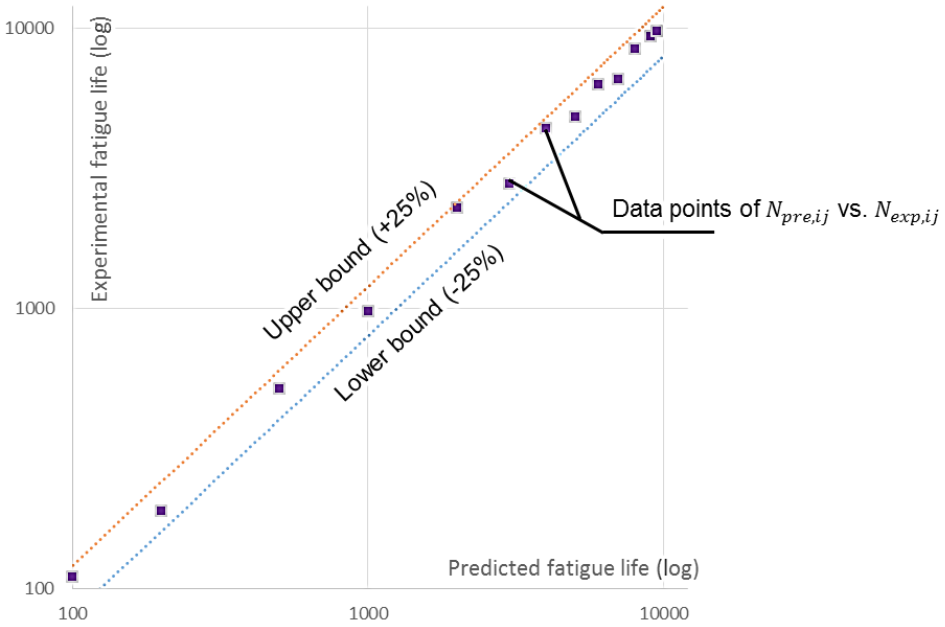

Figure 4.3 An acceptable range of prediction ratio

4.4.2 Evaluation through reference-condition transformation

The strain-based unified creep-fatigue equation is based on the concept of fatigue capacity, and thus it theoretically reflects a process of gradual consumption of the full fatigue capacity by the creep effect. In this case, we believe that the creep-fatigue data can be ideally transformed/restored to the reference condition (the pure-fatigue condition), and this transformation can be numerically conducted using Eq.4.28:

$$\varepsilon_{p,ref} = C_0 N^{-\beta_0} = \varepsilon_p / c(\sigma, T, t_c) \tag{4.28}$$

An effective numerical description of creep effect shown by function $c(\sigma, T, t_c)$ can cause all transformed creep-fatigue data to collapse into a single power-law curve with good quality, and the coefficient and exponent of this trendline can agree well with C_0 and β_0 respectively. This is further explained in Fig.4.4 as an example, where the creep-fatigue data for three different situations are transformed to the reference condition through Eq.4.28, and all the transformed data are well fitted in a power-law relation whose coefficient and exponent agree well with the values of C_0 and β_0 respectively. This demonstrates an effective description of creep effect by function $c(\sigma, T, t_c)$, and implies a high quality to predict fatigue life by using the unified formulation.

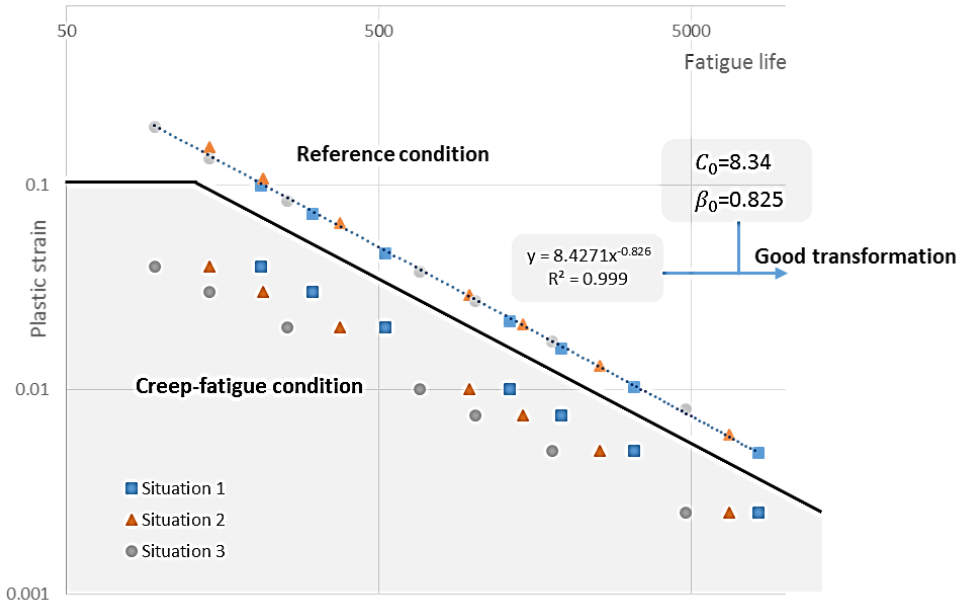

Figure 4.4 Reference-condition transformation

4.5 Validation on metals

The development of the new creep-fatigue equation attempts to find a unified formulation to predict creep-fatigue life for multiple temperatures and cyclic times for multiple materials. This is defined as the unified characteristic, and the validation is conducted on materials with low melting point (63Sn37Pb solder and 96.5Sn3.5Ag solder), medium melting point (AL2024T3 aluminium alloy) and high melting point (stainless steel 316 and stainless steel 304). The empirical data of creep rupture and creep fatigue are extracted from the literature. According to the definition of the unified creep-fatigue equation, the reference temperature is defined as 35% of the melting temperature and the reference cyclic time is suggested as a small value.

4.5.1 Validation on 63Sn37Pb solder

The reference temperature for 63Sn37Pb solder was chosen as 160K and the reference cyclic time was defined as 1s. The creep-rupture data [82] are plotted in Fig.4.5, and the point of convergence (T_{ref}, log t_a) is evaluated as (160K, 8.232). This gives

$$c_2 = \frac{1}{\log(t_a/t_{ref})} = \frac{1}{\log(10^{8.232}/1)} = 0.1215 \tag{4.29}$$

and the relationship between stress and the Manson-Haferd Parameter:

$$-\frac{1}{P_{MH}(\sigma)} = 8.1979 \times 10^{-3} + 8.3244 \times 10^{-4}\sigma + 6.6651 \times 10^{-6}\sigma^2 \tag{4.30}$$

Then, substituting into Eq.4.20, function $c_1(\sigma)$ is expressed as:

$$c_1(\sigma) = -\frac{c_2}{P_{MH}(\sigma)} = 9.9586 \times 10^{-4} + 1.01122 \times 10^{-4} \cdot f_m \cdot \sigma + 8.09657 \times 10^{-7} \cdot {f_m}^2 \cdot \sigma^2 \tag{4.31}$$

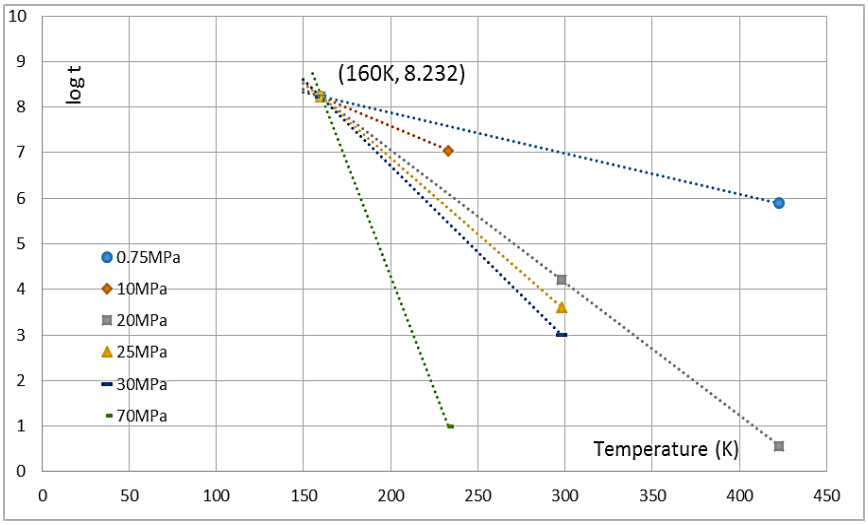

Figure 4.5 Creep-rupture characteristics of 63Sn37Pb solder

and the magnitude of f_m is given as 0.6366 for the sinusoidal wave.

The creep-fatigue coefficients [53] obtained from the literature are tabulated in Table 4.2. Minimizing the difference between the predicted creep-fatigue life ($N_{pre,ij}$) and the experimental creep-fatigue life ($N_{exp,ij}$) yields C_o=7.894 and β_o=0.825, and returns an average error (δ_a) (Eq.4.26) of 0.003301.

Table 4.2 Creep-fatigue data for 63Sn37Pb solder

Temperature (K)	Frequency (Hz)	Cyclic time (s)	Creep-fatigue Coefficients $\varepsilon_p = \varepsilon_f' N_f^{-\beta}$		Strain-stress Coefficients $\sigma/2 = K(\varepsilon_p/2)^n$	
			ε_f'	β	K	n
233	1	1	2.98	0.773	129.5	0.0652
298	1	1	2.28	0.756	110.89	0.0833
348	1	1	1.86	0.743	95.433	0.0962
398	1	1	1.45	0.723	84.026	0.1199
423	1	1	1.05	0.703	70.854	0.1261
298	0.1	10	1.57	0.719	108.43	0.1173
298	0.01	100	1.28	0.712	102.49	0.1316
298	0.001	1000	1.01	0.708	90.437	0.1438

The prediction ratio (N_{pre}/N_{exp}) under multiple temperatures and cyclic times are plotted in Fig.4.6, where all data points fall between the upper bound (+25%) and the lower bound (-25%). This implies that the unified creep-fatigue equation provides a high quality for fatigue-life prediction, specifically, a relatively high correlation between predicted and experimental creep-fatigue life.

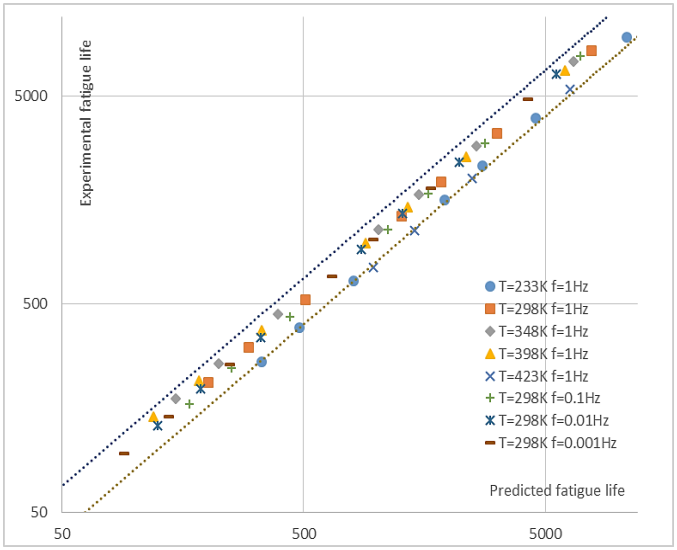

Figure 4.6 Prediction ratio for 63Sn37Pb solder

With the results obtained above, the experimental creep-fatigue data (ε_p-N_{exp}) (shadow area in Fig.4.7) is transformed to the reference condition (the pure-fatigue condition) ($\varepsilon_{p,ref}$-N_{exp}) by using Eq.4.28. Fig.4.7 shows that the transformed data collapse into one power-law curve of $\varepsilon_{p,ref} = 7.4485N^{-0.817}$ with the quality of fit as R^2=0.9896. The coefficients of the trendline, C_0=7.4485 and β_0=0.817, are very close to the results obtained through numerical optimization. This suggests good consistency with the reference condition, and the function $c(\sigma, T, t_c)$ represents a good numerical description of the creep characteristics.

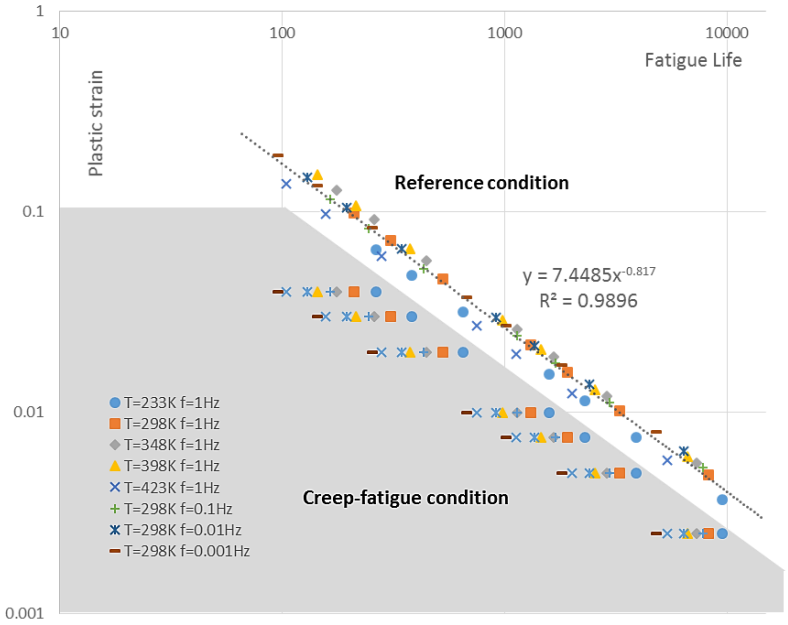

Figure 4.7 The transformed data ($\varepsilon_{p,ref}$-N_{exp}) for 63Sn37Pb

Consequently, the coefficients of the unified creep-fatigue equation for 63Sn37Pb solder are collected in Table 4.3:

Table 4.3 The coefficients of the unified formulation for 63Sn37Pb solder

C_0	β_0	c_2	T_{ref} (K)	t_{ref} (s)	f_m	δ_a
7.894	0.825	0.1215	160	1	0.6366	0.0033
$c_1(\sigma, f_m)$	$9.9586 \times 10^{-4} + 1.01122 \times 10^{-4} \cdot f_m \cdot \sigma + 8.09657 \times 10^{-7} \cdot {f_m}^2 \cdot \sigma^2$					

4.5.2 Validation on 96.5Sn3.5Ag solder

The reference temperature for 96.5Sn3.5Ag solder was chosen as 170K and the reference cyclic time was defined as 1s. The creep-rupture data [83] are plotted in Fig.4.8, and the point of convergence (T_{ref}, log t_a) is evaluated as (170K, 11.346). This gives

$$c_2 = \frac{1}{\log(t_a/t_{ref})} = \frac{1}{\log(10^{11.346}/1)} = 0.08814 \tag{4.32}$$

and the relationship between stress and the Manson-Haferd Parameter:

$$-\frac{1}{P_{MH}(\sigma)} = 0.0056 + 4.28 \times 10^{-3}\sigma - 1.44 \times 10^{-4}\sigma^2 \tag{4.33}$$

Then, substituting into Eq.4.20, function $c_1(\sigma)$ is expressed as:

$$c_1(\sigma) = -\frac{c_2}{P_{MH}(\sigma)} = 4.93581 \times 10^{-4} + 3.77237 \times 10^{-4} \cdot f_m \cdot \sigma - 1.26921 \times 10^{-5} \cdot {f_m}^2 \cdot \sigma^2 \tag{4.34}$$

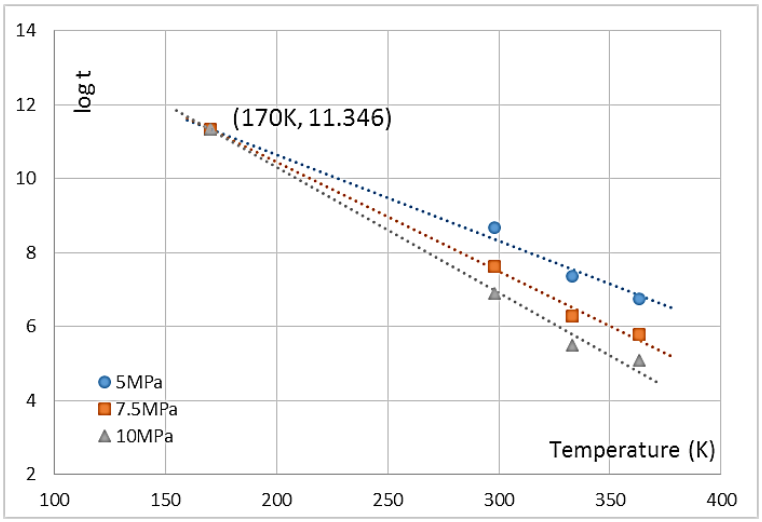

Figure 4.8 Creep-rupture characteristics of 63Sn37Pb solder

and the magnitude of f_m is given as 0.5 for the triangular wave.

The creep-fatigue coefficients [84, 85] obtained from the literature are tabulated in Table 4.4. Minimizing the difference between the predicted creep-fatigue life ($N_{pre,ij}$) and the experimental creep-fatigue life ($N_{exp,ij}$) yields C_o=28.425 and β_o=0.90, and returns an average error (δ_a) (Eq.4.26) of 0.008557.

Table 4.4 Creep-fatigue data for 96.5Sn3.5Ag solder

Temperature (K)	Frequency (Hz)	Cyclic time (s)	Creep-fatigue Coefficients $\varepsilon_p = \varepsilon_f' N_f^{-\beta}$		Strain-stress Coefficients $\sigma/2 = K(\varepsilon_p/2)^n$	
			ε_f'	β	K	n
293	0.1	10	17.749	0.912	103.4	0.0752
358	0.1	10	3.8811	0.795	82.978	0.1066
393	0.1	10	13.061	1.04	43.581	0.0217
293	1	1	32.017	0.952	108.53	0.078

293	0.01	100	36.454	1.072	72.801	0.035
293	0.001	1000	18.009	1.016	73.976	0.0652

The prediction ratio (N_{pre}/N_{exp}) under multiple temperatures and cyclic times are plotted in Fig.4.9, where all data points fall between the upper bound (+25%) and the lower bound (-25%). This implies that the unified creep-fatigue equation provides a high quality for fatigue-life prediction, specifically, a relatively high correlation between predicted and experimental creep-fatigue life.

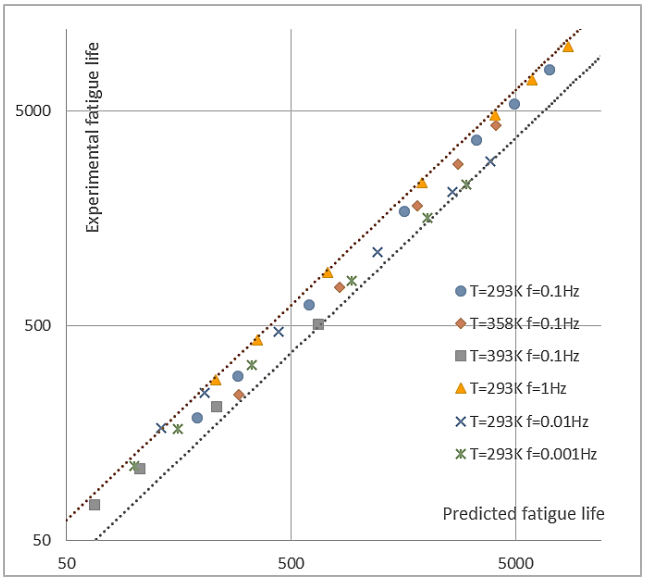

Figure 4.9 Prediction ratio for 96.5Sn3.5Ag solder

With the results obtained above, the experimental creep-fatigue data (ε_p-N_{exp}) (shadow area in Fig.4.10) is transformed to the reference condition (the pure-fatigue condition) ($\varepsilon_{p,ref}$-N_{exp}) by using Eq.4.28. Fig.4.10 shows that the transformed data collapse into one power-law curve of $\varepsilon_{p,ref} = 27.166N^{-0.90}$ with the quality of fit as R^2=0.9787. The coefficients of the trendline, C_0=27.166 and β_0=0.90, are very close to the results obtained through numerical optimization. This suggests good consistency for the reference condition, and the function $c(\sigma, T, t_c)$ represents a good numerical description of the creep characteristics.

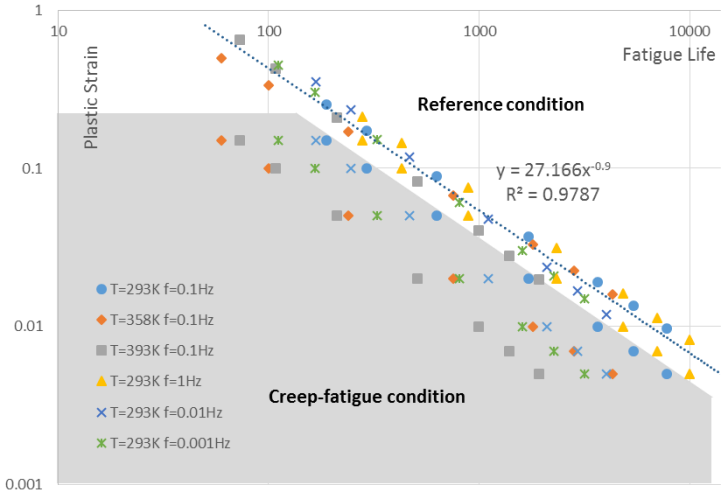

Figure 4.10 The transformed data ($\varepsilon_{p,ref}$-N_{exp}) for 96.5Sn3.5Ag solder

Consequently, the coefficients of the unified creep-fatigue equation for 96.5Sn3.5Ag solder is collected in Table 4.5:

Table 4.5 The coefficients of the unified formulation for 96.5Sn3.5Ag solder

C_0	β_0	c_2	T_{ref} (K)	t_{ref} (s)	f_m	δ_a
28.425	0.90	0.08814	170	1	0.5	0.008557
$c_1(\sigma, f_m)$	$4.93581 \times 10^{-4} + 3.77237 \times 10^{-4} \cdot f_m \cdot \sigma - 1.26921 \times 10^{-5} \cdot {f_m}^2 \cdot \sigma^2$					

4.5.3 Validation on AL2024T3 alumina alloy

The reference temperature for AL2024T3 was chosen as 270K and the reference cyclic time was defined as 1s. The creep-rupture data [86] are plotted in Fig.4.11, and the point of convergence (T_{ref}, log t_a) is evaluated as (270K, 10.078). This gives

$$c_2 = \frac{1}{\log(t_a/t_{ref})} = \frac{1}{\log(10^{10.078}/1)} = 0.09922 \tag{4.35}$$

and the relationship between stress and the Manson-Haferd Parameter:

$$-\frac{1}{P_{MH}(\sigma)} = 0.00498 + 9.64 \times 10^{-5}\sigma - 8.0 \times 10^{-8}\sigma^2 \tag{4.36}$$

Then, substituting into Eq.4.20, function $c_1(\sigma)$ is expressed as:

$$c_1(\sigma) = -\frac{c_2}{P_{MH}(\sigma)} = 4.85203 \times 10^{-4} + 9.56515 \times 10^{-6} \cdot f_m \cdot \sigma - 7.93789 \times 10^{-9} \cdot {f_m}^2 \cdot \sigma^2 \tag{4.37}$$

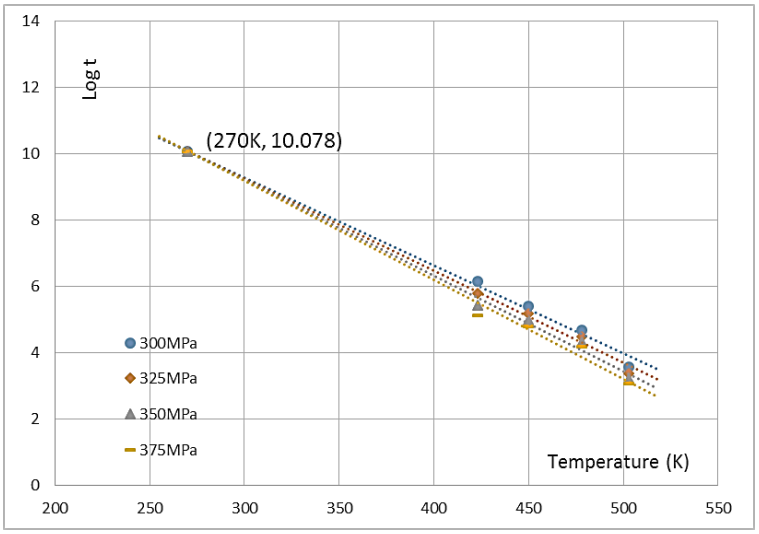

Figure 4.11 Creep-rupture characteristics of AL2024T3

and the magnitude of f_m is given as 0.5 for the triangular wave.

The creep-fatigue coefficients [87] obtained from the literature are tabulated in Table 4.6. Minimizing the difference between the predicted creep-fatigue life ($N_{pre,ij}$) and the experimental creep-fatigue life ($N_{exp,ij}$) yields C_o=0.7988 and β_o=0.5502, and returns an average error (δ_a) (Eq.4.26) of 0.003301.

Table 4.6 Creep-fatigue data for AL2024T3

Temperature (K)	Frequency (Hz)	Cyclic time (s)	Creep-fatigue Coefficients $\varepsilon_p = \varepsilon_f' N_f^{-\beta}$		Strain-stress Coefficients $\sigma/2 = K(\varepsilon_p/2)^n$	
			ε_f'	β	K	n
373	1	1	0.5874	0.55	652.57	0.0893
473	1	1	0.2443	0.46	996.42	0.1881
573	1	1	0.3429	0.544	492.98	0.0602
433	0.2	5	0.4357	0.532	953.97	0.1757

The prediction ratio (N_{pre}/N_{exp}) under multiple temperatures and cyclic times are plotted in Fig.4.12, where all data points fall between the upper bound (+25%) and the lower bound (-25%). This implies that the unified creep-fatigue equation provides a high quality for fatigue-life prediction, specifically, a relatively high correlation between predicted and experimental creep-fatigue life.

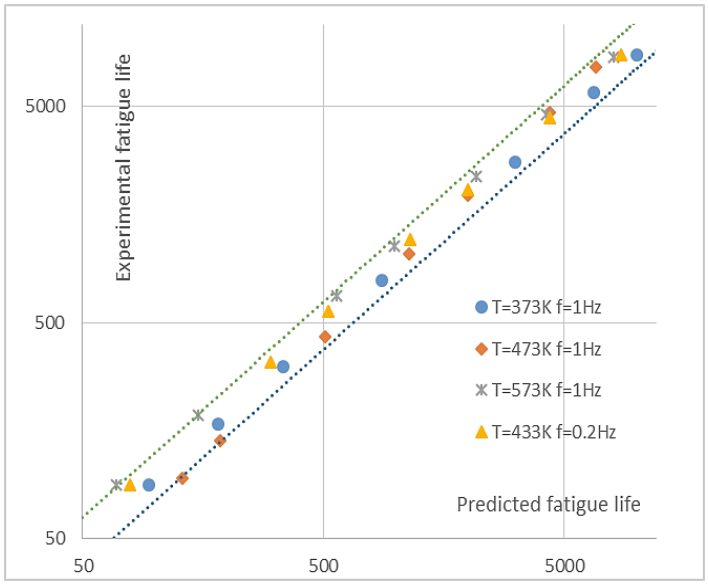

Figure 4.12 Prediction ratio for AL2024T3

With the results obtained above, the experimental creep-fatigue data (ε_p-N_{exp}) (shadow area in Fig.4.13) is transformed to the reference condition (the pure-fatigue condition) ($\varepsilon_{p,ref}$-N_{exp}) by using Eq.4.28. Fig.4.13 shows that the transformed data collapse into one power-law curve of $\varepsilon_{p,ref} = 0.7771N^{-0.546}$ with the quality of fit as R^2= 0.9927. The coefficients of the trendline, C_0=0.7771 and β_0=0.546, are very close to the results obtained through numerical optimization. This suggests good consistency with the reference condition, and the function $c(\sigma, T, t_c)$ represents a good numerical description of the creep characteristics.

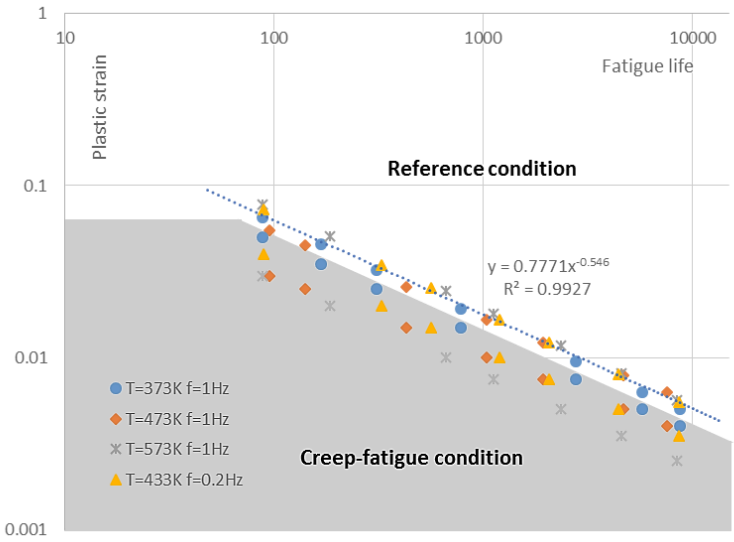

Figure 4.13 The transformed data ($\varepsilon_{p,ref}$-N_{exp}) for AL2024T3

Consequently, the coefficients of the unified creep-fatigue equation for AL2024T3 alumina alloy is collected in Table 4.7:

Table 4.7 The coefficients of the unified formulation for AL2024T3

C_0	β_0	c_2	T_{ref} (K)	t_{ref} (s)	f_m	δ_a
0.7988	0.5502	0.09922	270	1	0.5	0.004422
$c_1(\sigma, f_m)$	$4.85203 \times 10^{-4} + 9.56515 \times 10^{-6} \cdot f_m \cdot \sigma - 7.93789 \times 10^{-9} \cdot {f_m}^2 \cdot \sigma^2$					

4.5.4 Validation on stainless steel 316

The reference temperature for stainless steel 316 was chosen as 585K and the reference cyclic time was defined as 1s. The creep-rupture data [88] are plotted in Fig.4.14, and the point of convergence (T_{ref}, log t_a) is evaluated as (585K, 10.783). This gives

$$c_2 = \frac{1}{\log(t_a/t_{ref})} = \frac{1}{\log(10^{10.783}/1)} = 0.09274 \tag{4.38}$$

and the relationship between stress and the Manson-Haferd Parameter:

$$-\frac{1}{P_{MH}(\sigma)} = 0.006011 + 7.0286 \times 10^{-5}\sigma - 1.1429 \times 10^{-7}\sigma^2 \tag{4.39}$$

Then, substituting into Eq.4.20, function $c_1(\sigma)$ is expressed as:

$$c_1(\sigma) = -\frac{c_2}{P_{MH}(\sigma)} = 5.575 \times 10^{-4} + 6.5184 \times 10^{-6} \cdot f_m \cdot \sigma - 1.05994 \times 10^{-8} \cdot {f_m}^2 \cdot \sigma^2 \tag{4.40}$$

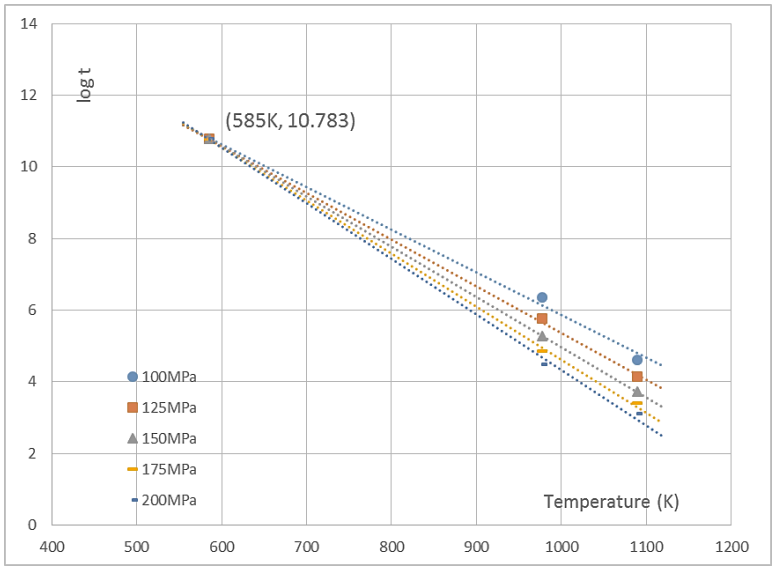

Figure 4.14 Creep-rupture characteristics of stainless steel 316

and the magnitude of f_m is given as 0.5 for the triangular wave.

The creep-fatigue coefficients [89] obtained from the literature are tabulated in Table 4.8. Minimizing the difference between the predicted creep-fatigue life ($N_{pre,ij}$) and the

experimental creep-fatigue life ($N_{exp,ij}$) yields C_o=0.7284 and β_o=0.6098, and returns an average error (δ_a) (Eq.4.26) of 0.00619.

Table 4.8 Creep-fatigue data for stainless steel 316

Temperature (K)	Strain rate (%/min)	Creep-fatigue Coefficients $\varepsilon_p = \varepsilon_f' N_f^{-\beta}$		Strain-stress Coefficients $\sigma/2 = K(\varepsilon_p/2)^n$	
		ε_f'	β	K	n
723	0.4	0.279	0.522	444	0.338
723	4	0.369	0.521	458	0.368
873	4	0.347	0.578	175	0.173
873	40	0.408	0.563	193	0.201
973	0.4	0.246	0.555	125	0.202
973	4	0.470	0.615	99.4	0.138
973	40	0.425	0.578	150	0.211

The prediction ratio (N_{pre}/N_{exp}) under multiple temperatures and cyclic times are plotted in Fig.4.15, where all data points fall between the upper bound (+25%) and the lower bound (-25%). This implies that the unified creep-fatigue equation provides a high quality for fatigue-life prediction, specifically, a relatively high correlation between the predicted and experimental creep-fatigue life.

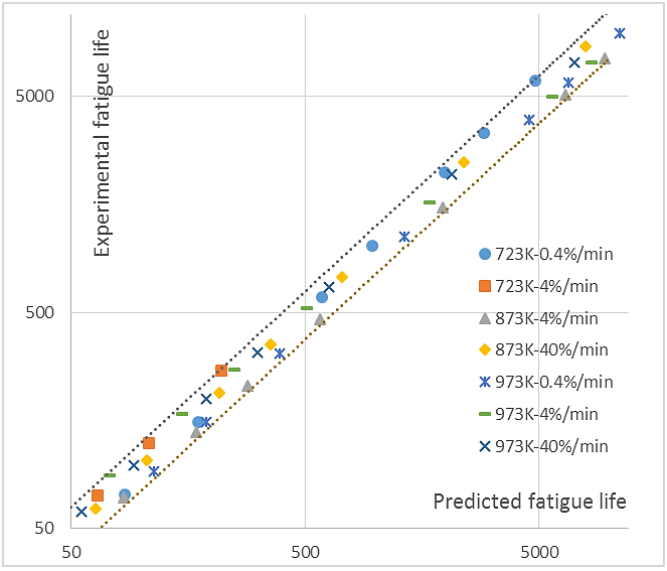

Figure 4.15 Prediction ratio for stainless steel 316

With the results obtained above, the experimental creep-fatigue data (ε_p-N_{exp}) (shadow area in Fig.4.16) is transformed to the reference condition (the pure-fatigue condition) ($\varepsilon_{p,ref}$-N_{exp}) by using Eq.4.28. Fig.4.16 shows that the transformed data collapse into one power-law curve of $\varepsilon_{p,ref} = 0.6934N^{-0.602}$ with the quality of fit as R^2=0.9876. The coefficients of the trendline, C_0=0.6934 and β_0=0.602, are very close to the results obtained through numerical optimization. This suggests good consistency with the reference condition, and the function $c(\sigma, T, t_c)$ represents a good numerical description of the creep characteristics.

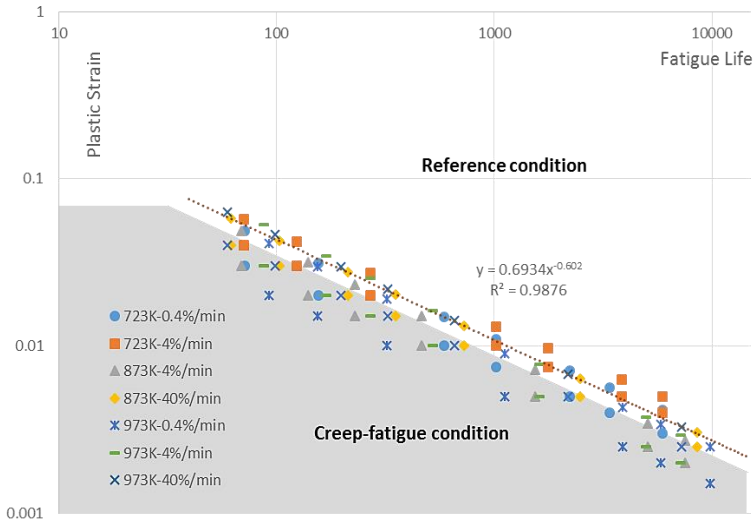

Figure 4.16 The transformed data ($\varepsilon_{p,ref}$-N_{exp}) for stainless steel 316

Consequently, the coefficients of the unified creep-fatigue equation for stainless steel 316 is collected in Table 4.9:

Table 4.9 The coefficients of the unified formulation for stainless steel 316

C_0	β_0	c_2	T_{ref} (K)	t_{ref} (s)	f_m	δ_a
0.7284	0.6098	0.09274	585	1	0.5	0.00619
$c_1(\sigma, f_m)$	$5.575 \times 10^{-4} + 6.5184 \times 10^{-6} \cdot f_m \cdot \sigma - 1.05994 \times 10^{-8} \cdot {f_m}^2 \cdot \sigma^2$					

4.5.5 Validation on stainless steel 304

The reference temperature for stainless steel 304 was chosen as 600K and the reference cyclic time was defined as 1s. The creep-rupture data [88] are plotted in Fig.4.17, and the point of convergence (T_{ref}, log t_a) is evaluated as (600K, 15.01). This gives

$$c_2 = \frac{1}{\log(t_a/t_{ref})} = \frac{1}{\log(10^{15.01}/1)} = 0.0666 \tag{4.41}$$

and the relationship between stress and the Manson-Haferd Parameter:

$$-\frac{1}{P_{MH}(\sigma)} = 0.012885 + 1.462 \times 10^{-4}\sigma - 2.80 \times 10^{-7}\sigma^2 \tag{4.42}$$

Then, substituting into Eq.4.20, function $c_1(\sigma)$ is expressed as:

$$c_1(\sigma) = -\frac{c_2}{P_{MH}(\sigma)} = 8.5843 \times 10^{-4} + 9.74017 \times 10^{-6} \cdot f_m \cdot \sigma - 1.86542 \times 10^{-8} \cdot {f_m}^2 \cdot \sigma^2 \tag{4.43}$$

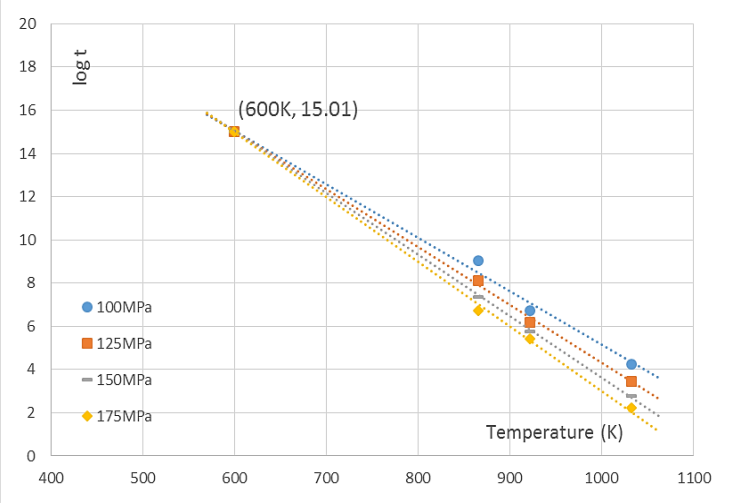

Figure 4.17 Creep-rupture characteristics of stainless steel 304

and the magnitude of f_m is given as 0.5 for the triangular wave.

The creep-fatigue coefficients [89] obtained from the literature are tabulated in Table 4.10. Minimizing the difference between the predicted creep-fatigue life ($N_{pre,ij}$) and the experimental creep-fatigue life ($N_{exp,ij}$) yields C_o=0.852 and β_o=0.5777, and returns an average error (δ_a) (Eq.4.26) of 0.00426.

Table 4.10 Creep-fatigue data for stainless steel 304

Temperature (K)	Strain rate (%/min)	Creep-fatigue Coefficients $\varepsilon_p = \varepsilon_f' N_f^{-\beta}$		Strain-stress Coefficients $\sigma/2 = K(\varepsilon_p/2)^n$	
		ε_f'	β	K	n
723	0.4	0.696	0.613	323	0.306
723	4	0.596	0.55	378	0.372
873	4	0.421	0.556	165	0.214
873	40	0.519	0.555	229	0.288
973	0.4	0.302	0.524	66.2	0.146
973	4	0.259	0.489	96.1	0.192
973	40	0.386	0.541	68	0.143

The prediction ratio (N_{pre}/N_{exp}) under multiple temperatures and cyclic times are plotted in Fig.4.18, where all data points fall between the upper bound (+25%) and the lower bound (-25%). This implies that the unified creep-fatigue equation provides a high quality for fatigue-life prediction, specifically, a relatively high correlation between predicted and experimental creep-fatigue life.

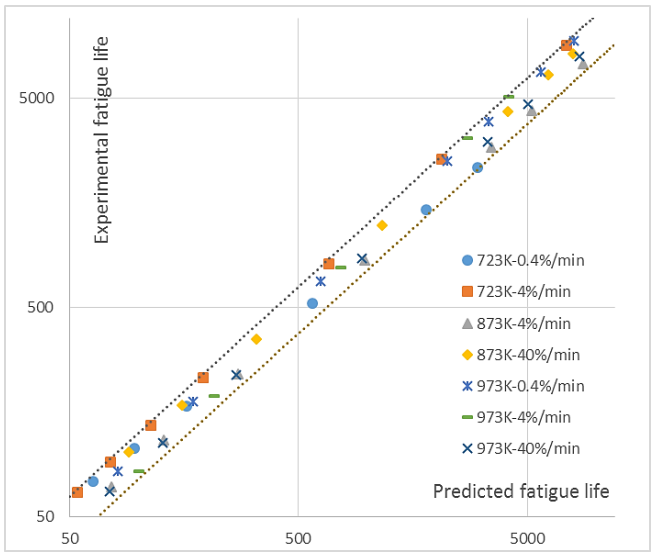

Figure 4.18 Prediction ratio for stainless steel 304

With the results obtained above, the experimental creep-fatigue data (ε_p-N_{exp}) (shadow area in Fig.4.19) is transformed to the reference condition (the pure-fatigue condition) ($\varepsilon_{p,ref}$-N_{exp}) by using Eq.4.28. Fig.4.19 shows that the transformed data collapse into one power-law curve of $\varepsilon_{p,ref} = 0.8288N^{-0.573}$ with the quality of fit as R^2=0.9927. The coefficients of the trendline, C_0=0.8288 and β_0=0.573, are very close to the results obtained through numerical optimization. This suggests good consistency with the reference condition, and the function $c(\sigma, T, t_c)$ represents a good numerical description of the creep characteristics.

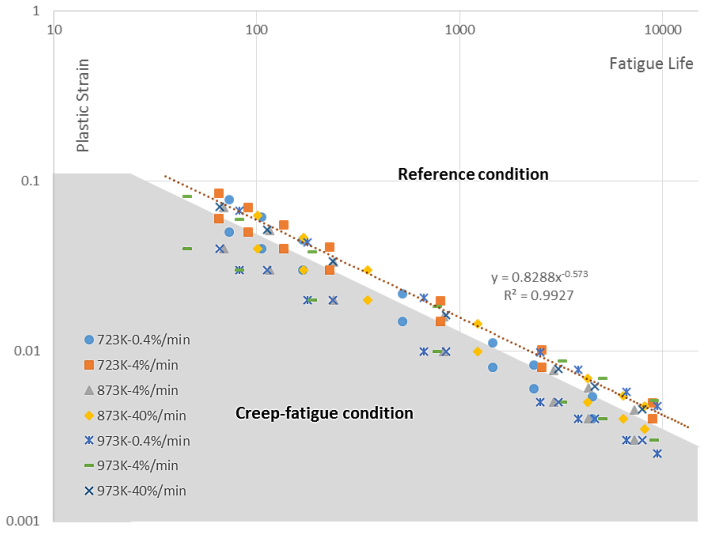

Figure 4.19 The transformed data ($\varepsilon_{p,ref}$-N_{exp}) for stainless steel 304

Consequently, the coefficients of the unified creep-fatigue equation for stainless steel 304 is collected in Table 4.11:

Table 4.11 The coefficients of the unified formulation for stainless steel 304

C_0	β_0	c_2	T_{ref} (K)	t_{ref} (s)	f_m	δ_a
0.852	0.5777	0.0666	600	1	0.5	0.00426
$c_1(\sigma, f_m)$	$8.5843 \times 10^{-4} + 9.74017 \times 10^{-6} \cdot f_m \cdot \sigma - 1.86542 \times 10^{-8} \cdot {f_m}^2 \cdot \sigma^2$					

Overall, the validation of the materials of solder (low-melting-temperature material), alumina alloy (medium-melting-temperature material) and stainless steel (high-melting-temperature material) demonstrates that the strain-based unified creep-fatigue equation has the ability to be applied to multiple temperatures and cyclic times for multiple materials. In this case, we conclude that the unified characteristic is accommodated into this new creep-fatigue equation.

4.6 Summary

The strain-based unified creep-fatigue equation started from the investigation of fatigue and creep phenomena. Then, based on the concept of fatigue capacity, relevant variables (including temperature, cyclic time, applied loading and fatigue life) are numerically constituted into a new creep-fatigue formulation (Eq.4.44):

$$\varepsilon_p = C_0 c(\sigma, T, t_c) {N_f}^{-\beta_0} \tag{4.44}$$

with

$$c(\sigma, T, t_c) = 1 - c_1(\sigma)\left(T - T_{ref}\right) - c_2 \log\left(t_c / t_{ref}\right)$$

$$T - T_{ref} = \begin{cases} T - T_{ref} & for \;\; T > T_{ref} \\ 0 & for \;\; T \le T_{ref} \end{cases} \tag{4.45}$$

$$t_c / t_{ref} = \begin{cases} t_c / t_{ref} & for \;\; t_c > t_{ref} \; and \; T > T_{ref} \\ 1 & for \;\; t_c \le t_{ref} \; or \; T \le T_{ref} \end{cases}$$

Function $c_1(\sigma)$ and constant c_2 are directly extracted from creep-rupture data (Eq.4.20 and Eq.4.18). In particular, a moderating factor (f_m) is introduced to transform the cyclic-loading situation to an equivalently constant-loading situation (Eq.4.22). Then, creep-fatigue data give the constants of C_0 and β_0 through minimizing the difference (Eq.4.24) between the predicted life and the experimental result. The goodness of the unified formulation on fatigue-life prediction can be evaluated through the prediction ratio where the acceptable values should be between 0.75 and 1.25, and the reference-condition transformation where all raw creep-fatigue data are transformed into the reference condition by collapsing into a single power-law curve.

The strain-based unified creep-fatigue equation was validated on the materials from a low melting point to those with a high melting point (63Sn37Pb solder, 96.5Sn3.5Ag solder, AL2024T3 alumina alloy, stainless steel 316 and stainless steel 304), where accepted prediction ratios were presented, and good transformation from the creep-fatigue condition to the reference condition was shown. This implies that the new creep-fatigue equation has the ability to be applied at multiple temperatures and cyclic times for multiple materials. Meanwhile, the numerical structure of this unified formulation is demonstrated, specially, the creep function $c(\sigma, T, t_c)$ presents a good performance of the description of creep behaviour. In addition, the strain-based unified creep-fatigue equation is based on the concept of fatigue capacity, and thus ideally it presents the ability to cover the full range of conditions from the pure-fatigue condition to the pure-creep condition. The advantages of this unified approach will be further discussed in Chapter 6.

Chapter 5

5. Strain-based unified creep-fatigue equation with grain-size dependence

This results chapter gives an extension of the model proposed in Chapter 4, where the grain-size dependence is introduced to describe creep-fatigue behaviour at a microstructural level. Then, the method to extract the coefficients is presented, and this formulation is validated on the materials of Inconel 718 and GP91 casting steel.

Publications relevant to this chapter are as follows (see Appendix A for details):

(1) Liu, D. and D.J. Pons, Development of a unified creep - fatigue equation including heat treatment. Fatigue & Fracture of Engineering Materials & Structures, 2017: p. 1-13.

The development and validation of the strain-based unified creep-fatigue equation were presented in Chapter 4, where the macroscopic dependencies of temperature and cyclic time are accommodated into this unified formulation. However, the microstructural-based effect, which is believed to have a significant influence on material properties, is not included. In this case, as a measurable parameter, grain-size dependence is introduced to further improve the unified formulation. Consequently, this modification gives the strain-based unified approach ability to describe creep-fatigue phenomenon in microstructural level.

5.1 Development of the strain-based unified creep-fatigue equation with grain-size dependence

The strain-based unified creep-fatigue formulation developed in Chapter 4 accommodates macroscopic variables (including temperature, cyclic time and applied loading), but cannot represent creep-fatigue behaviour at a microstructural level. This is a significant limitation for

the unified formulation when the creep-fatigue investigation of one specific material across multiple microstructures due to heat treatment. Normally, heat treating has significant influences on the mechanical properties, such as elasticity, ductility, strength, and hardness. This is microstructurally achieved through rearrangement of crystal structure and the change of homogeneity. This process can be evaluated through different variables, such as lattice structure, grain size, and the formation of precipitation, martensite, ferrite, cementite, and pearlite. However, most of them are unmeasurable as a parameter, thus are impractical to be introduced into a numerical formulation for engineering application. In this case, as a measurable parameter, the grain size is selected and then introduced to further modify the strain-based unified creep-fatigue equation (proposed in Chapter 4).

Other dependences at microstructural level, such as grain shape and its distribution, are also influenced by heat treatment. For example, the grain shape could be quantified by the key shape parameters, such as circularity, roundness, compactness, sphericity, aspect ratio, etc. These are left for future work. In principle it might in the future be possible to include grain morphology factors by further extension of the unified model. Challenges to be overcome in the future would be the need for a substantial amount of empirical testing, and the need to find mathematical representations of how the factors affect outcome variables. There is a paucity of existing models to connect grain morphology with life properties under creep-fatigue, so it wold be necessary to determine these relationships before including them into the unified model. Alternatively a brute force method such as high order polynomial data-fitting, or perhaps even neural networks, might be used – though neither of these methods provides any explanation of the effects.

The grain-size effect is presented in both fatigue and creep behaviours, and gives completely opposite situations. Generally, the material with smaller grain size is more beneficial for fatigue capacity but leads to poorer resistance to creep damage. This phenomenon results from the different failure mechanisms shown by fatigue and creep, where the fatigue damage occurs via cracks through the grains, while creep damage involves the grain boundary cracking [8]. The influence of grain size will be further discussed in Section 10.1.3.

The process to derive the modified formulation is presented below.

5.1.1 Strain-based unified creep-fatigue equation with grain-size dependence

Starting position

Chapter 4 gives the strain-based unified creep-fatigue equation:

$$\varepsilon_p = C_0 c(\sigma, T, t_c) {N_f}^{-\beta_0} \tag{5.1}$$

with

$$c(\sigma,T,t_c) = 1 - c_1(\sigma)\left(T - T_{ref}\right) - c_2 \log\left(t_c/t_{ref}\right)$$

$$T - T_{ref} = \begin{cases} T - T_{ref} & for \;\; T > T_{ref} \\ 0 & for \;\; T \le T_{ref} \end{cases} \tag{5.2}$$

$$t_c/t_{ref} = \begin{cases} t_c/t_{ref} & for \;\; t_c > t_{ref} \; and \;\; T > T_{ref} \\ 1 & for \;\; t_c \le t_{ref} \; or \; T \le T_{ref} \end{cases}$$

where the dependences of temperature and cyclic time are accommodated. To describe creep-fatigue behaviour at a microstructural level, the modified formulation of this unified equation (Eq.5.1) is constructed through incorporating the grain-size dependence. The same method for developing the unified formulation (shown in Chapter 4) is taken to introduce the parameter of grain size into this model. Specifically, the grain-size effect is numerically related to creep-fatigue behaviour based on the conventional grain-size-related equations, including the Hall-Petch equation for fatigue and the equation of steady-state creep rate for creep. By this means, the grain-size dependence is introduced into the fatigue component ($C_0 N^{-\beta_0}$) and creep component ($c(\sigma,T,t_c)$) respectively.

Note that we cannot assume creep-fatigue failure occurs at the steady stage for creep damage in the low-cycle fatigue regime, which was addressed in Chapter 4 to develop the strain-based unified creep-fatigue equation. However, we believe that the grain-size dependence is independent of creep stage, and thus it is reasonable to extract the relationship of grain size vs. creep strain from the equation of steady-state creep rate.

Existing formulations for grain size

On the one hand, in the situation where creep is dormant, the grain size is frequently related to yield stress through the Hall-Petch equation, where a power-law relation between them is presented. Then this relationship was extended to describe the fatigue characteristic by Mutoh & Radhakrishnan [90], Alexandre et al. [91], and Thompson & Backofen [92], and was physically derived from observing the plastic zone size around the crack tip at the fatigue limit. Consequently, the grain-size effect on fatigue capacity is numerically described by the Hall-Petch-type relation (Eq.5.3) [90, 91]:

$$\sigma_s = \sigma_0{}' + \frac{k}{\sqrt{d}} \tag{5.3}$$

where d is the grain size, σ_s is the fatigue strength (fatigue limit), and $\sigma_0{}'$ and k are constants.

On the other hand, for the creep condition, the grain size is always related to creep strain in a power-law relation, which is numerically represented by the equation of the steady-state creep rate:

$$\dot{\varepsilon} = \frac{A\sigma^m}{d^q} e^{-\frac{Q}{RT}} \tag{5.5}$$

where $\dot{\varepsilon}$ is the strain rate, σ is the applied stress, d is the average grain size, Q is the activation energy, T is the temperature, R is the Boltzmann's constant, and A, m and q are constants obtained from the creep test.

Development of a grain size model

Reforming this equation as $\sigma_s - \sigma_0{}' = \frac{k}{\sqrt{d}}$ gives a power-law relation between fatigue capacity (ε_p) and grain size, $\varepsilon_p \propto d^m$. Specifically, fatigue strength is physically defined as the stress below which no fatigue failure occurs, and is numerically identified as the stress at 10^7 cycles. In this case, fatigue strength could be ideally calculated through letting N_f=10^7 in the Basquin equation (Eq.2.1).

This implies that the power-law relation between fatigue strength and grain size could be extended to relate the fatigue strength coefficient (σ_0) with grain size, and the same to the fatigue ductility coefficient (C_0) and grain size. As a result, the modifying function ($b'(d)$) for the fatigue component is defined as:

$$b'(d) = Bd^n \tag{5.4}$$

where B and n are constants.

Creep damage is physically regarded as a diffusion-based behaviour which is generally described by diffusion flux. Since diffusion flux is defined as the substance flow through a unit area (grain-sized-related parameter) which is changeless during the whole process of creep rupture, it is believed that grain-size dependence is independent of creep stage.

Therefore, it is proposed that the power relation between creep-related damage and grain size shown by the steady stage of creep also could be applied to the initial stage of creep. In this case, the grain-size dependence can be related to the creep-related strain in a power-law relation, and the modifying function ($a'(d)$) for creep component is given as:

$$a'(d) = Ad^m \tag{5.6}$$

where A and m are constants.

Introducing the reference grain size into Eq.5.4 and Eq.5.6 gives the grain-size-related modifying functions, $B\left(d/d_{ref}\right)^n$ for the fatigue component and $A\left(d/d_{ref}\right)^m$ for the creep component. This completes the development of the grain size component to the model. The originality here is the inclusion of grain size in a combined creep/fatigue model.

Application

For the reference condition, we assume that these two modifying functions are both restored to 1, which gives a baseline to evaluate the grain-size effect on fatigue capacity. In addition, the introduction of the reference grain size provides an opportunity to remove the coefficient of modifying functions (A), which will be discussed in Chapter 6. Then these two modifying

functions are integrated into the strain-based unified creep-fatigue model (Eq.5.1), and then the modified formulation is given as:

$$\varepsilon_p = C_0 b(d) c(\sigma, T, t_c, d) N^{-\beta_0} \tag{5.7}$$

with

$$\begin{gathered} c(\sigma, T, t_c) = 1 - \left[c_1(\sigma)\left(T - T_{ref}\right) + c_2 \log\left(t_c / t_{ref}\right)\right] \cdot \left[A\left(d/d_{ref}\right)^m\right] \\ b(d) = B\left(d/d_{ref}\right)^n \end{gathered} \tag{5.8}$$

where, *A*, *B*, *m*, and *n* are grain-size-related constants.

A further modification and simplification are in order; specifically, the research [92, 93] on the relationship between grain size and fatigue life shows that grain size has only a slight influence on the pure-fatigue damage under the strain-controlled loading in the low-cycle fatigue regime. Therefore, for the reason of simplification, function $b(d)$ is removed from Eq.5.7.

Finally, the strain-based unified creep-fatigue equation (with grain-size dependence) is regenerated as:

$$\varepsilon_p = C_0 c(\sigma, T, t_c, d) N^{-\beta_0} \tag{5.9}$$

with

$$\begin{gathered} c(\sigma, T, t_c, d) = 1 - \left[c_1(\sigma)\left(T - T_{ref}\right) + c_2 \log\left(t_c / t_{ref}\right)\right] \cdot \left[A\left(d/d_{ref}\right)^m\right] \\ T - T_{ref} = \begin{cases} T - T_{ref} & for \;\; T > T_{ref} \\ 0 & for \;\; T \le T_{ref} \end{cases} \\ t_c / t_{ref} = \begin{cases} t_c / t_{ref} & for \;\; t_c > t_{ref} \; and \; T > T_{ref} \\ 1 & for \;\; t_c \le t_{ref} \; or \; T \le T_{ref} \end{cases} \end{gathered} \tag{5.10}$$

where ε_p is the plastic strain which reflects fatigue capacity, N_f is the creep-fatigue life, C_0 and β_0 are fatigue ductility coefficient and fatigue ductility exponent respectively, which are related to fatigue capacity at the pure-fatigue condition, T is the temperature, t_c is the cyclic time which is the reciprocal of loading frequency, d is the grain size, T_{ref} is the reference temperature which is defined as 35% of the melting temperature, t_{ref} is the reference cyclic time which is advised as a small value, d_{ref} is the reference grain size which is suggested as an arbitrary value but recommended to be selected from the values among the experimental range, σ reflects the applied loading which can be related to plastic strain through the cyclic strain-stress relation, $c_1(\sigma)$ and c_2 are the creep-related function and constant, and A and m are the grain-size-related constants.

5.1.2 Method of extracting the coefficients

This modified formulation should have the ability to cover the full range of conditions from pure fatigue to pure creep. In this case, the equation should have the ability to be restored to the conventional creep model in the pure-fatigue condition and be regenerated to the well-known time-temperature model in the pure-creep condition. All of these models are independent of grain size, which results in an assumption that:

The grain-size component $A\left(d/d_{ref}\right)^{m}$ equals 1 for both the pure-fatigue and the pure-creep conditions.

This assumption introduces a baseline to evaluate the grain-size effect on fatigue and creep behaviours. With this assumption, the same method shown in section 4.3 is applied to obtain the coefficients of the modified unified creep-fatigue formulation. In general, function $c_1(\sigma)$ and constant c_2 are derived from the creep-rupture data, and the magnitudes of C_0, β_0, A and m are obtained from the empirical data of creep fatigue. Significantly, C_0 and β_0 could be theoretically extracted from the pure-fatigue data, but for the reason of demanding higher fitting quality, the numerical optimization based on the creep-fatigue data is applied to extract C_0 and β_0 together with A and m.

Specifically, the pure-creep condition ($\varepsilon_p = 0$) gives the formula of constant c_2 (Eq.5.11) by letting T=T_{ref}, and suggests function $c_1(\sigma)$ (Eq.5.12) by letting t_c=t_{ref}.

$$c_2 = \frac{1}{\log\left(t_a/t_{ref}\right)} \tag{5.11}$$

$$c_1(\sigma) = -\frac{c_2}{P_{MH}(\sigma)} \tag{5.12}$$

In addition, a moderating factor (f_m) is introduced into the unified formulation to express a transformation from the cyclic-loading situation to an equivalent consistent-loading situation (the detailed explanation of this factor is presented in section 4.3). Then, with the cyclic strain-stress relation, function $c_1(\sigma)$ is further modified to describe creep damage from the strain perspective. This transformation gives:

$$c_1(\sigma) = -\frac{c_2}{P_{MH}(\sigma)} \rightarrow -\frac{c_2}{P_{MH}(\varepsilon_P)} = -\frac{c_2}{P_{MH}[f_{\mathrm{m}} \cdot K(T,t_c) \cdot {\varepsilon_P}^{n(T,t_c)}]} \tag{5.13}$$

where $K(T,t_c)$ and $n(T,t_c)$ are the strength coefficient and strain hardening exponent respectively, and they are functions of temperature and cyclic time.

Finally, the numerical optimization is applied to obtain the magnitudes of C_0, β_0, A and m through minimizing the difference (δ_t) (Eq.5.14) between the predicted creep-fatigue life ($N_{pre,ij}$) and experimental creep-fatigue life ($N_{exp,ij}$) for the conditions of $\varepsilon_{p,j}$, T_i, $t_{c,i}$ and d_i.

$$\delta_t = \sum \left(\log N_{pre,ij} - \log N_{exp,ij}\right)^2 \tag{5.14}$$

with

$$N_{comp,ij} = \left[\frac{\varepsilon_{p,j}}{C_0 c\left(\varepsilon_{p,j}, T_i,\ t_{c,i}, d_i\right)}\right]^{-1/\beta_0} \tag{5.15}$$

The average error (δ_a) is defined through dividing the total error (Eq.5.14) by the number of data points (n_{data}):

$$\delta_a = \sum \left(\log N_{pre,ij} - \log N_{exp,ij}\right)^2 / n_{data} \tag{5.16}$$

5.1.3 Evaluation of the unified formulation

The same method shown in section 4.4 is applied to evaluate the unified creep-fatigue equation, whereby the quality describing the creep-fatigue behaviour by using this formulation is investigated. Generally, this can be conducted by evaluating the prediction ratio and performing the reference-condition transformation.

Specifically, the prediction ratio (Eq.5.16) gives the ratio of predicted creep-fatigue life ($N_{pre,ij}$) to experimental creep-fatigue life ($N_{exp,ij}$):

$$H_{ij} = \frac{N_{pre,ij}}{N_{exp,ij}} \tag{5.16}$$

In the present work, we define that:

An acceptable prediction ratio should be between 0.75 and 1.25.

This also can be illustratively presented, where all data points of N_{pre} vs. N_{exp} under multiple temperatures and cyclic times should fall between the upper bound (+25%) and the lower bound (-25%) relative to ideal correlation (H=1).

In addition, the concept of fatigue capacity implies that creep-fatigue data can be ideally transformed into the reference condition by using Eq.5.17:

$$\varepsilon_{p,ref} = C_0 N^{-\beta_0} = \varepsilon_p / c(\sigma, T, t_c, d) \tag{5.17}$$

An effective numerical description of creep effect by function $c(\sigma, T, t_c, d)$ can cause all transformed creep-fatigue data to collect into a single power-law curve with good quality, where the coefficient and exponent of this trendline can well agree with C_0 and β_0 respectively. By this means, the high quality of fatigue-life prediction by using the unified equation is demonstrated.

5.2 Validation on metals

The unified creep-fatigue equation attempts to be applied in multiple situations for multiple materials, which is defined as the unified characteristic. This is validated on the materials of Inconel 718 and GP 91 casting steel, and the empirical data of creep rupture and creep fatigue are extracted from literature. This formulation was only validated on these two materials because of the limited data we could get from literature, and we believe that this unified equation would be better validated even be further modified if more empirical data on different materials are involved. According to the definition of this unified formulation, the reference temperature is defined as 35% of the melting temperature, the reference cyclic time is suggested as a small value, and the reference grain size is determined from the value within the experimental range.

5.2.1 Validation on Inconel 718

The reference temperature for Inconel 718 was chosen as 560K, the reference cyclic time was defined as 1s, and the reference grain size is selected as 35μm. The creep-rupture data [94] are plotted in Fig.5.1, and the point of convergence (T_{ref}, log t_a) is evaluated as (560K, 12.7805). This gives:

$$c_2 = \frac{1}{\log(t_a/t_{ref})} = \frac{1}{\log(10^{12.7805}/1)} = 0.0782 \tag{5.18}$$

and the relationship between stress and the Manson-Haferd Parameter:

$$-\frac{1}{P_{MH}(\sigma)} = 0.03538 + 5.27 \times 10^{-5}\sigma + 5.0 \times 10^{-8}\sigma^2 \tag{5.19}$$

Then, substituting into Eq.5.12, function $c_1(\sigma)$ is expressed as:

$$c_1(\sigma) = -\frac{c_2}{P_{MH}(\sigma)} = 2.7679 \times 10^{-3} - 4.12347 \times 10^{-6} \cdot f_m \cdot \sigma + 3.91221 \times 10^{-9} \cdot {f_m}^2 \cdot \sigma^2 \tag{5.20}$$

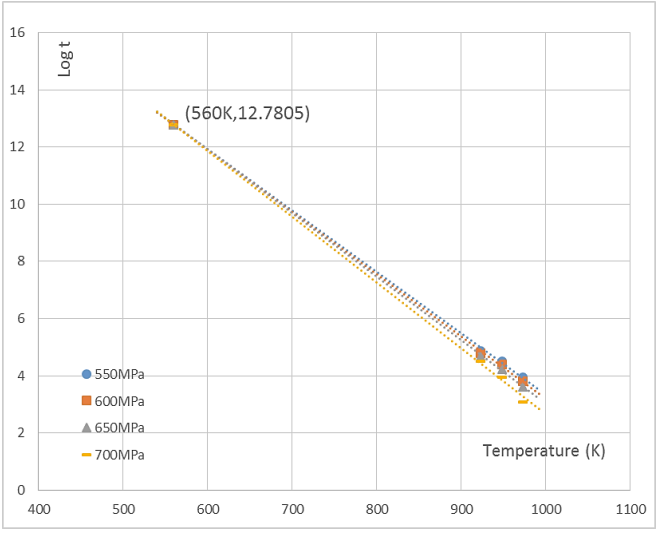

Figure 5.1 Creep-rupture characteristics of Inconel 718

and the magnitude of f_m is given as 0.6366 for the sinusoidal wave.

The creep-fatigue coefficients [95, 96] obtained from the literature are tabulated in Table 5.1, and the cyclic strain-stress relation [95, 96] is present by Eq.5.21 and Eq.5.22 (which were derived through curve fitting). Minimizing the difference between predicted creep-fatigue life ($N_{pre,ij}$) and experimental creep-fatigue life ($N_{exp,ij}$) yields C_o=0.4961, β_o=0.596, A=0.55005 and m=-0.5411, and returns an average error (δ_a) (Eq.5.14) of 0.00374.

Table 5.1 Creep-fatigue data for Inconel 718

Temperature (K)	Cyclic time (s)	Grain size (μm)	Creep-fatigue Coefficients $\varepsilon_p = \varepsilon_f' N_f^{-\beta}$	
			ε_f'	β
823	20	30	0.1642	0.588
873	20	30	0.1581	0.604
923	20	30	0.0981	0.558
700	3	11	0.7877	0.707
811	3	11	0.2545	0.579

$$K(T, t_c, d) = 1.7474 \times (10575.28663 - 7.64305T + 168.69826t)d^{-0.782457} \quad (5.21)$$

$$n(T, t_c, d) = 0.00593 \times (35.98325 - 0.03943T + 72.47165 \log t)d^{-0.41046} \quad (5.22)$$

The prediction ratio (N_{pre}/N_{exp}) under multiple temperatures, cyclic times and grain sizes are plotted in Fig.5.2, where all data points fall between the upper bound (+25%) and the lower bound (-25%). This implies that the unified creep-fatigue equation provides a high quality for fatigue-life prediction, specifically, a relatively high correlation between predicted and experimental creep-fatigue life.

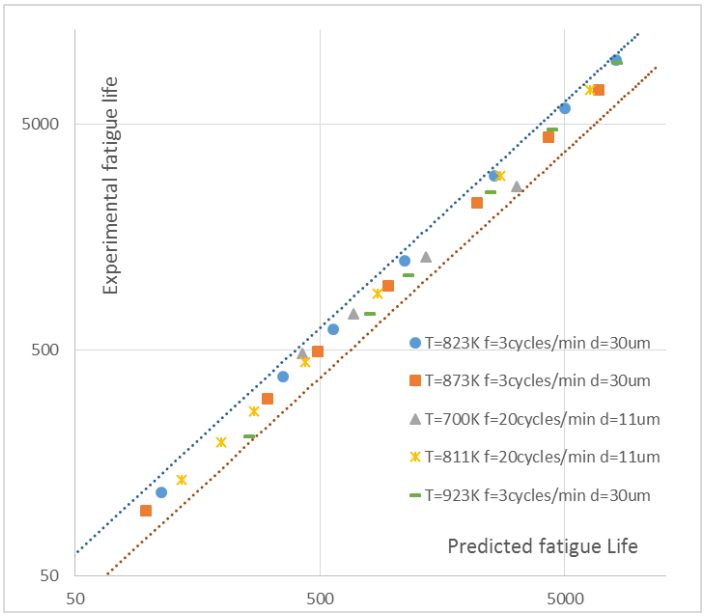

Figure 5.2 Prediction ratio for Inconel 718

With the results obtained above, the experimental creep-fatigue data (ε_p-N_{exp}) (shadow area in Fig.5.3) is transformed to the reference condition (the pure-fatigue condition) ($\varepsilon_{p,ref}$-N_{exp}) by using Eq.5.17. Fig.5.3 shows that the transformed data collapse into one power-law curve of $\varepsilon_{p,ref} = 0.477N^{-0.590}$ with the quality of fit as R^2=0.9905. The coefficients of the trendline, C_0=0.477 and β_0=0.590, are very close to the results obtained through numerical optimization. This suggests good consistency with the reference condition, and function $c(\sigma, T, t_c, d)$ represents a good numerical description of the creep characteristics.

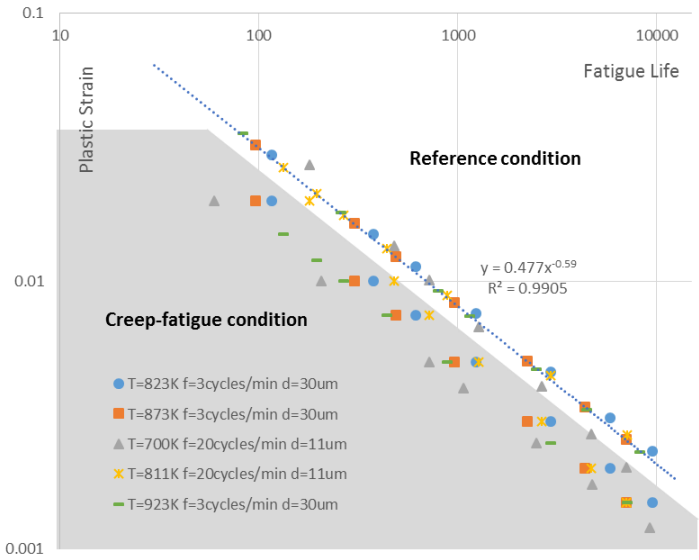

Figure 5.3 The transformed data ($\varepsilon_{p,ref}$-N_{exp}) for Inconel 718

Consequently, the coefficients of the unified creep-fatigue equation for Inconel 718 is collected in Table 5.2:

Table 5.2 The coefficients of the unified formulation for Inconel 718

C_0	β_0	c_2	A	m	T_{ref}(K)	t_{ref}(s)	d_{ref}(μm)	δ_a
0.4961	0.596	0.0782	0.55005	-0.5411	560	1	30	0.00374
$c_1(\sigma)$	$2.7679 \times 10^{-3} - 4.12347 \times 10^{-6} \cdot f_m \cdot \sigma + 3.91221 \times 10^{-9} \cdot {f_m}^2 \cdot \sigma^2$							

5.2.2 Validation on GP91 casting steel

The reference temperature for GP91 casting steel was chosen as 610K, the reference cyclic time was defined as 1s, and the reference grain size is selected as 25μm. The creep-rupture data [97] are plotted in Fig.5.4, and the point of convergence (T_{ref}, log t_a) is evaluated as (610K, 18.281). This gives:

$$c_2 = \frac{1}{\log(t_a/t_{ref})} = \frac{1}{\log(10^{18.281}/1)} = 0.0547 \tag{5.23}$$

and the relationship between stress and the Manson-Haferd Parameter:

$$-\frac{1}{P_{MH}(\sigma)} = 0.0174 + 2.20 \times 10^{-4}\sigma - 3.2 \times 10^{-7}\sigma^2 \tag{5.24}$$

Then, substituting into Eq.5.12, function $c_1(\sigma)$ is expressed as:

$$c_1(\sigma) = -\frac{c_2}{P_{MH}(\sigma)} = 9.51808 \times 10^{-4} + 1.20344 \times 10^{-5} \cdot f_m \cdot \sigma - 1.75045 \times 10^{-8} \cdot {f_m}^2 \cdot \sigma^2 \tag{5.25}$$

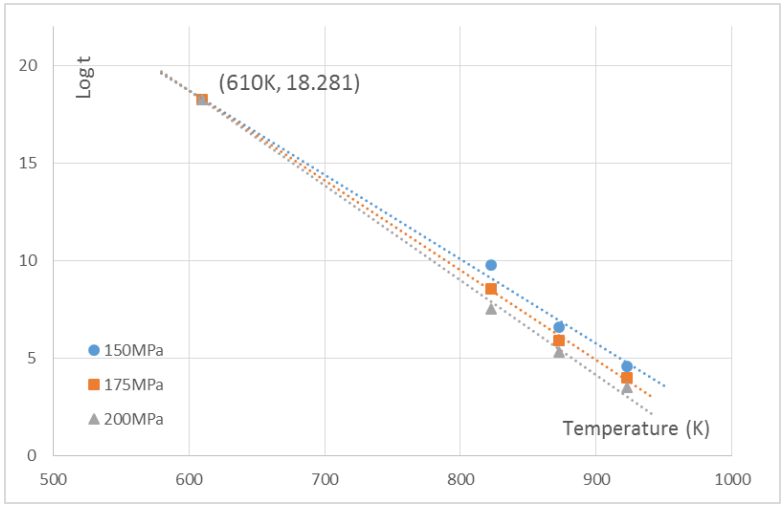

Figure 5.4 Creep-rupture characteristics of GP91 casting steel

and the magnitude of f_m is given as 0.6366 for the sinusoidal wave.

The creep-fatigue coefficients [98-100] obtained from the literature are tabulated in Table 5.3. Minimizing the difference between predicted creep-fatigue life ($N_{pre,ij}$) and experimental

creep-fatigue life ($N_{exp,ij}$) yields C_o=0.9532, β_o=0.669, A=0.5588 and m=-0.4053, and returns an average error (δ_a) (Eq.5.14) of 0.00334.

Table 5.3 Creep-fatigue data for GP91 casting steel

Temperature (K)	Frequency (Hz)	Cyclic time (s)	Grain size (μm)	Creep-fatigue Coefficients $\varepsilon_p = \varepsilon_f' N_f^{-\beta}$		Strain-stress Coefficients $\sigma/2 = K(\varepsilon_p/2)^n$	
				ε_f'	β	K	n
673	0.2	5	25	0.4609	0.5845	763.4	0.0956
823	0.2	5	25	0.9825	0.7279	416.15	0.0743
873	0.5	2	35	0.5990	0.6612	431.52	0.071

The prediction ratio (N_{pre}/N_{exp}) under multiple temperatures, cyclic times and grain sizes are plotted in Fig.5.5, where all data points fall between the upper bound (+25%) and the lower bound (-25%). This implies that the unified creep-fatigue equation provides a high quality for fatigue-life prediction, specifically, a relatively high correlation between predicted and experimental creep-fatigue life.

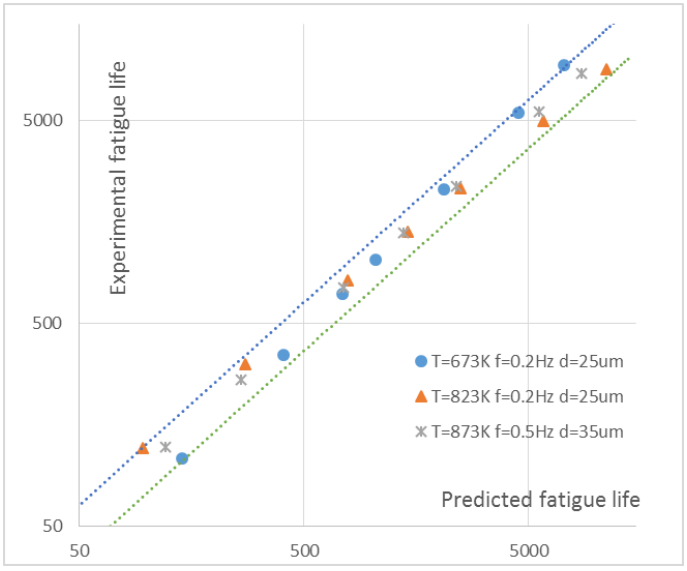

Figure 5.5 Prediction ratio for GP91 casting steel

With the results obtained above, the experimental creep-fatigue data (ε_p-N_{exp}) (shadow area in Fig.5.6) is transformed to the reference condition (the pure-fatigue condition) ($\varepsilon_{p,ref}$-N_{exp}) by using Eq.5.17. Fig.5.6 shows that the transformed data collapse into one power-law curve of $\varepsilon_{p,ref} = 0.9146N^{-0.663}$ with the quality of fit as R^2=0.9913. The coefficients of the trendline, C_0=0.9146 and β_0=0.663, are very close to the results obtained through numerical optimization. This suggests good consistency with the reference condition, and function $c(\sigma, T, t_c, d)$ represents a good numerical description of the creep characteristics.

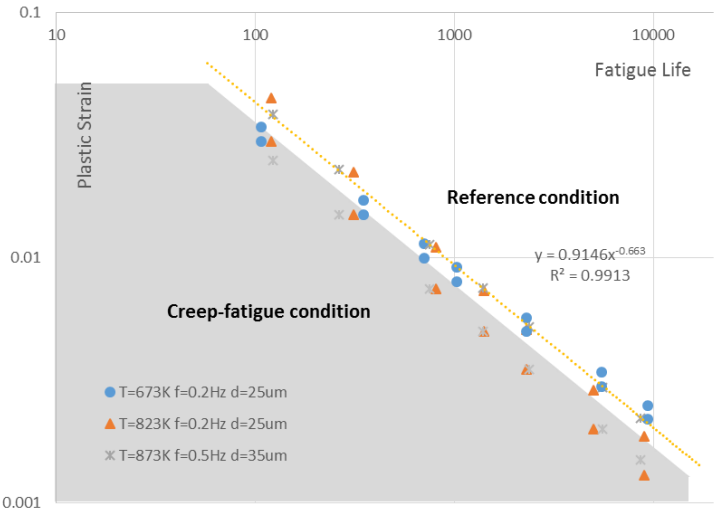

Figure 5.6 The transformed data ($\varepsilon_{p,ref}$-N_{exp}) for GP91 casting steel

Consequently, the coefficients of the unified creep-fatigue equation for GP91 casting steel is collected in Table 5.4:

Table 5.4 The coefficients of the unified formulation for GP91 casting steel

C_0	β_0	c_2	A	m	T_{ref}(K)	t_{ref}(s)	d_{ref}(μm)	δ_a
0.9532	0.669	0.0547	0.5588	-0.4053	610	1	25	0.00334
$c_1(\sigma)$	$9.51808 \times 10^{-4} + 1.20344 \times 10^{-5} \cdot f_m \cdot \sigma - 1.75045 \times 10^{-8} \cdot {f_m}^2 \cdot \sigma^2$							

Overall, the validation on the materials of Inconel 718 and GP91 casting steel demonstrated that the unified formulation with grain-size dependence has the ability to cover multiple situations and multiple materials; meanwhile, the structure of the creep function $c(\sigma, T, t_c, d)$ and the unified characteristic are proven. Note that because of the limited quality and quantity of empirical data which we could extract from the existing literature, the unified formulation may not be completely validated. Therefore, we believe that the unified creep-fatigue equation could be further validated even further modified if more empirical data could be obtained.

5.3 Summary

The strain-based unified equation presented in Chapter 4 was further modified to be given the ability to describe creep-fatigue behaviour at a microstructural level. In this case, the grain-size dependence was introduced and was related to fatigue capacity in a power-law relation based on the investigation of fatigue and creep mechanisms, then the modified formulation is represented as:

$$\varepsilon_p = C_0 c(\sigma, T, t_c, d) N^{-\beta_0} \tag{5.26}$$

with

$$c(\sigma, T, t_c, d) = 1 - \left[c_1(\sigma)\left(T - T_{ref}\right) + c_2 \log\left(t_c / t_{ref}\right)\right] \cdot \left[A\left(d/d_{ref}\right)^m\right]$$

$$T - T_{ref} = \begin{cases} T - T_{ref} & for \;\; T > T_{ref} \\ 0 & for \;\; T \le T_{ref} \end{cases} \tag{5.27}$$

$$t_c/t_{ref} = \begin{cases} t_c/t_{ref} & for \;\; t_c > t_{ref} \; and \;\; T > T_{ref} \\ 1 & for \;\; t_c \le t_{ref} \; or \; T \le T_{ref} \end{cases}$$

Function $c_1(\sigma)$ and constant c_2 are directly extracted from the creep-rupture data (Eq.5.11 and Eq.5.12), and the constants of C_0, β_0, A and m are numerical solved through minimizing the difference (Eq.5.14) between the predicted life and the experimental result. The unified formulation can be evaluated through the prediction ratio and the reference-condition transformation. Then, the unified creep-fatigue equation was validated on the materials of Inconel 718 and GP91 casting steel, where accepted prediction ratios were presented, and a good transformation from the creep-fatigue condition to the reference condition was shown. This implies that the modified formulation through introducing the grain-size dependence has the ability to be applied in multiple situations for multiple materials, and $c(\sigma, T, t_c, d)$ was proven to present an effective description of the creep effect. The grain-size dependence will be discussed in Chapter 6.

Chapter 6

6. Critique of the strain-based approach

This results chapter critiques the strain-based creep-fatigue approach. In this chapter, the Matlab-based and Excel-based numerical optimizations are compared, which indicates that both methods present the same quality for a solution, but the Excel-based method gives an easier method for engineering application. Then, by comparing with other existing creep-fatigue models proposed in Chapter 2, the new formulation presents significant advantages in the areas of unifying, integration, and economy. In particular, a grain-size-modified Manson-Haferd parameter and a simplified strain-based formulation are proposed. In addition, the introductions of the moderating factor and the grain-size dependence are also discussed in this chapter.

Publications relevant to this chapter are as follows (see Appendix A for details):

(1) Liu, D. and D.J. Pons, Development of a unified creep - fatigue equation including heat treatment. Fatigue & Fracture of Engineering Materials & Structures, 2017: p. 1-13.

(2) Liu, D. and D.J. Pons, A unified creep-fatigue equation with application to engineering design, in Creep, T. Tomasz, S. Marek, and A. Zieliński, Editors. 2017, InTechOpen: Rijeka, Croatia. (Accepted for publication)

The present work attempts to develop a unified creep-fatigue approach for engineering design, and thus this new model should be easy and practical for engineers to use. For example, this equation should be applied to multiple situations, and the coefficients of this equation should be obtained using a convenient and economical method. In this case, the strain-based unified creep-fatigue equation proposed above should be critiqued based on the needs of engineering design. In general, the unified model can be applied to make a material selection or to evaluate creep-fatigue capacity. The equation presented in Chapter 4 provides a more common approach for engineering design, where a material undergoing one specific heat treatment has been specified. The modified formulation through introducing grain-size dependence shown in

Chapter 5 provides a method to evaluate fatigue capacity for one specific material across multiple heat treatments. It is clear that the modified strain-based model is significantly better than other existing strain-based equations shown in Chapter 2 because this modified model has the ability to describe creep-fatigue behaviour at a microstructural level (across multiple heat treatments). There are also other advantages provided by this modified formulation which can be investigated through discussing its original formula. In addition, this original formulation presents a more common situation for engineering application, where one specified material has been assigned, and engineers only then need to input some macroscopic parameters (including temperature and cyclic time) to evaluate fatigue capacity. In this case, the critique shown in this chapter focuses on the strain-based creep-fatigue equation (without grain-size dependence) developed in Chapter 4.

6.1 Numerical optimization method

The strain-based unified creep-fatigue equation (shown in Chapter 4) is given as:

$$\varepsilon_p = C_0 c(\sigma, T, t_c) {N_f}^{-\beta_0} \tag{6.1}$$

with

$$\begin{aligned} c(\sigma, T, t_c) &= 1 - c_1(\sigma)\left(T - T_{ref}\right) - c_2 \log\left(t_c / t_{ref}\right) \\ T - T_{ref} &= \begin{cases} T - T_{ref} & for \;\; T > T_{ref} \\ 0 & for \;\; T \le T_{ref} \end{cases} \\ t_c / t_{ref} &= \begin{cases} t_c / t_{ref} & for \;\; t_c > t_{ref} \; and \; T > T_{ref} \\ 1 & for \;\; t_c \le t_{ref} \; or \; T \le T_{ref} \end{cases} \end{aligned} \tag{6.2}$$

where the constants of C_0 and β_0 can be derived from empirical data through the numerical optimization algorithm. In the present work, this is conducted by Excel which provides a more convenient method for engineering application without losing accuracy. Theoretically, this numerical operation also could be conducted by Matlab which is generally defined as a programming-language-based numerical computing software. However, although the accuracy of this method is incontrovertible, this method is significantly more complex than the Excel-based method. Therefore, the Matlab-based method is not suitable for engineering application. Note that the numerical optimizations conducted by Excel and Matlab are all based on the idea of:

Minimizing the difference between predicted fatigue life and experimental fatigue life.

The discussion and comparison between these two methods are presented below.

6.1.1 Matlab-based method

The software of Matlab [101] provides powerful numerical computing, which is operated by the programming language. Generally, to solve a specific variable, a possible range which

defines the boundary and the increment of this variable are first given, then the constraint condition is repeatedly verified through iterating with this incremental variable until it is satisfied, where the desired value of this variable is finally returned. The material of 63Sn37Pb solder is taken as an example to show the process of calculating the constants of C_0 and β_0. The programming code and its explanation are shown in appendix B. Then, the values of C_0 and β_0 are given as 7.90 and 0.8256 respectively, and the minimum error is 0.18486234.

In addition, the relationship among total error, C_0 and β_0 can be plotted in Fig.6.1 where the optimal solution is indicated:

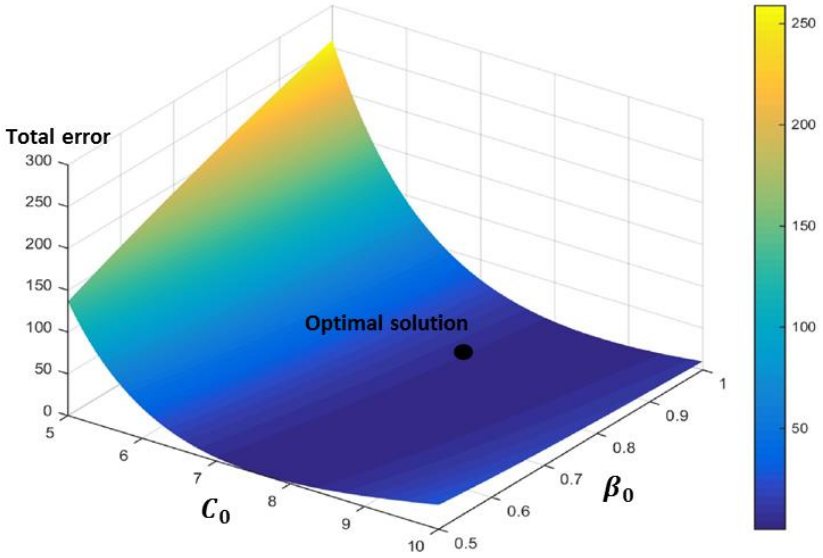

Figure 6.1 Relationship between total error, C_0 and β_0

6.1.2 Excel-based method

Excel is another software to conduct numerical computing (numerical optimization), which provides an easier tool for an engineer to use. This operation is based on a generalized reduced gradient (GRG) algorithm [102], which is one of the most robust nonlinear methods and has already been packaged into Excel. This approach provides a nonlinear optimization algorithm to find a locally optimal solution through numerical iteration. During this process, the derivatives (gradients) play an important role in convergence. Specifically, a positive/negative partial derivative of the optimum cell with respect to one adjustable cell implies that the value of this adjustable cell should be increased/decreased on the next iteration, and the iteration stops when the derivatives are zero.

The Excel-based method is generally manipulated by the following seven steps (Fig.6.2):

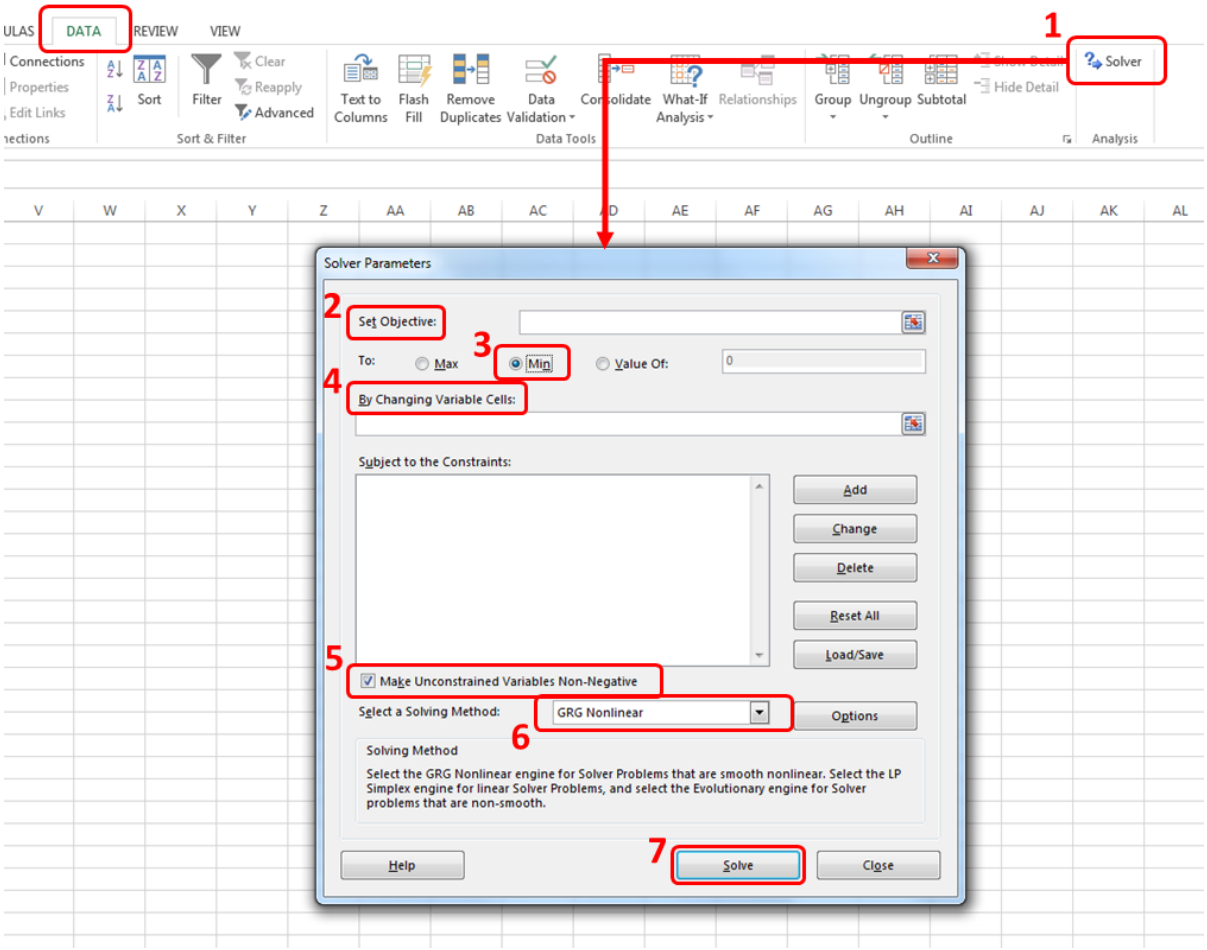

Figure 6.2 Excel-based method

(1) Opening Excel solver: DATA → Solver

(2) Selecting objective: selecting optimum cell in the spreadsheet. In the present work, the cell which shows total error is selected.

(3) Defining optimized condition: defining the criterion of numerical optimization for the value of the optimum cell. In the present work, the option of 'Min' is selected to find the minimum total error.

(4) Selecting variables: selecting adjustable cells in the spreadsheet. In the present work, the cells which give the value of C_0 and β_0 are selected.

(5) Ticking the option of 'Make Unconstrained Variables Non-Negative' since we do not accept negative values for either C_0 or β_0.

(6) Selecting solving method: selecting the numerical optimization algorithm. In the present work, we select the method of 'GRG Nonlinear' which is applied to the smooth-nonlinear situation.

(7) Clicking 'Solve' to get results.

Taking the material of 63Sn37Pb as an example, the Excel-based method gives C_0=7.894 and β_0=0.825, and the minimum error is suggested as 0.18485.

6.1.3 Discussion

Sections 6.1.1 and 6.1.2 present two different tools to do numerical optimization, and the results are collected in Table 6.1.

Table 6.1 Results obtained from Matlab-based method and Excel-based method

Methods	C_0	β_0	Minimum error
Matlab-based method	7.900	0.8256	0.18486
Excel-based method	7.894	0.8252	0.18485

Table 6.1 shows that the Matlab-based method nearly returns the same magnitudes of C_0 and β_0 as the Excel-based method, which significantly indicates that the result is independent of the tool which is used to do numerical optimization in the present work. In this case, both of them can be used to extract the constants of C_0 and β_0. However, for the purpose of engineering application, we recommend to use the Excel-based method. This is because:

(1) The Excel-based method provides a more convenient numerical method for engineers. Firstly, Excel is more popular software than Matlab regardless of the research field. In addition, Excel is easier to learn and use since no programming-language process is involved.

(2) The Excel-based method provides a more efficient process of numerical optimization for engineering application. Specifically, the Excel-based method presents a shorter time to return the results than the Matlab-based method. For example, in the present work, for the material of 63Sn37Pn solder, Excel takes no more than 5 seconds to get the results, but around 15 seconds are used to derive the results by Matlab (based on the programming code shown in section 6.1.1). It may be said that 15 seconds is also acceptable for engineering design, but this is based on the reasonable definitions of a possible range of variables and the number of incrementing steps. If the range of variables is widened to explore more possibilities, the number of incrementing steps then needs to be increased to maintain the accuracy. Alternatively, if the range of variables is retained, then the number of incrementing steps is increased to obtain better optimization results. As a result, the total time is significantly prolonged. For example, in order to obtain a smaller error, the number of steps is changed from 1000 to 3000 to explore more possibilities, then the total running time is remarkably increased to 140 seconds from 15 seconds even though a smaller minimum error is obtained (this smaller error is the same as the value obtained by the Excel-based method). We could imagine that the time would be further extended if further changes are conducted for the possible range of variables as well as the number of incrementing steps. In addition, the time is also influenced by the amount of empirical data. Specifically, the more data involved, then the more time is needed.

Consequently, we conclude that the numerical optimization conducted by Matlab is a time-consuming process, which is undesirable for engineering application.

Therefore, the Excel-based method provides a more convenient and efficient method for engineering design. This is because the method is easy to manipulate and can save significant time. In this case, Excel is suggested to conduct the numerical optimization for the present work.

6.2 Advantages of the strain-based unified creep-fatigue equation

The strain-based unified creep-fatigue formulation (Eq.6.3) was developed for engineering application, where the accuracy, coverage, and economy are equally important. In this case, the creep-fatigue approach should be applied at multiple temperatures and cyclic times for multiple materials, cover the full ranges of conditions from pure fatigue to pure creep and provide an economical method for fatigue-life prediction. The discussion shown below is presented by comparing this new model with the existing strain-based models (shown in Chapter 2), and the result shows that the strain-based creep-fatigue equation (developed in Chapter 4) has significant advantages for the aspects of unified characteristic, integrated feature, and economy.

$$\varepsilon_p = C_0 c(\sigma, T, t_c) {N_f}^{-\beta_0} \tag{6.3}$$

with

$$c(\sigma, T, t_c) = 1 - c_1(\sigma)\left(T - T_{ref}\right) - c_2 \log\left(t_c / t_{ref}\right)$$

$$T - T_{ref} = \begin{cases} T - T_{ref} & for \;\; T > T_{ref} \\ 0 & for \;\; T \le T_{ref} \end{cases} \tag{6.4}$$

$$t_c / t_{ref} = \begin{cases} t_c / t_{ref} & for \;\; t_c > t_{ref} \; and \; T > T_{ref} \\ 1 & for \;\; t_c \le t_{ref} \; or \; T \le T_{ref} \end{cases}$$

6.2.1 Unified characteristic

The unified characteristic is defined as the ability to predict fatigue life at multiple temperatures and cyclic times for multiple materials. In this case, the numerical representation which has this characteristic should include relevant variables, and should have the ability to be applied to multiple materials with high accuracy of fatigue-life prediction. Generally, the existing Coffin-Manson-based creep-fatigue models shown in Chapter 2 present good ability at fatigue-life prediction in the fields from which they were derived. However, the accuracy reduces when these models are extended to be applied to other materials. This limitation is improved by the strain-based unified creep-fatigue equation, which presents a general formulation based on the investigation of physical phenomena. Theoretically, the existing creep-fatigue models can be

modified to unified formulations through recalculating the coefficients for different materials. However, this results in poor economy since the more coefficients involved, then the more empirical data needed to obtain high accuracy of fitting. This is not desirable for engineering application.

The unified characteristic for the strain-based unified creep-fatigue equation was validated on multiple materials (including 63Sn37Pb solder, 96.5Sn3.5Ag solder, AL2024T3 alumina alloy, stainless steel 304, stainless steel 316, Inconel 718 and GP91 casting steel), which was presented in section 4.5 and section 5.2. In this chapter, the materials of 63Sn37Pb solder, stainless steel 304 and Inconel 718 are selected to demonstrate that the new creep-fatigue formulation is superior to the existing creep-fatigue models for the unified characteristic. The accuracy of fatigue-life prediction for these three materials by using different models is evaluated through average error, and the results are shown in Table 6.2.

Table 6.2 The accuracy of fatigue-life prediction for different models

No.	Creep-fatigue models	Average errors		
		63Sn37Pb	SS316	Inconel 718
1	Coffin's equation (Eq.2.31)	0.00910	0.06851	0.06770
2	Solomon's equation (Eq.2.32)	0.8747	23.9559	39.3992
3	Shi's equation (Eq.2.34)	0.002745	No result	No result
4	Jing's equation (Eq.2.36)	4.3435	No result	No result
5	Engelmaier's equation (Eq.2.38)	0.88304	0.07949	0.04423
6	Wong & Mai's equation (Eq.2.40)	0.000284	0.002810	0.001585
7	Strain-based creep-fatigue unified equation (Eq.6.3)	0.003301	0.004257	0.008643

Table 6.2 shows that Shi's equation provides the smallest average error compared to other models on 63Sn37Pb solder, but it cannot yield any result for the materials of stainless steel 304 and Inconel 718. Significantly, Shi's equation was directly derived from the creep-fatigue data of 63Sn37Pb solder by using curve fitting and thus provides the best fatigue-life prediction for this material. In addition, Table 6.2 also indicates that the fatigue-life prediction on materials of 63Sn37Pb solder, stainless steel 316 and Inconel 718 by using the equations of Coffin's, Solomon's, Engelmaier's and Jing's gives higher average errors (poor quality for fatigue-life prediction). This implies that although creep-fatigue behaviour may be well

represented by these models for their own applied areas from which they were derived, the accuracy strongly relies on the application area, but these models cannot be extended to other fields. This fundamentally results from the derivation method which is entirely based on curve fitting of empirical data, and thus the unified characteristic is not included.

The unified characteristic is represented by both Wong & Mai's equation and the strain-based unified creep-fatigue equation. Table 6.2 indicates that these two models give quite small average errors on materials of 63Sn37Pb solder, stainless steel 304 and Inconel 718, particularly, but Wong & Mai's equation has better performance. However, they present the unified characteristic based on remarkably different mechanisms. On the one hand, the strain-based unified creep-fatigue model was developed by including an element of physical justification, and thus the relationships between different variables are potential to be explained by the underlying physical mechanisms (this will be proved in Chapter 10). This is a typical advantage of the new model. In this case, the model theoretically has the ability to cover multiple materials. On the other hand, the unified characteristic also can be accommodated through the numerical method. This is normally achieved by introducing as many coefficients as possible to obtain a higher quality of fitting to the empirical data. This is the main principle for the smallest average error shown by using Wong & Mai's equation, even for any numerical-based formulation.

Structurally, both Wong & Mai's equation and the unified creep-fatigue equation present a general formulation for the creep-fatigue situation, where the coefficients are needed to be recalculated for different materials. In this case, the equations of Coffin's, Solomon's, Shi's, Engelmaier's and Jing's theoretically may also have the opportunity to represent the unified characteristic through transforming them into general formulations. For example, Solomon's equation can be rewritten as:

$$\varepsilon_p = C_1(T)\left(N_f f^{k-1}\right)^{-\beta_0} \tag{6.5}$$

with

$$C_1(T) = \mathrm{a} + \mathrm{b}T + \mathrm{c}T^2 + \mathrm{d}T^3 \tag{6.6}$$

where a, b, c, d, k and β_0 are the constants obtained from experiments. Then, this modified numerical formulation gives small errors (0.000529 for 63Sn37Pb and 0.00103 for stainless steel 316), and even represent better fatigue-life prediction than the unified formulation for some materials.

However, we cannot conclude that these modified formulations and Wong & Mai's equation are better than the strain-based unified creep-fatigue equation. Specifically, it is significant that these modified formulations and Wong & Mai's equation are introduced as many coefficients as possible to get a high quality of fitting to empirical data (such as modified Solomon's equation has six independent coefficients and Wong and Mai's equation has seven independent coefficients). Therefore, the representation of creep-fatigue behaviour is a numerical-based method and the goodness of extracting the coefficients highly relies on the number of empirical data. This means that the more empirical data result in more accurate fatigue-life prediction (better creep-fatigue description), which then gives poor economy. However, only two

independent coefficients in the strain-based unified creep-fatigue equation are derived by numerical optimization. This implies that less experimental effort is needed, thus giving a more economical method for fatigue-life prediction. The economy will be further discussed in section 6.2.3.

Overall, compared with other existing Coffin-Manson-based creep-fatigue formulations, the strain-based unified creep-fatigue equation provides a better method for fatigue-life prediction in multiple situations for multiple materials, wherein the small average errors are given, hence the unified characteristic is proven.

6.2.2 Integrated characteristic

The integrated characteristic refers to the ability to cover the full range of conditions from the pure-fatigue condition to the pure-creep condition. According to the concept of fatigue capacity, the full fatigue capacity (at the pure-fatigue condition) is gradually consumed by the increasing creep effect until it is completely consumed at the pure-creep condition. The comparison between different creep-fatigue models for the integrated characteristic is collected in Table 6.3, and then the discussion is shown in detail.

Table 6.3 The capacity of integrated characteristic

Creep-fatigue models	Pure-fatigue condition	Creep-fatigue condition	Pure-creep condition
Coffin's equation (Eq.2.31)	X	√	X
Solomon's equation (Eq.2.32)	X	√	X
Shi's equation (Eq.2.34)	X	√	X
Jing's equation (Eq.2.36)	X	√	X
Engelmaier's equation (Eq.2.38)	√	√	X
Wong & Mai's equation (Eq.2.40)	√√	√√	X
Strain-based creep-fatigue unified equation (Eq.6.3)	√√	√√	√√

√√: This equation can well describe the phenomena of this condition
√: This equation can partly describe the phenomena of this condition
X: This equation cannot describe the phenomena of this condition

Normally, the creep effect presents dependencies on temperature, cyclic time and applied loading, and thus the creep-fatigue model should accommodate these three relevant variables

in order to show a good description for creep-fatigue behaviour. In this case, creep effect in the existing Coffin-Manson-based creep-fatigue models (shown in Chapter 2) cannot be well-presented. Specifically, only the temperature and cyclic-time dependencies are included in the creep-fatigue models proposed by Solomon, Shi et al., and Engelmaier; only the cyclic-time dependence is presented in Coffin's equation, and only the temperature dependence is shown in Jing's equation. However, the Wong & Mai equation and the strain-based unified creep-fatigue equation accommodate these three variables, and they are believed to have a better ability to predict the fatigue-life under the creep-fatigue condition (the accuracy has been discussed in section 6.2.1). Further investigation of stress-related functions in these two equations shows that the stress function in the unified formulation is directly derived from the creep-rupture behaviour, but not for the Wong & Mai equation. Therefore, we believe that the strain-based unified creep-fatigue equation theoretically has a better description for creep effect.

In addition, a good numerical representation of creep fatigue also should be capable of covering two ends of the creep-fatigue condition: the pure-fatigue condition and the pure-creep condition. However, the equations proposed by Coffin, Solomon, Shi et al., Jing, Engelmaier and Wong & Mai do not totally satisfy this requirement.

On the one hand, the condition of pure fatigue is represented by letting $C_1(T)f^{\beta(1-k)} = C_0$ (C_0 is the ductility coefficient at the pure-fatigue condition) for the equation of Solomon, $C_2(T)f^{\beta[1-k(T)]} = C_0$ for the equation of Shi et al. and $\beta_0(\bar{T}, f) = \beta_0$ (β_0 is the ductility exponent at the pure-fatigue condition) for the equation of Engelmaier. When the extreme frequency is imposed, $f \to \infty$, the functions $C_i(T)$ and $\beta_0(\bar{T}, f)$ become infinitely small, which causes $T \to \infty$. In addition, the temperature component is not shown in Coffin's equation, thus the activation of creep effect in terms of temperature is ignored in this equation. The results shown above do not agree with the general understanding of pure fatigue, where the temperature should be lower than 35% of the melting point [57]. For Jing's equation, the derivation of function $C_3(T)$ is based on the material of 80Au/20Sn solder, thus a low temperature (where the creep effect is dormant) may return a reasonable value to describe the full fatigue capacity. When this equation is applied on steel, function $C_3(T)$ yields an impossible negative value since the temperature under the pure-fatigue condition is much higher than the situation for solder. However, the pure-fatigue condition can be well represented by both the Wong & Mai equation and the strain-based unified creep-fatigue equation by letting $T = T_{ref}$ and $t = t_{ref}$. In this case, these two equations are restored to the Coffin-Manson equation.

On the other hand, the condition of pure creep is presented by letting ε_p=0. This condition cannot be satisfied by the equation of Coffin because the coefficient C and exponent β_0 are constant, which leads to an impossible zero time or zero frequency. In addition, for the equation of Engelmaier, the pure-creep condition is satisfied by letting $\beta_0(\bar{T}, f) \to +\infty$, which implies $T \to +\infty$. The pure-creep condition for the equations of Solomon, Shi et al. and Jing et al. is satisfied by letting C_1=C_2=C_3=0, which returns T=172 ºC, 198 ºC and 249 ºC respectively. The equations of Solomon and Jing et al. imply that creep rupture only occur when the temperature is close to the melting temperature (186 ºC for 60Sn40Pb solder and 280 ºC for 80Au/20Sn

solder), while Shi's equation suggests that creep rupture only occurs above melting temperature (183 °C). The creep activation temperatures obtained from these four creep-fatigue equations do not agree with the general understanding of creep, where creep is activated at 35% of the melting temperature [57]. Although the Wong & Mai equation has a good description for pure fatigue, it cannot represent the pure-creep condition entirely. This is because letting $s(\sigma)c(T_R, f_R) = 0$ (at the pure-creep condition) cannot deduce any well-known time-temperature parameters, such as the Larson-Miller parameter (Eq.6.7), the Sherby-Dorn parameter (Eq.6.8) and the Manson-Haferd parameter (Eq.6.9):

$$P_{LM}(\sigma) = T(A + \log t_R) \tag{6.7}$$

$$P_D(\sigma) = t_R e^{-Q/(RT)} \tag{6.8}$$

$$P_{MH}(\sigma) = \frac{T - T_a}{\log t_R - \log t_a} \tag{6.9}$$

where $P_{LM}(\sigma)$ is the Larson-Miller parameter, $P_D(\sigma)$ is the Sherby-Dorn parameter, $P_{MH}(\sigma)$ is the Manson-Haferd parameter, A is the constant, t_R is the rupture time, R is the Boltzmann constant, Q is the activation energy, and $(log\ t_a, T_a)$ is the point of convergence of the $log\ t$-T lines. However, the Manson-Haferd parameter can be well-presented through letting $c(\sigma, T, t_c) = 0$ (at the pure-creep condition) for the strain-based unified creep-fatigue equation. In this case, the unified formulation has the ability to describe the pure-creep behaviour.

The integrated characteristic also can be illustratively presented by Fig.6.3, where the regimes of pure fatigue, creep fatigue and pure creep are shown based on the strain-based unified equation (proposed in Chapter 4).

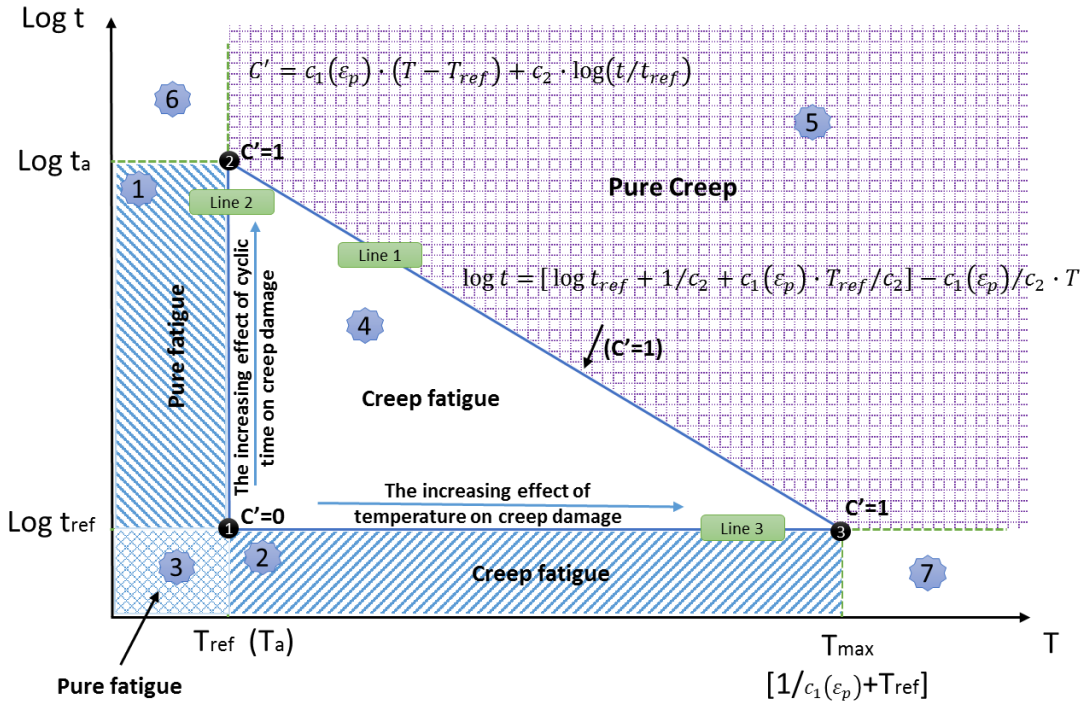

Figure 6.3 Illustration of the influence of creep damage on fatigue capacity

The discussion shown below is based on an assumption that is below the reference condition the change of cyclic time does not make significant influence on the creep-fatigue damage (this assumption was mentioned in Chapter 4). In the unified equation, function $c(T, t, \varepsilon_p)$ is presented as Eq.6.10, wherein function C' (Eq.6.11) describes the influence of temperature and cyclic time on creep fatigue. When $C' = 1$, damage is entirely caused by creep, while when $C' = 0$ the pure-fatigue behaviour leads to failure and the unified creep-fatigue equation is restored to the Coffin-Manson equation.

$$c(T, t, \varepsilon_p) = 1 - C' \tag{6.10}$$

with

$$C' = c_1(\varepsilon_p) \cdot (T - T_{ref}) + c_2 \cdot \log(t/t_{ref}) \tag{6.11}$$

According to the Manson-Haferd parameter, (T_a, $log\ t_a$) is the point of convergence of the T_a-$log\ t_a$ lines under different stresses, and $C' = 1$ at this point (Point 2 in Fig.6.3). This means that creep is active when the temperature is higher than T_a which is identified as the reference temperature. Therefore, when the temperature is lower than T_{ref} (T_a) and cyclic time is lower than t_a, no creep happens mainly due to low temperature (Area 1 and Area 3 in Fig.6.3) (the pure-fatigue condition). Based on the identification of reference time (t_{ref}), which is much lower than t_a and is regarded as the activation point of creep behaviour, another point (Point 3 in Fig.6.3) where $C' = 1$ is defined as (T_{max}, $log\ t_{ref}$), and T_{max} can be expressed as [$1/c_1(\varepsilon_p)+T_{ref}$]. When the cyclic time is lower than reference time (t_{ref}) and the temperature is between T_{ref} and T_{max}, the creep-fatigue situation is presented due to high temperature (Area 2 in Fig.6.3). In particular, Area 3 shows no creep happens due to both low temperature and low cyclic time, and $C' = 0$ at (T_{ref}, $log\ t_{ref}$) (Point 1 in Fig.6.3). The straight line (Line 1 in Fig.6.3) between Point 2 and Point 3 can be expressed as Eq.6.12:

$$\mathrm{Log}\, t = [\log t_{ref} + 1/c_2 + c_1(\varepsilon_p) \cdot T_{ref}/c_2] - c_1(\varepsilon_p)/c_2 \cdot T \tag{6.12}$$

which shows that any point on this line can deduce the function C' (Eq.6.11) to 1, and the area (Area 5 in Fig.6.3) which is above Line 1 represents the damage caused totally by creep. To be specific, in this area, the magnitude of function C' is higher than 1, which implies that the creep makes an enormous contribution to failure so that the contribution of cyclic fatigue can be neglected, and this area can be regarded as the pure-creep condition. The trigonal area (Area 4 in Fig.6.3), which is surrounded by Line 1, Line 2 and Line 3, represents the creep-fatigue condition. Specifically, according to Eq.6.11, any point in Area 4 can cause $0 < C' < 1$. In particular, the direction from Point 1 to Point 2 shows the increasing effect of cyclic time on creep contribution, and the direction from Point 1 to Point 3 represents the increasing effect of temperature on creep contribution.

Area 6 and Area 7 appear two different complex situations, and a supposition for these two areas are presented. To be specific, in Area 6, although the temperature too low to activate creep, the cyclic time may be enough long to break the atomic bonds in microstructure. Thus, a possible tensile fracture may be presented. In Area 7, the temperature is very high, even close

to the melting temperature, thus the behaviour of thermal viscoplasticity may be presented in this area.

Overall, comparing with other existing creep-fatigue models, the strain-based unified creep-fatigue equation can cover the full range of conditions from pure fatigue to pure creep. Specifically, this equation has the capability to model pure fatigue at $c(\varepsilon_p,T,t_c)=1$ where this equation is restored to the Coffin-Manson equation, model pure-creep rupture at $c(\varepsilon_p,T,t_c)=0$ where this equation is reorganized to the Manson-Haferd parameter, and model creep-fatigue damage at $0\leq c(\varepsilon_p,T,t_c)\leq 1$ where the creep effect is influenced by temperature, cyclic time and applied loading.

6.2.3 Economy

The process of fatigue-life evaluation in engineering design always requires good performance for both accuracy and economy [76]. The accuracy has been shown in section 6.2.1, and the economy will be discussed in this section. Both Wong & Mai's equation and the strain-based unified creep-fatigue equation can give a more accurate fatigue-life prediction than other existing creep-fatigue models in multiple situations for multiple materials, and thus the discussion of economy focuses on these two models. The results show that the unified formulation provides a more economical method for fatigue-life prediction since a minimum of experimental effort is involved.

Normally, the accuracy to predict a distribution (or a trend) by a numerical formulation partly depends on the number of coefficients, which implies that the formulation with more coefficients presents better fitting [102]. However, this factor is not isolated and is strongly related to the number of data points. Specifically, the more coefficients that are introduced, then the more data points that are needed, and then there is a better fit. This does not mean that a good formulation should contain as many coefficients as possible, because this may lead to redundancy of the empirical effort. Therefore, for deriving a numerical formulation, it is very important to keep a good balance between the accuracy and consumption. In this case, the strain-based unified creep-fatigue equation satisfies this requirement.

As mentioned in section 6.2.1, Wong & Mai's equation has seven independent coefficients which are obtained through numerical optimization, but only two independent coefficients are included in the strain-based unified creep-fatigue equation. This suggests that more empirical data are needed to give better fitting to the empirical data for Wong & Mai's equation, but this results in poor economy since performing a large number of creep-fatigue experiments is expensive and time-consuming. Significantly, this is not a good choice for engineering design due to the undesirable high cost. However, when fewer creep-fatigue tests are involved to control the total cost, the accuracy for the fatigue-life prediction reduces remarkably. This limitation is improved by the strain-based unified creep-fatigue equation, where a better balance between the accuracy and cost is given. A comparison between Wong & Mai's equation and the unified formulation for the accuracy of fatigue-life prediction regarding the empirical-data number is shown in Table 6.4, and the materials of 63Sn37Pb and stainless steel 304 are investigated.

Table 6.4 Accuracy of prediction regarding the empirical-data number

Materials	Number of data groups to derive coefficients	Average errors for predicting fatigue life	
		Wong & Mai's equation	Unified creep-fatigue equation
63Sn37Pb	Eight groups of data	0.000284	0.003301
	Three groups of data	0.2445	0.00355
Stainless steel 304	Seven groups of data	0.002810	0.004257
	Three groups of data	0.4684	0.007199

Taking the material of 63Sn37Pb as an example, Table 6.4 shows that Wong & Mai's equation gives better accuracy for the fatigue-life prediction than the unified formulation when all eight groups of creep-fatigue data are imposed (this has been discussed in section 6.2.1), wherein the average errors are 0.000284 for using Wong & Mai's equation and 0.003301 for using the unified formulation. Then, three groups of all creep-fatigue data (*T=233K, t_c=1s; T=298K, t_c=10s and T=298K, t_c=1000s*) were selected to obtain the coefficients, and the numerical optimization still yields quite small average errors for fitting. However, when Wong & Mai's equation with the coefficients obtained at this stage is extended to predict fatigue life at a total of eight creep-fatigue conditions, poor accuracy is given; specifically, the average error dramatically worsens to 0.2445 from 0.000284. This undesirable result is significantly improved by the strain-based unified creep-fatigue equation, wherein the difference between the average errors of the fatigue-life prediction under these two situations is very small (specifically, 0.003301 for the coefficients obtained from eight groups of creep-fatigue data and 0.00355 for the coefficients obtained from three groups of data). This indicates that fewer creep-fatigue experiments could be involved to obtain the coefficients of the unified formulation, and the accuracy of fatigue-life prediction by using Wong & Mai's equation is more sensitive to the amount of empirical data. As a result, the strain-based unified creep-fatigue equation provides a more economical method of fatigue-life prediction for engineering design because of the reduced number of creep-fatigue experiments. This conclusion is further demonstrated by the material of stainless steel 304, and the average errors under two situations are shown in Table 6.4.

Overall, it is clear that the good quality of the fatigue-life prediction provided by using Wong & Mai's equation (also other modified formulations from the original equations of Coffin's, Solomon's, Shi's, Engelmaier's and Jing's) is obtained through sacrificing economy. However, the strain-based unified creep-fatigue equation provides a more practical method of fatigue-life evaluation for engineering design, wherein a good balance between accuracy and economy is achieved.

Besides the advantages (unified characteristic, integrated feature and good economy) shown above, the strain-based unified creep-fatigue equation also can be explained by the underlying

physical mechanisms of fatigue and creep. However, the existing Coffin-Manson-based creep-fatigue models were derived through curve fitting, and thus they are completely numerically based formulations, and no physical explanation is included. Although this advantage (physical explanation) presented by the unified approach is not one of the essential requirements for engineering application, it is believed to be fundamental for three other advantages, thus it is highly important. The physical explanation of this unified formulation will be further discussed in Chapter 10.

6.2.4 The risk of model non-identifiability

The existing models (mentioned in Sections 2.2.2 and 2.2.3) are totally based on empirical data, specifically, both the relationships between different parameters and the coefficients in these models were extracted from empirical data by curve fitting. In this case, multiple power series were incorporated in the pursuit for high fitting-accuracy, and then multiple independent coefficients are included. Thus, these existing models may suffer from the problem of model non-identifiability or degeneracy: a different set of numerical coefficients might also solve the problem.

This risk is avoided by the unified model. This is because that the unified model has less independent coefficients which are determined by numerical optimization. Therefore, only one set of coefficients are given by the process of minimizing the difference between empirical data and predicted data. This was proved by Excel-based and Matlab-based numerical optimizations shown in Section 6.1.

6.3 Simplified form of the unified creep-fatigue equation

The research conducted by Manson indicated that the Coffin-Mansion equation can be modified to a universal slopes formulation (Eq.6.13) [103] by introducing the parameter of ductility based on the investigation of 29 materials, and this formulation takes the form:

$$\Delta\varepsilon_p = D^{0.6} {N_f}^{-0.6} \tag{6.13}$$

with

$$D = \ln\left(\frac{100}{100 - RA}\right) \tag{6.14}$$

where D is the ductility and RA is the percent reduction in area for the reference condition. Then, this simplified form was further modified by him based on 47 materials, and the modified universal slopes equation [104] is represented as:

$$\Delta\varepsilon_p = 0.547 D^{0.43} {N_f}^{-0.5} \tag{6.15}$$

The development of the universal slopes equation indicates that the full fatigue capacity shown in the strain-based unified creep-fatigue equation could be taken as a power-law relationship with the parameter of ductility. By this means, the unified formulation is modified as:

$$\Delta\varepsilon_p = X \cdot D^Y c(\sigma, T, t_c) N_f{}^{-\beta_0{}'} \tag{6.16}$$

or

$$\Delta\varepsilon_p = X \cdot D^Y c(\sigma, T, t_c, d) N_f{}^{-\beta_0{}'} \tag{6.17}$$

where X and Y are constants. Briefly, the constants X, Y and $\beta_0{}'$ can be derived from the numerical-optimization results shown in Chapters 4 and 5 on the materials of stainless steel 316, stainless steel 304, AL2024-T3, Inconel 718 and GP91 casting steel. The coefficients (C_0 and β_0) of the unified formulation and the ductility (D) for these five materials are collected in Table 6.5. Note that solder materials are not included in this exploration of simplified forms, because solder has a more significant deformation at break [105, 106], thus it is presented as a remarkably different material characteristic compared to other materials. In this case, to develop a simplified unified creep-fatigue equation, the solder materials should be discussed separately.

Table 6.5 The coefficients of the unified formulation and ductility

Materials	C_0	β_0	RA	D
Stainless steel 316	0.7284	0.6098	69%	1.171183
Stainless steel 304	0.8524	0.5777	70%	1.203973
AL2024-T3	0.7988	0.5502	27%	0.31471
Inconel 718	0.4961	0.5959	32%	0.38566
GP 91 casting steel	0.9562	0.6690	63.4%	1.005122

Table 6.5 shows that the values of β_0 are between 0.55 and 0.66, thus we assume the exponent ($\beta_0{}'$) of the simplified unified creep-fatigue equation to be 0.60. Then, minimizing the difference between the fatigue lives obtained from the simplified unified creep-fatigue equation and the experimental data gives the magnitudes of A and B as 0.8127 and 0.185 respectively. Then, the average errors of the fatigue-life prediction (which reflects the difference between predicted fatigue life and experimental fatigue life) by using the simplified formulation is presented in Table 6.6.

Table 6.6 Average errors of the fatigue-life prediction

Materials	Stainless steel 316	Stainless steel 304	AL2024-T3	Inconel 718	GP 91 casting steel
Average errors	0.02783	0.01860	0.42601	0.04744	0.06592

It can be found that the average error for aluminium alloy is much higher than other materials. This may be because other materials are carbon-based metal, but AL2024-T3 is an aluminium-based metal. Therefore, AL2024-T3 presents significantly different material characteristics compared with other carbon-based materials. In this case, the material of AL2024-T3 should be discussed separately. Then, by performing the same process of numerical optimization on the materials of stainless steel 316, stainless steel 304, Inconel 718 and GP91 casting steel, the values of A, B and $\beta_0{}'$ are returned as 0.8965, 0.3995 and 0.629 respectively and the improved average errors are shown in Table 6.7.

Table 6.7 Improved average errors of the fatigue-life prediction

Materials	Stainless steel 316	Stainless steel 304	Inconel 718	GP 91 casting steel
Average errors	0.01676	0.03006	0.004984	0.02898

Table 6.7 implies that the accuracy of the fatigue-life prediction is significantly improved by getting rid of the result for the material of AL2024-T3. In this case, the unified creep-fatigue formulation is modified and simplified as:

$$\Delta\varepsilon_p = 0.8965D^{0.3995}c(\sigma, T, t_c){N_f}^{-0.629} \tag{6.18}$$

or

$$\Delta\varepsilon_p = 0.8965D^{0.3995}c(\sigma, T, t_c, d){N_f}^{-0.629} \tag{6.19}$$

In particular, the simplified formulation without grain-size dependence (Eq.6.18) provides a more economical and convenient way to extract the coefficients since no creep-fatigue test is needed and only the creep-rupture test is required. However, for the simplified formulation with the grain-size dependence (Eq.6.19), the creep-fatigue tests are still needed to determine the grain-size-related coefficients, but less creep-fatigue tests are needed because fewer constants should be determined through numerical optimization. Thus, a more economical method for the fatigue-life prediction is proposed.

In the present work, including the parameter of ductility is an attempt to introduce a representative mechanical property into the unified model, and build a link to the applicability for applying at multiple materials. However, the simplified formulations (Eqs.6.18 and 6.19) were developed only based on limited empirical data, and thus it is believed that this formulation could be further modified and improved if more materials are investigated. This opens an opportunity for future research to improve the accuracy of the simplified formulations by investigating larger quantities of empirical data. Although recalculating the coefficients of the ductility component for each material may give a better accuracy, more empirical data are required because more coefficients are included.

6.4 Discussion of moderating factor (f_m)

The statement shown in section 4.2 suggests that a moderating factor was introduced into the creep-related function ($c_1(\sigma)$) to compress the amplitude of the applied loading:

$$c_1(\sigma) = -\frac{c_2}{P_{MH}(\sigma)} \rightarrow c_1(f_m \cdot \sigma) = -\frac{c_2}{P_{MH}(f_m \cdot \sigma)} \tag{6.20}$$

By this means, creep damage caused by constant loading is transformed to an equivalent value for the cyclic-loading condition. This transformation is consistent with a general understanding of creep effect, where constant loading produces more damage than the damage caused by its cyclic form (shown in section 4.2). As a result, this transformation provides a better numerical description of creep-fatigue behaviour. This is demonstrated for the materials of 63Sn37Pb solder, stainless steel 316 and Inconel 718, and the average errors (between the predicted fatigue life and the empirical result) in the situations with and without the moderating factor are collected in Table 6.8. Note that the fatigue-life prediction for the materials of 63Sn37Pb solder and stainless steel 316 are conducted by using the strain-based unified creep-fatigue equation without grain-size dependence:

$$\varepsilon_p = C_0 c(\sigma, T, t_c) {N_f}^{-\beta_0} \tag{6.21}$$

with

$$c(\sigma, T, t_c) = 1 - c_1(\sigma)\left(T - T_{ref}\right) - c_2 \log\left(t_c / t_{ref}\right) \tag{6.22}$$

and the fatigue-life prediction for Inconel 718 is conducted by using the unified formulation with grain-size dependence:

$$\varepsilon_p = C_0 c(\sigma, T, t_c, d) N^{-\beta_0} \tag{6.23}$$

with

$$c(\sigma, T, t_c) = 1 - \left[c_1(\sigma)\left(T - T_{ref}\right) + c_2 \log\left(t_c / t_{ref}\right)\right] \cdot \left[A\left(d / d_{ref}\right)^m\right] \tag{6.24}$$

Table 6.8 Average errors of the fatigue-life prediction in the situations with and without f_m

Situations	Average errors		
	63Sn37Pb solder	stainless steel 316	Inconel 718
With f_m	0.003301	0.00619	0.00374
Without f_m	0.02623	0.00541	0.00437

Table 6.8 shows that the average errors are significantly increased when the moderating factor (f_m) is removed for the unified creep-fatigue equation. In particular, for the material of 63Sn37Pb solder, the goodness of the fatigue-life prediction is made much worsen in the

situation without considering the moderating factor. Meanwhile, the numerical optimization returns C_0=589.366 and β_0=1.271, which are remarkably unreasonable. Specifically, C_0 and β_0 reflect the fatigue behaviour for the pure-fatigue condition. Thus, the numerical result implies that the plastic strain of 589.366 results in fatigue failure in the first loading cycle, which indicates an unreasonably huge value. In addition, the value of β_0 is normally between 0 and 1, but numerical optimization gives an absurd value (1.271).

For the material of stainless steel 316, although the average error is slightly improved when the moderating factor (f_m) is ignored, we could not conclude that the introduction of the moderating factor reduces the accuracy of the fatigue-life prediction. As discussed in Chapters 4 and 5, C_0 and β_0 somewhat reflect the fatigue capacity for the pure-fatigue condition, and thus can be used to roughly predict pure-fatigue life. In this case, the ability to describe the pure-fatigue behaviour by using C_0 and β_0 obtained from the situations with and without the moderating factor are evaluated, where the difference between predicted and experimental fatigue life (plotting empirical data gives that C_0=0.1986 and β_0=0.45) [89] are presented. Specifically, the average error is 0.009248 by using the coefficients obtained in the situation with the moderating factor, while removing the moderating factor gives a reduced accuracy of pure-fatigue-life prediction where the average error is 0.01270.

Consequently, the introduction of the moderating factor (f_m) physically and numerically provides a more reasonable description of creep effect for the cyclic-loading condition. This is clearly demonstrated for the materials of 63Sn37Pb solder and Inconel 718. Although this modification does not significantly improve the fatigue-life prediction for the material of stainless steel 316, the magnitudes of C_0 and β_0 returned from the formulation with the moderating factor give a better description for the pure-fatigue behaviour.

6.5 Discussion of grain-size dependence

As mentioned in Chapter 5, the parameter of grain size was introduced to reflect the heat-treatment effect. By this means, the creep-fatigue behaviour is numerically described at the microstructural level through the modified formulation:

$$\varepsilon_p = C_0 c(\sigma, T, t_c, d) N^{-\beta_0} \tag{6.25}$$

with

$$c(\sigma, T, t_c) = 1 - \left[c_1(\sigma)\left(T - T_{ref}\right) + c_2 \log\left(t_c/t_{ref}\right)\right] \cdot \left[A\left(d/d_{ref}\right)^m\right] \tag{6.26}$$

where the reference grain size is included to build a bridge between the pure-fatigue condition and the creep-fatigue condition.

6.5.1 Selection of the reference grain size

As mentioned in Chapter 5, the method to extract function $c_1(\sigma)$ and constant c_2 is based on the assumption that the grain-size component, $A\left(d/d_{ref}\right)^m$, equals 1 for the pure-creep condition. Under this assumption, the unified creep-fatigue equation can be reorganized as the original Manson-Haferd parameter, and the grain size obtained for this situation could be named as the pure-creep-related grain size. Since the reference grain size is suggested as an arbitrary value, the selection of this parameter ideally influences the results of numerical optimization for constants A and m. In this case, the grain-size related coefficients under different reference grain sizes are explored for the material of Inconel 718 and are shown in Table 6.9.

Table 6.9 Grain-size-related coefficients under different reference grain sizes

d_{ref}	A	m	$d = d_{ref}\sqrt[m]{1/A}$
10	0.99676	-0.5411	9.9401
20	0.68500	-0.5411	9.9399
30	0.55005	-0.5411	9.9400
40	0.47075	-0.5411	9.9394
60	0.37800	-0.5411	9.9399

The results shown in Table 6.9 indicates that constant *A* is strongly influenced by the choice of the reference grain size, but both *m* and *d* are independent of the reference grain size. This provides an opportunity to reduce the number of coefficients for the unified formulation. If the reference grain size is chosen as 9.94, the magnitudes of *A* and *m* are given as 1 and -0.541 respectively. This implies that constant *A* could be removed from the unified creep-fatigue equation only when the reference grain size is identified as 9.94.

From this we extract the more general implication that other materials may have a reference grain size that also gives *A* = 1. It appears that, for a given material, *m* is independent of the reference grain size and the value of *A*. This is a reasonable phenomenon, where the intensity of the grain-size effect on creep stays constant regardless of the choice of the reference grain size. Physically, since creep damage involves crack propagation along the grain boundary, the decreased/increased grain size results in increased/decreased opportunity for crack growth within a set area. This process is significantly independent of the selection of the reference grain size. In addition, the reference grain size which results in a unit value of *A* may be generally defined as the grain size for creep rupture tests.

However, the reference temperature and the reference cyclic time do not share the same feature as the reference grain size, because the creep is addressed to be dormant below the reference temperature and the reference cyclic time based on the concept of fatigue capacity. Therefore,

the influence of temperature and cyclic time on creep effect has a strong dependency on the choice of the reference temperature and the reference cyclic time.

6.5.2 Conceptual formulation of the grain-size-modified Manson-Haferd parameter

If we ignore the assumption of the grain-size component ($A\left(d/d_{ref}\right)^m$=1 at the pure-creep condition), letting ε_p=0 for the pure-creep condition could transform the strain-based unified creep-fatigue equation into the form:

$$\left[c_1(\sigma)\left(T-T_{ref}\right)+c_2\log\left(t_c/t_{ref}\right)\right]\cdot\left[A\left(d/d_{ref}\right)^m\right]=1 \tag{6.27}$$

Then, substituting function $c_1(\sigma)$ (Eq.4.20) and constant c_2 (Eq.4.18) gives a Manson-Haferd-type parameter:

$$P_{MH}(\sigma,d)=\frac{T_{ref}-T}{A\left(d/d_{ref}\right)^m\log t_a-\log \mathrm{t}+\left[1-A\left(d/d_{ref}\right)^m\right]\log t_{ref}} \tag{6.28}$$

This parameter is named as the grain-size-modified Manson-Haferd parameter. In particular, it can be restored to the original Manson-Haferd parameter through letting $A\left(d/d_{ref}\right)^m$=1 (the assumption is applied). Although this conceptual model is proposed in the present work, validation on the multiple materials is not included. Thus, an opportunity for future research is provided.

6.6 Critical review of the Wong & Mai equation

It is significant that the strain-based unified equation numerically gives a similar form as the Wong & Mai equation (proposed by my initial supervisor) [56] to present the temperature and time effects on creep fatigue; specifically, a linear relation between temperature and strain and a logarithmic relation between temperature and time. However, these relations in the Wong & Mai equation were derived from the empirical data through curve fitting while these relations in the strain-based unified model were obtained through including an element of physical justification. Therefore, the unified model can be physically explained (will be discussion in Chapter 10) but the Wong & Mai equation cannot. In this case, we could not say that the new formulation is a modification or extension of the Wong & Mai equation. This is because the development of these two models are based on two different principles. Specifically, the Wong & Mai equation shows that the expressions of function $c(T,t)$ and $b(T,t)$ are derived by examining the data of Shi on solder, and the obtained functions like $x_0+x_1T+x_2\log f$ where *x* refers to either *c* or *b*. No underlying physical basis was offered as to why the structure of the two equations should be identical like this. This raises the question of whether or not the formulation is physically unified, but this question disappeared for the unified formulation. In addition, the discussion above also shows that this new creep-fatigue model is better than the

Wong & Mai equation in the areas of integration and economy. In particular, the unified creep-fatigue model gives a more economical method for the fatigue-life prediction as the coefficients can be obtained through minimum experimental effort, which is significantly important for engineering design.

Besides these, the Wong & Mai equation also shows several issues:

Firstly, the Wong & Mai equation:

$$\varepsilon_p = C_0 s(\sigma) c(T,f) N_f^{-\beta_0 b(T,f)} \tag{6.29}$$

with

$$s(\sigma) = \begin{cases} 1 & when\ creep\ is\ dormant \\ exp\left[-\left(\sigma_{yield}\varepsilon_p^{n'}\right)/A\right] & when\ creep\ is\ active \end{cases}$$
$$c(T,f) = 1 - c_1\left(T - T_{ref}\right) - c_2 \log\left(f/f_{ref}\right) \tag{6.30}$$
$$b(T,f) = 1 - b_1\left(T - T_{ref}\right) - b_2 \log\left(f/f_{ref}\right)$$

shows that $s(\sigma) = 1$ and $c(T,t) = 1$ when creep is dormant (the pure-fatigue condition). Therefore, according to the derivation of stress function $s(\sigma)$ ($s(\sigma) = exp\left(-\frac{\Delta\sigma - \Delta\sigma_y}{\lambda_c}\right)$) [56], in this situation, the applied stress should equal the yield stress. However, this is not consistent with our general understanding of creep fatigue, where the yield stress is not a factor to determine the activation of creep effect. In this case, function $s(\sigma)$ cannot show a good description of the influence of stress on creep fatigue. What is needed is a stress function that can present the stress effects; this effect could be related to the creep behaviour and be shown through time-temperature relation. This need is presented by the unified formulation.

Another related issue is that Wong & Mai indicated that $c_1/c_2 = b_1/b_2$, because function $c(T,t)$ and $b(T,t)$ share the same pattern and characteristics. However, no reason was provided for this assumption. Also, the method of extracting the coefficients of function $c(T,t)$ and $b(T,t)$ was not proposed.

Furthermore, Wong & Mai indicated that $s(\sigma) = 1$ for solder material. However, this expression only applied to SnPb solder, and even then only one grade. This expression also implies that stress has zero influence on the creep-fatigue damage for SnPb solder, but this is an unreasonable assumption and inconsistent with the general understanding of creep behaviour.

Overall, although the strain-based unified creep-fatigue equation gives a numerically similar method to present temperature and time components as the Wong & Mai formulation, two different principles of derivation were performed. In this case, we conclude that the strain-based approach shown in the present work gives a new method to predict fatigue life. In addition, the significant advantages presented by the unified model and the issues raised by the Wong & Mai equation further indicates that the strain-based approach is much superior to the Wong & Mai equation.

6.7 Summary

The strain-based unified creep-fatigue equation was developed for engineering application, where convenience, accuracy, and economy were considered. Firstly, a convenient and effective method should be used to conduct numerical optimization. In this case, the tools of Excel and Matlab are applied to return the values of the constants in the unified creep-fatigue model, where the Excel-based method provides an easier method for manipulation with a high quality of fitting.

In addition, for engineering design, the unified creep-fatigue equation presents more significant advantages than the existing Coffin-Manson-based creep-fatigue models in the areas of unifying, integration and economy. Specifically, the new creep-fatigue model can be applied in multiple situations for multiple materials, can cover the full range of conditions from pure fatigue to pure creep, and can provide an economical method for the fatigue-life prediction. A further simplification through introducing the parameter of ductility was then made, which provides a more economical method for the fatigue-life prediction since none or fewer creep-fatigue tests are required. In particular, including a moderating factor (f_m) into the unified formulation was proved to be representing better descriptions of the creep effect and pure-fatigue behaviour.

Furthermore, the introduction of grain size gives this unified model a chance to describe creep-fatigue behaviour at a microstructural level. The investigation of the reference grain size indicates that one of the grain-size-related coefficients could be removed when one particular reference grain size is chosen, which provides a chance to further simplify the unified model. Then, a grain-size-modified Manson-Haferd parameter (Eq.6.28) was initially proposed, which opens an opportunity for future research on its improvement and validation.

It is noticeable that although the strain-based unified creep-fatigue equation gives a numerically similar method to present temperature and time components as the Wong & Mai formulation, we cannot say that the strain-based approach is the extension or modification of Wong & Mai's approach. This is mainly because they were derived from two significantly different methods, and the Wong & Mai equation also presents several issues which are inconsistent with a general understanding of creep fatigue.

Chapter 7

7. Stress-based unified creep-fatigue equation

This results chapter gives a stress-based unified creep-fatigue equation, which is normally applied in the high-cycle regime. In this chapter, the derivation of this new formulation is present, and the extraction of the coefficients is given. Then, the stress-based approach is validated on the materials of Inconel 718 and GP91 casting steel. In particular, introducing the compatibility gives a better description of the pure-fatigue condition. In addition, comparing with the existing stress-based models indicates that this new formulation can well present the unified and integrated characteristics.

Publications relevant to this chapter are as follows (see Appendix A for details):

(1) Liu, D. and D.J. Pons, Development of a stress-based creep-fatigue equation: Accommodating pure-fatigue to pure-creep for the high-cycle loading regime. International Journal of Damage Mechanics, 2017: p. 1-19.

Generally, in the pure-fatigue condition, the strain-based fatigue formulation is applied in the low-cycle regime ($N_f \leq 10^4$), while the fatigue behaviour in the high-cycle regime ($N_f > 10^4$) is described by the stress-based formulation [8, 107]. This feature is logically extended to the creep-fatigue area. In this case, the strain-based unified creep-fatigue equation was developed for the low-cycle regime, thus there is a need to develop a stress-based creep-fatigue model to be applied in the high-cycle regime. The stress-life relation is the most classical method to describe fatigue behaviour, and illustratively presented by S-N curve. The development of the stress-based creep-fatigue equation shows an extension of the conventional fatigue model, and ideally gives the ability to describe creep-fatigue behaviour under controlled stress amplitude. Significantly, we named this creep-fatigue equation as the 'unified' model, where 'unified' implies this new model could be applied to more materials in multiple situations. Note that although the stress-based approach is less practical than the strain-based approach since creep-fatigue failure normally occurs at the low-cycle fatigue regime in service, amounts of

experimental-based research were still conducted to explore the stress-life relation. In this case, a new stress-based creep-fatigue model is still developed in the present work, but its importance is secondary to the strain-based creep-fatigue equation.

7.1 Development of the stress-based unified creep-fatigue equation

The discussion shown in Chapter 2 indicates that the existing stress-based creep-fatigue models have significant limitations. Specifically, they cannot be applied in multiple situations for multiple materials, cannot entirely cover the full range of conditions from pure fatigue to pure creep, and cannot be physically explained. These disadvantages result from the method of curve fitting which is applied to derive these models. In this case, a new stress-based creep-fatigue model is needed.

In the present work, the stress-based unified creep-fatigue equation was developed from the identification of the physical phenomena, and then the relationships between the relevant variables (temperature and cyclic time at a macrostructural level, and grain size at a microstructural level) were extracted from the conventional fatigue and creep models (this method was also applied to extract the relationships in the strain-based formulation). These conventional models have been well verified under multiple situations, and thus it is believed that the relationships presented by these models are highly reliable. In particular, the concept of fatigue capacity, which shows that the full fatigue capacity is gradually consumed by the creep effect, was introduced to construct the formulation. The numerical-based simplification may be applied to constitute a more convenient formulation for engineering application.

7.1.1 Principle of constitution

In general, the creep-fatigue damage is caused by reversed loading at elevated temperature, and thus it is macroscopically influenced by temperature, frequency/cyclic time and applied loading (the effects of these factors were generally described in Chapter 4). As mentioned in Chapter 5, heat treatment has a significant effect on fatigue behaviour, and a measurable parameter, grain size, can be introduced to numerically describe this influence at a microstructural level. In this case, the dependences of temperature, cyclic time, applied loading and grain size should be accommodated into the stress-based formulation, and the relationships between them then can be extracted from the conventional fatigue and creep models.

At the creep-fatigue condition, the fatigue capacity (σ_f) is negatively influenced by the creep effect. Because of the fatigue effect, the total time of creep-fatigue failure under cyclic loading is significantly shorter than the creep-rupture time under the same loading but constant form. We assume that:

The creep-fatigue failure occurs at the steady state of creep in the high-cycle fatigue regime.

This assumption was not applied to develop the strain-based model which is normally used in the low-cycle fatigue regime, which is because the total time for the low-cycle failure is relatively short. With this assumption, the creep damage at the creep-fatigue condition can be evaluated by creep behaviour at the steady state. Normally, this state is numerically described by the equation of steady-state creep rate [8]:

$$\dot{\varepsilon} = \frac{A\sigma^m}{d^q} e^{-\frac{Q}{RT}} \tag{7.1}$$

where $\dot{\varepsilon}$ is the strain rate, σ is the applied stress, d is the average grain size, Q is the activation energy, T is the temperature, R is the Boltzmann's constant, and A, m and q are constants obtained from the creep test. This equation suggests that the creep damage could be represented as a function of stress, temperature, time and grain size. In this case, the creep-related strain (damage) can be related to stress in a power-law relation ($\varepsilon \propto \sigma^m$), related to temperature in a natural exponential relation ($\varepsilon \propto e^{-1/T}$), related to time in a linear relation ($\varepsilon \propto t$), and related to grain size in a power-law relation ($\varepsilon \propto d^q$).

In addition, at the pure-fatigue condition, the fatigue capacity is influenced by heat treatment. The grain size is identified as a measurable parameter to represent the influence of heat treatment. Normally, the grain size is related to yield stress through the Hall-Petch equation, where a power-law relation between them is given. Then this relation was extended to describe fatigue behaviour by Mutoh [90], Alexandre [91] and Thompson [92], and was physically derived from observing the plastic zone size around the crack tip at fatigue limit. Consequently, the grain-size effect on fatigue capacity is numerically described by the Hall-Petch-type relation (Eq.7.2):

$$\sigma_s = \sigma_0{}' + \frac{k}{\sqrt{d}} \tag{7.2}$$

where σ_s is the fatigue strength (fatigue limit), and $\sigma_0{}'$ and k are constants. Reforming this equation as $\sigma_s - \sigma_0{}' = \frac{k}{\sqrt{d}}$ gives a power-law relation between fatigue capacity (σ_f) and grain size, $\sigma_f \propto d^m$. Specifically, fatigue strength is physically defined as the stress below which no fatigue failure occurs, and is numerically identified as the stress at 10^7 cycles. In this case, fatigue strength could be ideally calculated by letting N_f=10^7 in the Basquin equation (Eq.2.1). This implies that the power-law relation between fatigue strength and grain size could be extended to relate grain size with fatigue strength coefficient (σ_0) as well as fatigue capacity (σ_f).

Furthermore, fatigue behaviour is generally presented as a process of damage accumulation, which is macroscopically shown by crack growth. This process is normally described by the second stage of crack growth where the major damage for structural failure is produced, and is numerically represented by Paris' equation (Eq.7.3) [29]:

$$\frac{da}{dn} = C(\Delta K)^m \tag{7.3}$$

where $\frac{da}{dn}$ is crack growth rate which reflects the length of crack growing during the period of one cycle, ΔK is the range of stress intensity factor, and C and m are constants. This equation shows that fatigue damage is accumulated in a power-law relation with the applied loading. This relationship is also explained by the conventional fatigue models, such as the Basquin equation and the Coffin-Manson equation. The conventional models show that irreversible damage is gradually stored in a power-law relation with an increased number of cycles, and the structural failure then occurs when the total damage achieves a critical value. In this case, we conclude that fatigue capacity can be related to fatigue life in a power-law relation.

Overall, the possible relationships between the relevant variables were extracted from the conventional fatigue and creep models. These relationships are presented in Table 7.1, and then could be used to develop the stress-based creep-fatigue equation.

Table 7.1 Possible relationships between relevant variables

No.	Variables	Relationships
1	Creep strain vs. applied stress	Power-law relation
2	Creep strain vs. temperature	Natural exponential relation
3	Creep strain vs. grain size	Power-law relation
4	Creep strain vs. time	Linear relation
5	Pure-fatigue capacity vs. grain size	Power-law relation
6	Fatigue capacity vs. fatigue life	Power-law relation

7.1.2 Constructing the creep-fatigue formulation

In general, the stress-based unified creep-fatigue equation can be constructed through numerically integrating the relationships between relevant variables identified in section 7.1.1 based on the concept of fatigue capacity.

At the pure-fatigue condition where the creep effect is dormant, fatigue capacity is only influenced by grain size, and the relationship between them is numerically represented in a power-law form. In this case, a grain-size-modified Basquin equation is given as:

$$\sigma_f = \sigma_0 \cdot B(d) \cdot N_f^{-b_0} = \sigma_0 \cdot B' d^p \cdot N_f^{-b_0} \tag{7.4}$$

where σ_f is the fatigue capacity for the pure-fatigue condition, function $B(d)$ is the grain-size moderating function for pure fatigue, B' and p are constants, and σ_0 and b_0 are the constants to reflect the full fatigue capacity.

At the creep-fatigue condition, fatigue capacity is influenced by temperature, cyclic time, applied loading and grain size, then the residual fatigue capacity can be postulated to be given by Eq.7.5:

$$\sigma = C(T,t,\sigma,d)\sigma_f = \sigma_0 \cdot B(d) \cdot C(T,t,\sigma,d) \cdot N_f^{-b_0} \tag{7.5}$$

where σ is the residual fatigue capacity and function $C(T,t,\sigma,d)$ is the creep moderating function. This equation gives a general construction of the stress-based unified creep-fatigue equation, which presents a combined effect of fatigue and creep.

Chapter 5 gives a creep moderating function $c(\sigma,T,t_c,d)$ (Eq.7.6) to present the creep effect in the strain-based model. Significantly, this function provides a clearly and simply numerical formulation to present creep effect. Although the relationship between applied strain and cyclic time was not directly derived from the conventional models, introducing the Manson-Haferd parameter somewhat improves this problem. Eq.7.6 may be extended to the stress-based situation, but this numerical formulation should be modified since Eq.7.6 describes the creep effect in terms of strain.

$$c(\sigma,T,t_c,d) = 1 - \left[c_1(\sigma)\left(T - T_{ref}\right) + c_2 \log\left(t_c/t_{ref}\right)\right] \cdot \left[A\left(d/d_{ref}\right)^m\right] \tag{7.6}$$

According to the discussion shown in section 4.2.3, a natural exponential relationship of creep-related strain vs. temperature was simplified to a linear relationship. In this case, based on the relationship between creep-related strain and applied stress shown in Table 7.1, the temperature can be related to applied stress in a power-law relation. In addition, the logarithmic relationship between temperature and time also should be remained. This gives the stress-based model a possible chance to be reformed as a well-known temperature-time parameter at the pure-creep condition. Considering these two relationships presented above, Eq.7.6 is modified and hence function $C(T,t,\sigma,d)$ is given as:

$$C(T,t_c,\sigma,d) = 1 - \left[C_1(\sigma) \cdot X \cdot \left(T - T_{ref}\right)^x + C_2 \cdot Y \cdot \log^y\left(t_c/t_{ref}\right)\right] \cdot \left[A'\left(d/d_{ref}\right)^{m'}\right] \tag{7.7}$$

where X, Y, x, y, A' and m' are constants. This numerical representation may be not accepted in the present work. This is because:

Firstly, Eq.7.7 shows a complex formulation since more coefficients are included, which is undesirable for engineering application;

Secondly, the power-law relationship (shown in Table 7.1) between time and creep-related stress is not presented by this formulation. However, this relation should be considered because we assume that creep-fatigue failure normally occurs at the steady stage of creep for the high-cycle fatigue. Note that the linear relationship between time and creep-related strain is not included in the strain-based approach since this assumption is not applied to the low-cycle fatigue.

In this case, we cannot accept the formulation shown by Eq.7.7 and then need to look for another formulation to describe creep effect and improve the problems mentioned above. This

may be achieved by attempting a product relationship between the temperature component and the time component, and the logarithmic relation of temperature vs. time may also be removed from the stress-based model. This after was proved to give good results. The derivation of function $C(T,t,\sigma,d)$ is shown as follows:

The concept of fatigue capacity indicates that the reduced fatigue capacity is consumed by the creep effect. From a stress perspective, this reduction, when $N_f = 1$, can be expressed as:

$$\sigma\big(N_f = 1\big) = \sigma_0 \cdot B(d) \cdot C(T, t_c, \sigma, d) = \sigma_f\big(N_f = 1\big) - \sigma_c = \sigma_0 \cdot B' d^p - \sigma_c \qquad (7.8)$$

where σ_c presents the reduction of fatigue capacity due to the creep effect. By employing the strain-stress relation, this stress (σ_c) (Eq.7.9) could be transferred and extracted from the general creep strain rate-stress relation (Eq.7.1), where the period of the creep process for one cycle is identified as the cyclic time (t_c).

$$\dot{\varepsilon}(\sigma,T,d) \rightarrow \varepsilon_c(\sigma,T,t_c,d) \xrightarrow{strain-stress\ relation} \sigma_c(\sigma,T,t_c,d) \qquad (7.9)$$

Then, based on the relationships between relevant variables shown in Table 7.1 (specifically, the power-law relationships of creep-related strain vs. applied stress and creep-related strain vs. grain size, the linear relationship between creep-related strain and time, and the natural exponential relationship between creep-related strain and temperature), combining the temperature component and time component gives the numerical representation of function $\sigma_c(\sigma,T,t_c,d)$:

$$\sigma_c(\sigma,T,t,d) = K[\varepsilon_c(\sigma,T,t_c,d)]^{n'} = K\left(C'\sigma^c d^b t_c e^{-\frac{Q'}{T}}\right)^{n'} \qquad (7.10)$$

wherein the cyclic strain-stress relation provides a power-law transformation from strain to stress.

The derivation of Eq.7.10 is based on another assumption, that is:

The initial phase of creep is small enough to be neglected, and thus the total creep damage can be described by the steady stage of creep.

Substituting Eq.7.10 in Eq.7.8 gives:

$$\sigma_0 B(d) C(T,t_c,\sigma,d) = \sigma_0 B' d^p - K\left(C'\sigma^c d^b t_c e^{-\frac{Q'}{T}}\right)^{n'} = \sigma_0 B' d^p \left[1 - \frac{K C'^{n'}}{\sigma_0 B'}\left(\sigma^c d^{b-\frac{p}{n'}} t_c e^{-\frac{Q'}{T}}\right)^{n'}\right] \qquad (7.11)$$

Then, Eq.7.5 is further presented as:

$$\sigma = \sigma_0 B' d^p \left[1 - \frac{K C'^{n'}}{\sigma_0 B'}\left(\sigma^c d^{b-\frac{p}{n'}} t_c e^{-\frac{Q'}{T}}\right)^{n'}\right] N_f^{-b_0} \qquad (7.12)$$

Eq.7.12 shows that the constant σ_0 is multiplied by another constant, B'. This gives an unreasonable numerical representation for extracting the coefficients since one specific product of σ_0 and B' could be achieved by multiple choices of σ_0 and B', and then makes numerical

optimization more complex. In this case, the magnitude of B' is assumed to be 1. This assumption provides a more reasonable and simpler numerical formulation for engineering application, and the grain-size effect is somewhat incorporated into the fatigue strength coefficient (σ_0). This may reduce the accuracy of the fatigue-life prediction, but the decreased number of coefficients could reduce the experimental effort and the complexity of manipulation.

Then, through reorganizing the coefficients, Eq.7.12 is further expressed as:

$$\sigma = \sigma_0 d^m \left[1 - A\left(\sigma^a d^n t_c e^{-\frac{Q'}{T}}\right)^k\right] N_f^{-b_0} \tag{7.13}$$

The experiments conducted by Gary [79] indicates that for a given magnitude of stress, the creep damage is more intensive at the constant-stress condition than the cyclic-stress condition. Since the presentation of the creep effect in Eq.7.13 was derived from the pure-creep equation at constant stress (Eq.7.1), the cyclic stress in Eq.7.13 should be compressed to an equivalent value by introducing a moderating factor, f_m (this factor was also introduced into the strain-based creep-fatigue equation for the same purpose). In the present work, we focus on creep-fatigue behaviour under cyclic loading (regular-loading) with zero mean stress; thus this factor is valid for this situation. Generally, this moderating factor is related to the shape of the loading wave, and reflects the average level of the cyclic loading. This moderating factor is evaluated based on half-cycle loading, from which arises an assumption that the creep effect in the tensile portion is the same as in the compressive portion. This assumption may not be appropriate for some materials [80, 81], but it could simplify the method to extract this factor. A further description of this moderating factor has been presented in Chapter 4.

Then, Eq.7.13 is modified as:

$$\sigma = \sigma_0 d^m \left\{1 - A\left[(f_m\sigma)^a d^n t_c e^{-\frac{Q'}{T}}\right]^k\right\} N_f^{-b_0} \tag{7.14}$$

where A, a, n, Q', m and k are constants.

As discussed in Chapter 3, a desirable creep-fatigue model should have the ability to cover the full range of conditions from pure fatigue to pure creep. On the one hand, a bridge between the pure-fatigue condition and the creep-fatigue condition can be built by introducing the reference condition which reflects the activation of creep effect and provides a baseline to describe creep-fatigue behaviour. Numerically, the thermal component, time component, and grain-size component are removed from the unified formulation for the reference condition. Then, introducing the reference temperature (T_{ref}), the reference cyclic time (t_{ref}) and the reference grain size (d_{ref}) into Eq.7.14 gives:

$$\sigma = \sigma_0 \left(d/d_{ref}\right)^m \left\{1 - A\left[\left(d/d_{ref}\right)^n \cdot f_m^a \cdot \sigma^a \cdot e^{-\frac{Q'}{T-T_{ref}}} \cdot \left(t_c/t_{ref}\right)\right]^k\right\} N_f^{-b_0} \tag{7.15}$$

Significantly, for the reference condition, the stress-based creep-fatigue equation is restored into the Basquin equation to show the pure-fatigue behaviour.

On the other hand, fatigue capacity is totally consumed by the creep effect for the pure-creep condition, which gives σ=0. Then, the stress-based creep-fatigue equation is reorganized as:

$$\log\left[e^{-\frac{Q'}{T-T_{ref}}}\cdot\left(t/t_{ref}\right)\right]=-a\log\sigma+\log\left[\left(\frac{1}{A}\right)^{1/k}\left(d/d_{ref}\right)^{-n}f_m^{-a}\right] \tag{7.16}$$

This equation presents a time-temperature relation, which has the same formulation as the Sherby-Dorn parameter, and thus implies that the stress-based formulation has the ability to describe the pure-creep behaviour. This transformation also provides a possible method to extract the creep-related parameters of the stress-based model. Consequently, the integrated characteristic is included in this new creep-fatigue formulation (this characteristic will be further discussed in section 7.3.2).

Overall, the stress-based unified creep-fatigue equation is constituted as:

$$\sigma=\sigma_0\cdot B(d)\cdot C(T,t_c,\sigma,d)\cdot N_f^{-b_0} \tag{7.17}$$

with

$$\begin{gathered}B(d)=\left(d/d_{ref}\right)^m\\ C(T,t,\sigma,d)=1-A\cdot\left[\left(d/d_{ref}\right)^n\cdot f_m^a\cdot\sigma^a\cdot e^{-\frac{Q'}{T-T_{ref}}}\cdot\left(t_c/t_{ref}\right)\right]^k\\ T-T_{ref}=\begin{cases}T-T_{ref} & for\ \ T>T_{ref}\\ \rightarrow\ 0 & for\ \ T\le T_{ref}\end{cases}\\ t_c/t_{ref}=\begin{cases}t_c/t_{ref} & for\ \ t_c>t_{ref}\ and\ \ T>T_{ref}\\ 1 & for\ \ t_c\le t_{ref}\ or\ T\le T_{ref}\end{cases}\end{gathered} \tag{7.18}$$

where σ is the applied stress which reflects fatigue capacity, N_f is the creep-fatigue life, σ_0 and b_0 are the fatigue strength coefficient and fatigue strength exponent respectively which are related to fatigue capacity at the pure-fatigue condition, T is the temperature, t_c is the cyclic time which is the reciprocal of loading frequency, d is the grain size, T_{ref} is the reference temperature which is defined as 35% of the melting temperature, t_{ref} is the reference cyclic time which is advised as a small value, d_{ref} is the reference grain size which is suggested as an arbitrary value but recommended to be selected from the value among the experimental range, and A, Q', n, a and k are constants.

7.1.3 Method of extracting the coefficients

The stress-based unified creep-fatigue equation was developed based on the concept of fatigue capacity. Therefore, the full range of conditions from the pure-fatigue condition to the pure-

creep condition can be theoretically included in this new formulation, and some or all of the coefficients can be extracted from the empirical data of pure fatigue and pure creep.

The relationship between the pure-fatigue capacity and grain size was directly extracted from the Hall-Petch-type relation (Eq.7.2), and thus the magnitude of *m*, which reflects the intensity of the grain-size effect on fatigue capacity, is identified as -0.5. In addition, the stress-moderating factor f_m is defined as the equivalent constant stress factor to the cyclic loading. Specifically, $f_m = 0.6366$ for the sinusoidal wave and $f_m = 0.5$ for the triangular wave.

According to the concept of fatigue capacity, under the pure-creep condition, the fatigue capacity is totally consumed by the creep effect, and thus $\sigma = 0$. This gives:

$$C(T, t_c, \sigma, d) = 1 - A \cdot \left[\left(d/d_{ref}\right)^n \cdot f_m^a \cdot \sigma^a \cdot e^{-\frac{Q'}{T-T_{ref}}} \cdot \left(t_c/t_{ref}\right) \right]^k = 0 \tag{7.19}$$

Then, applying a logarithmic operation represents a temperature-time relation:

$$\log\left[e^{-\frac{Q'}{T-T_{ref}}} \cdot t_c \right] = -a \log\sigma + \log\left[\left(\frac{1}{A}\right)^{1/k} \left(d/d_{ref}\right)^{-n} t_{ref} f_m^{-a} \right] \tag{7.20}$$

This relation significantly has the same form as a well-known temperature-time relation, the Sherby-Dorn parameter (Eq.7.21):

$$P_{SD}(\sigma) = \log\left[t_R e^{-Q/(RT)}\right] = -\frac{Q}{RT}\log e + \log t_R \tag{7.21}$$

where $P_{SD}(\sigma)$ is the Sherby-Dorn parameter and t_R is the rupture time. This parameter can be extracted through creep-rupture tests, and also can be expressed as a linear relationship with the log of stress (Eq.7.22):

$$P_{SD}(\sigma) = a_1 \log\sigma + a_2 = \log\left[t_R e^{-Q/(RT)}\right] \tag{7.22}$$

where a_1 and a_2 are constants obtained from creep-rupture tests. Since the creep moderating function is not strictly derived from the general creep strain rate-stress relation (Eq.7.1) and the initial stage of creep is ignored, the magnitude of $\log\left[\left(\frac{1}{A}\right)^{1/k}\left(d/d_{ref}\right)^{-n} t_{ref} f_m^{-a}\right]$ in Eq.7.20 cannot be related to the magnitude of a_2 in Eq.7.22. However, the intensity of the stress effect (a) and the activation-energy-related parameter (Q') may be related to the Sherby-Dorn parameter by comparing Eq.7.20 with Eq.7.22, hence Eq.7.23 and Eq.7.24.

$$Q' = Q/R \tag{7.23}$$

and

$$a = -a_1 \tag{7.24}$$

where the coefficients, Q' and a, can be extracted from creep-rupture data. Note that the Sherby-Dorn parameter $(P_{SD}(\sigma))$ and the activation energy (Q) should be extracted from the creep-rupture data of $(T - T_{ref})$ vs. t_R in the present work.

Numerical optimization is applied to obtain the magnitudes of σ_0, b_0, A, k and n. Although this method could provide a solution with minimum error, numerical optimization may not present good consistency with the internal physical relations between these coefficients. Consequently, this potential risk may result in inaccurate fatigue-life prediction under the pure-fatigue condition, because the full-fatigue-capacity-related parameters (σ_0 and b_0) are directly derived from the numerical optimization. The possible solution for σ_0 covers a wide range, thus a small fluctuation of any coefficient in the stress-based model could lead to a large change for σ_0. However, a narrow potential range of C_0 is presented for the strain-based model. In this case, we believe that the magnitude of C_0 could reasonably describe the pure-fatigue situation (which has been somewhat discussed in Chapter 6). Therefore, in order to improve the results obtained through the numerical optimization, the compatibility (which will be further discussed in section 7.3.1) [107] is introduced to relate the stress-life relation with the strain-life relation.

The derivation of the stress-based creep-fatigue equation and the strain-based creep-fatigue equation is based on the concept of fatigue capacity. This is based on an assumption that:

The exponents (b_0 and β_0) of these two creep-fatigue equations are independent of temperature, cyclic time and grain size.

This assumption implies that the modified creep-fatigue coefficients ($\sigma_0 \cdot B(d) \cdot C(T, t, \sigma, d)$ for the stress-based equation and $C_0 c(\sigma, T, t_c, d)$ for the strain-based equation) could not strictly follow the compatibility, but the coefficients (σ_0 and C_0) and the exponents (b_0 and β_0) for the pure-fatigue condition (the reference condition) can be numerically related by the compatibility equations (Eq.7.25 and Eq.7.26) [107]:

$$\sigma_0 = K' {C_0}^{n'} \tag{7.25}$$

$$b_0 = n' \beta_0 \tag{7.26}$$

where K' and n' are the strength coefficient and strain hardening exponent at the reference condition. Through introducing the compatibility, the coefficients of the stress-based unified creep-fatigue equation (Eq.7.17) are solved by combining with the coefficients of the strain-based unified creep-fatigue equation. By this means, the internal relations between the coefficients and exponents are included, and the number of independent coefficients of the stress-based model is reduced. The numerical optimization is conducted through minimizing the difference (δ_t) (Eq.7.27) between the predicted creep-fatigue life ($N_{pre,ij}$) and experimental creep-fatigue life ($N_{exp,ij}$) for the conditions of σ_j, ε_{pj}, T_i, $t_{c,i}$ and d_i.

$$\delta_t = \sum \left(\log N_{pre,ij} - \log N_{exp,ij} \right)^2 \tag{7.27}$$

with

$$N_{comp,ij} = \left[\frac{\sigma_j}{\sigma_0 B(d) C\left(T_i, t_{c,i}, \sigma_j, d_i\right)} \right]^{-1/b_0} \tag{7.28}$$

and the average error (δ_a) is defined through dividing total error (Eq.7.27) by the number of data points (n_{data}):

$$\delta_a = \sum \left(\log N_{pre,ij} - \log N_{exp,ij}\right)^2 / n_{data} \tag{7.29}$$

Theoretically, the magnitudes of C_0 and β_0 (in Eq.7.25 and Eq.7.26) could be extracted from the strain-based unified creep-fatigue equation, and they also could be obtained from the pure-fatigue test (wherein the temperature is lower than the reference temperature, the cyclic time is selected as the reference cyclic time and the grain size is chosen as the reference grain size). In the present work, the former method is accepted.

7.1.4 Evaluation of the unified formulation

The same method shown in Chapter 4 is applied to evaluate the stress-based unified creep-fatigue equation. Specifically, the evaluation is conducted through the prediction ratio and the reference-condition transformation.

The prediction ratio (Eq.7.30) gives the ratio of predicted creep-fatigue life ($N_{pre,ij}$) to experimental creep-fatigue life ($N_{exp,ij}$):

$$H_{ij} = \frac{N_{pre,ij}}{N_{exp,ij}} \tag{7.30}$$

In the present work, we define that:

An acceptable prediction ratio should be between 0.75 and 1.25.

This also can be illustratively presented, where all data points of N_{pre} vs. N_{exp} in multiple situations (including temperature, cyclic time and grain size) should fall between the upper bound (+25%) and the lower bound (-25%) relative to ideal correlation (H=1).

In addition, the concept of fatigue capacity implies that creep-fatigue data can be ideally transformed to the reference condition by using Eq.7.31:

$$\sigma_{ref} = \sigma_0 N^{-b_0} = \sigma / [B(d) \cdot C(T, t_c, \sigma, d)] \tag{7.31}$$

An effective creep description by function $C(\sigma, T, t_c, d)$ can collect all creep-fatigue data into one power-law curve (the curve for the reference condition) with high quality of fitting, where the coefficient and exponent of this trendline can well agree with σ_0 and b_0 respectively. By this means, the goodness of fatigue-life prediction by applying the stress-based unified equation is demonstrated.

7.2 Validation on metals

The stress-based creep-fatigue equation was developed to be applied in multiple situations for multiple materials, which is defined as the unified characteristic. This was validated on the materials of GP91 casting steel and Inconel 718, where the empirical data of creep rupture and creep fatigue were extracted from the literature. This equation was only validated on these two materials because of limited empirical data which could be obtained from the literature. In particular, the creep-fatigue data under the stress-controlled loading on Inconel 718 was transformed from the empirical data of the strain-life relation by applying the idea of compatibility. We believe that the stress-based creep-fatigue equation would be better validated, and even further modified, if more empirical data on different materials are involved. According to the definition of this stress-based model, the reference temperature is defined as 35% of the melting temperature, the reference cyclic time is given as a small value, and the reference grain size is selected from the value from the experimental range.

7.2.1 Validation on GP91 casting steel

The reference temperature for GP91 casting steel is chosen as 610K, the reference cyclic time is defined as 1s, and the reference grain size is selected as 25μm. In addition, according to the relation between fatigue capacity and grain size in the pure-fatigue condition, the magnitude of m is given as -0.5. The stress-moderating factor f_m is suggested as 0.6366 for the sinusoidal wave.

On the one hand, based on the creep-rupture data obtained from the literature [97], the Sherby-Dorn parameter (Eq.7.21) is extracted by plotting *1/(T-T_{ref}) vs. logt* (Fig.7.1):

$$P_{SD}(\sigma) = \log\left[te^{-Q/[R(T-T_{ref})]}\right] = -\frac{Q\log e}{R}\cdot\frac{1}{T-T_{ref}} + \log t \tag{7.32}$$

The slope (3054.07) of *1/(T-T_{ref}) vs. logt* curves shown in Fig.7.1 gives Q, then the magnitude of Q' is obtained through Eq.7.23:

$$Q' = Q/R = 3054.07/\log e = 7032 \tag{7.33}$$

On the other hand, the Sherby-Dorn parameter can also be presented as a function of stress:

$$P_{SD}(\sigma) = -12.95\log\sigma + 23.307 \tag{7.34}$$

According to Eq.7.24, the magnitude of a is given as 12.95.

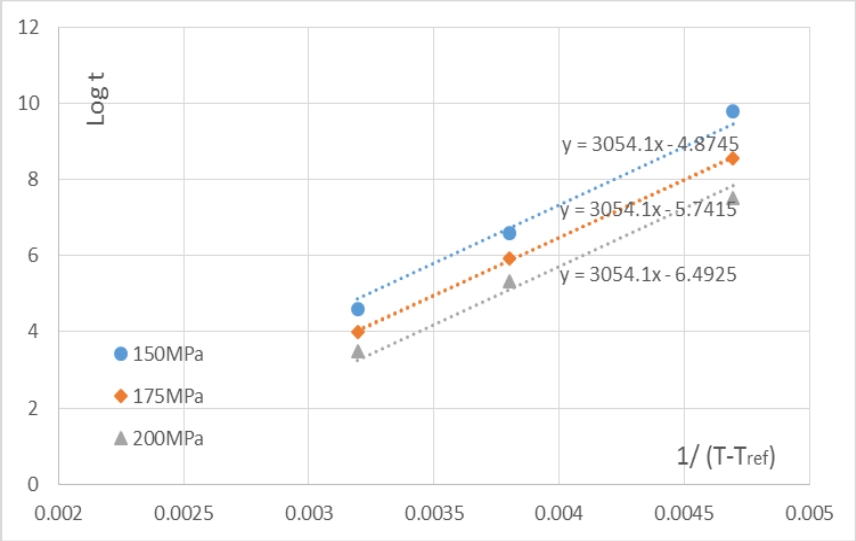

Figure 7.1 Creep-rupture characteristic of GP91 casting steel

The creep-fatigue coefficients and the strain-stress coefficients [98-100] obtained from the literature are tabulated in Table 7.2. Minimizing the difference between the predicted creep-fatigue life ($N_{pre,ij}$) and the experimental creep-fatigue life ($N_{exp,ij}$) yields $\sigma_0 = 1682.97$, $b_0 = 0.06995$, $A = 0.09356$, $k = 0.04628$ and $n = -61.114$, and returns an average error (δ_a) (Eq.7.29) of 0.001121.

Table 7.2 Creep-fatigue data for GP91 casting steel

Temperature (K)	Frequency (Hz)	Cyclic time (s)	Grain size (μm)	Creep-fatigue Coefficients $\sigma = \sigma_f' N_f^{-b}$		Strain-stress Coefficients $\sigma/2 = K(\varepsilon_p/2)^n$	
				σ_f'	b	K	n
673	0.2	5	25	1326.9	-0.056	763.4	0.0956
823	0.2	5	25	789.48	-0.054	416.15	0.0743
873	0.5	2	35	792.23	-0.048	431.52	0.071

The prediction ratio (N_{pre}/N_{exp}) under multiple temperatures, cyclic times and grain sizes are plotted in Fig.7.2, where all data points fall between the upper bound (+25%) and the lower bound (-25%). This implies that the stress-based unified creep-fatigue equation provides a high quality for the fatigue-life prediction, specifically, a relatively high correlation between the predicted and experimental creep-fatigue life.

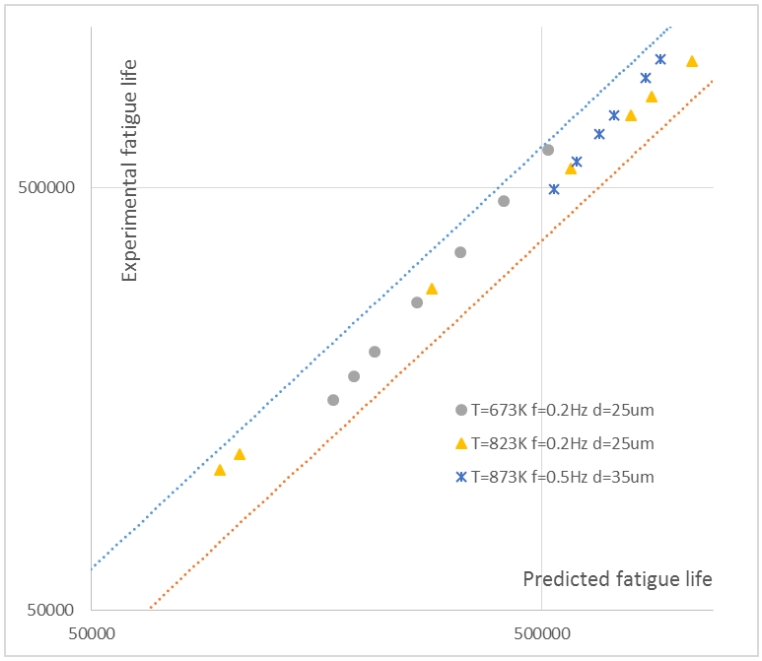

Figure 7.2 Prediction ratio for GP91 casting steel

With the results obtained above, the experimental creep-fatigue data (σ-N_{exp}) (shadow area in Fig.7.3) are transformed to the reference condition (the pure-fatigue condition) (σ_{ref}-N_{exp}), by using Eq.7.31. Fig.7.3 shows that the transformed data are collected into a single power-law curve of $\sigma_{ref} = 1612.2N^{-0.070}$ with a good quality of fit as R^2=0.9878. The coefficient and exponent of this trendline, σ_0=1612.2 and b_0=0.070, are close to the magnitudes of σ_0 and b_0 obtained through numerical optimization. This suggests good consistency with the reference condition, and implies the function $C(T, t, \sigma, d)$ represents a good numerical description of the creep characteristics.

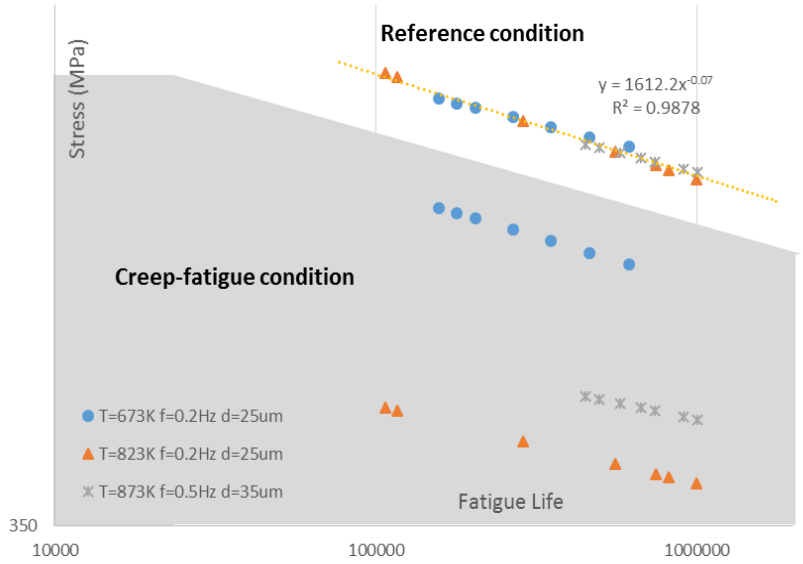

Figure 7.3 The transformed data (σ_{ref}-N_{exp}) for GP91 casting steel

Consequently, the coefficients of the unified creep-fatigue equation for GP91 casting steel is collected in Table 7.3:

Table 7.3 The coefficients of the unified formulation for GP91 casting steel

σ_0 (MPa)	b_0	a	A	m	T_{ref} (K)	t_{ref} (s)	d_{ref} (μm)
1682.97	0.06995	12.95	0.09356	-0.5	610	1	25
n	Q'	k	f_m			Error-average	
-61.114	7032	0.04628	0.6366			0.00112	

7.2.2 Validation on Inconel 718

The reference temperature for Inconel 718 is chosen as 560K, the reference cyclic time is defined as 1s, and the reference grain size is selected as 30μm. In addition, according to the relation between fatigue capacity and grain size in the pure-fatigue condition, the magnitude of m is given as -0.5. The stress-moderating factor f_m is suggested as 0.6366 for the sinusoidal wave.

On the one hand, based on the creep-rupture data [94] obtained from the literature, the Sherby-Dorn parameter (Eq.7.21) is extracted by plotting *1/(T-T_{ref}) vs. logt* (Fig.7.4):

$$P_{SD}(\sigma) = \log\left[te^{-Q/[R(T-T_{ref})]}\right] = -\frac{Q\log e}{R}\cdot\frac{1}{T-T_{ref}} + \log t \tag{7.35}$$

The slope (2974.4) of *1/(T-T_{ref}) vs. logt* curves shown in Fig.7.4 gives Q, then the magnitude of Q' may be obtained through Eq.7.23:

$$Q' = Q/R = 2974.4/\log e = 6849 \tag{7.36}$$

On the other hand, the Sherby-Dorn parameter also can be presented as a function of stress:

$$P_{SD}(\sigma) = -3.6069\log\sigma + 6.645 \tag{7.37}$$

According to Eq.7.24, the magnitude of a is given as 3.6069.

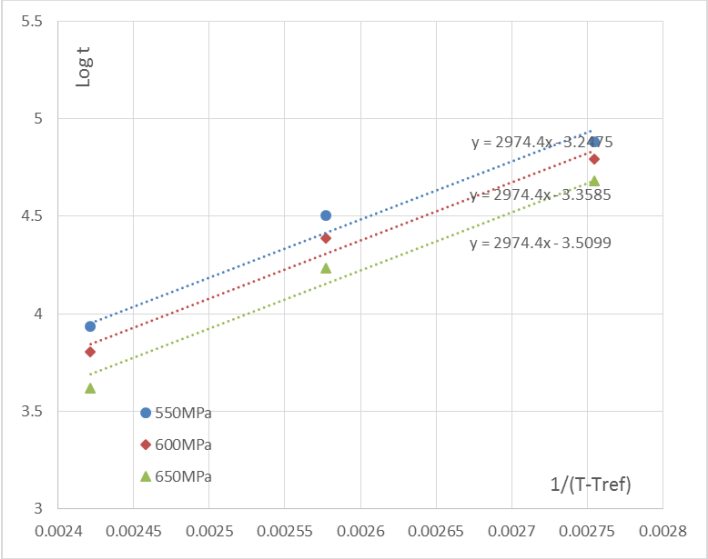

Figure 7.4 Creep-rupture characteristic for Inconel 718

The creep-fatigue coefficients [95, 96] obtained from the literature are tabulated in Table 7.4, and the strain-stress relation is calculated through Eq.7.38 and Eq.7.39. Minimizing the difference between the predicted creep-fatigue life ($N_{pre,ij}$) and the experimental creep-fatigue life ($N_{exp,ij}$) yields $\sigma_0 = 2321.593$, $b_0 = 0.0876$, $A = 0.694$, $k = 0.00364$ and $n = -56.929$, and returns an average error (δ_a) (Eq.7.29) of 0.003217.

Table 7.4 Creep-fatigue data for Inconel 718

Temperature (K)	Frequency (Hz)	Cyclic time (s)	Grain size (μm)	Creep-fatigue Coefficients $\sigma = \sigma_f' N_f^{-b}$	
				σ_f'	b
823	3	20	30	1442.6	0.084
873	3	20	30	1370.5	0.085
923	3	20	30	122.3	0.077
700	20	3	11	2998.9	0.067
811	20	3	11	2325.1	0.050

$$K(T,t,d) = 1.7474 \times (10575.28663 - 7.64305T + 168.69826t)d^{-0.782457} \quad (7.38)$$

$$n(T,t,d) = 0.00593 \times (35.98325 - 0.03943T + 72.47165\log t)d^{-0.41046} \quad (7.39)$$

The prediction ratio (N_{pre}/N_{exp}) under multiple temperatures, cyclic times and grain sizes are plotted in Fig.7.5, where all data points fall between the upper bound (+25%) and the lower bound (-25%). This implies that the stress-based unified creep-fatigue equation provides a high

quality for the fatigue-life prediction, specifically, a relatively high correlation between predicted and experimental creep-fatigue life.

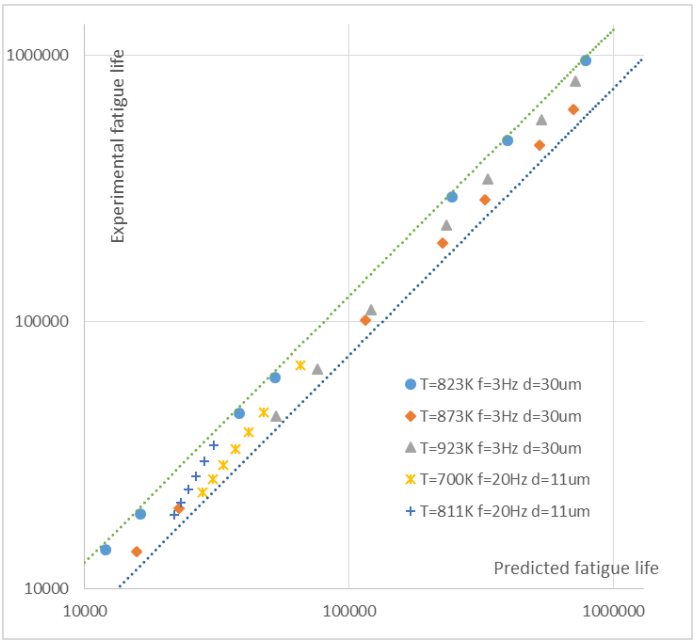

Figure 7.5 Prediction ratio for Inconel 718

With the results obtained above, the experimental creep-fatigue data (σ-N_{exp}) (shadow area in Fig.7.6) are transformed to the reference condition (the pure-fatigue condition) (σ_{ref}-N_{exp}), by using Eq.7.31. Fig.7.6 shows that the transformed data are collected into a single power-law curve of $\sigma_{ref} = 2267.1N^{-0.086}$ with a good quality of fit as R^2=0.9897. The coefficient and exponent of this trendline, σ_0=2267.1 and b_0=0.086, are close to the magnitudes of σ_0 and b_0 obtained through numerical optimization. This suggests good consistency with the reference condition, and implies that function $C(T, t, \sigma, d)$ represents a good numerical description of the creep characteristics.

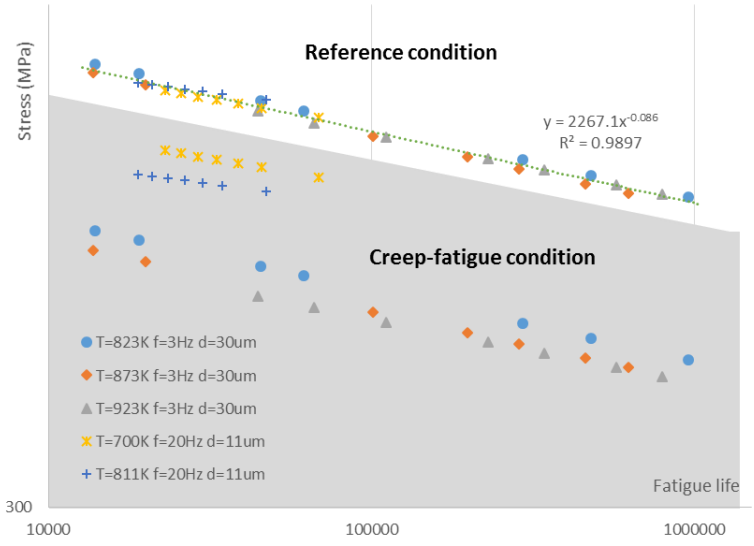

Figure 7.6 The transformed data (σ_{ref}-N_{exp}) for Inconel 718

Consequently, the coefficients of the unified creep-fatigue equation for Inconel 718 is collected in Table 7.5:

Table 7.5 The coefficients of the unified formulation for Inconel 718

σ_0 (MPa)	b_0	a	A	m	T_{ref} (K)	t_{ref} (s)	d_{ref} (μm)
2321.593	0.0876	3.6069	0.694	-0.5	560	1	30
n	Q'	k	f_m			Error-average	
-56.929	6849	0.00364	0.6366			0.003217	

Overall, the validation on the materials of GP91 casting steel and Inconel 718 demonstrates that the stress-based unified creep-fatigue equation has the ability to cover multiple situations and multiple materials. In addition, the formulation of the creep moderating function $C(\sigma, T, t_c, d)$ is verified. Note that because of the limited quality and quantity of the empirical data which could be extracted from the existing literature, the unified formulation may not be completely validated. In this case, we believe that this new model would be further validated, even improved, if more empirical data could be involved.

7.3 Discussion

The stress-based unified creep-fatigue equation was initially developed for the high-cycle regime under stress-controlled loading. In this case, by combining with the strain-based model which is applied to the low-cycle regime, these two creep-fatigue models construct a whole map for creep-fatigue behaviour. Although the stress-based formulation may not be completely validated due to limited empirical data, some significant ideas are still proposed which will be discussed in this section.

7.3.1 Introduction of compatibility

Generally, compatibility [107] presents the relationships between strain, stress and fatigue life, and gives the opportunity to link the Basquin equation (Eq.7.40) with the Coffin-Manson equation (Eq.7.41) through the Ramberg-Osgood equation (Eq.7.42):

$$\frac{\Delta\sigma}{2} = \sigma_f'(2N_f)^b \tag{7.40}$$

$$\frac{\Delta\varepsilon_p}{2} = \varepsilon_f'(2N_f)^c \tag{7.41}$$

$$\frac{\Delta\sigma}{2} = K\left(\frac{\Delta\varepsilon_p}{2}\right)^n \tag{7.42}$$

where $\Delta\sigma$ is the stress amplitude, σ_f' is the fatigue strength coefficient, b is the fatigue strength exponent, $\Delta\varepsilon_p$ is the plastic strain amplitude, ε_f' is the fatigue ductility coefficient and c is the fatigue ductility exponent, N_f is the number of cycles, K is the strain hardening coefficient and n is the strain hardening exponent. The relationships between the coefficients shown in these three conventional models are suggested as:

$$K = \frac{\sigma_f'}{\varepsilon_f'^n} \tag{7.43}$$

$$n = \frac{b}{c} \tag{7.44}$$

Eq.7.43 and Eq.7.44 are named as the compatibility equations.

As mentioned in section 7.1.3, the compatibility is applied to obtain the coefficients of the stress-based creep-fatigue formulation (σ_0 and b_0), which significantly provides a better description for the reference condition. Taking the material of GP91 casting steel as an example, the results obtained through the methods with and without employing the compatibility are collected in Table 7.6.

Table 7.6 Results obtained from method without and with applying the compatibility

Methods	Strain-based creep-fatigue equation		Stress-based creep-fatigue equation		Average error for stress-based model
	C_0	β_0	σ_0	b_0	
Experimental results	0.934	-0.644	1679.4	-0.0670	---
Method without compatibility	0.953	-0.669	2322.45	-0.0607	0.0000156
Method with compatibility	0.953	-0.669	1682.97	-0.0699	0.00112

The results shown in Table 7.6 suggest that the full fatigue capacity described by the stress-based model is enlarged by using the method without the compatibility, which may result from an artefact of the numerical optimization. Specifically, the method of numerical optimization aims to minimize the error, and thus the solution is only obtained from a numerical perspective that is disconnected from the physical situation. Although the method without the compatibility gives a smaller error compared to the method with the compatibility, the non-compatibility method ignores the internal relationship between the stress-life relation and the strain-life relation. This is a typical weakness of this method because a key constraint is removed during the numerical operation. However, the compatibility-based method results in a more reliable solution by involving a physically based constraint that cannot be ignored. Even though the average error increases compared to the situation with the non-compatibility method, the

validation shown in section 7.2.1 indicates that the accuracy of the fatigue-life prediction is still acceptable. In addition, the introduction of compatibility gives a better description of the reference condition. This is demonstrated by the evidence (see Table 7.6) that the pure-fatigue-related coefficients in the stress-based model (σ_0 and b_0) obtained from experiments are closer to the results given by the compatibility-based method than the results given by the non-compatibility method. Furthermore, Table 7.6 also indicates that the numerical optimization does not have a significant influence on the accuracy of presenting the reference condition for the strain-based model. This may result from the narrow potential range of C_0. However, this influence for the stress-based model becomes more significant because the possible solution for σ_0 covers a wide range, and a small fluctuation of any coefficient in the stress-based model could lead to a large change for σ_0.

The compatibility can be represented graphically as a set of relationships between the stress-life relation, the strain-life relation and the stress-strain relation (Fig.7.7), where the coefficients arising from the numerical optimization for GP91 casting steel are applied. Fig.7.7 presents a linear relation between logs of stress, strain and fatigue life in a 3-D space at the reference condition, and this straight curve can be projected onto the stress-life plane, the strain-life plane and the stress-strain plane. These projects represent the relations formulated by the Basquin equation, the Coffin-Manson equation and the Ramberg-Osgood equation respectively. This figure demonstrates that the compatibility is well accommodated between the strain-based and the stress-based creep-fatigue equation.

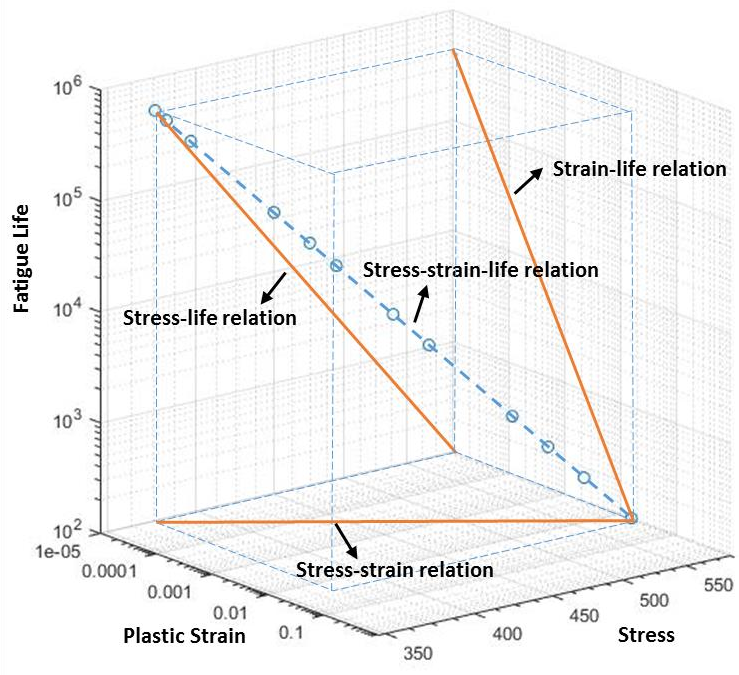

Figure 7.7 Stress-strain-life relation in a 3-D space

7.3.2 Advantages of the stress-based approach

The stress-based unified creep-fatigue equation was developed for engineering application, and thus this model should have the ability to be applied in multiple situations for multiple materials

and cover the full range of conditions from pure fatigue to pure creep. Comparing with other existing stress-based models shown in Chapter 2, the new stress-based model proposed in the present work presents significant advantages in these two areas (the unified and integrated characteristics). Fundamentally, these advantages result from the potential ability of presenting the underlying physical mechanisms of fatigue and creep, and this will be discussed in Chapter 10.

The economy is another requirement for a numerical formulation in engineering application. This has been discussed for the strain-based model in Chapter 6, where this new model shows an economical method for fatigue-life prediction since minimum empirical effort is involved. However, the economy is not discussed for the stress-based model. This is because the high-cycle fatigue regime described by the stress-based method firstly is not the main regime of creep-fatigue failure in service. In addition, although the stress-life relation in the creep-fatigue condition was explored by numbers of experiments, the numerical representation of this relation was not frequently proposed. The existing stress-based models cannot accommodate relevant variables, thus the accuracy of fatigue-life prediction in multiple situations for multiple materials is remarkably poorer than the new stress-based model. In this case, the most important indicator (accuracy) is lost from these existing models, and thus there is no need to further compare economy with the new model. Furthermore, the new stress-based equation has three independent coefficients (the number of independent coefficients is reduced from five to three by introducing the compatibility) which are obtained through numerical optimization based on the creep-fatigue test. In this case, we could believe that the consumption for obtaining the coefficients of the stress-based unified creep-fatigue equation is reduced to a significantly low level.

Overall, the critique of the stress-based model mainly focuses on the areas of unifying and integration. The discussion is shown as follows:

(1) Unified characteristic

As shown in Chapter 2, the existing stress-based creep-fatigue models, such as Kohout's equation and Mivehchi's equation, only accommodate the temperature dependence and were derived from the empirical data of one specific material through curve fitting. Therefore, it is believed that the existing models cannot provide an effective fatigue-life prediction for multiple materials in multiple situations (including temperature, cyclic time and grain size).

For example, when Kohout's equation:

$$\frac{\Delta\sigma}{2} = a\left(2N_f\right)^{-b}T^c \tag{7.45}$$

is applied to describe creep-fatigue behaviour on the material of GP91 casting steel, a poor situation of fatigue-life prediction is presented. Specifically, based on the empirical data of the creep fatigue (Table 7.2), the numerical optimization yields $a = 2.434$, $b = 2.972$ and $c = 6.768$, and the average error is 0.0699. However, the average error by applying the stress-based unified formulation was given as 0.00112 which is remarkably smaller than the error obtained by using Kohout's equation. In addition, this poor ability to predict fatigue life by using

Kohout's equation is also demonstrated by the prediction ratio (N_{pre}/N_{exp}), where most of the data points are out of the acceptable range of the prediction ratio (0.75-1.25). This is illustrated in Fig.7.8 which implies a poor correlation between the predicted and experimental creep-fatigue life.

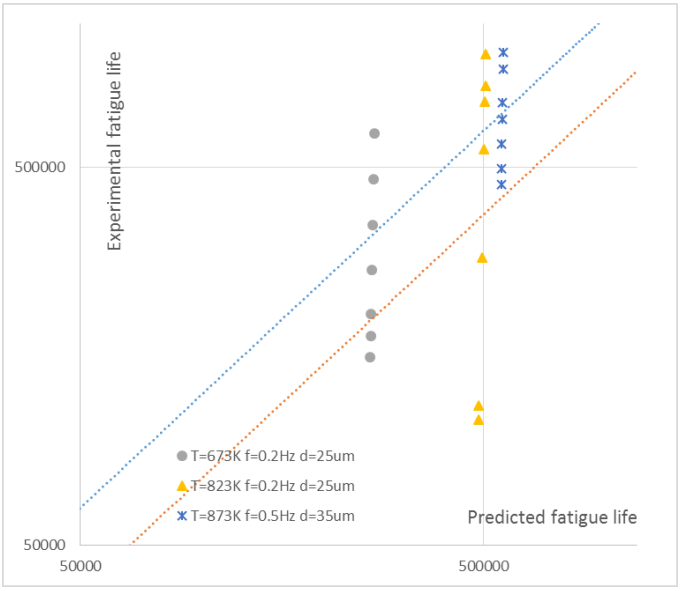

Figure 7.8 Prediction ratio for GP91 casting steel using Kohout's equation

However, this limitation is improved by the stress-based unified creep-fatigue equation, which has been verified in section 7.2. To be specific, the validation on the materials of GP91 casting steel and Inconel 718 presents small average errors, and the prediction ratios by using the new formulation are all within the acceptable range (0.75-1.25). In this case, the stress-based unified creep-fatigue equation presents the ability to be applied in multiple situations for multiple materials. We also realize that limited empirical data may not completely verify the unified characteristic for the unified stress-based model (further validation may be conducted in future research), but the results shown by the present work still indicate that this new stress-based model is more superior to other existing models for this characteristic.

(2) Integrated characteristic

The existing stress-based creep-fatigue formulations shown in Chapter 2, including Kohout's equation and Mivehchi's equation, have the opportunity to present the pure-fatigue condition. This is because both of them can be restored to the Basquin equation by letting the temperature component (T^c) equal 1 for Kohout's equation and defining the temperature as room temperature (a reference temperature where creep is activated) for Mivehchi's equation. However, Kohout's equation and Mivehchi's equation may not well represent creep-fatigue behaviour since only temperature dependence is included, and also it cannot be transformed to the pure-creep condition because letting $\Delta\sigma = 0$ cannot give any numerical formulation for creep mechanism. In this case, the integrated characteristic is not entirely presented by Kohout's equation and Mivehchi's equation.

This limitation is somewhat improved by the stress-based unified creep-fatigue equation, where the ability to cover the full range of conditions from the pure-fatigue condition to the pure-creep condition is presented.

Specifically, at the pure-fatigue condition, the temperature tends to the reference temperature, $T \to T_{ref}$, cyclic time is defined as the reference cyclic time, $t = t_{ref}$, and the grain size is given as the reference grain size, $d = d_{ref}$. This suggests that $e^{-Q'/(T-T_{ref})} \to 0$, and cyclic-time and grain-size components equal 1. Then, the stress-based creep-fatigue equation is restored to the Basquin equation, where the pure-fatigue behaviour is presented. The good consistency with the reference condition is demonstrated in section 7.3.1, where the magnitudes of σ_0 and b_0 (pure-fatigue-related coefficients, which are obtained through numerical optimization based on empirical data of creep fatigue) are close to the results obtained from the pure-fatigue test.

In addition, at the pure-creep condition, the fatigue capacity is totally consumed by the creep effect. This results in zero applied stress for fatigue ($\sigma = 0$). Then, the stress-based creep-fatigue equation is converted to Eq.7.46:

$$e^{-\frac{Q'}{T-T_{ref}}} \cdot \left(t/t_{ref}\right) = f_m^{-a} \cdot \sigma^{-a} \cdot \left(\frac{1}{A}\right)^{1/k} \left(d/d_{ref}\right)^{-n} \tag{7.46}$$

Doing the logarithmic operation gives:

$$\log\left[e^{-\frac{Q'}{T-T_{ref}}} \cdot \left(t/t_{ref}\right)\right] = -a \log\sigma + \log\left[\left(\frac{1}{A}\right)^{1/k} \left(d/d_{ref}\right)^{-n} f_m^{-a}\right] \tag{7.47}$$

Eq.7.47 indicates a time-temperature relation and has the same formulation as the Sherby-Dorn parameter. As shown in section 7.1.3, the intensity of the stress effect on creep damage is directly extracted from the creep-rupture test. This is presented in the Sherby-Dorn parameter by the coefficient of *a*. The last term of Eq.7.47 is related to the grain size, and its coefficients do not strictly follow the creep-rate equation (Eq.7.1), and thus this term cannot precisely present the creep behaviour. This is an inevitable problem caused by the bottom-up approach and the method of obtaining the coefficients, where the formulation is reorganized and simplified, and the creep characteristic is extracted from one given grain size. However, the connection between the creep-fatigue condition and the pure-creep condition could be achieved by letting $\log\left[\left(\frac{1}{A}\right)^{1/k} \left(d/d_{ref}\right)^{-n} f_m^{-a}\right] = 23.307$ (for GP91 casting steel), and a normalized grain size, 20μm, is then suggested. This normalized grain size relates to the material condition for performing the creep-rupture test, and thus varies with the change of heat treatment. This implies that the transformation of the stress-based creep-fatigue equation can only show the pure-creep condition where the creep effect is extracted. In theory, if the creep-rupture tests could be conducted with multiple materials, a better suggestion of the magnitude of *n* and a better creep description of the last term in Eq.7.47 could be given. The discussion shown above presents an opportunity to develop a grain-size-modified Sherby-Dorn parameter, and this modified parameter may take the same or similar form as Eq.7.48:

$$P_{SD} = td^n e^{-Q/RT} \tag{7.48}$$

Particularly, this grain-size-modified Sherby-Dorn parameter presents a good consistent with the creep-rate equation for the steady stage of creep.

Furthermore, the applicability of the stress-based unified equation at the creep-fatigue condition has been validated in section 7.2, where the creep function $C(T, t_c, \sigma, d)$ is between 0 and 1, and the creep-fatigue data can collapse into one power-law curve by transforming them into the reference condition. In addition, the high quality of the fatigue-life prediction is also demonstrated by the prediction ratio, where the differences between the predicted fatigue life and the experimental fatigue life in multiple situations lie within an acceptable zone.

Overall, comparing with other existing stress-based creep-fatigue models, the unified equation provides a more effective method of fatigue-life prediction for engineering application since it can be applied in multiple situations for multiple materials and can cover the full range of conditions from pure fatigue to pure creep.

7.4 Summary

The creep-fatigue damage in the low-cycle fatigue regime has been described by a strain-based creep-fatigue equation by integrating creep effect into fatigue damage. There is a need to develop a creep-fatigue equation which describes the stress-controlled creep-fatigue behaviour in the high-cycle fatigue regime. However, the importance of the stress-based model is secondary to the strain-based model because creep-fatigue failure frequently occurs in the low-cycle fatigue regime in service. Combining these two models gives a whole map from the low-cycle regime to the high-cycle regime.

By superposing a fatigue effect with a creep effect, the stress-based unified creep-fatigue equation was developed:

$$\sigma = \sigma_0 \cdot B(d) \cdot C(T, t_c, \sigma, d) \cdot N_f^{-b_0} \tag{7.49}$$

with

$$\begin{gathered} B(d) = \left(d/d_{ref}\right)^m \\ C(T,t,\sigma,d) = 1 - A \cdot \left[\left(d/d_{ref}\right)^n \cdot f_m^a \cdot \sigma^a \cdot e^{-\frac{Q'}{T-T_{ref}}} \cdot \left(t_c/t_{ref}\right)\right]^k \\ T - T_{ref} = \begin{cases} T - T_{ref} & for \;\; T > T_{ref} \\ \rightarrow 0 & for \;\; T \le T_{ref} \end{cases} \\ t_c/t_{ref} = \begin{cases} t_c/t_{ref} & for \;\; t_c > t_{ref} \; and \; T > T_{ref} \\ 1 & for \;\; t_c \le t_{ref} \; or \; T \le T_{ref} \end{cases} \end{gathered} \tag{7.50}$$

where the coefficients of Q' and a are extracted from the creep-rupture tests, and the constants of A, n and k are obtained from the creep-fatigue tests, and the pure-fatigue related coefficients of σ_0 and b_0 are derived by introducing the idea of compatibility.

Then, this stress-based creep-fatigue equation was validated on the materials of GP91 casting steel and Inconel 718, where accepted prediction ratios were presented and good transformation from the creep-fatigue condition to the reference condition (the pure-fatigue condition) was shown. Significantly, the introduction of compatibility gives a better description of the pure-fatigue condition.

In this unified model, the relationships between different variables were extracted from the conventional fatigue and creep models, which implies that these relationships are potential to be linked to the underlying physical mechanisms. This is the fundamental principle for this new stress-based model to be superior to other existing stress-based models in the areas of the unified and integrated characteristics.

Chapter 8

8. Attempt to adapt the unified creep-fatigue equations to situations with non-zero mean stress

This results chapter extends the formulations presented in Chapters 5 and 7 into the situation with a non-zero mean-stress effect. This extension is based on an assumption that the stress-strain relations under the situations with/without a mean-stress effect share the same characteristic, but this assumption may be ineffective.

The strain-based (proposed in Chapters 4 and 5) and stress-based (proposed in Chapter 7) unified creep-fatigue equations can only be applied in the condition with zero mean stress. However, for some practical engineering situations, the mean stress is non-zero. In this case, the mean-stress effect should be considered, and the modified creep-fatigue model with mean-stress effect needs to be proposed. The transformation from the zero-mean-stress situation to the non-zero-mean-stress situation is based on Morrow's mean stress equation and the concept of compatibility (an existing well-accepted method). This chapter presents the initial attempt of the unified creep-fatigue equations with a mean-stress effect, which is an extension of our present work and is a conceptual proposal. We realize that the creep-fatigue models with a mean-stress effect may not be effective for the fatigue-life prediction since the compatibility may need to be modified under the situation of non-zero mean stress, which provides an opportunity for future research.

8.1 Existing method for transformation

8.1.1 Fatigue models with mean-stress effect

Generally, the conventional pure-fatigue models, such as the Basquin equation and the Coffin-Manson equation, can only be applied in the situation with zero mean stress. However, for some engineering situations where the mean stress is non-zero, the mean-stress effect should be considered. In order to describe the fatigue behaviour under the condition of non-zero mean stress, the concept of equivalent stress was introduced and then formulated by different forms, such as the Soderberg relation (Eq.8.1) [20], the Morrow relation (Eq.8.2) [21], the Goodman relation (Eq.8.3) [23] and the Gerber relation (Eq.8.4) [24].

$$\sigma_{ar} = \frac{\sigma_a}{1 - \frac{\sigma_m}{\sigma_y}} \tag{8.1}$$

$$\sigma_{ar} = \frac{\sigma_a}{1 - \frac{\sigma_m}{\sigma_f'}} \tag{8.2}$$

$$\sigma_{ar} = \frac{\sigma_a}{1 - \frac{\sigma_m}{\sigma_u}} \tag{8.3}$$

$$\sigma_{ar} = \frac{\sigma_a}{1 - \left(\frac{\sigma_m}{\sigma_u}\right)^2} \tag{8.4}$$

where σ_{ar} is the equivalent stress amplitude, σ_a is the stress amplitude, σ_m is the mean stress, σ_y is the yield stress, and σ_u is the ultimate stress, σ_f' is the fatigue strength coefficient.

The transformation [8] between two stress conditions (zero mean-stress and non-zero mean-stress situations) started from the stress-life relation, the Basquin equation. This starting point provides an opportunity to involve the existing mean stress models shown by Eq.8.1-8.4. In this case, Morrow's equation (Eq.8.2), which shares the same coefficients (σ_f') with the Basquin equation, is selected. Then, the stress amplitude in the Basquin equation is replaced by Morrow's equivalent stress amplitude. By this means, the mean-stress effect is introduced, and the modified Basquin equation is given as:

$$\sigma_a = \left(\sigma_f' - \sigma_m\right)\left(2N_f\right)^b = \sigma_f'\left[\left(1 - \frac{\sigma_m}{\sigma_f'}\right)^{1/b}\left(2N_f\right)\right]^b \tag{8.5}$$

Comparing Eq.8.5 with the Basquin equation indicates that the fatigue life (N_f) in the Basquin equation is replaced by the stress-based equivalent fatigue life ($N_{f-\sigma}{}^*$):

$$N_{f-\sigma}{}^* = \left(1 - \frac{\sigma_m}{\sigma_f'}\right)^{1/b} N_f \tag{8.6}$$

This modification for fatigue life could also be applied to the strain-life relation, the Coffin-Manson equation. Then, the modified Coffin-Manson equation is organized as Eq.8.7 for the situation with non-zero mean stress.

$$\varepsilon_p = \varepsilon_f'\left(2N_f{}^*\right)^c = \varepsilon_f'\left[\left(1-\frac{\sigma_m}{\sigma_f'}\right)^{1/b}\left(2N_f\right)\right]^c = \varepsilon_f'\left(1-\frac{\sigma_m}{\sigma_f'}\right)^{c/b}\left(2N_f\right)^c \tag{8.7}$$

Eq.8.6 and Eq.8.7 are based on the controlled-stress situation, but for the strain-controlled situation, the fatigue equation with mean-stress effect should be derived by involving the parameter of mean strain. In this case, Morrow's mean stress equation (Eq.8.2) could be analogized to the mean plastic strain equation (equivalent plastic strain amplitude):

$$\varepsilon_{ar} = \frac{\varepsilon_a}{1-\frac{\varepsilon_{pm}}{\varepsilon_f'}} \tag{8.8}$$

where ε_a is the plastic strain amplitude in the zero-mean-stress situation, ε_f' is the fatigue ductility coefficient, ε_{pm} is the mean plastic strain and ε_{ar} is the equivalent plastic strain amplitude. Then, introducing the equivalent plastic strain into the Coffin-Manson equation gives the modified formulation with mean-stress effect:

$$\varepsilon_p = \varepsilon_f'\left(1-\frac{\varepsilon_{pm}}{\varepsilon_f'}\right)\left(2N_f\right)^c \tag{8.9}$$

This equation gives the strain-based equivalent life ($N_{f-\varepsilon}{}^*$):

$$N_{f-\varepsilon}{}^* = \left(1-\frac{\varepsilon_{pm}}{\varepsilon_f'}\right)^{1/c} N_f \tag{8.10}$$

Then, this equivalent life is introduced into the Basquin equation, and the modified formulation with mean-stress effect is shown as:

$$\sigma_a = \frac{\sigma_f'}{E}\left(1-\frac{\varepsilon_{pm}}{\varepsilon_f'}\right)^{b/c}\left(2N_f\right)^b \tag{8.11}$$

8.1.2 Compatibility in the non-mean-stress fatigue models

As mentioned in Chapter 7, the compatibility shows the internal relationship between the stress-life relation and the strain-life relation, and the bridge between them is built through the stress-strain relation. In the situation with zero mean stress, the compatibility is numerically represented as:

$$n' = \frac{b}{c} \tag{8.12}$$

$$K' = \frac{\sigma_f'}{\left(\varepsilon_f'\right)^{n'}} \tag{8.13}$$

where K' and n' are the strain hardening coefficient and exponent for the situation with zero mean stress under cyclic loading respectively. These two equations are named as compatibility equations.

The compatibility is also presented in the non-zero-mean-stress condition. Specifically, the stress amplitude can normally be related to the strain amplitude by the formulation of:

$$\varepsilon_p = \left(\frac{\sigma_a}{K''}\right)^{1/n''} \tag{8.14}$$

where K'' and n'' are the strain hardening coefficient and exponent for the situation with non-zero mean stress respectively. Then, substituting the stress amplitude and strain amplitude in Eq.8.14 with Eq.8.5 and Eq.8.7 respectively gives:

$$\sigma_f'\left(1-\frac{\sigma_m}{\sigma_f'}\right)(2N_f)^b = K''{\varepsilon_f'}^{n''}\left(1-\frac{\sigma_m}{\sigma_f'}\right)^{cn''/b}(2N_f)^{cn''} \tag{8.15}$$

Comparing two sides of Eq.8.15 results in Eq.8.16 and Eq.8.17:

$$b = cn'' \tag{8.16}$$

$$\sigma_f'\left(1-\frac{\sigma_m}{\sigma_f'}\right) = K''{\varepsilon_f'}^{n''}\left(1-\frac{\sigma_m}{\sigma_f'}\right)^{cn''/b} \tag{8.17}$$

Finally, reorganizing Eq.8.16 and Eq.8.17 gives the following equations:

$$n'' = \frac{b}{c} \tag{8.18}$$

$$K'' = \frac{\sigma_f'}{\left(\varepsilon_f'\right)^{n''}} \tag{8.19}$$

Eq.8.18 and Eq.8.19 are named as the compatibility equations for the situation with non-zero mean stress. Obviously, these two equations are the same as the compatibility equations for the zero-mean-stress condition (Eq.8.12 and Eq.8.13). This consistency implies that the stress-strain relation is independent of the mean-stress effect. In addition, this consistency also indicates a fundamental assumption for this well-accepted method (shown in section 8.1.1) of transforming between these two stress conditions, that is:

The stress-strain relations under situations with zero and non-zero mean stress present the same characteristic.

The same behaviour of compatibility is also shown at the strain-controlled situation, where the assumption presented above is applied.

8.2 Adapting the unified creep-fatigue equations to the situation with non-zero mean stress

8.2.1 Unified creep-fatigue equations with mean-stress effect

The same approach which is shown in section 8.1.1 is accepted to develop the unified creep-fatigue equation for the non-zero-mean-stress situation. Firstly, the transformation started from the stress-based unified creep-fatigue equation, and Morrow's mean stress equation (Eq.8.2) is integrated. By this means, replacing the stress amplitude in the stress-based unified creep-fatigue equation by the equivalent stress gives Eq.8.20:

$$\frac{\sigma}{1-\frac{\sigma_m}{\sigma_0}} = \sigma_0 \cdot B(d) \cdot C(T,t,\sigma,d) \cdot N_f^{-b_0} \tag{8.20}$$

Then, rearranging the form of Eq.8.20 gives the stress-based non-zero-mean-stress unified creep-fatigue equation:

$$\sigma = \sigma_0 \cdot \left(1-\frac{\sigma_m}{\sigma_0}\right) \cdot B(d) \cdot C(T,t,\sigma,d) \cdot N_f^{-b_0} = \sigma_0 \cdot B(d) \cdot C(T,t,\sigma,d) \cdot \left[\left(1-\frac{\sigma_m}{\sigma_0}\right)^{-1/b_0} \cdot N_f\right]^{-b_0} \tag{8.21}$$

Comparing this equation with the stress-based unified creep-fatigue equation gives the equivalent fatigue life (Eq.8.22), where the mean-stress effect is introduced:

$$N_f{}' = \left(1-\frac{\sigma_m}{\sigma_0}\right)^{-1/b_0} \cdot N_f \tag{8.22}$$

This modification for fatigue life also could be applied to the strain-based unified creep-fatigue equation. Then, this results in its modified form for the situation of non-zero mean stress:

$$\varepsilon_p = C_0 c(\sigma,T,t_c,d)\left[\left(1-\frac{\sigma_m}{\sigma_0}\right)^{-1/b_0} \cdot N_f\right]^{-\beta_0} = C_0\left(1-\frac{\sigma_m}{\sigma_0}\right)^{\frac{\beta_0}{b_0}} c(\sigma,T,t_c,d){N_f}^{-\beta_0} \tag{8.23}$$

For the situation with the strain-controlled situation, the same approach is applied, and then the modified creep-fatigue equations in terms of mean plastic strain are given as:

$$\varepsilon_p = C_0\left(1-\frac{\varepsilon_{pm}}{C_0}\right) c(\sigma,T,t_c,d){N_f}^{-\beta_0} \tag{8.24}$$

$$\sigma = \sigma_0 \cdot \left(1-\frac{\varepsilon_{pm}}{C_0}\right)^{\frac{b_0}{\beta_0}} \cdot B(d) \cdot C(T,t,\sigma,d) \cdot N_f^{-b_0} \tag{8.25}$$

8.2.2 Discussion of the compatibility

The discussion shown in Chapter 7 indicates that compatibility exists between the stress-based and strain-based unified creep-fatigue equations (the zero mean-stress situation), and the compatibility equations are given as:

$$K' = \frac{\sigma_0}{(C_0)^{n'}} \tag{8.26}$$

$$n' = \frac{b_0}{\beta_0} \tag{8.27}$$

The same compatibility equations are also presented for the situation with non-zero mean stress. Specifically, at the pure-fatigue condition, the coefficients of Eq.8.21 could be related to the coefficients of Eq.8.23 through the stress-strain relation:

$$\sigma_0 \cdot \left(1 - \frac{\sigma_m}{\sigma_0}\right) \cdot N_f^{-b_0} = K'' \left[C_0 \left(1 - \frac{\sigma_m}{\sigma_0}\right)^{\frac{\beta_0}{b_0}} N_f{}^{-\beta_0} \right]^{n''} \tag{8.28}$$

Comparing the two sides of Eq.8.28 gives Eq.8.29 and Eq.8.30:

$$\sigma_0 \cdot \left(1 - \frac{\sigma_m}{\sigma_0}\right) = K'' \left[C_0 \left(1 - \frac{\sigma_m}{\sigma_0}\right)^{\frac{\beta_0}{b_0}} \right]^{n''} \tag{8.29}$$

$$b_0 = n''\beta_0 \tag{8.30}$$

Rearranging Eq.8.29 and Eq.8.30 results in compatibility equations for the situation with non-zero mean stress condition:

$$K'' = \frac{\sigma_0}{(C_0)^{n''}} \tag{8.31}$$

$$n'' = \frac{b_0}{\beta_0} \tag{8.32}$$

It is clear that the compatibility equations shown above are the same as the equations in the situation with zero mean stress (Eq.8.26 and Eq.8.27). This implies that, in the creep-fatigue condition, the stress-strain relation is independent of the mean-stress effect, which is consistent with the phenomenon presented by the conventional fatigue models (discussed in section 8.1.2). In addition, the assumption shown in section 8.1.2 is also applied in the creep-fatigue condition to perform the transformation between two stress conditions.

The same behaviour of compatibility is also shown in the strain-controlled situation, where the same assumption is applied to the stress-controlled situation.

8.3 Critique of the unified creep-fatigue equations with mean-stress effect

Based on the statement shown in section 8.1 and section 8.2, the fatigue models at the zero-mean-stress condition and the non-zero-mean-stress condition are collected in Table 8.1.

Table 8.1 Fatigue models with/without mean-stress effect

Names	Zero-mean-stress condition	Non-zero-mean-stress condition
	The conventional fatigue models	
The stress-life relation	$\frac{\Delta\sigma}{2} = \sigma_f'(2N_f)^b$	$\frac{\Delta\sigma}{2} = \sigma_f'\left(1-\frac{\sigma_m}{\sigma_f'}\right)(2N_f)^b$ $\frac{\Delta\sigma}{2} = \frac{\sigma_f'}{E}\left(1-\frac{\varepsilon_{pm}}{\varepsilon_f'}\right)^{b/c}(2N_f)^b$
The strain-life relation	$\frac{\Delta\varepsilon_p}{2} = \varepsilon_f'(2N_f)^c$	$\frac{\Delta\varepsilon_p}{2} = \varepsilon_f'\left(1-\frac{\sigma_m}{\sigma_f'}\right)^{c/b}(2N_f)^c$ $\frac{\Delta\varepsilon_p}{2} = \varepsilon_f'\left(1-\frac{\varepsilon_{pm}}{\varepsilon_f'}\right)(2N_f)^c$
The stress-strain relation	$\Delta\varepsilon_p = \left(\frac{\Delta\sigma}{K'}\right)^{1/n'}$	$\Delta\varepsilon_p = \left(\frac{\Delta\sigma}{K''}\right)^{1/n''}$
Compatibility equations	$n' = n'' = \frac{b}{c}\ ;\ K' = K'' = \frac{\sigma_f'}{(\varepsilon_f')^{b/c}}$	
	The unified creep-fatigue models	
The stress-based equation	$\sigma = \sigma_0 \cdot B(d) \cdot C(T,t,\sigma,d) \cdot N_f^{-b_0}$	$\sigma = \sigma_0 \cdot \left(1-\frac{\sigma_m}{\sigma_0}\right) \cdot B(d) \cdot C(T,t,\sigma,d) \cdot N_f^{-b_0}$ $\sigma = \sigma_0 \cdot \left(1-\frac{\varepsilon_{pm}}{C_0}\right)^{\frac{b_0}{\beta_0}} \cdot B(d) \cdot C(T,t,\sigma,d) \cdot N_f^{-b_0}$
The strain-based equation	$\varepsilon_p = C_0 c(\sigma,T,t_c,d) N_f^{-\beta_0}$	$\varepsilon_p = C_0\left(1-\frac{\sigma_m}{\sigma_0}\right)^{\frac{\beta_0}{b_0}} c(\sigma,T,t_c,d) N_f^{-\beta_0}$ $\varepsilon_p = C_0\left(1-\frac{\varepsilon_{pm}}{C_0}\right) c(\sigma,T,t_c,d) N_f^{-\beta_0}$
The stress-strain relation	$\varepsilon_p = \left(\frac{\sigma}{K'}\right)^{1/n'}$	$\varepsilon_p = \left(\frac{\sigma}{K''}\right)^{1/n''}$
Compatibility equations	$n' = n'' = \frac{b_0}{\beta_0};\ K' = K'' = \frac{\sigma_0}{(C_0)^{b_0/\beta_0}}$	

Significantly, the compatibility equations imply that the transformation between two stress conditions is based on an assumption (mentioned in section 8.1.2), that is:

The stress-strain relations under situations with zero and non-zero mean stress present the same characteristic.

Although this assumption has been well accepted by previous research [8], it may not be correct.

Generally, non-zero mean stress leads to the tips of stable hysteresis loops of cyclic stress-strain curves deviating from the original curve (the curve in the situation of zero mean stress). This suggests two different behaviours, cycle-dependent relaxation and cycle-dependent creep. Specifically, cycle-dependent relaxation results from the constrained strain amplitude, and the mean stress drops toward zero with the increasing number of cycles, while cycle-dependent creep is caused by the constrained stress amplitude. For this behaviour, the mean strain increases over increased cycles, but the increasing rate decreases with the increasing number of cycles and the mean strain shift finally stops in a stable situation.

On the one hand, it is clear that the transformation of the stress-controlled situation reflects the behaviour of cycle-dependent creep where the mean stress is fixed. In this case, the tips of stable hysteresis loops departed from the previous track, and form a different cyclic stress-strain curve. This was also proved by experiments, where the experiments conducted by Lukas and Kunz (Table 8.2) [108] show that the cyclic stress-strain curve with zero mean stress is different from the cyclic stress-strain curve with non-zero mean stress (n"≠ n' and K"≠K'). Therefore, as the essential medium of the transformation between two stress situations, the stress-strain relations shown in Table 8.2 demonstrate that the assumption applied in the transformation may not be reasonable, and thus may lead to an imperfect description of creep fatigue in the situation of non-zero mean stress.

Table 8.2 Constants of the cyclic stress-strain and fatigue life curves

Stress ratio	strain hardening coefficient (K' or K'')	strain hardening exponent (n' or n'')
R= -1 ($\sigma_m = 0$)	408 MPa	0.163
R=0 ($\sigma_m \neq 0$)	51200 MPa	0.633

On the other hand, the transformation at the strain-controlled situation reflects the behaviour of cycle-dependent relaxation where the mean strain is controlled. According to results from our ANSYS results (a Chaboche Kinematic Hardening material model was applied to simulate the strain-stress behaviour), it was found that the tips of stable hysteresis loops follow the path of the stress-strain curve with zero mean strain if the strain range is small (Fig.8.1 a and b, elastic range and zero mean plastic strain). However, the tips deviate from this curve when the strain range is sufficiently large (plastic range and non-zero mean plastic strain) so that cycle-

dependent relaxation occurs (Fig.8.1 c and d). This is evidence for different stress-strain relations for zero and non-zero mean stress.

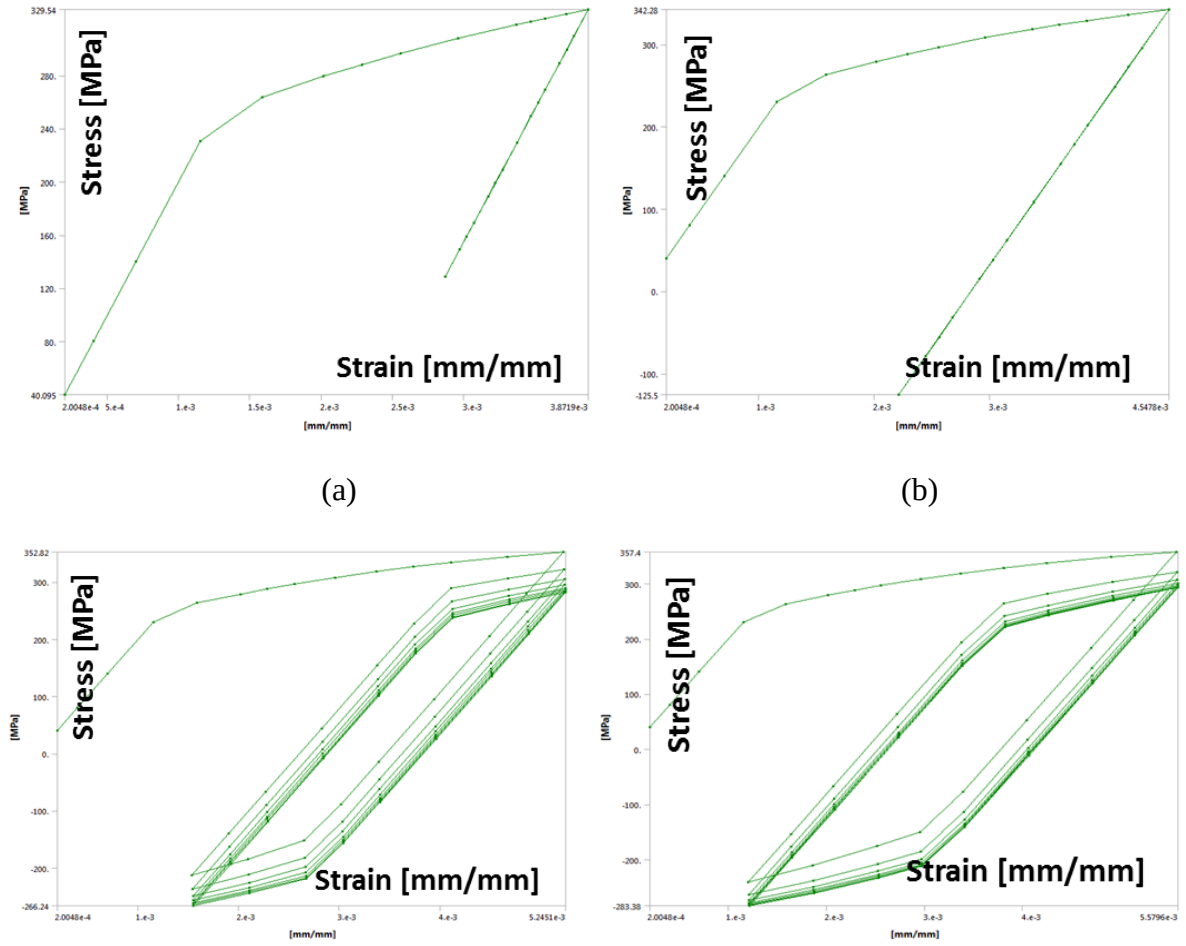

Figure 8.1 The hysteresis loops with non-zero mean strain. ANSYS results.

Discontinuity of the strain-stress curve is also observed at the point where the plastic strain is activated. In addition, experiments conducted by Yung-Chuan Chiou and Ming-Chuen Yip [109] show that different strain hardening coefficients and strain hardening exponents could be obtained under the different mean strains (Table 8.3), which implies that the cyclic stress-strain curves under situations of zero mean strain and non-zero mean strain are not consistent when the material experiences the strain-controlled cyclic loading.

Table 8.3 Constants of cyclic stress-strain curves with different mean strains

Mean strain	strain hardening coefficient (K' or K'')	strain hardening exponent (n' or n'')
0%	722.571 MPa	0.1507
0.4%	587.699 MPa	0.1170

Overall, the implication is that the strain-stress relation in the situation of zero mean stress is different from the relation in the situation with a non-zero mean stress. This may result in poor fatigue-life prediction when applying the unified mean-stress creep-fatigue equations. This is because the creep-fatigue equations with mean-stress effect were derived from the commonly held assumption that the strain-stress relation shares the same behaviour between situations with and without mean-stress effect. This issue implies that once non-zero mean stress is included, the complexity is presented by an ongoing tension-compression stress loading and method to include this behaviour in the formulation. This raised the further discussion of tension-compression process (Chapter 9).

8.4 Summary

Outcomes

The stress-based and strain-based unified creep-fatigue formulations were extended to the situation of non-zero mean stress:

$$\sigma = \sigma_0 \cdot \left(1 - \frac{\sigma_m}{\sigma_0}\right) \cdot B(d) \cdot C(T, t, \sigma, d) \cdot N_f^{-b_0} \tag{8.33}$$

$$\varepsilon_p = C_0 \left(1 - \frac{\sigma_m}{\sigma_0}\right)^{\frac{\beta_0}{b_0}} c(\sigma, T, t_c, d) {N_f}^{-\beta_0} \tag{8.34}$$

or

$$\sigma = \sigma_0 \cdot \left(1 - \frac{\varepsilon_{pm}}{C_0}\right)^{\frac{b_0}{\beta_0}} \cdot B(d) \cdot C(T, t, \sigma, d) \cdot N_f^{-b_0} \tag{8.35}$$

$$\varepsilon_p = C_0 \left(1 - \frac{\varepsilon_{pm}}{C_0}\right) c(\sigma, T, t_c, d) {N_f}^{-\beta_0} \tag{8.36}$$

The original form of the equation did not include the mean stress σ_m (or mean strain ε_{pm}). The above results show that it is possible to derive equations that do include mean stress (or strain), based on the application of the principle of compatibility.

Findings

This extension started from the stress-based unified equation; then the mean-stress effect was integrated by importing Morrow's mean-stress equation. Then introducing the equivalent fatigue life gave the strain-based unified equation with mean-stress effect. This process was based on the assumption that the strain-stress relation in the zero-mean-stress situation shares

the same characteristic when there is a non-zero mean stress, i.e. the value of the mean stress does not affect the stress-strain relationship. Hence there is an assumption of compatibility. This premise of compatibility is widely assumed in the literature.

However, the present analysis identifies that the stress-strain relationship is NOT the same for zero and non-zero mean stress. This claim is based on our analysis of the empirical data in the literature and finite element analysis results. We propose that the deviation is caused by a hysteresis effect. Hence, we question whether compatibility is universally valid. We suggest that the compatibility, which relates the stress-life relation to the strain-life relation, is not necessarily a conservative assumption in the creep-fatigue regime.

Potential future research directions

Based on the findings above, we propose that a modified compatibility relationship needs to be developed. Possibly this might be achieved by including a mean-stress effect. This could be worth doing for the potential to further improve the unified creep-fatigue formulations. This is a complex problem and an opportunity for future research.

Chapter 9

9. Conceptual model of the creep-fatigue-damage process

This results chapter gives a conceptual graphical-based model, which illustrates the whole process of damage accumulation from crack initiation to crack propagation then to structural failure.

Publications relevant to this chapter are as follows (see Appendix A for details):

(1) Liu, D. and D.J. Pons, Conceptual model of crack growth for creep fatigue. 2017. (In submission)

Normally, the process of fatigue failure is physically and macroscopically described by crack-growth behaviour. The theory indicates that an engineering structure fails when crack length achieves a critical value, and the total damage is gradually accumulated by the increasing number of cycles. Generally, the process of crack growth under cyclic loading is divided into three phases (Fig.9.1) [8]: crack initiation, crack propagation and structural fracture. Specifically, the first stage presents a threshold, below which there is no crack growth. The second stage shows a relatively steady state, in which the crack growth rate increases steadily with the increasing number of cycles (this is always described by Paris' Law [29]). The finial stage represents an unstable situation, where the engineering structure fails within a small number of cycles.

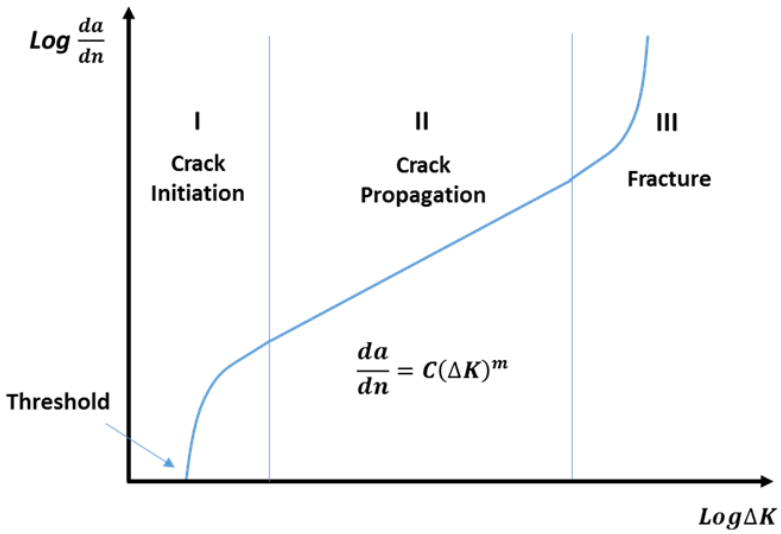

Figure 9.1 Three stages of crack growth

In this chapter, a conceptual graphical-based description of the crack-growth process of creep fatigue is presented at a grain-based level (a microstructural level). This was achieved by imagining the process from the perspective of atoms in orderly grains and at the grain boundaries (where the orderly arrangement between atoms breaks down). The bonds between atoms inside a grain are strong, relative to the bonds between atoms at grain boundaries. We sought to identify a coherent set of mechanisms that would affect the bonds between atoms, for all the loading regimes. This was based on integration of multiple concepts at the microstructural level, such as the plastic blunting process, the mechanisms of dislocation, and the diffusion creep process. These process are extant in the literature, and our contribution is to integrate and apply them to the fine scale to give a new understanding of the interaction between the underlying mechanisms. In addition, a number of new mechanisms for crack growth were also proposed to construct a comprehensive model.

Since the principles of crack growth of fatigue and creep are different (fatigue effect occurs via cracks through the grains while creep effect involves the grain boundary cracking), the fatigue and creep crack-growth behaviours were discussed and illustrated separately. In this conceptual model, three stages of crack growth from crack initiation to structural fracture were included. The second stage of steady crack growth is the primary focus. This is where the majority of the lifetime is consumed. It also presents multiple situations regarding the position of the crack relative to the grain boundary. The result is a proposed theory of the failure mechanisms, and this is represented in the form of a schematic representation.

9.1 Proposed principles of crack growth

In the present work, the crack-growth behaviours of fatigue and creep are discussed separately because of the different damage principles. Specifically, fatigue-crack growth results from the effect of dislocations, and creep-crack growth is based on diffusion. In this case, the fatigue

effect results in crack growth across (through) grains, while creep preferentially follows grain boundaries.

Crack growth caused by fatigue effect is attributed to plastic deformation at a crack-tip plastic zone, wherein the plastic deformation occurs via dislocations [110]. Ordinarily there is a preferred plane, and in that plane there are specific directions along which dislocation motion occurs, the slip plane. The axial (tension or compression) loading is decomposed into a normal stress which is perpendicular to the slip plane and a shear stress which is parallel to the slip plane. This shear stress then results in the movements along the slip plane. This implies that shear stress contributes to plastic dislocation, and then results in crack growth. In this case, the axial loading is transformed into the shear stress to produce the fatigue propagation.

The simplest form of dislocation is edge dislocation, see Fig.9.2 which represents a simplistic grain unit [110]. Specifically, the dislocation starts from the extra half-plane of atoms (plane I) which is identified as a defect. When a shear stress is applied, and its magnitude is sufficient, the bond between atom A and atom B is cut. Then, the bottom of all planes move to the right, and atom B is bonded with its neighbouring atom (atom C). In this case, a new half-plane of atoms (plane II) is generated. Under the shear stress, this irreversible process is successively and repeatedly presented, with the final result being the creation of a step at the edge of this unit. The process is irreversible because the other atoms in the grain also move into new positions (not shown in the figure) due to other disturbances, hence the atoms do not spontaneously revert to their original positions (plastic deformation). Hence the dislocation is an enduring feature of the grain. It can however be sent in a new direction should the orientation of the shear stress change, as occurs in reversed loading. By this means, the plastic deformation is produced due to the motion of numbers of dislocations. In addition there may be atomic displacement perpendicular to the plane, hence causing a screw dislocation. In practical situations, the behaviours of edge and screw dislocations are mixed, and both contribute to the overall plastic deformation of the grain and ultimately of the macroscopic deformation of the part.

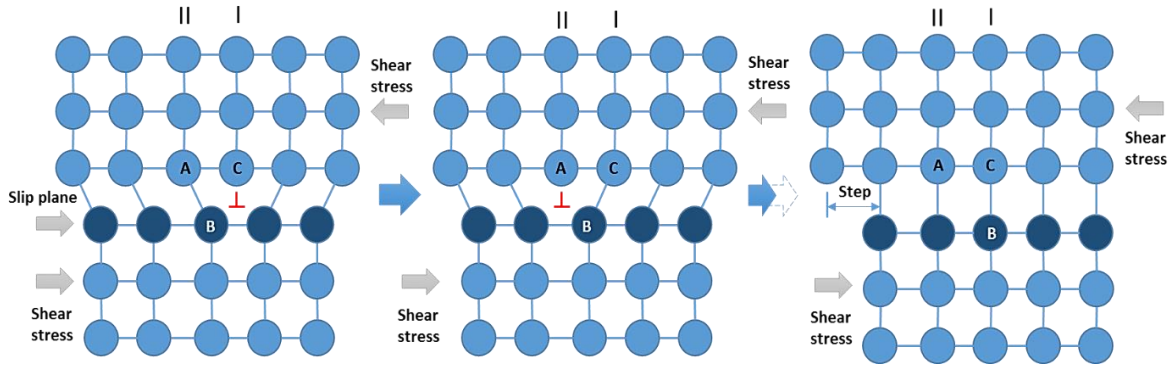

Figure 9.2 Edge dislocation for fatigue. Adapted from [110]

As mentioned above, the half-plane of atoms is regarded as the source of dislocation. The edge of this half plane is terminated within a grain; hence a large number of dislocations are piled up and then plastic deformation arises for the grain as a whole. This implies that the cracks

caused by fatigue are initiated within the grains and then are propagated through the grains, causing the observed transgranular fracture phenomenon.

However, the creep mechanism gives a different crack-growth behaviour, which is crack growth along the grain boundary. In general, crack growth caused by creep is attributed to diffusion behaviour, which is presented as the movements of vacancies [111, 112]. Under the creep situation, a constant applied loading leads to stress concentration at the triple points which are formed by the three adjacent grains (Fig.9.3). Normally, diffusion is a behaviour of atomic shifts from an area with high stress concentration to an area with low stress concentration. In this case, the atomic movements due to the diffusion mechanism results in the convergence of vacancies at the triple points, which then segregate the triple grain boundaries.

By this means, the micro-crack is initiated at the grain boundary. After the process of micro-crack initiation, the localized stress is highly concentrated at the crack tip, which then recruits more vacancies from the bulk of the grain, and these are diffused to the crack tip along the grain boundary. This leads to further propagation of the creep crack along the grain boundary. High temperature provides more favourable conditions for diffusion behaviour, hence advances the creep crack along grain boundaries. Thus creep failure is strongly temperature dependent.

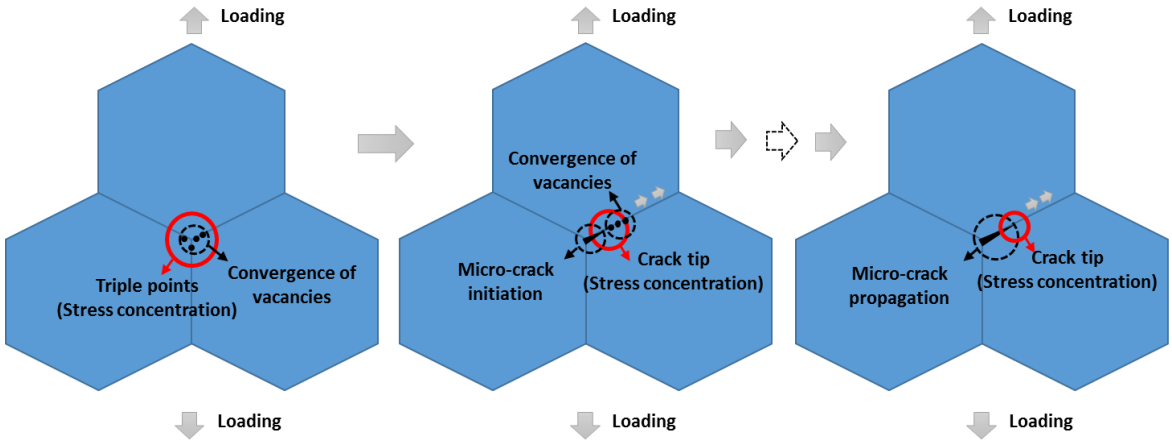

Figure 9.3 Crack growth by diffusion mechanism

Overall, crack-growth behaviours of fatigue and creep follow the different principles; specifically, fatigue effect occurs via cracks through the grains while the creep effect involves fracture along the grain boundary.

In the present work,

we assume that the fatigue effect makes more contribution to structural failure than creep effect since the cyclic time is not long enough to produce major creep damage.

Under this assumption, we could believe that the dislocation behaviour (plastic deformation at the crack-tip plastic zone) may play a more important role in creep-fatigue damage, and the diffusion behaviour (creep effect) takes an assistant position to further promote the crack

caused by fatigue. This concept is embedded into the conceptual graphical-based model proposed in the following section.

9.2 Conceptual graphical-based model

The conceptual model (Fig.9.5-9.17) mainly focuses on the second stage of crack growth because the majority of the lifetime is consumed at this stage, and this stage presents a stable process of crack growth. In this conceptual model, the crack-growth behaviours under the tensile partition and compressional partition are discussed separately, and crack-growth behaviours caused by the fatigue effect and creep effect are described separately.

In the present work, we integrate multiple mechanisms, which are proposed in the literature and exist at the microstructural level, to describe crack-growth process. Specifically, it is proposed that the following major mechanisms operate at the three stages. We note these as *premises*:

Stage I: Crack initiation

a) That dislocation behaviour [113] is a key mechanism at crack initiation. This effect causes the slip planes to extrude or intrude, which results in stress concentration at the surface and then leads to crack nucleation.

b) That the strain energy release rate [114, 115] determines the crack-growth rate . This mechanism underpins the unstable stage after the threshold of crack initiation. In this stage, increased energy accelerates the increase of crack-growth rate at the beginning phase, which is then retarded due to reduced energy and finally achieves a stable state.

c) That shear effects [116, 117] provide opportunistic directions for crack growth. This mechanism is that the direction oriented at 45^{o} gives a more favourable condition for crack growth at the initial phase of stage I.

Stage II: Crack propagation

d) That the plastic blunting process [9, 118-120] has asymmetrical effects in the tensile and compressive loading cycles. This mechanism describes crack-growth behaviour in one loading cycle. The tensile loading blunts the crack tip, and the new crack surface is created due to a shearing effect. Then, when the loading is reversed, the surface created under tensile loading remains (crack extension) because of a crushing effect.

e) That the crack tip plastic zone [121-123] enhances crack growth. This mechanism involves a highly localized stress around the crack tip. This, on the one hand, results in plastic deformation (crack opening) at the crack tip; on the other hand, gives a more favourable situation for diffusion.

f) That diffusion creep [111, 112] provides a mechanism that leads to grain elongation and then further crack opening. In addition, since atoms diffuse from a high to a low concentration region, more vacancies are generated and converged at the crack tip

where highly localized stress is presented, which provides a more favourable situation for creep damage.

g) That existing precipitates [124] cause fatigue resistance. The mechanism is mainly that precipitates are the obstacle to dislocation, hence restrain the process of crack propagation.

h) That crack deflection (change of direction) [125] preferentially occurs at the grain boundary. This is determined by the twist angle and the tile angle.

i) That triple-points [126-128] provide a mechanism for significant stress concentration, which provides a more favourable stress field for creep damage.

j) That a region with high density of micro-cracks is particular weak and supports crack branching activities [129].

k) That the slip bands within grains [130] may cause the crack to re-direct within grains.

Stage III: Structural failure

l) That the plastic energy [117] available exceeds the need for producing the new crack surface. The excess energy is applied to form voids, and thus further worsens creep-fatigue resistance.

The challenge is showing how these multiple premises are integrated together at the microstructural level. There are no models in the literature that provide such integration. To solve this problem, we make the following new *propositions* of mechanisms that operate at the microstructural level during crack growth:

A. That **energy dynamics** explain the crack initiation and the unstable phase after this, and is based on a liberation of energy due to coalescence of strain. In general, when the internal energy stored in the structure due to cyclic loading arrives at a critical value, the barrier to initiate the crack is overwhelmed. After this, the released energy is gradually consumed to produce new crack surfaces in an accelerated crack growth rate.

B. That **grain-mismatch** occurs due to grain elongation under the tensile loading, resulting in relative movement between two neighbouring grains. Then the shear stress along the grain boundary is increased and a weaker region along the grain boundary is created. This results in a mismatch band at the grain boundary. This widens the crack body and enhances its growth.

C. That **bonding crushing effects** exist at the finer scale. During the process of compression, the atomic bonds, which are distorted and rearranged in the tensile phase, may be further damaged and become potential failure sites for next loading cycle. This process is irreversible since the atoms cannot return to their original position under the compressional loading.

D. That a **crack net** is caused by the aggregation of micro-cracks. This crack net probes a larger volume of material for weaknesses, and then promotes the main crack.

E. That **irregular configuration of the grain boundary** causes stress/strain pile up at the grain boundary, and then results in large driving force for extending crack tip into the neighbouring grain.

Furthermore, it is proposed that these mechanisms are integrated by the following assumptions:

F. That the **primary mechanism** for failure in the creep-fatigue loading regime is crack growth by mechanisms of crack blunting (including shearing and crushing), hence fatigue effects.

G. That the **supporting mechanisms** that augment the extent of damage are grain elongation and diffusion, hence creep effects.

The application of these premises and propositions is detailed below**.**

9.2.1 Stage I: Crack initiation

Stage I (shown in Fig.9.1) presents the initiation of fatigue crack [113], and a threshold is given below which crack growth is dormant. In this stage, unstable (which is difficult to describe numerically) crack-growth rate above the threshold is shown. Specifically, the rate starts from a relatively high value, which reflects that a large amount of damage is rapidly produced within a few cycles at the initial stage, and then gradually decreases with the increasing number of cycles. This remarkable high crack-growth rate may result from a break in the stable situation (perfect structure), where amounts of energy are needed, and thus a blasting effect is presented. Then, the process of re-balance reduces the crack-growth rate to a relatively steady situation.

9.2.1.1 The threshold of crack initiation

The first stage (stage I) is that of crack initiation. We summarise the crack initiation mechanics as follows. Fundamentally, crack initiation is caused by stress concentration, where two situations are presented. A typical situation is that the crack starts at a surface defect such as a machining mark. This provides a highly localized stress concentration, hence a pre-existing micro-crack [8]. By this means, a crack is initiated at this specific point, and then the localized plastic strain caused by the ductile micro-tearing events provides opportunity for further propagation.

Second, for the situation with perfect surfaces (defect-free), dislocations play an important role [113] for the initiation of a fatigue crack [131] (Figure 1.9 therein), [132] (Figure 1 therein). During this process, loading cycles cause dislocations to pile up at the microstructural level. These dislocations are in the crystal lattice at the nanoscale. Under loading they align and coalesce to produce thicker slip planes through the crystal and eventually slip bands at the macrostructural level [133]. Under cyclic loading there is more relative movement between the bands so the effect becomes more pronounced – the bands displace further. We suggest this is due to irreversibility caused by the localised hardening effects of the dislocations. In the area of persistent slip bands, the slip planes extrude or intrude to the surface of the object, see Fig.9.4. This gives tiny steps in the surface, where the stress concentration then results in crack nucleation.

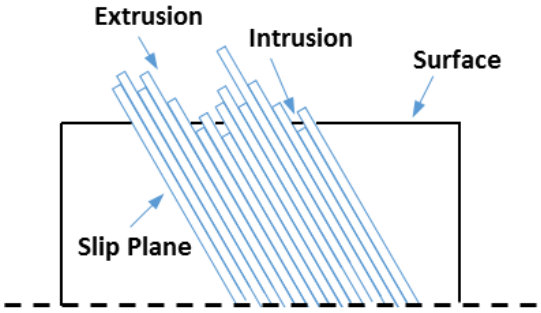

Figure 9.4 Crack initiation due to dislocation

In the stage I (crack-initiation stage), a stress-intensity threshold exists below which there is no crack growth. We attribute this to the cracks being too short to result in a meaningful stress concentration effect (which is primarily an effect of proportional geometry). Also, if there are many superficial defects - which is usually the case - then the material does not have a geometrically exact boundary at the nanoscale, and hence the stress avoids this region: the many small defects effectively decrease the stiffness of the superficial layer, and hence this layer is to some extent unloaded.

9.2.1.2 Crack growth after the threshold

After the threshold stress intensity is exceeded, there is a regime of high acceleration of crack-growth rate. Then, following this high acceleration regime, a transition to a slower acceleration of crack-growth rate is presented.

On the one hand, this process is attributed to the concept of strain energy release rate which describes the energy consumed to create per unit of new crack surface. This implies that the more strain energy is released, the more new crack surfaces are produced. Normally, the strain energy release rate could be numerically related to the M-integral [114, 115]. The relationship between the number of cycles and M-integral was investigated by Margaritis [134] (Figure 7 therein), where M-integral increases with the increasing number of cycles at the early phase, then it decreases over the peak, and finally it reaches a constant situation. This trend is consistent with observation of the initiation stage shown in Fig.9.1. Specifically, after the threshold, increased energy (released strain energy) accelerates the increase of crack-growth rate at the beginning phase, then reduced energy retards the acceleration of the crack-growth rate, and finally a steadily increased crack-growth rate is achieved under the situation with constant energy (this is viewed as the crack-propagation stage).

We suggest that the underlying energy dynamics are based on a rapid liberation of energy due to coalescence of strain. Specifically, the internal energy, which is stored in the structure in the form of the irreversible formation of dislocations that increase in number due to cyclic loading. Then, when this energy arrives at a critical value, the vacancies in the dislocations coalesce and form a crack – hence barrier to initiate the crack is broken through. This qualitative leap from perfection to imperfection requires internal energy. This process is accomplished during a short time period by releasing large amounts of energy. After this, the released energy is consumed

to produce new crack surfaces in a high acceleration of crack-growth rate, and the whole system is forced into an unsteady condition. Naturally, the need to re-balance this system gradually reduces the amount of released energy (caused by applied loading) until a balanced condition is reached. During this process, the high acceleration of crack-growth rate is gradually retarded, and then this acceleration reaches stabilization (the whole system is re-balanced). The growth of the crack causes further large scale deformation of the grain as a whole, which causes more dislocations to occur within the grain, and repeats the cycle.

An alternative explanation is that the unstable behaviour of crack growth in stage I is due to shear mechanisms [116, 117]. Generally, a crack is propagated through two different methods: the plastic deformation around the crack tip and the shear-stress effect at the planes oriented at 45^o. At the initial phase of crack growth, a small plastic zone and a small stress field are presented around the crack tip because of the small magnitude of stress intensity. In this case, the mechanism of plastic deformation around the crack tip may not be significant enough to become the driving force for crack growth. Instead the shear stress at the planes oriented at 45^o provides a more favourable condition for crack growth. This is because the shear stress at these planes and the relative movements between these planes under cyclic loading provide more vulnerable areas for crack growth. In this case, a crack grows along the planes oriented at 45^o with a minimum of effort, hence a high acceleration of crack-growth rate is given. As the stress intensifies, the shear-stress effect is gradually suppressed by the plastic-deformation mechanism hence the acceleration of crack-growth rate is reduced. This is because, during this process, the direction of the crack growth gradually deviates from the surface of the planes oriented at 45^o, and then the behaviour of penetrating the grain boundary results in the deceleration of crack-growth rate. Finally, crack-growth behaviour is stably caused by the crack-tip plastic zone, and a steady situation is achieved (stage II is initiated).

The crack initiation mechanics is summarised in Fig.9.5:

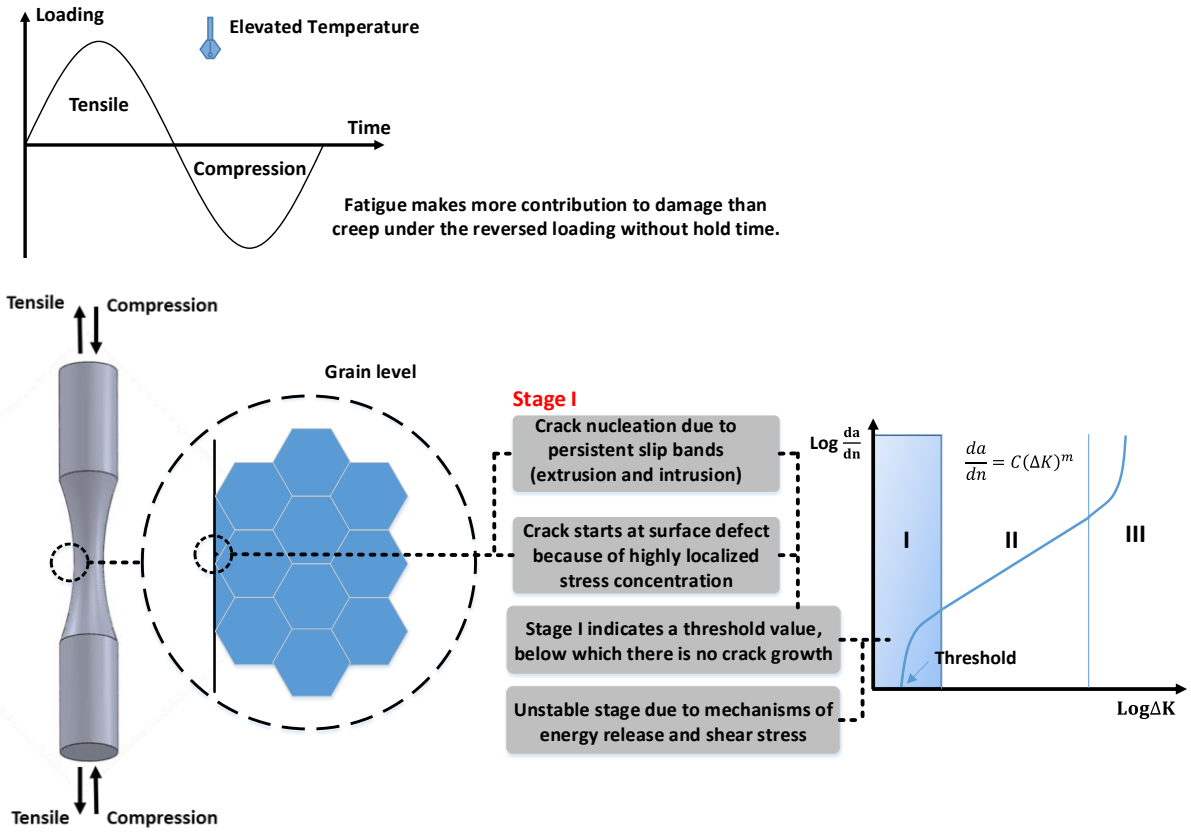

Figure 9.5 Stage I: Crack initiation

We suggest that both mechanisms apply, and complement each other. We summarise the crack initiation mechanics as follows, see Fig.9.5. Crack nucleation starts at the surface due to highly localized stress concentration. In the case of smooth surfaces, it is attributed to the presence of persistent slip bands (extrusion and intrusion). Stage I (that stage of crack initiation) has a threshold value, below which no crack growth occurs. Once a crack is initiated, it grows quickly at the early phase, then the acceleration of crack-growth rate is reduced, and the crack-growth behaviour finally becomes steady (see next section). This process is proposed to be underpinned by the above mechanisms of strain energy release and shear stress.

9.2.2 Stage II: Crack propagation

The second stage (stage II) shown in Fig.9.1 presents the behaviour of crack propagation, wherein the crack growth experiences a relatively steady process. This stage is numerically presented by Paris' Law (Eq.9.1) [29], which shows a power-law relationship between the crack growth rate ($\frac{da}{dn}$) and the range of the stress intensity factor during the fatigue cycle (ΔK):

$$\frac{da}{dn} = C(\Delta K)^m \tag{9.1}$$

where C and m are constants.

The crack-growth process of creep fatigue is mainly discussed under the second stage of crack growth, and this discussion is based on the idea of the plastic blunting process (illustrated in Fig.9.6 based on one cycle loading) [9, 118-120].

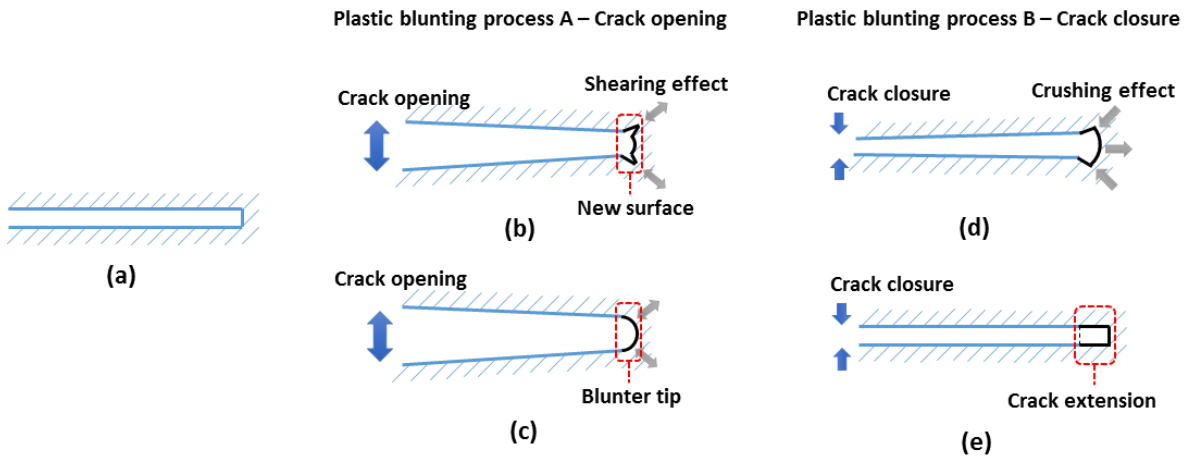

Figure 9.6 Plastic blunting process

At the beginning of loading cycle, the crack tip is sharp (Fig.9.6a). Then, the applied tensile stress leads to crack opening, and the stress concentration at crack tip causes the slip along planes at 45° (Fig. 9.6b). This leads to the gradual increase of crack-tip area, and finally the crack tip widens to its maximum plastic deformation (Fig. 9.6c) due to the plastic shear effect. At the same time, the crack tip becomes blunt and grows longer because a new crack surface is created. When the loading is changed to compressional situation, the crack is closed, and the slip at the crack tip is reversed (Fig. 9.6d). Finally, the crack surfaces are crushed together, and the new crack surface created under tensile loading remains (Fig. 9.6e) (crack extension). Consequently, the sub-cracks promoted by each loading cycle are accumulated, and the structure fails as the total damage achieves a critical value.

The idea of plastic blunting process was integrated with a general understanding of creep mechanism to show crack-growth behaviour of creep fatigue. The process of crack propagation (Fig.9.7-9.16) is described (in a grain-based level) by three typical situations: (1) crack tip within a grain (section 9.2.2.1); (2) crack tip at the grain boundary (section 9.2.2.2 (1)) or at the triple point (section 9.2.2.2 (2)); and (3) crack tip through grain boundary (section 9.2.2.3).

In the present work, fatigue is identified as crack growth by *overloaded local atomic bonds*, and creep is regarded as the *flow of atoms relative to each other* with transfer of bonding to new partners.

9.2.2.1 Crack tip within a grain

Model for crack growth in the tensile regime

Under tensile loading (Fig.9.7), the fatigue component follows the idea of the plastic blunting process. In this process (1A in Fig.9.7), tensile stress leads to crack opening, and shear behaviour is presented at the crack tip. Then, by the plastic shear effect, the new surface is

created; meanwhile, the crack tip widens and becomes blunt (the blunting behaviour was illustrated by Figure 12 in Ref [135] and Figure 32 in Ref [136], where a stretch region is presented). Diffusion creep is identified as the main creep mechanism for creep-fatigue damage in the present work. It is generally believed that diffusion creep leads to grain elongation, which then results in a further opportunity for crack opening (1B in Fig.9.7).

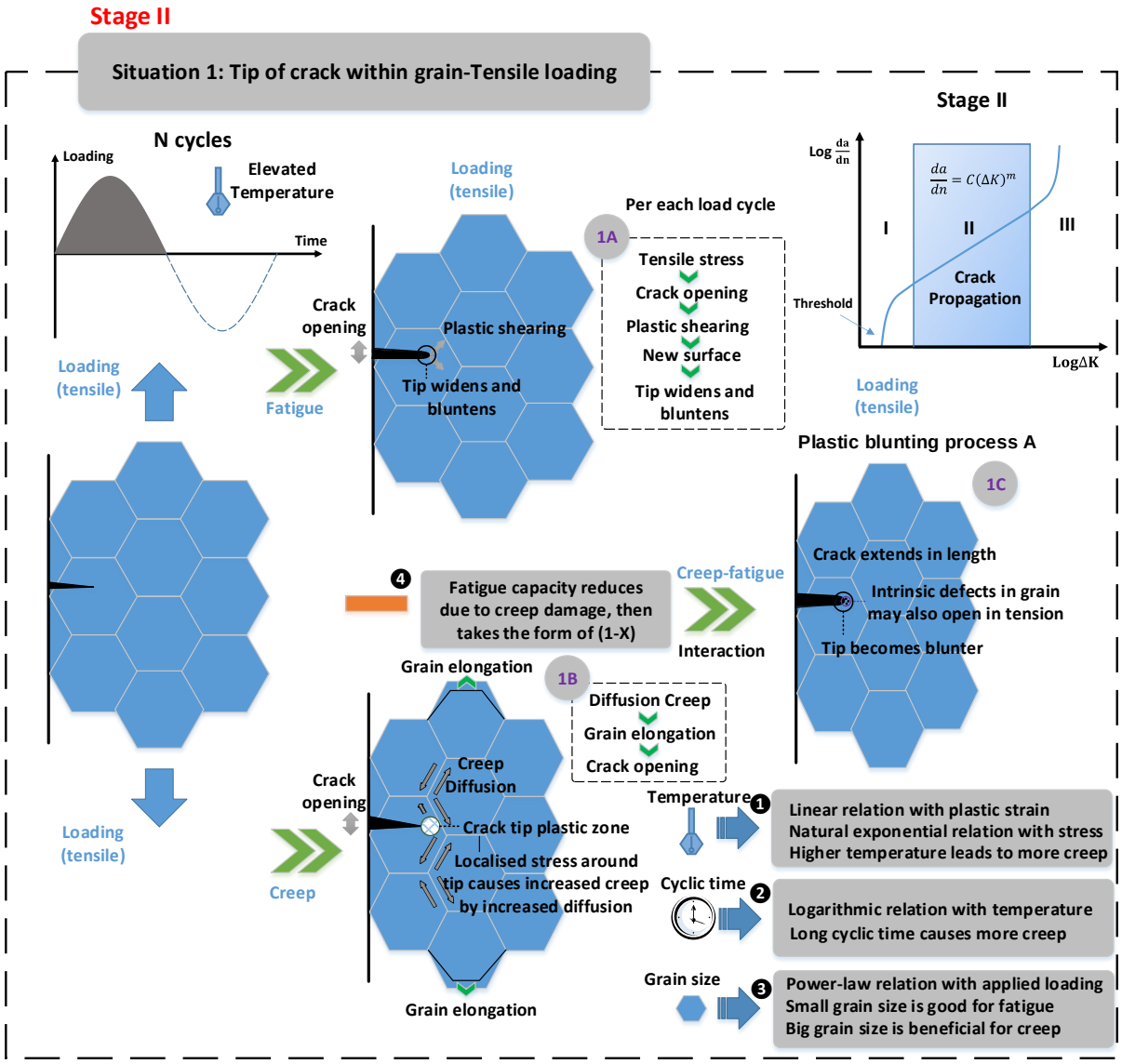

Figure 9.7 Crack tip within a grain-Tensile loading

In addition, diffusion creep has a dependency on applied loading, and larger loading produces more creep damage. Specifically, the idea of a crack tip plastic zone [121-123] indicates that the localized stress is highly significant around the crack tip, and gradually decreases in the direction of crack growth (Fig.9.8). This is consistent with the numerical representation (Eq.9.2) of stress distribution around the crack tip:

$$\sigma_{ij} = \sigma\sqrt{\frac{a}{2r}}f(\theta) = \frac{K}{2\pi r}f(\theta) \tag{9.2}$$

where σ_{ij} is the stress distribution, a is the crack length, K is the stress intensity factor, and r and θ are polar coordinates. Higher localized stress around crack tip causes more creep damage due to increased diffusion, and thus contributes to crack opening. Specifically, atoms normally diffuse from a region of high concentration to a region of low concentration. In this case, more vacancies are generated and converged at the crack tip, and then a more favourable situation for creep damage is presented.

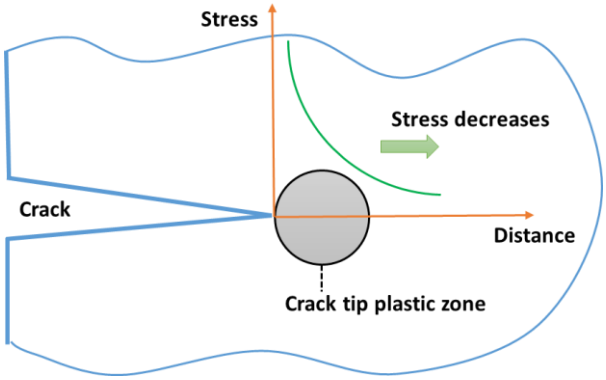

Figure 9.8 Stress around crack tip

Consequently, the crack tip surface caused by the fatigue effect is further extended and becomes blunter due to the creep effect (1C in Fig.9.7), which implies the combined effects of fatigue and creep. A defected-related state, such as intrinsic defects, around the crack tip may also promote crack growth (negative to fatigue resistance), where the weakest zone of atomic bonds is represented. An example of presenting a defected-related effect is shown in Figure 32 from [136], where the crack is promoted due to void coalescence and the bridges between voids are sheared off. In addition, precipitates may also be considered as a defected-related effect, but which are normally beneficial to fatigue resistance. On the one hand, this benefit results from the obstacle to further dislocation [124], whereby the precipitates restrain the process of crack propagation. On the other hand, this benefit could also be explained by the fatigue-softening behaviour [95]. Generally, softening behaviour is caused by disordering the stacking sequence of precipitates due to reversed loading, whereby the crack encounters a tougher situation to penetrate this area. In addition, the fatigue-softening behaviour can also be attributed to the reduced area intercepted by the dislocation of the slip planes due to the gradual consumption of precipitates under the reversed loading (the precipitates are cut into smaller sizes under reversed loading, and thus are dissolved).

Normally, the creep effect has strong dependencies on temperature, cyclic time and grain size, and these variables are accommodated in the unified creep-fatigue equations, and the relationships between these variables can be linked to the underlying physical mechanisms (see Chapter 10). Generally, a higher temperature leads to more creep damage; this effect will be described in section 10.1.1. The strain-based formulation shows a linear relation between temperature and applied loading, and the stress-based formulation presents a natural exponential relation between them (❶ in Fig.9.7). The underlying physical mechanisms of temperature dependence will be presented in section 10.2.1. In addition, a longer cycle time gives more creep damage, and this influence will be shown in section 10.1.2. A logarithmic

relation between cyclic time and temperature is presented by the unified creep-fatigue equations (❷ in Fig.9.7), and the underlying physical mechanism of this relationship will be discussed in section 10.2.2. Furthermore, a small grain size is positive for fatigue while a big grain size is beneficial for creep resistance; this will be discussed in section 10.1.3. A power-law relationship between grain size and applied loading (❸ in Fig.9.7) is shown in the unified creep-fatigue equations, and the underlying physical mechanisms of which will be discussed in section 10.2.3. Consequently, the negative creep effect caused by elevated temperatures, or prolonged cyclic time, or smaller grain size gives weaker atomic bonds, then this results in the adversely affected material. According to the concept of 'fatigue capacity', the total fatigue capacity is gradually consumed by the creep effect. This behaviour is numerically represented in the unified creep-fatigue equations by taking the form of '1-X' (❹ in Fig.9.7), which will be discussed in section 10.2.5.

Model for crack growth in the compressional regime

Under compressional loading (Fig.9.9), crack closure is presented based on the idea of the plastic blunting process. In this process, crack surface, especially the tip zone, is crushed together. Since the crushing process is inelastic and irreversible, the new crack surface created under tensile loading remains (1E in Fig.9.9). This implies that compressional loading also contributes to crack growth.

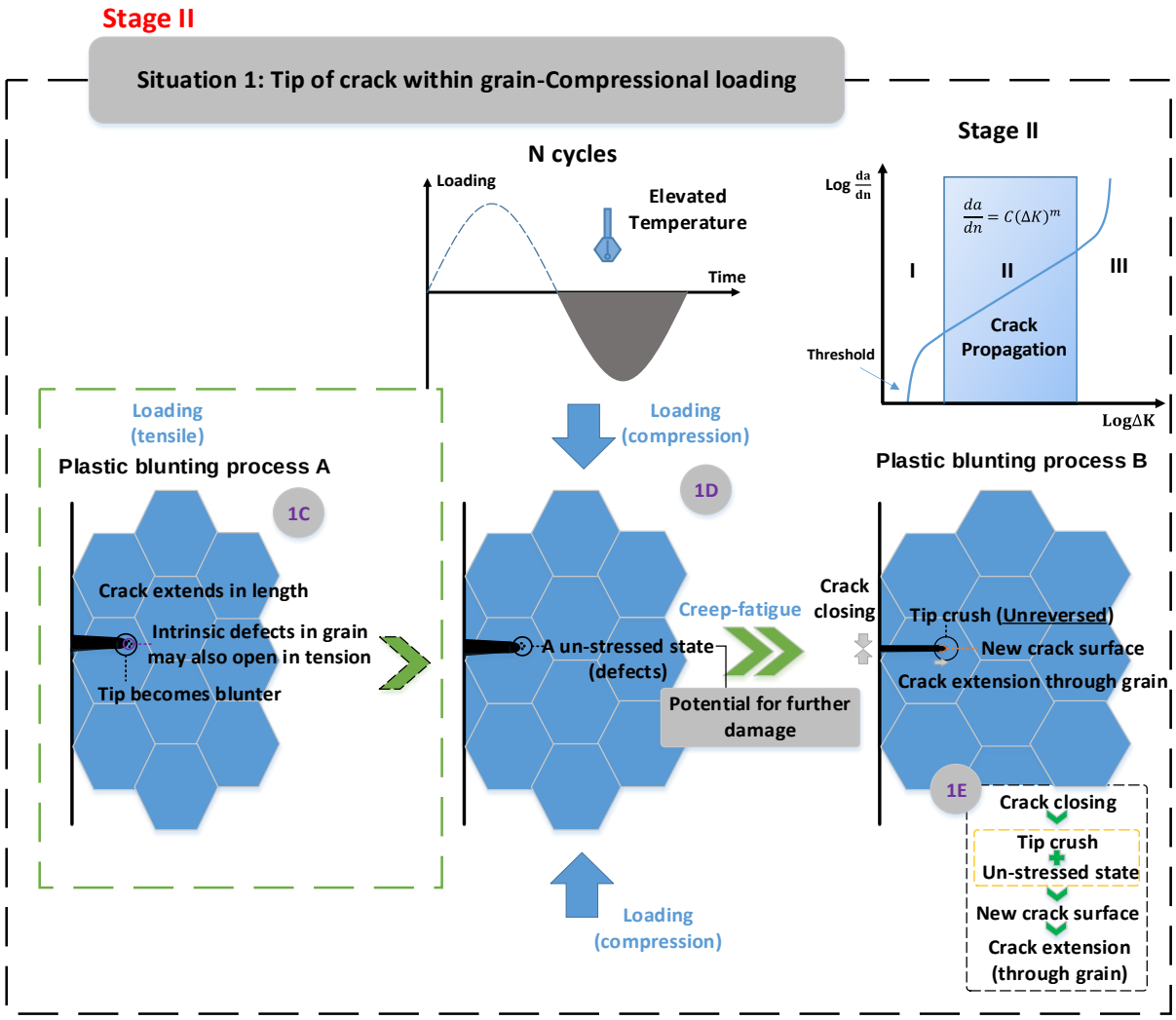

Figure 9.9 Crack tip within a grain-Compressional loading

This phenomenon may be explained by the observation of the crack tip opening displacements [137, 138] under compressional loading, where the crack is not entirely closed in this loading regime due to the plastic effect (this is illustrated by Figure 3 of Ref [137]).

In addition, the contribution of compressional loading may also be explained by the behaviour of atomic bonds. Specifically, creep fatigue does its damage in the tensile phase by changing the landscape of atom arrangements and hence the bond vulnerability (which implies the bonds are extended and become weaker). During the process of compression, because of the crushing effect, some of these partly broken bonds may be further damaged and become potential failure sites for the next loading cycle, while others may be totally damaged and then lead to crack extension. This is significantly not a reversible process since the atoms cannot return to their original positions after one tension-compression cycle. Furthermore, the defect-related state around the crack tip may further propagate cracks due to the crushing effect. Specifically, the crushing effect causes the crack tip to be squeezed, and then the tip is possibly extruded towards the zone with the weak atomic bonds. In this case, the crack is further extended (1D in Fig.9.9) by cutting these vulnerable bonds with the assistance of the crushing effect. Consequently, the sub-crack under one loading cycle is formed, which makes a contribution to the final fracture.

After N cycles, the accumulated crack arrives at the grain boundary or it encounters the triple point. This reaches the following situation.

9.2.2.2 Crack tip at grain boundary or triple point

(1) Crack tip at grain boundary

Model for crack growth in the tensile regime

Under tensile stress (Fig.9.10), the fatigue component experiences the same process shown in 'situation 1-1A', wherein the new crack surface is created due to the plastic shearing effect. Then, this causes the crack tip to widen and become blunt. For the creep component (2B-1 in Fig.9.10), diffusion creep results in grain elongation along the stress direction. On the one hand, this gives crack opening, which has been discussed in section 9.2.2.1; on the other hand, shear stress, which results from grain elongation, leads to elongation of the grain boundary, which then causes the crack tip to widen; meanwhile, a mismatch band appears [139, 140]. Specifically, the grain boundary presents a zone of irregular atomic bonds, and thus the bonds at the grain boundary present an anisotropic behaviour. Therefore, the relative movement of points caused by grain elongation at the grain boundary may present different results, the extension or break of atomic bonds. This gives a zone of material where bonds are partly weakened, and provides a potential for further damage. Consequently, creep intensifies the plastic blunting process caused by the fatigue effect, and a blunter crack tip arises.

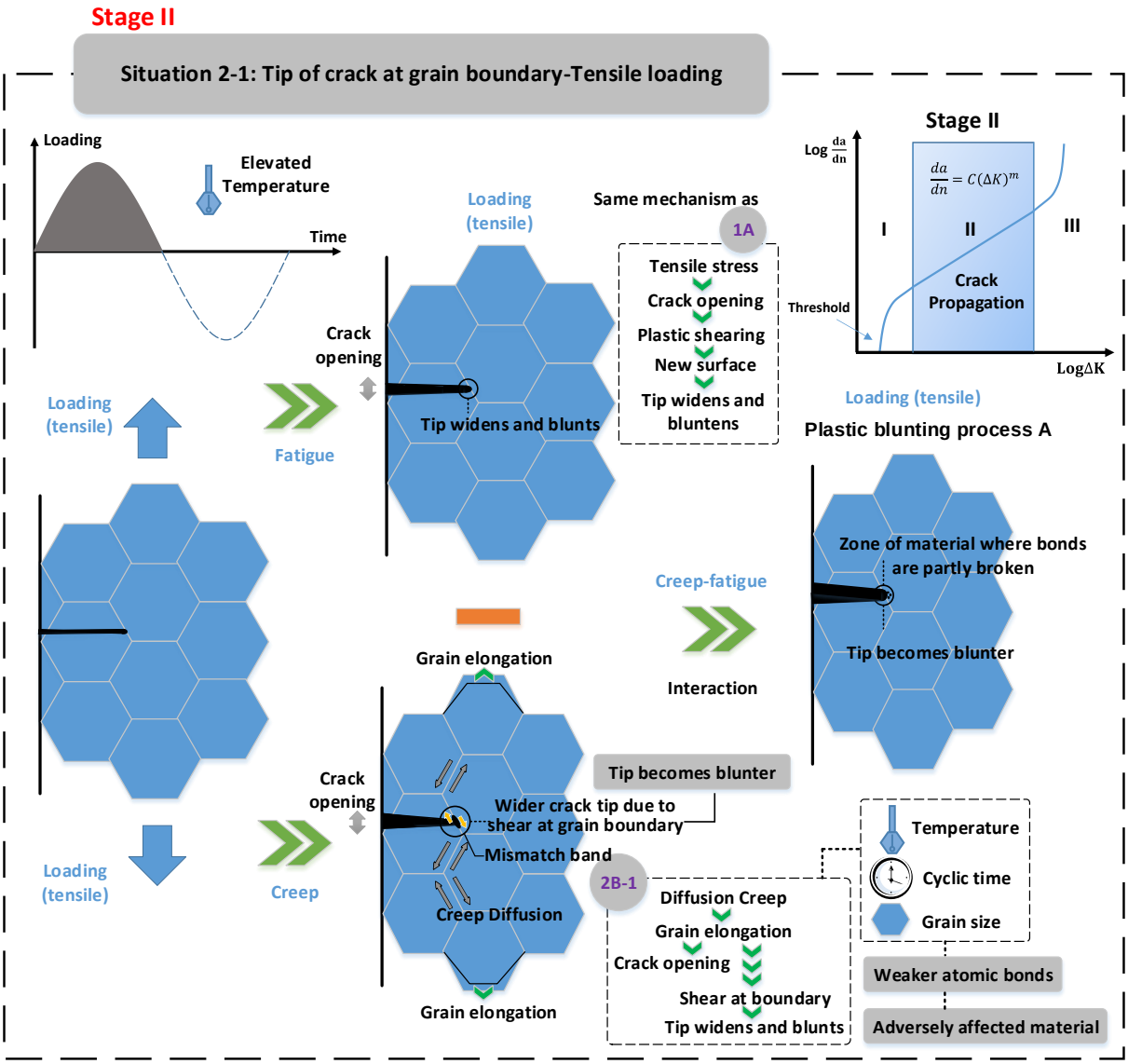

Figure 9.10 Crack tip at grain boundary-Tensile loading

Model for crack growth in the compressional regime

Under the situation with compressional loading (Fig.9.11), the same creep-fatigue process shown in 'situation 1- 1E' is presented, where reversed loading crushes the material ahead of the crack, even across the grain boundary. As a result, the new crack surface caused by the tensile loading remains by the tip-crush effect, and the crack is further extended across the grain boundary.

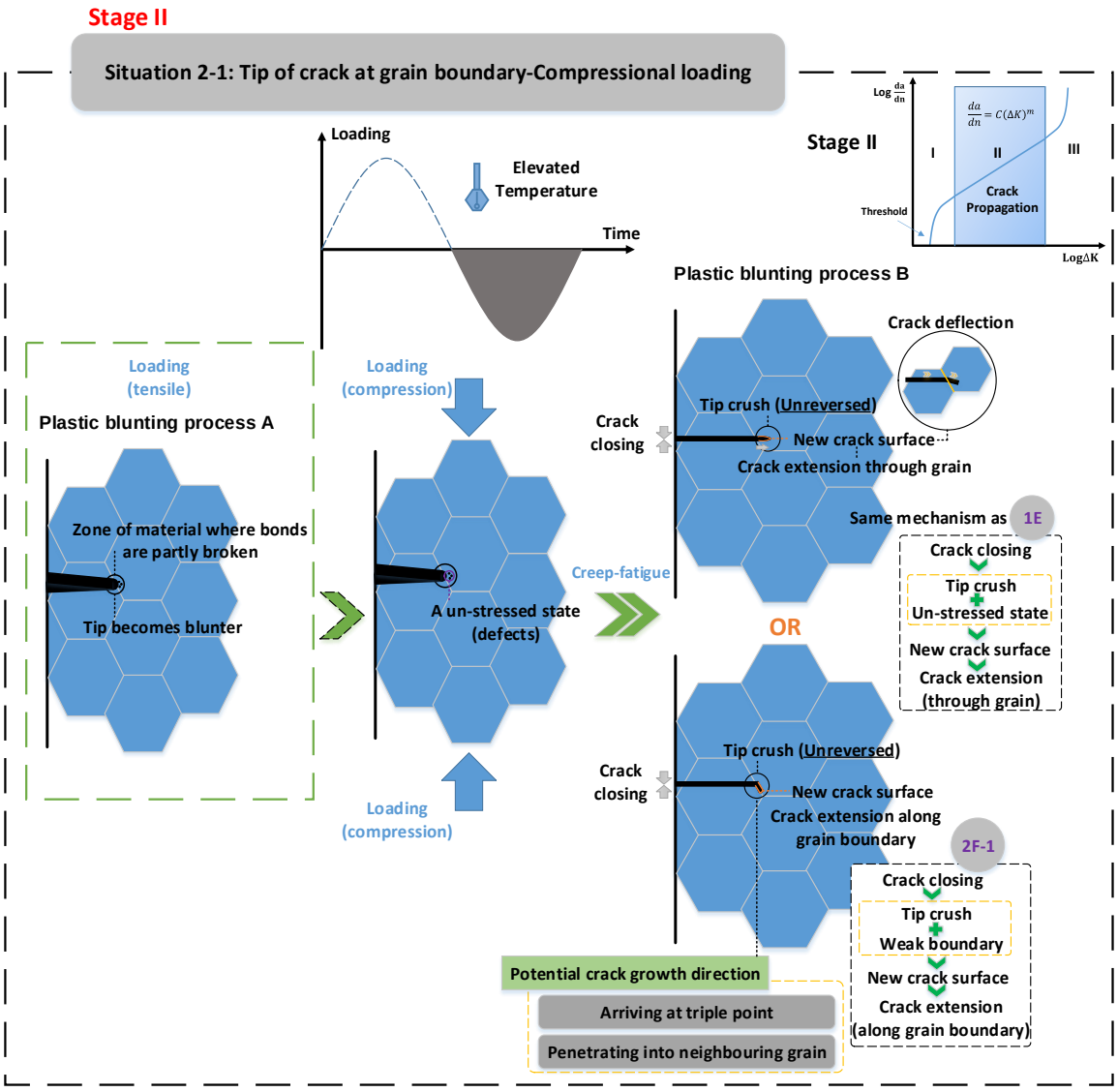

Figure 9.11 Crack tip at grain boundary-Compressional loading

In particular, the crack path may be deflected (this behaviour is illustrated by Figure 12 in [141]) at the boundary. Specifically, crack deflection at the grain boundary is generally determined by the twist angle *(a)* between two slip planes on the grain boundary and the tilt angle *(b)* between the intersection lines of two slip planes on the cross section [125]. This behaviour is illustrated by Fig.9.12, where the crack path is redirected at the grain boundary of the sample surface.

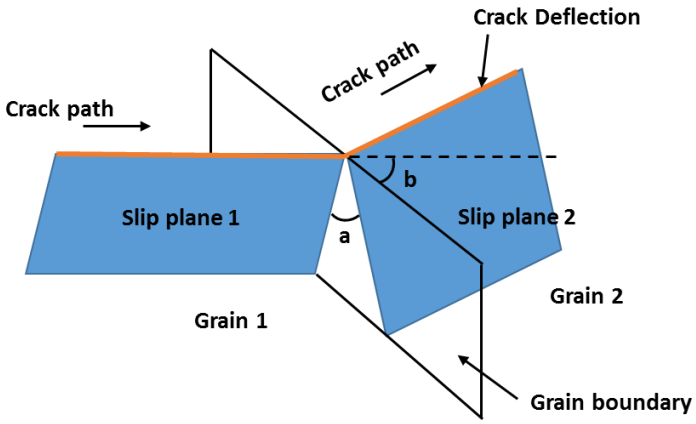

Figure 9.12 Crack deflection

Alternatively, the tip-crush effect during the process of crack closure may lead to crack growth along the grain boundary. Specifically, grain band sliding, which occurs during crack opening, may result in a weaker region along the grain boundary. This then provides a more likely direction for crack propagation than the direction passing through the grain boundary. After this, the crack may arrive at a triple point or may penetrate into the neighbouring grain (deviated progression along the grain boundary). These two situations will be discussed in the next section.

(2) Crack tip at triple point

Model for crack growth in the tensile regime

The triple point, which is defined as the connection point among three adjacent grains, provides a different crack-growth mechanism for fatigue and creep. Specifically, fatigue effect under tensile stress (Fig.9.13) presents the same process shown in 'situation 1-1A', where a blunt tip is presented at the triple point according to the idea of plastic blunting process. Comparing with the situation shown in section 9.2.2.2 (1), creep presents a different behaviour at the triple point. On the one hand, diffusion creep gives grain elongation along the direction of tensile stress, and then this leads to crack opening (2B-2 in Fig.9.13); on the other hand, the triple point presents a significant stress concentration [126-128], which provides an effective stress field for crack growth along the grain boundary (2B-2 in Fig.9.13). In this situation, multiple opportunities arise for crack propagation along the grain boundary. Generally, the weakest microstructural zone may finally determine the direction of crack growth. Specifically, the weakest zone shows an intensified state, which is normally caused by defects. These include vacancies which are beneficial to diffusion creep [142, 143], and micro-cracks which aggravate the concentration of stress and hence provide favourable conditions for diffusion. These defect-related effects may also change the direction of crack growth. In addition, according to the idea of the crack tip plastic zone (shown in Fig.9.8), the stress concentration is presented at the crack tip, where a strong high-stress field is provided hence more creep damage is produced. This implies that this area/direction may have more potential for crack growth. As a result, with the combined effect of fatigue and creep, a blunter crack tip is presented. The crack grows

opportunistically in the direction where the grain boundaries are most vulnerable (for propagation into the grain see below).

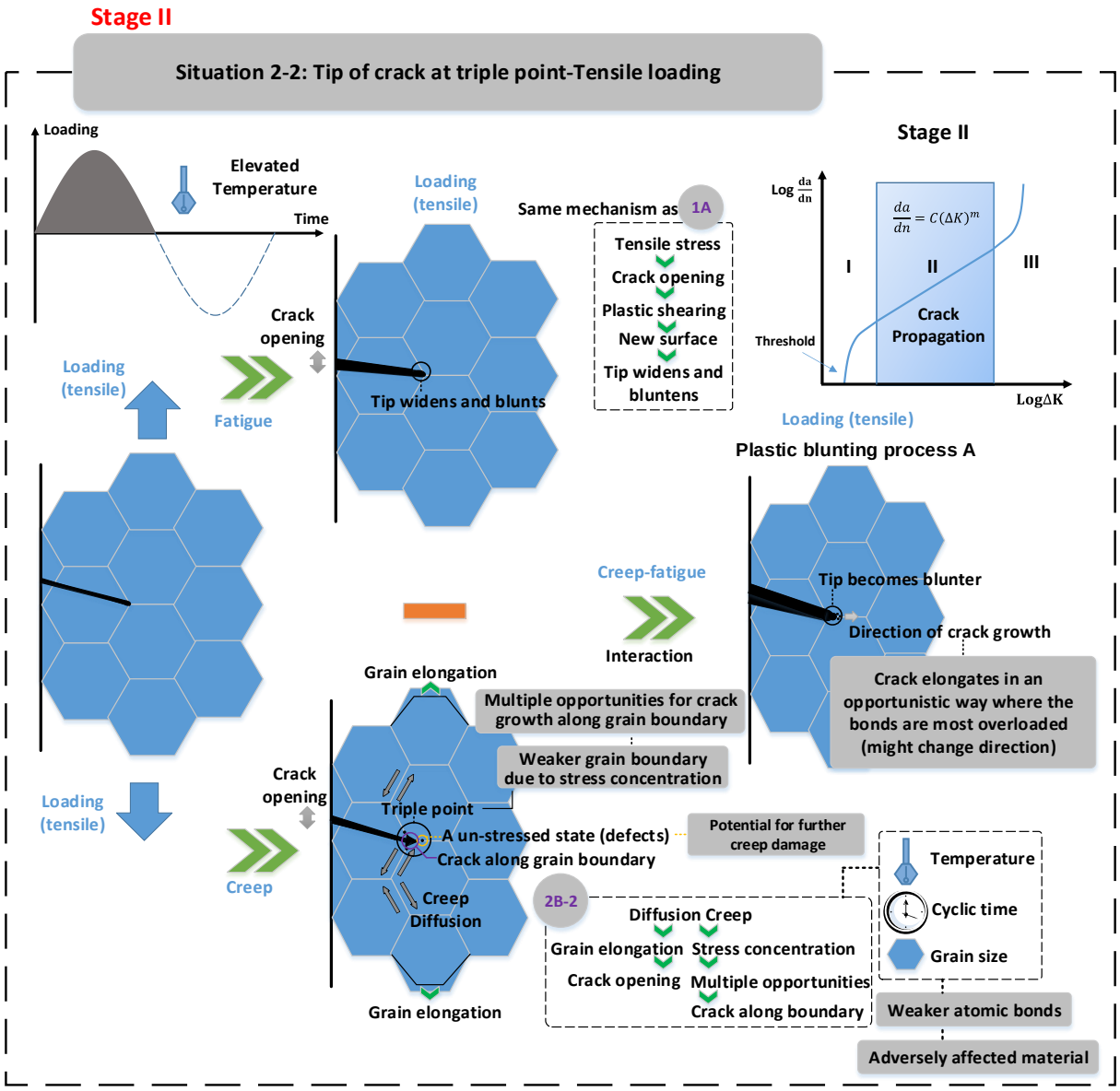

Figure 9.13 Crack tip at triple point-Tensile loading

Model for crack growth in the compressional regime

Under compressional loading (Fig.9.14), according to the idea of plastic blunting process, the crushing effect maintains the new crack surface created under the tensile situation, and thus the crack is extended along the grain boundary (2E-2 in Fig.9.14).

Crack growth at next cycle or next few cycles may have two possible paths (2F-2 in Fig.9.14). Specifically, on the one hand, a crack may grow traverse (or along) the grain boundary, where weakest atomic bonds are presented. This may be attributed to stress concentration at the grain boundary since the existence of the stress gradient results in the convergence of vacancies [111, 112], and in particular, the vacancies at the grain boundary give a favourable condition for diffusion creep [142, 143]. In this case, the crack along the grain boundary gradually

accumulates, and then reaches the next triple point, where the opportunity for re-direction is provided.

On the other hand, the crack may be deflected away from the grain boundary [144]. This behaviour is illustrated by Figure 3 from [139] and Figure 7 from [140]. This phenomenon may result from defects, such as vacancies in the grain or on its boundary and micro-cracks in the vicinity of the crack. These provide locations for re-direction of crack growth. Specifically, vacancies provides better conditions for diffusion creep, which has been discussed in the previous sections. In addition, the aggregation of micro-cracks, which are attached to the main crack, also contributes to crack deflection at the grain boundary. This phenomenon is identified as branching activities, and is illustrated by Figure 10 of Ref [145] and Figure 13 of Ref [146]. In this situation, a crack-based tree is constructed at the microstructural level, where the main crack is the trunk of this tree and micro-cracks form the branches. The weakest area normally appears at the region with the high density of the micro-cracks, and plays an important role in crack propagation. This is because the aggregation of micro-cracks weaves a crack net which offers multiple sites for shear strain under tensile loading. The shear stress at the inter-atomic level for any one crack is not decreased by having more micro-cracks. Consequently the crack net probes a larger volume of material for weaknesses than a single crack could do on its own. This promotes the main crack to automatically grow in a direction most favourable to increasing the total strain (hence most injurious to the integrity of the part).

In addition, the deviated progression may also be caused by the stress concentration at the grain boundary due to irregular configuration thereof. Specifically, this grain-boundary condition results in stress/strain pileup at the boundary (weak boundary condition is presented) and then leads to larger driving force for extending crack tip into the neighbouring grain, whereby the barrier of the grain boundary is overcome. This is consistent with the general understanding that cracks always propagate towards the direction which requires the minimum energy (stress).

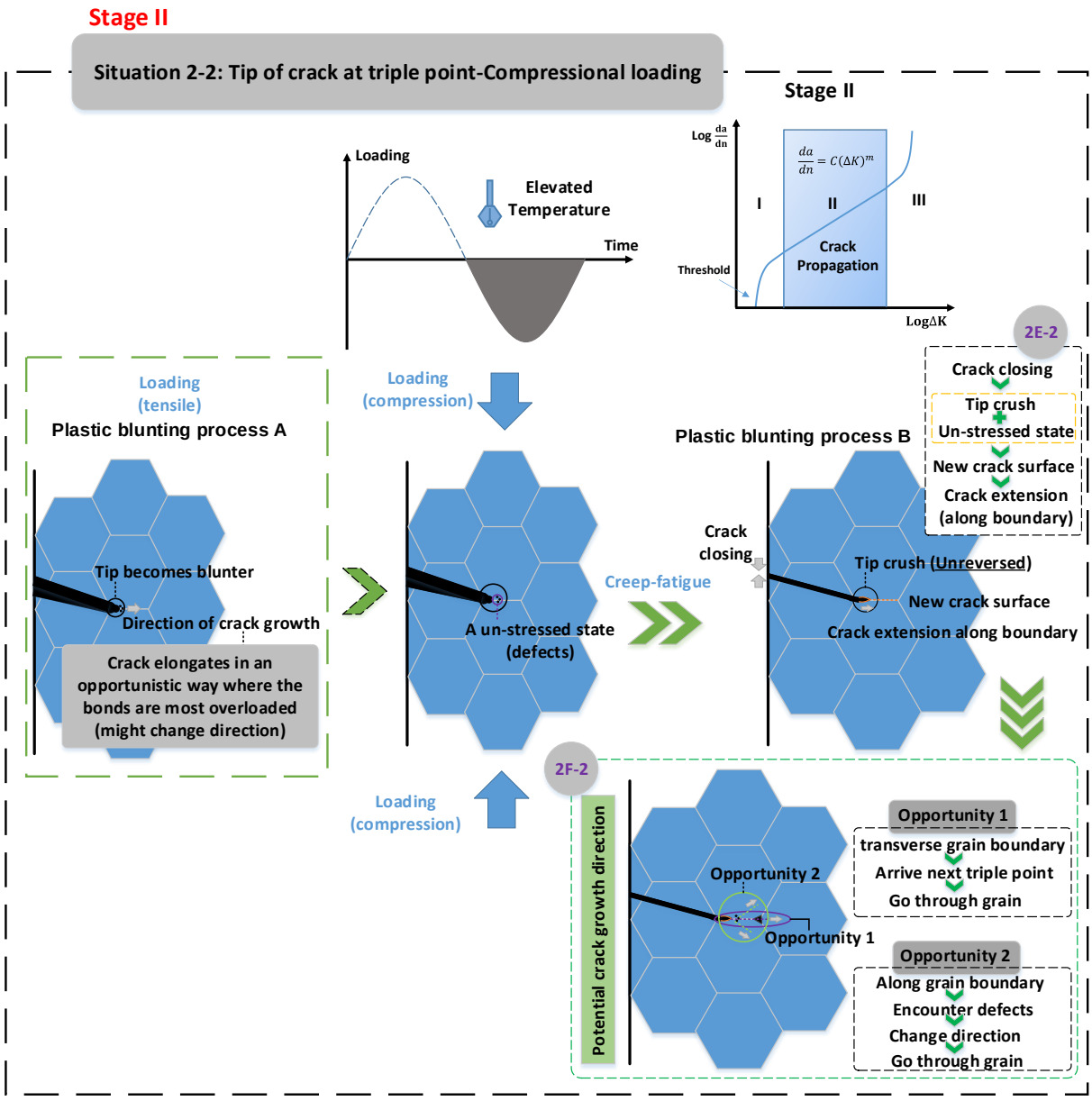

Figure 9.14 Crack tip at triple point-Compressional loading

These two situations reflect the fact that fatigue makes more contribution than creep in the present case (cyclic loading without hold time). Specifically, the first option implies that the tensile stress, which is perpendicular to grain boundary, provides a tearing stress to peel off the surface at the grain boundary. This is a significant fatigue behaviour, where the bonds at the grain boundary are further overloaded and then broken due to the previous damage caused by creep. In addition, the surface of grain boundary is normally not ideally smooth; the geometric anisotropy or defects at the grain boundary may cause that plastic strain to pile up at one specific point, which means that less stress is needed at this point to break the barrier and penetrate the grain boundary, thereby providing for re-direction for crack growth [147]. This transgranular behaviour is illustrated by Figure 4 of Ref [148].

After this process, crack goes through the grain boundary, and the crack tip is extended to the next grain, which is the third situation and examined below.

9.2.2.3 Crack tip through grain boundary

Model for crack growth in the tensile regime

Under tensile loading (Fig.9.15), the fatigue component experiences the same process shown in 'situation 1-1A' (Fig.9.7), where the new crack surface is produced due to plastic shearing effect, and then the crack tip widens and becomes blunt. For the creep partition (3B in Fig.9.15), on the one hand, diffusion creep gives grain elongation, which leads to crack opening due to configurational effect of the grain. On the other hand, the extension of the grain boundary caused by grain elongation gives a relative movement between two neighbouring grains, which generates shear stress along the grain boundary. In this case, a mismatch band at the grain boundary is generated due to the distortion of the existing crack under shearing conditions. This band may be further intensified due to pre-existing damage caused by the grain-boundary effect (shown in section 9.1.2.2 (1), situation 2-1). As a result, this mismatch band widens the crack body and further promotes the crack opening. Finally, the combination of fatigue and creep gives a blunter crack tip.

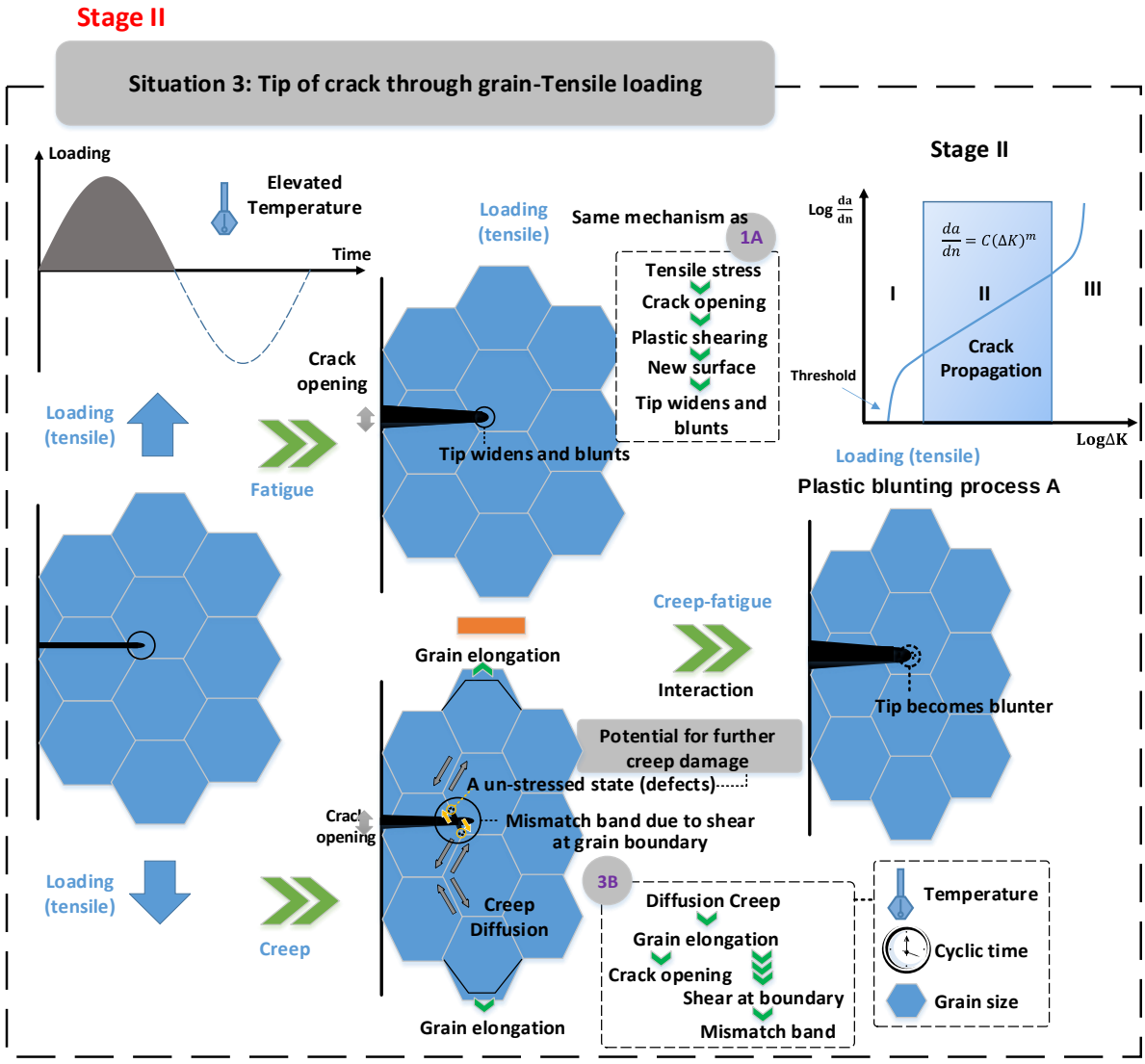

Figure 9.15 Crack tip through grain boundary-Tensile loading

Model for crack growth in the compressional regime

Under compressional loading (Fig.9.16), the crack-closure process maintains the new crack surface created under tensile loading. Meanwhile, the fatigue crack is extended during the process of crushing, and this is enhanced by any nearby defects in the material.

It is notable that the slip band may result in a re-direction of the crack within grains, following the slip bands inside the grain. We propose this is caused by the relative movements between slip planes under cyclic loading, which gives a better condition for crack growth along the slip planes. Microstructurally, at the surfaces of the slip bands, the atomic bonds are distorted and elongated under the reversed loading. Thus, these bonds become vulnerable, and then the weakest region (the surfaces of the slip bands) is formed. In this case, at these surfaces, the atomic bonds require the least effort to cut, which then results in crack propagation along the slip bands. The slip band activities are illustrated in Figure 11 of Ref [130], wherein the crack behaviour of re-direction within a grain is presented.

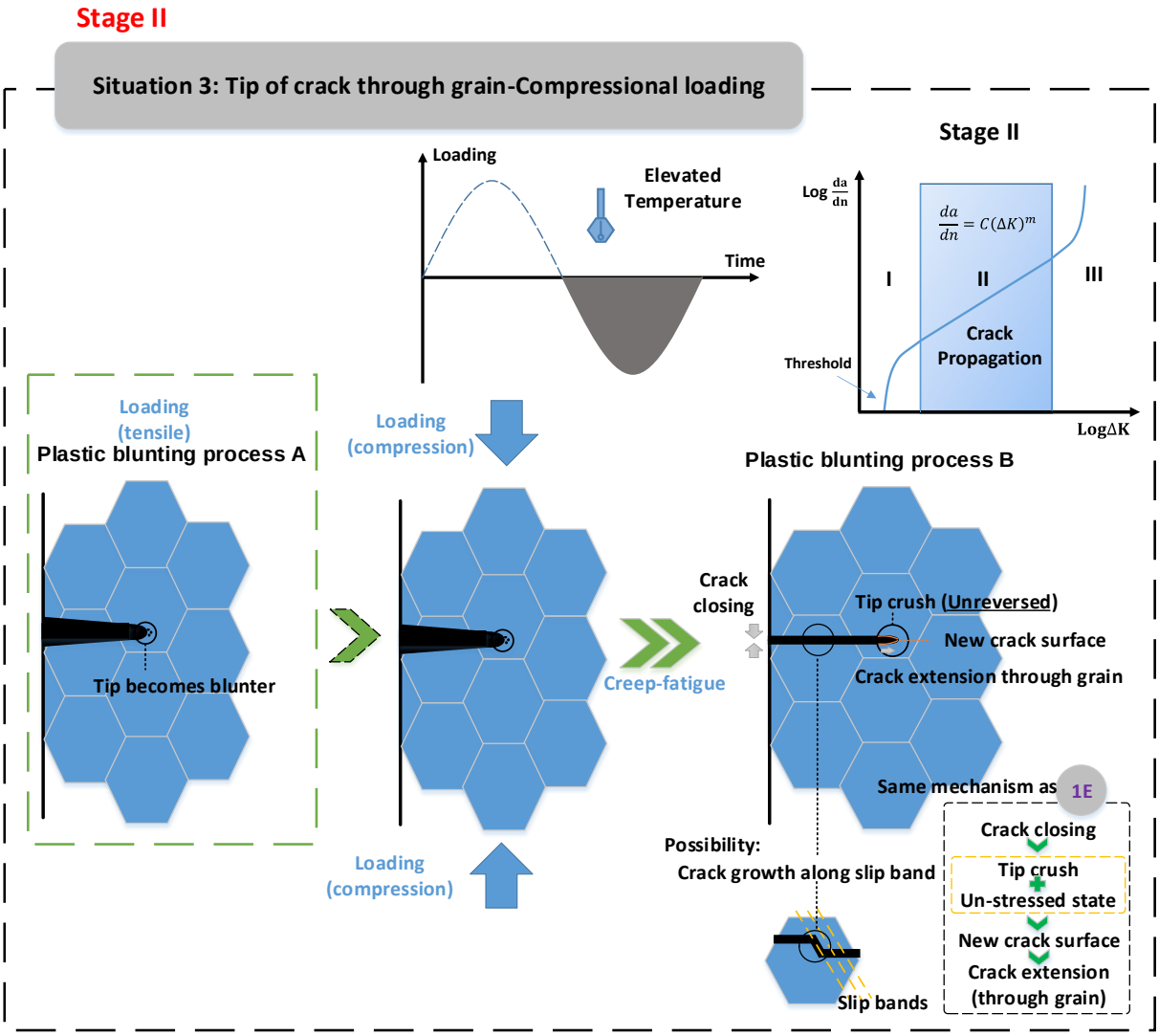

Figure 9.16 Crack tip through grain boundary-Compressional loading

9.2.3 Stage III: Structural failure

The final stage shown in Fig.9.17 illustrates the fracture of the engineering structure:

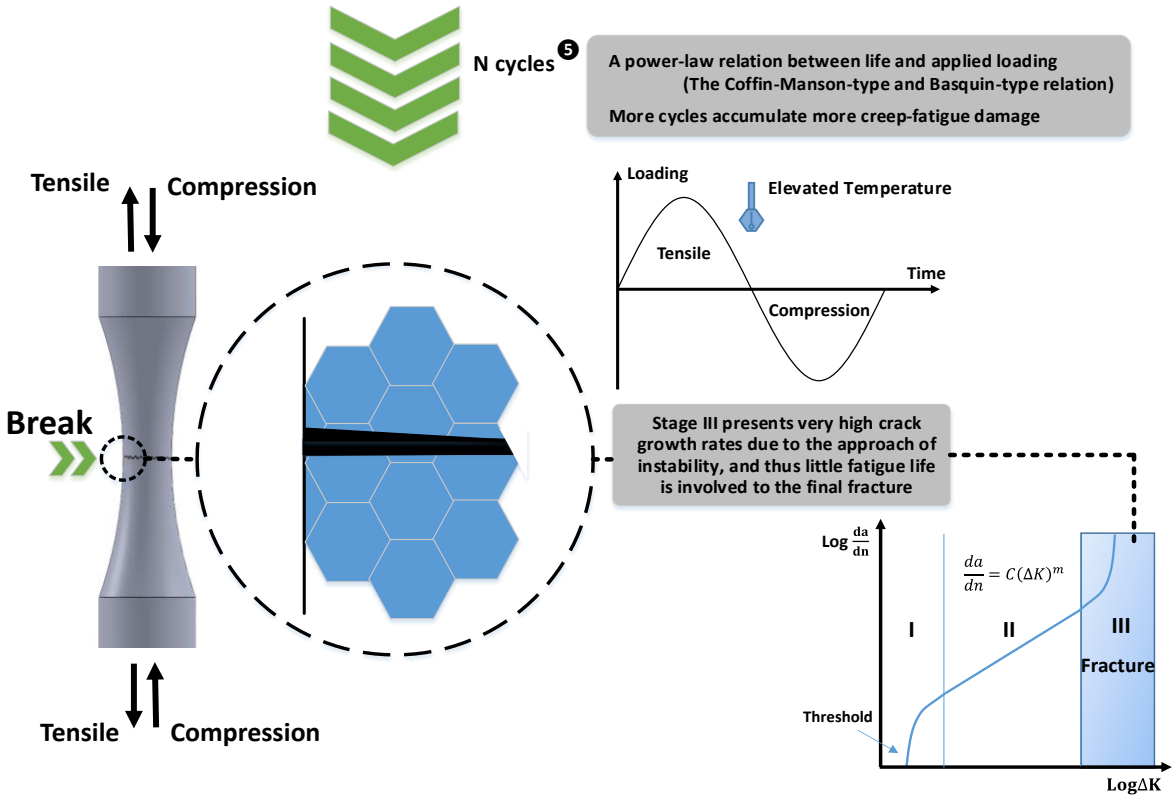

Figure 9.17 Structural failure

In this stage, crack growth rate rapidly increases, and part-separation commences when the total crack length reaches a critical value (final facture). This stage represents an unstable state, where the equilibrium shown in the second stage of crack growth is broken due to intensified accumulation of damage and reduction of remaining cross sectional area. This is attributed to a high stress field at the crack tip due to high stress intensity [117], hence the plastic zone becomes large compared to the crack size. Under this stress state, the plastic energy available exceeds that needed for producing the new crack surface. In this case, on the one hand, a part of the plastic energy is applied to create new crack surface; one the other hand, the rest of plastic energy is applied to form voids [117] (see Figure 4.11). Then, under the applied stress, these voids are further expanded and then coalesced by internal necking [149]. This phenomenon worsens the creep-fatigue resistance, and then leads to rapid growth of the crack. Therefore, in this stage, a small contribution of loading cycles leads to big creep-fatigue damage, which then results in failure.

During the process of crack growth, the creep-fatigue damage gradually accumulates with the increasing number of cycles, and this process is presented in a power-law relation (❺ in Fig.9.17). This is accommodated in the unified creep-fatigue equations, where a power-law relationship between life and the applied loading is shown. As discussed in section 9.2.2.1, the idea of crack tip plastic zone implies that the stress concentration around the crack tip plays an important role in crack growth. Specifically, the more stress is concentrated, the larger the

plastic zone, and then the more the crack is promoted. Therefore, we assume that the crack growth is a geometry-related behaviour, and the crack growth rate (crack growth in one cycle) may be related to the size of the plastic zone. Normally, the area of a zone can be presented as a second-order-power relation with a certain dimension, such as radius for circle and the length of a side for square. In this case, since the stress amplitude is directly related to size of the plastic zone, we believe that the applied loading can be related to the crack growth rate in a power-law form. In addition, this relation is also consistent with the idea of damage accumulation shown in Fig.9.18. In the first stage, the original steady state (a perfect body) is suddenly broken due to the large amount of accumulated energy, which implies at this stage a small amount of damage is produced with a large number of loading cycles (stage I in Fig.9.18). Then, after the process of re-balancing, the damage accumulation gives a relatively steady state, where the rate of accumulation stably increases (stage II in Fig.9.18). Finally, when the totally damage arrives at or close to a critical value, the load bearing capacity collapse in a short time. This stage implies that much damage is produced within a small number of loading cycles (stage III in Fig.9.18). The detailed physical explanation of this power-law relation will be represented in section 10.2.4.

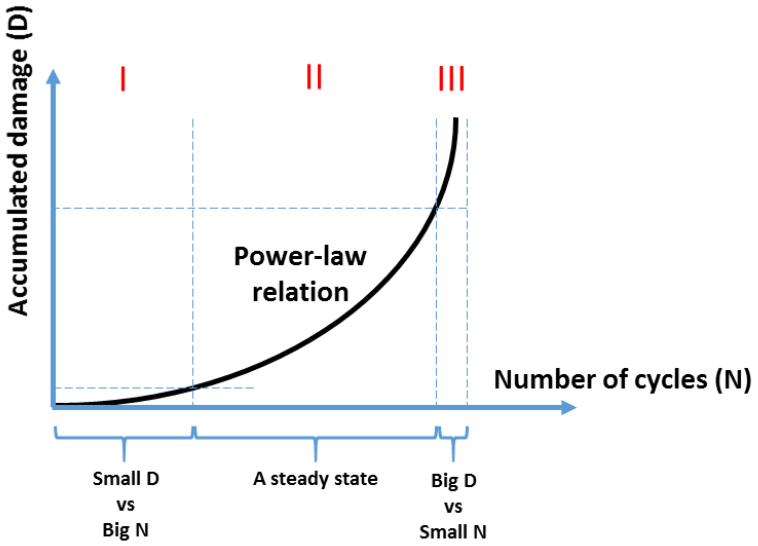

Figure 9.18 Damage accumulation

9.3 Summary

In this chapter, Based on the general understanding of crack-growth behaviour, a conceptual model has been proposed, and represented graphically, wherein fatigue and creep effects are treated separately due to the different damage principles. This conceptual model illustrates the process of damage accumulation from crack initiation to crack propagation then to structural failure. In particular, the analysis of crack propagation is mainly based on existing mechanisms of plastic blunting and diffusion creep. The possible grain-boundary behaviours, such as the mismatch behaviour at grain boundary due to creep deformation, are included. This model is

consistent with the various creep and fatigue microstructure observations in the literature, but goes further by integrating these premises and our proposed propositions together into a logically consistent framework that describes the overall failure process.

While the ideas of crack growth are well known, the literature does not provide a comprehensive explanation of the process from initiation to failure. The novel contribution of the above model is therefore the integration of multiple mechanisms at the microstructural level, inclusion of the grain boundary effect, and coverage of the stages from initiation to failure.

We have proposed a number of new mechanisms for crack growth (propositions A-G in section 9.2). Using these it has been possible to construct a comprehensive model of the crack growth process at the microstructural level. This model is also consistent with the existing concepts in the literature (premises a-l in section 9.2). Of itself this does not *prove* that these propositions are true, but it does show that these concepts are useful in better understanding the creep-fatigue mechanisms.

During the process of crack growth, the creep-related dependencies of temperature, cyclic time and grain size were mentioned, and the influences of them on creep-fatigue behaviour and the relationships between them (at a microstructure level) will be discussed in the next chapter (Chapter 10). In addition, we believe that this conceptual model still has the opportunity to be further modified as a deeper investigation of the creep-fatigue mechanism.

Chapter 10

10. Conceptualization of a general physical explanation of the unified creep-fatigue equation

This results chapter links the unified models to the underlying physical mechanisms, which is identified as the fundamental principle to make the unified creep-fatigue models superior to the existing models. In this chapter, the influences of temperature, cyclic time and grain size on creep-fatigue behaviour are discussed. Then the consistency between the unified formulations and the microstructural phenomena is investigated. This chapter strongly proves that the unified creep-fatigue model can present a better physical explanation.

Publications relevant to this chapter are as follows (see Appendix A for details):

(1) Liu, D. and D.J. Pons, Physical-Mechanism Exploration of the Low-Cycle Unified Creep-Fatigue Formulation. Metals, 2017. 7(9): p. 379.

The unified creep-fatigue equations were developed based on the combination of empirical-based and constitutive-based methods with a deliberate attempt throughout that was based on the underlying physical mechanisms. In this case, the unified equations are potential to be linked to the underlying physical mechanisms. This was proven in this chapter. Specifically, the investigation of fatigue and creep at a microstructural level indicates that elevated temperature or prolonged time produces more creep damage, and a larger grain size has a negative influence on fatigue resistance but is beneficial for creep. In particular, the grain-size effects on fatigue and creep were conceptually simulated by finite element analysis (FEA), which presents the same result as the physical phenomenon. Then, the relationships between the relevant variables (including temperature, cyclic time, applied loading and grain size) were linked to the physical mechanisms. For example, the linear relation between fatigue capacity and the temperature was derived from diffusion creep, and the applied loading is related to life

in a power-law relation based on the crack-growth behaviour. Consequently, the unified creep-fatigue equations were physically explained. To do this, we consider each of the main relationships (temperature dependence, etc.) for these two equations, and explore what the literature says about the mechanisms.

10.1 Underlying principle of creep fatigue at microstructural level

The creep-fatigue process presents the fatigue behaviour at elevated temperature, where the creep effect is active. Thus, a combined effect of fatigue and creep is presented. At the microstructural level, fatigue and creep behaviours show different principles. Generally, fatigue damage occurs via cracks through the grains, while creep damage involves the grain boundary cracking. This was simply explained in section 9.1. In the present work, the influences of temperature, frequency/cyclic time and grain size on creep fatigue were considered, and these factors were numerically formulated by the unified creep-fatigue models; the individual discussion follows.

10.1.1 Temperature dependence

Creep-fatigue damage is identified as the combined effect of creep and fatigue. According to the concept of fatigue capacity, the full fatigue capacity (for the pure-fatigue condition) is consumed due to increased creep damage. Temperature has a significant influence on creep, but presents a negligible effect on pure fatigue [76]. Therefore, the discussion of temperature dependence focuses on creep behaviour which is activated at 35% of the melting temperature [57]. In general, increasing temperature accelerates the process of creep damage, thus reduces the creep-fatigue capacity. This has been verified by numbers of creep-fatigue tests, such as the experiments conducted by Shi on 63Sn37Pb solder [53], Karakas on 2024-T3 aluminium alloy [87] and Fournier on Inconel 718 [95]. In addition, the influence of temperature on creep is also shown by a numerical formulation, the general creep equation:

$$\dot{\varepsilon} = \frac{A\sigma^m}{d^q} e^{-\frac{Q}{RT}} \tag{10.1}$$

This equation is consistent with the experimental results in the literature, where the increasing temperature is associated with greater plastic strain hence there is more creep damage.

Creep mechanisms are normally divided into Nabarro-Herring creep, Coble creep, grain boundary sliding and dislocation creep [8, 150]. Nabarro-Herring creep and Coble creep show a strong dependency on temperature, where the diffusional flow of atoms occurs under conditions of relatively high temperature. Grain boundary sliding involves displacements of grains against each other. This is the main mechanism for the creep failure of ceramics at high temperature because of the glassy-phase formation which provides a good sliding condition along the grain boundary. Therefore, this creep behaviour is not a major contributor to metals and hence is removed from further consideration here. Dislocation creep presents a drastic

dislocation through the crystal lattice, which results from both line defects and point defects at relatively low temperature. Therefore, high stress is needed, and small diffusional flow is involved. This process is highly sensitive to the applied stress on the material, but not temperature. This is indicated in Ref.[8], wherein a higher stress sensitive exponent is presented compared to the other three creep mechanisms. Based on the brief description of these four creep mechanisms shown above, the diffusion creep (including Nabarro-Herring creep and Coble creep), which has strong temperature dependence, is used to explain the influence of temperature on creep.

The temperature effect on creep fatigue is attributed to elevated temperature leading to weaker bonding between atoms at the grain boundary. This is due to better conditions for diffusion. Then this causes the movements of vacancies [142, 151, 152]. This transfer finally results in the overall deformation of the material. Specifically, a vacancy is defined as a point defect in a crystal, where an atom is missing from its original lattice site. During this process, an atom needs to overcome the energy barrier to move from its current site to the nearby vacant site. In this case, the high temperature can provide atoms enough energy to break the bonds with neighbouring atoms and then lead to the location transfer of atoms. This process can be identified as a thermodynamic system with a strong driving force of temperature for diffusion [150].

In addition, diffusion basically is a net movement of atoms from a high concentration region to a low concentration region. This reflects the initial driving force for the transfer of atoms. During this process, temperature is an important factor for determining the rate of diffusion, wherein elevated temperature speeds up the random atom motion, which gives the atom access to a greater physical volume of space, and the new atomic configuration opportunities that are provided. Consequently, increasing the temperature accelerates the process of diffusion (more creep damage occurs) and then reduces the fatigue capacity for the creep-fatigue condition.

Creep-fatigue damage occurs when material experiences reversed loading at high temperatures (higher than 0.35 of the melting temperature), where the reduction of fatigue capacity is mainly due to the creep effect. This is the regime (the creep-fatigue condition) discussed in our research. When the temperature is lower than 0.35 of the melting temperature (the reference temperature), the temperature shows a slight effect on fatigue, thus creep effect is identified as being dormant. This is consistent with the investigation on 21 different carbon and alloy steels, wherein a temperature factor was introduced to modify the fatigue life [76]. Specifically, the magnitude of this factor decreases drastically from 1 (such as 0.549 at 600℃) when the temperature is higher than the reference temperature, and this regime, the creep-fatigue condition, has been discussed above. While the temperature factor only varies between 1 and 1.025 under the reference temperature, this regime is defined as the pure-fatigue condition where fatigue is slightly influenced by temperature. Hence temperature dependence is ignored (not the field in our research). The weak temperature dependence for pure fatigue could be related to oxidation. At elevated temperature, the crack surface is oxidized, and then the material becomes more brittle. This results in further crack propagation. The rate of oxidation at low temperature is much lower than the situation at high temperature, which implies weak influence on fatigue due to the low diffusivity of oxygen. To be specific, the diffusivity depends on the temperature

in the way of *exp(-C/T)*, where the oxidant diffusivity exponentially increases at high temperature while exponentially decreases at low temperature. This physically results in the dramatic deduction of fatigue capacity under high temperature (the creep-fatigue condition). In addition, the activation and acceleration of the creep effect could also be attributed to the behaviour of atomic vibrations [110]. Specifically, atomic vibration is accelerated (also the internal energy is increased) with rising temperature, where a favourable condition to break the bonds between atoms is provided. By this means, the creep effect is intensified, and fatigue capacity is reduced with increased temperature. In particular, the threshold temperature above which creep effect is active is identified as 35% of the melting temperature, and is included in the unified models as the reference temperature.

Consequently, the increasing temperature accelerates the process of diffusion (more creep damage occurs), and then reduces the fatigue capacity at the creep-fatigue condition.

10.1.2 Frequency/cyclic time dependence

In the present work, the frequency/cyclic time is limited to a range typical for general engineering situations. Thus, the influence of frequency/cyclic time on the pure-fatigue life is ignored [76], and the discussion of frequency/cyclic time effect is based on the creep behaviour.

Creep is normally defined as a time-dependent deformation under constant loading, which indicates that creep damage is intensified with increasing time. This general influence of frequency/cyclic time on fatigue capacity could be explained through the transient-creep-plus-elastic model shown in Fig.10.1 [8], where σ [MPa] is the applied stress. In this model, a high frequency load (which is related to elastic strain rate) primarily causes deformation of spring S_2. This is because of the dynamic resistance effect of dashpot (η_1[MPa]). Hence the slope of the stress-strain curve is S_2[N/m]. However, low frequency loads (events over longer time) cause the deformation of both springs S_1 and S_2, and the dashpot is relatively inconsequential. In this case, the strain (ε[m/m]) may be expressed as:

$$\varepsilon = \frac{\sigma}{S_1} + \frac{\sigma - \eta_1}{S_2} \tag{10.2}$$

Eq.10.2 shows that the slope (S_e[N/m]) of the stress-strain curve is $S_1S_2/(S_1+S_2)$, which is smaller than S_2. This implies that a longer time can reduce stiffness, and then increase strain (at a given stress) and lead to more creep damage.

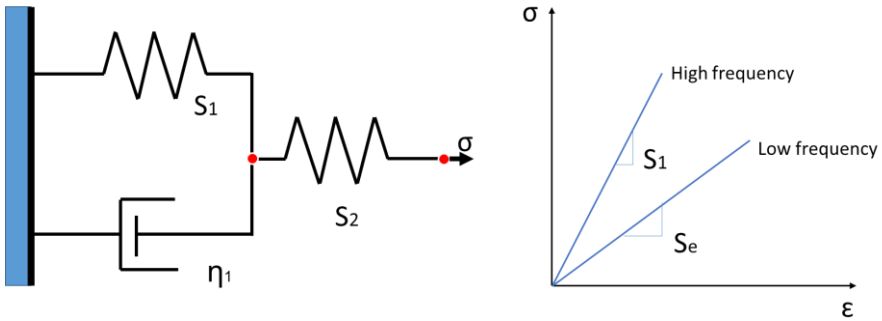

Figure 10.1 The transient-creep-plus-elastic model

The influence of frequency/cyclic time was initially formulated by the frequency-modified Coffin-Manson equation based on the experimental results at elevated temperature, wherein the creep effect in terms of time was involved.

$$\varepsilon_p = C\left(N_f f^{k-1}\right)^{-\beta_0} \tag{10.3}$$

where ε_p is the plastic strain, N_f is the number of cycles, C is the fatigue strength coefficient, β_0 is the fatigue strength exponent, f is the frequency and k is a constant obtained from experiments. This equation implies that decreased frequency (increased cyclic time) reduces fatigue capacity due to the increased contribution of creep damage.

Consequently, low frequency (large cyclic time) gives more accumulation of creep under a given temperature and loading. In other words, longer time leads to more diffusion in microstructure when a material is exposed to high temperature under constant applied loading, and then produces more creep-fatigue damage.

10.1.3 Grain-size dependence

Grain size has a significant influence on both fatigue damage and creep damage, but the opposite effects are presented. Generally, smaller grain size is more positive for the pure-fatigue resistance, while bigger grain size is more beneficial for the pure-creep ductility [8]. This phenomenon results from the different failure mechanisms shown by fatigue and creep.

Fatigue failure is caused by the progressive accumulation of plastic deformation under cyclic loading. During fatigue process, cracks initiate at the early stage and then gradually propagate through grain boundary with the increasing number of cycles. It is easy to understand that the propagation of the crack needs to penetrate the grain boundary to extend to the next grain, and this may also require a reorientation of the crack growth direction. This means that the more grains the crack encounters the slower the progression of fatigue failure, and hence greater loading (stress or strain) is required to make the crack achieve the critical length of failure. This relation is also formulated through the Hall-Petch-type equation (Eq.10.4):

$$\sigma_s = \sigma_0{}' + \frac{k}{\sqrt{d}} \tag{10.4}$$

where σ_s is the fatigue strength (fatigue limit), and $\sigma_0{}'$ and k are constants. This equation shows that the fatigue strength increases with decreased grain size.

As mentioned above, the grain boundary is the barrier for the propagation of the crack under the pure-fatigue condition. However, the grain boundary becomes the source of creep damage at the pure-creep condition [150]. Since the stress concentration is intensive in the intersection point among three adjacent grains (a geometric stress concentration effect), the crack growth along the grain boundary is promoted at these triple points [126-128]. Consequently, the triple point provides an opportunity for further crack propagation under creep, even on the grounds of geometric considerations alone. Also relevant to note is that the triple point contains crystalline defects, where multiple directional opportunities for crack propagation along the

grain boundaries are provided. In this way, the finer the grain size, the greater the internal area of grain boundaries and volumetric density of triple points, hence enhancing the opportunity for crack propagation under creep. In contrast a body with a few grains, or even only one grain, presents fewer such boundary opportunities. In addition, the influence of grain size on creep could also be explained by the physical mechanism of diffusion creep. Specifically, atomic diffusion causes the elongation of grain along the stress axis, which implies finer grain size produces more significant deformation than coarse grain size under a given stress within the same area. In particular, the influence of grain size on creep is numerically formulated through the general creep equation (Eq.10.1), where a bigger grain size results in a smaller strain rate, and thus less creep damage is given during a given time.

We propose, based on considerations of how the element-based cracks are structured, that the extended finite element method (XFEM) is suitable for modelling fatigue, and the Cohesive Zone Material (CZM) method for creep. This novel proposition is justified below.

The FEA literature shows that XFEM-based and CZM-based methods are used interchangeably for both creep and fatigue loading situations [153, 154]. There is no prior article identifying that XFEM-based and CZM-based methods may be specific to fatigue and creep behaviours respectively. Our reasoning is that the XFEM crack-growth simulation technique is suitable for simulating fatigue crack propagation because it shows the crack propagating through elements (shown in Appendix C). We believe this is comparable to crack propagation through grains in the pure-fatigue situation. On the other hand, the CZM (Cohesive Zone Material) model, which presents a crack, grows along the boundaries of elements, is applied to simulate creep-crack growth (shown in Appendix D). During the process of simulation, the grain is modelled by an element, and thus the coarse element presents a big grain size and the finer element shows a small grain size. Compared to coarse element, the finer element was obtained through increasing the number of divisions in the length or width direction, hence relatively smaller sizes were used for the elements, as well as the grains. Then, the geometries with small grain size and big grain size are used to perform simulation under the same applied force (7.5N).

On the one hand, at the pure-fatigue condition, the results (obtained through the XFEM-based method) for coarse and finer grain sizes under the applied force are shown in Table 10.1.

Table 10.1 Simulation results for grain-size effect on fatigue

Condition: fatigue	The same applied force [7.5N]		
	Max Strain	Max Pseudo Deformation	Max Pseudo Stress
Small grain size	0.003198	0.091784	417.36
Big grain size	0.005022	0.199358	638.07

Table 10.1 shows that small grain size benefits the fatigue capacity. Specifically, when the same applied force is applied, the material with small grain size gives smaller damage (strain/deformation) and presents smaller stress than the material with large grain size. This implies that the material with small grain size has better ability against deformation and better

stress response against fracture. The results are consistent with the general understanding of grain-size effect on fatigue.

On the other hand, at the pure-creep condition, the results (obtained through the CZM-based method) for coarse and finer grain sizes under the same force are shown in Table 10.2.

Table 10.2 Simulation results for grain-size effect on creep

Condition: creep	The same applied force [7.5N]		
	Max Strain	Max Deformation	Max Stress
Small grain size	0.0042559	0.9311 mm	745 MPa
Big grain size	0.0029548	0.77826 mm	510 MPa

Table 10.2 indicates that large grain size benefits the creep capacity, specifically, the material with large grain size gives smaller damage (strain/deformation) and presents smaller stress than the material with small grain size under the same applied force. This implies that the material with large grain size has better ability against deformation and better stress response against fracture. The results are consistent with the general understanding of grain-size effect on creep.

Our proposed explanation is that for small grains the amount of grain boundary is larger relative to the internal area/volume enclosed. The coupling between adjacent elements occurs through the element boundary and the vertices (which correspond to triple points in real grains). The more the (linear) area of element boundaries, and the closer these vertices, the *stiffer* the structure. Hence for smaller elements (or grains) more of the imposed load is carried by the boundary structure, and correspondingly less stress (or strain) is experienced *inside* the grain. This idealisation explains the simulation results, which indicate that the smaller elements are more beneficial for trans-element crack-growth behaviour and more negative for crack-growth behaviour along element boundary. Consequently, the grain-size effects obtained from FEA are consistent with the general understanding of the creep and fatigue phenomena.

According to the above discussion, it is clear that the influences of grain size on fatigue and creep are contrary, and thus the combined effect of fatigue and creep on the creep-fatigue life should be determined by the proportion of fatigue contribution and creep contribution. The research conducted by Hatanaka & Yamada [155], Hattori et al. [156] and Pieraggi & Uginet [157] show that the fatigue strength (fatigue capacity) reduces with increasing grain size. This implies that the fatigue effect makes more contribution to the creep-fatigue damage than creep effect at the creep-fatigue condition with the zero-hold-time cyclic loading and relatively short cyclic time (the situation presented in the present work). This may be because the total failure time is too short to produce major creep damage in the low-cycle regime. We could imagine that, for the situation of cyclic loading with hold time or relatively long cyclic time, the contribution of creep effect would increase. In particular, this contribution would be further intensified by the prolongation of hold time or cyclic time. Finally, if the creep effect becomes more significant than the fatigue effect, the bigger grain size would have more benefits for creep-fatigue behaviour.

The grain-size effect on creep-fatigue behaviour also could be expressed through a numerical relation. Generally, according to previous research into the grain-size effect on creep-fatigue behaviour, fatigue capacity can be related to grain size in a power-law relation: $N_{creep-fatigue} \propto d^n$. The exponent of this relation (n) depends on the contribution ratio of creep to fatigue ($D_{creep}/D_{fatigue}$). Specifically, when $\frac{D_{creep}}{D_{fatigue}} < 1$, then $n < 0$, which implies that fatigue makes more of a contribution to creep-fatigue damage, and small grain size is positive for life; when $\frac{D_{creep}}{D_{fatigue}} > 1$, then $n > 0$, which shows that creep contributes more damage to creep fatigue, and big grain size is beneficial for life; when $\frac{D_{creep}}{D_{fatigue}} = 1$, then $n = 0$, and this presents a balanced situation between the contributions of creep and fatigue.

Overall, creep-fatigue behaviour has significant dependencies of temperature, frequency /cyclic time and grain size. In general, elevated temperature or prolonged cyclic time intensifies creep damage, then reduces fatigue capacity at the creep-fatigue situation. In addition, the grain-size dependence presents opposite effects on fatigue and creep. Specifically, the smaller grain size is beneficial for fatigue but is negative for creep. In this case, the grain-size effect on creep-fatigue behaviour depends on the contribution ratio of creep to fatigue.

10.2 Analysis of the relationships in the unified creep-fatigue equations

The conventional creep and fatigue models were normally derived from empirical data and were then fully verified in multiple situations for multiple materials. Since the relationships between different variables shown in the unified creep-fatigue equations were derived from conventional models, we assume that these relationships are potential to well agree with the underlying physical mechanisms. This assumption was proved in this section. Note that this discussion mainly focuses on the strain-based model since the low-cycle loading regime is more common in service.

10.2.1 Relationship between temperature and applied loading

(1) The strain-based unified creep-fatigue equation

There is a need to explain why this equation shows a linear relationship between temperature and strain, and to identify whether there is any physical basis for this. The unified creep-fatigue equation can be reorganized to the form:

$$\varepsilon_p = C_0 N^{-\beta_0} - \left[c_1(\sigma)\left(T - T_{ref}\right) + c_2 \log\left(t_c/t_{ref}\right)\right] \cdot \left[A\left(d/d_{ref}\right)^m\right] C_0 N^{-\beta_0} \qquad (10.5)$$

The first term in Eq.10.5 shows the full fatigue capacity, and the second term reflects the strain caused by the creep effect. Significantly, a linear relationship is presented between temperature

and applied plastic strain ε_p (also creep-related strain), which is consistent with creep behaviour shown by empirical data and the physical mechanism.

On the one hand, a linear relationship between temperature and strain (ε_p) is presented through experimental data, which is validated for 63Sn37Pb solder [53] and GP91 casting steel [100] materials. The data on these two materials at a life of 5000 cycles are tabulated in Table 10.3. Then, the linear relationship between temperature and strain is well represented in Fig.10.2 with a good quality of linear fitting, wherein R^2 is 0.9932 for 63Sn37Pb solder and 0.9946 for GP91 casting steel.

Table 10.3 Data of temperature-strain relation for 63Sn37Pb and GP91 casting steel

Materials	Temperature (K)	Strain	Cyclic time (s)	Life (cycles)
63Sn37Pb	233	0.00412	1	5000
	298	0.00364		
	248	0.00332		
	398	0.00307		
GP91 casting steel	673	0.00317	20	5000
	823	0.00199		
	873	0.00174		

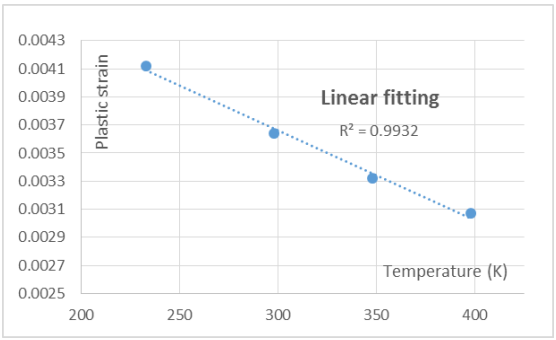

(a) 63Sn37Pb

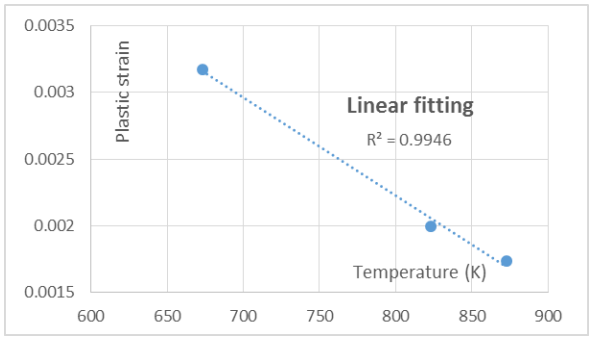

(b) GP91 casting steel

Figure 10.2 Curve fitting of temperature vs. strain: (a) 63Sn37Pb; (b) GP91 casting steel

On the other hand, this linear relationship between temperature and strain is also represented by the underlying physical mechanism. According to the brief description of four different creep mechanisms (including Nabarro-Herring creep, Coble creep, grain boundary sliding and dislocation creep) in section 9.2, the diffusion creep (including Nabarro-Herring creep and Coble creep) is regarded as the main creep mechanism for creep-fatigue behaviour since it has a strong temperature dependence. Therefore, the discussion of temperature-strain relation is built on the mechanism of diffusion. Generally, diffusion is caused by movement due to vacancy. During this process, the bonds between an atom and its neighbours are cut, and then

new bonds are built when this atom moves to the nearby vacant site. This process can be identified as a thermodynamic system due to the strong driving force of temperature for diffusion. In this case, a piece of crystal containing *n* atoms is selected, wherein an atom inside is transferred to the surface due to diffusion (Fig.10.3), and thus a vacancy is formed [151]. Gibbs free energy, which shows the thermodynamic potential to form this vacancy under the situation with a given pressure and a given temperature, is represented by Eq.10.6.

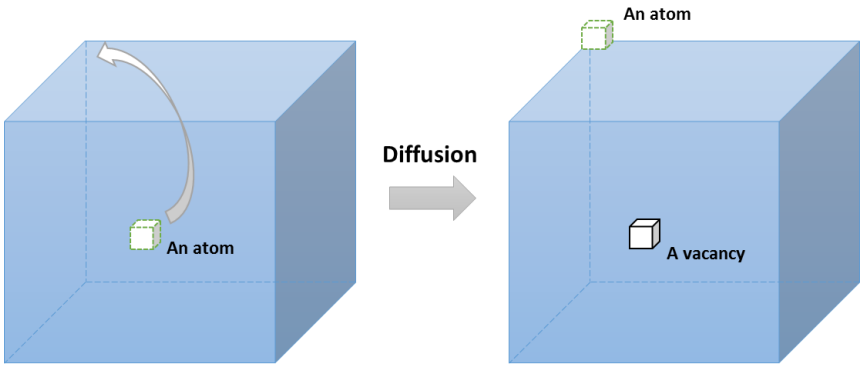

Figure 10.3 A movement of an atom

$$\Delta G_f = \Delta E_f + P\Delta V_f - T\Delta S_f \tag{10.6}$$

where ΔG_f is the Gibbs free energy for formation of a vacancy, ΔE_f is the change in internal energy due to formation of a vacancy, ΔV_f is the volume of a vacancy, ΔS_f is the entropy for formation of a vacancy, P is the pressure and T is the temperature. If n_v vacancies are formed during the process of diffusion, the total change in free energy is presented by Eq.10.7:

$$\Delta G = n_v \Delta G_f - T\Delta S_c \tag{10.7}$$

where ΔG is the total change in free energy and ΔS_c is configurational entropy. This configurational entropy is caused by the fact that n_v vacancies can be located among the *n* sites with *W* different ways, and thus ΔS_c is given by Eq.10.8:

$$\Delta S_c = k \ln W \tag{10.8}$$

where *k* is the Boltzmann's constant. According to the definition of configurational entropy, *W* can be defined as:

$$W = C_n^{n_v} = \frac{n!}{(n-n_v)!\,n_v!} \tag{10.9}$$

Then, the free energy shown by Eq.10.7 is reorganized as:

$$\Delta G = n_v \Delta G_f - kT \ln\left[\frac{n!}{(n-n_v)!\,n_v!}\right] \tag{10.10}$$

By using Stirling's equation:

$$\ln(x!) \approx x \ln x - x + O(\ln x) \tag{10.11}$$

Eq.10.10 can be simplified and approximated as Eq.10.12 by assuming $n \ll n_v$:

$$\Delta G \approx n_v \Delta G_f - kTn_v \left(1 + \ln \frac{n}{n_v}\right) \tag{10.12}$$

This equation shows that the total free energy has a vacancy-number dependence, and thus this free energy varies during the process of transfer. Normally, the minimum value occurs at the two ends of movements, where an equilibrium situation is achieved and is numerically represented through letting $\partial \Delta G / \partial n_v = 0$. Then, this operation gives the equilibrium atomic fraction of vacancies:

$$N_v = \frac{n_v}{n} = exp\left(-\frac{\Delta G_f}{kT}\right) \tag{10.13}$$

Normally, diffusion is numerically described by Fick's law [158]:

$$J = -D \frac{d\varphi}{dx} \tag{10.14}$$

where J is the diffusion flux which shows that the amount of substance flowing through a unit area at a unit time, D is the diffusion coefficient, x is the position and φ reflects the concentration of vacancies. In particular, φ is defined as the number of vacancies per unit volume, and thus is related to the atomic fraction by Eq.10.15:

$$\varphi = \frac{N_v}{\Omega} \tag{10.15}$$

where Ω is the atomic volume. Therefore, a natural exponential relation between the diffusion flux and the temperature component can be presented:

$$J \propto exp(-1/T) \tag{10.16}$$

Since the creep process indicates that diffusion finally leads to overall deformation, the strain caused by creep is related to temperature dependence in a natural exponential relation. Then, based on the concept of fatigue capacity, this relation is reasonably extended to show the relationship between temperature and applied loading (strain):

$$\varepsilon \propto exp(-1/T) \tag{10.17}$$

The expression of $exp(1/T)$ can be simplified as a linear dependence when the temperature is relatively high enough and within the application range (normally the range of experimental investigation). For example, for the GP91 casting steel, with a temperature range of 650K to 1000K, a linear relation between temperature and $exp(1/T)$ is illustrated (Fig.10.4), wherein a small linear fitting error (R^2=0.9849) is given.

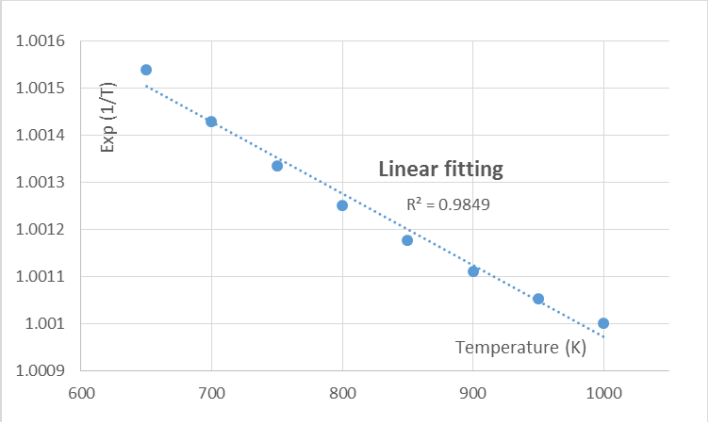

Figure 10.4 A linear relation between temperature (T) and $exp(1/T)$

Therefore, we conclude that the underlying physical mechanism is that diffusion of atoms is based on considerations of free energy and vacancies formation. The literature shows that this mechanism is represented by an exponential dependence of the form $\varepsilon \propto exp(-1/T)$. We propose that the physical explanation is that the ability of an atom to diffuse is based on the volume of space containing vacancies that it can recruit (hence an exponential relationship), and on the rate at which vacancies form within that space. The latter requires an activation energy, hence is dependent on temperature to achieve the necessary mobility at the atomic level. The formation of vacancies is therefore retarded at low temperatures, becomes active at intermediate temperatures, and is saturated at sufficiently high temperature (all available vacancies have been formed), hence the $exp(-1/T)$ form of the relationship. At sufficiently high temperature the saturation causes this to simplify to a linear relation. Therefore, the creep-related strain is linearly proportional to temperature, and the overall fatigue capacity is reduced by a thermal effect, hence giving rise to the $c_1(\sigma)(T - T_{ref})$ term in the unified formulation:

$$\varepsilon_p = C_0\left\{1 - \left[c_1(\sigma)(T - T_{ref}) + c_2(\sigma)\log(t_c/t_{ref})\right]\cdot\left[A(d/d_{ref})^m\right]\right\}N^{-\beta_0}$$

Linear relation

Hence, we conclude that the strain-based unified creep-fatigue equation has a plausible physical basis for the temperature relationship. However, the stress-based form of the equation has a different representation for temperature, and this is explained next.

(2) The stress-based unified creep-fatigue equation

A numerical simplification was not applied to the stress-based formulation to present the relationship of temperature vs. stress (applied loading). This is because a different structure (compared to the strain-based formulation) was constituted to describe creep-fatigue behaviour in terms of stress. In the stress-based unified creep-fatigue equation, the temperature term is presented in a natural-exponent form. Since this presentation was extracted from the creep behaviour, thus the natural-exponent formula shown here gives the relation between temperature and stress that causes creep damage.

On the one hand, this natural exponent relationship is consistent with the empirical data of creep, which is well represented by the Arrhenius equation:

$$\dot{\varepsilon} = Ae^{-\frac{Q}{RT}} \tag{10.18}$$

where $\dot{\varepsilon}$ is the creep strain rate, Q is the activation energy, R is the universal gas constant, T is the temperature and A is the constant. This equation has good physical basis, and was verified in multiple situations for multiple materials. Therefore, it is believed that the natural exponential relationship agrees well with empirical data.

On the other hand, according to Eq.10.17, there is a natural exponential relationship between strain and temperature, and this relationship can be extended to the stress-temperature relation (Eq.10.19) by introducing the proportional relation between stress and strain (the Ramberg–Osgood relation). Fundamentally, this transformation is based on the concept of compatibility. In this case, it can be concluded that this natural exponential relationship is consistent with the underlying physical mechanism of creep, and a natural exponential relationship of temperature vs. stress (applied loading) is presented.

$$\varepsilon \xrightarrow{stress-strain\ relation} \sigma \propto exp(1/T) \tag{10.19}$$

Overall, we conclude that the phenomenon of diffusion creep presents a natural exponential relationship between temperature and stress: $\sigma \propto exp(1/T)$, which is consistent with the relationship shown in our unified formulation:

$$\sigma = \sigma_0 \cdot (d/d_{ref})^m \left\{1 - A \cdot \left[(d/d_{ref})^n \cdot f_m^a \cdot \sigma^a \cdot e^{\frac{Q'}{T-T_{ref}}} \cdot (t_c/t_{ref})\right]^k\right\} \cdot N_f^{-b_0}$$

National exponential relation

Hence, the stress-based unified creep-fatigue equation has a plausible physical explanation for the temperature relationship.

10.2.2 Relation between temperature and cyclic time

(1) The strain-based unified creep-fatigue equation

The dependencies of temperature and cyclic time have a significant influence on creep-fatigue behaviour, and a logarithmical relation between them is presented in the strain-based creep-fatigue equation. This is consistent with the relation obtained from experimental data and reflects the underlying creep mechanism.

On the one hand, the logarithmical relation between temperature and cyclic time can be derived from empirical data, and this is verified by the data on the materials of 63Sn37Pb solder [53] and stainless steel 316 [89]. Although it is difficult to directly derive this relation through the experimental data extracted from the literature, this relation could be indirectly proved by fitting cyclic time against the strain. The creep-fatigue data on the materials for the life of 5000 cycles are tabulated in Table 10.4, and the curve-fitting results are then presented in Fig.10.5.

Table 10.4 Data of cyclic time/strain rate-strain relation for 63Sn37Pb and SS316

Materials	Cyclic time (s)	Strain	Temperature (K)	Life (cycles)
63Sn37Pb	10	0.00344	298	5000
	100	0.00298		
	1000	0.00243		
Materials	Strain rate (%/min)	Strain	Temperature (K)	Life (cycles)
Stainless steel 316	0.4	0.00218	973	5000
	4	0.00253		
	40	0.00309		

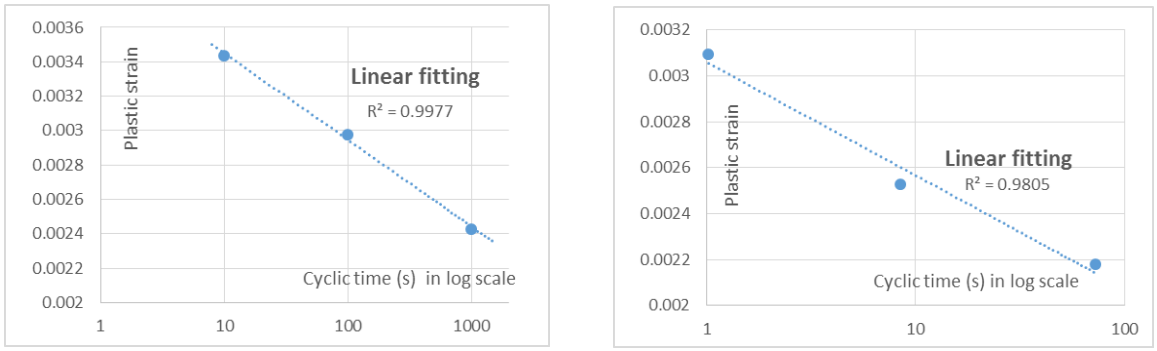

(a) 63Sn37Pb (b) Stainless steel 316

Figure 10.5 Curve fitting of cyclic time vs. strain: (a) 63Sn37Pb; (b) stainless steel 316

Fig.10.5 illustrates a good linear fitting between strain and the log of cyclic time, which implies a logarithmical relation between cyclic time and strain. Then, this logarithmical relation can be extended to the temperature-cyclic time relation based on the linear relationship between strain and temperature, which has been proven in section 10.2.1.

On the other hand, this logarithmical relation between temperature and cyclic time is also represented by the underlying creep mechanism. As shown in section 10.2.1, the diffusion-creep behaviour gives the logarithmical relationship between temperature and diffusion flux (shown in Eq.10.16). The definition of 'diffusion flux' indicates that this term measures the amount of substance (such as atoms) flowing through a cross sectional area during a unit time. Thus, a time dependence is included in this parameter in the form of a rate function. Then, Eq.10.16 can be presented as:

$$J = \frac{dD_v}{dt} \propto exp(-1/T) \tag{10.20}$$

where D_v reflects the amount of substance flowing through a unit area. Significantly, Eq.10.20 gives a logarithmical relation between temperature and cyclic time, and this is consistent with

the relationship shown by the strain-based unified creep-fatigue equation. In addition, this logarithmical relationship is also presented by a well-known time-temperature parameter, the Larson-Miller Parameter. In particular, this parameter is built on the principle shown by Eq.10.18 (the Arrhenius equation), and thus has a strong physical basis. This implies that it is reasonable to present the temperature-time relation in a logarithmical relation.

The logarithmical relation for cyclic time is also represented by another conventional time-temperature parameter, the Manson-Haferd Parameter, wherein the time dependence is addressed as rupture time. Specifically, the integrated characteristic indicates that the strain-based unified equation can be reorganized to the Manson-Haferd Parameter under the pure-creep condition, where a logarithmical temperature-time relation is presented. Although this time-temperature parameter was totally derived from empirical data (no physical basis) [8], it has been successfully validated on different materials and thus is believed to have a good ability for describing creep behaviours [35]. In addition, the pure-creep condition could be regarded as the idealisation of a creep-fatigue situation with extremely prolonged cyclic time. In this case, the consistency between the unified formulation and the Manson-Haferd Parameter on the temperature-time relation indicates that it is reasonable for the unified formulation to present the creep mechanism in a logarithmical relation between temperature and cyclic time.

In the specific case of cyclic creep, the load fluctuates between tension and compression. The cyclic time is a measure of the duration of time to which the material is exposed to the diffusion flow under tension and compression. Under tensile loading, we propose that the flow is in practice limited by dislocation pinning, grain boundaries, and other flow-limiting effects at the microstructural level. This causes the rate of diffusion to be reduced over longer periods, and hence the total plastic strain due to this component has the form $c_2 \log(t_c/t_{ref})$. When the cycle is reversed, and the load moves into the compression stage, the diffusion is not undone (reversed). This is because changes have occurred at the microstructural level, such that it is not the same geometric system as before, thus the system is inelastic. Consequently, the compression part of the cycle does not completely undo the inelastic strain of the previous stage (during a limited time range imposed for a general engineering case). Also, the compression is proposed to undo or at least disturb the flow-limiting effects that arose in the tension stage. Hence the next tension cycle permits further diffusion to occur. We therefore propose that the cyclic time reduces the fatigue capacity per $1 - [c_2 \log(t_c/t_{ref})]$. Although the cycle time provides a limited opportunity for the creep effect to operate, it is still reasonable to assume that the amount of creep that occurs within one part of the cycle follows the logarithmic time-temperature dependence.

Theoretically, the temperature and cyclic time both affect the fatigue capacity. In this case, we propose that to a first approximation they are independent of each other rather than convoluted with each other, hence the overall effect is additive. This statement is only one aspect of describing temperature-time relation, which is based on the situation with unspecified creep damage. If creep is included, then temperature can be related with time under one specific damage to show an inversely proportional relation. For example, for one specific creep damage, the effect caused by increased temperature could be compensated through decreasing cyclic time. Consequently, considering these two situations, the numerical representation of creep

effect is given as the sum of the temperature and cyclic time effects, and the logarithmical relation between them is included, hence the form: $\left[c_1(\sigma)\left(T - T_{ref}\right) + c_2 \log\left(t_c/t_{ref}\right)\right]$.

Consequently, based on the investigation of diffusion creep, which is physically described by the amount of substance flowing through a specific area during a unit time, we conclude that the logarithmic relation between temperature and cyclic time is consistent with the relation shown in the unified formulation:

$$\varepsilon_p = C_0\left\{1 - \left[c_1(\sigma)\left(T - T_{ref}\right) + c_2(\sigma)\log\left(t_c/t_{ref}\right)\right]\cdot\left[A\left(d/d_{ref}\right)^m\right]\right\}N^{-\beta_0}$$

Logarithmic relation

Similarly, the stress-based creep-fatigue formulation gives a natural exponential relationship of temperature vs. cyclic time, and this is explained next.

(2) The stress-based unified creep-fatigue equation

The relationship between temperature and time for the stress-based formulation was directly derived from the conventional creep model. By this means, a natural exponential relationship between them is accommodated. According to the derivation of this unified formulation, the relationship reflects the creep-rupture behaviour; thus it should be consistent with the empirical data of creep rupture and the physical mechanism of creep.

On the one hand, this natural exponential relationship is consistent with the observation of creep-rupture behaviour, and is validated on the materials of Inconel 718 [95] and GP91 casting steel [100]. The creep-rupture data on these two materials at a given stress (650MPa for Inconel 718 and 200MPa for GP91 casting steel) are tabulated in Table 10.5, and the curve-fitting results are then presented in Fig.10.6.

Table 10.5 Creep-rupture data of Inconel 718 and GP91 casting steel

Inconel 718			GP91 casting steel		
Temperature (K)	Stress (MPa)	Rupture time (H)	Temperature (K)	Stress (MPa)	Rupture time (H)
923	650	13.28	823	200	9000
948	650	4.74	873	200	60.9
973	650	1.15	923	200	0.87

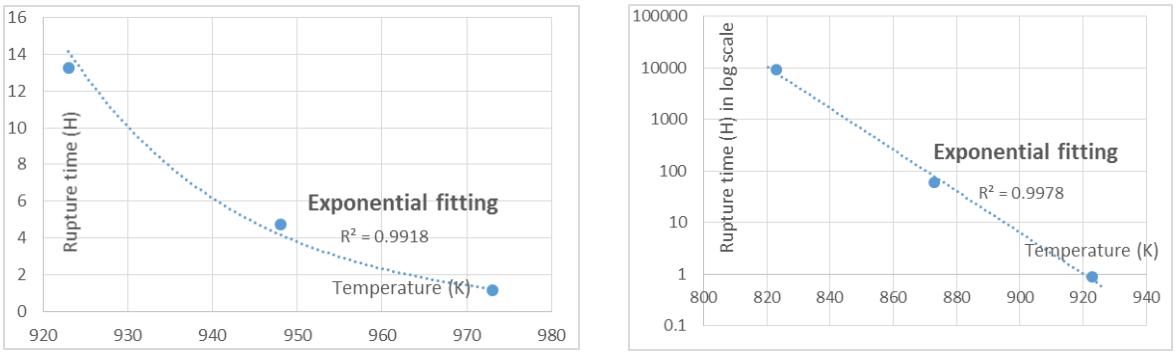

(a) Inconel 718 (b) GP91 casting steel

Figure 10.6 Curve fitting of temperature vs. rupture time: (a) Inconel 718; (b) GP91 casting steel

Fig.10.6 illustrates good exponential fitting between temperature and creep-rupture time; specifically, fitting errors are 0.9918 for Inconel 718 and 0.9978 for GP91 casting steel. Therefore, the natural exponential relationship between temperature and time shown in the stress-based unified creep-fatigue equation is consistent with the experimental data of creep rupture.

On the other hand, a natural exponential relationship (Eq.10.21) between temperature and time is observed through reorganizing Eq.10.16; thus it is believed that this relation shown in the unified formulation is consistent with the diffusion creep mechanism at the microstructural level.

$$J = \frac{dD_v}{dt} \propto exp(-1/T) \rightarrow t \propto exp(-1/T) \tag{10.21}$$

In addition, this natural exponential relation is also accommodated in the conventional creep-related formulations, such as the Arrhenius equation and the Sherby-Dorn parameter. This consistency further verifies that the natural exponential relationship shown in the stress-based unified creep-fatigue equation is consistent with the underlying physical mechanism of creep.

Consequently, we conclude that the natural exponential relationship between temperature and time is observed from diffusion creep, and is also consistent with the empirical data. This relationship is represented in our unified equation:

$$\sigma = \sigma_0 \cdot \left(d/d_{ref}\right)^m \left\{1 - A \cdot \left[\left(d/d_{ref}\right)^n \cdot f_m^a \cdot \sigma^a \cdot e^{\frac{Q'}{T-T_{ref}}} \cdot \left(t_c/t_{ref}\right)\right]^k\right\} \cdot N_f^{-b_0}$$

Logarithmic relation
(Natural exponential relation)

This section strongly proves that the relationship of temperature vs. time in the stress-based unified creep-fatigue equation is based on the underlying physical mechanisms and can be explained at a microstructural level.

10.2.3 The power-law relation between grain size and strain

(1) The strain-based unified creep-fatigue equation

The grain-size dependence was only introduced into the creep component since it has a more significant influence on creep damage than fatigue damage under strain-controlled loading. The derivation of the strain-based unified creep-fatigue equation shows that the grain-size component is directly extracted from the general creep equation for steady state, wherein a power-law relation between strain (fatigue capacity) and grain size is presented. This relation has been well verified by empirical data and thus appears to accurately represent creep behaviour. However, it is still necessary to identify the underlying physical mechanisms.

The power-law relation between grain size and fatigue capacity is consistent with the creep mechanism. Generally, creep behaviour is described by diffusion flux which is numerically formulated by Fick's equation (Eq.10.14). The term 'diffusion flux' is not only related to the time (discussion in section 10.2.2) but also related to the unit area where the substance is flowing through (Eq.10.22):

$$J = \frac{dD_t}{dA} \propto exp(1/T) \tag{10.22}$$

where D_t reflects the amount of substance flowing during a unit time and A is the area where substance is flowing through. This area can be obtained by the product of the number of grains per unit area and the average area of a grain, wherein the average area has a strong dependence on grain size. Generally, the area of a geometry can be numerically related to the key dimension in the form of a second power order. In the present work, a complex situation for the creep-fatigue condition, wherein creep and fatigue are interacting, may cause the intensity of grain-size effect to deviate from the power of two, but the power-law relation is retained. Consequently, based on the general creep mechanism, it is logical that a power-law relation is applied to relate grain size to creep-related strain, the same order as the applied strain (fatigue capacity). This is included in the unified formulation.

In addition, bigger grain size is always beneficial for pure creep. This grain-size effect on creep is consistent with the presentation of the strain-based unified creep-fatigue equation. According to the validations on the materials of Inconel 718 and GP91 casting steel, the negative exponent to grain size shows the benefit of big grain size on creep resistance.

We propose that the physical explanation for the grain-size dependence is that the diffusion creep phenomenon involves effects at the (irregular) grain boundaries, and to a lesser extent movement within the crystalline structure of the grain. However, the latter mechanism becomes stalled once the available dislocations have run their courses. Hence the steady creep loading purges the internal structure of the grain of imperfections. Consequently, the larger the grain, the lower the opportunity for diffusion creep to occur. Thus, it is to be expected that plastic strain would be inversely related to grain size, and hence m is negative in $\left[A\left(d/d_{ref}\right)^{m}\right]$. For very small grains the effect becomes disproportionately worse, because a small change in grain size results in a large change in the number of grains in the section. This means more grain

boundaries and opportunity for creep. A similar change in size for a large grain has a much smaller effect.

We note that *m* is approximately -0.5 for both materials considered (Inconel 718 and GP91 casting steel). Since creep damage involves crack propagation along a grain boundary, the decreased grain size results in increased opportunity for crack growth within a given area. For example, one square grain is identified to have four sides, hence four crack-growth potentials, then halving or quartering of the grain size gives two more or six more potential directions for crack growth respectively for the same total area.

Note that the size of one square grain is a reference condition, based on which the grain is halved or quartered. In this case, the grain size of 1 is not specified as 1μm, but should rather be considered as a mathematical origin for the scaling effect, hence we refer to this as the pseudo grain size.

The relationship between pseudo grain size *d'* and the number of crack-growth planes is shown in Fig.10.7. This relationship may be formulated numerically as a power-law relation, with exponent -0.68. In practical situations, the grain boundaries are not flat planes but are instead more irregular. The effect of this is to (a) increase the planar area available, and (b) provide more opportunities for an element of the boundary to be aligned with the preferred crack-growth direction. Hence practical situations are expected to provide greater opportunity for crack growth as the grain size decreases. The effect of this is to change the exponent closer to zero, e.g. if there were two additional planes at each stage then the exponent becomes -0.523. We, therefore, propose that there are natural reasons for the exponent in the formulation $\left[A\left(d/d_{ref}\right)^{m}\right]$ to be of the order *m* = -0.68 or larger, and this is compatible with the empirically determined values of -0.5411 for Inconel 718 and -0.4053 for GP91 casting steel.

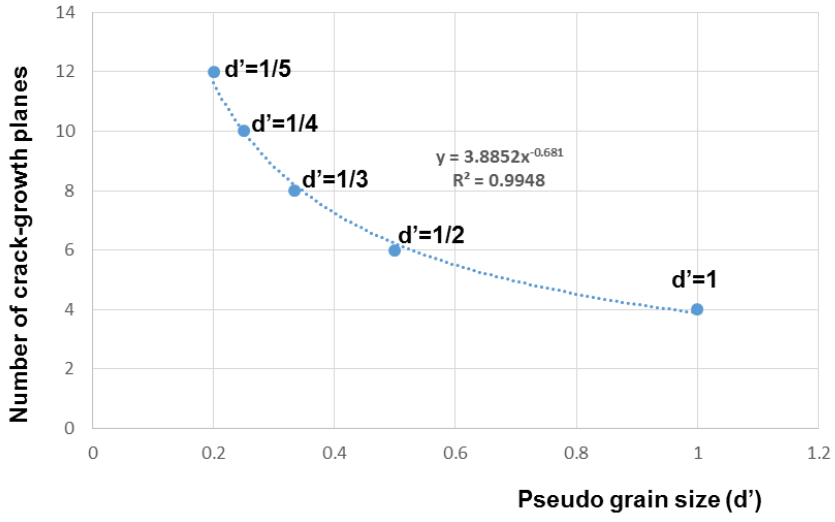

Figure 10.7 Relationship between pseudo grain size and the number of potential crack-growth planes

Consequently, diffusion-creep behaviour gives a power-law relation between grain size and strain (fatigue capacity), which is consistent with the observation of empirical data and

investigation of conventional models. This physical-based relationship is also numerically represented in our unified creep-fatigue equation:

$$\varepsilon_p = C_0\left\{1-\left[c_1(\sigma)(T-T_{ref})+c_2(\sigma)\log(t_c/t_{ref})\right]\cdot\left[A(d/d_{ref})^{m}\right]\right\}N^{-\beta_0}$$

Power-law relation

where the grain-size dependence was introduced into the creep component in a power-law relation.

(2) The stress-based unified creep-fatigue equation

The grain-size dependence was introduced into both the creep component and the fatigue component for the stress-based formulation in the form of a power-law relation. In this case, the unified formulation has the capacity to describe creep-fatigue behaviour at a microstructural level under the stress-controlled loading. Significantly, the power-law relation is consistent with the underlying physical mechanisms of fatigue and creep, and the discussion of consistency on the fatigue and creep phenomena is conducted separately.

On the one hand, the discussion shown above for the strain-based unified creep-fatigue equation is based on a general understanding of the creep mechanism and thus can be extended to the stress-based situation based on the concept of compatibility. In this case, it is reasonable to believe that the power-law relation between grain size and creep-related stress can well present the underlying physical mechanism of creep (consistent with the creep mechanism).

On the other hand, the power-law relation also is presented in the fatigue component. According to the discussion shown in the section of derivation (Chapter 7), this power is normally selected as -0.5. This has been well verified by amounts of empirical data for multiple materials and is numerically shown as the Hall-Petch-type equations through curve fitting. In addition, this power-law relation is also consistent with the fatigue mechanism, where the cracks grow through the grain boundary. In this case, the grain-size effect on fatigue can generally be explained through the theory of grain boundary strengthening. Specifically, according to the concept of dislocation pile-up (shown in Fig.10.8) [159], the grains with bigger size pile up more dislocations, and have a bigger driving force for moving dislocations from one grain to adjacent grains. As a result, less force could be applied, which then exhibits lower yield stress. This implies the beneficial effect of small grain size on fatigue behaviour.

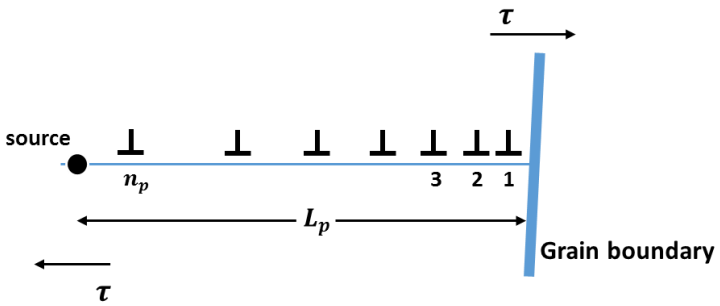

Figure 10.8 The concept of dislocation pile-up

According to the model shown in Fig.10.8, the pile-up length L_p can be presented as:

$$L_p = n_p \mu b / A \tau_e \tag{10.23}$$

where n_p is the number of dislocations, μ is the shear modulus, b is the Burgers vector, A is a constant and τ_e is the shear stress which makes dislocation pile up. Stress concentration occurs at the front of the pile-up, where the magnitude of stress is defined as the product of n_p and τ_e. When the stress concentration arrives at a critical value (τ_c), a new dislocation develops between two adjacent grains. Therefore, this condition of yielding is presented as:

$$\tau_c = n_p \tau_e \tag{10.24}$$

Then, introducing Eq.10.24 into Eq.10.23 gives:

$$\tau_e = \sqrt{\frac{\tau_c \mu b}{A L_p}} \tag{10.25}$$

The pile-up length can be defined as proportional to grain size:

$$L_p = Bd \tag{10.26}$$

where B is the scale of pile-up length to grain size and d is the grain size. Substituting Eq.10.25 with Eq.10.26 gives the relationship between grain size and stress:

$$\tau_e \propto \sqrt{\frac{1}{d}} \tag{10.27}$$

Significantly, Eq.10.27 shows that the stress which causes fatigue damage can be related to grain size in a power-law relation, and the power is selected as -0.5. The discussion shown above well demonstrates the power-law relation presented by the fatigue component in the stress-based unified equation is consistent with the physical mechanism of fatigue (dislocation pile-up).

The validations on the materials of Inconel 718 and GP91 casting steel further demonstrate the grain-size effect for fatigue and creep. Specifically, the negative exponent to grain size for the fatigue component implies the benefit of small grain size on fatigue capacity, and the negative exponent to grain size for the creep component shows the benefit of big grain size on creep resistance.

Consequently, diffusion-creep behaviour gives a power-law relationship between grain size and fatigue capacity for creep damage, and the concept of dislocation pile-up presents the same relation to fatigue behaviour. Both of these numerical representations are accommodated into the stress-based unified equation:

$$\sigma = \sigma_0 \cdot (d/d_{ref})^m \left\{1 - A \cdot \left[(d/d_{ref})^n \cdot f_m^a \cdot \sigma^a \cdot e^{\frac{Q'}{T - T_{ref}}} \cdot (t_c/t_{ref})\right]^k\right\} \cdot N_f^{-b_0}$$

Power-law relation

Significantly, the magnitudes of *m* and *n* present consistency with a general understanding of the grain-size effect on fatigue and creep respectively.

10.2.4 The power-law relation between life and applied loading

(1) The strain-based unified creep-fatigue equation

The derivation of the strain-based unified creep-fatigue equation is based on the concept of 'fatigue capacity', and shows the extension of a conventional strain-life equation, the Coffin-Manson equation. Therefore, the power-law relation shown in the Coffin-Manson equation is extended to the creep-fatigue condition and is accommodated in the unified formulation. This relation has been well demonstrated by the empirical data shown in the validation on different materials, wherein the creep-fatigue data follow the Coffin-Manson-type relation (a power-law relation). Since the Coffin-Manson equation has been well verified on multiple materials and is successfully applied in engineering design, it is believed that the power-law relation between reversed loading and the number of cycles could well present the process of damage accumulation in fatigue perspective.

Normally, fracture mechanics can be presented by three independent cracking models. In general, Model I is an opening model showing direct apart between two crack surfaces, Model II is a sliding model showing one crack surface sliding over another surface in the perpendicular direction to the edge of the crack, and Model III is a tearing model showing one crack surface moving apart from another surface in the parallel direction to the edge of the crack. Model I presents the simplest loading situation, and also is the situation shown by the present research [123]. In this situation, the stress intensity factor is normally shown by Eq.10.28:

$$K = \sigma\sqrt{\frac{\pi a}{2}} \tag{10.28}$$

During the process of crack growth, plastic deformation normally occurs around the crack tip due to high stress concentration, where a circular plastic zone ahead of the crack tip is formed (Fig.10.9). Combining with the stress intensity factor (Eq.10.28), the stress distribution near the crack tip can be represented as:

$$\sigma_{ij} = \sigma\sqrt{\frac{a}{2r}}f(\theta) = \frac{K}{2\pi r}f(\theta) \tag{10.29}$$

where σ is the applied stress, a is the crack length, K is the stress intensity factor, and r and θ are polar coordinates located in the plastic zone. This equation shows that when *r* tends towards zero, the stress around the crack tip becomes singular. This proves the existence of the plastic zone, and implies that the yield stress (σ_y) is presented at the boundary of the plastic zone. Then, through letting $\sigma_{ij} = \sigma_y$ and $f(\theta) = 1$, Eq.10.29 gives the size of the plastic zone [123]:

$$r_y = \frac{1}{2\pi}\left(\frac{K}{\sigma_y}\right)^2 \tag{10.30}$$

where r_y is the radius of the plastic zone.

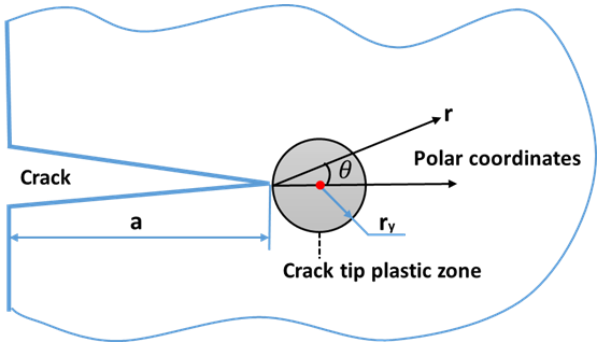

Figure 10.9 The plastic zone around crack tip

For the situation with cyclic loading, Eq.10.28 shows that the stress intensity factor varies with the change of loading, and then results in expansion or shrinkage of the plastic zone. In this situation, the effective stress intensity factor is defined as:

$$K_{eff} = K_{max} - K_{min} = \Delta K \tag{10.31}$$

where ΔK is the difference between the maximum and minimum stress intensity factors, and K_{eff}, K_{max} and K_{min} are the effective, maximum and minimum stress intensity factors for one cycle, respectively. Then, based on Eq.10.30, an equivalent radius of the plastic zone ($\overline{r_y}$) can be given by Eq.10.32:

$$\overline{r_y} = \frac{1}{2\pi}\left(\frac{\Delta K}{\sigma_y}\right)^n \tag{10.32}$$

This equation shows that the second power order in Eq.10.30 is reasonably replaced by a general exponent (n) due to the equivalent transformation, but the power-law relation is retained. Then, it is believed that the larger plastic zone gives longer crack growth [123], and thus the crack growth in one cycle can be related to ΔK in a power-law relation. This relation is well represented and proven by Paris [29], who proposed the crack growth law:

$$\frac{da}{dN} = C(\Delta K)^m \tag{10.33}$$

where $\frac{da}{dN}$ reflects the crack-growth rate and gives the increased crack length in one cycle, and C and m are constants. According to Eq.10.28, the difference between the stress intensity factors at the maximum stress and the minimum stress (the effective stress intensity factor) can be expressed as:

$$\Delta K = X\Delta\sigma\sqrt{\pi a} \tag{10.34}$$

where X is a constant. Then, introducing Eq.10.34 into Eq.10.33 gives:

$$\frac{da}{dN} = C\left(X\Delta\sigma\sqrt{\pi a}\right)^m \tag{10.35}$$

Applying the integral operation for life gives:

$$\int_0^{N_f} dN = \int_{a_i}^{a_c} \frac{da}{C\left(X\Delta\sigma\sqrt{\pi a}\right)^m} = \frac{1}{C\left(X\Delta\sigma\sqrt{\pi}\right)^m} \int_{a_i}^{a_c} a^{-m/2} da \tag{10.36}$$

Then, the result of integration is presented as:

$$N_f = \frac{2\left(a_c^{\frac{2-m}{2}} - a_i^{\frac{2-m}{2}}\right)}{(2-m)C\left(X\Delta\sigma\sqrt{\pi a}\right)^m} \tag{10.37}$$

where a_c is the critical crack length at which fracture occurs, and a_i is the initial crack length at which the crack starts to grow under a given stress range $\Delta\sigma$. Significantly, this equation shows a typical power-law relation between fatigue life and applied stress range (applied loading). Reasonably, this relationship can be extended to relate plastic strain with fatigue life due to the concept of compatibility.

Therefore, the discussion above indicates that the existence and size of the plastic zone at the crack tip is the physical basis given by the crack growth for the power-law relationship between the applied loading and the number of cycles. This relationship is also included in our new creep-fatigue equation:

$$\boxed{\varepsilon_p} = C_0\left\{1 - \left[c_1(\sigma)(T - T_{ref}) + c_2(\sigma)\log(t_c/t_{ref})\right] \cdot \left[A\left(d/d_{ref}\right)^m\right]\right\}\boxed{N}^{-\beta_0}$$

Power-law relation

Overall, we conclude that the relationship of life vs. plastic strain in the strain-based creep-fatigue equation is consistent with the physical phenomena of fatigue-damage accumulation.

(2) The stress-based unified creep-fatigue equation

The stress-based unified creep-fatigue model was also derived from the concept of 'fatigue capacity', and presents an extension of the conventional stress-life relation, the Basquin equation. Therefore, a power-law relationship between fatigue life and cyclic loading is well accommodated in this unified formulation. This relationship is believed to be consistent with the observation of empirical data. In addition, the investigation of the fracture mechanism shown above (for the strain-based model) also indicates a power-law relation between fatigue life and applied stress (Eq.10.37). This relation is numerically represented in the stress-based formulation:

$$\boxed{\sigma} = \sigma_0 \cdot \left(d/d_{ref}\right)^m \left\{1 - A \cdot \left[\left(d/d_{ref}\right)^n \cdot f_m^a \cdot \sigma^a \cdot e^{\frac{Q'}{T - T_{ref}}} \cdot \left(t_c/t_{ref}\right)\right]^k\right\} \cdot \boxed{N_f}^{b_0}$$

Power-law relation

Consequently, we conclude that the power-law relationship of life vs. stress in the stress-based unified creep-fatigue equation is consistent with the physical behaviour, and a physical-based explanation of the damage accumulation is numerically represented.

This power-law relationship can also be applied to numerically explain the process of damage accumulation. Normally, this process can be divided into three stages based on the rate of damage accumulation. For a given applied cyclic loading, at the first stage, the damage is initiated and then accumulates with cycles at a relatively slow speed. This stage presents the break of an equilibrium situation from the ideally perfect body, and thus more work is needed to break through the threshold. This implies that more cycles result in small damage, i.e. a small rate of damage accumulation is given. At the second stage, damage accumulation enters a relatively steady situation at an intermediate speed. Although this stage is smooth, it consumes the most of lifetime. The third stage presents the finally fracture, where the steady situation shown in the second stage is broken and the rate of damage accumulation is suddenly increased. The instability presented in this stage may result from the arriving of critical damage, where the whole system completely loses stability during a quite short time and then collapses. This implies that a small number of cycles leads to dramatic damage accumulation. Based on the description shown above, it is believed that the damage-accumulation process, which experiences the stages of slow growth rate, relatively stable growth and sudden fracture, can be numerically well represented by a power-law form. This process has been somewhat described in section 9.2.3 and illustrated in Fig.9.18.

10.2.5 The numerical representation of creep effect on fatigue capacity

(1) The strain-based unified creep-fatigue equation

The development of the strain-based unified creep-fatigue equation is based on the concept of 'fatigue capacity'. Briefly, this concept indicates that the full fatigue capacity is gradually consumed by the creep effect, and this process can be numerically represented by the form of '1-x'. This form is also accommodated in the unified formulation:

$$\varepsilon_p = C_0\left\{1-\underbrace{\left[c_1(\sigma)\left(T-T_{ref}\right)+c_2(\sigma)\log\left(t_c/t_{ref}\right)\right]\cdot\left[A\left(d/d_{ref}\right)^m\right]}_{\text{Creep damage}}\right\}N^{-\beta_0}$$

The form of (1-X)

Reorganizing the strain-based unified formulation gives Eq.10.38:

$$\varepsilon_p = C_0N^{-\beta_0}-\left[c_1(\sigma)\left(T-T_{ref}\right)+c_2(\sigma)\log\left(t_c/t_{ref}\right)\right]\left[A\left(d/d_{ref}\right)^m\right]N^{-\beta_0} \qquad (10.38)$$

The first term of Eq.10.38 reflects the full fatigue capacity, where the fatigue behaviour under the pure-fatigue condition is represented by the Coffin-Manson equation. The second term of Eq.10.38 reflects the creep effect, which has the temperature, cyclic time and grain size dependences. This term takes a Coffin-Manson-type formulation and shows the creep-related-damage accumulation under cyclic loading. The combination of these two terms shows the gradual consumption of full fatigue capacity due to creep effect, and then the residual fatigue capacity is given. In this case, this expression of '1-x' represents a good numerical explanation

of the negative effects of increased temperature and cyclic time and decreased grain size on the creep-fatigue life.

In addition, the reference condition is introduced to show the threshold between pure fatigue and creep fatigue, and present a baseline for evaluating creep fatigue.

$$\varepsilon_p = C_0\left\{1-\left[c_1(\sigma)\left(T-\boxed{T_{ref}}\right)+c_2(\sigma)\log\left(t_c/\boxed{t_{ref}}\right)\right]\cdot\left[A\left(d/\boxed{d_{ref}}\right)^m\right]\right\}N^{-\beta_0}$$

Reference condition

At the reference condition, the full fatigue capacity is represented (the second term of Eq.10.38 equals to zero), and the strain-based unified creep-fatigue equation is restored to the Coffin-Manson equation. Therefore, the introduction of the reference condition builds a bridge between pure fatigue and creep fatigue.

Consequently, representation of '1-x' shown in the unified model numerically represents the concept of fatigue capacity, which provides an effective description of the negative creep effect on fatigue capacity. Significantly, the introduction of the reference condition builds a bridge between the pure-fatigue condition and the creep-fatigue condition, where the physical phenomenon of activating the creep effect is numerically represented.

(2) The stress-based unified creep-fatigue equation

Based on the concept of fatigue capacity, the stress-based unified creep-fatigue equation also takes the form of '1-x' to show the gradual consumption of creep to the full fatigue capacity.

$$\sigma = \sigma_0\cdot\left(d/d_{ref}\right)^m\left\{\underline{1}-\boxed{A\cdot\left[\left(d/d_{ref}\right)^n\cdot f_m^a\cdot\sigma^a\cdot e^{-\frac{Q'}{T-T_{ref}}}\cdot\left(t_c/t_{ref}\right)\right]^k}\right\}\cdot N_f^{-b_0}$$

Creep damage

The form of (1-X)

Reorganizing the stress-based unified formulation gives Eq.10.39:

$$\sigma = \sigma_0\cdot\left(d/d_{ref}\right)^m\cdot N_f^{-b_0}-\sigma_0\cdot\left(d/d_{ref}\right)^m A\cdot\left[\left(d/d_{ref}\right)^n\cdot f_m^a\cdot\sigma^a\cdot e^{-\frac{Q'}{T-T_{ref}}}\cdot\left(t_c/t_{ref}\right)\right]^k\cdot N_f^{-b_0} \quad (10.39)$$

The first term of Eq.10.39 gives the full fatigue capacity, which shows the fatigue behaviour under the pure-fatigue condition. This is represented by the grain-size modified Basquin equation. The second term of Eq.10.39 reflects the creep effect, which accommodates relevant variables, including temperature, stress, time and grain size. This term also takes the form of the Basquin-type equation to show accumulation of creep-related damage under the cyclic loading. The combination of these two terms gives the residual fatigue capacity due to the consumption of creep damage. Therefore, the formulation of '1-x' gives a good numerical explanation of the negative effect of creep.

In addition, the reference condition is also introduced into the stress-based unified creep-fatigue equation to show the threshold between pure fatigue and creep fatigue, and present a baseline for evaluating creep fatigue.

$$\sigma = \sigma_0 \cdot (d/d_{ref})^m \left\{1 - A \cdot \left[(d/d_{ref})^n \cdot f_m^a \cdot \sigma^a \cdot e^{-\frac{Q'}{T+T_{ref}}} \cdot (t_c/t_{ref})\right]^k\right\} \cdot N_f^{-b_0}$$

Reference condition

At the reference condition, the full fatigue capacity is represented, wherein the grain-size components are defined as 1, and the second term of Eq.10.39 equals zero. Then, the unified formulation is restored to the Basquin equation. Therefore, the introduction of the reference condition builds a bridge between pure fatigue and creep fatigue.

Consequently, the negative effect of creep on fatigue capacity is numerically formulated as the form of '1-x', and the introduction of the reference condition shows the threshold for the activation of the creep effect. In this case, the stress-based unified formulation represents a high consistency with the physical phenomenon.

Overall, the discussion shown above indicates that the unified creep-fatigue equations (both strain-based and stress-based) can be well explained by the underlying physical mechanisms of fatigue and creep. The relationships between different variables and their physical bases are collected in Table 10.6.

Table 10.6 Relationships between different variables and their physical bases

Mechanisms	Variables	Strain-based model	Stress-based model
Diffusion creep	Temperature vs. applied loading	Linear relation (simplification)	Natural exponential relation
Diffusion creep	Temperature vs. cyclic time	Logarithmical relation	Natural exponential relation
Diffusion creep	Grain size vs. applied loading (creep component)	Power-law relation	Power-law relation
Dislocation pile-up	Grain size vs. applied loading (fatigue component)	---	Power-law relation
Crack growth	Life vs. applied loading	Power-law relation	Power-law relation
Fatigue capacity	Negative effect of creep	Form of '1-x'	Form of '1-x'
Activation of creep effect	Temperature, cyclic time and grain size	The reference condition	The reference condition

10.3 Summary

Creep-fatigue behaviour is identified to be influenced by temperature, cyclic time and grain size. Generally, elevated temperature or prolonged cyclic time gives more creep damage, then reduces fatigue capacity. The grain-size effect presents opposite effects on fatigue and creep. Specifically, the bigger grain size is negative for the pure-fatigue capacity but is beneficial for creep resistance.

These variables were considered to constitute the strain-based and stress-based unified creep-fatigue equations, and the relationships between these variables were extracted from the conventional fatigue and creep models. Since these conventional models have been well demonstrated in multiple situations for multiple materials, we assume that they have the ability to numerically represent the underlying physical mechanisms of fatigue and creep. This consistency was proven in the present chapter, where creep-related relationships reflect the behaviour of diffusion creep and the fatigue-related relationships were derived from the phenomena of dislocation pile-up and crack growth. In addition, the concept of fatigue capacity gives a numerical representation of '1-x' to describe the negative effect of creep damage. Significantly, the introduction of the reference condition builds a bridge between pure fatigue and creep fatigue, which numerically shows the activation of creep effect.

Taking the strain-based formulation as an example, the fundamental mechanisms, which are at work to determine creep-fatigue behaviour of a material, are illustrated by Fig.10.10:

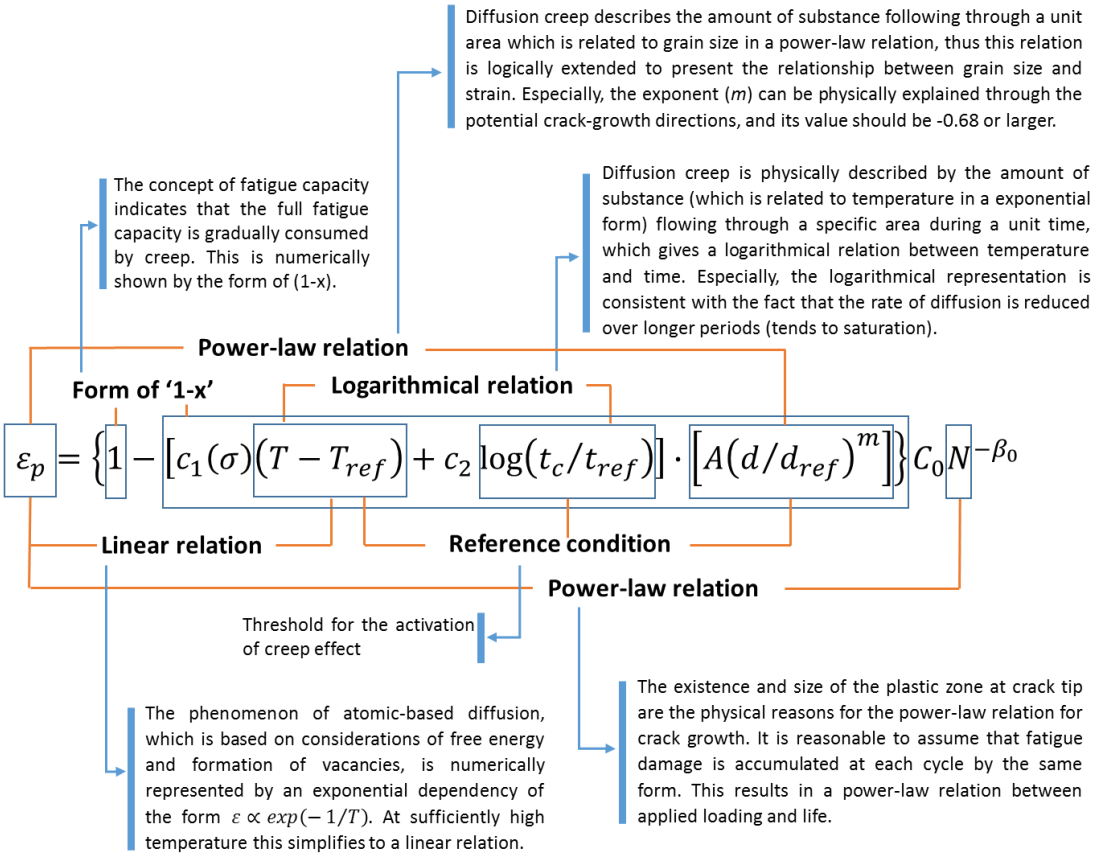

Figure 10.10 Main relationships and fundamental mechanisms in the strain-based model

Consequently, we conclude that the strain-based and stress-based unified creep-fatigue equations show good consistency with the underlying physical mechanisms, and thus can be explained at a microstructural level. This is a very important characteristic for the unified creep-fatigue models since this fundamentally gives them the ability to cover multiple situations and multiple loading regimes.

Chapter 11

11. Application to engineering design

This chapter demonstrates the applicability of the unified creep-fatigue approach. It provides a guide to application from the perspective of an engineering designer, and is illustrated with a case study on a gas turbine blisk. It is shown that the combination of the unified approach and FEA can significantly reduce the complexity of creep-fatigue simulation.

Publications relevant to this chapter are as follows (see Appendix A for details):

(1) Liu, D. and D.J. Pons, A unified creep-fatigue equation with application to engineering design, in Creep, T. Tomasz, S. Marek, and A. Zieliński, Editors. 2018, InTechOpen: Rijeka, Croatia.

In this chapter, the strain-based unified creep-fatigue equation (proposed in Chapter 4) is selected to represent the application for engineering design. This unified equation was developed for engineering application, and thus the accuracy and economy are equally important. This has been demonstrated in Chapter 6, and specifically the accuracy of fatigue-life prediction was proven through validating on multiple materials, and the investigation on the economy shows that the coefficients of the unified equation can be extracted by minimal experimental effort. This chapter gives a general guide to apply this unified formulation to the fatigue-life prediction, and then a practical case study on the gas turbine blisk is represented to determine the appropriate material.

11.1 Guide to apply the strain-based unified creep-fatigue equation

This section gives a general guide for the application of the unified creep-fatigue equation, and the description shown here focuses on the strain-based approach (without grain size) which

reflects a more common situation for engineering case in service. In this general guide, the requirement of experiments, the derivation of coefficients and the multiple application situations are presented (flow chart is shown in Fig.11.1).

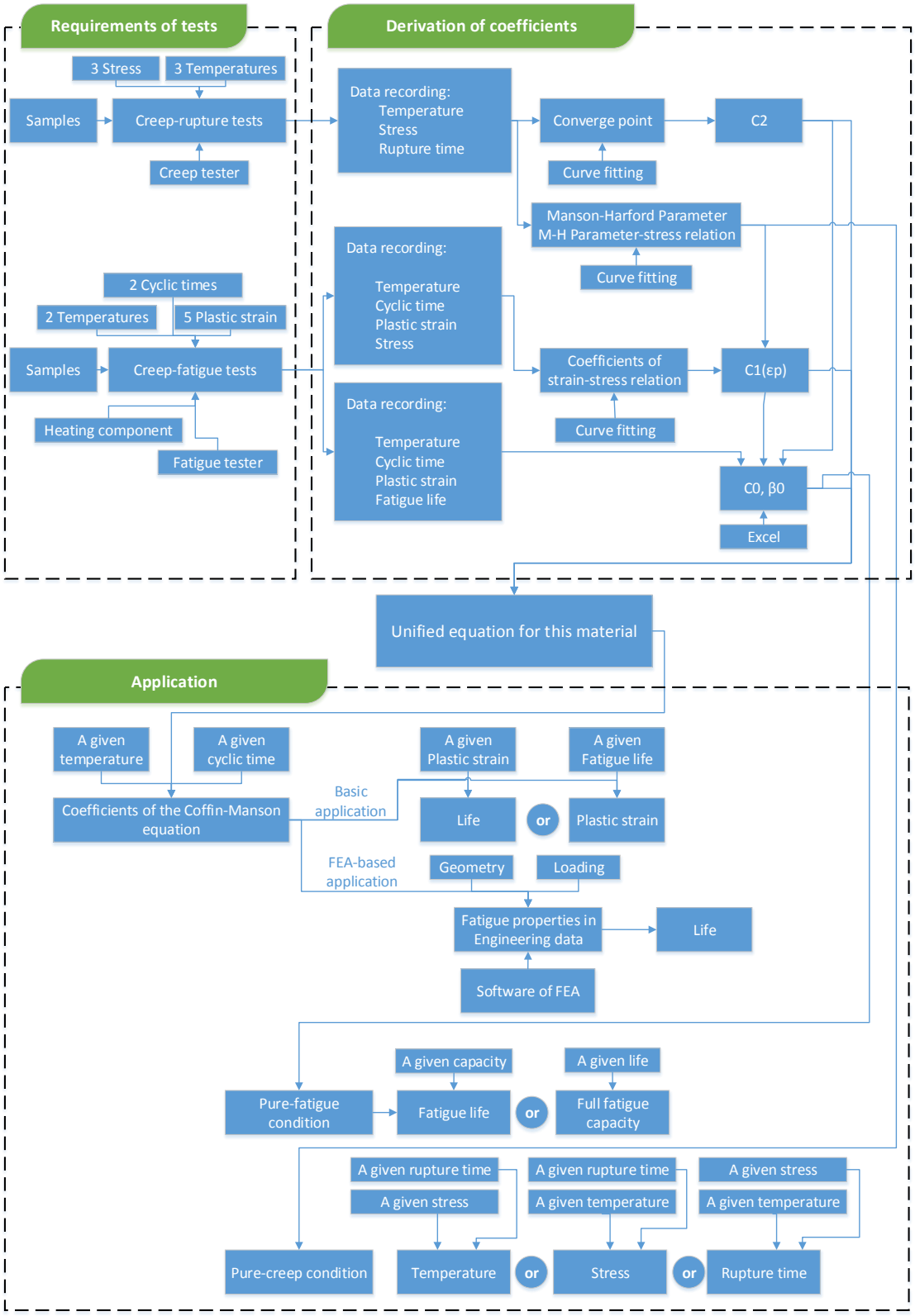

Figure 11.1 Flow chart of the guide to application

The unified model has a clear structure that is understandable by engineering practitioners, includes the general variables at the engineering scale, is easily mathematically solved, and provides accuracy and economical method for fatigue-life prediction. In this case, the bridge between academic knowledge and engineering practice is built.

In particular, the coefficients of the unified model can be easily obtained. Specifically, the coefficients are determined by empirical data on a specific material that engineers use in their company, including the creep-rupture data and creep-fatigue data. Less creep-fatigue data are needed compared to other methods (See Section 6.1). On the one hand, the creep-related coefficients could be derived by the time-temperature parameter. This process is conducted through curving fitting by Excel. One the other hand, the creep-fatigue related coefficients are determined by minimizing the difference between the predicted data and empirical data. This is an interpolation and regression analysis, and this numerical optimization can be conducted by Excel. We compared the results given by Excel and Matlab, and both of them result in the same solution. However, Excel is more economical, popular and convenient to be used for engineers (See Section 6.1). Thus, the method of extracting the coefficients is easily learnt and operated by the engineering practitioners.

11.1.1 Requirements of tests

As discussed in Chapter 6, comparing with the existing creep-fatigue models, minimal experimental effort is involved to get the coefficients of the strain-based unified model. In this case, only simple creep-rupture test and a small number of creep-fatigue tests are needed, and thus this model provides a more commercial method for fatigue-life prediction.

11.1.1.1 Creep rupture tests

Generally, creep is active above 35% of the melting temperature (the reference temperature), and thus the creep rupture tests should be conducted higher than this temperature. The creep-rupture tests are performed under at least three different temperatures and stresses (shown in Table 11.1), and then the rupture times are recorded.

Table 11.1 The situations for creep-rupture tests

Test No.	Temperature (K)	Stress (MPa)
1	Temperature 1 (Higher than 35% of melting temperature)	Stress 1
2		Stress 2
3		Stress 3
4	Temperature 2 (Higher than 35% of melting temperature)	Stress 1
5		Stress 2

6		Stress 3
7	Temperature 3 (Higher than 35% of melting temperature)	Stress 1
8		Stress 2
9		Stress 3

11.1.1.2 Creep-fatigue tests

As shown in Chapter 6, a more commercial method for deriving coefficients is represented by using the strain-based unified creep-fatigue equation. This is because the number of creep-fatigue tests (which is expensive and time-consuming) is significantly reduced. The discussion shown in Chapter 6 implies that only two sets of creep-fatigue tests are needed (shown in Table 11.2), where the temperatures (Temperature 1 < Temperature 2) and cyclic times (Cyclic time 1 < Cyclic time 2) are selected from two ends of the general application range. Each set of creep-fatigue tests is conducted under five different plastic strains. Note that the number of creep-fatigue tests could be further reduced by selecting three or four different plastic strains for each set of creep-fatigue test. However, the accuracy of the fatigue-life prediction may be reduced.

Table 11.2 The situations for creep-fatigue tests

Test No.	Temperature (K)	Frequency (Hz) / Cyclic time (s)	Plastic strain
1	Temperature 1	Cyclic time 1	Plastic strain 1
2			Plastic strain 2
3			Plastic strain 3
4			Plastic strain 4
5			Plastic strain 5
6	Temperature 2	Cyclic time 2	Plastic strain 1
7			Plastic strain 2
8			Plastic strain 3
9			Plastic strain 4
10			Plastic strain 5

11.1.2 Derivation of coefficients

The derivation of the coefficients in the stain-based unified model (Eq.11.1) has been described in Chapter 4, where $c_1(\sigma)$ and c_2 are obtained through creep-rupture tests, and creep-fatigue tests give the magnitudes of C_0 and β_0. In this section, this process is briefly presented.

$$\varepsilon_p = C_0\{1 - [c_1(\sigma)(T - T_{ref}) + c_2 \log(t_c/t_{ref})]\}N^{-\beta_0} \quad (11.1)$$

(1) Selection of the reference condition

The reference temperature is defined as 35% of the melting temperature, and the cyclic time is suggested as a small value, normally 1 second. The creep damage is assumed to be active above the reference temperature and the reference cyclic time.

(2) Derivation of creep-related coefficients

During the creep-rupture tests (shown in Table 11.2), the temperatures (T), stresses (σ) and rupture times (t) are recorded (totally, nine groups of data are recorded). Then, the relationships between T and $log\ t$ under three different stresses are plotted (Fig.11.2), wherein the temperature at the point of convergence is identified as the reference temperature, and the value of $log\ t$ at this convergence point ($log\ t_a$) is given by the average value of the $logt(T_{ref})$ at three different stresses. The value of $log\ t_a$ then gives c_2 through Eq.11.2.

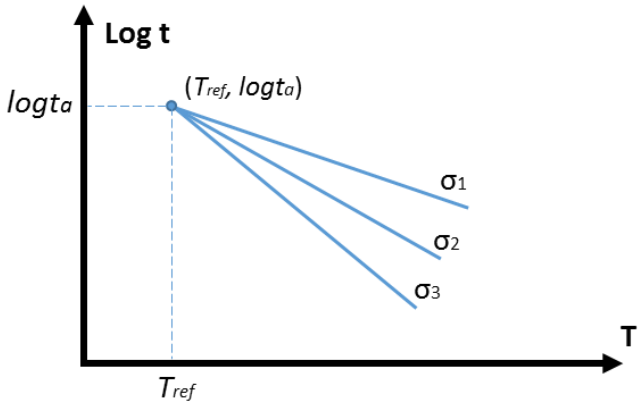

Figure 11.2 Plotting of *T vs. log t*

$$c_2 = \frac{1}{\log(t_a/t_{ref})} \quad (11.2)$$

According to Fig.11.2, the Manson-Haferd parameters under three different stresses are given, then the relationship between the Manson-Haferd parameter and applied stress ($P_{MH}(\sigma)$) can be obtained through curve fitting. Then, function $c_1(\sigma)$ is represented as the form of Eq.11.3.

$$c_1(\sigma) = -\frac{c_2}{P_{MH}(\sigma)} \quad (11.3)$$

(3) Derivation of fatigue-related coefficients

During the creep-fatigue tests (shown in Table 11.2), the temperatures (*T*), cyclic time (*t*), stresses (σ), plastic strain (ε_P) and fatigue life (*N*) are recorded (totally, 10 groups of data are recorded). In particular, with the empirical data of plastic strain vs. stress, the coefficients (*K* and *n*) of the strain-stress relation under two temperature-cyclic time conditions are obtained. These two coefficients then are involved in the function $c_1(\sigma)$ for transforming stress into plastic strain (Eq.11.4), where a moderating factor (f_{m}) is introduced to compress the stress effect on creep-related damage.

$$c_1(\sigma) = -\frac{c_2}{P_{MH}(\sigma)} \rightarrow c_1(\varepsilon_P) = -\frac{c_2}{P_{MH}[f_{\mathrm{m}} \cdot K(T, t_c) \cdot {\varepsilon_P}^{n(T,t_c)}]} \tag{11.4}$$

According to the discussion in Chapter 6, the Excel-based method is selected to derive the fatigue-related coefficients (C_0 and β_0) since Excel provides a more convenient tool to perform the numerical optimization for engineering application (compared to Matlab). In this case, by using Excel, minimizing the difference (δ_a) between the predicted fatigue life and the experimental results (Eq.11.5) yields the magnitudes of C_0 and β_0.

$$\delta_a = \sum \left(\log N_{comp,ij} - \log N_{exp,ij}\right)^2 \tag{11.5}$$

11.1.3 Application for strain-based unified approach

The strain-based unified equation can be simply represented as a Coffin-Manson-type equation (Eq.11.6). The coefficient (C') and the exponent (β_0) of this simplified form can be obtained under a given temperature and a given cyclic time.

$$\varepsilon_p = C' N^{-\beta_0} \tag{11.6}$$

with

$$C' = C_0\{1 - [c_1(\sigma)(T - T_{ref}) + c_2 \log(t_c/t_{ref})]\} \tag{11.7}$$

(1) The basic application

Eq.11.6 gives the strain-life relation under a given temperature-cyclic time condition. Then, this can be used to predict fatigue life for a given plastic strain or can be applied to evaluate the fatigue capacity under a given life. This represents the most fundamental application of the unified creep-fatigue model.

(2) The FEA-based application

The coefficient and exponent of Eq.11.6 can be imported into the software of finite element analysis, such as ANSYS, as the fatigue property in engineering data. Since they already contain the creep effect, the creep-related material property and loading can be removed from FEA. This significantly reduces the difficulty and complexity of analysis.

(3) The description of pure fatigue and pure creep

On the one hand, the strain-based unified creep-fatigue equation can be restored to the Coffin-Manson equation at the reference condition ($T = T_{ref}$ and t=t_{ref}), wherein the creep effect is dormant, and the full fatigue capacity is presented. In this case, this restored equation can be used to predict fatigue life or fatigue capacity at the pure-fatigue condition.

On the other hand, the strain-based unified model can be reformed as the Manson-Haferd parameter at the pure-creep condition. This reflects that the fatigue capacity is totally consumed by the creep effect, and the fatigue effect is too small to be ignored. The Manson-Haferd parameter can be used to evaluate creep behaviour, including rupture time, temperature and applied loading.

In the following section, a case study on a gas turbine blisk for material selection will be presented, where the FEA-based application of the strain-based unified creep-fatigue equation is discussed in detail.

11.2 Design case study – Fatigue-life evaluation for gas turbine blisk

A gas turbine blisk works at high temperatures, and experiences repeated starting up and shutting off. This is a typical creep-fatigue situation, where damage is caused by the combination of creep effect (elevated temperature) and fatigue effect (reversed loading). In this case study, the theory of highly accelerated life test is accepted to make a selection of material. In particular, the strain-based creep-fatigue equation is used to obtain the creep-fatigue-related parameters which are then imported into finite element analysis for evaluating the creep-fatigue damage.

11.2.1 The specification for this case study

11.2.1.1 The method of highly accelerated life test

This case study is based on the theory of highly accelerated life test, which is used at the initial stage of design to improve the reliability of the product, such as the selection of material, the optimization of structure and the decision of manufacturing processes. Normally, the accelerated life test is performed through intensifying the influence of stress-related factors on life. Therefore, the prediction of fatigue life and creep-rupture time in this case study cannot represent the real value of the failure under operating conditions. In the present work, we apply the theory of highly accelerated life test to select a material for the gas turbine blisk.

11.2.1.2 The application of the strain-based creep-fatigue equation

The strain-based unified creep-fatigue equation is used to give the creep-fatigue-related coefficients under the service condition; then these coefficients are introduced into finite element analysis (FEA) as engineering data. Obviously, the creep effect has been involved in the creep-fatigue-related coefficients, and thus FEA could be conducted under the situation without the creep effect to get the stress/strain distribution and fatigue life. In addition, the creep-fatigue life can also be calculated through Morrow's equation, where the stress/strain distribution obtained from FEA and the creep-fatigue-related coefficients obtained from the unified formulation were included.

11.2.1.3 The partition of creep-fatigue situation

In the real operation condition, the total damage is accumulated by the fatigue damage caused by repeated process of starting up and shutting off, the creep damage caused by elevated temperature and the damage caused by high-frequency vibration. The features of the operation period are shown below:

(1) This period always takes several hours and may be different for each operational unit.

(2) This period contains high-frequency vibration, which leads to fatigue damage. The amplitude of the loading caused by vibration is much smaller than the loading caused by the repeated process of starting up and shutting off. In addition, the loading caused by vibration is irregular, and thus the damage caused by this loading can be evaluated through Miner's linear damage rule or the Rainfall method.

(3) The creep damage is accumulated due to the elevated temperature during the period of operation, and the majority creep damage is caused by the loading under the maximum operational velocity.

According to these features and for the reason of simplification, we then assume that:

(1) The creep-fatigue evaluation based on each operational unit is divided into three parts. They are: regular-loading fatigue partition (repeated process of starting up and shutting off); creep partition (elevated temperature); and irregular-loading partition (high-frequency vibration) (Fig.11.3). In this case, the overall evaluation is split into three different partitions, and their individual evaluation is conducted separately.

(2) The partition which includes high-frequency vibration is not considered in this case study. This is because comparing the loading at the maximum operational velocity, the amplitude of loading caused by vibration is so small that it can be ignored. In this case, the overall evaluation focuses on the regular-loading partition and creep partition (Fig.11.3).

(3) The constant loading for creep damage is defined as the applied loading at the maximum rotational velocity.

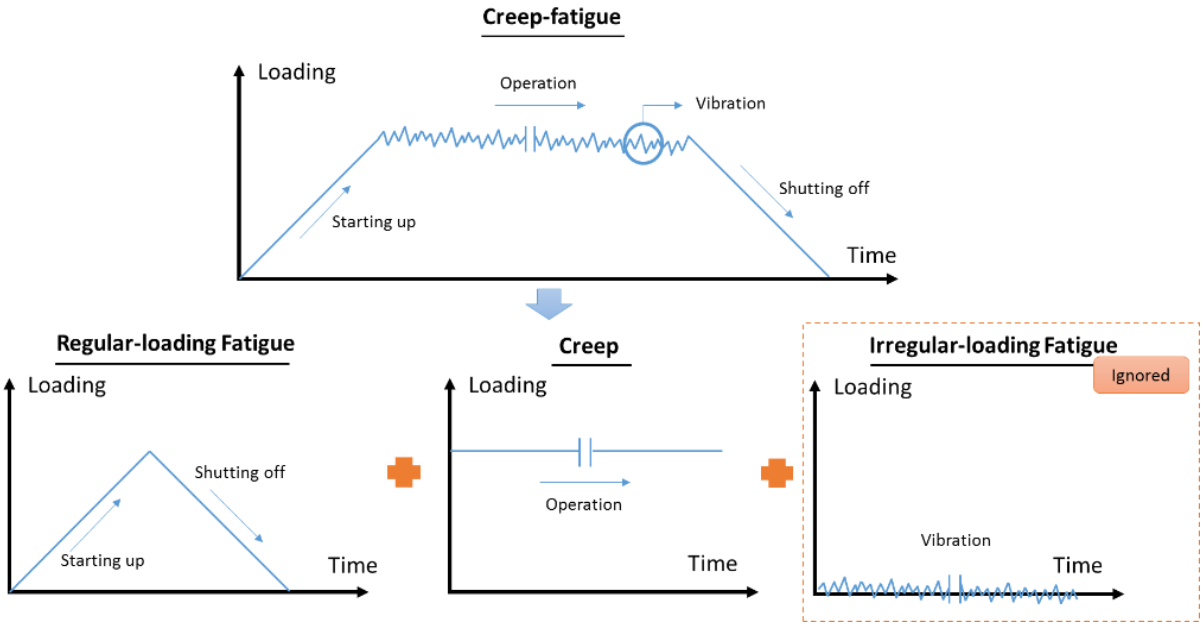

Figure 11.3 The partition of creep fatigue

As shown in Fig.11.3, the fatigue damage is caused by the repeated process of starting up and shutting off, and the maximum loading appears at 100% rotational velocity. The waveform for the loading is a triangle. Normally, the creep-fatigue test could be accelerated through increasing temperature, or frequency or loading. In this case study, the factor to accelerate the process of fatigue failure is identified as the cyclic time (the reciprocal of frequency). Thus, the cyclic time is defined as 1s, which could be identified as the reference cyclic time in the strain-based creep-fatigue equation. Obviously, this cyclic time is higher than the real situation, where it is impossible for the gas turbine blisk to start up and then shut off within one second. However, the choice of frequency does not influence the result of stress/strain distribution for FEA.

It is notable that, in the present case study, the fatigue-life prediction for fatigue partition is conducted at the pure-fatigue condition (the creep effect is dormant), but not at the creep-fatigue condition under loading without hold time. This is because the fatigue-related coefficients (obtained from the unified model), which are applied to evaluate fatigue partition, has included the creep effect. In this case, the evaluation of fatigue partition gives the number of repeated processes of starting up and shutting off under loading without hold time at elevated temperature. The creep damage which occurs during the hold time is considered in the creep partition, where creep-rupture time could be evaluated by the Manson-Haferd parameter.

11.2.1.4 The advantages of applying the coefficients derived from the strain-based creep-fatigue equation

FEA methods such as ANSYS can accommodate creep, fatigue, and creep-fatigue but only with data. Normally, FEA-based creep-fatigue evaluation [160-162] is based on the exploration of creep and fatigue behaviour by experiments, where the relationships of creep strain vs. time and applied loading vs. fatigue life are imported into FEA software as engineering data to

simulate creep-fatigue behaviour. Then, the simulation is conducted under cyclic loading and elevated temperature. Generally, this is a complex process. This is first because amounts of empirical experiment are required, and especially there is a need to redo the creep test when the applied loading is changed. In addition, the introduction of a creep effect may result in non-convergence for FEA, and then the analysis settings may need to be repeatedly modified to get solution convergence. Consequently, it is difficult to apply FEA to early design stages, especially when the creep-fatigue material properties are not yet established empirically.

However, the complexity can be improved by using the strain-based unified creep-fatigue equation. Specifically, this new formulation is used to get the creep-fatigue-related coefficients under the service condition; then these coefficients are introduced into FEA as the engineering data. The key concept is that the unified equation provides a method to transfer the creep effect into the creep-fatigue-related coefficients. Therefore, FEA can be conducted without the need for obtaining explicit creep data. This significantly reduces the complexity of simulation. This process of substitution is described below.

In addition, the creep-rupture time for creep evaluation can be directly obtained through the Manson-Haferd parameter, and this temperature-time relation has already been included in the strain-based creep-fatigue equation. Therefore, the creep-rupture test for evaluating the creep behaviour can be eliminated.

Overall, applying the coefficients obtained from the strain-based unified creep-fatigue equation could significantly reduce the total cost consumed on the creep and fatigue tests.

11.2.2 The methodology

This case study is based on the theory of a highly accelerated life test, and then the material of the gas turbine blisk is determined by combining the unified model and FEA. In particular, the strain-based unified equation gives the coefficients/parameters for evaluating the fatigue and creep damage under service conditions.

11.2.2.1 The flowchart for the whole process

Based on the validation of the strain-based unified creep-fatigue equation, the creep-fatigue-related coefficients for Inconel 718 and GP 91 casting steel were used to evaluate the creep-fatigue damage. The material which has better fatigue and creep capacity is selected for the gas turbine blisk. The design process is presented by Fig.11.4.

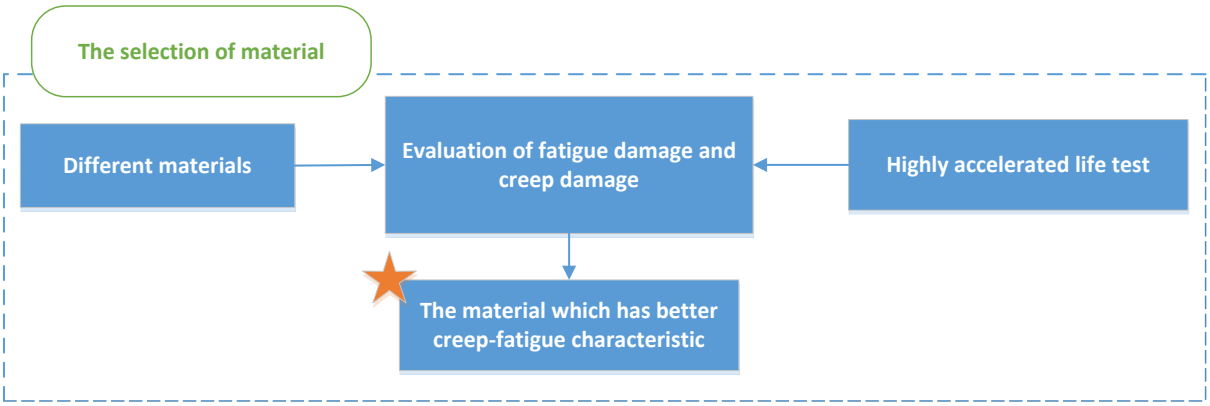

Figure 11.4 The process of design

11.2.2.2 The flowchart for the evaluation of fatigue damage and creep damage

The core (evaluation of fatigue damage and creep damage) shown in Fig.11.4 is detailed in Fig.11.5, where the fatigue damage caused by repeated process of starting up and shutting off (fatigue partition), and creep damage caused by constant loading (creep partition) are evaluated separately. The partition of operation loading was discussed in section 11.2.1.3. In addition, as mentioned in section 11.2.1.1, this evaluation is based on the highly accelerated life test, where the results do not show the real damage under a practical operation situation, but provides an applicable method to improve the product at the initial phase of engineering design.

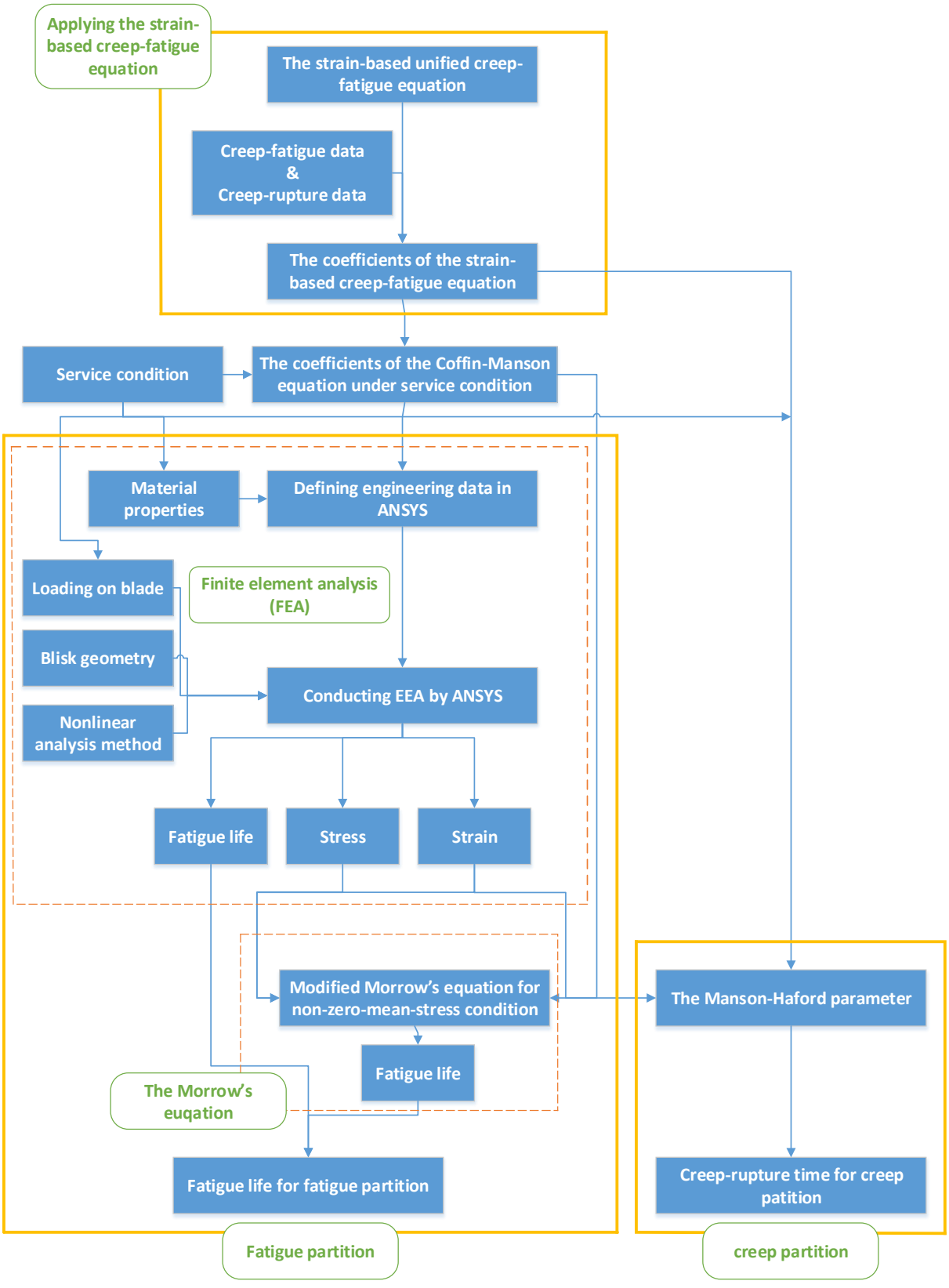

Figure 11.5 The evaluation of fatigue damage and creep damage

The fatigue damage was evaluated by two ways. On the one hand, the strain-based unified creep-fatigue equation gave the creep-fatigue-related coefficients, then these coefficients were

input into ANSYS WORKBENCH as engineering data to calculate the fatigue life. On the other hand, based on stress and strain distribution obtained through FEA, Morrow's equation resulted in another solution. Then, the results obtained by FEA and Morrow's equation were compared; meanwhile, a design decision was made. The fatigue life represents an equivalent number of cycles, which reflects the ability of the gas turbine blisk to accommodate the repeated loading during the process of starting up and shutting off.

The creep damage was evaluated by the Manson-Haferd parameter, which has been included in the strain-based unified creep-fatigue equation. With the stress and strain obtained from FEA, the Manson-Haferd parameter gave the creep-rupture time for creep partition. This presents an equivalent total time for the gas turbine blisk against the constant loading at 100% rotational velocity.

11.2.3 Geometry

The geometry of the gas turbine blisk (Fig.11.6) was downloaded from 'www.grabcad.com' [163] in Solidworks format. One of the blades (Fig.11.7) was selected to conduct finite element analysis in ANSYS WORKBENCH. The key dimensions are shown in Table 11.3.

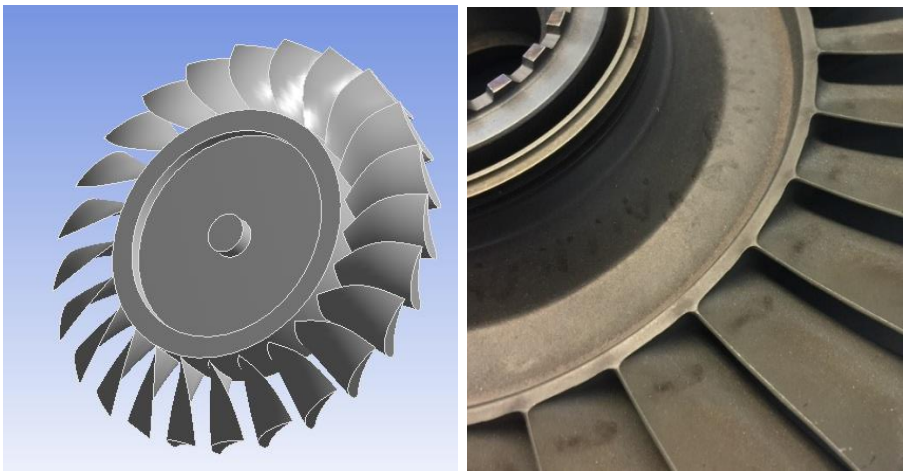

Figure 11.6 Gas turbine blisk

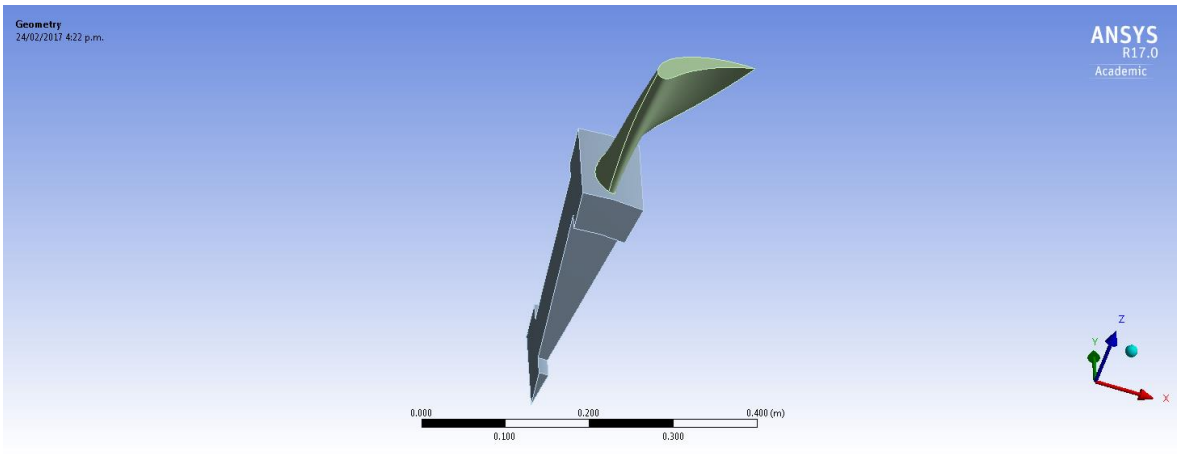

Figure 11.7 The geometry in ANSYS WORKBENCH

Table 11.3 Key dimensions of geometry

No.	Items	Dimensions
1	R_1 (the distance from centre to tip of the blade)	469mm
2	R_2 (the distance from centre to root of the blade)	295mm
3	Number of blades	24
4	The outlet anger for mean cross section	30°
5	The area of mean cross section	3036.45mm^2

11.2.4 Service conditions

The turbine blisk is working under cyclic loading and elevated temperature, and the service conditions are summarised in Table 11.4:

Table 11.4 Service conditions

Rotational velocity (n)	Temperature (T)	Mass flow rate ($\dot{M}$)	Nozzle angle (α)
3000 rpm	811K (538°C)	31.6 kg/s	14°

11.2.5 Material properties (at temperature of 811K)

The design decision on the material is considered between Inconel 718 [164] and GP91 casting steel [100]. The material properties of these two materials at the temperature of 811K are shown in Table 11.5, and they are input into ANSYS WORKBENCH as engineering data and are introduced into Morrow's equation.

Table 11.5 The material properties at 811K for Inconel 718 and GP91 casting steel

Material	Density (kg/m^3)	Yield stress (MPa)	Tensile stress (MPa)	Young's modules (MPa)	Grain size (μm)
Inconel 718	8220	1069	1276	179000	30
GP91 casting steel	7700	342	402	161500	25

11.2.6 The coefficients for creep-fatigue condition

The numerical description of creep-fatigue behaviour is represented by the unified formulation (shown in Chapter 5):

$$\varepsilon_p = C_0 c(\sigma, T, t_c, d) N^{-\beta_0} \tag{11.8}$$

with

$$c(\sigma, T, t_c) = 1 - \left[c_1(\sigma)\left(T - T_{ref}\right) + c_2(\sigma)\log\left(t_c/t_{ref}\right)\right] \cdot \left[A\left(d/d_{ref}\right)^m\right] \tag{11.9}$$

According to the validation shown in Chapter 5 on the materials of Inconel 718 and GP91 casting steel, the coefficients in the unified creep-fatigue formulation with grain-size effect (Eq.11.8) are collected in Table 11.6:

Table 11.6 Coefficients of unified equation for Inconel 718 and GP91 casting steel

Inconel 718							
C_0	β_0	c_2	A	m	T_{ref}(K)	t_{ref}(s)	d_{ref}(μm)
0.4961	0.596	0.0782	0.55005	-0.5411	560	1	30
$c_1(\sigma)$	$2.7679 \times 10^{-3} - 4.12347 \times 10^{-6} \cdot f_m \cdot \sigma + 3.91221 \times 10^{-9} \cdot {f_m}^2 \cdot \sigma^2$						
GP91 casting steel							
C_0	β_0	c_2	A	m	T_{ref}(K)	t_{ref}(s)	d_{ref}(μm)
0.9532	0.669	0.0547	0.5588	-0.4053	610	1	25
$c_1(\sigma)$	$9.51808 \times 10^{-4} + 1.20344 \times 10^{-5} \cdot f_m \cdot \sigma - 1.75045 \times 10^{-8} \cdot {f_m}^2 \cdot \sigma^2$						

Based on the statement of fatigue partition in section 11.2.1.3, the cyclic time is chosen as 1s and f_m is defined as 0.5 for the triangular loading waveform. In addition, the temperature is identified as 811K which is consistent with the service condition shown in section 11.2.4. Then, according to the coefficients shown in Table 11.6, the coefficients of the Coffin-Manson equation (strain-life-related coefficients) are given through the strain-based unified equation. Then, integrating the strain-life-related coefficients with the strain-stress relation, the coefficients of the Basquin equation (stress-life-related coefficients) are represented through the concept of compatibility. These coefficients (at 811K) for Inconel 718 and GP91 casting steel are shown in Table 11.7, and are input into ANSYS WORKBENCH as engineering data.

Table 11.7 The creep-fatigue-related coefficients for Inconel 718 and GP91 casting steel

Material	Coefficients for the Coffin-Manson equation $\Delta\varepsilon_p/2 = C(2N_f)^{\beta}$		Coefficients for the Basquin equation $\Delta\sigma/2 = \sigma(2N_f)^{b}$		Coefficient for the strain-stress relation $\Delta\sigma/2 = K(\Delta\varepsilon_p/2)^{n}$	
	C	β	σ	b	K	n
Inconel 718	0.4828	-0.636	851.6	-0.091775	946	0.1443
GP91 casting steel	0.5093	-0.662	382	-0.0422	398.5	0.0638

11.2.7 Loading

The centrifugal force, tangential force and axial force are the main loadings which cause creep-fatigue damage at elevated temperature during the repeated process of starting up and shutting off. The maximum loading is calculated at the situation of 100% rotational velocity.

11.2.7.1 Centrifugal force

The centrifugal force can be obtained through Eq.11.10 [165]:

$$F_c = 0.5\rho A\omega^2\left({R_1}^2 - {R_2}^2\right) \tag{11.10}$$

where F_c is the centrifugal force, ρ is the density, A is the area of cross section and ω is the rotational velocity in rad/s.

According to the rotational velocity, the magnitude of ω is given by Eq.11.11:

$$\omega = \frac{2\pi n}{60} = \frac{2\pi \times 3000}{60} = 314.2\ rad/s \tag{11.11}$$

Then, the centrifugal force is represented by Eq.11.12:

$$F_c = 0.5 \times 8220 \times 0.00303645 \times 314.2^2 \times (0.469^2 - 0.295^2) = 163780.776\ N \tag{11.12}$$

11.2.7.2 Tangential force and axial force

The tangential force and axial force are calculated by the velocity triangle (Fig.11.8) [160], which is a well-accepted method for the force calculation of a blade.

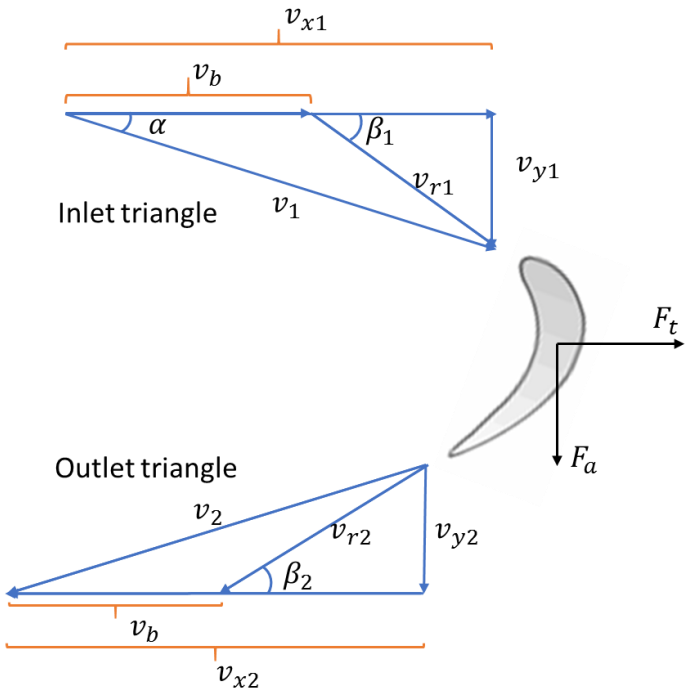

Figure 11.8 Velocity triangle for blade

The mean cross section is selected to calculate the tangential force and axial force. The detailed calculation is shown below:

▪ In the inlet triangle (Eq.11.13-11.18)

$$v_b = \frac{\pi D_m N}{60} = \frac{\pi \times [2 \times 0.295 + (0.469 - 0.295)] \times 3000}{60} = 120.01\ m/s \tag{11.13}$$

$$v_1 = \frac{2v_b}{\cos\alpha} = \frac{2 \times 120.01}{\cos 14°} = 247.55\ m/s \tag{11.14}$$

$$\tan\beta_1 = \frac{v_{y_1}}{v_{x_1}} = \frac{v_1 \sin\alpha}{v_1 \cos\alpha - v_b} = \frac{v_1 \sin\alpha}{v_b} = \frac{247.55 \times \sin 14°}{120.01} = 0.499 \rightarrow \beta_1 = 26.519° \tag{11.15}$$

$$v_{r_1} = \frac{v_1 \sin\alpha}{\sin\beta_1} = \frac{247.55 \times \sin 14°}{\sin 26.519°} = 134.129\ m/s \tag{11.16}$$

$$v_{x_1} = v_1 \cos\alpha = 247.55 \times \cos 14° = 240.1967\ m/s \tag{11.17}$$

$$v_{y_1} = v_1 \sin\alpha = 247.55 \times \sin 14° = 59.8878\ m/s \tag{11.18}$$

▪ In the outlet triangle (Eq.11.19-11.22)

$$v_{r_2} = v_{r_1} = 134.129\ m/s \tag{11.19}$$

$$\beta_2 = 30° \tag{11.20}$$

$$v_{x_2} = v_{r_2} \cos\beta_2 + v_b = 134.129 \times \cos 30° + 120.01 = 67.0645\ m/s \tag{11.21}$$

$$v_{y_2} = v_{r_2} \sin\beta_2 = 134.129 \times \sin 30° = 236.17\ m/s \tag{11.22}$$

Then, the tangential force is given as (Eq.11.23 and Eq.11.24):

$$F_t = \dot{M}\Delta v_x = 31.6 \times (240.1667 + 236.17) = 15052.23972\ N \tag{11.23}$$

$$F_t/blade = \frac{15052.23972}{24} = 627.177\ N \tag{11.24}$$

and the axial force is represented as (Eq.11.25 and Eq.11.26):

$$F_a = \dot{M}\Delta v_y = 31.6 \times (67.0645 - 59.8878) = 226.78372\ N \tag{11.25}$$

$$F_a/blade = \frac{226.78372}{24} = 9.449\ N \tag{11.26}$$

11.2.8 Evaluation of fatigue damage

11.2.8.1 Finite element analysis results

The finite element analysis is conducted through the nonlinear analysis method [160-162, 165]. The material properties shown in Table 11.5 and the creep-fatigue-related coefficients shown in Table 11.7 are input into ANSYS WORKBENCH as engineering data. The boundary condition (force) presented in section 11.2.7 is imposed. Finally, the maximum stress, maximum total strain, and fatigue life are given. The results are tabulated (Table 11.8) and shown in Figs.11.9-11.14.

Table 11.8 FEA results for Inconel 718 and GP91 casting steel

Material	Maximum stress	Maximum total strain	Minimum fatigue life
Inconel 718	1311.8 MPa	0.011597	2350 cycles
GP91 casting steel	755.27MPa	0.029661	327 cycles

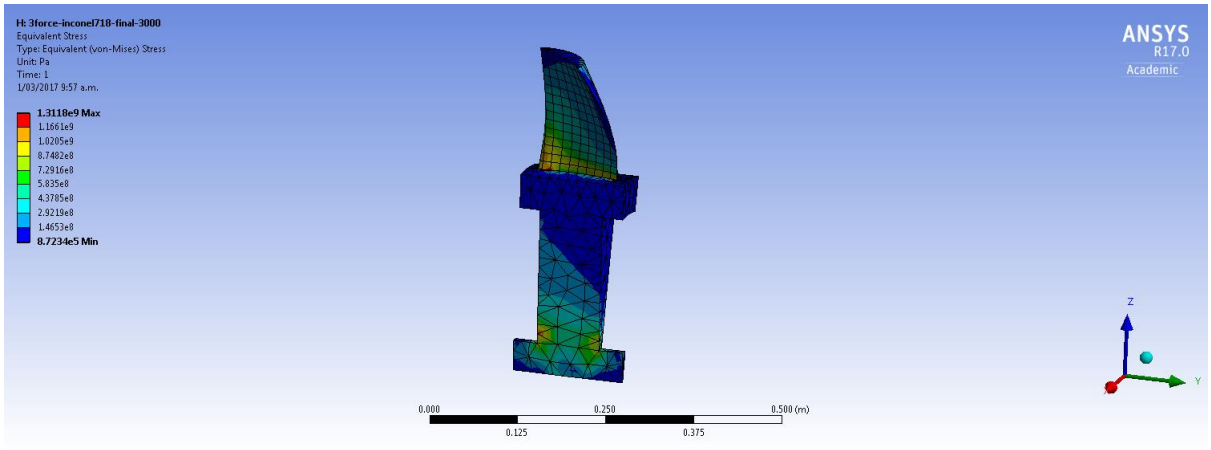

Figure 11.9 The stress distribution for Inconel 718

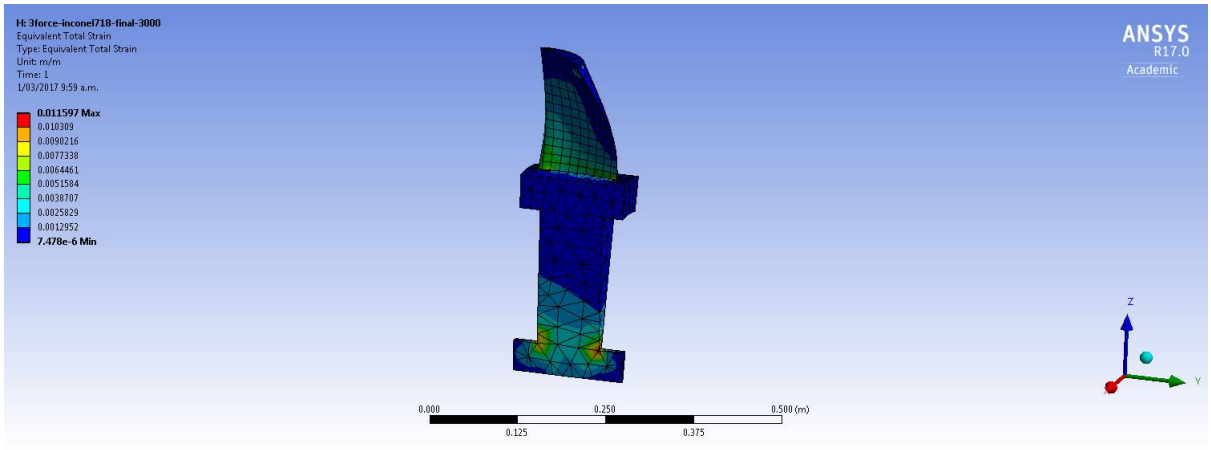

Figure 11.10 The total strain distribution for Inconel 718

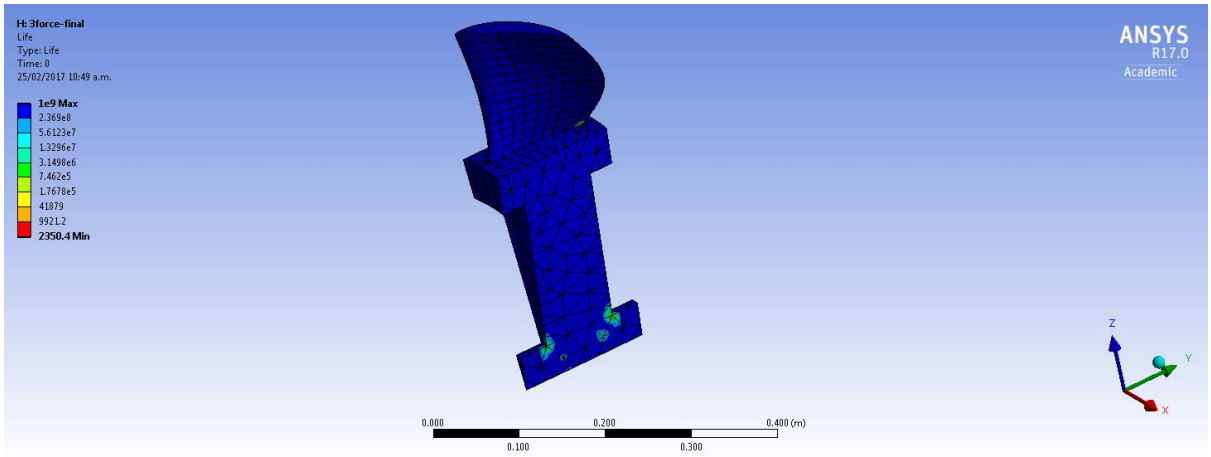

Figure 11.11 The fatigue life distribution for Inconel 718

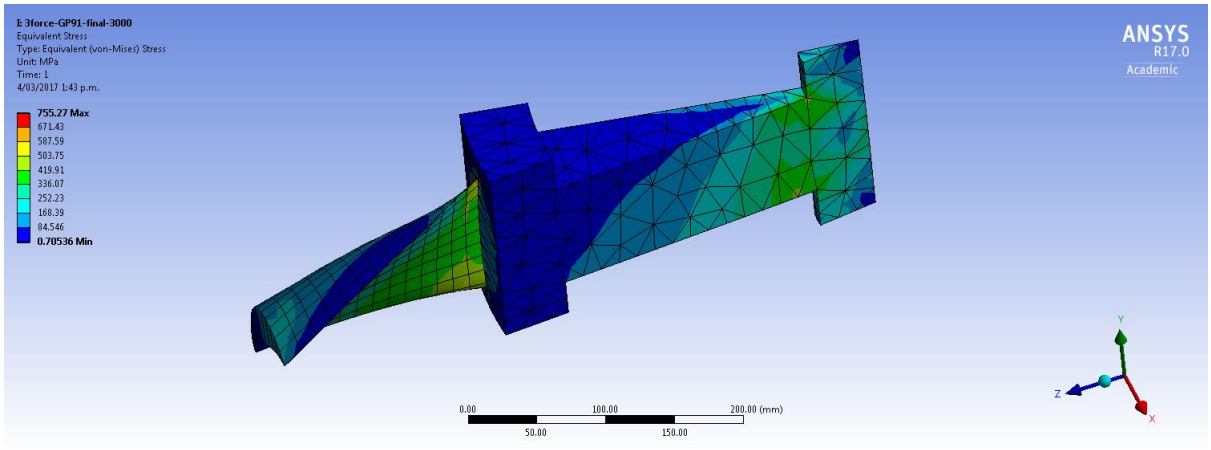

Figure 11.12 The stress distribution for GP91 casting steel

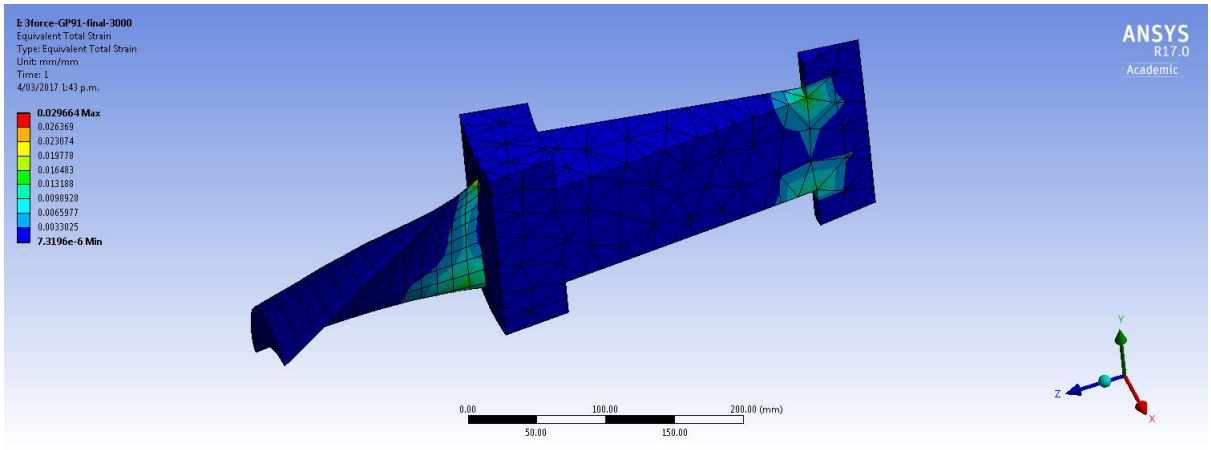

Figure 11.13 The total strain distribution for GP91 casting steel

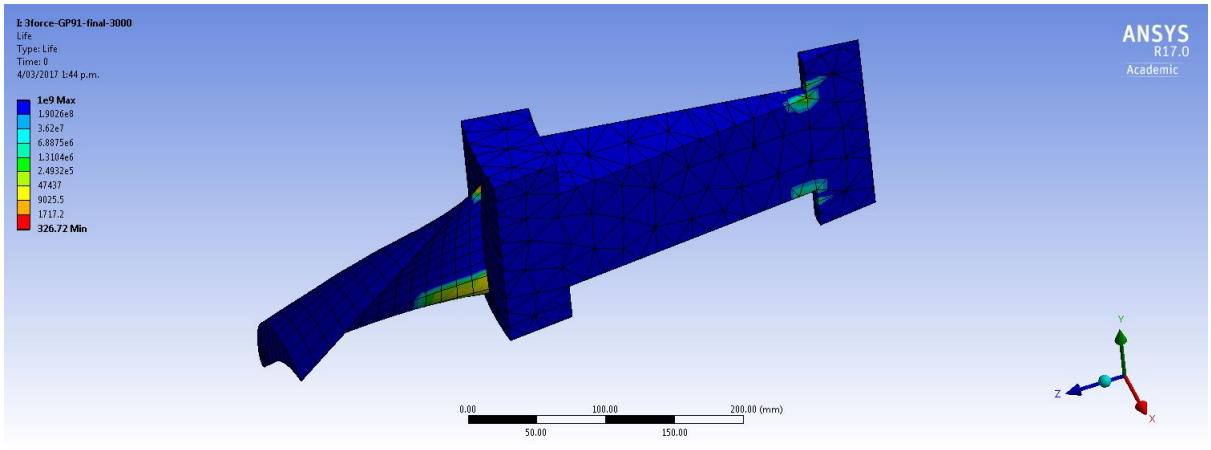

Figure 11.14 The fatigue life distribution for GP91 casting steel

11.2.8.2 The results obtained through Morrow's equation

Based on the stress and strain obtained from FEA, the fatigue life can be calculated through Morrow's equation (non-zero-mean-stress condition) (Eq.11.27):

$$\varepsilon_t = 3.4\left(\frac{\sigma_s - \sigma_m}{E}\right){N_f}^{-0.12} + {C_0}^{0.6}{N_f}^{-0.6} \tag{11.27}$$

where ε_t is the total strain, σ_s is the tensile stress, E is the Young's modulus, C_0 is the fatigue ductility coefficient based on $\Delta\varepsilon_p - N$ relation (0.6215 for Inconel 718 and 0.9757 for GP91 casting steel), and σ_m is the mean stress which is defined as half of the maximum stress obtained from EFA.

Substituting Eq.11.27 with the values obtained from EFA gives following results:

• Inconel 718

$$0.011597 = 3.4\left(\frac{1276 - 1311.8/2}{179000}\right){N_f}^{-0.12} + {0.6215}^{0.6}{N_f}^{-0.6} \tag{11.28}$$

Then, we get:

$$N_f = 2440\ cycles \tag{11.29}$$

• GP91 casting steel

$$0.029661 = 3.4\left(\frac{402 - 755.27/2}{161500}\right){N_f}^{-0.12} + {0.9757}^{0.6}{N_f}^{-0.6} \tag{11.30}$$

Then, we get:

$$N_f = 348\ cycles \tag{11.31}$$

11.2.8.3 Comparing the results

The fatigue damage is evaluated through both FEA and Morrow's equation, and the results are tabulated in Table 11.9. The error (δ) between these two results is given by Eq.11.32.

$$\delta = \frac{N_{f-Morrow} - N_{f-FEA}}{N_{f-FEA}} \times 100\% \tag{11.32}$$

Table 11.9 The results obtained through FEA and the Morrow's equation

Material	The results obtained by FEA	The results obtained by Morrow's equation	δ
Inconel 718	2350 cycles	2440 cycles	3.83%
GP91 casting steel	327 cycles	348 cycles	6.42%

As shown in Table 11.9, the fatigue life obtained through Morrow's equation is higher than the result obtained from FEA. This is because the mean stress dependence is removed from the second term (plastic strain), which reduces the mean-stress effect on the fatigue capacity and hence obtains a longer fatigue-life prediction. In order to get a more reliable prediction, the results obtained by FEA are accepted.

11.2.9 The evaluation of creep damage

According to the FEA results, the maximum plastic strain can be obtained, and it could then be transformed to stress by the stress-strain relation. Note that we do not directly apply the maximum stress obtained from FEA. This is because the stress theoretically was derived from the applied loading, but no creep effect was involved. Thus, the stress obtained from FEA is extremely high. However, the strain or the deformation obtained through including the material properties (which accommodate the creep effect) is not strongly influenced by the process of FEA. In this case, the plastic strain given by FEA is applied to be transformed into stress through the empirical data of the strain-stress relation. By this means, the transformed stress is used to get the rupture time through the Manson-Haferd parameter to evaluate the creep damage. The transformation from plastic strain to stress is shown in Table 11.10.

Table 11.10 The transformation from plastic strain to stress

Material	Maximum plastic strain	Strength coefficient	Strain hardening exponent	Stress (MPa)
Inconel 718	0.0054062	946	0.1443	445.4
GP91 casting steel	0.02498	398.5	0.0638	314.9

According to the validation of the strain-based unified creep-fatigue equation, the Manson-Haferd parameters for Inconel 718 and GP91 casting steel are represented as Eq.11.33 and Eq.11.34 respectively:

$$\frac{1}{P_{MH-718}(\sigma)} = -5.0 \times 10^{-8}\sigma^2 + 5.27 \times 10^{-5}\sigma - 3.5375 \times 10^{-2} \tag{11.33}$$

$$\frac{1}{P_{MH-91}(\sigma)} = 3.2 \times 10^{-7}\sigma^2 - 2.2 \times 10^{-4}\sigma - 1.74 \times 10^{-2} \tag{11.34}$$

Then, substituting the stress with the values shown in Table 11.10 gives the Manson-Haferd parameters. They are -0.0218 for Inconel 718 and -0.0549 for GP91 casting steel. According to the definition of the Manson-Haferd parameter (Eq.11.35), the rupture times for these two materials under the loading of creep partition are given through Eq.11.36. The results are shown in Table 11.11.

$$P_{MH} = \frac{T_a - T}{\log t_a - \log t} \tag{11.35}$$

$$t = 10^{\log t_a - \frac{T_a - T}{P_{MH}}} \tag{11.36}$$

Table 11.11 Creep damage for Inconel 718 and GP91 casting steel

Material	Manson-Haferd parameter	T_a	$\log t_a$	Rupture time
Inconel 718	-0.0218	560 K	12.7805	5588.6 hours
GP91 casting steel	-0.0549	610 K	18.281	4791.9 hours

11.2.10 Design decision

The evaluations of fatigue damage (fatigue partition) and creep damage (creep partition) are collected in Table 11.12. The results shown in Table 11.12 indicate that Inconel 718 has better fatigue capacity and creep capacity than GP91 casting steel. Therefore, Inconel 718 is selected for this gas turbine blisk.

Table 11.12 The evaluation of fatigue damage and creep damage

Material	Evaluation of fatigue damage	Evaluation of creep damage
Inconel 718	2350 cycles	5588.6 hours
GP91 casting steel	327 cycles	4791.9 hours

11.2.11 Discussion

11.2.11.1 Determining total deformation

In this case study, the fatigue damage and creep damage were evaluated separately. Therefore, we propose that the total deformation could be ideally accumulated by the deformations caused by fatigue and creep. The gas turbine blisk mainly operates during the period of constant loading with high temperature, and thus we assume that the total deformation is largely contributed by the creep, and the deformation caused by the fatigue is ignored. This assumption also could be determined according to the result shown by FEA, where the deformation for the fatigue partition is small enough (4mm) to be removed from the total deformation. Therefore, the total deformation could be calculated from the creep-rupture time described in section

11.2.9. Specifically, a creep test under a given temperature and a given stress (which are consistent with service conditions) needs to be done, and then the total creep strain can be obtained through the creep strain-time curve. By this means, the total deformation is evaluated through total creep strain.

11.2.11.2 The relationship between the fatigue and creep partitions

In the present case, the times for each operation unit are normally different. Therefore, we could not give the exact number of operation units to failure under real loading conditions by combining the fatigue damage with creep damage. In this case, the individual fatigue and creep evaluation may be more reasonable.

In addition, as mentioned in section 11.2.1, the theory of the highly accelerated life test is applied for fatigue-damage evaluation. This implies that the fatigue-related result shown in this case study cannot present the real damage in service conditions. Specifically, the fatigue damage is enlarged because of the intensified frequency/time effect. In contrast, the evaluation of creep damage may present a more reasonable result. However, the interaction between creep and fatigue is not considered. Therefore, it is improper to linearly combine these two damages to evaluate the total damage since this method may result in overestimating the creep-fatigue capacity.

A general guide for engineering design could be shown as follows:

(1) If the gas turbine blisk experiences a frequent process of starting up and shutting off, but the time for running under constant loading is very short compared to the total rupture time, the evaluation of fatigue partition would be more important.

(2) If the gas turbine blisk works under constant loading and high temperature for a long time at each operational unit, the evaluation of creep partition would be regarded as a more crucial item.

(3) Between these two situations shown above, the fatigue damage and the creep damage should be considered equally, and a recommended improvement/optimization for the gas turbine blisk should give both high fatigue capacity and high creep resistance.

11.3 Summary

The results demonstrate that the unified creep-fatigue equation may readily be applied to engineering design. In general, the coefficients of the unified model can be extracted with minimum experimental effort. Then, with the coefficients, the unified equation can be applied to evaluate fatigue capacity under multiple situations. In addition, the unified model can be combined with FEA, whereby a simpler method of creep-fatigue simulation is presented since the creep-related parameters could be removed from simulation (this reduces the complexity).

To verify the applicability of the unified model for engineering design, a case study of a gas turbine blisk for material selection was conducted. In this case study, the fatigue damage and creep damage were evaluated separately. For the fatigue partition, the creep-fatigue-related coefficients obtained from the unified model were imported into FEA as engineering data, which significantly reduces the complexity of the creep-fatigue simulation. In addition, the creep damage was evaluated through the Manson-Haferd parameter (this parameter is included in the unified formulation). Consequently, this case study indicates that the unified creep-fatigue equation provides a convenient method for engineering design.

Chapter 12

12. Discussion

This chapter evaluates the results given by the present work. In this chapter, the outcomes are collected. Then, an overall evaluation on the usefulness of the unified creep-fatigue models is conducted by applying a four-level maturity model. Finally, the limitations of the present work are identified, and the future directions of research are proposed.

The review of existing creep-fatigue models indicates that there is a need to develop a new creep-fatigue model (for engineering design) which could be applied in multiple situations for multiple materials, cover the full range of conditions from pure fatigue to pure creep, and provide an economical method for fatigue-life prediction. In this case, based on the concept of fatigue capacity, a strain-based unified creep-fatigue equation was developed through the combination of the constitutive-based and empirical-based method. This equation was then modified to describe creep-fatigue behaviour at a microstructural level by introducing the parameter of grain size. The strain-based model was validated on materials with low melting points to those with high melting points in multiple situations. This strain-based approach normally is applied at the low-cycle fatigue regime. In this case, to construct a whole map, a stress-based unified creep-fatigue equation, which is normally applied at the high-cycle fatigue regime, was then developed by using the same principle of derivation. Comparing with the existing creep-fatigue models, the new creep-fatigue models show significant advantages in the areas of unifying, integration and economy, which are strongly desirable for engineering design. The fundamental principle to have these advantages results from the physical-justification-based constitution of the unified formulations. The relationships accommodated in the unified formulation were verified to be consistent with the physical mechanisms of fatigue and creep, such as diffusion creep and crack growth. Then, a conceptual graphical-based mode was proposed based on the understanding of crack growth, which illustrates the whole process of damage accumulation from crack initiation to crack propagation then to fracture. Finally, a guide for applying the unified creep-fatigue model to engineering design

was given, and a case study on a gas turbine blisk for material selection was presented. Significantly, introducing the unified model into FEA reduces the complexity of the creep-fatigue simulation. Overall, the development of the unified creep-fatigue equations provides a convenient and applicable method for fatigue-life prediction for engineering design, where both accuracy and economy are considered.

12.1 Outcomes

In general, the present work successfully answered the questions which were proposed in Chapter 3. This is summarised in Table 12.1:

Table 12.1 General results

No.	Questions	Results
1	Does this model accurately represent the empirical data for multiple situations and multiple materials?	YES. The new model can be applied in multiple situations for multiple materials with the high quality of fitting to empirical data.
2	Does this model have the ability to cover the pure-fatigue condition, the creep-fatigue condition, and the pure-creep condition?	YES. The new model has the ability to cover the full range of conditions from pure fatigue to pure creep.
3	Is this model practicable and useful for engineering design?	YES. The new model presents a good balance between accuracy and economy, particularly when applied to a case study.
4	Is this model consistent with the underlying physical mechanisms?	YES. The relationships between different variables present good consistency with the underlying physical mechanisms, such as diffusion creep and crack growth.

In addition, the unified model developed in the present work presents a clear structure that is understandable by engineering practitioners, includes the general variables at the engineering scale (such as temperature, time and loading), and can be easily mathematically solved by Excel. These are important for application by engineering practitioners.

More details for these outcomes are shown below.

12.1.1 Development of a strain-based unified creep-fatigue equation

The literature review shown in Chapter 2 indicates that the existing creep-fatigue equations represent significant limitations (including non-unifying, non-integration, poor economy and poor physical explanation) for engineering application.

In the present work, the concept of fatigue capacity has been proposed. This concept was then combined with the relationships extracted from the conventional models to develop a strain-based unified creep-fatigue equation (Eq.12.1):

$$\varepsilon_p = C_0 c(\sigma, T, t_c) N_f^{-\beta_0} \tag{12.1}$$

with

$$\begin{gathered} c(\sigma, T, t_c) = 1 - c_1(\sigma)\left(T - T_{ref}\right) - c_2 \log\left(t_c / t_{ref}\right) \\ T - T_{ref} = \begin{cases} T - T_{ref} & for \;\; T > T_{ref} \\ 0 & for \;\; T \le T_{ref} \end{cases} \\ t_c / t_{ref} = \begin{cases} t_c / t_{ref} & for \;\; t_c > t_{ref} \; and \; T > T_{ref} \\ 1 & for \;\; t_c \le t_{ref} \; or \; T \le T_{ref} \end{cases} \end{gathered} \tag{12.2}$$

where ε_p is the plastic strain which reflects fatigue capacity, N_f is the creep-fatigue life, C_0 and β_0 are fatigue ductility coefficient and fatigue ductility exponent respectively which are related to the fatigue capacity at the pure-fatigue condition, T is the temperature, t_c is the cyclic time which is the reciprocal of loading frequency, T_{ref} is the reference temperature which is defined as 35% of the melting temperature, t_{ref} is the reference cyclic time which is suggested as a small value, σ reflects the applied loading which can be related to plastic strain through the cyclic strain-stress relation, and $c_1(\sigma)$ and c_2 are the creep-related function and constant.

12.1.2 Introduction of heat-treatment effect into the creep-fatigue model

The heat-treatment effect was then included in the strain-based model by introducing the parameter of grain size, which results in the ability to describe creep-fatigue behaviour at a microstructural level. The strain-based unified creep-fatigue equation with grain-size effect (Eq.12.3) is represented as:

$$\varepsilon_p = C_0 c(\sigma, T, t_c, d) N^{-\beta_0} \tag{12.3}$$

with

$$c(\sigma, T, t_c) = 1 - \left[c_1(\sigma)\left(T - T_{ref}\right) + c_2 \log\left(t_c/t_{ref}\right)\right] \cdot \left[A\left(d/d_{ref}\right)^m\right]$$

$$T - T_{ref} = \begin{cases} T - T_{ref} & for \;\; T > T_{ref} \\ 0 & for \;\; T \le T_{ref} \end{cases} \tag{12.4}$$

$$t_c/t_{ref} = \begin{cases} t_c/t_{ref} & for \;\; t_c > t_{ref} \; and \; T > T_{ref} \\ 1 & for \;\; t_c \le t_{ref} \; or \; T \le T_{ref} \end{cases}$$

where d is the grain size, d_{ref} is the reference grain size which is suggested as an arbitrary value but recommended to be selected from the value among the experimental range, and A and m are the grain-size-related constants.

12.1.3 Validation and critique of the strain-based model

The creep-related coefficients are derived from creep-rupture data, and especially the Manson-Haferd parameter is included. In addition, the fatigue-related coefficients are extracted from empirical data of creep fatigue through numerical optimization. In particular, a moderating factor (f_m) was applied to transform the creep-related damage under constant loading into an equivalent situation with cyclic loading. By the method shown above, the strain-based unified creep-fatigue equation was then validated on the materials of 63Sn37Pb solder, 96.5Sn3.5Ag solder, 2024T3 aluminium alloy, stainless steel 316, stainless steel 304, Inconel 718 and GP91 casting steel, and the experimental data in multiple situations (multiple temperatures, cyclic times and grain sizes) were extracted from the literature. The validation strongly demonstrates that the strain-based approach has the ability to predict the creep-fatigue life with high accuracy across multiple materials.

In addition, through comparing with existing creep-fatigue models, the strain-based model presents more significant advantages. Specifically, the strain-based unified formulation can be applied in multiple situations for multiple materials, can cover the full range of conditions from the pure-fatigue condition to the pure-creep condition, can provide an economical method for fatigue-life prediction and can avoid the risk of model non-identifiability or degeneracy.

Furthermore, based on the discussion and critique of the strain-based model shown above, the grain-size-modified Manson-Haferd parameter ($P_{MH}(\sigma, d)$) (Eq.12.5) was initially proposed as:

$$P_{MH}(\sigma, d) = \frac{T_{ref} - T}{A\left(d/d_{ref}\right)^m \log t_a - \log \mathrm{t} + \left[1 - A\left(d/d_{ref}\right)^m\right] \log t_{ref}} \tag{12.5}$$

and the strain-based formulations were further simplified as:

$$\Delta\varepsilon_p = 0.8965 D^{0.3995} c(\sigma, T, t_c) N_f{}^{-0.629} \tag{12.5}$$

or

$$\Delta\varepsilon_p = 0.8965D^{0.3995}c(\sigma, T, t_c, d)N_f{}^{-0.629} \tag{12.6}$$

through including the parameter of ductility (D). Especially, this simplified formulation implies that no or less creep-fatigue data are required to obtain the coefficients, which provides a more economical method for fatigue-life prediction but the accuracy may be reduced. We believe that the accuracy may be further improved as more materials are investigated.

12.1.4 Development and validation of a stress-based model

The strain-based approach is normally applied to the low-cycle fatigue regime. In this case, to construct a whole map for creep fatigue, a stress-based model (a classic method) was developed through including an element of physical justification and applying the concept of fatigue capacity. Particularly, the numerical simplification was applied during the process of derivation. The stress-based unified creep-fatigue equation (Eq.12.7) is represented as:

$$\sigma = \sigma_0 \cdot B(d) \cdot C(T, t_c, \sigma, d) \cdot N_f^{-b_0} \tag{12.7}$$

with

$$\begin{gathered} B(d) = \left(d/d_{ref}\right)^m \\ C(T,t,\sigma,d) = 1 - A \cdot \left[\left(d/d_{ref}\right)^n \cdot f_m^a \cdot \sigma^a \cdot e^{-\frac{Q'}{T-T_{ref}}} \cdot \left(t_c/t_{ref}\right)\right]^k \\ T - T_{ref} = \begin{cases} T - T_{ref} & for \;\; T > T_{ref} \\ \rightarrow 0 & for \;\; T \le T_{ref} \end{cases} \\ t_c/t_{ref} = \begin{cases} t_c/t_{ref} & for \;\; t_c > t_{ref} \; and \; T > T_{ref} \\ 1 & for \;\; t_c \le t_{ref} \; or \; T \le T_{ref} \end{cases} \end{gathered} \tag{12.8}$$

where σ is the applied stress which reflects fatigue capacity, σ_0 and b_0 are the fatigue strength coefficient and fatigue strength exponent respectively which are related to fatigue capacity at the pure-fatigue condition, and A, Q', n, a and k are constants.

In general, the Sherby-Dorn parameter was included to derive the creep-related coefficients, and the creep-fatigue data were applied to extract the fatigue-related coefficients through numerical optimization. In the same way as the strain-based approach, a moderating factor (f_m) was also introduced to conduct an equivalent transfer for creep damage. Particularly, the numerical optimization for the stress-based model was conducted by combining with the strain-based model, where the compatibility was included. This provides a better description for the pure-fatigue condition. The stress-based unified creep-fatigue equation was then validated on the materials of Inconel 718 and GP91 casting steel. The validation shows that the stress-based formulation has the ability to predict fatigue life in multiple situations for multiple materials, and can cover the full range of conditions from the pure-fatigue condition to the pure-creep condition.

12.1.5 Extension to the situation with non-zero mean stress

The strain-based and stress-based unified formulations shown above are only applied to the situation with zero mean stress. However, for some practical engineering situations, the mean stress is not zero. In this case, based on the well-accepted method presented in the previous research, the unified formulations were extended to the situation with non-zero mean stress. The stress-based modified formulation is represented as:

$$\sigma = \sigma_0 \cdot \left(1 - \frac{\sigma_m}{\sigma_0}\right) \cdot B(d) \cdot C(T, t, \sigma, d) \cdot N_f^{-b_0} \tag{12.9}$$

and the strain-based modified formulation is represented as:

$$\varepsilon_p = C_0 \left(1 - \frac{\sigma_m}{\sigma_0}\right)^{\frac{\beta_0}{b_0}} c(\sigma, T, t_c, d) {N_f}^{-\beta_0} \tag{12.10}$$

where σ_m is the mean stress.

The well-accepted method which was applied to develop the modified creep-fatigue models is based on an assumption that the strain-stress relations in the situations with zero and non-zero mean stress are the same. However, the investigation into the empirical data and FEA results implies that this assumption may not be accurate. Further improvement is a complex issue, and thus is not included in the present work but opens an opportunity for future research.

12.1.6 Explanation of the underlying physical mechanisms

As mentioned above, the unified creep-fatigue models present more significant advantages than the existing creep-fatigue models in the areas of unifying, integration and economy. In general, these advantages fundamentally result from the consistency between the unified models and the underlying physical mechanisms, such as diffusion creep and crack growth. In addition, the concept of fatigue capacity numerically presents the negative effect of creep damage in the form of '1-x', and the introduction of the reference condition builds a bridge between pure fatigue and creep fatigue (numerically presents the activation of creep effect). Therefore, we conclude that the unified creep-fatigue models can numerically reflect physical phenomena and can be well explained by physical mechanisms. The relationships between different variables and the corresponding physical mechanisms are shown in Table 12.2:

Table 12.2 Relationships between different variables and their physical bases

Mechanisms	Variables	Strain-based model	Stress-based model
Diffusion creep	Temperature vs. applied loading	Linear relation (simplification)	Natural exponential relation

Diffusion creep	Temperature vs. cyclic time	Logarithmical relation	Natural exponential relation
Diffusion creep	Grain size vs. applied loading (creep component)	Power-law relation	Power-law relation
dislocation pile-up	Grain size vs. applied loading (fatigue component)	---	Power-law relation
Crack growth	Life vs. applied loading	Power-law relation	Power-law relation
Fatigue capacity	Negative effect of creep	Form of (1-x)	Form of (1-x)
Activation of creep effect	Temperature, cyclic time and grain size	the reference condition	the reference condition

In addition, based on the physical phenomena of crack growth and diffusion, a conceptual graphical-based model was initially proposed. Specifically, this conceptual model illustrates the creep-fatigue damage accumulation from the crack initiation to crack propagation then to structural failure, and especially the concept of plastic blunting caused by cyclic loading and the mismatch behaviour at the grain boundary caused by creep were included. We believe that this model still has opportunities to be further modified by an intensified investigation into the creep-fatigue mechanism.

12.1.7 Application to engineering design

The unified creep-fatigue model was applied to an engineering application. In this case, a guide to apply this unified model to engineering design was described, which includes the requirements for tests, derivation of coefficients and application of a practical situation.

Then, a case study of a gas turbine blisk for material selection was given, particularly, the theory of highly accelerated life test was applied and the creep-fatigue-related coefficients calculated from the unified model were imported into the simulation as engineering data. The result shows that the combination of the unified formulation and FEA reduces the complexity of the creep-fatigue simulation. The case study indicates that the unified creep-fatigue equation provides a convenient and applicable method for engineering design.

12.2 Evaluating the maturity of the model

Generally, the goodness of a numerical model can be evaluated through the concept of 'maturity'. In the present work, we propose a four-level maturity model to evaluate a numerical model. Specifically, the maturity level is divided into four sub-levels: accurate level (lowest level), unified level, comprehensive level and universal level (highest level). The description of maturity level is shown in Table 12.3:

Table 12.3 Description of maturity level

Levels	Level 1	Level 2	Level 3	Level 4
Name	**Accurate level**	**Unified level**	**Comprehensive level**	**Universal level**
Formulation	Unexplained power or polynomial formulation	Partially consistent with the expected underlying mechanisms	Plausible explanation based on physical realism	Consistent with physical mechanisms
Coefficients	No link to physical meaning, and are entirely model calibration factor or statistical variables	Qualitatively link to physical meaning, thus can be derived through combination of physical phenomena and empirical data	Quantitatively link to physical meaning, and thus can be totally derived from physical phenomena	Based on physically independently measurable parameters (such as yield stress, Young's modules, and Poisson's ratio)
Parameters	The simplest assumption of parameters, such as temperature or frequency	All environment-related parameters (temperature and frequency/time/strain rate)	All environment-related parameters, and the parameters for groups of materials	All relevant parameters (including all environment-related and material-related parameters)
Construct validity	Only applicable for one specific material is included	Recalculate coefficients for different materials in one group of materials are included	Applicable to one group of materials (such as metal and plastic) are included	Applicable to new materials are included

Range of failure mechanism	Only covers pure fatigue, or creep fatigue, or pure creep	Covers two of these three ranges	Partially covers all these three ranges	Covers pure fatigue, creep fatigue and pure creep
Testing for accuracy	Requires comprehensive testing across full range of the variables (maximum experimental effect)	Economical tests but reasonably degraded accuracy (Economical-test process means fewer testing groups are involved, and thus lower cost.)	Economical tests with high accuracy	Simple & economical tests with high accuracy (minimal experimental effect) (Simple test refers to the test with a simple process, such as creep-rupture test and tensile test.)
Sensitivity	Strongly sensitive to the quantity and quality of empirical data	Reduced quantity and quality of empirical data with reasonably degraded accuracy	Reduced quantity and quality of empirical data with high accuracy	No dependence on the empirical data of creep fatigue

Taking the strain-based unified equation as an example, the goodness of this equation is evaluated by comparing with other existing creep-fatigue models. The scores, which are necessarily subjective, given by different formulations are shown in Table 12.4:

Table 12.4 Evaluation of different models based on the maturity level

Models	**Coffin's equation**	**Shi's equation**	**Wong & Mai's equation**	**Strain-based unified equation**
Formulation	1	1	2	2
Coefficients	1	1	1.5	2
Parameters	1	2	2	2.5
Construct validity	1	1	2	2
Range of failure mechanism	1	1	3	4
Testing for accuracy	1.5	1	1	2.5
Sensitivity	1.5	1	1	2.5

Total	**8**	**8**	**12.5**	**17.5**

Table 2 shows that the strain-based unified creep-fatigue equation is more mature than other existing models but still has the opportunity to be further improved. This method also can be applied to evaluate the stress-based unified creep-fatigue equation, and the outcomes are about the same.

12.3 Limitations and Opportunities for further development

Based on the evaluation of maturity, we realize that the research (development of the creep-fatigue models) conducted in the present work suggests opportunities for further improvement (towards achieving the 'universal' level):

(1) The unified creep-fatigue models were validated using limited empirical data and limited metallic materials. Thus, the new model may not be applied for plastics and composites since they present totally different materials characteristics and failure mechanisms. In this case, the relationships between different variables in the unified models may not be extended to other material categories. However, we believe that this new model may be further improved as more empirical data on more materials are included. The improved formulation may have opportunity to cover extensive situations. *To achieve this, it may be necessary to explore more empirical data on more materials. In addition, more microstructural-level-based parameters may be included, and a corresponding inclusion of new terms into the unified formulation.*

(2) The unified creep-fatigue equation is applicable to cyclic loading without hold time. In this loading condition, fatigue makes more of a contribution than creep on failure, because the total time is too small to produce remarkable creep damage. However, for the cyclic loading with the hold time, the creep effect gradually intensifies as the hold time increases. Then, more creep damage is produced than fatigue damage, and the failure finally occurs due to the creep effect. We could imagine that in the situation with a relatively short hold time, the unified formulation may still present a reasonable prediction of fatigue life, but the accuracy of this prediction may become worse when the hold time is prolonged. This implies that the unified formulation has an opportunity to be further modified to cover the situation with hold time or relatively long cyclic time. In this case, the modified formulation could be extended to more engineering situations and even directly give the fatigue-life prediction for the whole of (say) a turbine operational cycle. *To achieve this, it would seem necessary to modify the formulation (especially, the creep component in this unified model) to include new terms of as yet-unknown mathematical form.*

(3) The existing creep-fatigue models are lacking physical meaning due to curve-fitting-based derivation. The unified creep-fatigue equation has somewhat reduced this problem. This is because the relationships between different variables were derived from the conventional

models, the well-known time-temperature parameter (creep) was included, and the reference condition which indicates the threshold of the creep effect was introduced. However, the coefficients still cannot be derived without performing any creep-fatigue test, and thus this unified formulation cannot be fully explained from a physical perspective. However, it is difficult to quantitatively relate the coefficients with microstructural behaviour because of the unknown way of mathematically determining the impact intensity of macro-variables on creep fatigue at the fundamental level (see Chapter 3). In this case, the unified creep-fatigue models have an opportunity to be further improved to reduce the dependence on empirical data. Then, the coefficients in the unified formulation can be partly predicted without any experiments or with fewer experiments. Thus, a more economical method for the fatigue-life prediction would be advantageous, and this would also reduce the sensitivity to the quality and quantity of empirical data. *To achieve this, it would be necessary to find a way to relate the coefficients to the general material properties, possibly starting from first principles by using the modelling method.*

An ideal future state would be to find a creep-fatigue model that included the mechanical materials properties (such as elastic modulus, yield stress, hardness, etc.). No existing model does this satisfactorily. A similar problem applies to microstructure – it too cannot currently be used to predict the life of a part. In section 2.4.4 we explore why there may be intrinsic limitations in the ability of all existing models to describe the relationships between microstructure, mechanical properties, and part life.

An approximate formulation might be achievable if sufficient creep-fatigue data could be obtained for a variety of mechanical and microstructural properties. In which case curve fitting would be the simplest method to represent these properties. For example the coefficients in the unified equation could be replaced with power series functions of mechanical and microstructural properties. This would be likely to give an accurate representation, providing sufficient data could be collected. However there are two limitations. The first is the practical difficulty of collecting this amount of data. Even then the results would only be valid for the specific situations covered, and would not generalise to other conditions of loading etc, or to other materials. The second limitation is that the model would become more abstract. The current unified equation can be linked, at a broad level, to physical mechanisms. However if additional power series were added then there would potentially be difficulty providing a physical explanation for the relationships.

It is not even certain that an explicit formulism exists at all. Instead it appears that the damage caused by thermal (creep) and cyclic (fatigue) loading is a complex emergent property, i.e. arises progressively and is high dependent on the immediate prior state of the microstructure in a chaotic manner. This is consistent with the observed cascade nature of the failure process. If so, then the ‘true’ solution for creep-fatigue may be none of the existing approaches but perhaps instead a simulation system based on molecular dynamics applied to the part as a whole and covering the full life of the part.

(4) The unified creep-fatigue formulations with mean-stress effect are based on a conventional underlying premise that the strain-stress relations under the situations with and without mean-stress effect share the same characteristics. The present work has identified that this is strictly not the case (see Chapter 8). Thus, there is a need for a better stress-strain model. *To achieve this, it would be necessary to apply a mathematical approach based on first principles to represent the underlying material science mechanics.*

(5) In addition, the graphical-based crack-growth model proposed in the present work is a conceptual model. Some of the fatigue and creep behaviours have been well demonstrated and explained in previous research, such as stress distribution at the crack tip for fatigue and the stress concentration at the triple point for creep. However, there are still some behaviours which are difficult to validate through experiments, such as the situation with the crack tip at the grain boundary. Our conceptual model of fatigue and creep has offered an explanation of these behaviours, but this work is conjectural. It would be valuable to test the validity of this at the microstructural level. *To achieve this, it would be necessary to combine fractography and fatigue tests. However, it is difficult and complex to empirically examine and investigate the phenomena at the grain boundary since it will be difficult to dynamically capture those moments when the crack tip arrives at the grain boundary. A new experimental method may also need to be developed.*

(6) A potential criticism of the unified formulation is that it is incomplete to constitute a unified model disregard the microstructural properties. These properties include grain size & morphology, chemical composition, precipitates, dislocation dynamics, sub-grain boundaries, cracks and voids.

It is true that both fatigue and creep damage occur via effects at the level of the grain and their boundaries. However the relationships of these individual factors to fatigue, creep, or creep-fatigue, are only partially understood, do not link to mechanical properties, and are not formulated in ways useful to design engineers. Even the energy models (section 2.2.4) and physical-damage based models (section 2.1.3) have these limitations.

From a design perspective there is no existing model or theory that integrates all the microstructural variables to the point of being able to predict the life of a specific material under the load conditions anticipated by the design engineer.

Furthermore, these factors are difficult to measure, and neither do vendors of material provide these characteristics. Consequently design engineers have to make decisions based on the imperfect information they have, hence the *complexity* issue (section 2.4.5). Design engineers assume that the material they are working with is in a default as-supplied state. They assume there is a default microstructure in place, e.g. that heat treatment has developed some type of grain size and morphology. They have no specific knowledge or mathematical expression of how that microstructure affects the fatigue-creep properties of their part. Instead they merely assume that the vendor has developed the microstructure to the extent necessary to deliver the specified mechanical properties. Additional microstructural information may become available to a design engineer from optical-, electron-microscopy or spectroscopy, e.g. knowledge of the actual grain morphology, distribution of precipitates, development of boundary migration or

sub-grain boundaries, variation in chemical composition, or crack growth. However this information is of no value to the design engineer as there is no method to reliably use this as part of the design considerations. This is a consequence of the imperfect body of knowledge connecting the microstructure to the level at which the design of machine elements occurs.

Hence engineering designers rely on simple formulations such as the Marin equation (Eq.1.1), where all the parameters are based on variables that they can observed, such as ultimate tensile strength and surface condition (among others).

We acknowledge that the unified equation presented here also suffers from these same limitations. It does not link the microstructural properties to the mechanical properties. Thus we do not claim that the model is complete. Nonetheless the model does have features that are unique and which improve the situation from an engineer design perspective. First, the model integrates all of creep, fatigue, and creep-fatigue into one convenient formulation. The alternative would be for designers to use multiple different formulations in a disjointed manner. Second, the model does demonstrate the feasibility of including one microstructural property, namely grain size.

12.4 Summary

The unified creep-fatigue model proposed in the present work suggests significant advantages for engineering application. Specifically, this unified model has the ability to be applied in multiple situations for multiple materials, cover the full range of conditions from pure fatigue to pure creep, provide an economical method for fatigue-life prediction and show a physical-based explanation. In particular, this new model is applicable to engineering design, and can be combined with finite element analysis to give a more convenient method for simulation. Based on the four-level maturity model, we also realize that the present work still implies that there are some possible opportunities for future research.

Chapter 13

13. Conclusions

Key explanations

The present work aimed to develop a unified creep-fatigue model for engineering purposes, thus the most important is that this unified model should be easily used by day-to-day engineers, e.g. those working in design. From the perspective of formulating such a model, it is desirable that the creep-fatigue model should have a clear structure that is understood by engineering practitioners, include the general variables at the engineering scale (temperature, period, and loading), be easily mathematically solved, and provide an accurate and economical method for life prediction.

Existing models cannot be applied at multiple situations on multiple materials, and require large amounts of empirical data. Specifically, the existing models are purely empirical-based models, and thus the relationships between different variables are totally numerical-based, and no physical meaning is involved. Therefore, the existing models cannot be extended to other materials. In addition, the existing models normally take the polynomial form, and the accuracy of curve fitting strongly depends on the number of power series. Large quantities of empirical data are involved, and thus poor economy results.

The current work overcomes these limitations by the development of a unified model, and hence moves the field forward regarding empirical-based models of creep-fatigue. Key attributes are:

- The ability to be applied in multiple situations (loading, temperature, and cycling time) for multiple metallic materials.
- Covers the full range of conditions from pure creep to creep-fatigue to pure fatigue.
- Provides a method of extracting the coefficients and hence an economical method for fatigue-life prediction based on limited empirical data.

- Shows the basics of a physical-based explanation that connects the formulation to underlying physical mechanisms of fatigue and creep, at least to some degree.
- Furthermore this new model is applicable to engineering design, and can be combined with finite element analysis to give a more convenient method for simulation by engineering practitioners.

The unified models (strain and stress version) provide improved formulations for creep-fatigue. In the present work, we continue the tradition of applying curve fitting to derive the coefficients in the unified model. Nonetheless the unified model is fundamentally different to existing models. The improvements are achieved by integration of components of conventional fatigue and creep models into a new formulation. The formulation as a whole is novel.

Physical basis of creep fatigue

While it is desirable that creep and fatigue be fully explained from a physical perspective, the current model only makes a start at this. A particularly difficult fundamental problem is to quantitatively relate the coefficients with microstructural behaviour – this is currently intractable by any theory because of the unknown way of mathematically determining the influence of fundamental physics variable on the microstructure and onwards to the macro-variables at the engineering level. The current work introduces some partial solutions by including grain size and ductility into the formations, which is novel. Specifically, the parameter of grain size was introduced into the unified models to reflect the influence of heat treatment (see sections 5.1 and 7.1), and then the grain-size modified strain-based and stress-based models were developed. In addition, we introduced the parameter of ductility into the unified model (see section 6.3), and then developed a simplified strain-based model. However, this simplification is an empirical-based process, and the coefficients for the ductility component still require empirical data.

Introducing the material properties, elastic modulus, yield strength and hardness, into the unified model could further improve the applicability of the model to engineering practitioners. However this would increase the complexity of the mathematical formulation. With the current state of the body of knowledge of creep and fatigue, it is not apparent how this might be achieved. This is because of the gap between the grain scale and the engineering scale.

Ideally, the attempted model (the relationships between the relevant variables and the coefficients in this model) should be totally based on the observation at the microstructural level, but it is difficult to quantitatively relate the coefficients with the microstructure. The problem is one of multiscale modelling (see Fig.13. 1 - reproduction of Figure 3.1), whereby the phenomena of creep-fatigue emerges at the engineering scale from effects at the grain level, which in turn derive from effects at the atomic scale and deeper fundamental physics. It would be valuable to build a bridge between the grain and engineering scales, whereby the description at the microstructural level is upgraded to the macroscopic level. However, it is unclear how

this may be done. While qualitative explanations and quantitative formulations exist for some of the processes at the individual levels, there is no existing theory that cover this whole scale.

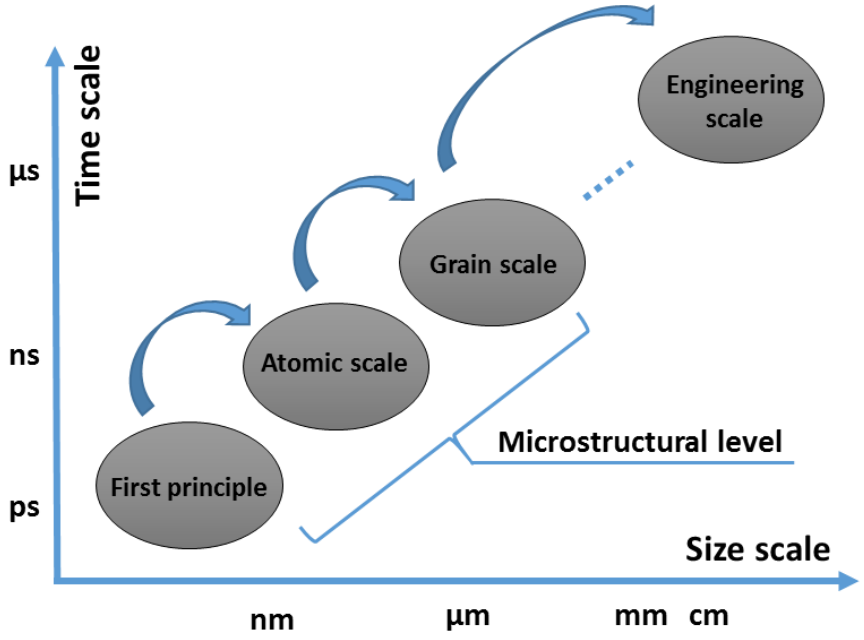

Figure 13.1 Presentation of multi-scale modelling

The contribution of the present work to this problem is to relate the formulation of the model to microstructural phenomena. For example, the mechanism of diffusion creep gives a linear relationship between temperature and plastic deformation, and the behaviour of dislocation pile up gives a power-law relationship between grain size and plastic deformation. Although these relationships are extant in conventional models, the present work integrated them holistically. In addition, to further modify the unified model, we included the parameter of grain size into the model.

It is true agree that microstructural events, such as intra, trans granular defects, dislocation dynamics and boundary effects, also control creep-fatigue behaviour. However, these factors were not included, primarily because measurements of these parameters are difficult and not readily available for engineering practitioners. We were attempting to develop a method that would improve the design process for engineers, hence focussed on grain size exclusively. Nonetheless there is value in attempting to include other measurements of grain morphology in future developments.

Nonetheless the model does have features that are unique: it demonstrates the feasibility of including one microstructural property, namely grain size. Furthermore, it is effective for use by design engineers, as demonstrated in the published case study (Chapter 11).

Therefore, while the model does not meet the ultimate goal of connecting the microstructure to the mechanical properties, it does achieve the important and valuable goal of bringing a solution method to design engineer for the full range of creep/fatigue effects. The advantages of the new model are significant in terms of engineering application (Section 6.2). In addition, the inclusion of grain size takes the model beyond other models, and is also strategically

significant because grain size is connected to heat treatment, and the latter is something that design engineers know and have some control over.

Summary of the formulation

Taking the strain-based formulation as an example, the fundamental mechanisms, which are worked to determine creep-fatigue behaviour of a material, are illustrated below in Figure 13.2 (reproduction of Figure 10.10):

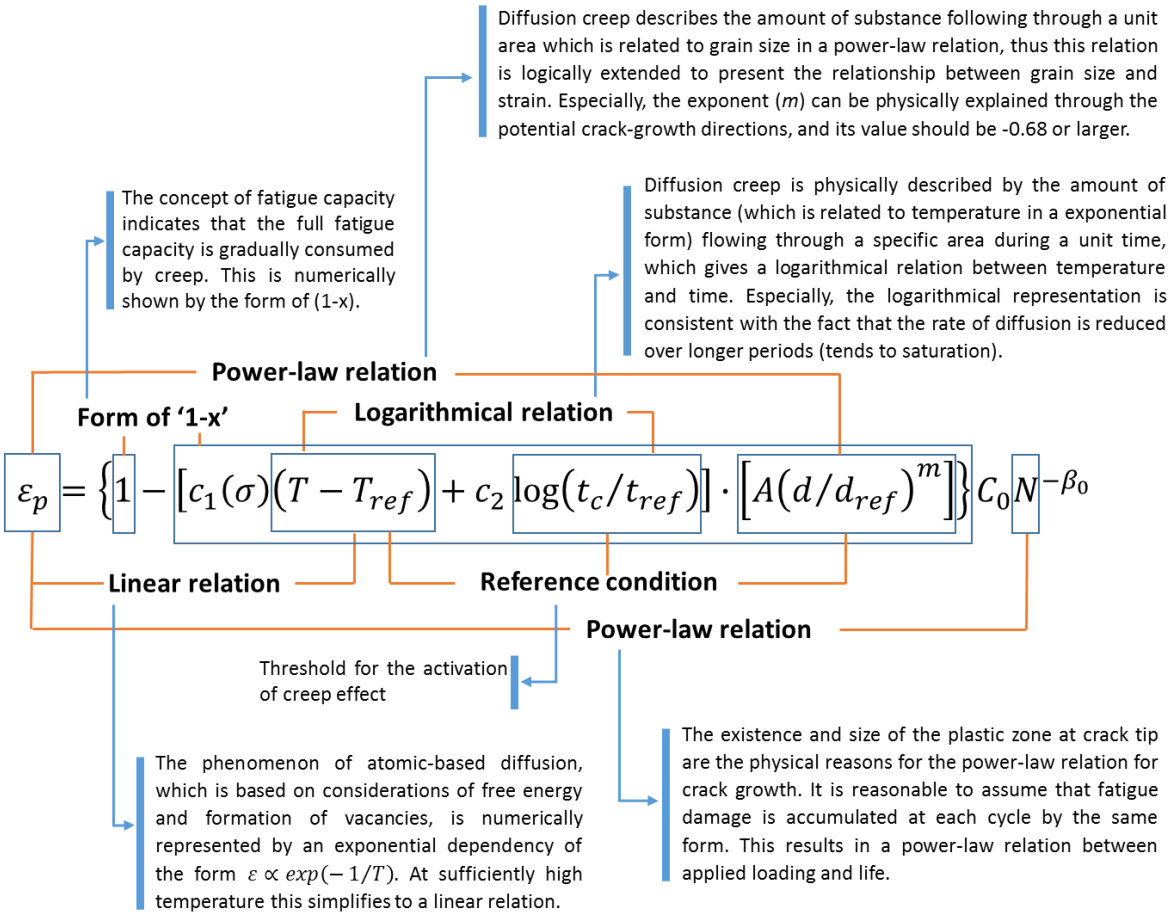

Figure 13.2 Main relationships and fundamental mechanisms in the strain-based model

Statement of novel contributions

In summary, the present work makes several original intellectual contributions:

(1) The concept of 'fatigue capacity' was further explained and numerically applied. This introduces a fundamental principle: that the material has a capacity to carry strain, and this capacity is progressively degraded by microstructural damage due to creep, fatigue, and

potentially other damage mechanisms. This provided a basis to develop the unified model, and gave a means to link the three loading conditions.

(2) We developed the unified creep-fatigue models. Three forms were developed:

• The strain-based unified creep-fatigue equation (without grain-size effect) for the low-cycle fatigue regime;

• The strain-based unified creep-fatigue equation with grain-size effect (which shows the ability to predict fatigue life at a microstructural level) for the low-cycle fatigue regime;

• The stress-based unified creep-fatigue equation for the high-cycle fatigue regime (the importance is secondary to the strain-based approach).

(3) The method for extracting the coefficients of the unified creep-fatigue equations was proposed. In particular, a moderating factor (f_m) was introduced to transfer the creep damage under the situation with constant loading into the equivalent situation with cyclic loading. In addition, the compatibility was included to extract the coefficients of the stress-based model.

(4) The unified creep-fatigue models were validated on multiple materials, and the advantages of this unified model were investigated. Specifically, the unified formulations can be applied in multiple situations for multiple materials (the unified characteristic), can cover the full range of conditions from the pure-fatigue condition to the pure-creep condition (the integrated characteristic), can provide an economical method for the fatigue-life prediction (minimum experimental effort), and can show better consistency with the underlying physical mechanisms of fatigue and creep (a good physical explanation).

(5) The unified equations were linked to the underlying physical mechanisms. Specifically, the influences of temperature, cyclic time and grain size on creep fatigue were investigated, and the relationships between these variables were partially explained at a microstructural level.

(6) The grain-size-modified Manson-Haferd parameter. Grain size is an important parameter that differentiates between grades of material and heat treatment. It is relatively easy for practitioners to obtain this information via sample preparation, etching, and microscopy.

(7) The simplified strain-based formulation were proposed. Ductility was included in the formulation. Ductility is a general material property at the engineering level, i.e. is relatively easy for practitioners to obtain this data.

(8) The unified creep-fatigue models were extended to the situation with non-zero mean-stress effect. The present work has identified that this method is not strictly appropriate.

(9) A conceptual graphical-based model was proposed. Specifically, this conceptual model illustrates the whole process of damage accumulation from crack initiation to crack propagation then to structural failure.

(10) The unified creep-fatigue equation was applied to engineering design. In the present work, a guide to apply the unified formulation to engineering design was developed. Then, a case study for material selection was given for a gas turbine blisk, which shows that the combination of the unified model and FEA can significantly reduce the complexity of simulation.

Short form conclusion

The present work overcomes several of the limitations evident in the existing empirical models for creep-fatigue. The work makes multiple original contributions. The first is the development of validated unified creep-fatigue models covering both the strain and stress based situations. The second is the inclusion of grain-size – this is important as it provides a means to include heat-treatment effect into the formulations. The third contribution is the partial extension to the situation with non-zero mean-stress effect, and an identification of potential issues with stress-strain compatibility under this loading regime. A fourth contribution is the development of proposed underlying physical mechanisms for creep-fatigue at the microstructural level. Application of the method to engineering design has been demonstrated. The unified model can be applied in multiple situations for multiple materials, can cover the full range of conditions from pure fatigue to pure creep, offers an economical method for fatigue-life prediction, and is underpinned conceptually by physical mechanisms at the microstructural level.

References

1. Liu, D. and D.J. Pons, *Development of a unified creep‐fatigue equation including heat treatment.* Fatigue & Fracture of Engineering Materials & Structures, 2018. **41**(1): p. 170-182. DOI: http://dx.doi.org/10.1111/ffe.12670.
2. Liu, D. and D.J. Pons, *A unified creep-fatigue equation with application to engineering design*, in *Creep*, T. Tomasz, S. Marek, and A. Zieliński, Editors. 2018, InTechOpen: Rijeka, Croatia.
3. Liu, D. and D.J. Pons, *Development of a stress-based creep-fatigue equation: Accommodating pure-fatigue to pure-creep for the high-cycle loading regime.* International Journal of Damage Mechanics, 2017: p. 1-19. DOI: https://dx.doi.org/10.1177/1056789517735678.
4. Liu, D. and D.J. Pons, *Physical-Mechanism Exploration of the Low-Cycle Unified Creep-Fatigue Formulation.* Metals, 2017. **7**(9): p. 379. DOI: http://dx.doi.org/10.3390/met7090379.
5. Liu, D., D.J. Pons, and E. Wong, *Proposal for a unified creep-fatigue equation*, in *International Conference on Innovative Design and Manufacturing (ICIDM)*. 24-26 January 2016: Auckland, New Zealand.
6. Liu, D., D.J. Pons, and E. Wong, *Creep-integrated fatigue equation for metals.* International Journal of Fatigue, 2017. **98**: p. 167-175. DOI: http://dx.doi.org/10.1016/j.ijfatigue.2016.11.030.
7. Liu, D., D.J. Pons, and E.-h. Wong, *The Unified Creep-Fatigue Equation for Stainless Steel 316.* Metals, 2016. **6**(9): p. 219. DOI: http://dx.doi.org/10.3390/met6090219.
8. Dowling, N.E., *Mechanical behavior of materials: engineering methods for deformation, fracture, and fatigue*. 2012, London, UK: Pearson. 954.
9. Chowdhury, P. and H. Sehitoglu, *Mechanisms of fatigue crack growth–a critical digest of theoretical developments.* Fatigue & Fracture of Engineering Materials & Structures, 2016. **39**(6): p. 652-674. DOI: https://doi.org/10.1111/ffe.12392.
10. Marin, J., *Mechanical behavior of engineering materials*. 1962, New Jersey, USA: Prentice Hall.
11. Schütz, W., *A history of fatigue.* Engineering fracture mechanics, 1996. **54**(2): p. 263-300. DOI: https://doi.org/10.1016/0013-7944(95)00178-6.
12. Basquin, O., *The exponential law of endurance tests.* American Society of Testing Materials, 1910. **10**: p. 625-630.
13. Wöhler, A., *Theorie rechteckiger eiserner Brückenbalken mit Gitterwänden und mit Blechwänden.* Zeitschrift für Bauwesen, 1855. **5**(1855): p. 121-166.
14. Coffin Jr, L.F., *A study of the effects of cyclic thermal stresses on a ductile metal.* 1953, Knolls Atomic Power Lab.: New York, USA
15. Manson, S. *Behavior of materials under conditions of thermal stress*. 1954; Available from: https://ntrs.nasa.gov/archive/nasa/casi.ntrs.nasa.gov/19930092197.pdf.

16. Morrow, J., *Cyclic plastic strain energy and fatigue of metals*, in *Internal friction, damping, and cyclic plasticity*. 1965, ASTM International: Pennsylvania, USA.
17. Magnin, T., L. Coudreuse, and J. Lardon, *A quantitative approach to fatigue damage evolution in FCC and BCC stainless steels.* Scripta metallurgica, 1985. **19**(12): p. 1487-1490. DOI: https://doi.org/10.1016/0036-9748(85)90156-5.
18. Polak, J. and P. Liškutían, *Nucleation and short crack growth in fatigued polycrystalline copper.* Fatigue & Fracture of Engineering Materials & Structures, 1990. **13**(2): p. 119-133. DOI: https://doi.org/10.1111/j.1460-2695.1990.tb00584.x.
19. Suh, C. and H. Kitagawa, *Crack growth behaviour of fatigue microcracks in low carbon steels.* Fatigue & Fracture of Engineering Materials & Structures, 1987. **9**(6): p. 409-424. DOI: https://doi.org/10.1111/j.1460-2695.1987.tb00468.x.
20. Soderberg, C.R. and V. Sweden, *Factor of safety and working stress.* Transactions of American Mathematics Society, 1930. **52**(2): p. 13-28.
21. Morrow, J., *Fatigue properties of metals, Section 3.2 of Fatigue Design Handbook Experimental Mechanics, Pub. AE-4.* Society for Automotive Engineers, Warrendale, PA, 1964.
22. Morrow, J., *Fatigue properties of metals.* Fatigue design handbook, 1968: p. 21-30.
23. Goodman, J., *Mechanics applied to engineering*. 1918, London, UK: Longmans, Green & Co. 845.
24. Gerber, H., *Bestimmung der zulässigen spannungen in eisen-constructionen*. 1874, Germany: Wolf. 27.
25. Manson, S., *Inversion of the strain-life and strain-stress relationships for use in metal fatigue analysis.* Fatigue & Fracture of Engineering Materials & Structures, 1979. **1**(1): p. 37-57. DOI: https://doi.org/10.1111/j.1460-2695.1979.tb00366.x.
26. Manson, S., *Thermal stress in design, Part 19, cyclic life of ductile materials.* Machine Design, 1960. **32**: p. 139-144.
27. Palmgren, A., *Die lebensdauer von kugellagern.* Zeitschrift des Vereines Deutscher Ingenieure, 1924. **68**(14): p. 339-341.
28. Miner, M.A., *Cumulative damage in fatigue.* J. Appl. Mech., 1945. **12**(3): p. 159-164.
29. Paris, P. and F. Erdogan, *A critical analysis of crack propagation laws.* Journal of Basic Engineering, 1963. **85**(4): p. 528-533. DOI: http://dx.doi.org/10.1115/1.3656900.
30. Arrhenius, S., *Über die Dissociationswärme und den Einfluss der Temperatur auf den Dissociationsgrad der Elektrolyte.* Zeitschrift für physikalische Chemie, 1889. **4**(1): p. 96-116. DOI: https://doi.org/10.1515/zpch-1889-0408.
31. Arrhenius, S., *Über die Reaktionsgeschwindigkeit bei der Inversion von Rohrzucker durch Säuren.* Zeitschrift für physikalische Chemie, 1889. **4**(1): p. 226-248. DOI: https://doi.org/10.1515/zpch-1889-0416.
32. Orr, R.L., O.D. Sherby, and J.E. Dorn, *Correlations of rupture data for metals at elevated temperatures.* 1953, Institue of Engineering Research, University of California: Berkeley, USA
33. Larson, F.R. and J. Miller, *A time-temperature relationship for rupture and creep stresses.* Transactions ASME, 1952. **74**(5): p. 765-775.
34. Manson, S. and A. Haferd, *A linear time-temperature relation for extrapolation of creep and stress-rupture data.* 1953, Lewis Flight Propulsion Lab.: Ohio, USA. http://ntrs.nasa.gov/archive/nasa/casi.ntrs.nasa.gov/19930083803.pdf
35. Penny, R.K. and D.L. Marriott, *Design for creep*. 1995, Berlin/Heidelberg, Germany: Springer Science & Business Media. 430.

36. Kiran, R. and K. Khandelwal, *A micromechanical cyclic void growth model for ultra-low cycle fatigue.* International Journal of Fatigue, 2015. **70**: p. 24-37. DOI: https://doi.org/10.1016/j.ijfatigue.2014.08.010.
37. Maurel, V., L. Rémy, F. Dahmen, and N. Haddar, *An engineering model for low cycle fatigue life based on a partition of energy and micro-crack growth.* International Journal of Fatigue, 2009. **31**(5): p. 952-961. DOI: https://doi.org/10.1016/j.ijfatigue.2008.09.004.
38. Xue, Y., M. Horstemeyer, D. McDowell, H. El Kadiri, and J. Fan, *Microstructure-based multistage fatigue modeling of a cast AE44 magnesium alloy.* International journal of fatigue, 2007. **29**(4): p. 666-676. DOI: https://doi.org/10.1016/j.ijfatigue.2006.07.005.
39. Taira, S., *Lifetime of structures subjected to varying load and temperature*, in *Creep in structures*. 1962, Springer: Berlin/Heidelberg, Germany. p. 96-124.
40. Robinson, E.L., *Effect of temperature variation on the long-time rupture strength of steels.* ASME Transactions, 1952. **74**(5): p. 777-781.
41. Takahashi, Y., *Study on creep-fatigue evaluation procedures for high-chromium steels—Part I: Test results and life prediction based on measured stress relaxation.* International Journal of Pressure Vessels and Piping, 2008. **85**(6): p. 406-422. DOI: https://doi.org/10.1016/j.ijpvp.2007.11.008.
42. Takahashi, Y., B. Dogan, and D. Gandy, *Systematic evaluation of creep-fatigue life prediction methods for various alloys.* Journal of Pressure Vessel Technology, 2013. **135**(6): p. 061204. DOI: https://doi.org/10.1115/1.4024436.
43. Halford, G., M. Hirschberg, and S. Manson, *Creep fatigue analysis by strain-range partitioning.* 1971, National Aeronautics and Space Administration: Washington, D.C., USA. https://ntrs.nasa.gov/archive/nasa/casi.ntrs.nasa.gov/19710018469.pdf
44. Neu, R. and H. Sehitoglu, *Thermomechanical fatigue, oxidation, and creep: Part II. Life prediction.* Metallurgical Transactions A, 1989. **20**(9): p. 1769-1783. DOI: https://doi.org/10.1007/bf02663208.
45. Ainsworth, R., M. Ruggles, and Y. Takahashi, *Flaw assessment procedure for high-temperature reactor components.* Journal of Pressure Vessel Technology, 1992. **114**(2): p. 166-170. DOI: http://dx.doi.org/10.1115/1.2929024.
46. Janson, J., *Damage model of creep-fatigue interaction.* Engineering Fracture Mechanics, 1979. **11**(2): p. 397-403. DOI: https://doi.org/10.1016/0013-7944(79)90014-6.
47. Mao, H. and S. Mahadevan, *Reliability analysis of creep–fatigue failure.* International journal of fatigue, 2000. **22**(9): p. 789-797. DOI: https://doi.org/10.1016/S0142-1123(00)00046-3.
48. Deguchi, M., H. Tobe, and E. Sato, *Damage propagation mechanism in low-cycle creep fatigue of Cu–Cr–Zr alloy.* International Journal of Fatigue, 2016. **87**: p. 351-358. DOI: https://doi.org/10.1016/j.ijfatigue.2016.02.025.
49. Liu, H., R. Bao, J. Zhang, and B. Fei, *A creep–fatigue crack growth model containing temperature and interactive effects.* International Journal of Fatigue, 2014. **59**: p. 34-42. DOI: https://doi.org/10.1016/j.ijfatigue.2013.09.017.
50. Xuan, F., S. Tu, and Z. Wang, *Time-dependent fatigue fracture theory and residual life assessment techniques for defective structures.* Advances in Mechanics, 2005. **35**(3): p. 391-403.
51. Coffin, L., *Fatigue at high temperature*, in *Fatigue at elevated temperatures*. 1973, ASTM International: Pennsylvania, USA.

52. Solomon, H., *Fatigue of 60/40 solder.* IEEE Transactions on Components, Hybrids, and Manufacturing Technology, 1986. **9**(4): p. 423-432. DOI: http://dx.doi.org/10.1109/tchmt.1986.1136672.
53. Shi, X., H. Pang, W. Zhou, and Z. Wang, *Low cycle fatigue analysis of temperature and frequency effects in eutectic solder alloy.* International journal of fatigue, 2000. **22**(3): p. 217-228. DOI: http://dx.doi.org/10.1016/s0142-1123(99)00124-3.
54. Jing, H., Y. Zhang, L. Xu, G. Zhang, Y. Han, and J. Wei, *Low cycle fatigue behavior of a eutectic 80Au/20Sn solder alloy.* International Journal of Fatigue, 2015. **75**: p. 100-107. DOI: https://doi.org/10.1016/j.ijfatigue.2015.02.005.
55. Engelmaier, W., *Fatigue life of leadless chip carrier solder joints during power cycling.* IEEE Transactions on Components, Hybrids, and Manufacturing Technology, 1983(3): p. 232-237. DOI: http://dx.doi.org/10.1109/tchmt.1983.1136183.
56. Wong, E. and Y.-W. Mai, *A unified equation for creep-fatigue.* International Journal of Fatigue, 2014. **68**: p. 186-194. DOI: http://dx.doi.org/10.1016/j.ijfatigue.2014.05.004.
57. Ashby, M.F., H. Shercliff, and D. Cebon, *Materials: engineering, science, processing and design*. 2013, Oxford, UK: Butterworth-Heinemann. 784.
58. Kohout, J., *Temperature dependence of stress–lifetime fatigue curves.* Fatigue & Fracture of Engineering Materials & Structures, 2000. **23**(12): p. 969-977. DOI: https://doi.org/10.1046/j.1460-2695.2000.00276.x.
59. Mivehchi, H. and A. Varvani-Farahani, *Temperature dependence of stress–fatigue life data of FRP composites.* Mechanics of Composite Materials, 2011. **47**(2): p. 185-192. DOI: https://doi.org/10.1007/s11029-011-9197-7.
60. Feltner, C.E. and J.D. Morrow, *Microplastic strain hysteresis energy as a criterion for fatigue fracture.* Journal of Basic Engineering, 1961. **83**(1): p. 15-22. DOI: https://doi.org/10.1115/1.3658884.
61. Zhu, S.-P., Y.-J. Yang, H.-Z. Huang, Z. Lv, and H.-K. Wang, *A unified criterion for fatigue–creep life prediction of high temperature components.* Proceedings of the Institution of Mechanical Engineers, Part G: Journal of Aerospace Engineering, 2017. **231**(4): p. 677-688. DOI: https://doi.org/10.1177/0954410016641448.
62. Kumar, J., A. Singh, S.G.S. Raman, and V. Kumar, *Creep-fatigue damage modeling in Ti-6Al-4V alloy: A mechanistic approach.* International Journal of Fatigue, 2017. **98**: p. 62-67. DOI: https://doi.org/10.1016/j.ijfatigue.2017.01.016.
63. Gurumurthy, K., B. Srinivasan, P.S. Krishna, G. Achary, and S. Subramanyam, *Creep-fatigue design studies for process reactor components subjected to elevated temperature service as per ASME-NH.* Procedia Engineering, 2014. **86**: p. 327-334. DOI: https://doi.org/10.1016/j.proeng.2014.11.045.
64. Schafrik, R.E., D.D. Ward, and J.R. Groh, *Application of alloy 718 in GE aircraft engines: past, present and next five years.* Superalloys, 2001. **718**: p. 625-706. DOI: https://doi.org/10.7449/2001/superalloys_2001_1_11.
65. Williams, J.C. and E.A. Starke Jr, *Progress in structural materials for aerospace systems.* Acta Materialia, 2003. **51**(19): p. 5775-5799. DOI: http://dx.doi.org/10.1016/j.actamat.2003.08.023.
66. Tien, J.K., B. Hendrix, and A. Attarwala, *Creep-fatigue interactions in solders.* IEEE transactions on components, hybrids, and manufacturing technology, 1989. **12**(4): p. 502-505. DOI: https://doi.org/10.1109/ecc.1989.77759.
67. Frear, D.R., *Solder mechanics: a state of the art assessment*. Vol. 1. 1991, Pittsburgh, USA: The Minerals, Metals & Materials Society. 437.

68. Lee, W., L. Nguyen, and G.S. Selvaduray, *Solder joint fatigue models: review and applicability to chip scale packages.* Microelectronics reliability, 2000. **40**(2): p. 231-244. DOI: https://doi.org/10.1016/S0026-2714(99)00061-X.
69. Cailletaud, G., D. Nouailhas, J. Grattier, C. Levaillant, M. Mottot, J. Tortel, C. Escavarage, J. Héliot, and S. Kang, *A review of creep-fatigue life prediction methods: identification and extrapolation to long term and low strain cyclic loading.* Nuclear engineering and design, 1984. **83**(3): p. 267-278. DOI: https://doi.org/10.1016/0029-5493(84)90121-3.
70. June, W., *A continuum damage mechanics model for low-cycle fatigue failure of metals.* Engineering fracture mechanics, 1992. **41**(3): p. 437-441. DOI: https://doi.org/10.1016/0013-7944(92)90083-Q.
71. Chaboche, J.L., *Une loi différentielle d'endommagement de fatigue avec cumulation non linéaire*. 1974, Palaiseau, France: Office Nationale d'Etudes et de Recherches Aérospatiales. 12.
72. Metzger, M., B. Nieweg, C. Schweizer, and T. Seifert, *Lifetime prediction of cast iron materials under combined thermomechanical fatigue and high cycle fatigue loading using a mechanism-based model.* International Journal of Fatigue, 2013. **53**: p. 58-66. DOI: https://doi.org/10.1016/j.ijfatigue.2012.02.007.
73. Seifert, T. and H. Riedel, *Mechanism-based thermomechanical fatigue life prediction of cast iron. Part I: Models.* International Journal of Fatigue, 2010. **32**(8): p. 1358-1367. DOI: https://doi.org/10.1016/j.ijfatigue.2010.02.004.
74. Charkaluk, E., A. Bignonnet, A. Constantinescu, and K. Dang Van, *Fatigue design of structures under thermomechanical loadings.* Fatigue & Fracture of Engineering Materials & Structures, 2002. **25**(12): p. 1199-1206. DOI: https://doi.org/10.1046/j.1460-2695.2002.00612.x.
75. Constantinescu, A., E. Charkaluk, G. Lederer, and L. Verger, *A computational approach to thermomechanical fatigue.* International Journal of fatigue, 2004. **26**(8): p. 805-818. DOI: https://doi.org/10.1016/j.ijfatigue.2004.01.006.
76. Joseph Edward Shigley, C.R.M., *Mechanical engineering design*. 2001, New York, USA: McGraw-Hill Education. 1248.
77. Jiang, L., C. Brooks, P. Liaw, H. Wang, C.J. Rawn, and D. Klarstrom, *High-frequency metal fatigue: the high-cycle fatigue behavior of ULTIMET® alloy.* Materials Science and Engineering: A, 2001. **314**(1): p. 162-175. DOI: https://doi.org/10.1016/S0921-5093(00)01928-6.
78. Liaw, P., H. Wang, L. Jiang, B. Yang, J. Huang, R. Kuo, and J. Huang, *Thermographic detection of fatigue damage of pressure vessel steels at 1,000 Hz and 20 Hz.* Scripta Materialia, 2000. **42**(4): p. 389-395. DOI: https://doi.org/10.1016/S1359-6462(99)00358-9.
79. Halford, G.R., *Cyclic creep rupture behavior of three high temperature alloys.* 1971, National Aeronautics and Space Administration: Washington, D.C., USA. https://ntrs.nasa.gov/archive/nasa/casi.ntrs.nasa.gov/19710016169.pdf
80. Tsuno, N., S. Shimabayashi, K. Kakehi, C. Rae, and R. Reed. *Tension/compression asymmetry in yield and creep strengths of Ni-based superalloys*. in *The 11th International Symposium on Superalloys*. 14-18 September 2008. Champion, Pennsylvania.
81. Yamashita, M. and K. Kakehi, *Tension/compression asymmetry in yield and creep strengths of Ni-based superalloy with a high amount of tantalum.* Scripta materialia, 2006. **55**(2): p. 139-142. DOI: https://doi.org/10.1016/j.scriptamat.2006.03.048.

82. Shi, X.Q., Z.P. Wang, Q.J. Yang, and H.L.J. Pang, *Creep Behavior and Deformation Mechanism Map of Sn-Pb Eutectic Solder Alloy.* Journal of Engineering Materials and Technology, 2002. **125**(1): p. 81-88. DOI: http://dx.doi.org/10.1115/1.1525254.
83. Lin, C.-K. and D.-Y. Chu, *Creep rupture of lead-free Sn-3.5 Ag and Sn-3.5 Ag-0.5 Cu solders.* Journal of Materials Science: Materials in Electronics, 2005. **16**(6): p. 355-365. DOI: https://doi-org.ezproxy.canterbury.ac.nz/10.1007/s10854-005-1147-5.
84. Kanchanomai, C., Y. Miyashita, Y. Mutoh, and S. Mannan, *Influence of frequency on low cycle fatigue behavior of Pb-free solder 96.5 Sn–3.5 Ag.* Materials Science and Engineering: A, 2003. **345**(1): p. 90-98. DOI: https://doi.org/10.1016/S0921-5093(02)00461-6.
85. Kanchanomai, C. and Y. Mutoh, *Effect of temperature on isothermal low cycle fatigue properties of Sn–Ag eutectic solder*. Materials Science and Engineering: A, 2004. **381**(1): p. 113-120. DOI: https://doi.org/10.1016/j.msea.2004.04.018.
86. Kaufman, J.G., *Properties of aluminum alloys: tensile, creep, and fatigue data at high and low temperatures*. 1999, Ohio, USA: ASM international. 305.
87. Karakaş, Ö. and J. Szusta, *Monotonic and low cycle fatigue behaviour of 2024‐T3 aluminium alloy between room temperature and 300° C for designing VAWT components.* Fatigue & Fracture of Engineering Materials & Structures, 2016. **39**(1): p. 95-109. DOI: https://doi.org/10.1111/ffe.12336.
88. Fritz, L.J. and W. Koster, *Tensile and creep rupture properties of (1) uncoated and (2) coated engineering alloys at elevated temperatures.* 1977, Lewis Research Center: Ohio, USA. https://ntrs.nasa.gov/archive/nasa/casi.ntrs.nasa.gov/19770016292.pdf
89. Kanazawa, K. and S. Yoshida. *Effect of temperature and strain rate on the high temperature low-cycle fatigue behavior of austenitic stainless steels*. in *International conference on creep and fatigue in elevated temperature applications*. 23 Sep 1973. Philadelphia, USA: Institution of Mechanical Engineers.
90. Mutoh, Y. and V. Radhakrishnan, *Effect of yield stress and grain size on threshold and fatigue limit.* Journal of Engineering Materials and Technology, 1986. **108**(2): p. 174-178. DOI: https://doi.org/10.1115/1.3225857.
91. Alexandre, F., S. Deyber, and A. Pineau, *Modelling the optimum grain size on the low cycle fatigue life of a Ni based superalloy in the presence of two possible crack initiation sites.* Scripta Materialia, 2004. **50**(1): p. 25-30. DOI: https://doi.org/10.1016/j.scriptamat.2003.09.043.
92. Thompson, A.W. and W. Backofen, *The effect of grain size on fatigue.* Acta metallurgica, 1971. **19**(7): p. 597-606. DOI: https://doi.org/10.1016/0001-6160(71)90012-5.
93. Komotori, J. and M. Shimizu. *Grain size effect in low cycle fatigue of steel under mean strain*. in *7th International Conference On Fracture*. 24 March 1989. Houston, USA.
94. Sugahara, T., K. Martinolli, D.A. Reis, C. de Moura Neto, A.A. Couto, F.P. Neto, and M. Barboza, *Creep Behavior of the Inconel 718 Superalloy.* Defect and Diffusion Forum, 2012. **326-328**: p. 509-514. DOI: https://doi.org/10.4028/www.scientific.net/ddf.326-328.509.
95. Fournier, D. and A. Pineau, *Low cycle fatigue behavior of Inconel 718 at 298 K and 823 K.* Metallurgical and Materials Transactions A, 1977. **8**(7): p. 1095-1105. DOI: https://doi.org/10.1007/bf02667395.
96. Sanders, T., R. Frishmuth, and G. Embley, *Temperature dependent deformation mechanisms of alloy 718 in low cycle fatigue.* Metallurgical and Materials Transactions A, 1981. **12**(6): p. 1003-1010. DOI: http://dx.doi.org/10.1007/978-1-4899-1736-2_9.

97. Tabuchi, M., H. Hongo, Y. Li, T. Watanabe, and Y. Takahashi, *Evaluation of microstructures and creep damages in the HAZ of P91 steel weldment.* Journal of Pressure Vessel Technology, 2009. **131**(2): p. 021406. DOI: https://doi.org/10.1115/pvp2007-26495.
98. Golański, G. and J. Kępa, *The effect of ageing temperatures on microstructure and mechanical properties of GX12CrMoVNbN9-1 (GP91) cast steel.* Archives of Metallurgy and Materials, 2012. **57**(2): p. 575-582. DOI: https://doi.org/10.2478/v10172-012-0061-0.
99. Mishnev, R., N. Dudova, and R. Kaibyshev, *Low cycle fatigue behavior of a 10% Cr martensitic steel at 600 C.* ISIJ International, 2015. **55**(11): p. 2469-2476. DOI: https://doi.org/10.2355/isijinternational.isijint-2015-336.
100. Mroziński, S. and G. Golański, *Low cycle fatigue of GX12CrMoVNbN9-1 cast steel at elevated temperature.* Journal of Achievements in Materials and Manufacturing Engineering, 2011. **49**(1): p. 7-16.
101. Higham, D.J. and N.J. Higham, *MATLAB guide*. 2005, Philadelphia, USA: Society for Industrial and Applied Mathematics. 382.
102. Chapra, S.C. and R.P. Canale, *Numerical methods for engineers*. 2010, New York, USA: McGraw-Hill. 960.
103. Manson, S., *Fatigue: a complex subject—some simple approximations.* Experimental mechanics, 1965. **5**(7): p. 193-226. DOI: https://doi.org/10.1007/bf02321056.
104. Manson, S. and U. Muralidharan, *A modified universal slopes equation for estimation of fatigue characteristics of metals.* Journal of Engineering Materials and Technology, 1988. **110**: p. 55. DOI: https://doi.org/10.1115/1.3226010.
105. Kanchanomai, C., Y. Miyashita, and Y. Mutoh, *Low-cycle fatigue behavior of Sn-Ag, Sn-Ag-Cu, and Sn-Ag-Cu-Bi lead-free solders.* Journal of Electronic Materials, 2002. **31**(5): p. 456-465. DOI: https://doi.org/10.1007/s11664-002-0100-0.
106. Shohji, I., T. Yoshida, T. Takahashi, and S. Hioki, *Tensile properties of Sn–Ag based lead-free solders and strain rate sensitivity.* Materials Science and Engineering: A, 2004. **366**(1): p. 50-55. DOI: https://doi.org/10.1016/j.msea.2003.09.057.
107. Lee, Y.-L., *Fatigue testing and analysis: theory and practice*. Vol. 13. 2005, Oxford, UK: Butterworth-Heinemann. 402.
108. Lukáš, P. and L. Kunz, *Effect of mean stress on cyclic stress-strain response and high cycle fatigue life.* International Journal of Fatigue, 1989. **11**(1): p. 55-58. DOI: https://doi.org/10.1016/0142-1123(89)90048-0.
109. Chiou, Y.-C. and M.-C. Yip, *Effect of mean strain level on the cyclic stress–strain behavior of AISI 316 stainless steel.* Materials Science and Engineering: A, 2003. **354**(1): p. 270-278. DOI: https://doi.org/10.1016/S0921-5093(03)00016-9.
110. Callister, W.D. and D.G. Rethwisch, *Materials science and engineering*. Vol. 5. 2013, New Jersey, USA: John Wiley & Sons.
111. Liu, C., Y. Han, M. Yan, and M. Chaturvedi, *Creep crack growth behaviour of Alloy 718.* Superalloys, 1991. **178**(625): p. 537-548. DOI: https://doi.org/10.7449/1991/superalloys_1991_537_548.
112. Sadananda, K., *A theoretical model for creep crack growth.* Metallurgical and Materials Transactions A, 1978. **9**(5): p. 635-641. DOI: https://doi.org/10.1007/bf02659920.
113. Laird, C., *Mechanisms and theories of fatigue.* Fatigue and microstructure, 1979: p. 149-203.
114. Banks-Sills, L., Y. Motola, and L. Shemesh, *The M-integral for calculating intensity factors of an impermeable crack in a piezoelectric material.* Engineering Fracture

Mechanics, 2008. **75**(5): p. 901-925. DOI: https://doi.org/10.1016/j.engfracmech.2007.05.009.
115. Warzynek, P., B. Carter, and L. Banks-Sills, *The M-integral for computing stress intensity factors in generally anisotropic materials.* 2005, National Aeronautics and Space Administration: Washington, D.C., USA. https://ntrs.nasa.gov/archive/nasa/casi.ntrs.nasa.gov/20060002645.pdf
116. Miller, K., *Materials science perspective of metal fatigue resistance.* Materials science and technology, 1993. **9**(6): p. 453-462. DOI: https://doi.org/10.1179/mst.1993.9.6.453.
117. Rodopoulos, C.A., *Fatigue Damage Map as a Virtual Tool for Fatigue Damage Tolerance*, in *Virtual Testing and Predictive Modeling*. 2009, Springer: Berlin/Heidelberg, Germany. p. 73-104.
118. Laird, C., *The influence of metallurgical structure on the mechanisms of fatigue crack propagation*, in *Fatigue crack propagation*. 1967, ASTM International: Pennsylvania, USA.
119. Laird, C. and R. de La Veaux, *Additional evidence for the plastic blunting process of fatigue crack propagation.* Metallurgical and Materials Transactions A, 1977. **8**(4): p. 657-664. DOI: https://doi.org/10.1007/bf02676989.
120. Peralta, P., S.-H. Choi, and J. Gee, *Experimental quantification of the plastic blunting process for stage II fatigue crack growth in one-phase metallic materials.* International Journal of Plasticity, 2007. **23**(10): p. 1763-1795. DOI: https://doi.org/10.1016/j.ijplas.2007.03.009.
121. Shi, K., L. Cai, S. Qi, and C. Bao, *A prediction model for fatigue crack growth using effective cyclic plastic zone and low cycle fatigue properties.* Engineering Fracture Mechanics, 2016. **158**: p. 209-219. DOI: https://doi.org/10.1016/j.engfracmech.2016.02.046.
122. Wang, G., *The plasticity aspect of fatigue crack growth.* Engineering fracture mechanics, 1993. **46**(6): p. 909-930. DOI: https://doi.org/10.1016/0013-7944(93)90144-H.
123. Weertman, J., *Fatigue crack propagation theories*, in *Fatigue and microstructure*. 1979, American Society for Metals: Ohio, USA. p. 279-206.
124. Ham, R. and T. Broom, *The mechanism of fatigue softening.* Philosophical Magazine, 1962. **7**(73): p. 95-103. DOI: https://doi.org/10.1080/14786436208201860.
125. Zhai, T., X. Jiang, J. Li, M. Garratt, and G. Bray, *The grain boundary geometry for optimum resistance to growth of short fatigue cracks in high strength Al-alloys.* International journal of fatigue, 2005. **27**(10): p. 1202-1209. DOI: https://doi.org/10.1016/j.ijfatigue.2005.06.021.
126. Cocks, A. and A. Pontern, *Mechanics of creep brittle materials 1*. 1989, Berlin/Heidelberg, Germany: Springer Science & Business Media. 310.
127. Ejaz, N., I. Qureshi, and S. Rizvi, *Creep failure of low pressure turbine blade of an aircraft engine.* Engineering Failure Analysis, 2011. **18**(6): p. 1407-1414. DOI: https://doi.org/10.1016/j.engfailanal.2011.03.010.
128. Král, P., J. Dvořák, M. Kvapilová, M. Svoboda, and V. Sklenička. *Creep damage of Al and Al-Sc alloy processed by ECAP*. in *Acta Metallurgica Slovaca-Conference*. 2013.
129. Kinloch, A., C. Wang, S. Wu, R. Ladani, J. Zhang, E. Bafekrpour, K. Ghorbani, and A. Mouritz, *Aligning graphene nanoplatelets with an external electric field to improve multifunctional properties of epoxy nanocomposites.* 2015: p. 607-618. DOI: https://doi.org/10.1016/j.carbon.2015.07.026.

130. Villechaise, P., J. Cormier, T. Billot, and J. Mendez. *Mechanical behaviour and damage processes of Udimet 720Li: influence of localized plasticity at grain boundaries*. in *12th International Symposium on Superalloys*. 2012. Champion, Pennsylvania.
131. Claude Bathias, A.P., *Fatigue of materials and structures*. 2013, New Jersey, USA: John Wiley & Sons. 512.
132. Sangid, M.D., *The physics of fatigue crack initiation.* International journal of fatigue, 2013. **57**: p. 58-72. DOI: https://doi.org/10.1016/j.ijfatigue.2012.10.009.
133. Wang, Z., I. Beyerlein, and R. LeSar, *Slip band formation and mobile dislocation density generation in high rate deformation of single fcc crystals.* Philosophical Magazine, 2008. **88**(9): p. 1321-1343. DOI: http://dx.doi.org/10.1080/14786430802129833.
134. Margaritis, G. and J. Botsis, *Energy evaluations during crack initiation.* Engineering fracture mechanics, 1991. **40**(6): p. 1123-1134. DOI: https://doi.org/10.1016/0013-7944(91)90176-2.
135. Lach, R., R. Adhikari, R. Weidisch, T. Huy, G. Michler, W. Grellmann, and K. Knoll, *Crack toughness behavior of binary poly (styrene-butadiene) block copolymer blends.* Journal of materials science, 2004. **39**(4): p. 1283-1295. DOI: https://doi.org/10.1023/b:jmsc.0000013887.79570.33.
136. Zerbst, U., C. Klinger, and R. Clegg, *Fracture mechanics as a tool in failure analysis—Prospects and limitations.* Engineering Failure Analysis, 2015. **55**: p. 376-410. DOI: https://doi.org/10.1016/j.engfailanal.2015.07.001.
137. Pippan, R. and W. Grosinger, *Fatigue crack closure: from LCF to small scale yielding.* International Journal of Fatigue, 2013. **46**: p. 41-48. DOI: https://doi.org/10.1016/j.ijfatigue.2012.02.016.
138. Prasad, K., V. Kumar, K.B.S. Rao, and M. Sundararaman, *A comparative assessment of crack closure mechanisms in Timetal 834 near α titanium alloy under isothermal and thermomechanical fatigue loading.* Journal of Alloys and Compounds, 2016. **688**: p. 8-11. DOI: https://doi.org/10.1016/j.jallcom.2016.06.258.
139. Guo, Y., D. Collins, E. Tarleton, F. Hofmann, J. Tischler, W. Liu, R. Xu, A. Wilkinson, and T. Britton, *Measurements of stress fields near a grain boundary: Exploring blocked arrays of dislocations in 3D.* Acta Materialia, 2015. **96**: p. 229-236. DOI: https://doi.org/10.1016/j.actamat.2015.05.041.
140. McMurtrey, M., G. Was, B. Cui, I. Robertson, L. Smith, and D. Farkas, *Strain localization at dislocation channel–grain boundary intersections in irradiated stainless steel.* International Journal of Plasticity, 2014. **56**: p. 219-231. DOI: https://doi.org/10.1016/j.ijplas.2014.01.001.
141. Pineau, A., *Crossing grain boundaries in metals by slip bands, cleavage and fatigue cracks.* Philosophical Transactions of the Royal Society A, 2015. **373**(2038): p. 20140131. DOI: https://doi.org/10.1098/rsta.2014.0131.
142. Kassner, M.E., *Fundamentals of creep in metals and alloys*. 2015, Oxford, UK: Butterworth-Heinemann. 337.
143. Kumar, Y., S. Venugopal, G. Sasikala, S.K. Albert, and A. Bhaduri, *Study of creep crack growth in a modified 9Cr–1Mo steel weld metal and heat affected zone.* Materials Science and Engineering: A, 2016. **655**: p. 300-309. DOI: https://doi.org/10.1016/j.msea.2015.12.053.
144. Wen, J.-F. and S.-T. Tu, *A multiaxial creep-damage model for creep crack growth considering cavity growth and microcrack interaction.* Engineering Fracture Mechanics, 2014. **123**: p. 197-210. DOI: https://doi.org/10.1016/j.engfracmech.2014.03.001.

145. Kinloch, A., C. Wang, S. Wu, R. Ladani, J. Zhang, E. Bafekrpour, K. Ghorbani, and A. Mouritz, *Aligning graphene nanoplatelets with an external electric field to improve multifunctional properties of epoxy nanocomposites.* Carbon, 2015. **94**: p. 607-618. DOI: https://doi.org/10.1016/j.carbon.2015.07.026.
146. Pretty, C.J., M.T. Whitaker, and S.J. Williams, *Thermo-Mechanical Fatigue Crack Growth of RR1000.* Materials, 2017. **10**(1): p. 34. DOI: https://doi.org/10.3390/ma10010034.
147. Kacher, J., B. Eftink, B. Cui, and I. Robertson, *Dislocation interactions with grain boundaries.* Current Opinion in Solid State and Materials Science, 2014. **18**(4): p. 227-243. DOI: https://doi.org/10.1016/j.cossms.2014.05.004.
148. Benz, J.K. and R.N. Wright, *Fatigue and Creep Crack Propagation Behaviour of Alloy 617 in the Annealed and Aged Conditions.* 2013, Idaho National Laboratory (INL): Idaho, USA. https://www.osti.gov/biblio/1111504
149. Scheyvaerts, F., T. Pardoen, and P. Onck, *A new model for void coalescence by internal necking.* International Journal of Damage Mechanics, 2010. **19**(1): p. 95-126. DOI: https://doi.org/10.1177/1056789508101918.
150. Finnie, I. and W.R. Heller, *Creep of Engineering Materials*. 1959, New York, USA: McGraw-Hill. 341.
151. Poirier, J.-P., *Creep of crystals: high-temperature deformation processes in metals, ceramics and minerals*. 1985, Cambridge, UK: Cambridge University Press. 276.
152. Shewmon, P., *Diffusion in solids*. 2016, Berlin/Heidelberg, Germany: Springer. 238.
153. De Moura, M. and J. Gonçalves, *Cohesive zone model for high-cycle fatigue of adhesively bonded joints under mode I loading.* International Journal of Solids and Structures, 2014. **51**(5): p. 1123-1131. DOI: https://doi.org/10.1016/j.ijsolstr.2013.12.009.
154. Meng, Q. and Z. Wang, *Extended finite element method for power-law creep crack growth.* Engineering Fracture Mechanics, 2014. **127**: p. 148-160. DOI: https://doi.org/10.1016/j.engfracmech.2014.06.005.
155. HATANAKA, K. and T. YAMADA, *Effect of grain size on low cycle fatigue in low carbon steel.* Bulletin of Japan Society of Mechanical Engineers, 1981. **24**(196): p. 1692-1699. DOI: http://doi.org/10.1299/jsme1958.24.1692.
156. Hattori, H., M. Kitagawa, and A. Ohtomo, *Effect of Grain Size on High Temperature Low-Cycle Fatigue Properties of Inconel 617.* Tetsu-to-Hagane, 1982. **68**(16): p. 2521-2530. DOI: http://doi.org/10.2355/tetsutohagane1955.68.16_2521.
157. Pieraggi, B. and J. Uginet, *Fatigue and creep properties in relation.* 1994, The Minerals, Metals & Materials Society: Pittsburgh, USA. http://www.tms.org/superalloys/10.7449/1994/Superalloys_1994_535_544.pdf
158. Evans, R.W. and B. Wilshire, *Introduction to creep*. 1993, Michigan, USA: The Institute of Materials, University of Michiganb. 115.
159. Kato, M., *Hall–Petch relationship and dislocation model for deformation of ultrafine-grained and nanocrystalline metals.* Materials Transactions, 2014. **55**(1): p. 19-24. DOI: https://doi.org/10.2320/matertrans.ma201310.
160. Kumar, R.R. and K. Pandey, *Static Structural and Modal Analysis of Gas Turbine Blade*, in *International Conference on Advanced Material Technologies*. 27-28 December 2016: Visakhapatnam, Andhra Pradesh, India.
161. Madhu, P., *Stress Analysis and Life Estimation of Gas Turbine Blisk for Different Materials of a Jet Engine.* International Journal of Science and Research, 2016. **5**(6): p. 1103-1107. DOI: https://doi.org/10.21275/v5i6.nov164440.

162. Khan, S.B.a.A.R.A., *Fatigue and Creep Interaction in Steam Turbine Bladed Disk.* International Journal of Innovative Research in Science, Engineering and Technology, 2014. **3**(6).
163. vava, G. *Simple Rotor Blisk*. 2016; Available from: https://grabcad.com/library/simple-rotor-blisk-1.
164. *Inconel alloy 718.* 2007, Special Metals Corporation: New York, USA
165. Tulsidas, D., M. Shantharaja, and K. Kumar, *Design modification for fillet stresses in steam turbine blade.* International Journal of Advanced Engineering Technology, 2012. **3**: p. 343-346.

Appendix A

Appendix A: Publications

Publications that have arisen from the present work are presented in Table A.1:

Table A.1 Published and accepted papers

No.	Titel	Authors	Name of publisher	Year	Status
1	Proposal for a unified creep-fatigue equation	Dan Liu; Dirk John Pons; Ee-hua Wong	International Conference on Innovative Design and Manufacturing	2016	Published & Presented
2	The unified creep-fatigue equation for stainless steel 316	Dan Liu; Dirk John Pons; Ee-hua Wong	Metals	2016	Published
3	Creep-integrated fatigue equation for metals	Dan Liu; Dirk John Pons; Ee-hua Wong	International Journal of Fatigue	2017	Published
4	Development of a unified creep-fatigue equation including heat treatment	Dan Liu; Dirk John Pons	Fatigue and Fracture of Engineering Materials and Structures	2018	Published
5	A unified creep-fatigue equation with application to engineering design	Dan Liu; Dirk John Pons	InTechOpen-Creep (Book chapter)	2018	Published

6	Development of a Stress-based Creep-fatigue Equation: Accommodating Pure-fatigue to Pure-creep for the High-cycle Loading Regime	Dan Liu; Dirk John Pons	International Journal of Damage Mechanics	2017	Published
7	Physical-Mechanism Exploration of the Low-Cycle Unified Creep-Fatigue Formulation	Dan Liu; Dirk John Pons	Metals	2017	Published
8	Conceptual model of crack growth for creep fatigue	Dan Liu; Dirk John Pons	Engineering Fracture Mechanics	2017	Submitted

The papers listed in Table A.1 are attached as follows:

Paper 1: Proposal for a unified creep-fatigue equation

Dan Liu [1], Dirk John Pons [1] and Ee-hua Wong [2]

1. Department of Mechanical Engineering, University of Canterbury, Christchurch 8140, New Zealand; dan.liu@pg.canterbury.ac.nz

2. Energy Research Institute, Nanyang Technological University, 637553, Singapore; ehwong@ntu.edu.sg

Conference Paper (Pre-prints for the publication)

Please cite this paper as:

Liu, D., D.J. Pons, and E.H. Wong, Proposal for a unified creep-fatigue equation, in International Conference on Innovative Design and Manufacturing (ICIDM). 24-26 Jan, 2016: Auckland, New Zealand.

Abstract

Creep-fatigue implies the interaction between fatigue and creep, which is shown in many existing creep-fatigue models. However, these models cannot combine pure fatigue with creep-fatigue, and suffer from poor physical explanations. The proposed unified creep-equation can accommodate relevant variables and show sound underlying general principles of mechanics, and the parameters can be easy to obtain from empirical tests. The equation is of the form: $\Delta\varepsilon_p = C_0 C\left(T, t, \varepsilon_{p,ref}\right) N^{-\beta_0}$.

Keywords: creep-fatigue, creep-rupture, unified equation, fatigue model.

1. Introduction

Fatigue damage occurs when a material is subjected to cyclic loading. Although the term 'fatigue' first appeared in 1854, the history of fatigue could be traced as far back as 1837, when the first fatigue test results were published by Albert [1]. This period of almost two hundred years witnessed many significant milestones in fatigue theory, and the development of many models. However, these models cannot combine pure fatigue with creep-fatigue, and suffer from poor physical explanations of underlying causality. This paper develops a proposed unified creep-equation to accommodate relevant variables.

2. BACKGROUND

2.1 Fatigue models

The general fatigue models, like the Basquin equation (Eq.1) [2], the Coffin-Manson equation (Eq.2) [3, 4] and Morrow's energy-based equation (Eq.3) [5, 6], have been used in different areas successfully. The general form is:

$$\frac{\Delta\sigma}{2} = \sigma_f'(2N_f)^b \tag{1}$$

$$\frac{\Delta\varepsilon_p}{2} = \varepsilon_f'(2N_f)^c \tag{2}$$

$$\Delta W_P = W_f'(2N_f)^\beta \tag{3}$$

where, $\Delta\sigma$ is the stress amplitude, σ_f' is the fatigue strength coefficient, b is the fatigue strength exponent, $\Delta\varepsilon_p$ is the plastic strain amplitude, ε_f' is the fatigue ductility coefficient, c is the fatigue ductility exponent, ΔW_P is the plastic energy, W_f' is the energy coefficient, β is the energy exponent and N_f is the number of cycles.

2.2 Creep models

Creep damage occurs when a material is exposed to high levels of stress for a long term. Generally, creep is divided into three stages: primary creep, secondary creep and tertiary stage. Early work mainly focused on the effect of temperature on creep, and the Arrhenius equation (Eq.4) [7, 8] was proposed by Svante in 1889 to describe the relationship between strain rate and temperature. Then, combined with the effect of stress, a general equation (Eq.5) [9] was produced.

$$\dot{\varepsilon} = Ae^{\frac{-Q}{RT}} \tag{4}$$

$$\dot{\varepsilon} = \frac{A_2 \sigma^m}{d^q T} e^{\frac{-Q}{RT}} \tag{5}$$

where, $\dot{\varepsilon}$ is the strain rate, A and A_2 are constants dependent on the material and the particular creep mechanism, Q is the activation energy of the creep mechanism, σ is the applied stress, T is the absolute temperature, m and q are the exponents dependent on the creep mechanism, d is the grain size of the material and R is the Boltzmann's constant.

In addition, because of test-time limitations, the creep rupture test cannot be sustain for a long time, such as more than one year. Therefore, the accelerated test which employs a higher temperature is conducted to build the time-temperature relation, such as the Sherby-Dorn Parameter (Eq.6) [10], Larson-Miller Parameter (Eq.7) [11] and [12] (Eq.8) [13].

$$P_{SD} = te^{-Q/RT} \tag{6}$$

$$P_{LM} = T(\log t + C) \tag{7}$$

$$P_{MH} = \frac{T - T_a}{\log t - \log t_a} \tag{8}$$

where, P_{SD} is the Sherby-Dorn Parameter, P_{LM} is the Larson-Miller Parameter, P_{MH} is the Manson-Haferd Parameter, Q is the activation energy of the creep mechanism, R is the Boltzmann's constant, t is the time, T is the absolute temperature, C is a constant and ($\log t_a$, T_a) is the point of convergence of the $\log t$-T lines.

2.3 Creep-fatigue

Creep-fatigue can be regarded as the interaction of both fatigue and creep mechanisms of failure. Failure is negatively influenced by temperature, frequency and stress. Based on a number of creep rupture tests and creep-fatigue tests, various creep-fatigue models have been developed through curve fitting or numerical methods.

2.3.1 Models based on Coffin-Manson equation

To explore the influence of temperature and/or frequency on creep-fatigue, a large number of creep-fatigue tests have been conducted at different temperatures and/or frequencies. Then, different modified Coffin-Manson relationships were developed. For example, Jing's creep-fatigue model (Eq.9) [14] employs the influence of temperature on fatigue life,

$$\frac{\Delta\varepsilon_p}{2} = \varepsilon_f'\left(2N_f\right)^c \tag{9}$$

with

$$\varepsilon_f' = 68.79 - 0.34T + 250.56/\sqrt{T}$$
$$c = 1.29 - 0.0053T + 2.5/\sqrt{T}$$

and Shi's models (Eq.10) [15] and Engel Maier's model (Eq.11) [16] present the effects of both temperature and frequency on fatigue life.

$$\left[N_f f^{(k-1)}\right]^m \Delta\varepsilon_p = C \tag{10}$$

with

$$f^{(k-1)} = \begin{cases} f^{(k_1-1)} \; for & 1Hz \geq v \geq 10^{-3}Hz \\ \left[\frac{f}{10^{-3}}\right]^{(k_2-1)} (10^{-3})^{(k_1-1)} \; for & 10^{-3}Hz > v \geq 10^{-4}Hz \end{cases}$$

$$k_2 = 0.437 - 3.753 \times 10^{-4}T - 8.04 \times 10^{-7}T^2$$

$$k_1 = 0.919 - 1.765 \times 10^{-4}T - 8.634 \times 10^{-7}T^2$$

$$m = 0.731 - 1.63 \times 10^{-4}T + 1.392 \times 10^{-6}T^2 - 1.515 \times 10^{-8}T^3$$

$$C = 2.122 - 3.57 \times 10^{-3}T + 1.329 \times 10^{-5}T^2 - 2.502 \times 10^{-7}T^3$$

$$N_f = 0.5\left(\Delta\varepsilon_p/\varepsilon_f'\right)^{(1/c)} \tag{11}$$

with

$$c = -0.442 - 6 \times 10^{-4}T + 1.74 \times 10^{-2}\ln(1+f)$$

where, f is the frequency, k is the frequency exponent, m is the fatigue exponent, C is the material ductility coefficient and T is temperature.

In addition, besides temperature and frequency, another factor, cracking energy density (CED), was introduced into a new creep-fatigue equation (Eq.12) [17] by Lee. This equation can show good consistency with real situations, because cracking energy density can provide the information related to not only the location but also the direction of a crack nucleation.

$$\left[N_f f^{(k-1)}\right]^m \Delta\left(\frac{CED}{aT+b}\right) = C \tag{12}$$

2.3.2 Models based on linear accumulation damage rule

Given that the accumulation of creep and fatigue damage happen at different stages, the Coffin-Manson equation (fatigue) and Monkman-Grant equation (creep) were employed to develop a new creep-fatigue model (Eq.13) [18] through the linear damage rule. The contributions of fatigue and creep need to be calculated respectively by using this model.

$$N_f = \frac{1}{D_f + D_C} = \frac{1}{\left(\varepsilon_f'/\Delta\varepsilon_p\right)^{-1/\alpha} + \Delta t \cdot \dot{\varepsilon}_s^m / C} \tag{13}$$

where, D_f is the fatigue damage, D_C is the creep damage, α is the fatigue ductility exponent, Δt is the creep time, $\dot{\varepsilon}_s$ is the stable creep deformation rate, m is the exponent and C is the constant depends on the material.

In addition, the Coffin-Manson equation was extended in 1950s to creep-fatigue by inserting the plastic strain range into the inelastic strain range. The inelastic strain range is presented as the sum of the plastic strain range and the creep strain range. To future develop this theory, the inelastic strain range is divided into four components: completely reversed plasticity, tensile plasticity reversed by compressive creep, tensile creep reversed by compressive plasticity and completely reversed creep. Then, based on the Coffin-Manson equation and linear accumulation damage rule, an equation (Eq.14) [19] is developed which combines the effects of above four components.

$$\frac{1}{N} = \frac{\Delta\varepsilon_{pp}}{\Delta\varepsilon_{in}N_{pp}} + \frac{\Delta\varepsilon_{cc}}{\Delta\varepsilon_{in}N_{cc}} + \frac{\Delta\varepsilon_{cp}}{\Delta\varepsilon_{in}N_{cp}} + \frac{\Delta\varepsilon_{pc}}{\Delta\varepsilon_{in}N_{pc}} \tag{14}$$

where, $\Delta\varepsilon_{in}$ is the inelastic strain, $\Delta\varepsilon_{pp}$ is the plastic strain reversed by plastic strain, $\Delta\varepsilon_{cc}$ is the tensile creep strain reversed by compressive creep, $\Delta\varepsilon_{cp}$ is the tensile creep reversed by compressive plasticity and $\Delta\varepsilon_{pc}$ is the tensile plasticity reversed by compressive creep. N_{pp}, N_{cc}, N_{cp} and N_{pc} are the fatigue life of individual strain components, and follow the Coffin-Manson equation.

2.3.3 Other creep-fatigue models

As another form to present the influence of frequency, strain rate was introduced into a creep-fatigue equation (Eq.15) [20]. This equation was derived from both dynamic viscosity equation and toughness equation, so it can describe relationships between more parameters, such as stress, strain range, strain rate and cyclic stress-strain relation.

$$N_f = K(\Delta\varepsilon_P)^{n-1}(\Delta\varepsilon_t/\dot{\epsilon})^m\sigma_{sat} \tag{15}$$

Where, $\Delta\varepsilon_t$ is the total strain amplitude, $\dot{\epsilon}$ is the strain rate, σ_{sat} is the saturated tension stress, and K, n and m are the material parameters.

In addition, based on the ductility exhaustion theory which proposes the continuous consumption of ductility caused by fatigue and creep can lead to damage when accumulated strain reaches a critical ductility, and given the influence of loading waveform, creep and mean stress on fatigue life, a fatigue life prediction methodology (Eq.16) [21] for low cycle fatigue-creep was developed.

$$N_f = C_2\left(\Delta W_p\sigma_{max}^{1+n'}\right)^{\frac{-1}{\beta(1+n')}}\left(E_p - T_0\Delta W_{FL}\right)^{\frac{\alpha}{\beta(1+n')}} \tag{16}$$

where, ΔW_p is the plastic strain energy density, n' is cyclic strain hardening exponent, T_0 is the total time period per cycle, E_p is the viscosity-based parameter, ΔW_{FL} is the tensile elastic energy per cycle, σ_{max} is the maximum stress, α and β are model parameters, C_2 is the material-specific constant and N_f is the number of cycles.

Furthermore, according to the crack growth laws, a fracture mechanism-based method (Eq.17) [12] is produced to describe fatigue damage and predict fatigue life through calculating the

amount of crack extension. In this equation, the fatigue and creep crack growth per cycle are obtained separately, and the total damage is calculated through the sum of the two contributions.

$$\frac{da}{dN} = \left(\frac{da}{dN}\right)_f + \left(\frac{da}{dN}\right)_c \tag{17}$$

with

$$\left(\frac{da}{dN}\right)_f = C\left(\Delta J_{eff}\right)^l \text{ and } \left(\frac{da}{dN}\right)_c = \int_0^{t_h} AC^{*q}\,dt$$

where, $\frac{da}{dN}$ is the total crack growth per cycle, $\left(\frac{da}{dN}\right)_f$ is the crack growth per cycle due to cyclic load changes, $\left(\frac{da}{dN}\right)_c$ is the crack growth per cycle due to hold time, ΔJ_{eff} is the effective range of J-integral, t_h is the hold time, C^* is the time-dependent fracture parameter, and C, l, A and q are material constants obtained from experiments.

2.4 Limitations in the creep-fatigue models

These creep-fatigue models mentioned above are derived from existing fatigue models, such as the Coffin-Manson equation and the assumption of linear accumulation damage. Through a large number of experiments, the influence of different factors, like frequency/strain rate, temperature and stress, are presented in some models. Because the development of these models is based on many creep-fatigue tests, these models are highly reliable. However, it is time-consuming and expensive for industries to perform these tests. In addition, for some models which do not include the factors of temperature and/or frequency, the coefficients obtained from specific temperature and frequency cannot be used to predict fatigue life in other situations. Furthermore, some equations which come from curve fitting or mathematical methods cannot be explained from a physical perspective, so they are not meaningful and not easy to understand. For those models based on linear damage rule, it is noted that the linear addition of damage is inconsistent with the microstructural characteristics of fatigue damage and creep damage. To be specific, cyclic strain/stress cause the slips between lattices, which can lead to the persistent slip bands, then these deformations lead to cracks. The damage caused by creep comes from diffusion and dislocation along the grain boundaries and within the lattice, which lead to the accumulation of voids. Last but not least, it is significant that the existing fatigue models (like the Coffin-Manson equation) only work without creep while these creep-fatigue equations above only can be used when creep is active, which means that these creep-fatigue equations cannot build a bridge between pure fatigue and creep fatigue.

3. Approach

The purpose of this work was to derive a unified creep-fatigue equation that can accommodate relevant variables. This should ideally also show sound underlying general principles of mechanics, and the parameters should be easy to obtain from empirical tests.

A theoretical approach was taken by starting from the Coffin-Manson equation, and extending it conceptually by the addition of parameters to represent the creep behaviour. Experimental data from the literature for 63Sn37Pb solder was used to establish a suitable formulation of the model.

The resulting formulation accommodates both fatigue and creep, with variables for life (N), frequency of applied load (f) or cyclic time (t), temperature (T), material properties, and four coefficients.

4. The proposal of the unified creep-fatigue equation

4.1 Starting points

The approach for finding this model was to start with the Coffin-Manson equation for pure fatigue. This formulation was selected because it is the only one that can be used in the low-cycle regime to describe fatigue behaviours between plastic strain and fatigue life. This equation has excellent fit to empirical observations. Also, it is physically plausible that the plastic strain should be a simple power function of the number of cycles, for the following reason. Each load cycle has the potential to initiate or propagate a crack, and every cycle causes progressive damage. Hence the more the load cycles the less residual strong material left to carry the load, and the more intense the effect of subsequent load cycles. There is a progressive recruitment of the load-bearing cross-section by the crack. Phenomena whereby an effect progressively recruits the whole of a volume of space are typically well-described by exponential formulations. In the case of a crack across a cross section, it is not unreasonable to expect that a power relationship, which is a more general form of the exponential, could be a good starting point. Also, this formulation has been well-accepted in the literature, and has been the basis for a number of other models which have been effective in their areas.

Nonetheless this formulation does not include temperature and cycle time. Given the influence of temperature and cycle time which have been verified in Shi's paper [15], the parameters of temperature (T) and cycle time (t) need to be employed. At this point, the term 'fatigue capacity' needs to be introduced to describe the relation between pure fatigue and creep. For creep fatigue, the fatigue capacity is reduced because of the increasing influence of creep damage. This can be shown in Fig.1, to be specific, the creep-fatigue curves between pure fatigue curve and pure creep curve show the residual fatigue capacities, and the reductions are caused by creeps at different plastic strains/stresses. Therefore, given the contribution of creep on the reduction of fatigue capacity, the time-temperature-stress relation should be employed to develop the unified creep-fatigue equation. This relation (stress-time-temperature relation) is frequently referred to be the time-temperature parameter, such as Sherby-Dorn Parameter (Eq.6), Larson-Miller Parameter (Eq.7) and Manson-Haferd Parameter (Eq.8). Among these three parameters, the Manson-Haferd Parameter is regarded to be the best description of stress-time-temperature relation [22]. Therefore, this parameter should be employed to describe the contribution of creep on fatigue damage and develop the unified creep-fatigue equation.

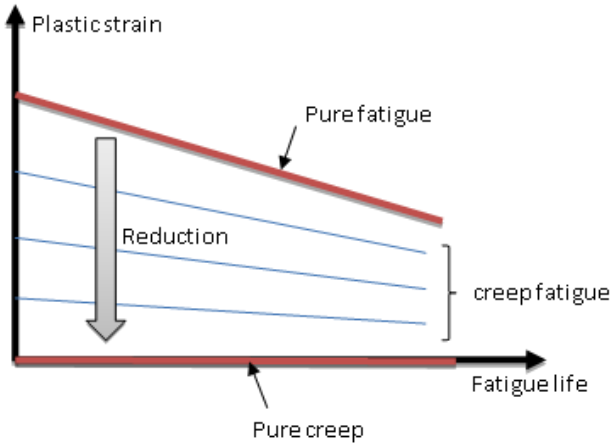

Fig.1 The description of 'fatigue capacity'

To develop the unified creep-fatigue equation, the influences of frequency and temperature on fatigue life are discussed separately, and the derivation [23] of this equation is based on the experiments conducted by Shi [15]. Firstly, according to the experimental data of 63Sn37Pb solder, the ductility exponent βo is slightly affected by the cyclic frequency, then the assumption of plastic strain-frequency-fatigue life relation can be obtained:

$$\Delta\varepsilon_p = C_f(f)N^{-\beta_0} \tag{18}$$

Plotting C_f versus f (Fig.2), it shows that a logarithmic function presents a much better fit than a power-law function. Then, the function $C_f(f)$ can be presented as:

$$C_f(f) = a_2' + a_2 \log f = a_2' - a_2 \log t \tag{19}$$

where, t is the cycle time.

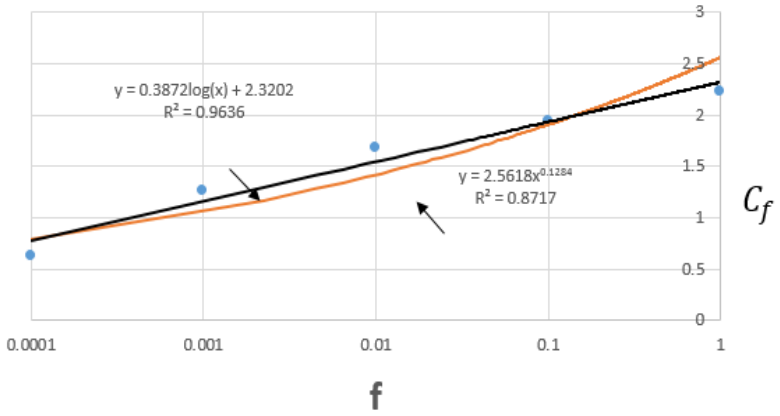

Fig.2 C_f versus f at 25°C for the proposed unified creep-fatigue equation against the experimental data for 63Sn37Pb solder. Data adapted from Shi [15].

In addition, the ductility exponent β_o is slightly affected by the temperature, then the assumption of plastic strain-temperature-fatigue life relation can be obtained:

$$\Delta\varepsilon_p = C_T(T)N^{-\beta_0} \tag{20}$$

Plotting C_T versus T (Fig.3), it shows a linear relation between C_T and temperature. Then, the function $C_T(T)$ can be presented as:

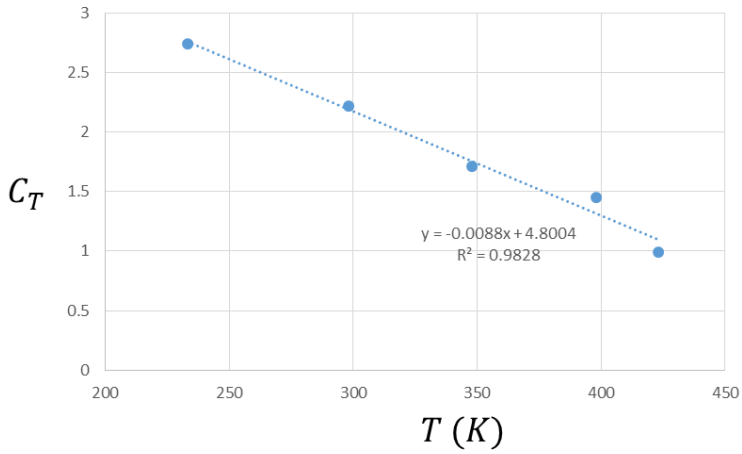

Fig.3 C_T versus T at 1Hz for the proposed unified creep-fatigue equation against the experimental data for 63Sn37Pb solder. Data adapted from Shi [15].

$$C_T(T) = a_1' + a_1 T \tag{21}$$

Combining Eq.19 and Eq.21 gives:

$$C(T,t) = a_0 + a_1 T - a_2 \log t \tag{22}$$

which shows a linear relation between T and $\log t$. It is noted that this relation is consistent with the Manson-Haferd Parameter (Eq.8). Therefore, the assumptive form of $C(T,t)$ is reasonable, and the coefficients could be obtained through creep rupture tests.

Furthermore, the Manson-Haferd Parameter shows that both temperature and time are function of stress, thus Eq. 22 can be presented as:

$$C\big(T(\sigma),t(\sigma)\big) = a_0 + a_1 T(\sigma) - a_2 \log t(\sigma) = a_0 + a_1(\sigma)T - a_2\,(\sigma)\log t \tag{23}$$

Then, stress can be converted to plastic strain through strain-stress relation, and Eq.23 can be further presented as:

$$C\big(T,t,\varepsilon_{p,ref}\big) = a_0 + a_1\big(\varepsilon_{p,ref}\big)T - a_2\,\big(\varepsilon_{p,ref}\big)\log t \tag{24}$$

where, $\varepsilon_{p,ref}$ is the plastic strain at pure fatigue.

4.2 Basic form of the unified creep-fatigue equation

The unified creep-fatigue equation should be used for both pure fatigue and creep fatigue, and the pure fatigue can be regarded as the special situation of creep fatigue. For this reason and comparing this equation with the Coffin-Manson equation, Eq.24 can be deduced to be Eq.25, and the unified equation can be presented to be Eq.26.

$$C(T,t,\varepsilon_{p,ref}) = a_0\left(1+\frac{a_1(\varepsilon_{p,ref})}{a_0}T-\frac{a_2(\varepsilon_{p,ref})}{a_0}\log t\right) = C_0\,(1+c_1(\varepsilon_{p,ref})T+c_2(\varepsilon_{p,ref})\log t) \tag{25}$$

$$\Delta\varepsilon_p = C_0C(T,t,\varepsilon_{p,ref})N^{-\beta_0} = C_0\left(1+c_1(\varepsilon_{p,ref})T+c_2(\varepsilon_{p,ref})\log t\right)N^{-\beta_0} \tag{26}$$

It is significant that pure fatigue happens when both T=0 and $\log t$=0, under this condition the creep-fatigue equation restores to the Coffin-Manson equation. This condition is regarded as the reference condition, and introducing the terms 'reference temperature' and 'reference time' into Eq.26 gives:

$$\Delta\varepsilon_p = C_0C(T,t,\varepsilon_{p,ref})N^{-\beta_0} = C_0[1+c_1(\varepsilon_{p,ref})(T-T_{ref})+c_2\,(\varepsilon_{p,ref})\log(t/t_{ref})]N^{-\beta_0} \tag{27}$$

This Equation shows that the creep is dormant at reference temperature and reference time.

Finally, the basic form of the unified creep-fatigue equation can be presented as:

$$\Delta\varepsilon_p = C_0C(T,t,\varepsilon_{p,ref})N^{-\beta_0} \tag{28}$$

with

$$C(T,t,\varepsilon_{p,ref}) = 1+c_1(\varepsilon_{p,ref})(T-T_{ref})+c_2\,(\varepsilon_{p,ref})\log(t/t_{ref}) \tag{29}$$

To sum up the origin and underpinning mechanics of this, we propose that plastic strain is a linear function of temperature, that the frequency function is logarithmic, that the thermal and frequency effects may be added, and that the number of cycles has power relationship.

The creep part of this equation is provided by the thermal component. This was derived from observation of empirical data, which shows a simple linear relationship. This is consistent with the idea that creep is largely a combination of diffusion and dislocation effects. Both of these are known to have a temperature dependency. This dependency is typically expressed as exp(c/T) where c is a constant, as in the Nabarro-Herring and Coble creep formulations. A formulation like exp(c/T) simplifies to a linear dependency when the temperature is very high (Fig.4). Our equation is also consistent with the evidence that many materials have a threshold temperature below which creep does not materially occur. The explanation of this may be found in activation energy for diffusion and dislocation events.

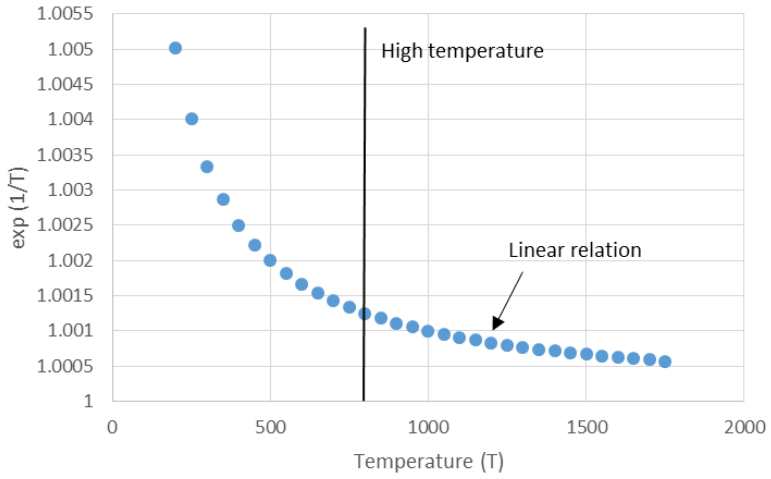

Fig.4 Linear relation at high temperature

The frequency part of this equation is presented by logarithmic cyclic time in the unified creep-fatigue equation, which shows a linear relation with temperature. Similar to the creep part, this was also derived from observation of empirical data. This relation is consistent with the temperature-time relation in the Manson-Haferd Parameter. In addition, for the Arrhenius equation, performing logarithmic operation can present a linear relation between log $\dot{\varepsilon}$ and T-1, which also can be expressed as a linear relation between log t and T. In particular, the identification of this relation is regarded as the method for defining the activation energy for creep damage, which means that this dependency can imply the activation of creep.

According to the expression of Eq.29, temperature and simple superposition with frequency effect through a plus sign. We found that the magnitude of $c_1(\varepsilon_{p,ref})$ and $c_2(\varepsilon_{p,ref})$ are negative in the subsequent research, which shows that the fatigue capacities decrease when creep is active. This is consistent with empirical data, and can be shown in Fig.1. Furthermore, this expression (decrease of fatigue capacities) gives a good numerical explanation of the negative effects of temperature and frequency on fatigue life.

5 Conclusion

The existing creep-fatigue models are excessive tuned and non-universal, and have poor explanations and economy. This work proposes a new formulation that accommodates both fatigue and creep, with variables for life (N), frequency of applied load (f) or cyclic time (t) (which is a measure of strain rate), temperature (T), material properties, and four coefficients.

The equation is of the form: $\Delta\varepsilon_p = C_0 C(T, t, \varepsilon_{p,ref}) N^{-\beta_0}$, which is based on the Coffin-Manson equation, and considers the influence of temperature and frequency on fatigue life. In addition, the coefficients in this equation can be obtained through minimum experimental efforts. In particular, the derivation of this equation shows a reasonable temperature-time relation, and the explanation of this may be found in activation energy for diffusion and

dislocation events. Hence the equation is consistent with what is known about the underlying facture mechanics.

Contribution statement: The work was conducted by DL, supervised by DP and EW. The form of the equation was proposed by DL and EW, The explanations were developed by DL and DP. The literature review was conducted by DL.

References

1. Schütz, W., A history of fatigue. Engineering fracture mechanics, 1996. 54(2): p. 263-300.
2. Basquin, O. The exponential law of endurance tests. in Proc. Astm. 1910.
3. Coffin Jr, L., A study of the effect of cyclic thermal stresses on a ductile metal. American Society of Mechanical Engineers, 1954. 76: p. 931-950.
4. Manson, S.S., Behavior of materials under conditions of thermal stress. 1953: NACA TN 2933.
5. MORROW, J.D., Miaroplastio Strain Hysteresis Energy as a Criterion for Fatigue Fracture. 1961.
6. Morrow, J., Cyclic plastic strain energy and fatigue of metals. 1965.
7. Arrhenius, S., Über die Dissociationswärme und den Einfluss der Temperatur auf den Dissociationsgrad der Elektrolyte. 1889: Wilhelm Engelmann.
8. Arrhenius, S., Über die Reaktionsgeschwindigkeit bei der Inversion von Rohrzucker durch Säuren. Zeitschrift für physikalische Chemie, 1889. 4: p. 226-248.
9. Dowling, N.E., Mechanical behavior of materials: engineering methods for deformation, fracture, and fatigue. 1993: Prentice hall.
10. Orr, R.L., O.D. Sherby, and J.E. Dorn, Correlations of rupture data for metals at elevated temperatures. 1953, DTIC Document.
11. Larson, F. and J. Miller, A time-temperature relationship for rupture and creep stresses. 1952.
12. Ainsworth, R., M. Ruggles, and Y. Takahashi, Flaw assessment procedure for high-temperature reactor components. Journal of pressure vessel technology, 1992. 114(2): p. 166-170.
13. Manson, S. and A.M. Haferd, A linear time-temperature relation for extrapolation of creep and stress-rupture data. 1953, Lewis Flight Propulsion Lab., NACA.
14. Jing, H., et al., Low cycle fatigue behavior of a eutectic 80Au/20Sn solder alloy. International Journal of Fatigue, 2015. 75: p. 100-107.
15. Shi, X., et al., Low cycle fatigue analysis of temperature and frequency effects in eutectic solder alloy. International Journal of Fatigue, 2000. 22(3): p. 217-228.
16. Engelmaier, W., Fatigue life of leadless chip carrier solder joints during power cycling. IEEE transactions on components, hybrids, and manufacturing technology, 1983(3): p. 232-237.
17. Lee, J. and H.-Y. Jeong, Fatigue life prediction of solder joints with consideration of frequency, temperature and cracking energy density. International Journal of Fatigue, 2014. 61: p. 264-270.
18. Zhu, Y., et al., A new creep–fatigue life model of lead-free solder joint. Microelectronics Reliability, 2015.
19. Manson, S., et al., Creep-fatigue analysis by strain-range partitioning. 1971.
20. Goswami, T., Development of generic creep–fatigue life prediction models. Materials & design, 2004. 25(4): p. 277-288.

21. Zhu, S.-P., et al., An efficient life prediction methodology for low cycle fatigue–creep based on ductility exhaustion theory. International Journal of Damage Mechanics, 2012: p. 1056789512456030.
22. Pelleg, J., Mechanical properties of materials. 2012.
23. Wong, E. and Y.-W. Mai, A unified equation for creep-fatigue. International Journal of Fatigue, 2014. 68: p. 186-194.

Paper 2: The Unified Creep-Fatigue Equation for Stainless Steel 316

Dan Liu [1], Dirk John Pons [1,*] and Ee-hua Wong [2]

1. Department of Mechanical Engineering, University of Canterbury, Christchurch 8140, New Zealand; dan.liu@pg.canterbury.ac.nz

2. Energy Research Institute, Nanyang Technological University, 637553, Singapore; ehwong@ntu.edu.sg

*****Correspondence: dirk.pons@canterbury.ac.nz

Published Paper (Pre-prints for the publication)

Please cite this paper as:

Liu, D., D.J. Pons, and E.H. Wong, The Unified Creep-Fatigue Equation for Stainless Steel 316. Metals, 2016. 6(9): p. 219. DOI: http://dx.doi.org/10.3390/met6090219

Abstract

Background—The creep-fatigue properties of stainless steel 316 are of interest because of the wide use of this material in demanding service environments, such as the nuclear industry. **Need**—A number of models exist to describe creep-fatigue behaviours, but they are limited by the need to obtain specialized coefficients from a large number of experiments, which are time-consuming and expensive. Also, they do not generalize to other situations of temperature and frequency. There is a need for improved formulations for creep-fatigue, with coefficients that determinable directly from the existing and simple creep-fatigue tests and creep rupture tests. **Outcomes**—A unified creep-fatigue equation is proposed, based on an extension of the Coffin-Manson equation, to introduce dependencies on temperature and frequency. The equation may be formulated for strain as $\varepsilon_p = C_0 c\left(T, t, \varepsilon_p\right) N^{-\beta_0}$, or as a power-law $\varepsilon_p = C_0 c(T,t) N^{-\beta_0 b(T,t)}$. These were then validated against existing experimental data. The equations provide an excellent fit to data (r^2 = 0.97 or better). **Originality**—This work develops

a novel formulation for creep-fatigue that accommodates temperature and frequency. The coefficients can be obtained with minimum experimental effort, being based on standard rather than specialized tests.

Keywords: creep-fatigue; creep-rupture; unified equation; fatigue model

1. Introduction

The life of nuclear power plants has been a major issue because it strongly relates to safety and economy [1]. Stainless steel 316 is widely used for the making of components, such as turbine blades and piping, because of its excellent corrosion resistance.

As the two main fatigue evaluation and design methods in the nuclear industry, the linear damage rule and the crack growth law have been used for many years. However, microstructural characteristics lead to imperfect prediction of fatigue failure. The coefficients in these models are obtained from a large number of experiments, which are time-consuming and expensive for industry to perform. When these models are employed, the coefficients are normally obtained from specific temperature and frequency, so these coefficients cannot be used to predict fatigue life in other situations. Therefore, there is a need to develop a creep-fatigue model that can largely avoid the influence of microstructure, present the influence of creep effects on fatigue behaviour, and be generalized to other situations of temperature and frequency. Ideally, the parameters in this model should be easy to obtain from empirical tests with minimum effort.

In this paper, the strain-form unified creep-fatigue equation and power-law form will be introduced and will be verified on stainless steel 316. As part of the validation, the simple experimental methods of extracting coefficients will be presented.

2. Existing Approaches

In the case of pure fatigue, three general fatigue models are used to predict the fatigue life of this material: the Basquin equation (Eq.1) [2], the Coffin-Manson equation (Eq.2) [3,4] and Morrow's energy-based equation (Eq.3) [5,6].

$$\frac{\Delta\sigma}{2} = \sigma_f'(2N_f)^b \tag{1}$$

$$\frac{\Delta\varepsilon_p}{2} = \varepsilon_f'(2N_f)^c \tag{2}$$

$$\Delta W_P = W_f'(2N_f)^\beta \tag{3}$$

where $\Delta\sigma$ is the stress amplitude, σ_f' is the fatigue strength coefficient, b is the fatigue strength exponent, $\Delta\varepsilon_p$ is the plastic strain amplitude, ε_f' is the fatigue ductility coefficient, c is the fatigue ductility exponent, ΔW_p is the plastic energy, W_f' is the energy coefficient, β is the energy exponent and N_f is the number of cycles. The coefficients in Eq.1 and Eq.2 can be related through the compatibility (Eq.4) [7] and cyclic stress-strain relation (Eq.5) [8]

$$K' = \frac{\sigma_f'}{\left(\varepsilon_f'\right)^{n'}} \; n' = \frac{b}{c} \tag{4}$$

$$\varepsilon_p = \left(\frac{\sigma_a}{K'}\right)^{1/n'} \tag{5}$$

where σ_a is the stress amplitude, K' is the strain hardening coefficient and n' is the strain hardening exponent.

In nuclear power plants, some components which are made of stainless steel 316 are subjected to fatigue at elevated temperature, at which the mechanism of creep is active. The failure of these components is caused by the combination of fatigue damage and creep damage. Two major rules are used to evaluate creep-fatigue life: the linear damage rule and the crack growth law.

2.1 The Linear Damage Rule

The linear damage theory was proposed by Palmgren [9] in 1924; it was further developed by Miner [10] in 1945 and called the Palmgren–Miner rule. This rule is widely used in the nuclear industry to design and evaluate the life of nuclear power plants [11-14]. According to this rule, damage can be calculated through using Eq.6, and the engineering structure fails when D equals 1.

$$D = \sum_{i=1}^{k} \frac{n_i}{N_i} \tag{6}$$

where D is the accumulated fatigue damage, k is the number of block loading, n_i is the number of constant amplitude cycles under the ith strain/stress range, and N_i is the number of cycles to fatigue failure under the ith strain/stress range.

Combined with the creep effects, the total damage is divided into fatigue damage and creep damage at the elevated temperature (Eq.7) [15], which shows that the accumulation of fatigue and creep damage happens at different stages.

$$D = D_f + D_c \tag{7}$$

where D_f is the fatigue damage and D_c is the creep damage.

However, as one of the simplified methods which are used to predict life in the nuclear industry, the linear damage rule can lead to inaccurate results because of the neglect of loading sequences [13]. This problem was also realized in other industries. Therefore, many studies were

conducted to improve the accuracy of this rule. For example, Richard and Newmark [16] proposed a power-law damage rule. Manson [17] demonstrated that failure can still happen when D is less than 1 and the linear damage rule was modified to double linear damage rule. Although these models can improve the results, these modifications do not change the character of linear accumulation of damage. Therefore, when creep is active, the inaccuracy which comes from the linear accumulation of creep damage and fatigue damage still cannot be solved, because the linear addition of damage is inconsistent with the microstructural characteristics. To be specific, cyclic strain/stress causes the slips between lattices, which can lead to the persistent slip bands. These deformations then lead to cracks. Meanwhile, the damage caused by creep comes from diffusion and dislocation along the grain boundaries and within the lattice, which leads to the accumulation of voids.

2.2 The Linear Damage Rule

The crack growth law is also used in the nuclear industry to predict fatigue life of some components [18,19], such as piping and tanks. The crack growth law shows that the fatigue life is the number of loading cycles which is required to achieve the final crack size, and this process is divided into two stages: initiation and propagation. Therefore, the total crack size can be presented as the linear addition of initial crack size and propagative crack size. Normally, the initial crack is identified as the real crack size in the structures before loading, and the propagative crack (Eq.8) [19,20] can be obtained through Paris's model [21]:

$$\frac{\mathrm{d}a}{\mathrm{d}N} = C(\Delta J_{\mathrm{eff}})^l \tag{8}$$

where $\frac{\mathrm{d}a}{\mathrm{d}N}$ is the total crack growth per cycle, ΔJ_{eff} is the effective range of J-integral, and C is a material constant obtained from experiments. When creep is active, the total damage is calculated through the sum of fatigue and creep crack growth (Eq.9) [21]:

$$\frac{\mathrm{d}a}{\mathrm{d}N} = \left(\frac{\mathrm{d}a}{\mathrm{d}N}\right)_f + \left(\frac{\mathrm{d}a}{\mathrm{d}N}\right)_c \tag{9a}$$

$$\left(\frac{\mathrm{d}a}{\mathrm{d}N}\right)_f = C(\Delta J_{\mathrm{eff}})^l \text{ and } \left(\frac{\mathrm{d}a}{\mathrm{d}N}\right)_c = \int_0^{t_h} AC^{*q}\mathrm{d}t \tag{9b}$$

where $\left(\frac{\mathrm{d}a}{\mathrm{d}N}\right)_f$ is the crack growth per cycle due to cyclic load changes, $\left(\frac{\mathrm{d}a}{\mathrm{d}N}\right)_c$ is the crack growth per cycle due to hold time, t_h is the hold time, C^* is the time-dependent fracture parameter, and l, A and q are material constants obtained from experiments.

The crack growth law provides a good physical explanation of damage. However, the quantitative summation between the cracks caused by fatigue and the cracks caused by creep does not consider the directions of these cracks. This means that two parallel cracks can cause the same damage as two non-parallel cracks, which is inconsistent with the microstructure, because the angle between two cracks plays an important role in the total damage.

2.3 Recent Developments towards a Unified Creep-Fatigue Equation

As identified above, the limitations of these methods are that they do not fully accommodate the observed microstructural characteristics, they require extensive testing to determine the coefficients, and the results cannot be generalized to other situations of temperature and frequency.

In an attempt to address these problems, Wong and Mai [22] proposed a formalism to accommodate fatigue and creep-fatigue, which they called a unified creep-fatigue equation (hereafter WM equation); see Eq.10. The unified creep-fatigue equation takes into account the influence of temperature and frequency on fatigue life. This equation was developed by extension of the Coffin-Manson equation.

$$\varepsilon_p = C_0 s(\sigma) c(T,t) N^{-\beta_0 b(T,t)} \quad (10)$$

where σ is the stress, T is the temperature, t is the cyclic time (1/frequency), C_0 is the fatigue ductility coefficient, β_0 is the fatigue ductility exponent, ε_p is the plastic strain and N is the fatigue life. The basic premise of the WM formulation is that 'all fatigue phenomenon are indeed creep-fatigue, and "pure fatigue" is just a special case of creep-fatigue' [22]. They reasoned that the Coffin–Manson equation was "a special case of a unified creep-fatigue equation".

The general principles of this were shown for the case of SnPb solder [22]. However there are several issues with the WM formulation. They did not provide the method to get the stress function s (σ). This means that this unified equation still cannot be used to predict fatigue life. A related issues is that they assumed that functions c (T, t) and b (T, t) share the same pattern and characteristics, such that internal coefficients $c_1/c_2 = b_1/b_2$, but no reason was provided for this assumption. Also, the method of extracting the coefficients of function c (T, t) and b (T, t) was not proposed.

The WM equation has potential, but the concept needs further development. It has not been applied other than to solder, so its universal applicability is uncertain. There is a need to further validate or modify and the relationships between the coefficients, or improve the formulation.

3. Methods

3.1 Research Question

The purpose of this paper was to extend and modify the WM unified creep-fatigue equation. The WM equation provided some helpful initial starting points for the present work. Firstly, they showed that the creep-fatigue behaviour is negatively influenced by temperature, frequency and stress. Secondly, the unified creep-fatigue equation could be deduced from the Coffin–Manson equation and the experimental data of Shi [23] on solder, and the reference

condition could be introduced into this unified equation. Thirdly, function c (T, t) and b (T, t) could be related to Manson–Haferd parameter, at least numerically.

3.2 Approach

Work in progress towards a further conceptual development has been to show how plastic strain (ε_p) may be theoretically related, in the creep-fatigue situation, to conditions at the reference temperature (T_{ref}) and reference cycle time (t_{ref}) at which tests are performed [24]. This line of thinking results in two forms of the unified creep-fatigue equation. The first form (strain form) represents the plastic strain as a function of cycle time, number of cycles, and temperature: $\varepsilon_p = C_0 c\left(T, t, \varepsilon_p\right) N^{-\beta_0}$. The second form (power-law form) does the same, but is simplified to a power-law relationship: $\varepsilon_p = C_0 c(T,t) N^{-\beta_0 b(T,t)}$. Definitions of variables are provided below.

In this paper both forms are verified by application to stainless steel 316. As part of the validation, the simple experimental methods of extracting coefficients are presented. The approach is to take published empirical data for creep rupture tests and creep-fatigue tests. The experimental data for creep-fatigue are from [25] and the creep rupture data are from [26] for stainless steel 316. From the data which were obtained at an arbitrary temperature and reference cycle time, we extract coefficients for the strain-form unified creep-fatigue equation (Section 4.3.1), and validate them through the empirical data at other conditions (Section 4.3.2). Then, the empirical data at two temperatures and reference cycle time are used to extract the coefficients for the power-law form (Sections 4.4.1.1 and 4.1.2.1), and validate it through the empirical data at other conditions (Sections 4.4.1.2 and 4.4.2.2).

The unified creep-fatigue equations were originally developed for solder, a material that is very different to stainless steel. Results show that the two forms of the unified creep-fatigue equation provide excellent representation of the stainless steel 316 creep fatigue data. A temperature modified Coffin–Manson equation was derived from the combination of the power-law unified creep-fatigue equation and the frequency modified Coffin–Manson equation.

4. Results: Theory and Calculation

4.1 Introduction to the Unified Creep-Fatigue Equation

At this point, the term "fatigue capacity" needs to be introduced to describe the relation between pure fatigue and creep. For creep-fatigue, the fatigue capacity is reduced because of the increasing influence of creep damage. This can be seen in Figure 1: the creep-fatigue curves between pure fatigue curve and pure creep curve show the residual fatigue capacities, and the reductions are caused by creeps at different plastic strains/stresses.

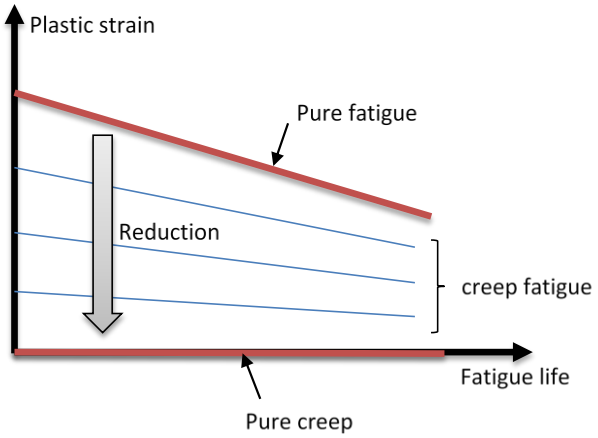

Figure 1 The relation between pure fatigue and pure creep.

Therefore, given the contribution of creep to the reduction of fatigue capacity, it is reasonable that the time-temperature-stress relationship, such as the Sherby–Dorn Parameter (Eq.11) [27], the Larson–Miller Parameter (Eq.12) [28] and the Manson–Haferd Parameter (Eq.13) [29], is involved in the unified creep-fatigue equation.

$$P_{\mathrm{SD}}(\sigma) = te^{-Q/RT} \tag{11}$$

$$P_{\mathrm{LM}}(\sigma) = T(\log t + C) \tag{12}$$

$$P_{\mathrm{MH}}(\sigma) = \frac{T - T_a}{\log t - \log t_a} \tag{13}$$

where P_{SD} is the Sherby–Dorn Parameter, P_{LM} is the Larson–Miller Parameter, P_{MH} is the Manson–Haferd Parameter, Q is the activation energy of the creep mechanism, R is the Boltzmann's constant, t is the time, T is the absolute temperature, C is a constant and ($\log t_a$, T_a) is the point of convergence of the $\log t$-T lines. Among these three parameters, the Manson–Haferd Parameter is regarded as the best description of stress-time-temperature relation [30].

It can be found that the unified creep-fatigue equation (Eq.14 and Eq.15) [24] shows a linear relationship between T and log$t$:

$$\varepsilon_p = C_0 c(T, t, \varepsilon_p) N^{-\beta_0} \tag{14}$$

with

$$c(T, t, \varepsilon_p) = 1 - c_1(\varepsilon_p)(T - T_{\mathrm{ref}}) - c_2 \log(t/t_{\mathrm{ref}}) \; (T > T_{\mathrm{ref}}, t > t_{\mathrm{ref}}) \tag{15}$$

Note that this relationship is consistent with the form of the P_{MH} parameter.

The *reference condition* refers to the threshold temperature T_{ref} at which creep first occurs (below this temperature no creep occurs), and cycle time (period) t_{ref} (arbitrary set as 1 second for comparing different data sets). The reference temperature and cyclic time for stainless steel 316 are identified as T_{ref} = 670 K and t_{ref} = 1 s. This temperature is 0.4 of the melting temperature and corresponds to the widely held assumption that below this temperature no creep occurs.

We then determine the plastic strain at reference condition, by transforming Eq.14:

$$\varepsilon_{p,\mathrm{ref}} = C_0 N^{-\beta_0} = \frac{\varepsilon_p}{c(T,t,\varepsilon_p)} \tag{16}$$

This transformation would result in all ε_p: N data reducing into one single $\varepsilon_{p,\mathrm{ref}}$: N curve if the creep function (Eq.15) could describe the influence of creep on fatigue well.

However, the strain form returns an equation that is not power-law. Because power-law relation is expressed as a straight line on a log-log plot, it can provide an easy and clear way to present the creep-fatigue behaviours between different temperatures and cyclic times through translation and rotation. For this reason, the unified creep-fatigue equation is represented as a power-law form (Eq.17) [24] through fitting the ε_p-N data with a power-law relation.

$$\varepsilon_p = C_0 c(T,t) N^{-\beta_0 b(T,t)} \tag{17}$$

with

$$c(T,t) = 1 - c_1(T - T_{ref}) - c_2 \log(t/t_{ref}) \; (T > T_{\mathrm{ref}},\, t > t_{\mathrm{ref}}) \tag{18}$$

$$b(T,t) = 1 - b_1(T - T_{\mathrm{ref}}) - b_2 \log(t/t_{\mathrm{ref}}) \; (T > T_{\mathrm{ref}},\, t > t_{\mathrm{ref}}) \tag{19}$$

Then, the plastic strain at reference condition is determined by transforming Eq.17:

$$\varepsilon_{p,\mathrm{ref}} = C_0 N^{-\beta_0} = C_0 \left[\frac{\varepsilon_p}{C_0 c(T,t)}\right]^{1/b(T,t)} \tag{20}$$

This transformation would cause all ε_p:N data to collapse into one $\varepsilon_{p,\mathrm{ref}}$:$N$ curve if the creep function (Eq.18) and stress function (Eq.19) could present the influence of creep on fatigue well.

It can be seen that the unified creep-fatigue equation is restored to the Coffin–Manson equation at reference condition (T_{ref}, t_{ref}), which builds a bridge between pure fatigue and creep fatigue. The deduction of coefficients (Eq.A1-A13) in the strain-form unified creep-fatigue equation and power-law form is shown in Appendix A.

Next, the relatively simple methods of obtaining the coefficients will be verified on stainless steel 316.

4.2. Extracting the Creep-Rupture Properties of Stainless Steel 316

The Manson–Haferd parameter was extracted through plotting creep-rupture data [26] as log *(time)* vs. *temperature*. According to the Manson–Haferd parameter, all log$t$-T lines at different stresses should converge to one point, where the temperature is regarded as the Creep Initiation Temperature, below which no creep occurs. We determine this temperature as 40% of the melting temperature. This corresponds to the reference temperature. In this case the reference temperature is found to be T_{ref} = 670 K. At this temperature, the rupture times at different stresses were found. According to Manson–Haferd parameter, these rupture times should be

the same. However, because the accuracy of experiments is influenced by many factors, such as facilities and environment, the points (rupture time, reference temperature) at different stresses cannot be collected into one point. Therefore, the average of these rupture times is employed to define the rupture time at the point of convergence, and the point of convergence is identified to be (670, 9.54) (shown in Figure 2). The Manson–Haferd parameter is stress dependent, and the values are obtained as the inverse of the slope from the fitted lines. Then, the relationship between Manson–Haferd parameter and stress can be extracted from Figure 2, and Eq.21 is given through curve-fitting:

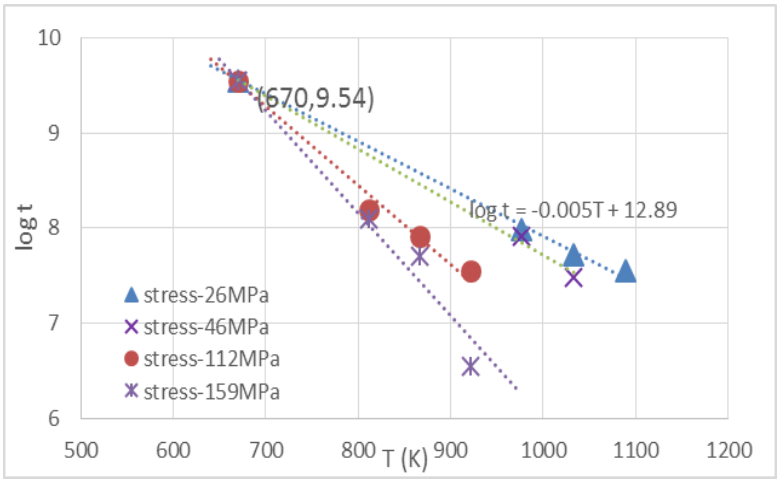

Figure 2 The P_{MH} (σ, T, t) parameter of AISI stainless steel 316. Data extracted from [26].

$$-\frac{1}{P_{\mathrm{MH}}(\sigma)} = 4.50 \times 10^{-3} + 1.26 \times 10^{-5}\sigma + 1.70 \times 10^{-7}\sigma^2 \tag{21}$$

To convert P_{MH} (σ) to P_{MH} (ε_p), the data of stress, total strain, temperature and Young's modulus are extracted from [31]. Because the time of tension tests is much less than the creep-rupture time, the influence of time (creep) on tension tests can be neglected. The temperature-dependent plastic strain-stress relationship (Eq.22–24) can be developed through curve-fitting.

$$\varepsilon_p = \left(\frac{\sigma}{K(T)}\right)^{1/n(T)} \tag{22}$$

$$K(T) = -0.4875T + 769.79 \tag{23}$$

$$n(T) = 7.04 \times 10^{-2} + 1.94 \times 10^{-4}T - 1.22 \times 10^{-7}T^2 \tag{24}$$

Then, substituting Eq.22-24 into Eq.21 gives Eq.25:

$$-\frac{1}{P_{\mathrm{MH}}(\varepsilon_p, T)} = 4.50 \times 10^{-3} + 1.26 \times 10^{-5}K(T)\,\varepsilon_p^{n(T)} + 1.70 \times 10^{-7}K(T)\,\varepsilon_p^{2n(T)} \tag{25}$$

4.3 Evaluation of the Coefficients of the Strain-Form Unified Creep-Fatigue Equation $\varepsilon_p = C_0 c(T, t, \varepsilon_p) N^{-\beta_0}$ for the Stainless Steel 316 and Validation

4.3.1 Evaluation of Creep-Fatigue Coefficients

Based on the Eq.A1-A6 shown in Appendix A, the coefficients of the creep function, c (T, t, ε_p), for the stainless steel 316 are established as follows.

Substituting log t_a = 9.54 and t_{ref} = 1s into Eq.A2, the coefficient c_2 is evaluated as:

$$c_2 = \frac{1}{\log(t_a/t_{\text{ref}})} = \frac{1}{\log(10^{9.54}/1)} = 0.105 \tag{26}$$

Substituting Eq.26 into Eq.A4, coefficient c_1 (σ) and c_1 (ε_p) are developed respectively:

$$c_1(\sigma, T) = 4.73 \times 10^{-4} + 1.32 \times 10^{-6}\sigma(T) + 1.79 \times 10^{-8}\sigma^2(T) \tag{27}$$

$$c_1(\varepsilon_p, T) = 4.73 \times 10^{-4} + 1.32 \times 10^{-6}K(T)\,\varepsilon_p^{n(T)} + 1.79 \times 10^{-8}K^2(T)\,\varepsilon_p^{2n(T)} \tag{28}$$

The fatigue coefficients C_0 and β_0 of the stainless steel 316 can be extracted from fatigue test at an arbitrary temperature at the reference cycle time. Selecting the data point (T = 873 K, t_{ref}), at which ε_p (T=873K, t_{ref}, N=1) = 2.1705, C_o is extracted through using Eq.A6, which is 2.95, and β_0 is given as 0.663. However, a big error ($\sum(N_{f-\text{exp}} - N_{f-\text{equ}})^2 = 49.85$) is given through comparing the fatigue life obtained from experiments with the result obtained from unified model. Therefore, the C_0 is resolved as 0.959 through minimizing the error (0.312).

4.3.2 Validations

Using the fatigue and the creep coefficients evaluated in Section 4.3.1, namely, C_0 = 0.959, β_0 = 0.663, c_2 = 0.105, and c_1 (ε_p,T) as described by Eq.28, the generated raw fatigue data (ε_p-N) obtained from [25] (T = 723 K, 873 K and 973 K) are transformed to the reference condition ($\varepsilon_{p,\text{ref}}$-$N$) through Eq.16. The transformed data are plotted in Figure 3.

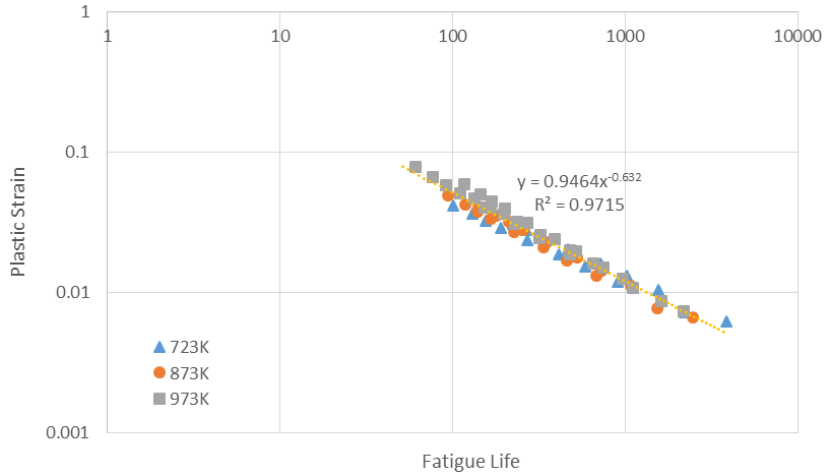

Figure 3 Transformed $\varepsilon_{p,\text{ref}}$-$N$ data of SS316 using Eq.14 with creep function c (T, t, ε_p).

Significantly, these data are collected into a power-law curve of $\varepsilon_{p,\mathrm{ref}} = 0.9464N^{-0.632}$ with the quality of fit as R^2 = 0.9715. This good transformation verifies the unified equation, $\varepsilon_p = C_0 c(T, t, \varepsilon_p) N^{-\beta_0}$, the form of creep function c (T, t, ε_p), and the methods of extracting the fatigue and the creep coefficients. The error between fatigue life from experiments and creep-fatigue equation is 0.312.

4.3.3 Application

This shows that the mathematical representation provided by the strain-form unified creep-fatigue equation accommodates the data for multiple temperatures, fatigue life, and plastic strain.

$$\varepsilon_p = 0.959\left[1 - c_1(\varepsilon_p, T)(T - 670) - 0.105\log(t)\right]N^{-0.663} \tag{29}$$

with

$$\begin{aligned} c_1(\varepsilon_p, T) = {} & 4.73 \times 10^{-4} + 8.712 \times 10^{-7} \times (769.79 - 0.4875T)\, \varepsilon_p^{7.04\times10^{-2} + 1.94\times10^{-4}T - 1.22\times10^{-7}T^2} \\ & + 7.797 \times 10^{-9} \times (769.79 - 0.4875T)^2 \varepsilon_p^{0.1408 + 3.88\times10^{-4}T - 2.44\times10^{-7}T^2} \end{aligned} \tag{30}$$

This could be used to determine fatigue life for given plastic strain, temperature and cycle time. Alternatively, to determine plastic strain by numerical solution of the equation.

4.4 Evaluation of the Coefficients of the Power-Law Unified Creep-Fatigue Equation $\varepsilon_p = C_0 c(T, t) N^{-\beta_0 b(T,t)}$ for the Stainless Steel 316 and Validation

The fatigue behaviour of stainless steel 316 presents an inflection point at the temperature of 873 K [25]. Below this temperature, the fatigue life decreases with the increasing temperature, while, increases above this temperature. Given that the power-law unified creep-fatigue equation is built on the assumption of continual increasing/decreasing fatigue life with increasing temperature, the evaluation and validation of the power-law unified creep-fatigue equation are conducted at two temperature regimes (below 873 K and above 873 K).

4.4.1 Evaluation of Creep-Fatigue Coefficients and Validation below 873 K

4.4.1.1 Evaluation of Creep-Fatigue Coefficients

Based on the Eq.A7-A13 shown in Appendix A, the coefficients of c function and b function for the stainless steel 316 are established as follows.

The creep coefficient c_2 is identical as 0.105.

Substituting Eq.18 with the data points (T = 873 K, $t = t_{\mathrm{ref}}$) and (T = 873 K, t = 10 s), where ε_p (T = 873 K, $t = t_{\mathrm{ref}}$, N = 1) = 1.0296 (Eq.A8) and ε_p (T = 873 K, t = 10 s, N = 1) = 0.5987 (Eq.A9), gives $C_0 c_2$ = 0.4309. Then, C_0 is solved as 4.1038. In addition, substituting Eq.19 with these two data points, where $\beta_0 b$ (873 K, $t = t_{\mathrm{ref}}$) = 0.663 (Eq.A10) and $\beta_0 b$ (T = 873 K, t = 10 s) = 0.651(Eq.A11), gives $\beta_0 b_2$ = 0.012.

Substituting Eq.18 with the data points (T = 723 K, $t = t_{ref}$) and (T = 873 K, $t = t_{ref}$), where ε_p (T = 723 K, $t = t_{ref}$, N = 1) = 2.1705 (Eq.A12) and ε_p (T = 873 K, $t = t_{ref}$, N = 1) = 1.0296 (Eq.A8), gives c_1 = 0.001853. Then, substituting Eq.19 with these two data points, where $\beta_0 b$ (723 K, $t = t_{ref}$) = 0.634 (Eq.A13) and $\beta_0 b$ (873 K, $t = t_{ref}$) = 0.663 (Eq.A10), gives β_0 = 0.624 and b_1 = -0.00031, then b_2 is solved as 0.01924.

The error between the fatigue life from experiments and creep-fatigue equation is 52.88. As shown in the evaluation of coefficients for strain-form unified creep-fatigue equation, this poor prediction is caused by the inaccuracy of C_0. Therefore, the C_0 is resolved as 0.876 through minimizing the error (0.792).

4.4.1.2 Validations

Using the fatigue and creep coefficients found in Section 4.4.1.1, namely, C_0=0.876, β_0=0.624, c_1=0.001853, c_2=0.105, b_1=-0.0003094 and b_2=0.01924, the raw fatigue data (ε_p-N) obtained from [25] (T = 723 K and 873 K) are transformed to the reference condition ($\varepsilon_{p,ref}$-N) through Eq.20. The transformed data are plotted in Figure 4, which shows that these data can be collapsed into a power-law curve of $\varepsilon_{p,ref} = 0.5959N^{-0.556}$ with the quality of fit as R^2 = 0.9583. This transformation has verified the unified equation, $\varepsilon_p = C_0 c(T,t) N^{-\beta_0 b(T,t)}$, the form of creep function c (T, t) and stress function b (T, t), and the methods of extracting the coefficients. The error between fatigue life from experiments and unified equation is 0.792.

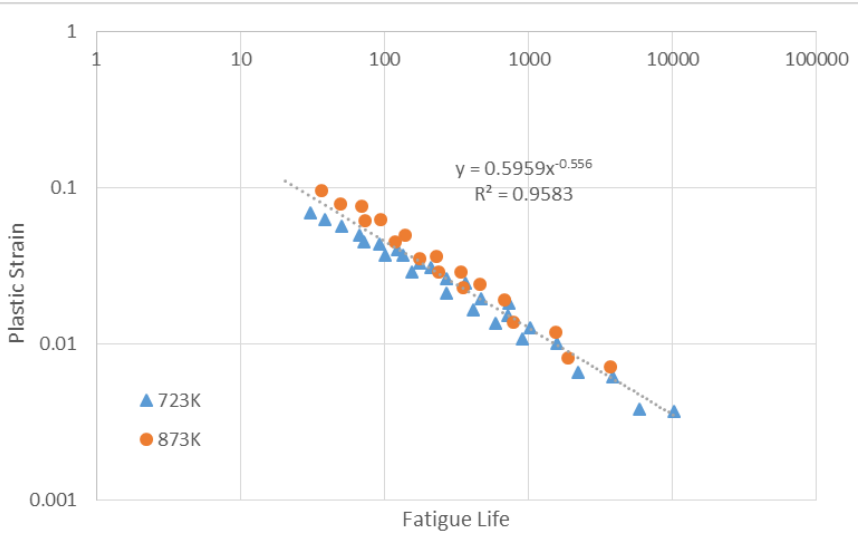

Figure 4 Transformed $\varepsilon_{p,ref}$-N data (below 873 K) of stainless steel 316 using Eq.17 with functions c (T, t) and b (T, t).

4.4.2 Evaluation of Creep-Fatigue Coefficients and Validation above 873 K

4.4.2.1 Evaluation of Creep-Fatigue Coefficients

The data points (T = 873 K, $t = t_{ref}$), (T = 873 K, t = 10 s) and (T = 973 K, $t = t_{ref}$) are selected to evaluate the coefficients. These coefficients are obtained through the same method shown in

Section 4.4.1.1: C_0= 0.879, β_0 = 0.807, c_1 = 0.00146, c_2 = 0.105, b_1 = 0.00088 and b_2 = 0.01487.

4.4.2.2 Validations

Using the fatigue and creep coefficients found in Section 4.4.2.1, the raw fatigue data (ε_p-N) obtained from [25] (T = 873 K and 973 K) are transformed to the reference condition ($\varepsilon_{p,\mathrm{ref}}$-$N$) through Eq.20. The transformed data plotted in Figure 5, which shows that these data can be collapsed into a power-law curve of $\varepsilon_{p,\mathrm{ref}} = 0.9439N^{-0.82}$ with a quality of fit of R^2 = 0.9797. This transformation has verified the unified equation, $\varepsilon_p = C_0 c(T,t) N^{-\beta_0 b(T,t)}$, the form of creep function c (T, t) and stress function b (T, t), and the methods of extracting the coefficients. The error between fatigue life from experiments and creep-fatigue equation is 0.300.

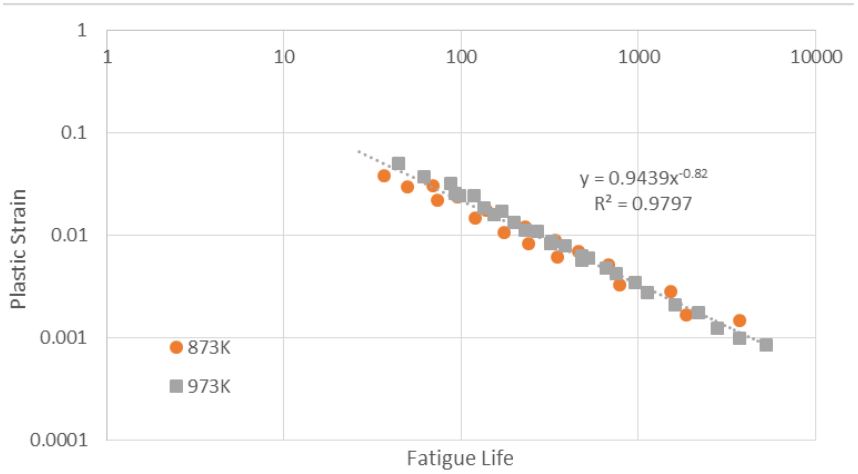

Figure 5 Transformed $\varepsilon_{p,\mathrm{ref}}$-$N$ data (above 873 K) of stainless steel 316 using Eq.17 with functions c (T, t) and b (T, t).

4.4.3 Application

The mathematical representation (Eq.31 for below 873 K and Eq.32 for above 873 K) provided by the unified creep-fatigue equation accommodates the data for multiple temperatures, fatigue life, and plastic strain. This could be used to determine fatigue life for given plastic strain, temperature and cycle time. Alternatively, to determine plastic strain by numerical solution of the equation:

$$\varepsilon_p = 0.876[2.2415 - 0.001853\mathrm{T} - 0.105\log(t)]\, N^{-0.624[0.7927+0.0003094T-0.01924\log(t)]} \quad (T < 873\ \mathrm{K}) \tag{31}$$

$$\varepsilon_p = 0.879[1.9782 - 0.00146\mathrm{T} - 0.105\log(t)]\, N^{-0.807[1.5896+0.00088T-0.01487\log(t)]} \quad (T \geq 873\ \mathrm{K}) \tag{32}$$

5. Discussion

5.1 The Moderating Factor

As shown above, C_0 in the strain-form unified creep-fatigue equation was obtained from data point (T = 723 K, t_{ref}). However, this result is different from C_0 obtained from data point (T = 873 K, t_{ref}) and (T = 973 K, t_{ref}). To improve the accuracy of C_0, these three data points are used to regress the magnitude of C_0, which is 2.517 (Eq.33).

$$\varepsilon_p(T, t_{\text{ref}}, N = 1) = C_0' = C_0[1 - c_1(C_0')(T - T_{\text{ref}})] = 2.517[1 - 0.00278(T - T_{\text{ref}})] \quad (33)$$

At data point (T = 723 K, t_{ref}), substituting C_0' into the Eq.28 cannot yield to 2.1705, and the magnitude of $c_1(2.1705)$ is bigger than 0.00278. Thus, according to the Eq.27, it appears that the big contribution of stress leads to higher magnitude of c_1 function. Therefore, mathematically, the amplitude of stress should be compressed in order to reduce the magnitude of $c_1(C_0')$ into the result of regression (0.00278). Then, a moderating factor, f, is introduced into Eq.27 to modify stress, and Eq.27 and Eq.28 can be expressed as

$$c_1(\sigma, f) = 4.73 \times 10^{-4} + 1.32 \times 10^{-6} f\sigma + 1.79 \times 10^{-8} f^2\sigma^2 \quad (34)$$

$$c_1(\varepsilon_p, T, f) = 4.73 \times 10^{-4} + 1.32 \times 10^{-6} fK(T)\, \varepsilon_p^{n(T)} + 1.79 \times 10^{-8} f^2 K(T)\, \varepsilon_p^{2n(T)} \quad (35)$$

This moderating factor is solved as 0.69, and C_0 is given as 0.846 through minimizing the error (0.276).

Using the fatigue and the creep coefficients, namely, C_0 = 0.846, β_0 = 0.663, c_2 = 0.105, c_1 (ε_p,T, f) as described by Eq.35 and f = 0.69, the generated raw fatigue data (ε_p-N) obtained from [25] (T = 723 K, 873 K and 973 K) are transformed to the reference condition ($\varepsilon_{p,\text{ref}}$-$N$) through Eq.16. The transformed data are plotted in Figure 6.

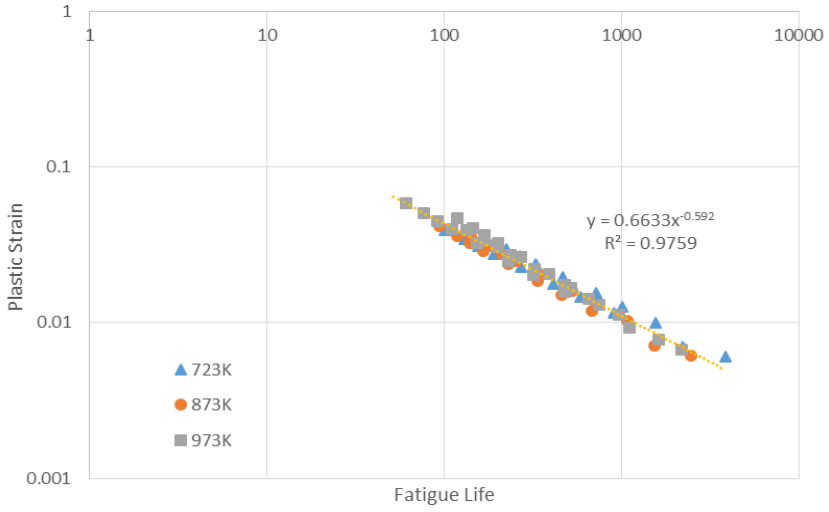

Figure 6 Transformed $\varepsilon_{p,\text{ref}}$-$N$ data of stainless steel 316 using Eq.14 with creep function c (T, t, ε_p) and moderating factor.

Figure 6 illustrates how the transformed data are collected into a power-law curve of $\varepsilon_{p,\mathrm{ref}} = 0.6633N^{-0.592}$ with the quality of fit R^2 = 0.9759. The error between fatigue life from experiments and creep-fatigue equation is 0.276. Comparing this result with the transformation in Section 4.3.2 shows that the introduction of moderating factor can provide a better description of creep effect through c_1 function and prediction of creep-fatigue behaviour.

The research conducted by Gary shows that the stress vs. creep rupture time curves under cyclic loading lie above the curves under constant loading [32]. This means that cyclic stress is higher than constant stress at the same rupture time. Because c_1 function is based on the time-temperature relation under constant stress (Manson–Haferd parameter), the creep effect is enlarged when the cyclic stress is imposed. Therefore, it is reasonable to introduce a moderating factor to compress the cyclic stress to an equivalent constant stress.

5.2 The Heat Treatment

Heat treatment can change fatigue behaviour through hardening or softening. However, stainless steel 316 cannot be hardened by heat treatment, and this is proved by [33], where fatigue life changes slightly between aged condition and annealed condition [33]. This makes the unified creep-fatigue equation more universal for stainless steel 316 under different heat treatments. For example, the creep-fatigue data of aged stainless steel obtained from [33] (T = 839 K and 922 K) and quenched stainless steel 316 obtained from [25] (T = 723 K, 873 K and 973 K) can be collected into one power-law curve $\varepsilon_{p,\mathrm{ref}} = 0.6533N^{-0.588}$ with a quality of fit of R^2 = 0.9827 (Figure 7).

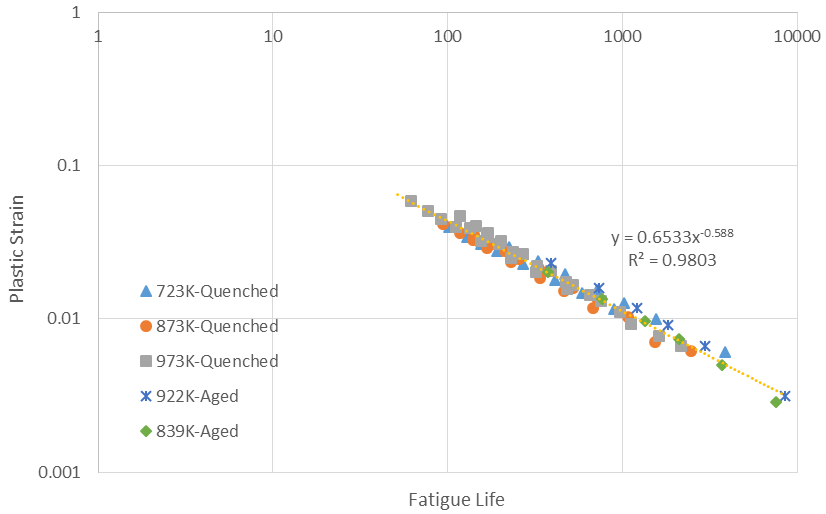

Figure 7 Transformed $\varepsilon_{p,\mathrm{ref}}$-$N$ data of quenched and aged stainless steel 316 using Eq.14 with creep function c (T, t, ε_p).

Although the unified creep-fatigue equation shows a good universality for stainless steel 316 under different heat treatments, the potential limitation for this equation still cannot be ignored. For example, this strong influence of heat treatment on fatigue life is shown on Inconel 718, and the aged condition can provide better fatigue strength than annealed condition [33]. Therefore, if the unified creep-fatigue equation is imposed on Inconel 718, the coefficients

obtained at one specified heat treatment condition cannot be used to predict the fatigue life of this material under other heat treatments. This is an opportunity for future development of the formulation.

5.3 Reliability

The proposed new equations were validated against existing experimental data in the literature. The equations provide an excellent fit to data (r^2 = 0.97 or better). This demonstrates that the equations provide the desired level of fidelity to the original experimental data.

The validation only can show these selected data follow the unified creep-fatigue equation, but not all data. Hence it is important to consider the degree of reliability. In this section, the strain-form unified creep-fatigue equation was used to explore the reliability.

The fatigue life, temperature and strain rate are defined as random variables, and then 100 random creep-fatigue data points (*plastic strain* vs. *fatigue life*) were derived from [25] and the Coffin–Manson equation. These random data then were transformed into a reference condition through Eq.16. The transformation of 10 sets of random data (1000 data points) shows that these creep-fatigue data can collapse into almost one straight line at log-log scale (two of them are shown in Figure 8) with the quality of fit R^2 = 0.975–0.985. This transformation based on random data has further verified the unified equation, $\varepsilon_p = C_0 c(T, t, \varepsilon_p) N^{-\beta_0}$ and the form of creep function c (T, t, ε_p).

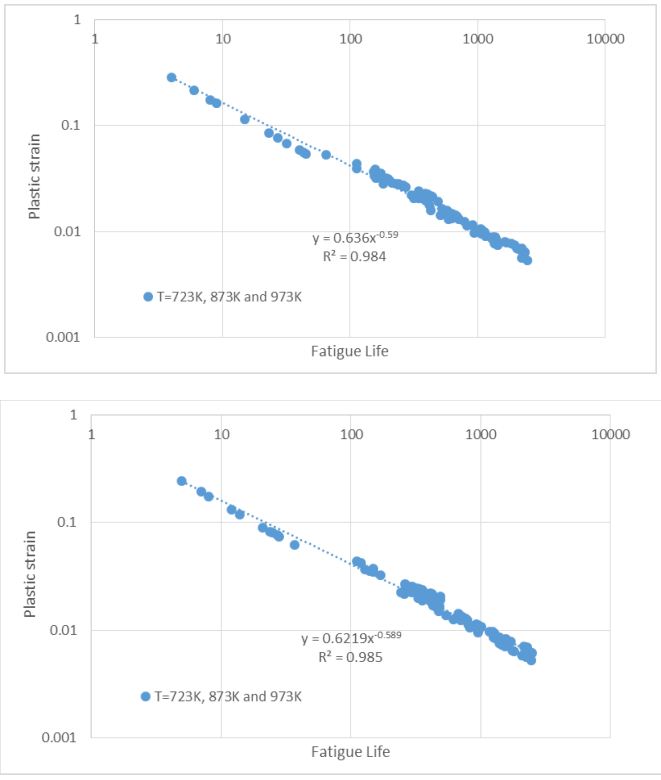

Figure 8 Transformed $\varepsilon_{p,\mathrm{ref}}$-$N$ data of SS316 using Eq.14 with creep function c (T, t, ε_p) and random variables. Data shown are for two of ten sets, as evidence of a consistent transformation process.

5.4 The Initial Proposal of Creep-Fatigue-Equation-Based Temperature Modified Coffin–Manson Equation

Frequency modified Coffin–Manson equation can be expressed as Eq.36 [34]:

$$\Delta\varepsilon_p = C_0\left[N_f \nu^{k-1}\right]^m \tag{36}$$

where ν is the frequency, and k and m are the constant determined by experiments. Comparing this equation with the conventional Coffin–Manson equation (Eq.2), the $N_f \nu^{k-1}$ can be defined as the frequency modified fatigue life. Similarly, comparing the unified creep-fatigue equations (Eq.14 and Eq.17) with the conventional Coffin–Manson equation (Eq.2), $\left[c\left(T,t,\varepsilon_p\right)\right]^{-1/\beta_0} N$ and $[c(T,t)]^{-1/\beta_0 b(T,t)} N$ can be defined as the temperature-frequency modified fatigue life (creep-fatigue life). If we get rid of frequency effect from the unified creep-fatigue equations, the creep-fatigue life ($N_{f-\text{creep+fatigue}}$) can be transformed to temperature modified fatigue life ($N_{f-\text{temp}}$) through Eq.37, then the temperature modified Coffin–Manson equation could be developed through this transformation.

$$N_{f-\text{temp}} = N_{f-\text{creep+fatigue}} \cdot \nu^{k-1} \tag{37}$$

Because c_1 function in the strain-form unified creep-fatigue equation related to time-temperature relation, it is difficult to remove the frequency effect from this function. Therefore, the power-law unified creep-fatigue equation is used to develop the temperature modified Coffin-Manson equation (Eq.38) through removing the frequency-related items and transforming creep-fatigue life to temperature modified fatigue life.

$$\varepsilon_p = C_0[1 - c_1(T - T_{\text{ref}})]N_{f-\text{temp}}{}^{-\beta_0[1-b_1(T-T_{\text{ref}})]} \tag{39}$$

Based on the creep-fatigue data [25], the coefficients of this equation are evaluated (shown in Table 1). Then, using the coefficient shown in Table 1, the generated raw fatigue data (ε_p-N) obtained from [25] (T = 723 K, 873 K and 973 K) are transformed to the reference condition ($\varepsilon_{p,\text{ref}}$-$N$) through Eq.16. The transformed data at "723 K and 873 K", and "873 K and 973 K" are plotted in Figures 9 and 10 respectively.

Table 1 The coefficients of Eq.38.

Temperature Regimes	C_0	c_1	β_0	b_1	k
723 K−873 K	1.997	0.002955	0.62375	−0.000309	723 K: 0.728 873 K: 0.758
873 K−973 K	2.452	0.002668	0.80713	0.00088	873 K: 0.758 973 K: 0.873

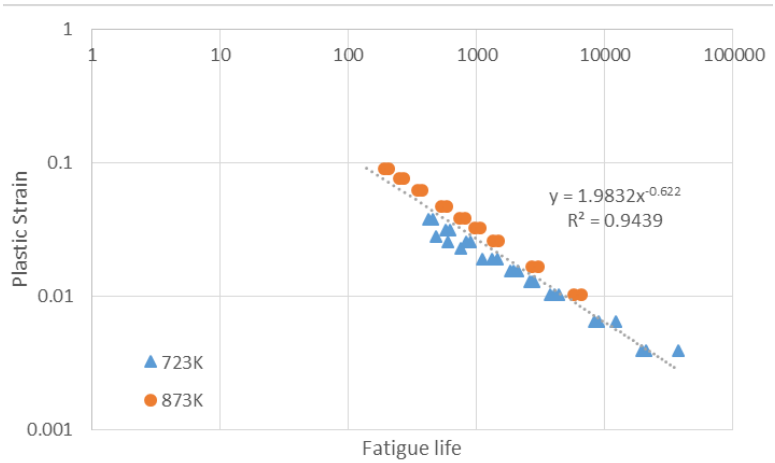

Figure 9 Transformed $\varepsilon_{p,\mathrm{ref}}$-$N$ data (below 873 K) of stainless steel 316 using Eq.17.

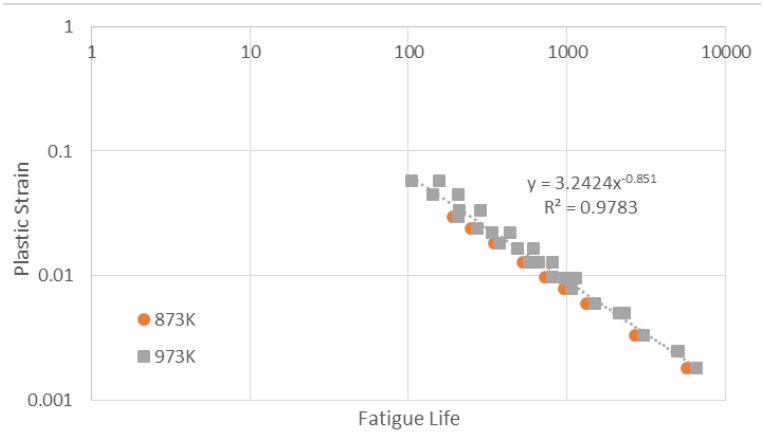

Figure 10 Transformed $\varepsilon_{p,\mathrm{ref}}$-$N$ data (above 873 K) of stainless steel 316 using Eq.17.

Figures 9 and 10 show that the creep-fatigue data below 873 K and above 873 K can be collapsed into power-law curves of $\varepsilon_{p,\mathrm{ref}} = 1.9832N^{-0.622}$ with the quality of fit as R^2 = 0.9439 and $\varepsilon_{p,\mathrm{ref}} = 3.2424N^{-0.851}$ with the quality of fit as R^2 = 0.9783 respectively. The errors between fatigue life from experiments and creep-fatigue equation for these two temperature regimes are 0.814 and 0.294. This transformation has verified the creep-fatigue-equation-based temperature modified Coffin–Manson equation.

5.5 Application and Future Research

The results have provided a derivation of the equations and the methods for determining the coefficients. While this may appear mathematically complex, it is a necessary feature of the work as it provides reproducibility and assists other researchers in applying and adapting the work.

The implications for practitioners, e.g., nuclear industry, are given in Sections 4.3.3 and 4.4.3, using the two forms of the unified creep-fatigue equation. The equations are provided for stainless steel 316 and encapsulate the data for multiple temperatures, fatigue life, and plastic strain. In application, the equation might be used to determine fatigue life for given conditions

(plastic strain, temperature and cycle time), or to determine acceptable plastic strain for a given life and other conditions.

6. Conclusions

The following major results were obtained:

(1) The strain-form unified creep-fatigue equation: $\varepsilon_p = C_0 c\left(T, t, \varepsilon_p\right) N^{-\beta_0}$ and power-law form: $\varepsilon_p = C_0 c(T, t) N^{-\beta_0 b(T,t)}$ have been verified on stainless steel 316, and the methods of extracting the fatigue and the creep coefficients by limited creep-fatigue tests and creep rupture tests have been presented. The equations are efficient as they represent a whole range of conditions, in contrast to some other formulations which have to be calibrated separately for each set of environmental conditions.

(2) A moderating factor is introduced into the unified creep-fatigue equation to compress the amplitude of cyclic stress, and leads to a more reasonable result than the situation without moderating factor.

(3) The reliability of this unified creep-fatigue equation is verified through random variables.

(4) The creep-fatigue equation-based, temperature-modified Coffin-Manson equation is proposed, and this equation is validated through transforming raw data to the reference condition.

(5) However, there is a potential limitation. For the materials whose fatigue behaviour is strongly influenced by heat treatment, the coefficients obtained from one specific material condition cannot be used to predict the fatigue life of the same material at material conditions. This is identified as an area for future development of the theory.

Author Contributions: The work was conducted by DL and supervised by DP and EW. The initial form of the unified creep-fatigue equation was proposed by DL and EW, and the method of extracting the coefficients was then developed by DL and EW. The discussion on the moderating factor, heat treatment and reliability was developed by DL and DP. The review of creep-fatigue models in the nuclear industry and the evaluation and validation of the unified creep-fatigue equation for stainless steel 316 were conducted by DL. The initial form of the creep-fatigue equation–based, temperature-modified Coffin–Manson equation was proposed by DL.

Conflicts of Interest: The authors declare no conflict of interest. The research was conducted without personal financial benefit from any funding body, and no such body influenced the execution of the work.

Appendix A

A.1 The coefficients in the strain-form unified creep-fatigue equation

At pure creep-rupture condition, plastic strain $\varepsilon_p = 0$, then *c* function can be presented as:

$$c(T,t,\sigma) = 1 - c_1(\sigma)(T_R - T_{\mathrm{ref}}) - c_2(\sigma)\log(t_R/t_{\mathrm{ref}}) = 0 \tag{A1}$$

where T_R is rupture temperature and t_R is rupture time. According to Manson-Haferd Parameter (Eq.8), the creep occurs at the point of convergence. At this point, $T_R = T_a = T_{\mathrm{ref}}$ and $t_R = t_a$, then Eq.A1 can be deduced to Eq.A2:

$$c_2 = \frac{1}{\log(t_a/t_{\mathrm{ref}})} \tag{A2}$$

This equation shows that c_2 is independent of stress/strain, and it can be obtained through creep rupture test.

In addition, creep rupture also occurs at the reference cyclic time, where $t = t_{\mathrm{ref}}$, then Eq.A1 can be deduced to Eq.A3:

$$c_1(\sigma) = \frac{1}{T_R - T_{\mathrm{ref}}} \tag{A3}$$

The Manson–Haferd Parameter shows the gradients of *T* vs. log*t* curves at different stresses, and keeps constant at one specific stress. The Manson–Haferd Parameter can be regarded as a function of stress $P_{\mathrm{MH}}(\sigma)$. When the stress is converted into plastic strain through Ramberg–Osgood relation, the *T* vs. log*t* curves at different strains become nonlinear, and the Manson–Haferd Parameter is presented as the gradient of tangents at one specific strain and temperature. In this case, the Manson–Haferd Parameter can be shown as a function of strain and temperature $P_{\mathrm{MH}}(\varepsilon_p, T)$.

Invoking the Manson–Haferd Parameter (Eq.8) and Eq.A2 and Eq.A3 can be reduced to Eq.A5:

$$c_1(\sigma) = -\frac{c_2}{P_{\mathrm{MH}}(\sigma)} = -\frac{c_2}{P_{\mathrm{MH}}(\varepsilon_p, T)} \tag{A4}$$

Then, the *c* function can be defined through Eq.A2 and Eq.A4:

$$c(T,t,\varepsilon_p) = 1 + \frac{T - T_{\mathrm{ref}}}{P_{\mathrm{MH}}(\varepsilon_p, T)\cdot\log(t_a/t_{\mathrm{ref}})} - \frac{\log(t/t_{\mathrm{ref}})}{\log(t_a/t_{\mathrm{ref}})} \tag{A5}$$

If plastic strain is expressed as C_0' when $N = 1$ and $t = t_{\mathrm{ref}}$, Eq.14 can be presented as:

$$C_0[1 - c_1(C_0')(T - T_{\mathrm{ref}})] = \varepsilon_p(T, t_{\mathrm{ref}}, N = 1) = C_0' \tag{A6}$$

Because C_0' can be obtained from a single fatigue test performed at an arbitrary temperature and reference cyclic time, C_0 can be solved numerically. Meanwhile, β_0 also can be evaluated from this single fatigue test.

A.2 The coefficients in the power-law unified creep-fatigue equation

In Eq.18, the coefficient c_2 can be evaluated through Eq.A2.

When $N = 1$, Eq.17 can be represented as:

$$\varepsilon_p(T, t, N = 1) = C_0[1 - c_1(T - T_{\text{ref}}) - c_2 \log(t/t_{\text{ref}})] \quad \text{(A7)}$$

The coefficient C_0 can be extracted through performing fatigue tests at one arbitrary temperature (T_1) at t_{ref} and one arbitrary cyclic time (t_1). Substituting these fatigue data into Eq.A7 gives Eq.A8 and Eq.A9, then C_0 can be solved.

$$\varepsilon_p(T, t_{\text{ref}}, N = 1) = C_0[1 - c_1(T_1 - T_{\text{ref}})] \quad \text{(A8)}$$

$$\varepsilon_p(T, t_1, N = 1) = C_0[1 - c_1(T - T_{\text{ref}}) - c_2 \log(t_1/t_{\text{ref}})] \quad \text{(A9)}$$

The same fatigue experiments performed for the magnitude of C_0 can be used to extract $\beta_0 b_2$ through Eq.A10 and Eq.A11

$$\beta_0 b(T_1, t_{\text{ref}}) = \beta_0[1 - b_1(T_1 - T_{\text{ref}})] \quad \text{(A10)}$$

$$\beta_0 b(T_1,\ t_1) = \beta_0[1 - b_1(T_1 - T_{\text{ref}}) - b_2 \log(\ t_1/t_{\text{ref}})] \quad \text{(A11)}$$

Next, another set of fatigue testes at another arbitrary temperature (T_2) at t_{ref} is performed to obtain coefficient c_1. When $N = 1$ and $t = t_{\text{ref}}$, Eq.17 can be represented as:

$$\varepsilon_p(T, t_{\text{ref}}, N = 1) = C_0[1 - c_1(T_2 - T_{\text{ref}})] \quad \text{(A12)}$$

The combination of Eq.A8 and Eq.A12 gives $-C_0 c_1$, then c_1 can be solved.

In addition, when $T = T_2$ and $t = t_{\text{ref}}$, the exponent of the power-law unified creep-fatigue equation can be represented as:

$$\beta_0 b(T, t) = \beta_0[1 - b_1(T_2 - T_{\text{ref}})] \quad \text{(A13)}$$

The combination of Eq.A10 and Eq.A13 gives β_0 and b_1. Then β_0 can be used to solve b_2.

References

1. Holmström, S.; Pohja, R.; Nurmela, A.; Moilanen, P.; Auerkari, P. Creep and creep-fatigue behaviour of 316 stainless steel. Procedia Eng. **2013**, 55, 160–164.
2. Basquin, O. The Exponential Law of Endurance Tests. Am. Soc. Test. Mater. Proc. **1910**, 10, 625–630.
3. Coffin, L.F., Jr. A Study of the Effects of Cyclic Thermal Stresses on a Ductile Metal; Knolls Atomic Power Lab.: Niskayuna, NY, USA, 1953.
4. Manson, S.S. Behavior of Materials under Conditions of Thermal Stress; National Advisory Committee for Aeronautics: Cleveland, OH, USA, 1954.
5. Feltner, C.E.; Morrow, J.D. Microplastic strain hysteresis energy as a criterion for fatigue fracture. J. Basic Eng. **1961**, 83, 15–22.

6. Morrow, J. Cyclic plastic strain energy and fatigue of metals. In Internal Friction, Damping, and Cyclic Plasticity; ASTM International: West Conshohocken, PA, USA, 1965.
7. Dowling, N.E. Mechanical Behavior of Materials: Engineering Methods for Deformation, Fracture, and Fatigue; Prentice Hall: Upper Saddle River, NJ, USA, 1993.
8. Ramberg, W.; Osgood, W.R. Description of Stress-Strain Curves by Three Parameters; National Advisory Committee for Aeronautics: Cleveland, OH, USA, 1943.
9. Palmgren, A. Die lebensdauer von kugellagern . ZVDI **1924**, 68, 339–341.
10. Miner, M.A. Cumulative damage in fatigue. J. Appl. Mech. **1945**, 12, 159–164.
11. Chopra, O.K. Environmental Effects on Fatigue Crack Initiation in Piping and Pressure Vessel Steels; Argonne National Lab.: Argonne, IL, USA, 2000.
12. Gosselin, S.R.; Deardorff, A.F.; Peltola, D.W. Fatigue assessments in operating nuclear power plants. In Changing Priorities of Codes and Standards: Failure, Fatigue, and Creep. Pvp-vol. 286; American Society of Mechanical Engineers: New York, USA, 1994.
13. Rodabaugh, E. Comparisons of Asme-Code Fatigue-Evaluation Methods for Nuclear Class 1 Piping with Class 2 or 3 Piping; Rodabaugh (EC) and Associates: Hilliard, OH, USA, 1983.
14. Rudolph, J.; Heinz, B.; Jouan, B.; Bergholz, S. Areva Fatigue Concept-a Three Stage Approach to the Fatigue Assessment of Power Plant Components. INTECH Open Access Publisher: Rijeka, Croatia, 2012.
15. Zhu, Y.; Li, X.; Wang, C.; Gao, R. A new creep-fatigue life model of lead-free solder joint. Microelectron. Reliab. **2015**, 55, 1097–1100.
16. Richart, F.; Newmark, N. An Hypothesis for the Determination of Cumulative Damage in Fatigue; Selected Papers By Nathan M. Newmark@ sCivil Engineering Classics; ASCE: Reston, VA, USA, 1948; pp. 279–312.
17. Manson, S. Interfaces between fatigue, creep, and fracture. Int. J. Fract. Mech. **1966**, 2, 327–327.
18. Gosselin, S. Fatigue Crack Flaw Tolerance in Nuclear Power Plant Piping: A Basis for Improvements to ASME Code Section XI Appendix L; US Nuclear Regulatory Commission, Office of Nuclear Regulatory Research, Division of Fuel, Engineering and Radiological Research: Washington, DC, USA, 2007.
19. Rudolph, J.; Bergholz, S.; Willuweit, A.; Vormwald, M.; Bauerbach, K. Methods of detailed thermal fatigue evaluation of nuclear power plant components. Mater. Werkst. **2011**, 42, 1082–1092.
20. Ainsworth, R.; Ruggles, M.; Takahashi, Y. Flaw assessment procedure for high-temperature reactor components. J. Press. Vessel Technol. **1992**, 114, 166–170.
21. Paris, P.; Erdogan, F. A critical analysis of crack propagation laws. J. Basic Eng. **1963**, 85, 528–533.
22. Wong, E.; Mai, Y.-W. A unified equation for creep-fatigue. Int. J. Fatigue **2014**, 68, 186–194.
23. Shi, X.; Pang, H.; Zhou, W.; Wang, Z. Low cycle fatigue analysis of temperature and frequency effects in eutectic solder alloy. Int. J. Fatigue **2000**, 22, 217–228.
24. Wong, E.H.; Liu, D. The unified equations for creep-fatigue—Deriving creep function from creep-rupture parameters. International Journal of Fatigue , submitted for publication, 2016.
25. Kanazawa, K.; Yoshida, S. Effect of Temperature and Strain Rate on the High Temperature Low-Cycle Fatigue Behavior of Austenitic Stainless Steels. In Proceedings of the International Conference on Creep and Fatigue in Elevated Temperature Applications, Philadelphia, PA, USA, 23–27 September 1973; Institution of Mechanical Engineers: London, UK, 1975; Volume 1.
26. Nickel Development Institute. High Temperature Characteristics of Stainless Steels; Nickel Development Institute: Toronto, ON, Canada, Year.
27. Orr, R.L.; Sherby, O.D.; Dorn, J.E. Correlations of Rupture Data for Metals at Elevated Temperatures; DTIC Document: Fort Belvoir, VA, USA, 1953.

28. Larson, F.R.; Miller, J. A Time-Temperature Relationship for Rupture and Creep Stresses; Trans ASME, New York, USA, 1952; 74: 765-771.
29. Manson, S.; Haferd, A. A Linear Time-Temperature Relation for Extrapolation of Creep and Stress Rupture Data; NaCA TN 2890; Lewis Flight Propulsion Laboratory Cleveland: Cleveland, OH, USA, 1953.
30. Penny, R.K.; Mariott, D.L. Design for Creep; Chapman & Hall : London, UK, 1995.
31. Engineering Virtual Organization for CyberDesign. 316 Stainless Steel. Available online: https://icme.hpc.msstate.edu/mediawiki/index.php/316_Stainless_Steel (accessed on 6 September 2016).
32. Halford, G. Cyclic creep-rupture behavior of three high-temperature alloys. Metall. Trans. **1972**, 3, 2247–2256.
33. Jaske, C.; Mindlin, H.; Perrin, J. Development of Elevated Temperature Fatigue Design Information for Type 316 Stainless Steel; Battelle Columbus Labs.: Columbus, OH, USA, 1975.
34. Coffin, L., Jr. Predictive Parameters and Their Application to High Temperature, Low Cycle Fatigue; ICF2: Brighton, UK, 1969.

Paper 3: Creep-Integrated Fatigue Equation for Metals

Dan Liu [1], Dirk John Pons [1,*] and Ee-hua Wong [2]

1. Department of Mechanical Engineering, University of Canterbury, Christchurch 8140, New Zealand; dan.liu@pg.canterbury.ac.nz

2. Energy Research Institute, Nanyang Technological University, 637553, Singapore; ehwong@ntu.edu.sg

*****Correspondence: dirk.pons@canterbury.ac.nz

Published Paper (Pre-prints for the publication)

Please cite this paper as:

Liu, D., D.J. Pons, and E.H. Wong, Creep-integrated fatigue equation for metals. International Journal of Fatigue, 2017. 98: p. 167-175. DOI: http://dx.doi.org/10.1016/j.ijfatigue.2016.11.030.

Abstract

Background - The existing creep-fatigue models are valid over limited ranges of temperatures and frequencies. **Need** - There is a need to develop a creep-fatigue equation that covers the full range of phenomena from pure fatigue to pure creep rupture, and all the intermediate failures. **Method** - By integrating the Manson-Haferd parameter into the Coffin-Manson equation, the creep-integrated fatigue equation is developed and further is validated on three metal alloys: 63Sn37Pb solder, Sn3.5Ag solder and stainless steel 316. **Results** - This new formulation collapses the dispersed strain-life data of the alloys obtained at diverse temperatures and cycle times into a cohesive strain-life formulaic representation. Supported by this result, the method of establishing the material parameters for the creep-integrated fatigue equation is demonstrated, and the resulting equation is capable of modelling the full range of creep-fatigue interaction from pure fatigue to pure creep rupture.

Keywords: creep-fatigue, creep rupture, linear time-temperature parameter, strain-life.

1. Introduction

The challenge in creep-fatigue modelling is in compounding the damages due to creep and fatigue. The common practice is to assume that creep damage and fatigue damage act independently such that creep-fatigue damage is the linear sum of the two damages [1]. However, this simple and convenient assumption has been found to be invalid. Creep and fatigue damages in metals are known to interact, and then lead to aggregated damage [2]. The construction of a creep-fatigue interaction relation for a metal requires the metal to undergo fatigue experiments at multiple temperatures and multiple cycle times [3]. The effort required for such characterisation is prohibitively demanding and this has discouraged the exploration of alternative alloys. One particular example is the selection of lead-free solder in electronic applications; it is impractical to perform creep-fatigue experiments for the vast possibilities of lead-free solder alloys. Moreover, the characterised creep-fatigue interaction relation is frequently valid over only limited ranges of temperatures and cycle times.

This paper presents a creep-fatigue interaction model that can be constructed from a creep rupture test [4] together with a very limited creep-fatigue test. The experimental data of creep rupture and fatigue are readily available in the literature for many alloys and these can be used to establish the creep-fatigue interaction model. By integrating creep-rupture into the fatigue equation, this model is capable of modelling creep-fatigue interaction between pure fatigue and pure creep.

The paper is organised into five sections. The basic models of pure fatigue and pure creep are introduced in this section. This is followed by a brief review of creep-fatigue models in Section 2. Section 3 details the derivations of the creep-integration fatigue equation. The equation is demonstrated on three metal alloys in Section 4. This is followed by a brief discussion in Section 5 and conclusion in Section 6.

In the absence of mean stress, the fatigue life of a material which is experiencing pure fatigue may be expressed either in the form of stress-life [5,6],

$$\sigma_{ref} = C_\sigma N^{-\beta_\sigma} \tag{1}$$

or strain-life [7,8],

$$\varepsilon_{p,ref} = C_0 N^{-\beta_0} \tag{2}$$

or energy-life [9],

$$w_{p,ref} = C_w N^{-\beta_w} \tag{3}$$

where σ_{ref} and $\varepsilon_{p,ref}$ are the alternating amplitudes of stress and plastic strain, respectively; $w_{p,ref}$ is the hysteretic plastic work density enclosed by a stable cyclic stress-strain locus; σ_{ref}, $\varepsilon_{p,ref}$,

and $w_{p,ref}$ are effectively the fatigue capacities for N cycles of fatigue life; C_σ, C_o, and C_w are the fatigue capacities for one cycle of fatigue life; and β_σ, β_o, and β_w are fatigue exponents, which describe the sensitivity of the fatigue capacities to increasing fatigue life. The subscript "*ref*" emphasizes the condition of pure fatigue in the absence of any other damage driving forces such as creep.

Rearranging Eq.2 into

$$d_f = \frac{1}{N} = \left(\frac{\varepsilon_{p,ref}}{C_0}\right)^{1/\beta_0} \tag{4}$$

gives a linearized estimate of the damage induced by a single fatigue cycle. In the case of fatigue under non-constant amplitudes of cycling and assuming that the linear accumulation of damage is independent of the sequence of loadings, the cumulative damage is given by

$$D_f = \sum_i n_i d_{f(i)} = \sum_i \frac{n_i}{N_i} \tag{5}$$

where n_i represents the number of cycles at cyclic strain amplitude, $\varepsilon_{p,ref(i)}$. This was first proposed by Palmgren [10] and subsequently by Miner [11], and is frequently referred to as the Palmgren-Miner cumulative damage rule.

Robinson [12] postulated that materials have a limiting capacity of creep life before rupture, t_R, which is a function of the applied stress and temperature; that is, $t_R(\sigma, T)$. Assuming further that the cumulative damage is independent of the sequence of the applied stress, Robinson suggested the linear damage accumulation rule:

$$D_c = \sum_i \frac{t_i}{t_{R(i)}} \tag{6}$$

where t_i represents the duration of creep under the applied stress σ_i at temperature T_i. Eq. **Error! eference source not found.** is known as the time fraction rule.

Along a similar line of thought as Robinson, Goldhoff [13] and Oding [14] have separately postulated that materials have a limiting creep strain capacity before rupture, ε_R, which is a function of the applied stress (or strain rate) and temperature; that is, $\varepsilon_R(\sigma, T)$; and assuming further that the cumulative damage is independent of the sequence of the applied stress, they proposed the linear accumulation rule:

$$D_c = \sum_i \frac{\varepsilon_{c(i)}}{\varepsilon_{R(i)}} \tag{7}$$

where $\varepsilon_{c(i)}$ represents the magnitude of creep strain at the applied stress σ_i at temperature T_i. This is referred to as the creep ductility exhaustion rule.

There have been many variances in the proposed form of the function $t_R(\sigma, T)$. The most well-known are the linear time-temperature parameters. Among these, the three most common parameters are the Larson-Miller parameter [15],

$$P_{LM}(\sigma) = T(A + \log t_R) \tag{8}$$

the Manson-Haferd parameter [16],

$$P_{MH}(\sigma) = \frac{T - T_{ref}}{\log(t_R/t_a)} \tag{9}$$

and the Sherby-Dorn parameter [17],

$$P_D(\sigma) = t_R e^{-Q/(k_b T)} \tag{10}$$

wherein A is a constant, T_{ref} is the reference temperature below which the mechanism of creep is considered to be inactive, t_a is the duration above which creep rupture would occur independent of temperature, Q is the activation energy, and k_b is the Boltzmann constant. Among these three, the Manson-Haferd parameter, P_{MH}, has been found to give the best description for engineering metal alloys [18].

2. A brief review of creep-fatigue models

In the presence of both fatigue and creep in a single cycle, materials simultantaneously experience damages due to creep and fatigue. A number of models have been proposed to compound these two damages. The major models are reviewed.

2.1 Linear and bi-linear damage summation

The damages caused by creep and fatigue in a creep-fatigue cycle are assumed to obey the respective damage relations of pure creep and pure fatigue. In the case of creep-fatigue under steady cycles, the fatigue damage per cycle, d_f, is given by Eq.4 while the creep damage per cycle is given by

$$d_c = \int_0^{t_c} \frac{\dot{\varepsilon}_c(t,T)dt}{\varepsilon_R(\dot{\varepsilon}_c,T)} \quad \text{or} \quad d_c = \int_0^{t_c} \frac{dt}{t_R(\sigma,T)} \tag{11}$$

where t_c is the cycle time. Assuming the damages due to creep and fatigue are linearly additive in nature, the creep-fatigue damage per cycle is accumulated:

$$d = d_f + d_c \tag{12}$$

In the case of creep-fatigue under non-steady cycles, d_f and d_c in Eq.12 can be substituted with the Palmgren-Miller cumulative damage rule, Eq.5, and either the time-fraction rule, Eq.6, or the creep strain exhaustion rule, Eq.7. Creep-fatigue failure occurs when

$$D_f + D_c = 1 \tag{13}$$

Eq.13 is known as the linear damage summation (LDS) rule [1]. The validity of the LDS rule requires that creep and fatigue induce microstructually identical damages. In actuality, creep tends to induce intergranular damage while fatigue tends to induce transgranular damage [19].

The invalid linear accumulation of datigue damage and creep damage is also proved by Masaya et al. [20].

In practice, failures have frequently been observed to occur at $D_f + D_c < 1$ [20,21]. It is suggested that the interaction of creep damage and fatigue damage has induced additional damage, which shall be referred to as creep-fatigue interaction (CFI) damage, D_{cf}, such that failure occurs when

$$D_f + D_c + D_{cf} = 1 \tag{14}$$

There is no known mathematical model for D_{cf}. Creep-fatigue interaction of a metal is frequently described using a bi-linear D_f-D_c diagram [22,23] that could only be established through laborious experimental characterisation.

2.2 Crack growth law

The crack growth law states that the fatigue life is the number of loading cycles required to achieve the final crack size, and this process is divided into two stages: initiation and propagation. The total crack size can be presented as the linear addition of initial crack size and propagative crack size. Normally, the initial crack is identified as the real crack size in the structures before loading, and the propagative crack (Eq.15) can be obtained through Paris's model [24]:

$$\frac{da}{dN} = C\left(\Delta J_{eff}\right)^l \tag{15}$$

where $\frac{da}{dN}$ is the total crack growth per cycle, ΔJ_{eff} is the effective range of J-integral, and C is a material constant obtained from experiments. When creep is active, the total damage is calculated through the sum of fatigue and creep crack growth (Eq.16) [25]:

$$\begin{gathered} \frac{da}{dN} = \left(\frac{da}{dN}\right)_f + \left(\frac{da}{dN}\right)_c \\ \left(\frac{da}{dN}\right)_f = C\left(\Delta J_{eff}\right)^l \quad \text{and} \quad \left(\frac{da}{dN}\right)_c = \int_0^{t_h} AC^{*q} dt \end{gathered} \tag{16}$$

where $\left(\frac{da}{dN}\right)_f$ is the crack growth per cycle due to cyclic load changes, $\left(\frac{da}{dN}\right)_c$ is the crack growth per cycle due to hold time, t_h is the hold time, C^* is the time-dependent fracture parameter, and l, A and q are material constants obtained from experiments.

The crack growth law provides a good physical description of damage. However, the quantitative summation between the cracks caused by fatigue and creep does not consider the interaction effect [26,27]. For this reason, the total damage should be presented as the sum of the damage caused by fatigue, creep and the interaction effect between them.

2.3 Strain range partitioning

Manson et al. [28] proposed to partition the inelastic strain in a cyclic stress-strain hysteresis loop into three components ε_{pp}, ε_{cc}, ε_{cp} (or ε_{pc}), where "the first letter of the subscript (*c* for creep and *p* for plastic strain) refers to the type of strain imposed in the tensile portion of the cycle, and the second letter refers to the type of strain imposed during the compressive portion of the cycle". Each component is assumed to obey the power-law relation:

$$\varepsilon_{jk}=C_{jk}N_{jk}^{-\beta_{jk}} \tag{17}$$

Assuming linear accumulation of damage independent of the sequence of loadings, the cumulative damage of an individual component is given by

$$D_{jk}=\sum_i n_i\left(\frac{\varepsilon_{jk(i)}}{C_{jk}}\right)^{1/\beta_{jk}} \tag{18}$$

Assuming the damage due to an individual component adds up linearly, failure occurs when

$$D_{pp}+D_{cc}+D_{cp}\ or\ D_{pc}=1 \tag{19}$$

This is known as the strain range partitioning (SRP) model. In practice, it is near impossible to segregate the ε_{pp}, ε_{cc}, ε_{cp} (or ε_{pc}) components in a real-life cyclic stress-strain hysteresis loop.

2.4 Creep-modified fatigue equations

It is only intuitive to attempt to incorporate creep into the basic fatigue equations. The first attempt was made by Coffin [7]. This was to be followed by a number of researchers, principally from the electronic and microelectronic communities.

Assuming that the effects of frequency are only in modifying the fatigue life, *N*, in the Coffin-Manson equation, Coffin [7] incorporated cyclic frequency, *f*, as a modifier to the strain-life equation:

$$\varepsilon_p=C\left(Nf^{k-1}\right)^{-\beta_0} \tag{20}$$

where *k* is a fitting constant. Coffin referred to Nf^{k-1} as frequency-modified fatigue life.

Solomon [29] expressed the creep-fatigue relation for the Sn40Pb solder in the form of frequency-modified fatigue-life equation:

$$\varepsilon_p=C_m(T)\left(Nf^{k-1}\right)^{-\beta_0} \tag{21}$$

in which

$$C_m(T)=1.338-2\times10^{-4}T-1\times10^{-5}T^2-2\times10^{-7}T^3 \tag{22}$$

where T is in ^oC and β_o=0.5; and the frequency exponent, *k*, is found to be dependent on frequency: k=-0.42 for $6\text{x}10^{-5}$ Hz ≤ f ≤ $3\text{x}10^{-4}$ Hz and k=-0.84 for $3\text{x}10^{-4}$ Hz ≤ f ≤ 0.3 Hz.

Shi et al. [30] described the creep-fatigue relation of Sn37Pb solders in the form of frequency-modified fatigue-fatigue equation:

$$\varepsilon_p = C_s(T)\left(Nf^{k(T)-1}\right)^{-\beta_s(T)} \tag{23}$$

where C_s, β_s, and k are functions of temperatures given by

$$\begin{aligned} C_s(T) &= 2.122 - 3.57\times10^{-3}T + 1.329\times10^{-5}T^2 - 2.502\times10^{-7}T^3 \\ \beta_s(T) &= 0.731 - 1.63\times10^{-4}T + 1.392\times10^{-6}T^2 - 1.151\times10^{-8}T^3 \\ k_1(T) &= 0.919 - 1.765\times10^{-4}T - 8.634\times10^{-7}T^2 \\ k_2(T) &= 0.437 - 3.753\times10^{-4}T - 8.04\times10^{-7}T^2 \end{aligned} \tag{24}$$

where T is in ^oC; and k_1 and k_2 are the frequency exponents for 10^{-3} Hz < f <1 Hz and 10^{-4} Hz < f < 10^{-3} Hz, respectively. The frequency-modified relation is also used for predicting fatigue life on practical structures, such as solder joints [31,32] in electronic assemblies.

Not all researchers have followed the approach of frequency-modified fatigue-life. Kanchanomai et al. [33] established a power-law relation between the time to failure, t_f=Nt_c, and the strain rate, $\dot{\varepsilon}$. Assuming $\dot{\varepsilon} = \dot{\varepsilon}_p$=$2\varepsilon_p/t_c$, Kanchanomai et al. expressed the rate-time relation of Sn37Pb solder in the form of strain-life as

$$\varepsilon_p = C_k f^{\beta-1} N^{-\beta} \tag{25}$$

Analysing the thermomechanical fatigue of eutectic SnPb solder joints in electronic assemblies, Engelmaier [34] came to the following form of creep modified strain-life equation:

$$\varepsilon_p = C_E N^{-\beta(\bar{T},f)} \tag{26}$$

where C_E is a constant and

$$\beta(\bar{T},f) = 0.442 + 6\times10^{-4}\bar{T} - 1.74\times10^{-2}\ln(1+43200f) \tag{27}$$

where $\bar{T}$ is the mean cyclic solder joint temperature in ^oC.

Wong & Mai [35] proposed the equation:

$$\varepsilon_p = C_0 s(\sigma) c(T,f) N^{-\beta_0 b(T,f)} \tag{28}$$

where

$$\begin{aligned} s(\sigma) &= \begin{cases} 1 & when\ creep\ is\ dormant \\ exp\left[-\left(\sigma_{yield}\varepsilon_p^{n'}\right)/A\right] & when\ creep\ is\ active \end{cases} \\ c(T,f) &= 1 - c_1\left(T - T_{ref}\right) - c_2\log\left(f/f_{ref}\right) \\ b(T,f) &= 1 - b_1\left(T - T_{ref}\right) - b_2\log\left(f/f_{ref}\right) \\ T - T_{ref} &= \begin{cases} T - T_{ref} & for\ T \geq T_{ref} \\ 0 & for\ T \leq T_{ref} \end{cases} \end{aligned} \tag{29}$$

$$f/f_{ref} = \begin{cases} f/f_{ref} & for\ f \geq f_{ref} \\ 0 & for\ f \leq f_{ref} \end{cases}$$

n' is cyclic hardening index; *A*, c_1, c_2, b_1 and b_2 are positive constants; and T_{ref} is the reference temperature below which creep becomes dormant and f_{ref} is the reference frequency above which creep becomes dormant.

2.5 Future directions

The above results have all been based on curve fitting methods, where a basic structural equation is proposed and then coefficients are fitted based on empirical data. One of the limitations of this method is that it produces many different formulations. Indeed, there could be unlimited forms of creep-modified fatigue equations. With an adequate number of fitting parameters, any creep-modified fatigue equation can be quite easily fitted to experimental creep-fatigue data generated within a creep-fatigue condition.

However, a good creep-modified strain-life equation should be capable of covering the full spectrum of creep fatigue, including the two ends of the spectrum: pure fatigue and pure creep rupture. The equations of Coffin, Solomon, Shi et al., Kanchanomai et al., and Engelmier do not satisfy the above conditions. As an illustration, the condition of pure fatigue is given by letting $C(T)f^{\beta(1-k)} = C_0$ for the equations of Coffin, Solomon and Shi et al. At the condition of extreme cyclic frequency, $f \to \infty$, the function $C(T)$ must become infinitely small, which implies $T \to \infty$. The clearly does not agree with the generally accepted understanding of the physics of fatigue. On the other hand, the condition of pure creep rupture is given by letting ε_p=0. This condition cannot be satisfied for the equation of Coffin, because C and β_0 are constant. For the equation of Engelmaier, the condition of creep-rupture is satisfied by letting $\beta(\bar{T}, f) \to +\infty$, which suggests $T \to +\infty$. The condition of creep-rupture is satisfied for the equations of Solomon and Shi et al. by letting C_m=C_s=0, which returns T=172 °C and 198 °C, respectively. The equation of Solomon suggests that creep rupture is dependent solely on temperature, independent of stress and time. The equation of Shi et al. implies that the condition of creep rupture could only occur at a temperature that is above the melting temperature of the eutectic tin-lead solder, which is 183 °C. These conditions do not agree with our understanding of the physics of creep. While the equation of Wong & Mai is capable of modelling pure fatigue, it is not entirely capable of modelling the condition of creep rupture, because the function $s(\sigma)c(T_R, f_R) = 0$ does not agree with any of the forms of the known time-temperature parameters presented in Eqs.8-10.

There is a need to develop a creep-fatigue equation that covers the full range of phenomena from pure fatigue to pure creep rupture, and all the intermediate failures.

3. Method

The objective of this work was to develop an equation that integrates creep damage into the fatigue equation. The integrated equation should be capable of modelling pure fatigue and creep fatigue.

The approach started by taking the strain perspective, by assuming that the material has a fatigue capacity $\varepsilon_{p,ref}$. This is then reduced to $\varepsilon_p$by the action of creep. The effect is proposed to be moderated by the applied stress, temperature, and cyclic time, hence $c(\sigma, T, t_c)$. Then, a specific formulation for this c function based on a linear relationship between temperature and the log of the cyclic time was proposed. The Manson-Haferd parameter (P_{MH}) is used for the thermal component. The resulting formulation (Eqs.40) is capable of modelling pure fatigue and creep-fatigue damage.

This equation is then validated by application to three materials: (i) eutectic tin-lead solder, Sn37Pb, (ii) lead-free solder, Sn3.5Ag, and (iii) stainless steel, SS316. The data for these materials were obtained from the literature. Results show that this equation provides a good description of the creep effect on fatigue damage.

4. Creep-integrated fatigue equation

4.1 Derivations

4.1.1 The basic form of the equation

The presence of creep reduces the fatigue capacity, $\varepsilon_{p,ref}$. The reduced fatigue capacity is postulated to be given by

$$\varepsilon_p = c(\sigma, T, t_c)\varepsilon_{p,ref} \tag{30}$$

wherein $c(\sigma,T,t_c)$ is the creep-damage function, which is proposed to take the form:

$$c(\sigma, T, t_c) = 1 - c_1(\sigma)\left(T - T_{ref}\right) - c_2(\sigma)\log\left(t_c/t_{ref}\right)$$

$$T - T_{ref} = \begin{cases} T - T_{ref} & for\ T \geq T_{ref} \\ 0 & for\ T \leq T_{ref} \end{cases} \tag{31}$$

$$t_c/t_{ref} = \begin{cases} t_c/t_{ref} & for\ t_c \geq t_{ref} \\ 0 & for\ t_c \leq t_{ref} \end{cases}$$

The functions $c_1(\sigma)$ and $c_2(\sigma)$ are positive in values and should be referred to as creep functions. Substituting Eq.31 into Eq.2 gives the basic form of the creep-integrated fatigue equation:

$$\varepsilon_p = C_0 c(\sigma, T, t_c) N^{-\beta_0} \tag{32}$$

This equation shares several similarities with other equations - this is because they are all expansions of the Coffin-Manson equation [7,8]. The point of difference for Eq.32 is it has the potential to cover the whole spectrum from pure fatigue to pure creep rupture, and creep-fatigue in between, which is novel. The other equations, including those of [35] and [30], do not have this capability.

4.1.2 Relating creep functions to P_{MH} parameter

The P_{MH}-parameter described in Eq.9 is known to give one of the best descriptions of creep-rupture of metal alloys [18]. At pure creep-rupture condition, plastic strain equals to 0, then c function can be presented as:

$$c(T,t,\sigma) = 1 - c_1(\sigma)\left(T_R - T_{ref}\right) - c_2(\sigma)\log\left(t_R/t_{ref}\right) = 0 \tag{33}$$

where T_R is rupture temperature and t_R is rupture time. Then, according to the Manson-Haferd Parameter (Eq.9), and letting T=T_{ref} and t_R=t_{ref}, respectively, the following equations are given:

$$c_2 = \frac{1}{\log\left(t_a/t_{ref}\right)} \tag{34}$$

$$c_1(\sigma) = -\frac{c_2}{P_{MH}(\sigma)} \tag{35}$$

In order to integrate creep damage into a strain-life fatigue equation, the creep function $c_1(\sigma)$ ought to be expressed as a function of plastic strain amplitude, that is $c_1(\varepsilon_p)$. The research conducted by Gary [36] and Masaya et al. [20] shows that cyclic stress is higher than constant stress at the same rupture time. Because c_1 function is based on the time-temperature relation under constant stress (Manson-Haferd parameter), the creep effect is enlarged when the cyclic stress (σ_{ref}) is imposed. Therefore, it is reasonable to introduce a moderating factor, f_m, to compress the cyclic stress to an equivalent constant stress (σ_s), and this has been verified on stainless steel 316 [37]. Then, the P_{MH} parameter for cyclic stress rupture can be expressed as:

$$P_{MH}(\sigma_s) = P_{MH}\left(f_m\sigma_{ref}\right) \tag{36}$$

Through expressing the cyclic σ_{ref}-ε_p relation as

$$\sigma_{ref} = K(T,t_c)\varepsilon_p^{n(T,t_c)} \tag{37}$$

where $K(T,t_c)$ and $n(T,t_c)$ are functions of temperature and cycle time, $P_{MH}(\sigma_s)$ is transformed to $P_{MH}(\varepsilon_p)$ as

$$P_{MH}(\varepsilon_P) = P_{MH}\left[f_m K(T,t_c)\varepsilon_p^{n(T,t_c)}\right] \tag{38}$$

In order to preserve the linearity of the P_{MH}-parameter, $P_{MH}(\varepsilon_p)$ must be a function of only ε_p. Therefore, the $\overline{K}$ and $\bar{n}$ are defined as the mean coefficients of $K(T,t_c)$ and $n(T,t_c)$ over the ranges of temperature and cycle time of interest, then

$$P_{MH}(\varepsilon_P) = P_{MH}\left(\overline{K}^*\varepsilon_p^{\bar{n}}\right) \tag{39}$$

and $\overline{K}^* = f_m \overline{K}$.

4.1.3 The creep-integrated fatigue equation

The creep-integrated fatigue equation takes the form:

$$\varepsilon_p = C_0 c\left(\varepsilon_p, T, t_c\right) N^{-\beta_0} \tag{40}$$

where

$$c\left(\varepsilon_p, T, t_c\right) = 1 - c_1\left(\varepsilon_p\right)\left(T - T_{ref}\right) - c_2 \log\left(t_c / t_{ref}\right)$$
$$c_1\left(\varepsilon_p\right) = -\frac{c_2}{P_{MH}\left(\varepsilon_p\right)}$$
$$c_2 = \frac{1}{\log\left(t_a / t_{ref}\right)} \tag{41}$$
$$P_{MH}(\varepsilon_P) = P_{MH}\left(\overline{K}^* \varepsilon_p^{\bar{n}}\right)$$

Eq.40 is capable of modelling pure fatigue at $c(\varepsilon_p,T,t_c)$=1, modelling pure creep rupture at $c(\varepsilon_p,T,t_c)$=0, and modelling creep-fatigue damage at $0 \leq c(\varepsilon_p,T,t_c) \leq 1$.

4.2 Characterization

The creep-integrated fatigue equation is described by the fatigue coefficients, C_o and β_o, and the creep functions, $c_1(P_{MH}(\sigma_s),\overline{K}^*,\bar{n})$ and c_2. The coefficients, C_o and β_o, and $P_{MH}(\sigma_s)$ of many alloys are available in literature. Otherwise, these may be characterised rather economically using standard test procedures. The coefficients $\overline{K}^*$ and $\bar{n}$ can be established by performing creep-fatigue tests at two conditions above the reference condition, (T_{b1}, t_{b1}) and (T_{b2}, t_{b2}), and Eq.30 can be expressed as:

$$\varepsilon_p = c\left(\varepsilon_p, \overline{K}^*, \bar{n}, T_{bj}, t_{bj}\right)\varepsilon_{p,ref} \qquad j = 1,2 \tag{42}$$

where ε_p is obtained from the creep-fatigue experiment and $\varepsilon_{p,ref}(N)$ is evaluated using the relation $\varepsilon_{p,ref} = C_o N^{-\beta o}$. Alternatively, performing creep-fatigue tests at multiple conditions of (T, t_c)$_j$ above the reference condition yield multiple sets of (ε_{pi}, $N_{exp,i}$)$_j$, where ε_{pi} corresponds to strain amplitude i. The fatigue coefficients, C_o and β_o, and the stress-strain coefficients, $\overline{K}^*$ and $\bar{n}$, can be extracted simultaneously by regressing the computed creep-fatigue life,

$$N_{com,ij} = \left\{\frac{\varepsilon_{pi}}{C_0 c\left[\varepsilon_{pi}, \overline{K}^*, \bar{n}, (T, t_c)_j\right]}\right\}^{-1/\beta_0} \tag{43}$$

against the experimental life, $N_{exp,ij}$.

5. Demonstration on metal alloys

The creep-integrated strain-life equation, $\varepsilon_p = C_0 c(\varepsilon_p, T, t_c) N^{-\beta_0}$, will be demonstrated on the following metal alloys: (i) eutectic tin-lead solder, Sn37Pb, (ii) lead-free solder, Sn3.5Ag, and (iii) stainless steel, SS316.

5.1 Sn37Pb solder

The experimental creep-fatigue data of Shi et al. [30] and the creep-rupture data of Shi et al. [38] for the eutectic tin-lead solder, Sn37Pb are used to demonstrate the procedures of establishing the creep-integrated fatigue equation and to show the quality of the equation. The reference temperature is chosen to be 150 K, which is approximately $0.33T_m$. The reference cycle time is chosen to be 1s. The parameters to be established are the fatigue coefficients, C_o and β_o, and the creep functions, $c_1(\varepsilon_p)$ and c_2.

5.1.1 Evaluating creep functions, $c_1(\varepsilon_p)$ and c_2

The creep-rupture time of Sn37Pb solder as a function of the applied steady-stress, σ_s, and temperature are extracted from figures 2 and 3 of Shi et al. [38]. **Error! Reference source not ound.** shows the plots of log t_R versus T as a function of σ_s. The point of convergence, (T_{ref}, log t_a), is evaluated as (150 K, 10); thus,

$$c_2 = \frac{1}{\log(t_a/t_{ref})} = 0.1 \tag{44}$$

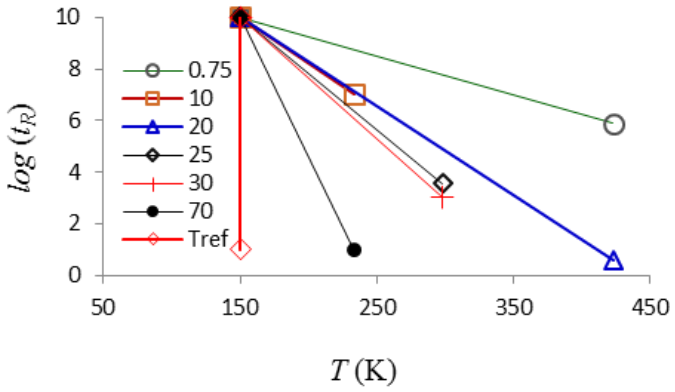

Figure 1 Creep-rupture characteristics of Sn37Pb solder (σ_s in MPa)

The gradients of the lines give -1/ $P_{MH}(\sigma_s)$, which have been evaluated as:

$$-\frac{1}{P_{MH}(\sigma_s)} = 1.34 \times 10^{-2} + 1.31 \times 10^{-3}\sigma_s \tag{45}$$

Substituting into Eq.34 gives

$$c_1(\varepsilon_p) = -\frac{c_2}{P_{MH}(\bar{K}^* \varepsilon_p^{\bar{n}})} = 1.34 \times 10^{-3} + 1.31 \times 10^{-4} \bar{K}^* \varepsilon_p^{\bar{n}} \tag{46}$$

5.1.2 Evaluating fatigue coefficients, C_o, and β_o, and stress-strain coefficients, $\bar{K}^*$ and $\bar{n}$

The creep-fatigue coefficients $(C_b, \beta_b)_j$ at five temperatures and five cycle times are extracted from figures 6 and 12, respectively, of Shi et al. [30] and these are tabulated in Table 1. The coefficients $(C_b, \beta_b)_j$ were used to generate pseudo experimental creep-fatigue data, $(\varepsilon_{pi}, N_{exp,i})_j$, where i=1 to 6. These were then regressed against $N_{com,ij}$ of Eq.43. Supported by $c_1(\varepsilon_p)$ and c_2 obtained in Eqs.44 and 46, the regression has led to C_o=4.06, β_o=0.778, $\bar{K}^*$ =11.9 MPa and $\bar{n}$=0.138.

Table 1 Creep-fatigue coefficients of Sn37Pb solder extracted from Ref. [30]

Creep-fatigue coefficients	Temperature (K), t_c = 1 sec				
	233	298	348	398	423
C_b	2.76	2.22	1.70	1.43	0.97
β_b	0.775	0.755	0.745	0.75	0.715
Creep-fatigue coefficients	Period, t_c (s), *T=298* K				
	10^0	10^1	10^2	10^3	10^4
C_b	2.22	1.92	1.67	1.23	0.60
β_b	0.755	0.735	0.715	0.715	0.670

5.1.3 Transforming to pure fatigue relation, $\varepsilon_{p,ref} = C_0 N^{-\beta_0}$

With the creep functions fully defined, the creep-fatigue data ε_p-N_{exp} is transformed to pure fatigue data $\varepsilon_{p,ref}$-N_{exp} using the relation: $\varepsilon_{p,ref} = \varepsilon_p / c(\varepsilon_p, T, t_c)$. Figure 2 shows the creep-fatigue data, ε_p-N_{exp} (shadow area), and the transformed pure-fatigue data, $\varepsilon_{p,ref}$-N_{exp}. It is noted that the transformed data collapsed into a single power-law curve. The coefficients of the trendline, C_o=3.97 and β_o=0.77 agree well with that obtained in Section 4.1.2.

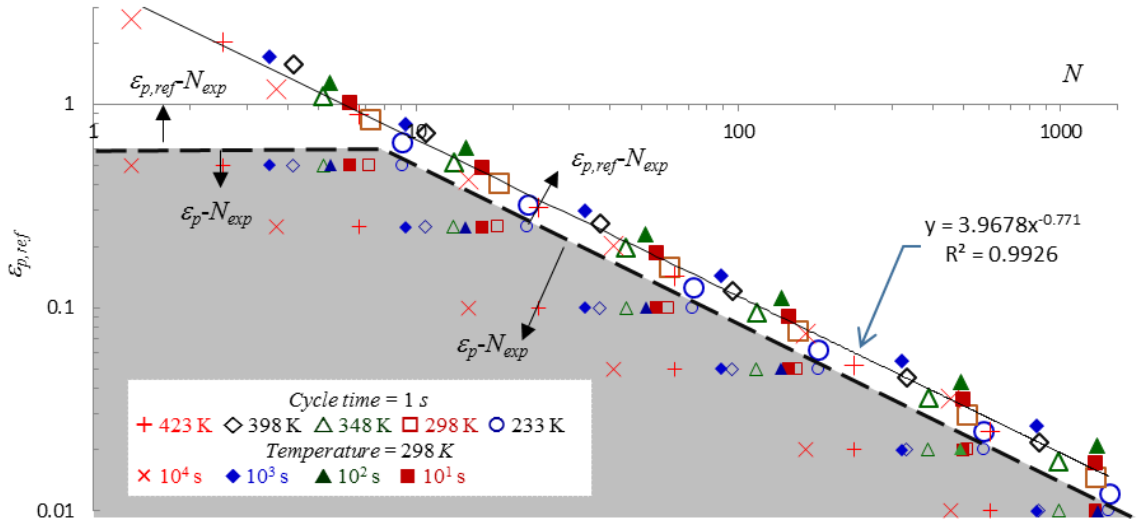

Figure 2 Creep-fatigue ε_p-N_{exp} data and the transformed $\varepsilon_{p,ref}$-N_{exp} data of Sn37Pb solder

5.2 Lead-free solder, Sn3.5Ag

The reference temperature for the Sn3.5Ag lead-free solder is chosen to be 150 K, which is approximately 0.3 T_m; and the reference cycle time is chosen to be 1 s.

5.2.1 Evaluating creep functions, $c_1(\varepsilon_p)$ and c_2

The creep-rupture time of Sn3.5Ag solder as a function of the applied steady-stress, σ_s, and temperature are extracted from figures 5 of Lin & Chu [39]. The point of convergence for the P_{MH} parameter is evaluated as (150 K, 10) giving c_2=0.1. The gradients, $1/P_{MH}(\sigma_s)$, and the creep function $c_1(\varepsilon_p)$ have been evaluated as:

$$-\frac{1}{P_{MH}(\sigma_s)} = 1.26\times10^{-2} + 1.02\times10^{-3}\sigma_s \tag{47}$$

$$c_1(\varepsilon_p) = 1.26\times10^{-3} + 1.02\times10^{-4}\bar{K}^*\varepsilon_p^{\bar{n}} \tag{48}$$

5.2.2 Evaluating fatigue coefficients, C_o, and β_o, and stress-strain coefficients, $\bar{K}^*$ and $\bar{n}$

The experimental creep-fatigue data, $(\varepsilon_{pi}, N_{exp,i})_j$, at four plastic strain amplitudes, at three temperatures and at four cyclic times are extracted from figure 8 of Kanchanomai & Mutoh [40] and from figure 4 of Kanchanomai et al. [41], respectively, and these are tabulated in Table 2. These were regressed against $N_{com,ij}$ of Eq.43 to yield C_o=12, β_o=0.86, $\bar{K}^*$ =12 MPa and $\bar{n}$= -0.07.

Table 1 Creep-fatigue coefficients of Sn3.5Ag solder evaluated from Ref. [40] and Ref. [41]

Creep-fatigue coefficients	Temperature (K), t_c = 10s			
	293	358	393	
C_b	10.3	2.0	6.5	
β_b	0.92	0.80	1.04	
Creep-fatigue coefficients	Period, t_c (s), *T=293* K			
	10^0	10^1	10^2	10^3
C_b	16.1	10.3	18.3	9.0
β_b	0.95	0.92	1.07	1.02

5.2.3 Transforming to pure fatigue relation, $\varepsilon_{p,ref} = C_0 N^{-\beta_0}$

Figure 3 shows the creep-fatigue data, ε_p-N_{exp}, and the transformed pure-fatigue data, $\varepsilon_{p,ref}$-N_{exp} (shadow area). The transformed data collapsed into a single power-law curve. However, the coefficients of the trend line, C_o=8.7 and β_o=0.82, do not agree well with that obtained in Section 4.2.2, which highlights inconsistency in the creep-fatigue data. The creep-fatigue coefficients, (C_b, β_b), at the three temperatures and the four cycle times were evaluated from the creep-fatigue data, ε_p-N_{exp}, of Refs. [40] and [41] (Table 2). The magnitudes of these coefficients fluctuate randomly, which confirms the creep-fatigue data are indeed relatively poor in quality.

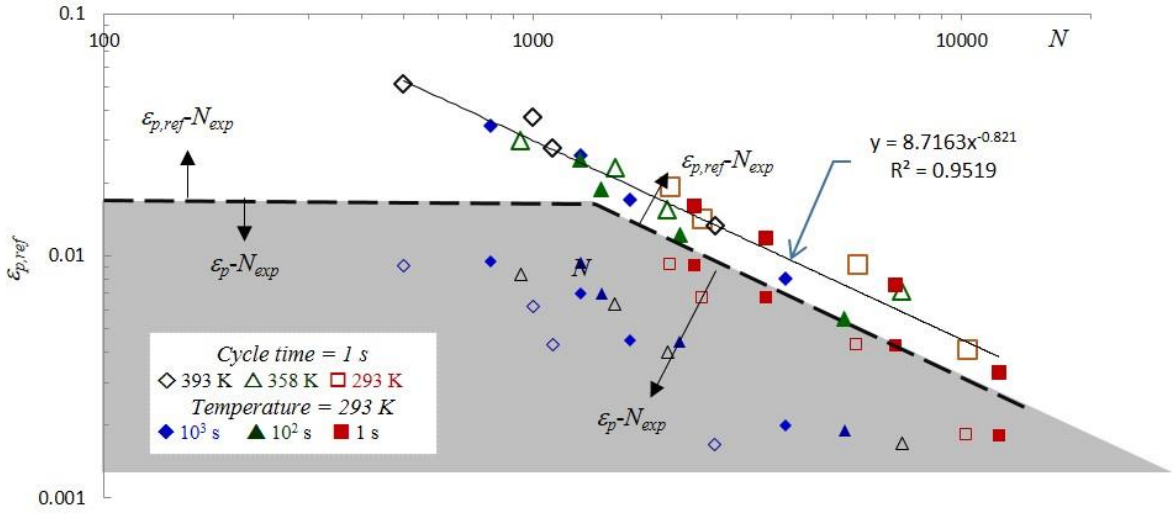

Figure 3 Creep-fatigue ε_p-N_{exp} data and the transformed $\varepsilon_{p,ref}$-N_{exp} data of Sn3.5Ag solder

5.3 Stainless steel, SS316

The reference temperature for the stainless steel 316 is chosen to be 500 K, which is approximately $0.33T_m$; and the reference cycle time is chosen to be 1 s.

5.3.1 Evaluating creep functions, $c_1(\varepsilon_p)$ and c_2

The creep-rupture time of SS316 as a function of the applied steady-stress (σ_s), and temperature are extracted from figure 12 of Ref. [42]. The point of convergence for the P_{MH} parameter is evaluated as (500 K, 10) giving c_2=0.1. The gradients, $1/P_{MH}(\sigma_s)$, and the creep function $c_1(\varepsilon_p)$ have been evaluated as:

$$-\frac{1}{P_{MH}(\sigma_s)} = 3.67 \times 10^{-3} + 1.95 \times 10^{-5}\sigma_s \tag{49}$$

$$c_1(\varepsilon_p) = 3.67 \times 10^{-4} + 1.95 \times 10^{-6}\bar{K}^*\varepsilon_p^{\bar{n}} \tag{50}$$

5.3.2 Evaluating fatigue coefficients, C_o, and β_o, and stress-strain coefficients, $\bar{K}^*$ and $\bar{n}$

The creep-fatigue coefficients $(C_b, \beta_b)_j$ at three temperatures and three strain rates are extracted from Table 266.3 of Kanazawa & Yoshida [37] and are tabulated in Table 3. At T=293 K, creep is inactive in SS316. The creep-fatigue coefficients $(C_b, \beta_b)_j$ at temperatures above T_{ref}=500 K were used to generate pseudo experimental creep-fatigue data, $(\varepsilon_{pi}, N_{exp,i})_j$, where i=1 to 5. These were then regressed against $N_{com,ij}$ of Eq.43 to yield C_o=0.60, β_o=0.54, $\bar{K}^*$ =31.47 MPa and $\bar{n}$=-0.401. In computing the creep-damage function, $c(\varepsilon_p,T,t_c)$, the cycle time was evaluated approximately as $t_c=2\varepsilon_p/\dot{\varepsilon}$.

Table 2 Creep-fatigue coefficients of SS316 extracted from Ref. [43]

Temperature (K)	Strain rate (min^{-1})	Creep-fatigue coefficients	
		C_b	β_b
293	0.04	0.907	0.568
	0.4	0.916	0.569
723	0.004	0.279	0.522
	0.04	0.369	0.521
	0.4	0.223	0.409
873	0.004	0.246	0.585
	0.04	0.347	0.578
	0.4	0.408	0.563

973	0.004	0.246	0.555
	0.04	0.47	0.615
	0.4	0.425	0.578

5.3.3 Transforming to pure fatigue relation, $\varepsilon_{p,ref} = C_0 N^{-\beta_0}$

Figure 4 shows the creep-fatigue data, ε_p-N_{exp} (shadow area), and the transformed pure-fatigue data, $\varepsilon_{p,ref}$-N_{exp} by using the relation: $\varepsilon_{p,ref} = \varepsilon_p / c(\varepsilon_p, T, t_c)$. It is noted that the transformed data collapsed into a single power-law curve, and the coefficients of the trend line, C_o=0.57 and β_o=0.53, do not agree well with but is close to the coefficients obtained in Section 4.3.2. This result could show the poor quality in the generated pseudo experimental creep-fatigue data, $(\varepsilon_{pi}, N_{exp,i})_j$. This is caused by the relatively poor quality of creep-fatigue data, where the coefficients fluctuate randomly but slightly, especially at 873K and 973K. In addition, if the fatigue data at room temperature (creep is dormant) were accepted, the magnitudes of C_o and β_o could be identified as 0.91 and 0.568 respectively, and the coefficients, $\bar{K}^*$and $\bar{n}$, could be regressed as 161MPa and -0.16 respectively. Then, the creep-fatigue data can collapse into a single power-law curve, and the coefficient of this trend line is shown as 0.77, which is deviated significantly from the pure fatigue coefficient (C_o=0.91). This deviation again implies the poor quality of creep-fatigue data because of the inconsistency between the pure-fatigue data and creep-fatigue data.

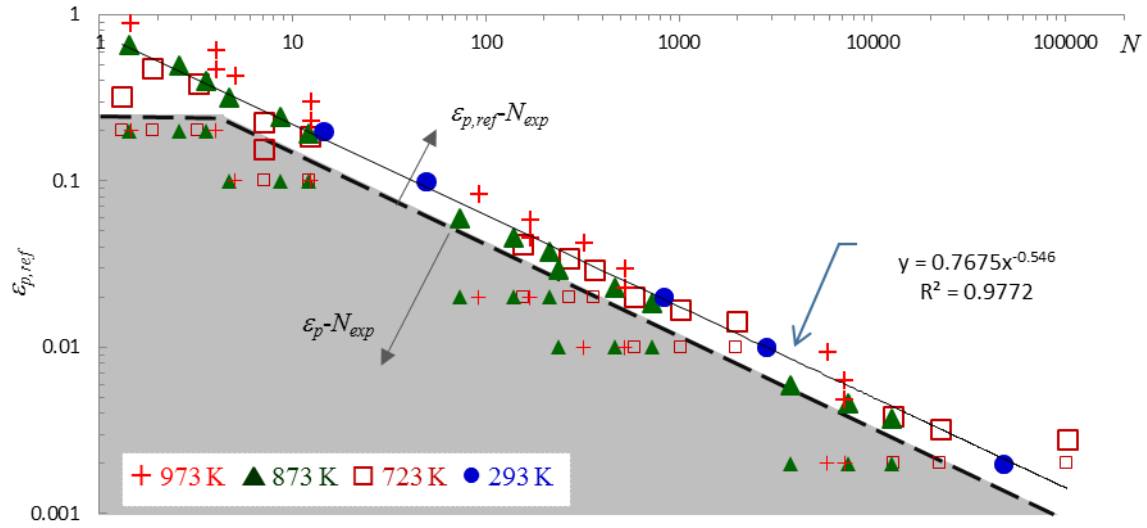

Figure 4 Creep-fatigue ε_p-N_{exp} data and the transformed $\varepsilon_{p,ref}$-N_{exp} data of SS316

In summary the equation for 316SS is:

$$\varepsilon_p = C_0 c(\varepsilon_p, T, t_c) N^{-\beta_0} \quad (51)$$

where

$$c(\varepsilon_p, T, t_c) = 1 - c_1(\varepsilon_p)(T - T_{ref}) - c_2 \log(t_c / t_{ref}) \quad (52)$$

$$c_1(\varepsilon_p) = -\frac{c_2}{P_{MH}(\varepsilon_p)}$$

$$c_2 = \frac{1}{\log(t_a/t_{ref})}$$

$$P_{MH}(\varepsilon_P) = P_{MH}(\bar{K}^* \varepsilon_p^{\bar{n}})$$

6. Discussion

6.1 Comparison of the materials

The fatigue coefficients and the creep functions for the three metal alloys are tabulated in Table 4. If the pure-fatigue data is involved, the stainless steel 316 has the worst (low-cycle) fatigue resistance but the best creep resistance, because lower magnitude of c_1 implies higher creep resistance against creep. The Sn3.5Ag solder shows significantly better fatigue resistance and marginally better creep resistance than the Sn37Pb solder. This explains the better thermomechanical fatigue reliability of the Sn3.5Ag solder joints in electronic assemblies [44].

Table 3 Fatigue coefficients and creep functions of Sn37Pb, Sn3.5Ag, and SS316

Alloys	Fatigue coefficients		Creep functions	
	C_o	β_o	$c_1(\varepsilon_p)$	c_2
Sn 37Pb	4.1	0.78	$1.34\text{x}10^{-3} + 1.56\text{x}10^{-3}\varepsilon_p^{0.14}$	0.1
Sn3.5Ag	12	0.86	$1.26\text{x}10^{-3} + 1.23\text{x}10^{-3}\varepsilon_p^{-0.07}$	0.1
SS316	0.91	0.57	$3.67\text{x}10^{-4} + 3.14\text{x}10^{-4}\varepsilon_p^{-0.16}$	0.1

The Sn3.5Ag solder and the SS316 have shown negative values of the cyclic stress hardening exponent, $\bar{n}$. This appears to suggest significant presence of creep in a creep-fatigue cycle leading to "stress softening". However, the cyclic stress-strain characteristics of the Sn3.5Ag solder (figure 5 of [40] and figure 3 of [41]) and SS 316 (figure 226.5 of [43]) have shown no evidence of stress softening even at elevated temperatures and cycle times. The negative stress exponents are believed to be the consequence of the relatively poor quality of the creep-fatigue data.

6.2 Physical interpretation of the formula

C_0 is the plastic strain when fatigue life is one cycle (N=1) (no creep). This is related to the ductility, i.e. that solder has greater plastic strain than stainless steel. Having a high C_0 is an

advantageous property, since it means that the material accepts high plastic strain, at least in the single cycle load case.

β_0 is the slope of the plastic strain vs. life at log-log scale. This property represents the material's resistance to the fatigue damage. For a given life N (and same C_0), a material with higher β_0 has less ability to accept imposed plastic strain.

$c(\varepsilon_p, T, t_c)$ is named as creep function since it accommodates creep rupture characteristics. The linear relationship between temperature and cyclic time is consistent with the Manson-Haferd parameter, and the derivation of the coefficients is built on this parameter. Particularly, in the function c, c_1 is shown as a function of applied loading, and for a given plastic strain, the higher magnitude of c_1 implies lower creep resistance against creep.

The reference condition is introduced into this equation, and shows threshold between pure fatigue and creep fatigue. This creep-fatigue equation is restored to the Coffin-Manson equation at reference condition, which builds a bridge between pure fatigue and creep fatigue.

6.3 Application to design

In a typical design application the typical workflow is that the engineer knows the applied stress, and then has to select a material and determine if the life is adequate (other permutations are possible). Given a candidate material with known yield strength and Young's Modulus, it is then possible to determine the applied strain. A material that is stronger and stiffer will have greater elastic strain, thereby reducing plastic strain. For the materials under consideration here, for a given applied load the stainless steel 316 would experience a lower plastic strain, due to its higher yield strength and Young's Modulus, than the solders.

In addition, according to the creep-fatigue equation proposed in this paper, desirable materials for longevity are those with high C_0, low β_0 and small c_1, and this creep-fatigue equation can be used to evaluate fatigue damage. Taking Sn37Pb solder as an example, fatigue life for given plastic strain would be necessary to solve the following equation (Eq.53) to determine life:

$$\varepsilon_p = 4.06\left[1 - \left(1.34 \times 10^{-3} + 1.56 \times 10^{-5}\varepsilon_p^{0.138}\right)(T - 150) - 0.1\log(t_c)\right]N^{-0.778} \qquad (53)$$

Alternatively, to determine plastic strain by numerical solution of the equation.

6.4 Contribution and limitations

The magnitude of the deviation between the fatigue coefficients, (C_o, β_o), of the transformed $\varepsilon_{p,ref}$-N data and those evaluated from regression using Eq.40 provides a measurement of the goodness of the fatigue coefficients and the creep functions. The resulting R^2 values present that the equation accommodates the empirical data to a high degree of fidelity. This shows that it has been possible to develop an equation capable of modelling the full spectrum of fatigue and creep, and the combinations thereof. This has not been shown previously in the literature, and is therefore a novel contribution. Also, compared to other approaches in the literature, the

present work explicitly shows how to determine the coefficients, and provides some explanation of their physical meaning. The concept of reference conditions is novel.

Limitations in the present work are that the model has only been demonstrated for these three materials. A future research activity could be to test the model against other materials, to check how well the formulation represented other classes of materials. Also, it is not easy to see how heat-treatment would be accommodated in this model, other than by changing the yield strength and hence changing the proportion of plastic to elastic strain. All the creep-fatigue equations in the literature have the problem of lacking a physical explanation for their coefficients. In the present work this problem is slightly reduced, in that the Manson-Haferd parameter has been used, and the reference conditions have been associated with physically plausible phenomena. Nonetheless a full physical explanation for creep-fatigue remains elusive. Thus it is still not possible to predict the coefficients for a material that has not been encountered before.

7. Conclusion

By integrating the Manson-Haferd creep-rupture parameter into the Coffin-Mason fatigue equation, the resulting equation has been shown to be capable of modelling creep-fatigue interaction from pure fatigue to pure creep rupture. The associated material parameters can be established very economically by performing a standard creep rupture test followed by very limited number of creep-fatigue tests. For many engineering metal alloys, such data are readily available in the literature. The creep-integrated fatigue equation for three metal alloys, namely Sn37Pb solder, Sn3.5Ag solder, and stainless steel 316 have been established using the available data in the literature. The equation has been shown to be capable of collapsing the dispersed strain-life data of the metal alloys obtained at diverse temperatures and cycle times into a cohesive strain-life formulaic representation. However, the heat-treatment effect is not accommodated into this equation and a full physical explanation for the coefficients needs to be further developed.

Conflict of interests: The authors declare no conflict of interest. The research was conducted without personal financial benefit from any funding body, nor did any such body influence the execution of the work.

Contribution statement: The work was conducted by DL, supervised by DP. The form of the creep-integrated fatigue equation was developed by DL and EW. The method to determine the coefficients was developed by DL based on guidance from DP. The explanation of the physical meaning was developed by DL and DP. The concept of reference conditions was developed by DL and EW. The first draft of the paper was written by DL. All authors contributed to writing the final paper.

References

1. Taira, S. Lifetime of structures subjected to varying load and temperature. In Creep in structures, Springer: 1962; pp 96-124.
2. Campbell, R. Creep/fatigue interaction correlation for 304 stainless steel subjected to strain-controlled cycling with hold times at peak strain. Journal of engineering for industry 1971, 93, 887-892.
3. International, A. Astm e2714-13, standard test method for creep-fatigue testing. 2013.
4. International, A. Astm e139-11, standard test methods for conducting creep, creep-rupture, and stress-rupture tests of metallic materials. 2011.
5. Basquin, O. In The exponential law of endurance tests, Proc. Astm, 1910; pp 625-630.
6. Wöhler, A. Theorie rechtekiger eiserner brückenbalken mit gitterwänden und mit blechwänden. Zeitschrift für Bauwesen 1855, 5, 121-166.
7. Coffin, L. Fatigue at high temperature. In Fatigue at elevated temperatures, ASTM International: 1973.
8. Manson, S.S. Behavior of materials under conditions of thermal stress. Lewis Flight Propulsion Lab.: 1954.
9. Morrow, J. Cyclic plastic strain energy and fatigue of metals. In Internal friction, damping, and cyclic plasticity, ASTM International: 1965.
10. Palmgren, A. Die lebensdauer von kugellagern. Zeitschrift des Vereins Deutscher Ingenieure 1924, 68, 339-341.
11. Miner, M.A. Cumulative damage in fatigue. Journal of applied mechanics 1945, 12, 159-164.
12. Robinson, E.L. Effect of temperature variation on the long-time rupture strength of steels. Trans. ASME 1952, 74, 777-781.
13. Goldhoff, R. Uniaxial creep-rupture behavior of low-alloy steel under variable loading conditions. Journal of Basic Engineering 1965, 87, 374-378.
14. Oding, I.A.; Kennedy, A.J. Creep and stress relaxation in metals. Oliver & Boyd: 1965.
15. Larson, F.R.; Miller, J. A time-temperature relationship for rupture and creep stresses. Trans. ASME 1952, 74, 765-775.
16. Manson, S.; Haferd, A. A linear time-temperature relation for extrapolation of creep and stress-rupture data. Lewis Flight Propulsion Lab.: 1953.
17. Dorn, J.; Orr, R.L.; Sherby, O. Creep correlations of metals at elevated temperatures. AIME TRANS 1954, 200, 71-80.
18. Penny, R.K.; Marriott, D.L. Design for creep. Springer Science & Business Media: 2012.
19. Hertzberg, R.W. Deformation and fracture mechanics of engineering materials. Wiley: 1996.
20. Deguchi, M.; Tobe, H.; Sato, E. Damage propagation mechanism in low-cycle creep fatigue of cu–cr–zr alloy. International Journal of Fatigue 2016, 87, 351-358.
21. Mao, H.; Mahadevan, S. Reliability analysis of creep–fatigue failure. International journal of fatigue 2000, 22, 789-797.
22. Code, R. Design and constriction rules for mechanical components of fbr nuclear islands. AFCEN: 2007.
23. Jetter, R.I. Subsection nh—class 1 components in elevated temperature service. In Companion guide to the asme boiler & pressure vessel code, volume 1, second edition, ASME Press: 2006.
24. Paris, P.; Erdogan, F. A critical analysis of crack propagation laws. Journal of basic engineering 1963, 85, 528-533.
25. Ainsworth, R.; Ruggles, M.; Takahashi, Y. Flaw assessment procedure for high-temperature reactor components. Journal of pressure vessel technology 1992, 114, 166-170.

26. Liu, H.; Bao, R.; Zhang, J.; Fei, B. A creep–fatigue crack growth model containing temperature and interactive effects. International Journal of Fatigue 2014, 59, 34-42.
27. Xuan, F.; Tu, S.; Wang, Z. Time-dependent fatigue fracture theory and residual life assessment techniques for defective structures. Chin J Adv Mech 2005, 35, 391-403.
28. Manson, S.; Halford, G.R.; Hirschberg, M.H. Creep-fatigue analysis by strain-range partitioning. Lewis Research Center: 1971.
29. Solomon, H. Fatigue of 60/40 solder. IEEE Transactions on Components, Hybrids, and Manufacturing Technology 1986, 9, 423-432.
30. Shi, X.; Pang, H.; Zhou, W.; Wang, Z. Low cycle fatigue analysis of temperature and frequency effects in eutectic solder alloy. International Journal of Fatigue 2000, 22, 217-228.
31. Lee, J.; Jeong, H.-Y. Fatigue life prediction of solder joints with consideration of frequency, temperature and cracking energy density. International Journal of Fatigue 2014, 61, 264-270.
32. Wong, E.; Seah, S.; Caers, J.; Lai, Y.-S. Frequency-dependent strain–life characteristics of sn1. 0ag0. 1cu solder on cupper pad at high cyclic frequency. International Journal of Fatigue 2014, 59, 43-49.
33. Kanchanomai, C.; Miyashita, Y.; Mutoh, Y. Strain-rate effects on low cycle fatigue mechanism of eutectic sn–pb solder. International Journal of Fatigue 2002, 24, 987-993.
34. Engelmaier, W. Fatigue life of leadless chip carrier solder joints during power cycling. IEEE transactions on components, hybrids, and manufacturing technology 1983, 232-237.
35. Wong, E.; Mai, Y.-W. A unified equation for creep-fatigue. International Journal of Fatigue 2014, 68, 186-194.
36. Halford, G. Cyclic creep-rupture behavior of three high-temperature alloys. Metallurgical Transactions 1972, 3, 2247-2256.
37. Liu, D.; Pons, D.; Wong, E.-h. The unified creep-fatigue equation for stainless steel 316. Metals 2016, 6, 219.
38. Shi, X.; Wang, Z.; Yang, Q.; Pang, H. Creep behavior and deformation mechanism map of sn-pb eutectic solder alloy. Journal of Engineering Materials and Technology 2003, 125, 81-88.
39. Lin, C.-K.; Chu, D.-Y. Creep rupture of lead-free sn-3.5 ag and sn-3.5 ag-0.5 cu solders. Journal of Materials Science: Materials in Electronics 2005, 16, 355-365.
40. Kanchanomai, C.; Mutoh, Y. Effect of temperature on isothermal low cycle fatigue properties of sn–ag eutectic solder. Materials Science and Engineering: A 2004, 381, 113-120.
41. Kanchanomai, C.; Miyashita, Y.; Mutoh, Y.; Mannan, S. Influence of frequency on low cycle fatigue behavior of pb-free solder 96.5 sn–3.5 ag. Materials Science and Engineering: A 2003, 345, 90-98.
42. High temperature characteristics of stainless steels. Nickel Development Institute.
43. Kanazawa, K.; Yoshida, S. In Effect of temperature and strain rate on the high temperature low-cycle fatigue behavior of austenitic stainless steels, Creep and fatigue in elevated temperature applications. International conference sponsored by the Institution of Mechanical Engineers, American Society of Mechanical Engineers, American Society for Testing Materials, Philadelphia, 23-27 September 1973 and Sheffield, 1-5 April 1974. Vol. 1, 1975.
44. Pang, J.H.L. Lead free solder: Mechanics and reliability. Springer Science & Business Media: 2011.

Paper 4: Development of a unified creep-fatigue equation including heat treatment

Dan Liu * and Dirk John Pons

Department of Mechanical Engineering, University of Canterbury, Christchurch 8140, New Zealand;

*Correspondence: dan.liu@pg.canterbury.ac.nz

Published Paper (Pre-prints for the publication)

Please cite this paper as:

Liu, D. and D.J. Pons, Development of a unified creep-fatigue equation including heat treatment. Fatigue & Fracture of Engineering Materials & Structures, 2018. 41(1): p. 170-182. DOI: http://dx.doi.org/10.1111/ffe.12670.

Abstract

Background – Creep and fatigue damages in metals are known to interact, and then lead to aggregated damage. While models exist for fatigue, creep and creep-fatigue, no models cover all three load regimes. Also, a heat-treatment-related parameter is not well included in most creep-fatigue models. **Need** – There is a need to develop a creep-fatigue equation which covers the full loading regime from pure fatigue to pure creep, and creep-fatigue. Also needed is inclusion of a heat-treatment-related parameter. **Approach** – The unified creep-fatigue equation was started from the Coffin-Manson equation and integrated with the Manson-Haferd parameter. This equation was validated on Inconel 718. **Outcomes** – The method of deriving the coefficients and the formula of the creep function are demonstrated, and the resulting equation shows a good ability to describe the grain-size effect and the fully integrated characteristics. **Originality** - Original contributions of this work are the development of a new formulation to represent creep, fatigue, and creep-fatigue in metals. Also the inclusion of grain size –which is a proxy for heat treatment – in the formulation of this equation and in a proposed modified Manson-Haferd parameter.

Keywords: creep-fatigue, creep rupture, strain-life, grain size

Nomenclature

Pure-fatigue condition: Under pure-fatigue condition, the creep effect is dormant and the damage is totally caused by the fatigue. The loading is completely reversed externally applied stress/strain with no hold (dwell) time.

Pure-creep condition: Under pure-creep condition, the fatigue effect is ignored and the damage is totally caused by the creep. The loading is a constant externally applied stress (with hold or dwell time).

Creep-fatigue condition: Under creep-fatigue condition, the creep effect is active and the damage is caused by the creep and fatigue, and the interaction between them. The loading experienced by the material is reversed loading (per pure fatigue condition), and the elevated temperature provides an additional creep effect even though there is no externally imposed hold (dwell) time.

1. Introduction

Creep-fatigue behaviour is identified as the interaction of pure fatigue and pure creep. The challenge of integrating creep effect into fatigue damage to describe creep-fatigue behaviour has been tried to solve through extending some conventional pure fatigue models, such as the linear damage rule (Eq.1) [1,2], the crack growth law (Eq.2) [3], and the Coffin-Manson equation (Eq.3) [4,5]:

$$\mathrm{D} = \sum_{\mathrm{i}=1}^{\mathrm{k}} \frac{\mathrm{n_i}}{\mathrm{N_i}} \tag{1}$$

$$\frac{da}{dN} = C\left(\Delta J_{eff}\right)^{l} \tag{2}$$

$$\frac{\Delta\varepsilon_p}{2} = \varepsilon_f'\left(2N_f\right)^{\beta} \tag{3}$$

where,D is the fatigue damage, $\mathrm{n_i}$ is the number of constant amplitude cycles under the $\mathrm{i^{th}}$ strain/stress range, $\mathrm{N_i}$ is the number of cycles to fatigue failure under the $\mathrm{i^{th}}$ strain/stress range, $\frac{da}{dN}$ is the total crack growth per cycle, ΔJ_{eff} is the effective range of J-integral, C and l are material constants obtained from experiments, $\Delta\varepsilon_p$ is plastic amplitude, ε_f' is fatigue ductility coefficient, β is the fatigue ductility exponent and N_f is cycles to failure.

However, the ignorance of interaction effect between fatigue and creep leads to inaccurate fatigue-life prediction, and the large dependence on curve fitting results in limited application scale. The present work proposes a fully integrated creep-fatigue equation, which provides a

good description of creep effect and covers full range of conditions from pure fatigue to pure creep. In particular, a heat-treatment-related parameter, grain size, is introduced to show the influence of heat treatment on creep-fatigue damage.

2. A brief review of existing creep-fatigue models

With the creep effect, the conventional pure fatigue models are extended into creep-fatigue field. A number of creep-fatigue models have been proposed to integrate the creep damage with fatigue damage. Some of these models are shown below.

2.1 Linear damage rule

The total creep-fatigue damage (Eq.4) [6,7] is defined as the linear summation of pure fatigue damage (Eq.5) [1,2] and pure creep damage (Eq.6) [8]. According to the linear damage summation rule, the engineering structure fails when D equals 1.

$$D = D_f + D_c \tag{4}$$

with

$$D_f = \sum_i \frac{n_i}{N_i} \tag{5}$$

$$D_c = \sum_i \frac{t_i}{t_{R(i)}} \tag{6}$$

where, D is the creep-fatigue damage, D_f is the fatigue damage, D_c is the creep damage, t_i is the duration of creep under the applied stress σ_i at temperature T_i, and $t_{R(i)}$ is the creep-rupture time under the applied stress σ_i at temperature T_i.

Under cyclic loading with a hold period, the creep damage for one cycle (d_c) can be described through a ductility exhaustion method (Eq.7) [9,10]:

$$d_c = \int_0^{t_h} \frac{\dot{\varepsilon}_{in}}{\delta(\dot{\varepsilon}_{in},T)} dt \tag{7}$$

where, t_h is the time of hold period, $\dot{\varepsilon}_{in}$ is the inelastic strain rate and δ is the rupture ductility (strain limit). This method indicates that inelastic strain plays an important role in creep damage, and reflects that failure occurs when the accumulated strain over multiple cycles achieves the strain limit (δ). Considering the high-strain-rate effect at the early stage during the hold period, where less creep damage is produced than the latter portion, a modified ductility exhaustion model was then proposed (Eq.8) [9,10]:

$$d_c = \int_0^{t_h} \left(\frac{1}{\delta(\dot{\varepsilon}_{in},T)} - \frac{1}{\delta_0(T)} \right) \dot{\varepsilon}_{in} dt \tag{8}$$

where, δ_0 is the ductility obtained under a sufficiently high strain rate. In this case, the fatigue damage for one cycle (d_f) (Eq.9) is defined as the reciprocal of the fatigue life under the same loading and zero hold time (N_{f0}).

$$d_f = \frac{1}{N_{f0}} \tag{9}$$

Then, based on the linear damage rule, the creep-fatigue life is given by Eq.10:

$$N_f = \frac{1}{d_c + d_f} \tag{10}$$

However, the linear summation of fatigue damage and creep damage ignores the interaction between fatigue and creep [11,12]. Failures frequently are observed to occur when $D_f + D_c < 1$ [12,13]. This indicates that the additional damage cause by the interaction between fatigue and creep (D_{cf}) should be included in the linear damage rule, and failure occurs when:

$$D_f + D_c + D_{cf} = 1 \tag{11}$$

However, the mathematical expression for D_{cf} is unknown, thus Eq.11 still cannot be used to predict fatigue life.

2.2 Crack growth law

The total crack growth (Eq.12) [14] is calculated through the summation of fatigue crack growth (Eq.13) [3] and creep crack growth (Eq.14) [14]. The failure occurs when the total crack achieve the final crack size.

$$\frac{da}{dN} = \left(\frac{da}{dN}\right)_f + \left(\frac{da}{dN}\right)_c \tag{12}$$

with

$$\left(\frac{da}{dN}\right)_f = C\left(\Delta J_{eff}\right)^l \tag{13}$$

$$\left(\frac{da}{dN}\right)_c = \int_0^{t_h} AC^{*q} dt \tag{14}$$

where, $\frac{da}{dN}$ is the total crack growth per cycle, $\left(\frac{da}{dN}\right)_f$ is the crack growth per cycle due to cyclic load changes, $\left(\frac{da}{dN}\right)_c$ is the crack growth per cycle due to hold time, t_h is the hold time, C^* is the time-dependent fracture parameter, and A and q are material constants obtained from experiments.

The limitation of the crack growth law is the lack of knowledge of the interaction between fatigue and creep. For the interaction effect between fatigue and creep it has been proposed [15,16] that the total crack growth takes the form:

$$\frac{da}{dN} = \left(\frac{da}{dN}\right)_f + \left(\frac{da}{dN}\right)_c + \left(\frac{da}{dN}\right)_{cf} \quad (15)$$

where, $\left(\frac{da}{dN}\right)_{cf}$ is the crack growth caused by the interaction effect between fatigue and creep. However, Eq.15 cannot be used to predict fatigue life because of the unknown mathematical expression for $\left(\frac{da}{dN}\right)_{cf}$.

2.3 The Coffin-Manson-based creep-fatigue models

2.3.1 The presentation of the Coffin-Manson-based creep-fatigue models

The extension of the Coffin-Manson equation is conducted by a number of researchers. The first attempt was made by Coffin [17], who proposed the frequency-modified Coffin-Manson equation (Eq.16):

$$\varepsilon_p = C\left(N_f f^{k-1}\right)^{-\beta_0} \quad (16)$$

where, f is the frequency and k is a constant obtained from experiments. In this equation, the fatigue life is modified by the frequency-related component, and is named as frequency-modified fatigue life.

Then, this frequency-modified Coffin-Manson equation (Eq.16) is further modified through incorporating the influence of temperature on creep-fatigue behaviours.

For example, Solomon [18] proposed a creep-fatigue model (Eq.17) for the Sn40Pb solder:

$$\varepsilon_p = C_1(T)\left(N_f f^{k-1}\right)^{-\beta_0} \quad (17)$$

with

$$C_1(T) = 1.338 - 2\times10^{-4}T - 1\times10^{-5}T^2 - 2\times10^{-7}T^3 \quad (18)$$

where T is the temperature, β_0=0.5, and k is the constant and related to the frequency: k=-0.42 for $6\text{x}10^{-5}\text{Hz} \le f \le 3\text{x}10^{-4}\text{Hz}$ and k=-0.84 for $3\text{x}10^{-4}\text{Hz} \le f \le 0.3\text{Hz}$.

In addition, Shi et al. [19] expressed a creep-fatigue relation (Eq.19) for the Sn37Pb solders:

$$\varepsilon_p = C_2(T)\left[N_f f^{k(T)-1}\right]^{-\beta_0(T)} \quad (19)$$

with

$$\begin{gathered} C_2(T) = 2.122 - 3.57\times10^{-3}T + 1.329\times10^{-5}T^2 - 2.502\times10^{-7}T^3 \\ \beta_0(T) = 0.731 - 1.63\times10^{-4}T + 1.392\times10^{-6}T^2 - 1.151\times10^{-8}T^3 \\ k_1(T) = 0.919 - 1.765\times10^{-4}T - 8.634\times10^{-7}T^2 \\ k_2(T) = 0.437 - 3.753\times10^{-4}T - 8.04\times10^{-7}T^2 \end{gathered} \quad (20)$$

where $k_1(T)$ and $k_2(T)$ are the frequency-exponent functions for 10^{-3}Hz <f <1Hz and 10^{-4}Hz <f < 10^{-3}Hz, respectively.

Not all strain-life-based creep-fatigue models follow the pattern of frequency-modified Coffin-Manson equation. For example, Jing et al. proposed a temperate-modified Coffin-Manson equation (Eq.21) [20], where the coefficient and exponent of the Coffin-Manson equation are functions of temperature.

$$\frac{\Delta\varepsilon_p}{2} = C_3(2N_f)^{\beta} \tag{21}$$

with

$$\begin{aligned} C_3 &= 68.79 - 0.34T + 250.56/\sqrt{T} \\ \beta &= 1.29 - 0.0053T + 2.5/\sqrt{T} \end{aligned} \tag{22}$$

With the influence of both temperature and frequency on the creep fatigue, the creep-fatigue model (Eq.23) [21] proposed by Engelmaier presents a linear relation between the fatigue ductility exponent and temperature, and a logarithmic relation between the fatigue ductility exponent and frequency.

$$\varepsilon_p = C_4 N_f^{-\beta_0(\bar{T},f)} \tag{23}$$

with

$$\beta_0(\bar{T},f) = 0.442 + 6\times10^{-4}\bar{T} - 1.74\times10^{-2}\ln(1+43200f) \tag{24}$$

where, $\bar{T}$ is the mean temperature and f is the cyclic frequency ($1 \le f \le 1000$ cycles/day).

In addition, Wong & Mai represented a unified creep-fatigue equation (Eq.25) [22]:

$$\varepsilon_p = C_0 s(\sigma) c(T,f) N_f^{-\beta_0 b(T,f)} \tag{25}$$

with

$$\begin{aligned} s(\sigma) &= \begin{cases} 1 & when\ creep\ is\ dormant \\ exp\left[-\left(\sigma_{yield}\varepsilon_p^{n'}\right)/A\right] & when\ creep\ is\ active \end{cases} \\ c(T,f) &= 1 - c_1(T - T_{ref}) - c_2\log(f/f_{ref}) \\ b(T,f) &= 1 - b_1(T - T_{ref}) - b_2\log(f/f_{ref}) \end{aligned} \tag{26}$$

where, n' is cyclic hardening index; A, c_1, c_2, b_1 and b_2 are positive constants; T_{ref} is the reference temperature below which creep becomes dormant and f_{ref} is the reference frequency above which creep becomes dormant.

2.3.2 Limitations of the Coffin-Manson-based creep-fatigue equation

A good creep-modified strain-life equation should cover the full range of conditions from pure-fatigue condition to pure-creep-rupture condition. However, the Coffin-Manson-based creep-fatigue models shown above cannot totally present this characteristic (Table 1).

Table 1 The ability of the Coffin-Manson-based creep-fatigue models to cover the full range of conditions

Creep-fatigue equation	Pure-fatigue condition	Creep-fatigue condition	Pure-creep condition
Coffin equation (Eq.16)	X	√	X
Solomon equation (Eq.17)	X	√√	X
Shi equation (Eq.19)	X	√√	X
Jing equation (Eq.21)	X	√	X
Engelmaier equation (Eq.23)	√	√	X
Wong & Mai equation (Eq.25)	√√	√√	X

√√: This equation can well describe the phenomena of this condition
√: This equation can partly describe the phenomena of this condition
X: This equation cannot describe the phenomena of this condition

The creep-fatigue equation should accommodate relevant variables, including temperature and frequency, this has been well-presented in creep-fatigue models proposed by Solomon, Shi et al., and Engelmaier and Wong & Mai. However, the influence of temperature is not presented in the Coffin equation and the influence of frequency is not shown in the Jing equation. Although the temperature and frequency are accommodated in Engelmaier equation, the possibility of inaccurate fatigue-life prediction could result from the constant coefficient (C_4), which implies that the plastic strains at different conditions share the same value (C_4) when $N_f = 1$.

The condition of pure fatigue is presented by letting $C_1(T)f^{\beta(1-k)} = C_0$ (C_0 is the ductility coefficient at pure-fatigue condition) for the equation of Solomon, and $C_2(T)f^{\beta[1-k(T)]} = C_0$ for the equation of Shi et al. When the extreme frequency is imposed, $f \to \infty$, the functions $C_i(T)$ become infinitely small, which causes $T \to \infty$. This does not agree with the general understanding of pure fatigue, where the creep effect should be dormant. However, the pure-fatigue condition can be well presented in the Wong & Mai equation through letting $T = T_{ref}$ and $t = t_{ref}$.

The condition of pure creep is presented by letting ε_p=0. This condition cannot be satisfied by the equation of Coffin, because the coefficient C and exponent β_0 are constant, which leads to impossible zero frequency. In addition, for the equation of Engelmaier, the pure creep condition is satisfied by letting $\beta_0(\bar{T}, f)\rightarrow+\infty$, which implies $T\rightarrow+\infty$. The pure creep condition for the equations of Solomon, Shi et al. and Jing et al. is satisfied by letting C_1=C_2=C_3=0, which returns T=172 ºC, 198 ºC and 249 ºC respectively. The equations of Solomon and Jing et al. implies that creep rupture only occur when the temperature closes to melting temperature (186ºC for 60Sn40Pb solder and 280 ºC for 80Au/20Sn solder), while the equation of Shi at el. suggests that creep rupture only occurs above melting temperature (183ºC). The creep activation temperatures obtained from these three creep-fatigue equations do not agree with general understanding of creep, where creep is typically active at 35% of melting temperature for metals [23]. Furthermore, the Wong & Mai equation cannot present the pure creep condition entirely. This is because letting $s(\sigma)c(T_R, f_R) = 0$ at pure creep condition cannot deduce any well-known time-temperature parameters, such as the Larson-Miller parameter [24], the Sherby-Dorn parameter [25] or the Manson-Haferd parameter [26].

Besides the limitations for linear damage rule, crack growth law and the Coffin-Manson-modified creep-fatigue equations mentioned above, the lack of heat-treatment-related parameter is another limitation. Generally, several metallurgical factors, such as grain size and precipitation size & shape, are involved, but the causality to fatigue and creep properties is poorly understood. From an engineering perspective, a general heat-treatment-related parameter for metals is the grain size. This parameter is known to be associated with fatigue and creep phenomena at the microstructure scale. Although the research relating the influence of grain size on creep and fatigue has been conducted [27-29], this parameter is not included in the creep-fatigue models shown in section 2.1, 2.2 and 2.3.

There is a need to develop a creep-fatigue equation that can incorporate the interaction effect between pure fatigue and pure creep, cover the full range of phenomena from pure fatigue to pure creep rupture, and show the influence of heat treatment on creep fatigue. To make this problem tractable, the present work uses grain size as the key parameter, while acknowledging that this is a simplification of a deeper and more complex set of heat treatment phenomena.

3. Research method

This work is the further development of the creep-fatigue equation [30,31], and aims to present the influence of heat treatment on creep fatigue and cover the full range of conditions from pure fatigue to pure creep.

The creep-fatigue equation shown in previous research [30,31] was started from the Coffin-Manson equation, then was extended to creep-fatigue condition by integrating creep damage. The parameters of temperature, cyclic time and applied loading were introduced to describe the action of creep, but the heat-treatment effect was not included. Therefore a heat-treatment-related parameter, grain size, is introduced to build the unified creep-fatigue equation. Through

assuming fatigue capacity is consumed by creep effect, a creep modifying function, $c(\sigma, T, t_c, d)$, is proposed to describe the reduction of fatigue capacity. This specific formulation for this c function is based on a linear relationship between temperature and the log of the cyclic time, and a power-law expression of grain size. The resulting formulation (Eq.31) has capability to model pure fatigue, creep fatigue and pure creep rupture.

This unified creep-fatigue equation is then validated on Inconel 718 in section 5.1. The experimental data, including creep-rupture data, creep-fatigue data and stress-strain data, were extracted from the literature. The coefficients of this creep-fatigue equation were derived through both experimental data and numerical method. Then, another group of creep-fatigue data was used to further evaluate this unified creep-fatigue equation through identifying the difference between experimental data and computed data. Supported by the results, this equation provides an excellent representation of creep fatigue behaviours and shows a fully integrated characteristic, and the method of extracting the coefficients is demonstrated.

4. Unified creep-fatigue equation

4.1 Development of the unified creep-fatigue equation

As shown in previous research [30,31], the fatigue capacity is reduced by creep effect, and the reduced fatigue capacity is assumed as:

$$\varepsilon_p = c(\sigma, T, t_c)\varepsilon_{p,ref} = C_0 c(\sigma, T, t_c) N^{-\beta_0} \tag{27}$$

with

$$c(\sigma, T, t_c) = 1 - c_1(\sigma)\left(T - T_{ref}\right) - c_2(\sigma)\log\left(t_c/t_{ref}\right) \tag{28}$$

where $\varepsilon_{p,ref}$ is the full fatigue capacity, ε_p is the reduced fatigue capacity, $c(\sigma, T, t_c)$ is the creep modifying function, and functions $c_1(\sigma)$ and $c_2(\sigma)$ are the stress functions related to creep.

The underlying principle of this formulation is that the material has a fatigue capacity $C_0 N^{-\beta_0}$, which is reduced by creep where the effect is assumed to be a multiplicative factor. The creep factor $c(\sigma, T, t_c)$ is a further function of thermal creep and cyclic loading time. The thermal creep is modelled as a linear dependency on the nominal applied stress and the temperature above a critical temperature, $c_1(\sigma)\left(T - T_{ref}\right)$. In a way, this assumes that stress and temperature contribute independently to the flow of material at the microstructural level. This flow occurs primarily as movement of grains along their boundaries, and it is reasonable to expect that such flow will be proportional to the shear stress (hence a function of σ), and the strength of the bonds will decrease linearly with temperature above a threshold.

The cyclic loading time is also modelled as reducing the capacity of the material. This is formulated as a dependency on the nominal applied stress σ and a log of the cycling time, hence

$c_2(\sigma)\log(t_c/t_{ref})$. The logarithmic relationship comes from the Manson-Haferd parameter, where a linear relation is shown between the log of time and temperature. In this way, the Manson-Haferd parameter is introduced into the creep-fatigue equation. This is a key characteristic for function $c(\sigma, T, t_c)$, because the introduction of the Manson-Haferd parameter gives this creep-fatigue equation (Eq.27) a possible ability to present a well-known time-temperature relation.

The next step is to extend the model by adding the heat-treatment-related parameter, grain size (d), into the creep-fatigue equation. The relationships between fatigue damage and grain size, and between creep damage and grain size are represented through Hall-Petch equation (Eq.29) [32,33] and general creep equation (Eq.30) [6] respectively.

$$\sigma_s = \sigma_0 + \frac{k}{\sqrt{d}} \tag{29}$$

$$\dot{\varepsilon} = \frac{A\sigma^m}{d^q} e^{-\frac{Q}{RT}} \tag{30}$$

where, σ_s is the fatigue strength, σ_0 and k are constants, $\dot{\varepsilon}$ is the strain rate, σ is the applied stress, d is the average grain size, Q is the activation energy, T is the temperature, R is the Boltzmann's constant, and A, m and q are constants obtained from creep test.

Consider the fatigue effect (Eq.29). Reformatting this to show the reduction in fatigue capacity as $\sigma_s - \sigma_0 = \frac{k}{\sqrt{d}}$, then it is evident that this shows a power-law relation with grain size. Likewise the creep effect (Eq. 30) may also be reformulated as a power-law effect. In addition, this power-law relation is also shown by Korth [34] for the creep-fatigue condition. These relationships are then expresses as grain-size-related modifying functions, $B\left(d/d_{ref}\right)^n$ for fatigue effect and $A\left(d/d_{ref}\right)^m$ for creep effect.

Then, the unified creep-fatigue equation is given as:

$$\varepsilon_p = C_0 b(d) c(\sigma, T, t_c, d) N^{-\beta_0} \tag{31}$$

with

$$c(\sigma, T, t_c) = 1 - \left[c_1(\sigma)\left(T - T_{ref}\right) + c_2(\sigma)\log\left(t_c/t_{ref}\right)\right] \cdot \left[A\left(d/d_{ref}\right)^m\right] \tag{32}$$

$$b(d) = B\left(d/d_{ref}\right)^n \tag{33}$$

where, A, B, m and n are grain-size-related constants.

However a further modification is in order. Function $b(d)$ is defined as a grain-size moderating function for pure fatigue condition. However, the research on the relation between grain size and fatigue life [35,36] shows that grain size has only a slight influence on pure fatigue damage. Therefore, for the reason of simplification, function $b(d)$ is removed from Eq.31.

Then, the unified creep-fatigue equation is regenerated as:

$$\varepsilon_p = C_0 c(\sigma, T, t_c, d) N^{-\beta_0} \tag{34}$$

with

$$c(\sigma, T, t_c) = 1 - \left[c_1(\sigma)\left(T - T_{ref}\right) + c_2(\sigma)\log\left(t_c/t_{ref}\right)\right] \cdot \left[A\left(d/d_{ref}\right)^m\right]$$

$$T - T_{ref} = \begin{cases} T - T_{ref} & for \quad T \geq T_{ref} \\ 0 & for \quad T \leq T_{ref} \end{cases} \tag{35}$$

$$t_c/t_{ref} = \begin{cases} t_c/t_{ref} & for \quad t_c \geq t_{ref} \\ 1 & for \quad t_c \leq t_{ref} \end{cases}$$

Briefly, this equation has capability to model pure fatigue at $c(\varepsilon_p,T,t_c)$=1, model pure creep rupture at $c(\varepsilon_p,T,t_c)$=0, and model creep-fatigue damage at $0 \leq c(\varepsilon_p,T,t_c) \leq 1$. This characteristic will be discussed in section 6.1.

4.2 The derivation of coefficients

The pure creep condition ($\varepsilon_p = 0$) gives the formulas of constant c_2 through letting $T=T_{ref}$, and gives function $c_1(\sigma)$ through letting $t_R=t_{ref}$ and introducing the Manson-Haferd parameter [30]:

$$c_2 = \frac{1}{\log(t_a/t_{ref})} \tag{36}$$

$$c_1(\sigma) = -\frac{c_2}{P_{MH}(\sigma)} \tag{37}$$

The research conducted by Gary [37] shows that the stress vs. creep rupture time curves under cyclic loading lie above the curves under constant loading. This implies that, compared to constant stress, higher cyclic stress is required to obtain the same rupture time. Because the function $c_1(\sigma)$ is related to the time-temperature relation (the Manson-Haferd parameter), the creep effect is enlarged when the cyclic stress is imposed. Therefore, it is reasonable to introduce a moderating factor, f_{m}, to compress the cyclic stress to an equivalent constant stress. This has be verified in previous research for solder and stainless steel [30,31]. This moderating factor is related to the shape of the loading wave, and can be defined as the average level of the cyclic loading to show an equivalent transformation from the cyclic loading to constant loading at the same time period. Illustratively, the area below the contour of the cyclic loading along the time dimension should be equal to area below the contour of the equivalent constant loading at the same time period. In particular, for a cyclic loading given by a function, $f(t)$, the equivalent constant loading is represented as Eq.38:

$$f_m = \frac{2\int_0^{t_c/2} f(t)dt}{t_c \cdot \sigma_{max}} \tag{38}$$

Eq.38 is built on an assumption that the creep effect in the tensile portion is the same as in the compressive portion, thus moderating factor (f_m) is evaluated based on half-cycle loading. Although this assumption may be not appropriate for some materials [38,39], it could simplify the method of extracting the moderating factor, which is important for engineering design.

With this moderating factor, function $c_1(\sigma)$ is converted to $c_1(f_{\mathrm{m}}\sigma)$. Then, the stress is converted into plastic strain through cyclic strain-stress relation for the reasons of expressing creep damage from the strain perspective and keeping the consistent with the Coffin-Manson equation. This transformation gives:

$$c_1(\sigma) = -\frac{c_2}{P_{MH}(\sigma)} = -\frac{c_2}{P_{MH}[f_{\mathrm{m}}\cdot K(T,t_c)\cdot {\varepsilon_P}^{n(T,t_c)}]} \tag{39}$$

where, $K(T,t_c)$ and $n(T,t_c)$ are the strength coefficient and strain hardening exponent respectively, and they are functions of temperature and cyclic time. It may also be said that the influence of temperature and cyclic time on material properties is presented through functions $K(T,t_c)$ and (T,t_c) . The derivation of the functions $c_1(\sigma)$ and $c_2(\sigma)$ is based on the experimental data of creep-rupture test and cyclic deformation tests.

The numerical method is used to obtain the magnitudes of C_0, β_0, A and m through minimizing the difference (Eq.40) between the computed creep-fatigue life ($N_{comp,ij}$) and experimental creep-fatigue life ($N_{exp,ij}$) at the conditions of $\varepsilon_{p,j}$, T_i and $t_{c,i}$.

$$error = \sum \left(\log N_{comp,ij} - \log N_{exp,ij}\right)^2 \tag{40}$$

with

$$N_{comp,ij} = \left\{\frac{\varepsilon_{pi}}{C_0 c[\varepsilon_{pi},K(T,t_c),n(T,t_c),(T,t_c)_j]}\right\}^{-1/\beta_0} \tag{41}$$

4.3 The evaluation of the unified creep-fatigue equation

The evaluation is processed through transforming the creep-fatigue data into reference condition, and this transformation is conducted by using Eq.42:

$$\varepsilon_{p,ref} = C_0 N^{-\beta_0} = \varepsilon_p / c(\sigma, T, t_c, d) \tag{42}$$

An effective description of creep effect can cause all transformed creep-fatigue data collapse into a single power-law curve with good quality, and the coefficient and exponent of this trend line can agree well with C_0 and β_0 respectively. Supported by the coefficients obtained from experimental data and numerical method, the fully integrated creep-fatigue equation is used to calculate the fatigue life at other situations. This results then are compared with the experimental data to further evaluate this creep-fatigue equation.

5. Validation on Inconel 718

The experimental creep-fatigue data, strain-stress data [40,41] and creep-rupture data [42] for Inconel 718 are used to validate and evaluate the fully integrated creep-fatigue equation. The creep-fatigue tests were conducted under cyclic loading without hold time. The reference temperature is defined as 35% of melting temperature, and the cyclic time is suggested as a

small value. The creep damage is assumed to be active above the reference temperature and the reference cyclic time. In addition, the reference grain size is arbitrarily selected based on the experimental range for the material, and should be consistent for all tests in the material family. Therefore, the reference temperature is chosen as 650K, the reference cyclic time is chosen as 1s, and the reference grain size is chosen as 30μm.

5.1 The derivation of the coefficients

The creep-rupture data are extracted from the Table 2 of ref.38, and the data points (log t_r, T) at different stresses are plotted in Figure 1. The point of convergence (T_{ref}, log t_a), is evaluated as (650 K, 10.539), thus,

$$c_2 = \frac{1}{\log(t_a/t_{ref})} = \frac{1}{\log(10^{10.539}/1)} = 0.09444 \tag{43}$$

and, the relationship between stress and the Manson-Haferd Parameter is given as:

$$-\frac{1}{P_{MH}(\sigma)} = 5.0517 \times 10^{-2} - 1.0789 \times 10^{-4}\sigma + 9.7143 \times 10^{-8}\sigma^2 \tag{44}$$

Then, substituting into Eq.37, function c_1 is expressed as:

$$c_1(\varepsilon_p) = -\frac{c_2}{P_{MH}(\varepsilon_p)} = 4.7708 \times 10^{-3} - 1.0189 \times 10^{-5} \cdot f_m \cdot K{\varepsilon_p}^n + 9.1742 \times 10^{-9} \cdot {f_m}^2 \cdot \left(K{\varepsilon_p}^n\right)^2 \tag{45}$$

and the magnitude of f_m is given as 0.6366 for the sinusoidal wave and 0.5 for triangular wave.

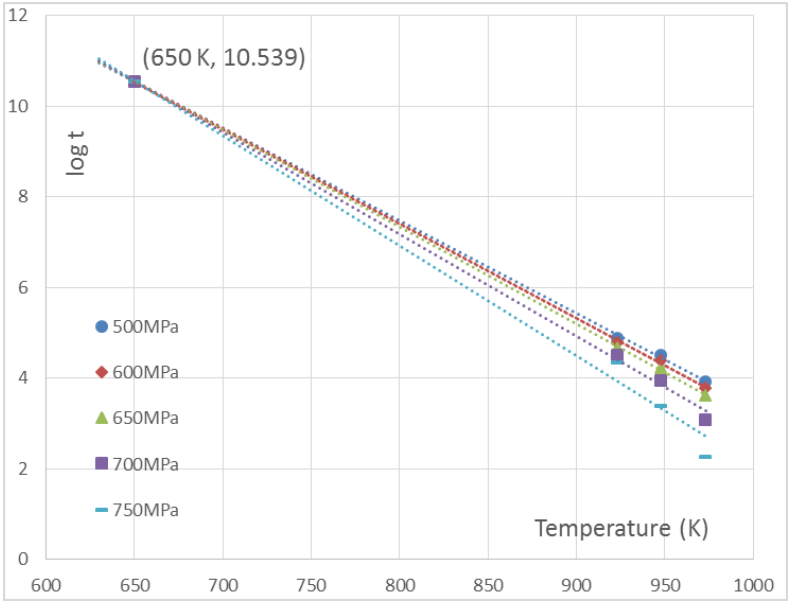

Figure 1 Creep-rupture characteristics of Inconel 718

The creep-fatigue coefficients at four temperatures, two cyclic times and two grain sizes obtained from ref.38 and ref.39 are tabulated in Table 2. Minimizing the difference between

computed creep-fatigue life ($N_{comp,ij}$) and experimental creep-fatigue life ($N_{exp,ij}$) regress that C_o=0.2888, β_o=0.583, A=1.1043 and m=1.3139.

Table 2 The creep-fatigue coefficients obtained from ref.38 and ref.39

Temperature (K)	Cyclic time (s)	Grain size (μm)	Creep-fatigue coefficients		f_m
			ε_f'	β	
823	20	30	0.1642	-0.588	0.6366
873	20	30	0.1581	-0.604	0.6366
700	3	11	0.7877	-0.707	0.6366
811	3	11	0.2545	-0.579	0.6366

5.2 Evaluation of the quality of the fully integrated creep-fatigue equation

With the results obtained in 5.1, the experimental creep-fatigue data, ε_p-N_{exp}, is transformed to reference condition (pure fatigue condition), $\varepsilon_{p,ref}$-N_{exp}, through using Eq.42. Figure 2 shows that the transformed data collapse into a one power-law curve of $\varepsilon_{p,ref} = 0.2626N^{-0.569}$ with the quality of fit as R^2= 0.9765. The coefficients of this trend line, C_o=0.2626 and β_o=0.569, very close to the results obtained in section 5.1. The error, which shows the difference between experimental fatigue life and computed fatigue life, is given as 0.1037 through using Eq.40.

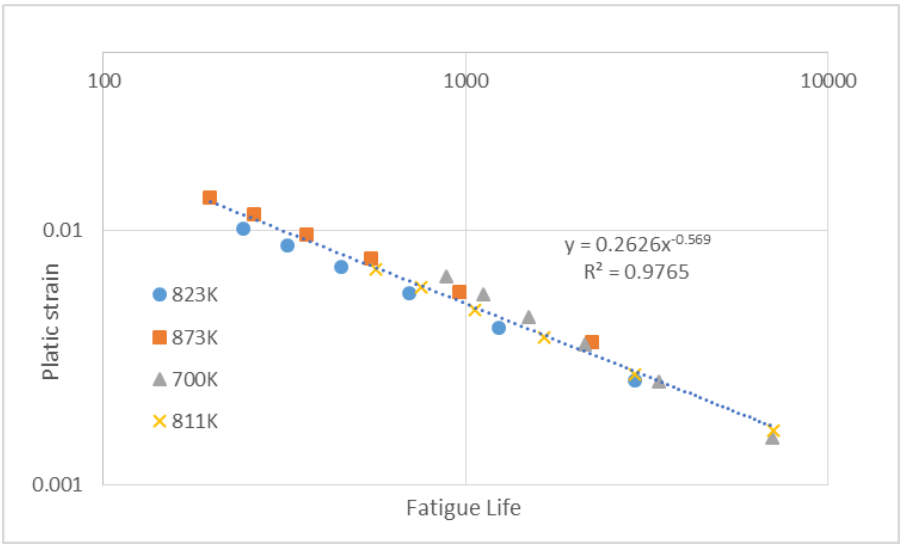

Figure 2 The transformed $\varepsilon_{p,ref}$-N_{exp} data of Inconel 718

To further evaluate the fully integrated creep-fatigue equation, another group of creep-fatigue data (Table 3) [40,43] are used to compare with computed fatigue life which is supported by the results shown in section 5.1. Figure 3 shows that the points of computed fatigue life vs. experimental fatigue life fall within the upper bound (+20%) and the lower bound (-20%).

Table 3 The creep-fatigue coefficients obtained from ref.38 and ref.41

Temperature (K)	Cyclic time (s) Or Strain rate (1/s)	Grain size (μm)	Creep-fatigue coefficients		f_m
			ε_f'	β	
823	Cyclic time: 200	30	0.3703	-0.640	0.6366
894	Strain rate: 0.004	22	0.351	-0.696	0.5
922	Strain rate: 0.004	22	0.0941	-0.546	0.5

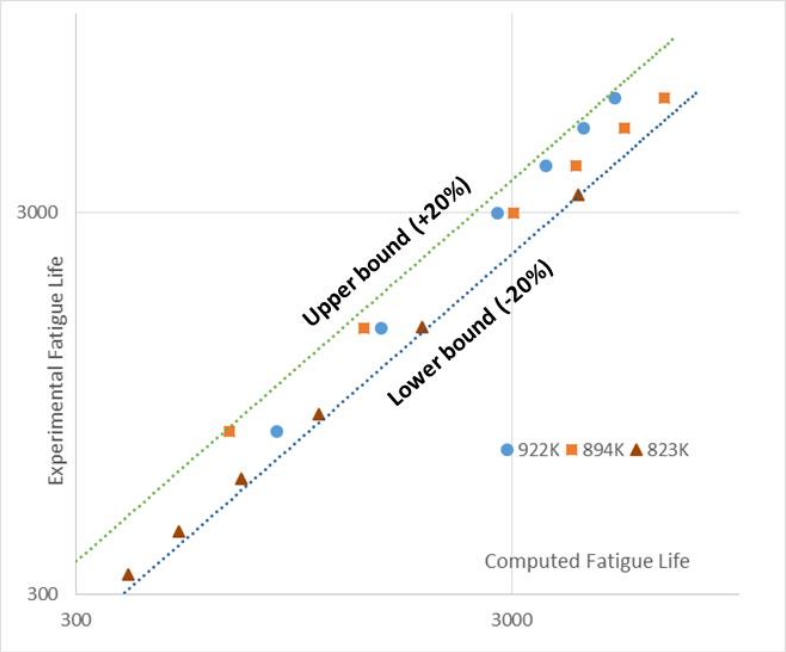

Figure 3 Computed fatigue life vs. experimental fatigue life for Inconel 718. The results show a relatively high correlation between computed and experimental fatigue life: all the data points are within 20% above and below (dotted lines) the ideal correlation.

The results presented above verify the method of extracting coefficients, suggest a good consistency with reference condition, and show that the unified creep-fatigue equation can provide a good description of creep effect through creep function $c(\varepsilon_p, T, t_c, d)$ and a good prediction of creep-fatigue life.

5.3 The reference grain size

The method of extracting function $c_1(\varepsilon_p)$ and constant c_2 is based on the assumption that grain-size component, $A(d/d_{ref})^m$, equals 1. With this assumption, the coefficients of grain-size component at four different reference grain sizes are calculated (Table 3).

The results shown in Table 4 suggest that constant A is strongly influenced by the choice of reference grain size, but both *m* and *d* are independent of reference grain size. This provides an opportunity to reduce the number of coefficients of the unified creep-fatigue equation. If the reference grain size is chosen as 27.82, the magnitudes of *A* and *m* are given as 1 and 1.314 respectively. This suggests that constant *A* could be removed from the unified creep-fatigue equation only when reference grain size is identified as 27.82.

Table 4 the coefficients of grain-size component

d_{ref}	A	m	$d = d_{ref}\sqrt[m]{1/A}$
10	0.260732	1.313872	27.8189
25	0.869030	1.313964	27.8188
40	1.611380	1.313609	27.8181
60	2.743848	1.313049	27.8165

From this we extract the more general implication that other materials may have a reference grain size that also gives A = 1. It appears that, for a given material, m is independent of the reference grain size and the value of A. This is a reasonable phenomenon, where the intensity of grain-size effect on creep remains constant regardless of the choice of reference grain size. In general the reference grain size may be defined as the grain size for creep rupture tests.

However, the reference temperature and the reference time do not share the same feature as the reference grain size, because the creep is assumed to be dormant below the reference temperature and the reference cyclic time. Therefore, the influence of temperature and cyclic time on creep effect has strong dependence on the choice of the reference temperature and the reference cyclic time.

6. Discussion

6.1 The fully integrated characteristics

The fully integrated characteristics refers that this unified creep-fatigue equation can cover the full range of conditions from pure fatigue to pure creep.

Pure fatigue

At pure fatigue condition, creep is dormant, and $T = T_{ref}$ and $t_c = t_{ref}$. This suggests that function $c(\varepsilon_p, T, t_c, d)$ equals 1; then, the fully integrated creep-fatigue equation is restored to the Coffin-Manson equation (Eq.3). The good consistency between the coefficients obtained from curve fitting (Figure 2) and the coefficients obtained from numerical solution has strongly verified the restoration of the creep-fatigue equation at pure fatigue condition.

Pure creep

At pure creep condition, fatigue effect is small enough to be ignored, and ε_p=0. Then, the function $c(\varepsilon_p, T, t_c, d)$ is expressed as Eq.46:

$$\left[c_1(\varepsilon_p)(T - T_{ref}) + c_2 \log(t_c/t_{ref})\right] \cdot \left[A(d/d_{ref})^m\right] = 1 \tag{46}$$

Through substituting Eq.36 and Eq.37 into Eq.46, the fully integrated creep-fatigue equation is simplified to a Manson-Haferd-type parameter:

$$P_{MH}(\sigma, d) = \frac{T_{ref} - T}{A(d/d_{ref})^m \log t_a - \log \mathrm{t} + \left[1 - A(d/d_{ref})^m\right] \log t_{ref}} \tag{47}$$

This parameter is named the *grain-size-modified Manson-Haferd Parameter*, and can be restored to the original Manson-Haferd Parameter through letting $A(d/d_{ref})^m = 1$. This implies that the fully integrated creep-fatigue equation can be converted to a well-known time-temperature relation to describe creep behaviours at pure-creep condition.

As this shows, the formulation (Eq. 34) reduces to the Manson-Haferd expression for pure creep, but with the addition of an optional grain-size parameter.

Combined creep and fatigue

Between pure fatigue condition and pure creep condition, the creep-fatigue condition is presented through letting $0< c(\varepsilon_p, T, t_c, d)<1$. This condition has been validated in section 5.2, where the transformed creep-fatigue data can be collected into a single power-law curve by using transforming equation (Eq.40) with minimum error.

These three conditions can be connected through the concept of fatigue capacity to represent the fully integrated characteristics. To be specific, the plastic strain at pure fatigue condition ($\varepsilon_{p,ref}$) is given through Eq.40, this presents the full fatigue capacity. With the influence of creep effect, the plastic strain (ε_p) obtained through Eq.34 gives the residual fatigue capacity (the creep-fatigue condition), and the reduction of fatigue capacity ($\varepsilon_{p,ref} - \varepsilon_p$) results from the consumption of creep effect. Then, with the increasing influence of creep effect, the total fatigue capacity is further consumed. Finally, the fatigue capacity is totally consumed by creep effect, and the creep-fatigue condition comes to the pure creep condition. This process is shown in Figure 4.

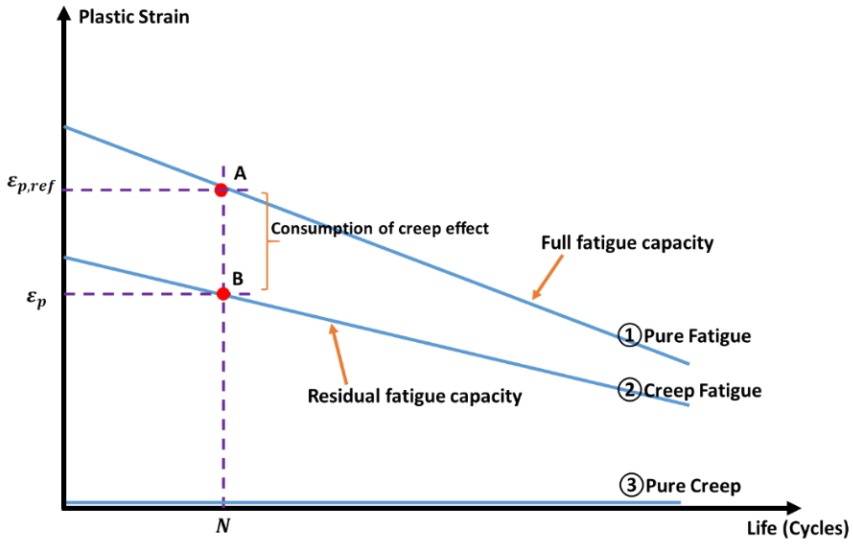

Figure 4 The description of the fatigue capacity

6.2 The consistency between the formulation and the physical meaning

In the creep-fatigue condition, the failure mode is occurring by multiple mechanisms, and this combined damage is described by the creep function $c(\varepsilon_p, T, t_c, d)$ through introducing grain size, the Manson-Haferd parameter, and the reference condition.

6.2.1 The introduction of grain size

The fatigue effect occurs via cracks through the grains [6,44], smaller grain size enhances fatigue capacity from the pure-fatigue perspective. While, the creep effect involves the grain boundary cracking [6,44], bigger grain size is more beneficial for creep, and results in longer rupture time. It seems that the influences of grain size on fatigue and creep are contrary, and the combined effect between fatigue and creep on the creep-fatigue life is determined by the proportion of fatigue contribution and creep contribution [28].

The grain-size component, $A(d/d_{ref})^m$, shows that, for a given fatigue life, the bigger grain size leads to smaller fatigue capacity under cyclic loading without hold time. This is consistent with the results shown by Hatanaka & Yamada [27], Hattori et al. [28] and Pieraggi & Uginet [29], where the fatigue strength (fatigue capacity) reduces with the increasing grain size. This implies that the fatigue effect makes more contribution to creep-fatigue damage than creep effect in the creep-fatigue condition under the zero-hold-time cyclic loading. This may be because that the total time to failure is too small to produce major creep damage in the low-cycle regime.

6.2.2 The introduction of time-temperature parameter

Function $c(\varepsilon_p, T, t_c, d)$ is named as the *creep function*, because it accommodates creep-rupture characteristics. To be specific, this function shows a linear relation between temperature and log of cyclic time, which is consistent with the relationship shown in the Manson-Haferd parameter. In particular, this parameter is mathematically represented through letting $c(\varepsilon_p, T, t_c, d) = 0$ at pure creep condition. This implies that there is a strong relation between function *c* and creep behaviours, and function *c* presents a link between pure creep and creep fatigue. In addition, the Manson-Haferd parameter represents that the creep behaviour is negatively influenced by the increasing temperature and cyclic time, and this is also mathematically presented through the creep function, $c(\varepsilon_p, T, t_c, d)$. The creep damage is intensified through increasing temperature and increasing cyclic time, where the higher temperature provides more energy to overcome the barrier to diffuse, and the longer cyclic time gives creep more time to contribute the damage.

6.2.3 The introduction of reference condition

The reference condition is introduced to show the threshold between pure fatigue and creep fatigue. At the reference condition, the fully integrated creep-fatigue equation is restored to the Coffin-Manson equation, and suggests the full fatigue capacity. Therefore, the introduction of the reference condition builds a bridge between pure fatigue and creep fatigue.

C_0 and β_0 are the presentation of fatigue capacity. C_0 is related to the fatigue ductility, and β_0 represents the material's resistance to fatigue damage. For a given β_0, higher C_0 implies better ability to accept plastic deformation, while, for a given C_0, higher β_0 suggests lower ability to resist fatigue damage.

6.3 Application of the unified creep-fatigue equation

The coefficients of the unified creep-fatigue equation are derived from numerical methods and experiments, including creep-rupture tests, creep-fatigue tests and strain-stress tests. Then, with the creep function, $c(\varepsilon_p, T, t_c, d)$, the raw creep-fatigue data are transformed into the reference condition and are collapsed into a single power-law curve ($\varepsilon_{p,ref}$-N curve). For a given applied plastic strain, the reference plastic strain can be calculated by using Eq.38; then, the corresponding fatigue life can be extracted from $\varepsilon_{p,ref}$-N curve. On the other hand, for a given required fatigue life, the reference plastic strain can be extracted from $\varepsilon_{p,ref} - N$ curve; then the corresponding plastic strain is computed through using Eq.38. In addition, this equation also provides us with a rough way to choose a material for an engineering structure. Specifically, desirable materials for longevity are those with high C_0, low β_0, and small c_1 and d.

6.4 Contributions and limitations

Based on the previous research [30,31], a heat-treatment-related parameter has been introduced to develop the fully integrated creep-fatigue equation, and the method of extracting the

coefficients has been shown in the present work. This is verified through transforming the creep-fatigue condition to the reference condition. In addition, the unified creep-fatigue equation shows a good ability to cover the full range of conditions from pure fatigue to pure creep rupture. Furthermore, this paper proposes a formulation of grain-size-modified Manson-Haferd Parameter. These results have not been shown previously in the literature, and are therefore the novel contributions.

All the creep-fatigue equations in the literature are lacking physical meaning, because they are based on the curve fitting. The present work has slightly reduced this problem, where the unified creep-fatigue equation shows an association with the Manson-Haferd Parameter, and the introduction of the reference condition indicates the threshold of creep-fatigue. However, limitations are that the derivation of the coefficient is based on the combination of experimental data and numerical solution; thus this creep-fatigue equation cannot be fully explained from a physical perspective. In addition, this unified creep-fatigue equation is developed for the situation of zero-hold-time cyclic loading. Therefore, for cyclic loading with hold time the equation may not present a good prediction of fatigue life. These limitations open future research opportunities.

7. Conclusion

The following major results were obtained:

(1) The unified creep-fatigue equation (Eq.34) has been validated on Inconel 718. With the transforming equation (Eq.38), the raw creep-fatigue data is transformed to reference condition, and collapse into a single power-law curve with good quality. This has verified the formula of creep function, $c(\varepsilon_p, T, t_c, d)$, and demonstrated the method of extracting the coefficients.

(2) A heat-treatment-related parameter, grain size, has been successfully introduced in to this creep-fatigue equation (Eq.34). The grain-size-related component describes creep damage through a power-law relation, which is consistent with that relation shown in the general creep equation. A formulation of grain-size-modified Manson-Haferd Parameter (Eq.47) is presented.

(3) The fully integrated characteristics of this creep-fatigue equation have been discussed. Function $c(\varepsilon_p, T, t_c, d)$ implies a link between pure-creep condition and creep-fatigue condition, while, the introduction of reference condition builds a bridge between the pure-fatigue condition and the creep-fatigue condition. However, the derivation of the coefficient is based on the combination of experimental data and numerical method, this means that this creep-fatigue equation cannot be fully explained from a physical perspective.

Original contributions of this work are the development of a new formulation to represent creep, fatigue, and creep-fatigue in metals. Also the inclusion of grain size – which is a proxy for heat treatment – in the formulation of this equation and in a proposed modified Manson-Haferd parameter.

Author Contributions: The work was conducted by DL and supervised by DP. The formula of the unified creep-fatigue equation was proposed and the method of extracting the coefficients was then developed by DL. The discussion on the fully integrated characteristic, reference grain size, the physical meaning and the application was conducted by DL and DP.

Acknowledgement: The author wishes to acknowledge the contribution of Dr. Ee-hua Wong, especially in helping to find the initial form of the creep-fatigue equation which does not accommodate a heat-treatment-related parameter.

Conflicts of Interest: The authors declare no conflict of interest. The research was conducted without personal financial benefit from any funding body, and no such body influenced the execution of the work.

References

1. Miner MA (1945) Cumulative damage in fatigue. J Appl Mech. 12: 159-164.
2. Palmgren A (1924) Die lebensdauer von kugellagern. Z Ver Dtsch Ing. 68: 339-341.
3. Paris P, Erdogan F (1963) A critical analysis of crack propagation laws. J Basic Eng. 85: 528-533.
4. Manson SS (1954) Behavior of materials under conditions of thermal stress. Lewis Flight Propulsion Lab.
5. Coffin Jr LF (1953) A study of the effects of cyclic thermal stresses on a ductile metal. Knolls Atomic Power Lab.
6. Dowling NE (1993) Mechanical behavior of materials: engineering methods for deformation, fracture, and fatigue. Prentice hall.
7. Taira S (1962) Lifetime of structures subjected to varying load and temperature. Creep in structures. Springer, 96-124.
8. Robinson EL (1952) Effect of temperature variation on the long-time rupture strength of steels. Trans ASME. 74: 777-781.
9. Takahashi Y (2008) Study on creep-fatigue evaluation procedures for high-chromium steels—Part I: Test results and life prediction based on measured stress relaxation. International Journal of Pressure Vessels and Piping. 85: 406-422.
10. Takahashi Y, Dogan B, Gandy D (2013) Systematic evaluation of creep-fatigue life prediction methods for various alloys. Journal of Pressure Vessel Technology. 135: 061204.
11. Janson J (1979) Damage model of creep-fatigue interaction. Engineering Fracture Mechanics. 11: 397-403.
12. Mao H, Mahadevan S (2000) Reliability analysis of creep–fatigue failure. Int J Fatigue. 22: 789-797.
13. Deguchi M, Tobe H, Sato E (2016) Damage propagation mechanism in low-cycle creep fatigue of Cu–Cr–Zr alloy. Int J Fatigue. 87: 351-358.
14. Ainsworth R, Ruggles M, Takahashi Y (1992) Flaw assessment procedure for high-temperature reactor components. J Pressure Vessel Technol. 114: 166-170.
15. Liu H, Bao R, Zhang J, Fei B (2014) A creep–fatigue crack growth model containing temperature and interactive effects. Int J Fatigue. 59: 34-42.

16. Xuan F, Tu S, Wang Z (2005) Time-dependent fatigue fracture theory and residual life assessment techniques for defective structures. Chin J Adv Mech. 35: 391-403.
17. Coffin L (1973) Fatigue at high temperature. Fatigue at elevated temperatures. ASTM International.
18. Solomon H (1986) Fatigue of 60/40 solder. IEEE Trans Compon Hybrid Manuf Technol. 9: 423-432.
19. Shi X, Pang H, Zhou W, Wang Z (2000) Low cycle fatigue analysis of temperature and frequency effects in eutectic solder alloy. Int J Fatigue. 22: 217-228.
20. Jing H, Zhang Y, Xu L, Zhang G, Han Y, Wei J (2015) Low cycle fatigue behavior of a eutectic 80Au/20Sn solder alloy. International Journal of Fatigue. 75: 100-107.
21. Engelmaier W (1983) Fatigue life of leadless chip carrier solder joints during power cycling. IEEE Trans Compon Hybrid Manuf Technol. 232-237.
22. Wong E, Mai Y-W (2014) A unified equation for creep-fatigue. Int J Fatigue. 68: 186-194.
23. Ashby MF, Shercliff H, Cebon D (2013) Materials: engineering, science, processing and design. Butterworth-Heinemann.
24. Larson FR, Miller J (1952) A time-temperature relationship for rupture and creep stresses. Trans ASME. 74: 765-775.
25. Dorn J, Orr RL, Sherby O (1954) Creep correlations of metals at elevated temperatures. AIME TRANS. 200: 71-80.
26. Manson S, Haferd A (1953) A linear time-temperature relation for extrapolation of creep and stress-rupture data. Lewis Flight Propulsion Lab.
27. HATANAKA K, YAMADA T (1981) Effect of grain size on low cycle fatigue in low carbon steel. Bull JSME. 24: 1692-1699.
28. Hattori H, Kitagawa M, Ohtomo A (1982) Effect of grain size on high temperature low-cycle fatigue properties of inconel 617. Tetsu To Hagane. 68: 2521-2530.
29. Pieraggi B, Uginet J FATIGUE AND CREEP PROPERTIES IN RELATION.
30. Liu D, Pons D, Wong E-h (2016) The Unified Creep-Fatigue Equation for Stainless Steel 316. Metals. 6: 219.
31. Liu D, Pons D, Wong E-h (2016) Creep-Integrated Fatigue Equation for Metals. Int J Fatigue.
32. Alexandre F, Deyber S, Pineau A (2004) Modelling the optimum grain size on the low cycle fatigue life of a Ni based superalloy in the presence of two possible crack initiation sites. Scr Mater. 50: 25-30.
33. Mutoh Y, Radhakrishnan V (1986) Effect of yield stress and grain size on threshold and fatigue limit. J Eng Mater Technol. 108: 174-178.
34. Korth GE (1991) Effects of various parameters on the fatigue life of alloy 718. EG and G Idaho, Inc., Idaho Falls, ID (USA).
35. Komotori J, Shimizu M (2013) Grain size effect in low cycle fatigue of steel under mean strain. ICF7, Houston (USA) 1989.
36. Thompson AW, Backofen W (1971) The effect of grain size on fatigue. Acta metallurgica. 19: 597-606.
37. Halford G (1972) Cyclic creep-rupture behavior of three high-temperature alloys. Metall Trans. 3: 2247-2256.
38. Tsuno N, Shimabayashi S, Kakehi K, Rae C, Reed R (2008) Tension/compression asymmetry in yield and creep strengths of Ni-based superalloys. Proceedings of the International Symposium on Superalloys, 433-442.
39. Yamashita M, Kakehi K (2006) Tension/compression asymmetry in yield and creep strengths of Ni-based superalloy with a high amount of tantalum. Scripta materialia. 55: 139-142.

40. Fournier D, Pineau A (1977) Low cycle fatigue behavior of Inconel 718 at 298 K and 823 K. Metall Trans A. 8: 1095-1105.

41. Sanders T, Frishmuth R, Embley G (1981) Temperature dependent deformation mechanisms of alloy 718 in low cycle fatigue. Metall Trans A. 12: 1003-1010.

42. Sugahara T, Martinolli K, Reis DA, et al. (2012) Creep Behavior of the Inconel 718 Superalloy. Defect and Diffusion Forum. Trans Tech Publ, 509-514.

43. Song Y, Lee M, Kim J (2005) Effect of grain size for the tensile strength and the low cycle fatigue at elevated temperature of alloy 718 cogged by open die forging press. Superalloys. 718: 625-706.

44. Finnie I, Heller WR (1959) Creep of Engineering Materials.

Paper 5: A unified creep-fatigue equation with application to engineering design

Dan Liu * and Dirk John Pons

Department of Mechanical Engineering, University of Canterbury, Christchurch 8140, New Zealand;

*Correspondence: dan.liu@pg.canterbury.ac.nz

Published Book Chapter (Pre-prints for the publication)

Please cite this paper as:

Liu, D. and D.J. Pons, A unified creep-fatigue equation with application to engineering design, in Creep, T. Tomasz, S. Marek, and A. Zieliński, Editors. 2018, InTechOpen: Rijeka, Croatia. DOI: http://dx.doi.org/10.5772/intechopen.70877

Abstract

Background - Creep-fatigue damage occurs under cyclic loading at elevated temperature, thus is influenced by temperature, frequency and applied loading. The existing creep-fatigue models have limited ability to cover the full combination of creep and fatigue behaviours, except with extensive prior empirical testing. Consequently they cannot effectively and efficiently be used for early engineering design. **Approach** – We present a unified formulation that overcomes these limitations. This is the *strain-based unified creep-fatigue equation*. We validate this equation against empirical data for 63Sn37Pb solder, stainless steel 304, Inconel 718, and GP91 casting steel. We show it is able to represent the creep, fatigue, and creep-fatigue behaviours of these materials. A simplified formulation is developed where the coefficients are extracted through simple creep-rupture tests. Although this degrades the precision somewhat, it significantly reduces the experimental cost, and makes it feasible to apply the equation more widely. We show how the equation may be used in a design situation, by application to a representative gas turbine blisk. Included here is a demonstration of how the equation may be integrated into finite element analysis, which is an important practical consideration in the design work flow. **Outcomes** – The usefulness of the simplified equation is the ability to

identify candidate materials for creep-fatigue loading situations. The ability to achieve this at relatively early design stages based on simple empirical tests, is advantageous because of the economy provided. The results demonstrate that the strain-based unified creep-fatigue equation evidences fidelity to empirical data for a range of creep-fatigue behaviours for multiple metallic materials, and may readily be applied to engineering design.

Keywords: creep fatigue, accuracy, economy, engineering design, turbine blisk

1. Introduction

Creep-fatigue failure results from the interaction of pure fatigue and creep, and is influenced by temperature, frequency and applied loading. The conventional strain-based creep-fatigue equations are quantitatively accurate in narrow areas of application, but suffer from poor ability to generalize to other materials and loading regimes. Consequently those equations are ineffective and inefficient for engineering design. A recent development in the field is a unified formulation of creep-fatigue. The advantages of this unified creep-fatigue equation are that it accommodates the crucial parameters (temperature, frequency and loading), covers different materials, represents the full range of conditions from pure fatigue to pure creep, and is economical in the testing regime to determine coefficients. This chapter describes the unified creep-fatigue equation and applies it to design. The theory can be applied to evaluate the fatigue capacity of candidate materials at the early stages of design.

2. Desirable characteristics of a creep-fatigue method for design

For the perspective of engineering design, the development of a creep-fatigue method should consider following four areas:

(1) Unified characteristic

The unified characteristic is defined as the ability to predict fatigue life for multiple temperatures and cyclic times for multiple materials. In this case, the desirable formulation should accommodate relevant variables (including temperature, cyclic time and applied loading), and should present small difference between predicted life and experimental result under multiple situations.

(2) Integrated characteristic

The integrated characteristic refers to the ability to cover full range of conditions from pure-fatigue condition to pure-creep condition. In this case, the desirable formulation should have

the ability to be transformed to the representations of pure fatigue and pure creep, and the transformed formulations should be consistent with the general understanding of fatigue and creep mechanisms.

(3) Economy

A desirable engineering method for fatigue-life prediction should present good balance between accuracy and economy. The economy of this theory can be assessed by evaluating the life-prediction error with overall experimental cost. Generally, the higher sensitive a numerical formulation has, the more experimental data are needed and the poorer economy is presented.

(4) Applicability to engineering design

An engineering-based creep-fatigue method should be effectively and efficiently applicable to practical design process, where an economical, convenient and accurate method is represented to engineers and designers. Such as, the creep-fatigue evaluation by using this formulation is applied to the initial stage of design to select material or optimize structure.

Overall, a desirable creep-fatigue formulation for engineering design should have unified and integrated characteristics, and present good economy and applicability to practical design.

3. Brief review of existing creep-fatigue models

Creep-fatigue behaviour is generally influenced by temperature and frequency/cyclic time, wherein increasing temperature or decreasing frequency results in reduced fatigue capacity due to intensified creep damage. Normally, the existing creep-fatigue equations were derived from empirical data through curve fitting, and present the extension of the Coffin-Manson equation (Eq.1) [1,2]:

$$\Delta\varepsilon_p/2 = \varepsilon_f'\left(2N_f\right)^{\beta} \tag{1}$$

where $\Delta\varepsilon_p$ is the plastic amplitude, ε_f' is the fatigue ductility coefficient, β is the fatigue ductility exponent and N_f is the cycles to failure. The development of creep-fatigue model was firstly attempted by Coffin, who proposed the frequency-modified Coffin-Manson equation (Eq.2) [3]:

$$\varepsilon_p = C\left(N_f f^{k-1}\right)^{-\beta_0} \tag{2}$$

where f is the frequency, and k is a constant obtained from experiments and is given different values for different temperatures (temperature dependency is indirectly introduced). Then, through directly integrating with temperature dependence, the frequency-modified Coffin-Manson equation (Eq.2) was further developed to show the combined influence of temperature on creep fatigue. For example, Solomon proposed a creep-fatigue equation (Eq.3) [4] for Sn40Pb solder:

$$\varepsilon_p = C_1(T)\left(N_f f^{k-1}\right)^{-\beta_0} \quad (3)$$

with

$$C_1(T) = 1.338 - 2\times10^{-4}T - 1\times10^{-5}T^2 - 2\times10^{-7}T^3$$

where T is the temperature, β_0=0.5, and k is the constant and related to the frequency: k=-0.42 for 6X10^{-5}Hz ≤f ≤ 3X10^{-4}Hz and k=-0.84 for 3X10^{-4}Hz ≤f ≤ 0.3Hz. In addition, based on the creep-fatigue tests on 63Sn37Pb solder, Shi et al. presented a creep-fatigue formulation (Eq.4) [5]:

$$\varepsilon_p = C_2(T)\left[N_f f^{k(T)-1}\right]^{-\beta_0(T)} \quad (4)$$

with

$$C_2(T) = 2.122 - 3.57\times10^{-3}T + 1.329\times10^{-5}T^2 - 2.502\times10^{-7}T^3$$
$$\beta_0(T) = 0.731 - 1.63\times10^{-4}T + 1.392\times10^{-6}T^2 - 1.151\times10^{-8}T^3$$
$$k_1(T) = 0.919 - 1.765\times10^{-4}T - 8.634\times10^{-7}T^2$$
$$k_2(T) = 0.437 - 3.753\times10^{-4}T - 8.04\times10^{-7}T^2$$

where $k_1(T)$ and $k_2(T)$ are the frequency-exponent functions for 10^{-3}Hz <f <1Hz and 10^{-4}Hz <f < 10^{-3}Hz, respectively.

Not all strain-based creep-fatigue models follow the pattern of the frequency-modified Coffin-Manson equation. For example, Jing et al. proposed a temperature-modified Coffin-Manson equation (Eq.5) [6], wherein the temperature dependence is incorporated into the coefficient and exponent of the Coffin-Manson equation respectively.

$$\Delta\varepsilon_p/2 = C_3\left(2N_f\right)^{\beta} \quad (5)$$

with

$$C_3 = 68.79 - 0.34T + 250.56/\sqrt{T}$$
$$\beta = 1.29 - 0.0053T + 2.5/\sqrt{T}$$

In addition, the creep-fatigue model (Eq.6) [7] developed by Engelmaier presents the influence of both temperature and frequency on creep fatigue, where a logarithmic relationship between temperature and frequency is included.

$$\varepsilon_p = C_4 {N_f}^{-\beta_0(\bar{T},f)} \quad (6)$$

with

$$\beta_0(\bar{T},f) = 0.442 + 6\times10^{-4}\bar{T} - 1.74\times10^{-2}\ln(1+43200f)$$

where $\bar{T}$ is the mean temperature and f is the cyclic frequency ($1 \le f \le 1000$ cycles/day).

Besides temperature and frequency, applied loading also contributes to creep damage. This factor was considered by Wong & Mai, and then they proposed a unified creep-fatigue equation (Eq.7) [8] which accommodates temperature, frequency and applied loading.

$$\varepsilon_p = C_0 s(\sigma) c(T,f) {N_f}^{-\beta_0 b(T,f)} \quad (7)$$

with

$$s(\sigma) = \begin{cases} 1 & when\ creep\ is\ dormant \\ exp\left[-\left(\sigma_{yield}\varepsilon_p^{n'}\right)/A\right] & when\ creep\ is\ active \end{cases}$$

$$c(T,f) = 1 - c_1\left(T - T_{ref}\right) - c_2\log\left(f/f_{ref}\right)$$

$$b(T,f) = 1 - b_1\left(T - T_{ref}\right) - b_2\log\left(f/f_{ref}\right)$$

where, *n'* is the cyclic hardening index, *A*, c_1, c_2, b_1 and b_2 are the positive constants, T_{ref} is the reference temperature below which creep becomes dormant and f_{ref} is the reference frequency above which creep becomes dormant.

Overall, the existing creep-fatigue formulations were developed through limited empirical data for specific materials, and not all models accommodate both temperature and frequency dependencies. Consequently these derivations and models may not be extended to predict fatigue life for multiple temperatures, frequencies, or different materials, thus cannot present a unified characteristic. Theoretically, the existing models may show the unified characteristic by recalculating the coefficients for each new material encountered. However, this would merely provide a numerical model without a fundamental physical theory. Furthermore such an approach would be poor economy due to the empirical effort involved.

In addition, these existing models only describe creep-fatigue behaviour, and cannot cover the full range of conditions from pure fatigue to pure creep. Taking Solomon's equation as an example, the pure-fatigue condition is presented by letting $C_1(T)f^{\beta(1-k)} = C_0$. When the extreme frequency is imposed, $f \to \infty$, the functions $C_1(T)$ becomes infinitely small, which causes $T \to \infty$. This does not agree with the general understanding of pure fatigue, where the temperature should be lower than 35% of the melting temperature [9]. The pure-creep condition is presented by putting $\varepsilon_p = 0$. This is satisfied by letting $C_1 = 0$, which returns T=172°C. This implies creep rupture only occur when the temperature closes to melting temperature (186°C for 60Sn40Pb), which does not agree with general understanding that creep is active at much lower temperature [9].

Furthermore, the existing creep-fatigue equations were derived from the method of curve fitting, where more coefficients were introduced to achieve high quality of fitting to empirical data. When these models are applied to describe creep-fatigue behaviour for another material, a large amount of empirical effort is involved to get high fitting accuracy. In this case the outcomes are strongly sensitive to the quality and quantity of empirical data.

Finally, per section 2, these disadvantages are significant in the case of engineering design, where decisions (such as material selection) must be made on incomplete information. Consequently the existing methods are often not applicable to practical design process except in narrowly defined areas.

These limitations have been recently improved by the *strain-based unified creep-fatigue* equation [10,11]. The next sections describe the advantages of this new model, and present a case study illustrating its applicability to engineering design.

4. Description of the strain-based unified creep-fatigue equation

The strain-based unified creep-fatigue equation (Eq.8) [10,11] is based on the underlying physical mechanisms of fatigue and creep. It provides a linear relationship between temperature and applied loading, based on the observation of creep-diffusion phenomenon [12], and it includes a power-law relation between number of cycles and applied loading which is consistent with crack-growth behaviour [13]. Structurally, this formulation presents an extension of the Coffin-Manson equation, and the creep effect is numerically incorporated based on the concept of *fatigue capacity*. This equation includes the variables of temperature, cyclic time and applied loading, and proposes that the full fatigue capacity is gradually consumed by the elevated temperature and prolonged cyclic time. The strain form is:

$$\varepsilon_p = C_0 c(\sigma, T, t_c) N^{-\beta_0} \tag{8}$$

with

$$c(\sigma, T, t_c) = 1 - c_1(\sigma)\left(T - T_{ref}\right) - c_2 \log\left(t_c / t_{ref}\right)$$

$$T - T_{ref} = \begin{cases} T - T_{ref} & for \quad T \geq T_{ref} \\ 0 & for \quad T \leq T_{ref} \end{cases}$$

$$t_c / t_{ref} = \begin{cases} t_c / t_{ref} & for \quad t_c \geq t_{ref} \\ 1 & for \quad t_c \leq t_{ref} \end{cases}$$

where ε_p is the plastic strain, N is the creep-fatigue life, T is the temperature, t_c is the cyclic time, T_{ref} is the reference temperature and is defined as 35% of melting temperature where the creep is active [9], t_{ref} is the reference cyclic time and is suggested as a small value, C_0 and β_0 are the constants which reflect the full fatigue capacity, and $c_1(\sigma)$ and c_2 are the creep-related function and constant respectively.

Function $c_1(\sigma)$ and constant c_2 are derived from creep-rupture tests which give the relationship of the Manson-Haferd parameter [14] against applied loading (σ), and the convergence point ($\log t_a$, T_a) of all $log\ t$-T lines at different stresses. Then, the pure-creep condition ($\varepsilon_p = 0$) gives the formula of constant c_2 (Eq.9) through letting T=T_{ref}, and suggests function $c_1(\sigma)$ (Eq.10) through letting t_c=t_{ref}.

$$c_2 = \frac{1}{\log\left(t_a / t_{ref}\right)} \tag{9}$$

$$c_1(\sigma) = -\frac{c_2}{P_{MH}(\sigma)} \tag{10}$$

For the same amplitude of applied loading, the creep damage caused by constant stress is significantly larger than the damage resulting from reversed loading [15], thus a moderating factor f_m is introduced to compress the constant stress, and then this presents an equivalent creep damage for the cyclic situation. This moderating factor is determined by the shape of loading wave, and is defined as the ratio of the average level to the peak value of applied cyclic loading. In this case, f_m is normally given as 0.6366 for the sinusoidal wave and 0.5 for a triangular wave. Then, with the strain-stress relation, function $c_1(\sigma)$ is converted into the form in terms of plastic strain (Eq.11):

$$c_1(\sigma) = -\frac{c_2}{P_{MH}(\sigma)} \rightarrow -\frac{c_2}{P_{MH}(\varepsilon_P)} = -\frac{c_2}{P_{MH}[f_{\mathrm{m}} \cdot K(T,t_c) \cdot {\varepsilon_P}^{n(T,t_c)}]} \tag{11}$$

where $K(T,t_c)$ and $n(T,t_c)$ are the strength coefficient and strain hardening exponent for cyclic-loading situation respectively, and they are functions of temperature and cyclic time.

Finally, creep-fatigue data are applied to obtain the magnitudes of C_0 and β_0 through minimizing the error (Eq.12) between the predicted creep-fatigue life ($N_{pre,ij}$) and experimental results ($N_{exp,ij}$):

$$error = \sum_{i,j} \left(\log N_{pre,ij} - \log N_{exp,ij}\right)^2 \tag{12}$$

5. Evaluation of creep-fatigue models for design

Next we show that the strain-based unified creep-fatigue equation is applicable to multiple situations, covers the full range of fatigue-to-creep, and provides an economical method for engineering design. Comparing with the existing models, this new model shows significant advantages on these three areas.

5.1 The unified characteristic

Generally, the existing creep-fatigue models shown in section 3 present good ability of fatigue-life prediction in the field where they were derived. However, the accuracy reduces when these models are extended to other materials at multiple temperatures and cyclic times. This limitation is improved by the strain-based creep-fatigue equation, which presents a general formulation based on physical mechanisms of fatigue and creep. Theoretically, the existing creep-fatigue models may also present unified characteristic through recalculating the coefficients for different materials, but the economy becomes poor which is not desired for engineering design.

The unified characteristic for the strain-based unified creep-fatigue equation is validated on multiple materials (including low melting temperature material: 63Sn37Pb solder, and high melting temperature materials: stainless steel 304, Inconel 718 and GP91 casting steel) at multiple temperatures and cyclic times. The coefficients of the unified formulation for these materials are obtained by the method shown in section 4, and the results are presented below.

• 63Sn37Pb solder

The coefficients of the unified formulation for 63Sn37Pb solder is shown in Table 1 based on the creep-rupture data [16] and creep-fatigue data [5]. This material was validated in our previous research [11], but the coefficients are recalculated here since the derivation method was further improved in the present work.

Table 1 Coefficients of the unified formulation for 63Sn37Pb solder

C_0	β_0	c_2	T_{ref} (K)	t_{ref}(s)	f_m	Convergent point	Average error
7.894	0.825	0.1215	160	1	0.6366	(160K, 8.232)	0.003301
$c_1(\sigma)$	$9.9586 \times 10^{-4} + 1.01122 \times 10^{-4} \cdot f_m \cdot \sigma + 8.09657 \times 10^{-7} \cdot {f_m}^2 \cdot \sigma^2$						

• Stainless steel 304

The coefficients of the unified formulation for stainless steel 304 is shown in Table 2 based on the creep-rupture data [17] and creep-fatigue data [18].

Table 2 Coefficients of the unified formulation for stainless steel 304

C_0	β_0	c_2	T_{ref} (K)	t_{ref} (s)	f_m	Convergent point	Average error
0.8524	0.578	0.0666	600	1	0.5	(600K, 15.01)	0.004257
$c_1(\sigma)$	$8.5843 \times 10^{-4} + 9.74017 \times 10^{-6} \cdot f_m \cdot \sigma - 1.86542 \times 10^{-8} \cdot {f_m}^2 \cdot \sigma^2$						

• Inconel 718

The coefficients of the unified formulation for Inconel 718 is shown in Table 3 based on the creep-rupture data [19] and creep-fatigue data [20].

Table 3 Coefficients of the unified formulation for Inconel 718

C_0	β_0	c_2	T_{ref} (K)	t_{ref} (s)	f_m	Convergent point	Average error
0.5658	0.608	0.0782	560	1	0.6366	(560K, 12.78)	0.008643
$c_1(\sigma)$	$2.7679 \times 10^{-3} - 4.12347 \times 10^{-6} \cdot f_m \cdot \sigma + 3.91221 \times 10^{-9} \cdot {f_m}^2 \cdot \sigma^2$						

• GP91 casting steel

The coefficients of the unified formulation for GP91 casting steel is shown in Table 4 based on the creep-rupture data [21] and creep-fatigue data [22].

Table 4 Coefficients of the unified formulation for GP91 casting steel

C_0	β_0	c_2	T_{ref} (K)	t_{ref} (s)	f_m	Convergent point	Average error

0.6879	0.667	0.0547	610	1	0.6366	(610K, 18.28)	0.00876
$c_1(\sigma)$	$9.51808 \times 10^{-4} + 1.20344 \times 10^{-5} \cdot f_m \cdot \sigma - 1.75045 \times 10^{-8} \cdot {f_m}^2 \cdot \sigma^2$						

The validation on the above four materials shows that the strain-based unified creep-fatigue equation has ability to cover multiple materials and presents good fatigue-life prediction at multiple temperatures and cyclic times. Structurally, Wong & Mai's equation also provides a general form, thus may have chance to present unified characteristic. In particular, the coefficients are not fixed across multiple materials, hence have to be determined in each case. The investigation indicates that Wong & Mai's equation presents smaller average errors on the materials of 63Sn37Pb solder (0.000284), stainless steel (0.002810) and Inconel 718 (0.001585) than the unified formulation. Normally, the equation with more coefficients has better fitting for empirical data. This is the main reason for smaller average error shown by using Wong & Mai's equation.

Theoretically, the equations of Coffin's, Solomon's, Shi's, Engelmaier's and Jing's may also have opportunity to present the unified characteristic through transforming them into general formulations. For example, Solomon's equation is rewritten as:

$$\varepsilon_p = C_1(T)\left(N_f f^{k-1}\right)^{-\beta_0} \tag{13}$$

with

$$C_1(T) = \mathrm{a} + \mathrm{b}T + \mathrm{c}T^2 + \mathrm{d}T^3$$

where a, b, c, d, k and β_0 are the constants obtained from experiments. Then, this modified formulation gives small errors (such as 0.000529 for 63Sn37Pb and 0.00103 for stainless steel 316), and even present better fatigue-life prediction than the unified formulation at some situations.

However, we cannot conclude that Wong & Mai's equation and those modified formulations are better than the strain-based unified creep-fatigue equation. To be specific, it is significant that Wong & Mai's equation and those modified formulations are introduced as many as coefficients to get good quality of fitting (such as seven independent coefficients for Wong and Mai's equation), thus the representation of creep-fatigue behaviour is a numerical-based method and the accuracy highly relies on the number of empirical data. This means that more empirical data gives more accurate prediction, and thus poor economy is presented. However, only two independent coefficients in the unified formulation are derived by curve fitting. This implies less experimental effort is needed, and then a more economical method for fatigue-life prediction is given. This will be discussed in section 5.3.

Overall, comparing with other existing creep-fatigue models, the strain-based unified creep-fatigue equation provides a better method for fatigue-life prediction at multiple situations, wherein the small average errors are given and the unified characteristic is proved.

5.2 The integrated characteristic

The integrated characteristic refers to the ability to cover full range of conditions from pure-fatigue condition to pure-creep condition. According to the concept of fatigue capacity, the full fatigue capacity (the pure-fatigue condition) is continuously consumed by the increasing creep effect to the condition of creep fatigue, and finally to the pure-creep condition as the fatigue capacity is completely consumed. The compare between different creep-fatigue models on the integrated characteristic is collected in Table 5 [23].

Table 5 The capacity of integrated characteristic

Creep-fatigue models	Pure fatigue	Creep fatigue	Pure creep
Coffin's equation (Eq.2)	X	√	X
Solomon's equation (Eq.3)	X	√	X
Shi's equation (Eq.4)	X	√	X
Jing's equation (Eq.5)	X	√	X
Engelmaier's equation (Eq.6)	√	√	X
Wong & Mai's equation (Eq.7)	√√	√√	X
Unified creep-fatigue equation (Eq.8)	√√	√√	√√

√√: This equation can well describe the phenomena of this condition
√: This equation can partly describe the phenomena of this condition
X: This equation cannot describe the phenomena of this condition

Normally, the creep effect presents the dependence on temperature, cyclic time and applied loading, thus the creep-fatigue model should accommodate these relevant variables to show a good description of creep fatigue. However, creep effect in the existing creep-fatigue models shown in section 2 cannot be totally presented, specifically, only the temperature and cyclic-time are included into the equations proposed by Solomon, Shi et al., and Engelmaier, only the cyclic-time is presented in Coffin's equation and only the temperature is shown in Jing's equation. While, Wong & Mai's equation and the unified formulation accommodate these three variables, thus they are believed to have a better fatigue-life prediction at the creep-fatigue condition (accuracy has been shown in section 5.1). Further investigation of stress-related functions in these two equations shows that function $c_1(\sigma)$ in the unified formulation is directly derived from creep-rupture behaviour, but is not for Wong & Mai's equation. Therefore, the strain-based unified creep-fatigue equation theoretically has better presentation of creep effect.

In addition, a good creep-fatigue equation also should be capable of covering two ends of creep-fatigue condition: pure-fatigue condition and pure-creep condition. However, the equations

proposed by Coffin, Solomon, Shi et al., Jing, Engelmaier and Wong & Mai do not totally satisfy this condition. On the one hand, the condition of pure fatigue is presented by letting $C_1(T)f^{\beta(1-k)} = C_0$($C_0$ is the ductility coefficient at pure-fatigue condition) for Solomon's equation, $C_2(T)f^{\beta[1-k(T)]} = C_0$ for Shi's equation and $\beta_0(\bar{T}, f) = \beta_0$ (β_0 is the ductility exponent at pure fatigue condition) for Engelmaier's equation. When the extreme frequency is imposed, $f \to \infty$, the functions $C_i(T)$ and $\beta_0(\bar{T}, f)$become infinitely small, which causes $T \to \infty$. In addition, the temperature component is not shown in Coffin's equation, thus the activation of creep effect in terms of temperature is ignored in this equation. These do not agree with the general understanding of pure fatigue, where the temperature should lower than 35% of melting temperature [9]. For Jing's equation, the derivation of function $C_3(T)$ is based on the material of 80Au/20Sn solder, thus a low temperature (where the creep effect is dormant) may return a reasonable value to describe full fatigue capacity. While, when this equation is applied on steel, function $C_3(T)$ yields to an impossible negative value since the temperature at the pure-fatigue condition is much higher than the situation for solder. However, the pure-fatigue condition can be well presented by both Wong & Mai's equation and the strain-based unified creep-fatigue equation through letting $T=T_{ref}$ *and* $t=t_{ref}$, where they can be restored to the Coffin-Manson equation.

On the other hand, the condition of pure creep is presented by letting $\varepsilon_p=0$. This condition cannot be satisfied by the equation of Coffin, because the coefficient C and exponent β_0 are constant, which leads to impossible zero time or zero frequency. In addition, for the equation of Engelmaier, the pure creep condition is satisfied by letting $\beta_0(\bar{T}, f) \to +\infty$, which implies $T \to +\infty$. The pure creep condition for the equations proposed by Solomon, Shi et al. and Jing et al. is satisfied by letting $C_1=C_2=C_3=0$, which returns T=172ºC, 198ºC and 249ºC respectively. The Solomon's and Jing's equations imply that creep rupture only occur when the temperature closes to melting temperature (186ºC for 60Sn40Pb solder and 280 ºC for 80Au/20Sn solder), while Shi's equation suggests that creep rupture only occur above melting temperature (183ºC). The creep activation temperatures obtained from these four creep-fatigue equations do not agree with general understanding of creep, where creep is active at 35% of melting temperature. Although Wong & Mai's equation has a good description for pure fatigue, it cannot present pure-creep condition entirely. This is because letting $s(\sigma)c(T_R, f_R) = 0$ cannot deduce any well-known time-temperature parameters, such as the Larson-Miller parameter [24], the Sherby-Dorn parameter [25] and the Manson-Haferd parameter [14]. However, the Manson-Haferd parameter can be well-presented through letting $c(\sigma, T, t_c) = 0$ for the strain-based unified creep-fatigue equation.

Overall, comparing with other existing creep-fatigue models, the strain-based unified creep-fatigue equation can cover the full range of conditions from pure fatigue to pure creep. Specifically, this equation has capability to model pure fatigue at $c(\varepsilon_p,T,t_c)=1$ where this equation is restored to the Coffin-Manson equation, model pure creep rupture at $c(\varepsilon_p,T,t_c)=0$ where this equation is transformed to the Manson-Haferd parameter, and model creep-fatigue damage at $0 \le c(\varepsilon_p,T,t_c) \le 1$ where the creep effect is influenced by temperature, cyclic time and applied loading.

5.3 The economy

Engineering design of fatigue-life evaluation always requires good performance on both accuracy and economy [26]. The accuracy has been shown in section 5.1 and the economy will be discussed in this section, where Wong & Mai's equation is select to compare with the strain-based unified creep-fatigue equation in terms of economy. The results show that the unified formulation provides a more economical method for fatigue-life prediction because the minimum experimental effort is involved.

Normally, the accuracy to predict or fit a distribution (or a trend) by a numerical formulation partly depends on the number of coefficients, which implies that the formulation with more coefficients presents better fitting [27]. However, this factor is not isolated, and is strongly related to the number of data points. Specifically, the more coefficients are introduced, then the more data points are needed to pick up, and then the better fitting can be gotten. This does not mean that a good formulation should contain as many as coefficients because this may lead to redundancy on the empirical effort. Therefore, is very important for deriving a formulation to keep a good balance between accuracy and consumption. In this case, the strain-based unified creep-fatigue equation satisfies this requirement.

As mentioned in section 5.1, Wong & Mai's equation has seven independent coefficients which are totally obtained through numerical method, but only two independent coefficients are included in the unified formulation. This suggests that more empirical data are needed to give better fitting for Wong & Mai's equation, but this results in poor economy since performing a large number of creep-fatigue experiments is expensive and time-consuming. This significantly is not a good choice for engineering design due to the undesirable high cost. However, when less creep-fatigue tests are involved to control the total cost, the accuracy for fatigue-life prediction remarkably reduces. This limitation is improved by using the strain-based unified creep-fatigue equation, where a better balance between accuracy and economy is given. The comparison between Wong & Mai's equation and the unified formulation on the accuracy of prediction in terms of empirical-data number is shown in Table 6, where the materials of 63Sn37Pb and stainless steel 304 are investigated.

Table 6 Accuracy of prediction in terms of empirical-data number

Materials	Number of data to derive coefficients	Average errors on predict fatigue life	
		Wong & Mai's equation	Unified creep-fatigue equation
63Sn37Pb	8 groups of data	0.000284	0.003301
	3 groups of data	0.2445	0.00355
Stainless steel 304	7 groups of data	0.002810	0.004257
	3 groups of data	0.4684	0.007199

Taking 63Sn37Pb solder as an example, Table 6 shows that Wong & Mai's equation gives better accuracy on fatigue-life prediction than the unified formulation when all eight groups of creep-fatigue data are imposed, wherein the average errors are 0.000284 for Wong & Mai's equation and 0.003301 for the unified formulation. Then, three groups of creep-fatigue data (*T=233K, t_c=1s*; *T=298K, t_c=10s; T=298K, t_c=1000s*) were selected to extract the coefficients, and the numerical method still yields to quite small errors for fitting. However, when Wong & Mai's equation with the coefficients obtained at this stage is extended to predict fatigue life at total eight creep-fatigue situations, a poor accuracy is given, where the average error dramatically worsens to 0.2445 from 0.000284. This undesirable result is significantly improved by the strain-based unified creep-fatigue equation, wherein the difference between the average errors of fatigue-life prediction under two situations is very small (specifically, 0.003301 for the coefficients obtained from eight groups of creep-fatigue data and 0.00355 for the coefficients obtained from three groups of data). This implies that less creep-fatigue experiments may be involved to obtain the coefficients of the unified formulation, and the accuracy of fatigue-life prediction by using Wong & Mai's equation is more sensitive on the number of empirical data. Consequently, the unified equation provides a more economical method for engineering design because of the reduced number of creep-fatigue experiments. This result is further demonstrated by the material of stainless steel 304, and the average errors under two situations are shown in Table 6.

Overall, it is clear that the better fatigue-life prediction provided by Wong & Mai's equation (also other modified formulations from the original equations of Coffin's, Solomon's, Shi's, Engelmaier's and Jing's) is obtained through sacrificing economy. However, the strain-based unified creep-fatigue equation provides a more practical method of fatigue-life evaluation for engineering design, wherein a good balance between accuracy and economy is achieved.

The research conducted by Manson indicated that the Coffin-Mansion equation can be modified to a universal slops formulation (Eq. (14)) through introducing the ductility (D) based on the observation of 47 materials [28]:

$$\Delta\varepsilon_p = 0.547D^{0.43}{N_f}^{-0.5} \tag{14}$$

Significantly, the coefficients of this equation can be directly derived from material properties, thus no fatigue test is involved. This remarkably reduces the cost spent on experiments, and thus could be introduced to simplify the unified creep-fatigue equation to eliminate creep-fatigue test. According to the empirical data on the materials of Stainless steel 316, Stainless steel 304, Inconel 718 and GP91 casting steel, the simplified formulation is presented as (Eq.15):

$$\Delta\varepsilon_p = 0.8965D^{0.3998}c(\sigma, T, t_c){N_f}^{-0.629} \tag{15}$$

This simplified form provide an easy way to extract the coefficients without any creep-fatigue tests, and only creep-rupture tests are needed. Therefore, a more economical method of fatigue-life prediction is proposed. This formulation could be further modified and improved if more materials are investigated. However, the solder materials are not included in this simplified form because solder materials present quite different material properties from carbon-based materials, where they has more significant deformation at break and higher full fatigue capacity

[29,30]. Therefore, the solder materials should be separately discussed to develop a simplified formulation.

6. Design application: Case study for gas turbine blisk

Evaluation shown in section 5 indicates that the strain-based unified creep-fatigue equation presents good characteristics on unify, integration and economy. This provides an effective and efficient creep-fatigue method for engineering design at initial stage, such as material selection, structure optimization and boundary-condition determination. Generally, during the process of design, the coefficients of this unified formulation can be extracted through minimum experimental effort. Then, the coefficients can be applied to numerically evaluate creep fatigue under service condition. In addition, FEA is frequently applied to conduct numerical analysis of creep fatigue in different engineering components, such as heat exchanger [31,32], turbine blade [33-35] and electronic package [36,37]. In this case, the coefficients obtained from the unified equation also can be imported into finite element analysis (FEA) software to reduce the complexity of analysis.

A gas turbine blisk works under high temperature, and experiences repeated starting up and shutting off. This is a typical creep-fatigue situation, where damage is caused by the combination of creep effect and fatigue effect. In this case study, the theory of highly accelerated life test is accepted to make a selection of material. In particular, the strain-based creep-fatigue equation is used to obtain the creep-fatigue-related parameters for the evaluation of creep-fatigue damage.

6.1 Methodology for fatigue-based design

This case study is based on the theory of highly accelerated life test, which is used at the initial stage of design to improve the reliability of product, such as the selection of material, the optimization of structure and the decision of manufacturing processes. Normally, the accelerated life test is done through intensifying the influence of stress-related factors on life. Therefore, the prediction of fatigue life and creep-rupture time in this case study cannot present the real value for the failure at the operation condition, but can provide effective guidance for engineering design, e.g. differentiating between different candidate solutions.

6.1.1 Loading characteristics

Generally, the total damage is accumulated by the fatigue damage caused by repeated process of starting up and shutting off, the creep damage due to elevated temperature and the damage results from vibration. Therefore, the creep-fatigue evaluation based on each operational unit is divided into three parts: regular-loading fatigue partition (repeated process pf starting up and

shutting off), creep partition (elevated temperature) and irregular-loading partition (vibration) (Figure 1).

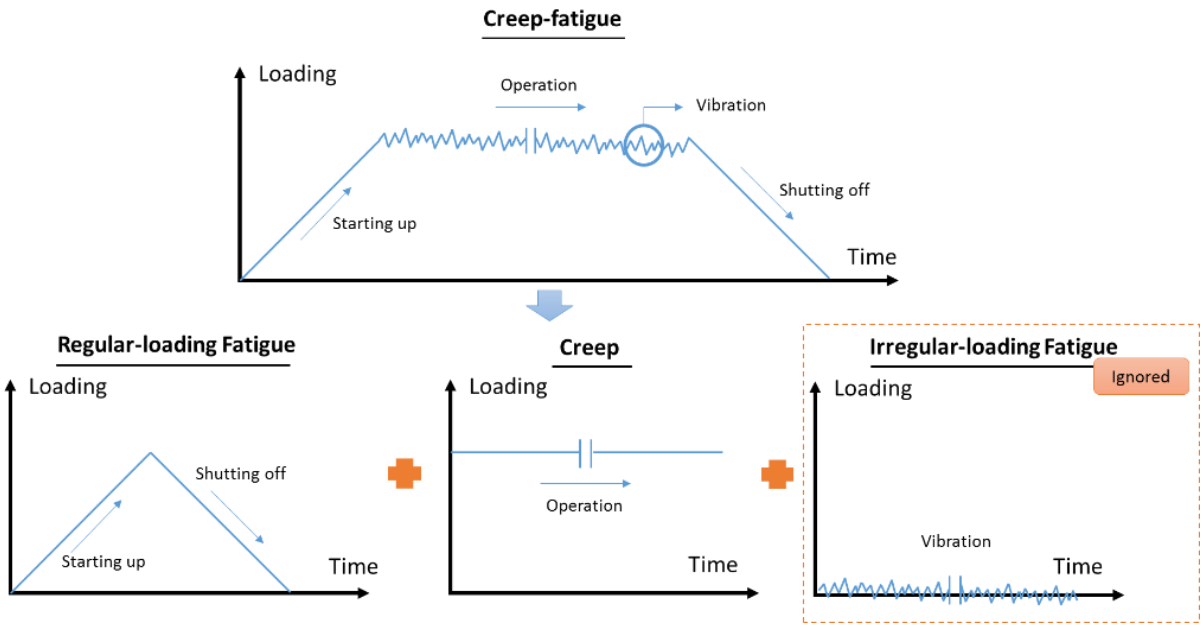

Figure 1 The partition of creep fatigue

The partition which includes vibration is not considered because the amplitude of this irregular-loading is so small that can be ignored. Therefore, this evaluation focuses on the regular-loading partition and creep partition. The fatigue damage is caused by the repeated process of starting up and shutting off, and the maximum loading appears at the 100% rotational velocity. The waveform for the loading is triangular. The cyclic time is arbitrarily defined as 1s, which is also defined as the reference cyclic time for the strain-based creep-fatigue equation. Significantly, this small cyclic time is much smaller than the real situation, where the gas turbine blisk is impossible to start up and then shut off within one second. However, the choice of frequency does not influence the result of stress/strain distribution for FEA. In addition, the constant loading for creep damage at elevated temperature is defined as the applied loading at the maximum rotational velocity.

6.1.2 FEA approach

FEA methods such as ANSYS can accommodate creep, fatigue, and creep-fatigue but only with data. Normally, FEA-based creep-fatigue evaluation [33,34,38] is based on the exploration of creep and fatigue behaviour by experiments, where the relationships of creep strain vs. time and applied loading vs. fatigue life are imported into FEA software as engineering data to simulate creep-fatigue behaviour. Then, the simulation is conducted under cyclic loading and elevated temperature. Generally, this is a complex process. This is firstly because the amount of empirical experiment required, especially the need to redo the creep test when the applied loading is changed. In addition, the introduction of a creep effect may result in non-convergence for FEA, and then the analysis settings may need to be repeatedly modified

to get solution convergence. This makes it difficult to apply FEA to early design stages where the creep-fatigue material properties are not yet established empirically.

However, the complexity can be improved through using the strain-based unified creep-fatigue equation (Eq.8). Specifically, this new formulation is used to get the creep-fatigue-related coefficients under the service condition, then these coefficients are introduced into FEA as the engineering data. The key concept is that equation provides a method to transfer the creep effect into the creep-fatigue-related coefficients. Therefore, FEA can be conducted without the need to obtain explicit creep data. This significantly reduces the complexity of simulation. This process of substitution is described below.

The process is that the unified equation gives the creep-fatigue-related coefficients for the candidate materials under consideration. Then, the coefficients were input into ANSYS as engineering data to evaluate fatigue life. The next stage was to take the maximum stress and strain obtained from FEA and substitute into Morrow's equation. This provides another estimate of the fatigue life. Finally, the results obtained by the two methods were compared, and design implications identified. The FEA stress and strain results were also used to evaluate the creep damage using the Manson-Haferd parameter. This gives an estimate of the creep-rupture time for the creep part of the loading. The evaluation was conducted on Inconel 718 and GP91 casting steel, and the ideal material should have good performance on both fatigue and creep.

6.2 Selection of material

6.2.1 Geometry

The geometry (Figure 2) of gas turbine blisk was structured by Solidworks [39], and one of blades was selected to conduct FEA by using ANSYS WORKBENCH. The key dimension are shown in Table 7.

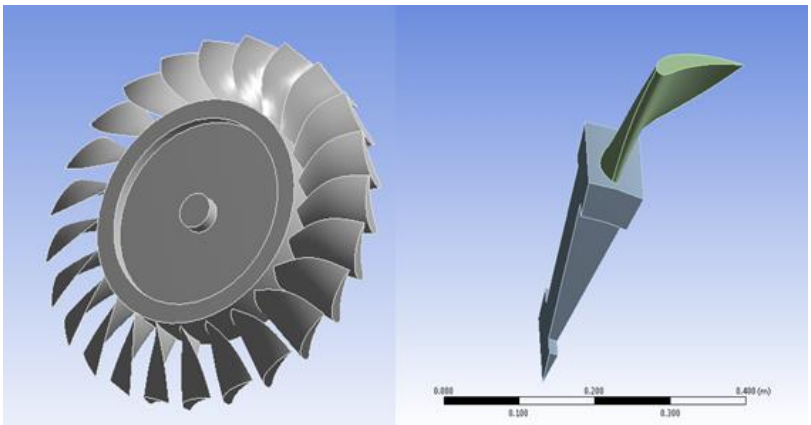

Figure 2 Geometry

Table 7 Key dimension of geometry

No.	Items	Dimensions

1	R_1 (the distance from center to tip of the blade)	469mm
2	R_2 (the distance from center to root of the blade)	295mm
3	Number of blades	24
4	The outlet anger for mean cross section	30°
5	The area of mean cross section	3036.45mm^2

6.2.2 Service condition

The turbine blisk is working under cyclic loading and elevated temperature, and the service condition is tableted in Table 8:

Table 8 Service condition

Rotational velocity (n)	Temperature (T)	Mass flow rate ($\dot{M}$)	Nozzle angle (α)
3000 rpm	811K (538°C)	31.6kg/s	14°

6.2.3 Coefficients for creep-fatigue condition and material properties

According to the coefficients of the strain-based unified creep-fatigue equation for the materials of Inconel 718 shown in Table 3 and GP 91 casting steel shown in Table 4, the fatigue-related coefficients at 811K which can be input into ANSYS as engineering data are presented in Table 9:

Table 9 The creep-fatigue-related coefficients for Inconel 718 and GP91 casting steel

Materials	Strain-life relation $\Delta\varepsilon_p/2 = C(2N_f)^{\beta}$		Stress-life relation $\Delta\sigma/2 = \sigma(2N_f)^{b}$		Strain-stress relation $\Delta\sigma/2 = K(\Delta\varepsilon_p/2)^{n}$	
	C	β	σ	b	K	n
Inconel 718	0.4828	-0.636	851.6	-0.09178	946	0.1443
GP91 casting steel	0.5093	-0.662	382	-0.0422	398.5	0.0638

In addition, the material properties of Inconel 718 [40] and GP91 casting steel [22] at 811K are shown in Table 10:

Table 10 Material properties of Inconel 718 and GP91 casting steel

Material	Density (kg/m^3)	Yield stress (MPa)	Tensile stress (MPa)	Young's modules (MPa)

Inconel 718	8220	1069	1276	179000
GP91 casting steel	7700	342	402	161500

6.2.4 Loading

The centrifugal force, tangential force and axial force to blades are the main loadings which cause creep-fatigue damage at elevated temperature during the repeated process of starting up and shutting off. The maximum loading is calculated at the situation of 100% rotational velocity.

(1) Centrifugal force

The centrifugal force can be obtained through Eq.16 [35]:

$$F_c = 0.5\rho A\omega^2\left({R_1}^2 - {R_2}^2\right) \tag{16}$$

where F_c is the centrifugal force, ρ is the density, A is the area of cross section and ω is the rotational velocity in rad/s. With the rotational velocity (3000 rpm), the magnitude of ω is given by Eq.17:

$$\omega = 2\pi n/60 = 2\pi \times 3000/60 = 314.2\ rad/s \tag{17}$$

Then, the centrifugal force is presented by Eq. (18):

$$F_c = 0.5 \times 8220 \times 0.00303645 \times 314.2^2 \times (0.469^2 - 0.295^2) = 163780.776\ N \tag{18}$$

(2) Tangential force and axial force

The tangential force and axial force are calculated through velocity triangle (Figure 3) [33], which is a well-accepted method for the force calculation of blade.

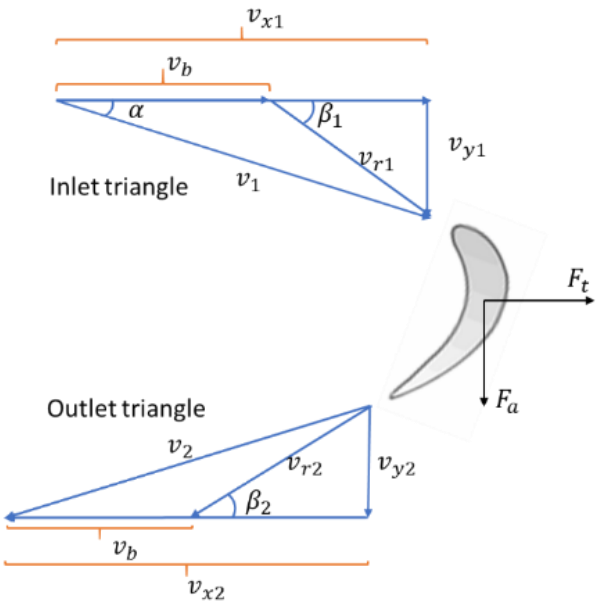

Figure 3 Velocity triangle for blade

The mean cross section is selected to calculate the tangential force and axial force, and the results in velocity triangle is shown in Table 11.

Table 11 The results in velocity triangle

In the inlet triangle						In the outlet triangle			
v_b (m/s)	v_1 (m/s)	β_1	v_{r_1} (m/s)	v_{x_1} (m/s)	v_{y_1} (m/s)	v_{r_2} (m/s)	β_2	v_{x_2} (m/s)	v_{y_2} (m/s)
120.01	247.55	26.519^0	134.129	240.197	59.888	134.129	30^0	67.065	236.17

Then, the tangential force (F_t) is give as (Eq.19 and Eq. 20):

$$F_t = \dot{M}\Delta v_x = 31.6 \times (240.1667 + 236.17) = 15052.23972\ N \quad (19)$$

$$F_t/blade = 15052.23972/24 = 627.177\ N \quad (20)$$

and the axial force (F_a) is presented as (Eq.21 and Eq.22):

$$F_a = \dot{M}\Delta v_y = 31.6 \times (67.0645 - 59.8878) = 226.78372\ N \quad (21)$$

$$F_a/blade = 226.78372/24 = 9.449\ N \quad (22)$$

6.2.5 The evaluation of fatigue damage

(1) Finite element analysis results

The finite element analysis is conducted through nonlinear analysis method [34,35,38]. The creep-fatigue-related coefficients from Table 9 and the material properties from Table 10 are input into ANSYS WORKBENCH as engineering data. The boundary condition (force) presented in section 6.2.4 is imposed. Finally, the maximum stress, maximum total strain and fatigue life are given. The results are tableted in Table 12, and fatigue-life prediction is shown in Figure 4 for Inconel 718 and Figure 5 for GP91 casting steel.

Table 12 FEA results for Inconel 718 and GP91 casting steel

Materials	Maximum stress	Maximum total strain	Minimum fatigue life
Inconel 718	1311.8 MPa	0.011597	2350 cycles
GP91 casting steel	755.27MPa	0.029661	327 cycles

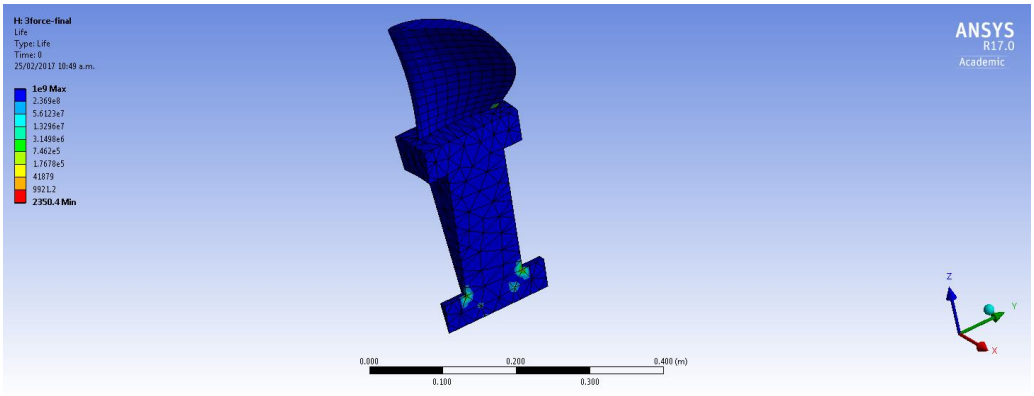

Figure 4 The fatigue life distribution for Inconel 718

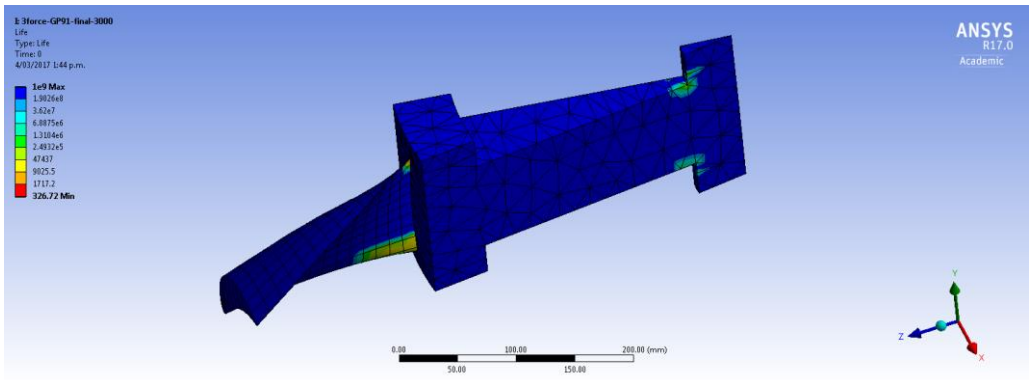

Figure 5 The fatigue life distribution for GP91 casting steel

(2) Predicted fatigue life through Morrow's equation

Based on the stress and strain obtained from FEA, the fatigue life can be calculated through Morrow's equation (non-zero-mean-stress condition) (Eq.23) [38,41]:

$$\varepsilon_t = 3.4\left(\frac{\sigma_s - \sigma_m}{E}\right) {N_f}^{-0.12} + {C_0}^{0.6} {N_f}^{-0.6} \tag{23}$$

where ε_t is the total strain, σ_s is the tensile stress, E is the Young's modulus, C_0 is the fatigue ductility coefficient based on $\Delta\varepsilon_p - N$ relation, and σ_m is the mean stress which is defined as the half of the maximum stress obtained from EFA.

Substituting Eq.23 with the values obtained from EFA gives the results: N_f=2440 for Inconel 718 and N_f=348 for GP91 casting steel.

(3) Comparing the results

The fatigue damage is evaluated through both FEA and the Morrow's equation, and the results are provided in Table 13. The error between these two results is given by Eq.24.

$$error = \frac{N_{f-Morrow} - N_{f-FEA}}{N_{f-FEA}} \times 100\% \tag{24}$$

Table 13 The results obtained through FEA and the Morrow's equation

Materials	FEA-based results	Morrow-based results	error
Inconel 718	2350 cycles to failure	2440 cycles to failure	3.83%
GP91 casting steel	327 cycles to failure	348 cycles to failure	6.42%

As shown in Table 13, the fatigue life obtained through Morrow's equation is higher than the result obtained from FEA. This may be because the influence of mean stress is removed from the second term (plastic strain), and thus reduces the mean-stress effect on fatigue capacity and obtains a longer fatigue-life prediction. The FEA results are more conservative, and most designers would want to proceed with them rather than the Morrow's results.

6.2.6 The evaluation of rupture time due to creep damage

According to the FEA results, the maximum plastic strain (0.005406 for Inconel 718 and 0.02498 for GP91 casting steel) can be obtained, and it could then be transformed to stress (445.4MPa for Inconel 718 and 314.9MPa for GP91 casting steel) by the stress-strain relation (Table 9). Finally, the stress is used to get the rupture time through the Manson-Haferd parameter (P_{MH}) obtained during the process of extracting the coefficients of the unified formulation. The results are shown in Table 14.

Table 14 Creep damage for Inconel 718 and GP91 casting steel at 811K

Materials	P_{MH}	$1/P_{MH} - \sigma$ relation	Rupture time
Inconel 718	-0.0218	$-5.0 \times 10^{-8}\sigma^2 + 5.27 \times 10^{-5}\sigma - 3.5375 \times 10^{-2}$	5588 hours
GP91 casting steel	-0.0549	$3.2 \times 10^{-7}\sigma^2 - 2.2 \times 10^{-4}\sigma - 1.74 \times 10^{-2}$	4791 hours

6.2.7 The design decision

The evaluation of fatigue damage (fatigue partition) and creep damage (creep partition) is collected in Table 15. The results indicate that Inconel 718 has better fatigue and creep capacity than GP91 casting steel. Therefore, Inconel 718 would be recommended as the material to take forward into the next stages of design. In safety critical situations it would still be prudent to conduct the empirical creep-fatigue tests to validate the selection. However it will be appreciated that conducting such tests for one material for the purposes of validation is more efficient than conducting the same tests for all candidate materials – some of which will not be taken forward.

Table 15 The evaluation of fatigue damage and creep damage

Materials	Evaluation of fatigue damage	Evaluation of creep damage
Inconel 718	2350 cycles to failure	5588 hours to failure
GP91 casting steel	327 cycles to failure	4791 hours to failure

7. Limitation

The strain-based unified creep-fatigue equation was developed for the situation of zero-hold-time cyclic loading. In this case, fatigue makes more contribution than creep on failure [42], because total time is too small to produce remarkable creep damage. However, for the cyclic loading with hold time, the creep effect gradually intensifies as the hold time increases. Then, creep damage makes more contribution and the failure finally occurs due to a creep effect. Therefore, at the situation with short hold time, the unified formulation may still present a reasonable prediction of fatigue life, but the accuracy of this prediction may become worse when the hold time is prolonged.

8. Conclusion

The unified creep-fatigue equation (Eq.8) presents an effective and efficient method for engineering design. The advantages of this equation are:

(1) Better fatigue-life prediction for multiple temperatures and cyclic times for multiple materials.

(2) Ability to cover the full range of conditions from pure fatigue to pure creep.

(3) Good economy since the coefficients may be determined through minimum experimental effort. Especially, a simplified form is presented where the coefficients can be obtained from simple creep-rupture tests without need for any creep-fatigue tests.

(4) Applicability to engineering design and FEA.

Author Contributions: The work was conducted by DL and supervised by DP. The validation on different materials, the integrated characteristic and the economy are analysed by DL. The case study on gas turbine blisk was conducted by DL with guidance from DP.

Conflicts of Interest: The authors declare no conflict of interest. The research was conducted without personal financial benefit from any funding body, and no such body influenced the execution of the work.

References

1. Coffin Jr LF. A study of the effects of cyclic thermal stresses on a ductile metal. Knolls Atomic Power Lab.; 1953.
2. Manson SS. Behavior of materials under conditions of thermal stress. 1954.
3. Coffin L. Fatigue at high temperature. Fatigue at elevated temperatures: ASTM International; 1973.
4. Solomon H. Fatigue of 60/40 solder. IEEE Trans Compon Hybrid Manuf Technol. 1986;9:423-32.
5. Shi X, Pang H, Zhou W, Wang Z. Low cycle fatigue analysis of temperature and frequency effects in eutectic solder alloy. International Journal of Fatigue. 2000;22:217-28.
6. Jing H, Zhang Y, Xu L, Zhang G, Han Y, Wei J. Low cycle fatigue behavior of a eutectic 80Au/20Sn solder alloy. International Journal of Fatigue. 2015;75:100-7.
7. Engelmaier W. Fatigue life of leadless chip carrier solder joints during power cycling. IEEE transactions on components, hybrids, and manufacturing technology. 1983:232-7.
8. Wong E, Mai Y-W. A unified equation for creep-fatigue. International Journal of Fatigue. 2014;68:186-94.
9. Ashby MF, Shercliff H, Cebon D. Materials: engineering, science, processing and design: Butterworth-Heinemann; 2013.
10. Liu D, Pons D, Wong E-h. The Unified Creep-Fatigue Equation for Stainless Steel 316. Metals. 2016;6:219.
11. Liu D, Pons D, Wong E-h. Creep-Integrated Fatigue Equation for Metals. Int J Fatigue. 2016.
12. Poirier J-P. Creep of crystals: high-temperature deformation processes in metals, ceramics and minerals: Cambridge University Press; 1985.
13. Weertman J. Fatigue crack propagation theories. Fatigue and Microstructure, ASM, Metals Park, Ohio. 1979:279-06.
14. Manson S, Haferd A. A linear time-temperature relation for extrapolation of creep and stress-rupture data: Lewis Flight Propulsion Lab.; 1953.
15. Halford G. Cyclic creep-rupture behavior of three high-temperature alloys. Metall Trans. 1972;3:2247-56.
16. Shi X, Wang Z, Yang Q, Pang H. Creep behavior and deformation mechanism map of Sn-Pb eutectic solder alloy. Journal of Engineering Materials and Technology. 2003;125:81-8.
17. Fritz LJ, Koster W. Tensile and creep rupture properties of uncoated and coated engineering alloys at elevated temperatures. 1977.
18. Kanazawa K, Yoshida S. Effect of temperature and strain rate on the high temperature low-cycle fatigue behavior of austenitic stainless steels. Creep and fatigue in elevated temperature applications International conference sponsored by the Institution of Mechanical Engineers, American Society of Mechanical Engineers, American Society for Testing Materials, Philadelphia, 23-27 September 1973 and Sheffield, 1-5 April 1974 Vol 11975.
19. Sugahara T, Martinolli K, Reis DA, de Moura Neto C, Couto AA, Neto FP, et al. Creep Behavior of the Inconel 718 Superalloy. Defect and Diffusion Forum: Trans Tech Publ; 2012. p. 509-14.
20. Fournier D, Pineau A. Low cycle fatigue behavior of Inconel 718 at 298 K and 823 K. Metall Trans A. 1977;8:1095-105.
21. Tabuchi M, Hongo H, Li Y, Watanabe T, Takahashi Y. Evaluation of microstructures and creep damages in the HAZ of P91 steel weldment. J Pressure Vessel Technol. 2009;131:021406.

22. Mroziński S, Golański G. Low cycle fatigue of GX12CrMoVNbN9-1 cast steel at elevated temperature. J Achiev Mater Manuf Eng. 2011;49:7-16.
23. Liu D, Pons D. Development of a unified creep-fatigue equation including heat treatment. Fatigue & Fracture of Engineering Materials & Structures. 2017.
24. Larson FR, Miller J. A time-temperature relationship for rupture and creep stresses. Trans ASME. 1952;74:765-75.
25. Dorn J, Orr RL, Sherby O. Creep correlations of metals at elevated temperatures. AIME TRANS. 1954;200:71-80.
26. Shigley JE, Mischke CR. Mechanical Engineering Design: McGraw-Hill; 2003.
27. Chapra SC, Canale RP. Numerical methods for engineers: McGraw-Hill New York; 2006.
28. Manson S. A modified universal slopes equation for estimation of fatigue characteristics of metals. Journal of Engineering Materials and Technology. 1988;110:55.
29. Kanchanomai C, Miyashita Y, Mutoh Y. Low-cycle fatigue behavior of Sn-Ag, Sn-Ag-Cu, and Sn-Ag-Cu-Bi lead-free solders. Journal of Electronic Materials. 2002;31:456-65.
30. Shohji I, Yoshida T, Takahashi T, Hioki S. Tensile properties of Sn–Ag based lead-free solders and strain rate sensitivity. Materials Science and Engineering: A. 2004;366:50-5.
31. Patil R, Anand S. Thermo-structural fatigue analysis of shell and tube type heat exchanger. International Journal of Pressure Vessels and Piping. 2017.
32. Zhao X, Zhou Y, Yuan K. Creep-fatigue damage evaluation of Ni-based superalloy inconel 617 based on finite element analysis. 23rd International Conference on Nuclear Engineering: Nuclear Power - Reliable Global Energy, ICONE 2015, May 17, 2015 - May 21, 2015. Chiba, Japan: American Society of Mechanical Engineers (ASME); 2015. p. et al.; GLSEQ, LLC/SCI Technologies. Inc; Hitachi-GE Nuclear Energy, Ltd.; Mitsubishi Heavy Industries, Ltd. (MHI); Toshiba Corporation; Westinghouse Electric Company.
33. Kumar RR, Pandey K. Static Structural and Modal Analysis of Gas Turbine Blade. International Conference on Advanced Material Technologies 2016.
34. Madhu P. Stress Analysis and Life Estimation of Gas Turbine Blisk for Different Materials of a Jet Engine. International Journal of Science and Research. 2016;5:1103-7.
35. Tulsidas D, Shantharaja M, Kumar K. Design modification for fillet stresses in steam turbine blade. Int J Adv Eng Technol. 2012;3:343-6.
36. Che F. Material characterization and low cycle fatigue model of low Ag content lead-free solder. IEEE Transactions on Device and Materials Reliability. 2017.
37. Hsieh M-C. Modeling correlation for solder joint fatigue life estimation in wafer-level chip scale packages. Microsystems, Packaging, Assembly and Circuits Technology Conference (IMPACT), 2015 10th International: IEEE; 2015. p. 65-8.
38. Khan SBaARA. Fatigue and Creep Interaction in Steam Turbine Bladed Disk. International Journal of Innovative Research in Science, Engineering and Technology. 2014;3.
39. Vava G. Simple Rotor Blisk. 2016; Available from: https://grabcad.com/library/simple-rotor-blisk-1
40. Metals S. Inconel alloy 718. Publication Number SMC-045 Special Metals Corporation. 2007.
41. Dowling NE. Mechanical behavior of materials: engineering methods for deformation, fracture, and fatigue: Pearson; 2012.
42. Hattori H, Kitagawa M, Ohtomo A. Effect of grain size on high temperature low-cycle fatigue properties of inconel 617. Tetsu To Hagane. 1982;68:2521-30.

Paper 6: Development of a stress-based creep-fatigue equation: Accommodating pure-fatigue to pure-creep for the high-cycle loading regime

Dan Liu * and Dirk John Pons

Department of Mechanical Engineering, University of Canterbury, Christchurch 8140, New Zealand;

*Correspondence: dan.liu@pg.canterbury.ac.nz

Published Paper (Pre-prints for the publication)

Please cite this paper as:

Liu, D. and D.J. Pons, Development of a stress-based creep-fatigue equation: Accommodating pure-fatigue to pure-creep for the high-cycle loading regime. International Journal of Damage Mechanics, 2017: p. 1-19. DOI: https://dx.doi.org/10.1177/1056789517735678.

Abstract

Background – The creep-fatigue damage in low-cycle regime has been described by a strain-based creep-fatigue equation through integrating creep effect into fatigue damage. **Need** – There is a need to develop a creep-fatigue equation which describes the stress-controlled creep-fatigue behaviour in high-cycle regime. **Approach** – This stress-based creep-fatigue equation was developed through superposing a fatigue mechanism with a creep mechanism. This creep-fatigue equation was then validated on GP91 casting steel. The creep-fatigue data were transformed to the reference condition and collapsed into one power-law curve with good quality. **Outcomes** – This result verified the formulas of the fatigue component and the creep component, and demonstrated the method of extracting the coefficients. The full-range characteristic of this creep-fatigue equation is discussed. In addition, the introduction of the compatibility presents a better description of the reference condition. **Originality** - A new creep-fatigue equation is provided with demonstrably good ability to cover the full range of

conditions from the pure-fatigue condition to the pure-creep condition for the high-cycle regime. The method of extracting the coefficients is also provided.

Keywords: Creep-fatigue, creep rupture, stress-life, grain size, compatibility

1. Introduction

Creep-fatigue damage is the combination of fatigue damage and creep damage. There are two regimes of interest: low- and high-cycle. The low-cycle regime is already described by a strain-based creep-fatigue equation (discussed below). This paper reports on the theoretical development of a creep-fatigue equation for the high-cycle regime, and provides a method for extracting the necessary coefficients.

The two conventional pure-fatigue models are the Coffin-Manson equation (strain-life relation) (Eq.1) [1,2] and the Basquin equation (stress-life relation) (Eq.2) [3].

$$\frac{\Delta\varepsilon_p}{2} = \varepsilon_f'(2N_f)^{-c} \tag{1}$$

$$\frac{\Delta\sigma}{2} = \sigma_f'(2N_f)^{-b} \tag{2}$$

where $\Delta\varepsilon_p$ is the plastic strain amplitude, ε_f' is the fatigue ductility coefficient, c is the fatigue ductility exponent, $\Delta\sigma$ is the stress amplitude, σ_f' is the fatigue strength coefficient, b is the fatigue strength exponent and N_f is the cycles to failure. These two models (Eq.1 and Eq.2) are not independent, but satisfy the stress-strain relation, the Ramberg-Osgood equation (Eq.3) [4]. This relationship between the stress-life relation, the strain-life relation and the stress-strain relation is defined as the compatibility [5]:

$$\Delta\varepsilon_p = \left(\frac{\Delta\sigma}{K'}\right)^{1/n'} \tag{3}$$

where K' is the strain hardening coefficient and n' is the strain hardening exponent.

Previous research has proposed a strain-based creep-fatigue equation (Eq.4) [6,7]:

$$\varepsilon_p = C_0 c(\varepsilon_p, T, t_c, d) N_f^{-\beta_0} \tag{4-1}$$

with

$$c(\varepsilon_p, T, t_c) = 1 - \left[c_1(\varepsilon_p)(T - T_{ref}) + c_2(\varepsilon_p)\log(t_c/t_{ref})\right] \cdot \left[A(d/d_{ref})^m\right] \tag{4-2}$$

where ε_p is the plastic strain, C_0 is the fatigue capacity for one cycle of fatigue life, β_0 reflects the rate of reduction of the fatigue capacity, T is the temperature, T_{ref} is the reference temperature, t_c is the cyclic time, t_{ref} is the reference cyclic time, d is the grain size, d_{ref} is the reference grain size, and A and m are grain-size-related constants.

This equation accommodates relevant variables, and covers the full range of conditions from the pure-fatigue condition to the pure-creep condition. Since this equation is an extension of the Coffin-Manson equation, it only provides a good fatigue-life prediction in the *low-cycle regime* for strain-controlled fatigue behaviour. Therefore, in order to constitute a complete mathematical formalism, there is a need to develop a creep-fatigue equation which could be used in the *high-cycle regime* for stress-controlled fatigue behaviour. In this case, we propose a new creep-fatigue formulation for the high-cycle regime, as an extension of the Basquin equation (a conventional stress-life relation for high-cycle regime). Significantly, the development of the stress-based creep-fatigue equation provides a new method to present creep-fatigue behaviour under controlled stress in high-cycle regime without a mean-stress effect. In addition, the compatibility implies that both stress-life relation and strain-life relation do not independently exist, instead they are coupled phenomena. Consequently, although the creep-fatigue damage normally occurs in the low-cycle regime and is always presented under the situation with strain-controlled loading, the stress-based creep-fatigue description is still necessary because it presents a more classic method (stress-controlled fatigue evaluation) for engineering design and is an indispensable part of the fatigue phenomenon.

This is a complex problem because of the difficulty in finding a suitable formulation. Ideally this formulation would accommodate all the variables (temperature, frequency, grain size), have general validity for multiple materials, and preferably also provides an economical way to determine the coefficients for engineering design. The existing literature shows that a number of empirical experiments [8-10] have been conducted to explore the fatigue behaviour at elevated temperature in the high-cycle regime, where the fatigue strength has a strong dependence on temperature. However, the results obtained from these experiments have not been formulated as an equation to predict the fatigue life at multiple situations. This problem has been somewhat addressed by Kohout [11], who proposed a temperature-modified Basquin equation (Eq.5):

$$\frac{\Delta\sigma}{2} = a\left(2N_f\right)^{-b}T^c \tag{5}$$

where *a* and *c* are constants obtained from experiments.

However the influence of other variables, such as frequency (cyclic time) and grain size, are not included into this equation. This limits the application range of Eq.5.

The present work proposes a stress-based creep-fatigue equation, which accommodates relevant variables, provides a good description of creep-fatigue damage under stress-controlled situation in the high-cycle regime, and has the ability to cover the full range of conditions from the pure-fatigue condition to the pure-creep condition.

2. Research method

Generally, the stress-life relation is the most classic method to describe fatigue behaviour, and is illustratively presented by the S-N curve. This provides a method of fatigue-life prediction

in terms of controlled stress amplitude. However this is limited in being unable to accommodate creep-fatigue at neither low nor high cycles.

The motivation for the current work is the need for a creep-fatigue equation for the high-cycle regime especially. In what follows we set out the development of a stress-based creep-fatigue equation, which is an extension of the Basquin equation. The latter presents fatigue behaviour under controlled stress in the high-cycle regime without mean-stress effect. Therefore, the new creep-fatigue formulation is applicable to the same situation. See also the section on limitations below.

The method for deriving stress-based creep-fatigue equation is present below.

The strain-based creep-fatigue equation (Eq.4) was developed by starting with the empirical data, and applying curve fitting. In contrast, the stress-based creep-fatigue equation shown in this paper started from the existing formulations for creep and fatigue, to which physical principles were applied, to then result in a new formulation. This method follows the established bottom-up process [12]. Our application of this is shown in Figure 1.

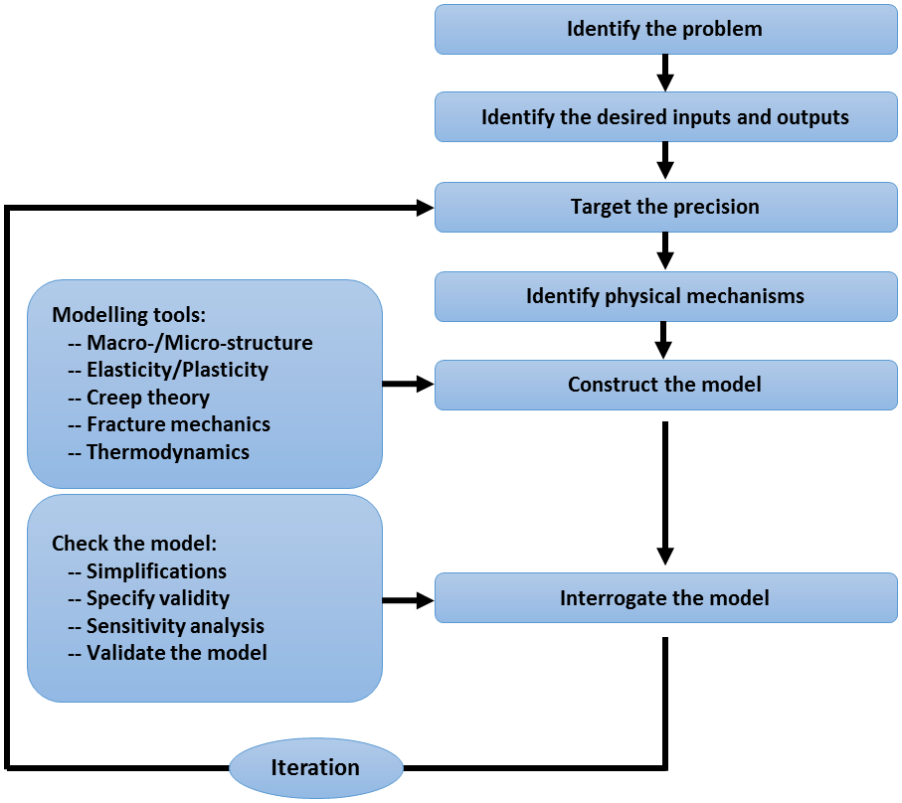

Figure 1 The process of bottom-up approach

This bottom-up process started with the identification of physical mechanisms of creep and fatigue, where the relationship between different variables were extracted. Then, these relationships were superimposed to construct the numerical formulation for creep-fatigue damage. During this process, the key variables were identified as temperature, cyclic time, and applied loading. These were then included in the formulation of the stress-based creep-fatigue equation. The relations between these variables were based on the structural relationships

embodied in the formulations of conventional fatigue and creep models. These others models have been well validated under multiple situations. In addition, we applied the concept of fatigue capacity [6], where the full fatigue capacity (the reference condition) is negatively influenced by temperature and cyclic time. A heat-treatment-related parameter, grain size, was introduced to describe the creep-fatigue damage from a micro-structure level. Significantly, introducing the concept of fatigue capacity gives the major structure of the stress-based creep-fatigue formulation, which is numerically presented as the form of '1-x'.

The stress-based creep-fatigue equation was validated on GP91 casting steel. The coefficients of this creep-fatigue equation were obtained by analysing experimental data. The experimental data, including the creep-rupture data, the creep-fatigue data and the strain-stress data, were extracted from the literature. Especially, the compatibility was introduced to extract the coefficients, and then the employment of the compatibility presented a better description of the reference condition.

The good representation of creep-fatigue behaviour formulated by the stress-based creep-fatigue equation was demonstrated through transforming all creep-fatigue data into the reference condition. The error of fatigue-life prediction was applied to evaluate the goodness of this creep-fatigue equation, and a small error was given. In particular, the stress-based creep-fatigue equation can be converted to the Basquin equation at the pure-fatigue condition, and can be reformed as a time-temperature parameter at the pure-creep condition.

3. The stress-based creep-fatigue equation

3.1 The derivation of the stress-based creep-fatigue equation

The stress-based creep-fatigue equation is a development of the conventional stress-life pure-fatigue equation, Basquin equation (Eq.2). This equation shows a relationship between fatigue life and applied stress without creep effect, and presents the full fatigue capacity for a given heat-treatment condition. The creep-fatigue damage is defined as the combined mechanisms of fatigue and creep, and is formulated through integrating the creep-related formulism into the Basquin equation.

At the pure-fatigue condition, the fatigue capacity is influenced by the heat treatment. The grain size is identified as a measurable parameter to represent the influence of heat treatment. Normally, grain size is related to yield stress through Hall-Petch equation, with a power-law relation between them. Then, this relation was extended to describe fatigue behaviour by Mutoh [13], Alexandre [14] and Thompson [15], and was physically derived from observing the plastic zone size around the crack tip at fatigue limit [16]. Consequently, the grain-size effect on fatigue capacity is numerically described by the Hall-Petch-type relation (Eq.6):

$$\sigma_s = \sigma_0{}' + \frac{k}{\sqrt{d}} \tag{6}$$

where σ_s is the fatigue strength (fatigue limit), and $\sigma_0{}'$ and k are constants. Reforming this equation as $\sigma_s - \sigma_0{}' = \frac{k}{\sqrt{d}}$ gives a power-law relation between fatigue capacity (σ_f) and grain size, $\sigma_f \propto d^m$. Specifically, fatigue strength is physically defined as the stress below which no fatigue failure occurs, and is numerically identified as the stress at 10^7 cycles. In this case, fatigue strength could be ideally calculated through letting N_f=10^7 in the Basquin equation (Eq.2). This implies that the power-law relation between fatigue strength and grain size could be extended to relate fatigue strength coefficient (σ_0) with grain size. Then, a grain-size-modified Basquin equation is given as:

$$\sigma_f = \sigma_0 \cdot B(d) \cdot N_f^{-b_0} = \sigma_0 \cdot B' d^p \cdot N_f^{-b_0} \tag{7}$$

where σ_f is the fatigue capacity for pure-fatigue condition, function $B(d)$ is the grain-size moderating function for pure fatigue, B' and p are constants, and σ_0 and b_0 are the constants to reflect the full fatigue capacity.

At the creep-fatigue condition, the fatigue capacity (σ_f) is negatively influenced by the creep effect. Because of the fatigue effect, the total time of creep-fatigue failure is significantly shorter than the creep-rupture time under applied loading [17]. Therefore, we assume that the creep damage for the creep-fatigue condition could be evaluated through the creep behaviour at the steady state, and this process is frequently presented by the equation of steady-state creep rate (Eq.8) [18,19]:

$$\dot{\varepsilon} = \frac{A\sigma^m}{d^q} e^{-\frac{Q}{RT}} \tag{8}$$

where $\dot{\varepsilon}$ is the strain rate, σ is the applied stress, d is the average grain size, Q is the activation energy, T is the temperature, R is the Boltzmennn's constant, and A, m and q are constants obtained from the creep test. This equation suggests that the creep damage could be presented as a function of stress, temperature, time and grain size. Therefore, we propose that the residual fatigue capacity (σ) can be formulated as Eq.9, through introducing a creep moderating function, $C(T, t, \sigma, d)$. This equation is termed the *stress-based creep-fatigue equation.* It provides a combination of the fatigue and creep mechanisms.

$$\sigma = C(T, t, \sigma, d)\sigma_f = \sigma_0 \cdot B(d) \cdot C(T, t, \sigma, d) \cdot N_f^{-b_0} \tag{9}$$

As discussed in the previous research [6,20], the reduction of fatigue capacity is consumed by the creep effect. From a stress perspective, this reduction, when $N_f = 1$, can be expressed as:

$$\sigma\big(N_f = 1\big) = \sigma_0 \cdot B(d) \cdot C(T, t_c, \sigma, d) = \sigma_f\big(N_f = 1\big) - \sigma_c = \sigma_0 \cdot B' d^p - \sigma_c \tag{10}$$

where σ_c presents the reduction of fatigue capacity due to the creep effect. Through employing the strain-stress relation [4], this stress (σ_c) (Eq.11) could be extracted from the general creep strain rate-stress relation (Eq.7), where the period of the creep process for one cycle is identified as the cyclic time (t_c).

$$\dot{\varepsilon}(\sigma, T, d) \rightarrow \varepsilon_c(\sigma, T, t, d) \xrightarrow{strain-stress\ relation} \sigma_c(\sigma, T, t_c, d) \tag{11}$$

Therefore, function $\sigma_c(\sigma, T, t_c, d)$ is assumed to take the form of Eq.12. This equation accommodates the power-law relations such as that shown in the general creep strain rate-stress relation (Eq.8), and retains the activation-energy component Q. In addition, the cyclic strain-stress relation provides a power-law transformation from strain to stress.

$$\sigma_c(\sigma, T, t, d) = K\left(C'\sigma^c d^b t_c e^{-\frac{Q}{RT}}\right)^{n'} \tag{12}$$

The derivation of Eq.12 is based on an assumptions, that is, the initial phase of creep is small enough to be neglected. Substituting Eq.10 with Eq.12 gives:

$$\sigma_0 B(d) C(T, t_c, \sigma, d) = \sigma_0 B' d^p - K\left(C'\sigma^c d^b t_c e^{-\frac{Q}{RT}}\right)^{n'} = \sigma_0 B' d^p \left[1 - \frac{KC'^{n'}}{\sigma_0 B'}\left(\sigma^c d^{b-\frac{p}{n'}} t_c e^{-\frac{Q}{RT}}\right)^{n'}\right] \tag{13}$$

Then, Eq.9 is shown as:

$$\sigma = \sigma_0 B' d^p \left[1 - \frac{KC'^{n'}}{\sigma_0 B'}\left(\sigma^c d^{b-\frac{p}{n'}} t_c e^{-\frac{Q}{RT}}\right)^{n'}\right] N_f^{-b_0} \tag{14}$$

Eq.14 shows that the constant σ_0 is multiplied with another constant B'. This gives an unreasonable numerical representation for extracting the coefficients since one specific product of σ_0 and B' could be achieved by multiple choices of σ_0 and B', and then makes empirical-data-based optimization operation more complex. In this case, the magnitude of B' is assumed as 1. This assumption provides a more reasonable and simpler numerical formulation for application, and the grain-size effect is somewhat incorporated into the fatigue strength coefficient (σ_0). This somewhat reduces the accuracy of fatigue-life prediction, but decreases the number of coefficients, and hence has the benefits of reduced experimental effort and complexity of operation.

Then, through re-organizing the coefficients, Eq.14 is further expressed as:

$$\sigma = \sigma_0 d^m \left[1 - A\left(\sigma^a d^n t_c e^{-\frac{Q'}{T}}\right)^k\right] N_f^{-b_0} \tag{15}$$

The experiments conducted by Gary [17] indicates that for a given magnitude of stress the creep damage is more intensive at the constant-stress condition than the cyclic-stress condition. Since the presentation of creep effect in Eq.15 comes from the pure-creep equation at constant stress (Eq.8), the cyclic stress in Eq.15 should be compressed to an equivalent constant stress through introducing a moderating factor, f_m. In the present work, we focus on the creep-fatigue behaviour under cyclic loading (regular-loading) with zero mean stress, thus this factor is valid in this situation. Generally, this moderating factor is related to the shape of the loading wave, and is defined as the average level of the cyclic loading to produce an equivalent transformation from the constant-loading situation to the cyclic-loading situation. This moderating factor is evaluated based on half-cycle loading, which arises as an assumption that the creep effect in the tensile portion is the same as in the compressive portion. This assumption may be not appropriate for some materials [21,22], but it simplifies the method of extracting this factor.

Then, Eq.15 is modified as:

$$\sigma = \sigma_0 d^m \left\{1 - A\left[(f_m\sigma)^a d^n t_c e^{-\frac{Q'}{T}}\right]^k\right\} N_f^{-b_0} \tag{16}$$

where A, a, n, Q', m and k are constants.

Finally, introducing the reference condition into Eq.16 gives the stress-based creep-fatigue equation:

$$\sigma = \sigma_0 \cdot B(d) \cdot C(T,t,\sigma,d) \cdot N_f^{-b_0} \tag{17-1}$$

with

$$\begin{aligned} B(d) &= \left(d/d_{ref}\right)^m \\ C(T,t,\sigma,d) &= 1 - A \cdot \left[\left(d/d_{ref}\right)^n \cdot f_m^a \cdot \sigma^a \cdot e^{-\frac{Q'}{T-T_{ref}}} \cdot \left(t_c/t_{ref}\right)\right]^k \\ T - T_{ref} &= \begin{cases} T - T_{ref} & for \;\; T > T_{ref} \\ \rightarrow 0 & for \;\; T \le T_{ref} \end{cases} \\ t_c/t_{ref} &= \begin{cases} t_c/t_{ref} & for \;\; t_c > t_{ref} \\ 1 & for \;\; t_c \le t_{ref} \end{cases} \end{aligned} \tag{17-2}$$

This completes the derivation of the stress-based creep-fatigue equation. Next we show how the coefficients may be derived.

3.2 The method of extracting coefficients

The coefficients of the stress-based creep-fatigue equation are extracted through experimental data and numerical method.

The relationship between fatigue capacity and grain size for pure fatigue is extracted from Eq.6, so the magnitude of m is identified as -0.5. In addition, the stress-moderating factor f_m is defined as the equivalent constant stress factor of the cyclic loading. Specifically, $f_m = 0.6366$ for the sinusoidal wave and $f_m = 0.5$ for the triangular wave.

According to the concept of fatigue capacity [6], at the pure-creep condition, the fatigue capacity is totally consumed by creep effect, thus $\sigma = 0$. This gives:

$$C(T,t_c,\sigma,d) = 1 - A \cdot \left[\left(d/d_{ref}\right)^n \cdot f_m^a \cdot \sigma^a \cdot e^{-\frac{Q'}{T-T_{ref}}} \cdot \left(t_c/t_{ref}\right)\right]^k = 0 \tag{18}$$

Then, applying a logarithmic operation presents a temperature-time relation:

$$\log\left[e^{-\frac{Q'}{T-T_{ref}}} \cdot t_c\right] = -a\log\sigma + \log\left[\left(\frac{1}{A}\right)^{1/k}\left(d/d_{ref}\right)^{-n} t_{ref} f_m^{-a}\right] \tag{19}$$

This relation has the same form as a well-known temperature-time relation, the Sherby-Dorn parameter (Eq.20) [23]:

$$P_{SD}(\sigma) = \log\left[t_R e^{-Q/(RT)}\right] = -\frac{Q}{RT}\log e + \log t_R \tag{20}$$

where $P_{SD}(\sigma)$ is the Sherby-Dorn parameter and t_R is the rupture time. This parameter can be extracted through creep-rupture tests, and can be also expressed as a linear relationship with the log of stress (Eq.21) [18]:

$$P_{SD}(\sigma) = a_1 \log \sigma + a_2 = \log\left[t_R e^{-Q/(RT)}\right] \tag{21}$$

where a_1 and a_2 are constants obtained from creep-rupture tests. Since the creep moderating function does not strictly derived from the general creep strain rate-stress relation (Eq.8) and the initial stage of creep is ignored, the magnitude of $\log\left[\left(\frac{1}{A}\right)^{1/k}\left(d/d_{ref}\right)^{-n} t_{ref} f_m^{-a}\right]$ in Eq.19 cannot be related to the magnitude of a_2 in Eq.21. However, the intensity of stress effect (a) and the activation-energy-related parameter (Q') , may be related with the Sherby-Dorn parameter through comparing Eq.19 with Eq.21, hence Eq.22.

$$Q' = Q/R \quad \text{and} \quad a = -a_1 \tag{22}$$

Therefore, the coefficients, Q' and a, can be extracted from creep-rupture data.

A numerical solution may be applied to obtain the magnitudes of σ_0, b_0, A, k and n. Although this method could provide a solution with minimum error, numerical optimization may not present good consistency with the internal physical relation between these coefficients. Consequently, this potential risk could lead to inaccuracy prediction for the pure-fatigue condition, because the full-fatigue-capacity-related parameters (σ_0 and b_0) are directly derived from the numerical method. Therefore, in order to improve the results obtained through the numerical method (the improvement will be shown in section 5.1), the compatibility [5] is introduced to relate the stress-life relation with the strain-life relation.

The derivation of the stress-based creep-fatigue equation and the strain-based creep-fatigue equation is based on the concept of fatigue capacity. This is based on an assumption that the exponents (b_0 and β_0) of these two creep-fatigue equations are independent of temperature, cyclic time and grain size. This assumption implies that the modified creep-fatigue coefficients ($\sigma_0 \cdot B(d) \cdot C(T, t, \sigma, d)$ for the stress-based equation and $C_0 c(\sigma, T, t_c, d)$ for the strain-based equation) could not strictly follow the compatibility, but the coefficients (σ_0 and C_0) and the exponents (b_0 and β_0) for the pure-fatigue condition (the reference condition) can be related through the compatibility equations (Eq.23 and Eq.24):

$$\sigma_0 = K' {C_0}^{n'} \tag{23}$$

$$b_0 = n'\beta_0 \tag{24}$$

In this way, the internal relation between the coefficients and exponents is included to reduce the number of independent coefficients, and then the coefficients of the stress-based creep-fatigue equation (Eq.17) is solved through combining with the strain-based creep-fatigue equations (Eq.3). The numerical method is conducted through minimizing the difference (Eq.25) between the computed creep-fatigue life ($N_{comp,ij}$) and experimental creep-fatigue life ($N_{exp,ij}$) at the conditions of σ_j, ε_{pj}, T_i and $t_{c,i}$.

$$error = \sum \left(\log N_{comp,ij} - \log N_{exp,ij}\right)^2 \tag{25-1}$$

with

$$N_{comp,ij} = \left[\frac{\sigma_j}{\sigma_0 B(d) C\left(T_i, t_{c,i}, \sigma_j, d\right)}\right]^{-1/b_0} \quad for\ stress - life\ relation \tag{25-2}$$

$$N_{comp,ij} = \left[\frac{\varepsilon_{pj}}{C_0 c\left(\varepsilon_{p,j}, T_i, t_{c,i}, d\right)}\right]^{-1/\beta_0} \quad for\ strain - life\ relation \tag{25-3}$$

3.3 The evaluation of the stress-based creep-fatigue equation

The method of evaluation is built on the concept of fatigue capacity. This implies that the creep fatigue data at multiple situations are transformed from one specific reference condition. Therefore, a good description of creep-fatigue damage can collect all creep-fatigue data into one power-law curve (the curve for the reference condition). This transformation from the creep-fatigue condition to the reference condition is progressed through Eq.26:

$$\sigma_{ref} = \sigma_0 N^{-b_0} = \sigma / [B(d) \cdot C(T, t, \sigma, d)] \tag{26}$$

In addition, the coefficient and exponent of the trend line in the reference condition should agree well with the magnitudes of σ_0 and b_0 respectively. This presents a good description on the reference condition. Finally, the ratio of experimental fatigue life to computed fatigue life should drop in a reasonable range, which verifies the goodness of fatigue-life prediction by using the stress-based creep-fatigue equation.

4. The validation on GP91 casting steel

The stress-based creep-fatigue equation is validated on GP91 casting steel, and the experimental data, including the creep-rupture data [24], the creep-fatigue data [25,26] and the stress-strain data [25,26], are obtained from literature. The reference temperature is defined as 35% of melting temperature [27], and the cyclic time is suggested as a small value. The creep effect is dormant below the reference temperature and the reference cyclic time. In addition, the reference grain size is arbitrarily selected based on the experimental range for the material. Therefore, the reference temperate is chosen as 610K, the reference cyclic time is given as 1s, and the reference grain size is chosen as 25μm.

4.1 The derivation of the coefficients

According to the relation between fatigue capacity and grain size in the pure-fatigue condition, the magnitude of *m* is given as -0.5. The stress-moderating factor f_m is suggested as 0.6366 for the sinusoidal wave.

4.1.1 The extracting of creep characteristic

On the one hand, based on the creep-rupture data obtained from Ref.19 (see Figure 3 therein), the Sherby-Dorn parameter (Eq.20) is extracted through plotting *1/(T-T_{ref}) vs logt* (Fig.2):

$$P_{SD}(\sigma) = \log\left[te^{-Q/[R(T-T_{ref})]}\right] = -\frac{Q\log e}{R}\cdot\frac{1}{T-T_{ref}} + \log t \tag{27}$$

The slope (3054.07) of *1/(T-T_{ref}) vs logt* curves shown in Fig.2 gives Q, then the magnitude of Q' may be obtained through Eq.22:

$$Q' = Q/R = 3054.07/\log e = 7032 \tag{28}$$

On the other hand, the Sherby-Dorn parameter is presented as a function of stress:

$$P_{SD}(\sigma) = -12.95\log\sigma + 23.307 \tag{29}$$

According to Eq.22, the magnitude of a is given as 12.95.

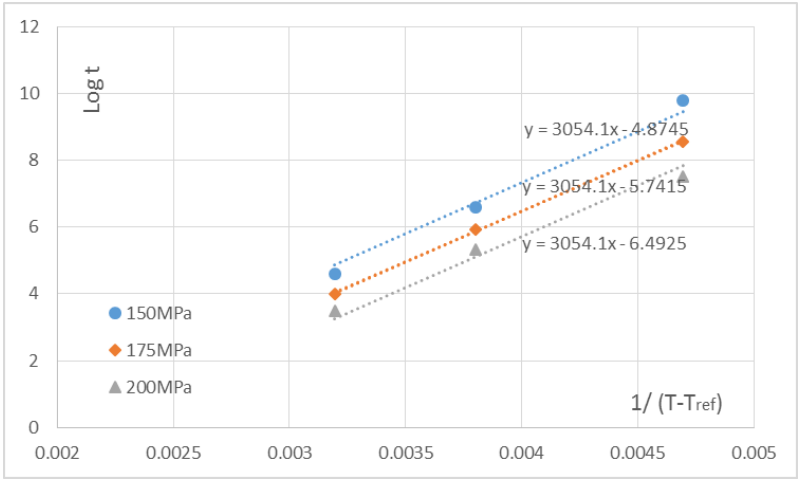

Figure 2 The creep-rupture characteristics for GP91 casting steel

The accuracy of the creep-related coefficients are limited by the data published in the literature, which in this case are sparse. Nonetheless there are sufficient data to establish the method, and accuracy may be improved as results from more creep-rupture tests become available in the future.

4.1.2 The extracting of coefficients through numerical method

The creep-fatigue coefficients and the strain-stress coefficients at three temperatures, two cyclic times and two grain sizes obtained from Ref.20 and Ref.21 are tabulated in Table 1. Minimizing the difference between computed creep-fatigue life ($N_{comp,ij}$) and experimental creep-fatigue life ($N_{exp,ij}$) yields $\sigma_0 = 874.40$, $b_0 = 0.0697$, $A = 0.1824$, $k = 0.02689$ and $n = -71.7328$.

Table 1 The creep-fatigue coefficients obtained from ref.20 and ref.21

Temperature (K)	Cyclic time (s)	Grain size (μm)	Creep-fatigue coefficients		Strain-stress coefficients	
			σ_f'	b	K'	n'
673	5	25	689.67	-0.056	763.4	0.0956
823	5	25	409.82	-0.054	416.15	0.0743
873	2	35	411.58	-0.048	431.52	0.071

4.2 The evaluation of the stress-based creep-fatigue equation

According to the results obtained in section 4.1, the experimental creep-fatigue data, σ-N_{exp}, are transformed to the reference condition (the pure-fatigue condition), σ_{ref}-N_{exp}, through using Eq.26. Figure 3 shows that the transformed data are collected into a single power-law curve of $\sigma_{ref} = 776.88N^{-0.06}$ with a good quality of fit as R^2= 0.9878. The coefficient and exponent of this trend line, 776.88 and 0.06 respectively, are close to the magnitudes of σ_0 and b_0 obtained in section 4.1.

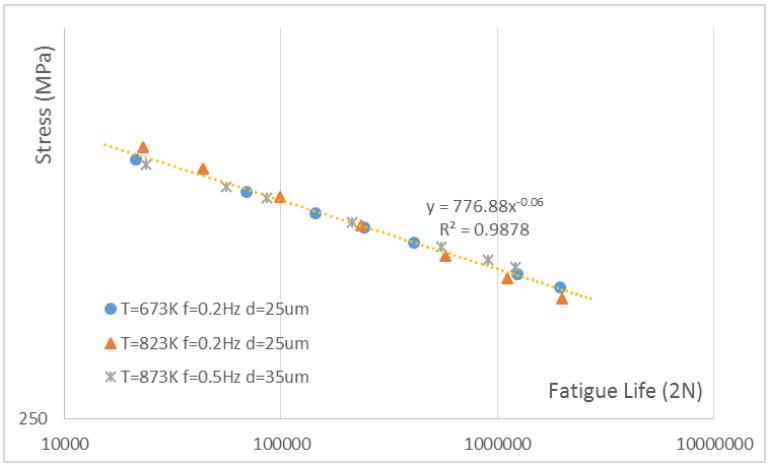

Figure 3 The transformed σ_{ref}-N_{exp} data of GP91 casting steel

In addition, the error, which shows the difference between experimental fatigue life and computed fatigue life, is calculated to be 0.2401 through Eq.12. The goodness of fatigue-life prediction is further illustrated in Fig.4, where the data points (N_{exp}, N_{comp}) fall within the upper bound (+30%) and the lower bound (-30%).

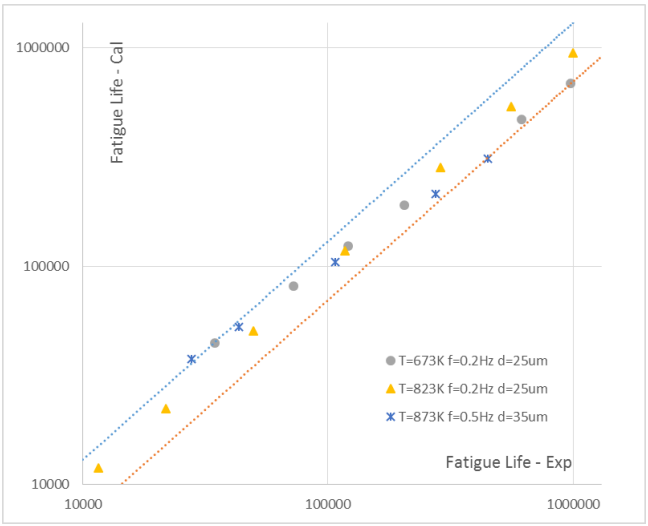

Figure 4 The plotting of computed fatigue life vs experimental fatigue life

The results obtained above verify the formulation of the stress-based creep-fatigue damage (Eq.17) and the method of extracting the coefficients. Specifically, the good transformation from multiple creep-fatigue conditions to the reference condition shows that this creep-fatigue equation provides a good description of creep effect through creep function $C(T, t, \sigma, d)$, and the small error between the computed fatigue life and experimental fatigue life represents an excellent fatigue-life prediction. In addition, the employment of compatibility provides a better description of the reference condition, and this will be discussed in section 5.1.

5. Discussion

5.1 The compatibility

The introduction of the compatibility presents the relationship between strain, stress and life. This provides a better description of the reference condition. The results obtained through the method with and without the compatibility are compared in Table 2.

Table 2 The results obtained from method without and with the compatibility

Methods	Strain-based creep-fatigue equation		Stress-based creep-fatigue equation		Error
	C_0	β_0	σ_0	b_0	
Experimental results	0.7297	-0.644	879.8	-0.0673	---
The method without compatibility	0.6879	-0.667	1740.36	-0.0576	0.05123
The method with compatibility	0.6879	-0.667	874.40	-0.0697	0.24008

The results shown in Table 2 suggest that the full fatigue capacity is enlarged by using the method without the compatibility. This may be an artefact of the numerical method. This method aims to minimize the error, thus the solution is obtained from a numerical perspective that is disconnected from the physical situation. Although the method without the compatibility gives a smaller error compared to the method with the compatibility, the non-compatibility method ignores the internal relationship (the compatibility) between the stress-life relation and the strain-life relation. This is a typical weakness for this method, because a key constraint is removed during the numerical operation. However, the compatibility-based method results in a more reliable solution by involving a physically based constraint that cannot be ignored, and then gives a more reasonable description for the reference condition.

The pure-fatigue-related coefficients [26] directly obtained from experiments are closer to the results given by the compatibility-based method than the results given by the non-compatibility method – this is evident in Table 2. In addition, Table 2 indicates that the numerical method does not have significant influence on the accuracy of presenting the reference condition for the strain-based creep-fatigue equation. This may result from the narrow potential range of C_0. However, this influence for the stress-based creep-fatigue equation becomes more significant, because the possible solution for σ_0 covers a wide range, and a small fluctuation of any coefficient in the stress-based creep-fatigue equation could lead to a large change for σ_0.

The compatibility may be represented graphically as a set of relationships between the stress-life relation, the strain-life relation, and the stress-strain relation see Figure 5. The values shown are for GP91 material and the coefficients arising from the numerical method applied to the experimental data. Figure 5 presents a linear relation between logs of stress, strain and fatigue life in a 3-D space at the reference condition, and this straight curve can be projected into the stress-life plane, the strain-life plane and the stress-strain plane. These projects represent the relations formulated by the Basquin equation, the Coffin-Manson equation and the Ramberg-Osgood equation respectively. This figure demonstrates that the compatibility is well accommodated in the stress-based creep-fatigue equation.

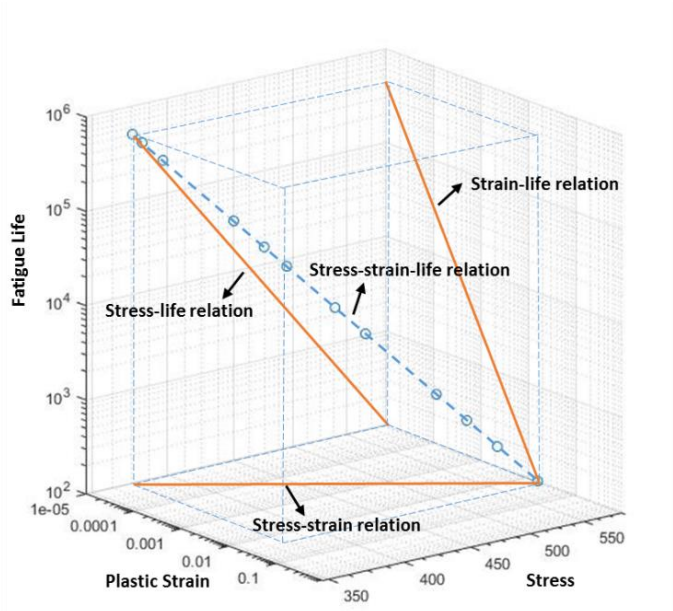

Figure 5 The stress-strain-life relation in a 3-D space

5.2 The full-scale characteristic

The stress-based creep-fatigue equation can cover the full range of conditions from the pure-fatigue condition to the pure-creep condition.

5.2.1 Pure fatigue

At the pure-fatigue condition, $T \to T_{ref}$, and the grain size is given as the reference grain size, $d = d_{ref}$. This suggests that $e^{-Q'/(T-T_{ref})} \to 0$ and grain-size component equals 1. Then, the stress-based creep-fatigue equation is restored to the Basquin equation, where the pure-fatigue damage is presented. The good consistency with the reference condition shown in section 4.2, where the creep-fatigue condition is transformed to the reference condition, strongly demonstrates this characteristic.

5.2.2 Pure creep

At the pure-creep condition, the fatigue capacity is totally consumed by creep effect. This results in the zero applied stress for fatigue ($\sigma = 0$). Then, the stress-based creep-fatigue equation is converted to Eq.30:

$$e^{-\frac{Q'}{T-T_{ref}}} \cdot \left(t/t_{ref}\right) = f_m^{-a} \cdot \sigma^{-a} \cdot \left(\frac{1}{A}\right)^{1/k} \left(d/d_{ref}\right)^{-n} \tag{30}$$

Doing logarithmic operation gives:

$$\log\left[e^{-\frac{Q'}{T-T_{ref}}} \cdot \left(t/t_{ref}\right)\right] = -a\log\sigma + \log\left[\left(\frac{1}{A}\right)^{1/k} \left(d/d_{ref}\right)^{-n} f_m^{-a}\right] \tag{31}$$

Eq.31 indicates a time-temperature relation, and has the same formulation as the Sherby-Dorn parameter. As shown in section 3.2, the intensity of stress effect on creep damage is directly extracted from the creep-rupture test. This is presented in the Sherby-Dorn parameter by the coefficient of *a*. The last term of Eq.31 is related to the grain size, and its coefficients do not strictly follow the creep-rate equation (Eq.8), thus this term cannot precisely present the creep behaviour. This is an inevitable problem caused by the bottom-up approach and the method of obtaining the coefficients, where the formulation is reorganized and simplified, and the creep characteristic is extracted from one given grain size. However, the connection between creep-fatigue condition and the pure-creep condition could be achieved through letting $\log\left[\left(\frac{1}{A}\right)^{1/k} \left(d/d_{ref}\right)^{-n} f_m^{-a}\right] = 23.307$, and a normalized grain size, 20μm, is then suggested. This normalized grain size relates to the material condition for creep-rupture test, and thus varies with the change of heat treatment. This implies that the transformation of the stress-based creep-fatigue equation only can show the pure-creep condition where the creep effect is extracted. In theory, if the creep-rupture tests could be conducted at different material conditions, a better suggestion of the magnitude of *n* and a better creep description of the last term in Eq.31 could be given. The limitation shown above presents a chance for developing a

grain-size-related Sherby-Dorn parameter, and this modified parameter may take the same or similar form as Eq.31.

5.2.3 Creep fatigue

The creep-fatigue condition has been validated in section 4, where the creep function, $C(T, t, \sigma, d)$, is between 0 and 1, and the creep-fatigue data can collapse into one power-law curve (the pure-fatigue condition) through transforming them into the reference condition. In addition, the good prediction of fatigue life is further illustrated by Figure 4, where the differences between the experimental fatigue life and computed fatigue life for multiple situations lie within an acceptable zone.

5.3 General physical explanation of the stress-based creep-fatigue equation

The Basquin equation is modified by the fatigue component, $B(d)$, and the creep component, $C(T, t, \sigma, d)$, to show the combination effect between fatigue and creep. In this way, the fatigue mechanism formulated by the Basquin equation (Eq.2) and the Hall-Petch-type relation (Eq.6), and the creep mechanism presented by the Sherby-Dorn parameter (Eq.20) and the equation of steady-state creep rate (Eq.8) are superposed.

5.3.1 The grain-size effect

The grain size effect is presented in both the fatigue component and the creep component, and shows that the material with small grain size presents a good pure-fatigue behaviour, but has poorer resistance to creep damage. This phenomenon results from the different failure mechanisms shown by fatigue and creep, where the fatigue effect occurs via cracks through the grains, while creep involves the grain boundary cracking [18].

For the fatigue component, the relationship between fatigue capacity and grain size in the pure-fatigue condition is consistent with the relation shown in Eq.6, where the fatigue capacity is reduced with increasing grain size. To be specific, fatigue failure is caused by the progressive accumulation of plastic deformation under cyclic loading. During this process, cracks initiate at the early stage and then gradually propagate through grain boundaries with the increasing number of cycles. The propagation of a crack needs to penetrate the grain boundary to extend to the next grain, and this may also require a reorientation of the crack growth direction. This means that more grains the crack encounters the slower growth, and hence the greater loading (stress or strain) is required to extend the crack to the critical length for final failure. Consequently, the material with smaller grain size presents a better pure fatigue behaviour, and accommodates high applied loading.

As shown above, grain boundary is a barrier for the propagation of a crack under pure-fatigue conditions. However, the grain boundary becomes the source of creep damage at pure-creep conditions. Since the stress concentration is worsened at the triple points (intersection among three adjacent grains), the crack growth along grain boundaries is promoted in these locations.

The triple point provides not only a geometric stress concentration effect, but also contains crystalline defects, where multiple directional opportunities for crack propagation along the grain boundaries are provided. In this way, the finer the grain size, the greater the internal area of grain boundaries and volumetric density of triple points, hence enhanced opportunity for crack propagation. In contrast a body with few grains, or even only one grain, presents fewer such boundary opportunities.

In addition, the influence of grain size on creep also involves the physical mechanism of diffusion creep. Specifically, the diffusion of atoms causes the elongation of a grain along the stress axis. As a result, a finer grain size undergoes more deformation opportunities than a coarse grain under a given stress.

Consequently, larger grain size is more beneficial for creep ductility, and results in longer rupture time.

5.3.2 The time-temperature relation

The creep behaviour is negatively influenced by temperature and cyclic time. This is mathematically presented through the creep component, $C(T, t, \sigma, d)$. This component accommodates the creep rupture characteristic, where the relation between temperature, time and stress is consistent with the Sherby-Dorn parameter and the equation of steady-state creep rate. The superposition between the Basquin equation and the well-known time-temperature relation presents a good link between the creep-fatigue condition and the pure-creep condition.

In general, the underlying mechanisms whereby temperature affects the creep-fatigue process are believed that elevated temperature leads to weaker atom bonding because of better conditions for diffusion, then causes the movements of vacancies. This transfer finally results in the overall deformation of the material. Specifically, an atom needs to overcome the energy barrier to move from its current site to the nearby vacant site. By this means, the high temperature can provide atoms enough energy to break the bonds with neighbour atoms and then lead to migration. In addition, diffusion basically is a net movement of atoms from a high to a low concentration region. This reflects the initial driving force for the transfer of atoms. During this process, temperature is an important factor to determine the rate of diffusion, wherein the elevated temperature speeds up the random atom motion. Consequently, the increasing temperature accelerates the process of diffusion (more creep damage occurs), and then reduces the fatigue capacity for the creep-fatigue condition.

Creep is defined as a time-dependent deformation under a constant loading, which indicates that creep damage is intensified with increasing time. The influence of frequency/cyclic time was initially formulated by the frequency-modified Coffin-Manson equation [28] based on the experimental results at elevated temperature, wherein the creep effect in terms of time was involved. This equation shows that the decreasing frequency (increasing cyclic time) decreases fatigue capacity due to the increasing contribution of creep damage. Specifically, slow frequency (large cyclic time) gives more accumulation of creep at a given temperature. In other words, the longer time leads to more diffusion in the microstructure when a material is exposed to high temperature under constant applied loading. In addition, the influence of

frequency/cyclic time on creep can also be explained through the stress-strain model shown in Fig.6 [18], where σ is the applied stress and η_1 reflects the yield strength. In this model, the small time can only lead spring E_1 to deform, and thus the slope of stress-strain curve is E_1. However, large time causes the deformation of both spring E_1 and E_2, and the strain (ε) may be expressed as:

$$\varepsilon = \frac{\sigma}{E_1} + \frac{\sigma - \eta_1}{E_2} \tag{32}$$

Eq.32 shows that the slope of stress-strain curve is $E_1E_2/(E_1+E_2)$, which is smaller than E_1. This implies that the large time can reduce stiffness, and increase strain and lead to more creep damage.

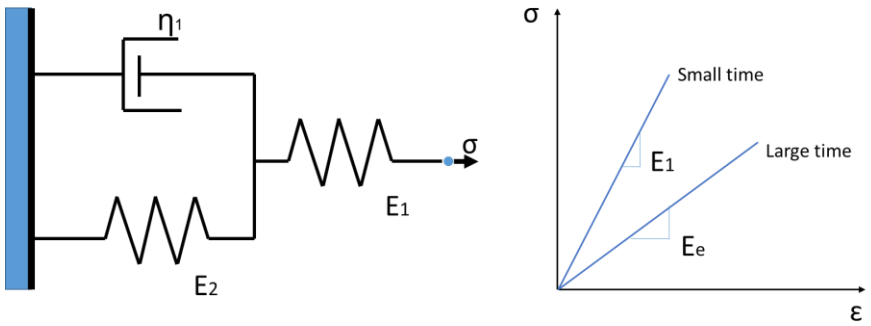

Figure 6 The stress-strain model. Image adapted from Ref.18.

5.3.3 The reference condition

The introduction of the reference condition shows the threshold between pure-fatigue condition and creep-fatigue equation, and the creep is dormant below the reference temperature and the reference cyclic time. Especially, at the reference condition, the stress-based creep-fatigue equation is restored to the Basquin equation, which builds a bridge between pure fatigue and creep fatigue. The full fatigue capacity is presented by σ_0 and b_0, wherein σ_0 is related to the fatigue strength and b_0 responds for the material's resistance to fatigue damage. For a given b_0, higher σ_0 implies better ability to accept applied stress, while, for a given σ_0, higher b_0 suggests lower ability to resist fatigue damage.

5.4 Contributions and limitations

The stress-based creep-fatigue equation was developed through integrating the fatigue mechanism (the Basquin equation and the Hall-Petch-type relation) with the creep mechanism (the Sherby-Dorn parameter and the equation of steady-state creep rate). The good R^2 values obtained through transforming the raw creep-fatigue data into the reference condition implies that this creep-fatigue equation accommodates the experimental data with a high degree of fidelity. In addition, this creep-fatigue equation has the capability to cover the full range of conditions from the pure-fatigue condition to the pure-creep condition. Especially, the introduction of the compatibility gives a more reasonable presentation of the reference

condition. These results have not been shown previously in the literature, hence are novel contributions.

However, extracting coefficients of this creep-fatigue equation partly relies on the numerical method. Although the temperature-time parameter and the reference condition have been involved in this creep-fatigue equation, the employment of the numerical method results in an incomplete physical explanation for the coefficients. This implies that it is difficult to predict the coefficients without the creep-fatigue experiments. This may not be completely solved, but opens an opportunity for future research to reduce this difficulty. In addition, the mean-stress effect has been thoroughly included in the pure-fatigue situation, such as the approach [18] based on the Morrow's mean stress equation and the formulation [29] based on Goodman's mean stress equation. However, the mean-stress effect is not included into the current stress-based creep-fatigue equation, thus the ratcheting phenomenon is not described by this equation. In this case, this limitation opens an opportunity for future research to accommodate mean-stress effect into the creep-fatigue formulation.

6. Conclusion

The strain-based creep-fatigue equation is applicable to the low-cycle regime (below 10^4 cycles), while the creep-fatigue behaviour in the high-cycle regime (between 10^4 cycles to 10^6 cycles) is described by the stress-based creep-fatigue equation. The combination of these two formulas presents a comprehensive model for creep-fatigue behaviour.

The following major results are obtained:

(1) The stress-based creep-fatigue equation (Eq.17) is proposed through superposing a fatigue mechanism with a creep mechanism.

(2) This creep-fatigue equation was validated on GP91 casting steel. The creep-fatigue data were transformed to the reference condition and collapsed into one power-law curve with good quality. This result verified the formulas of the fatigue component and the creep component, and demonstrated the method of extracting the coefficients.

(3) This creep-fatigue equation shows a good ability to cover the full range of conditions from the pure-fatigue condition to the pure-creep condition.

(4) The introduction of the compatibility provides a better description of the reference condition.

Author Contributions: The work was conducted by DL and supervised by DP. The formula of the stress-based creep-fatigue equation was proposed and the method of extracting the coefficients was then developed by DL. The discussion on the compatibility, the full-range characteristic and the physical explanation was conducted by DL and DP.

Conflicts of Interest: The authors declare no conflict of interest. The research was conducted without personal financial benefit from any funding body, and no such body influenced the execution of the work.

References

1. Coffin Jr LF. A study of the effects of cyclic thermal stresses on a ductile metal. Knolls Atomic Power Lab., 1953.
2. Manson SS. Behavior of materials under conditions of thermal stress. Lewis Flight Propulsion Lab., 1954.
3. Basquin O. The exponential law of endurance tests. Proc Astm. 1910, p. 625-30.
4. Ramberg W and Osgood WR. Description of stress-strain curves by three parameters. 1943.
5. Lee Y-L. Fatigue testing and analysis: theory and practice. Butterworth-Heinemann, 2005.
6. Liu D, Pons D and Wong E-h. The Unified Creep-Fatigue Equation for Stainless Steel 316. Metals. 2016; 6: 219.
7. Liu D, Pons DJ and Wong E. Creep-integrated fatigue equation for metals. Int J Fatigue. 2017; 98: 167-75.
8. Juijerm P and Altenberger I. Fatigue behavior of deep rolled Al–Mg–Si–Cu alloy at elevated temperature. Scr Mater. 2006; 55: 943-6.
9. Kawagoishi N, Chen Q and Nisitani H. Fatigue strength of Inconel 718 at elevated temperatures. Fatigue Fract Eng Mater Struct. 2000; 23: 209-16.
10. Liu Y, Yu J, Xu Y, Sun X, Guan H and Hu Z. High cycle fatigue behavior of a single crystal superalloy at elevated temperatures. Mater Sci Eng, A. 2007; 454: 357-66.
11. Kohout J. Temperature dependence of stress–lifetime fatigue curves. Fatigue Fract Eng Mater Struct. 2000; 23: 969-77.
12. Bhadeshia H and Honeycombe R. Steels: microstructure and properties. Butterworth-Heinemann, 2011.
13. Mutoh Y and Radhakrishnan V. Effect of yield stress and grain size on threshold and fatigue limit. J Eng Mater Technol. 1986; 108: 174-8.
14. Alexandre F, Deyber S and Pineau A. Modelling the optimum grain size on the low cycle fatigue life of a Ni based superalloy in the presence of two possible crack initiation sites. Scr Mater. 2004; 50: 25-30.
15. Thompson AW and Backofen W. The effect of grain size on fatigue. Acta metallurgica. 1971; 19: 597-606.
16. Mutoh Y and Radhakrishnan V. An Analysis of Grain Size and Yield Stress Effects on Stress at Fatigue Limit and Threshold Stress Intensity Factor. Journal of Engineering Materials and Technology(Transactions of the ASME). 1981; 103: 229-33.
17. Halford G. Cyclic creep-rupture behavior of three high-temperature alloys. Metall Trans. 1972; 3: 2247-56.
18. Dowling NE. Mechanical behavior of materials: engineering methods for deformation, fracture, and fatigue. Prentice hall, 1993.
19. Evans RW and Wilshire B. Introduction to creep. The Institute of Materials(UK), 1993. 1993: 115.
20. Liu D, Pons D and Wong E-h. Creep-Integrated Fatigue Equation for Metals. Int J Fatigue. 2016.

21. Tsuno N, Shimabayashi S, Kakehi K, Rae C and Reed R. Tension/compression asymmetry in yield and creep strengths of Ni-based superalloys. Proceedings of the International Symposium on Superalloys. 2008, p. 433-42.
22. Yamashita M and Kakehi K. Tension/compression asymmetry in yield and creep strengths of Ni-based superalloy with a high amount of tantalum. Scripta materialia. 2006; 55: 139-42.
23. Dorn J, Orr RL and Sherby O. Creep correlations of metals at elevated temperatures. AIME TRANS. 1954; 200: 71-80.
24. Tabuchi M, Hongo H, Li Y, Watanabe T and Takahashi Y. Evaluation of microstructures and creep damages in the HAZ of P91 steel weldment. J Pressure Vessel Technol. 2009; 131: 021406.
25. Mishnev R, Dudova N and Kaibyshev R. Low Cycle Fatigue Behavior of a 10% Cr Martensitic Steel at 600° C. ISIJ Int. 2015; 55: 2469-76.
26. Mroziński S and Golański G. Low cycle fatigue of GX12CrMoVNbN9-1 cast steel at elevated temperature. J Achiev Mater Manuf Eng. 2011; 49: 7-16.
27. Ashby MF, Shercliff H and Cebon D. Materials: engineering, science, processing and design. Butterworth-Heinemann, 2013.
28. Coffin L. Fatigue at high temperature. Fatigue at elevated temperatures. ASTM International, 1973.
29. Zghal J, Gmati H, Mareau C and Morel F. A crystal plasticity based approach for the modelling of high cycle fatigue damage in metallic materials. International Journal of Damage Mechanics. 2016; 25: 611-28.

Paper 7: Physical-Mechanism Exploration of the Low-Cycle Unified Creep-Fatigue Formulation

Dan Liu * and Dirk John Pons

Department of Mechanical Engineering, University of Canterbury, Christchurch 8140, New Zealand;

*Correspondence: dan.liu@pg.canterbury.ac.nz

Published Paper (Pre-prints for the publication)

Please cite this paper as:

Liu, D. and D.J. Pons, Physical-Mechanism Exploration of the Low-Cycle Unified Creep-Fatigue Formulation. Metals, 2017. 7(9): p. 379. DOI: http://dx.doi.org/10.3390/met7090379.

Abstract

Background—Creep-fatigue behaviour is identified as the incorporated effects of fatigue and creep. One class of constitutive-based models attempts to evaluate creep and fatigue separately, but the interaction of fatigue and creep is neglected. Other models treat the damage as a single component, but the complex numerical structures that result are inconvenient for engineering application. The models derived through a curve-fitting method avoid these problems. However, the method of curving fitting cannot translate the numerical formulation to underlying physical mechanisms. **Need**—Therefore, there is a need to develop a new creep-fatigue formulation for metal that accommodates relevant variables and where the relationships between them are consistent with physical mechanisms of fatigue and creep. **Method**—In the present work, the main dependencies and relationships for the unified creep-fatigue equation were presented through exploring what the literature says about the mechanisms. **Outcomes**—This shows that temperature, cyclic time and grain size have significant influences on creep-fatigue behaviour, and the relationships between them (such as linear relation, logarithmical relation and power-law relation) are consistent with phenomena of diffusion creep and crack

growth. Significantly, the numerical form of “1-x” is presented to show the consumption of creep effect on fatigue capacity, and the introduction of the reference condition gives the threshold of creep effect. **Originality**—By this means, the unified creep-fatigue equation is linked to physical phenomena, where the influence of different dependencies on creep fatigue was explored and relationships shown in this equation were investigated in a microstructural level. Particularly, a physical explanation of the grain-size exponent via consideration of crack-growth planes was proposed.

Keywords: creep fatigue; physical mechanism; temperature; cyclic time; grain size; fatigue capacity

1. Introduction

Creep-fatigue damage is physically explained as the combined effects of fatigue and creep, due to reversed loading and elevated temperature respectively. Historically, creep-fatigue models have been developed through either a constitutive-based method, or an empirically-based method.

The constitutive-based method is typically conducted by exploring the underlying physical mechanisms of fatigue and creep, and by including parameters representing the properties of the material. Some constitutive models have been extended from the conventional idea of continuum damage, including the linear damage rule [1,2] and the crack growth law [3]. Examples of such models are those proposed by Takahashi [4,5] and Warwick [6] which are based on ductility and energy exhaustion with the total damage being divided into fatigue damage and creep damage, the model proposed by Sehitoglu [7] that divides the total damage into three sub-damages caused by fatigue, oxidation and creep, and the model proposed by Ainsworth [8] that partitions the crack as a whole into sub-effects caused by fatigue and creep.

The constitutive models based on continuum damage are successful in evaluating creep and fatigue separately, but do not address the interaction of fatigue and creep, hence weakening the applicability. The deeper issue is that the interactive effect between fatigue and creep is complex and the numerical formulism is unknown. Thus, it is difficult to further improve the continuum-damage-based models by introducing an interactive effect. Some constitutive models try to avoid the need to evaluate the interactive component, by treating the total damage or the fatigue ability as a single component. Examples are the model [9,10] extended from the Chaboche model [11], the model [12,13] that described the crack-tip behaviour, and the model [14,15] that evaluated dissipated energy. Although these models present a comprehensive numerical representation of creep fatigue, they provide mathematically complex structures. Therefore, these models are not convenient to be used by engineers who need to obtain fatigue life through simpler physical parameters such as applied loading, temperature and cyclic time.

The empirical-based method is typically conducted by fitting mathematical formula to the empirical data, with the emphasis on high quality of fit. The empirical-based models might be

more favourable since these models provide simpler/clearer numerical representations. By the empirical-based method the creep-fatigue behaviour is numerically represented—this is achieved by incorporating the creep-related parameters into one of the conventional fatigue models, such as the Basquin equation [16] for the high-cycle regime, or the Coffin-Manson equation [17,18] for the low-cycle regime.

The low-cycle creep-fatigue behaviour has received much attention, and resulted in different strain-based creep-fatigue models. The first model developed by the empirical-based method was attempted by Coffin [19], who proposed the frequency-modified Coffin-Manson equation. Then, this formulation was further modified by Solomon [20] and Shi et al. [21] through directly introducing a temperature dependency. Discarding the family of equations based on the frequency-modified Coffin-Manson equation has given additional numerical representations of creep fatigue, such as the equations proposed by Jing et al. [22], Engelmaier [23] and Wong and Mai [24].

However, these creep-fatigue models have significant limitations. The issue is that there are multiple variables to model: failure mode (creep, creep-fatigue and fatigue), multiple temperatures, different cyclic times (frequency), and different materials (type of material and grade thereof). The existing curve-fitting models cover one or both of variable temperature and cyclic time, but are specific to one material grade. This is because these models were derived from one specific situation. In addition, these existing models cannot cover the full range of conditions from pure fatigue to pure creep, since they were derived from the empirical data of creep fatigue. In this case, the existing models cannot natively be extended to other materials or failure modes. Furthermore, these existing models cannot provide an economical method for engineering design because numerous creep-fatigue experiments are required to achieve high quality of curve fitting.

These three disadvantages arise as an intrinsic limitation of the method of curve fitting, since statistical fitting accuracy does not necessarily translate to a robust description of the underlying physical mechanisms. Therefore, these models are only numerical representations of creep-fatigue behaviour, and no underlying physical mechanisms of fatigue and creep are provided. The fitting method and related existing creep-fatigue models do not provide a route to achieve a unified formulation across multiple materials, integrated representation of failure modes, and engineering economy. However, these disadvantages are recently improved by the low-cycle unified creep-fatigue equation [25-27] (the description of this new model will be presented in Section 2). While this new model does not formalize the interactive effect between fatigue and creep, nonetheless the error of life prediction caused by this is within an acceptable range (we assume the ratio of predicted fatigue life to experimental result is between 0.75 and 1.25). This is because the coefficients in this new model are not solely derived from the empirical data of pure fatigue or/and pure creep, even though the relationships between different variables in this model are based on the mechanisms of fatigue and creep.

The purpose of the current paper is to link the low-cycle unified creep-fatigue equation to physical phenomena. To do this we considered each of the main dependencies (including temperature, cyclic time and grain size) and relationships for the unified creep-fatigue equation, and explored what the literature says about the mechanisms of fatigue and creep. Specifically,

the creep and fatigue mechanisms based on the underlying physical mechanisms in terms of temperature, cyclic time and grain size were discussed, then the consistency between the physical mechanisms and the structure of the unified creep-fatigue equation was investigated.

2. Brief Description of the Unified Model

The low-cycle unified creep-fatigue equation (Eq.1) [25-27] is presented as follow:

$$\varepsilon_p = C_0 c(\sigma, T, t_c, d) N^{-\beta_0} \tag{1}$$

with

$$c(\sigma, T, t_c, d) = 1 - \left[c_1(\sigma)\left(T - T_{ref}\right) + c_2 \log\left(t_c/t_{ref}\right)\right] \cdot \left[A\left(d/d_{ref}\right)^m\right]$$

$$T - T_{ref} = \begin{cases} T - T_{ref} \; for \; T > T_{ref} \\ 0 \; for \; T \le T_{ref} \end{cases}$$

$$t_c/t_{ref} = \begin{cases} t_c/t_{ref} \; for \; t_c > t_{ref} \\ 1 \; for \; t_c \le t_{ref} \end{cases}$$

where ε_p is the plastic strain, C_0 is the fatigue ductility coefficient, β_0 is the fatigue ductility exponent, N is the creep-fatigue life, σ is the stress, T is the temperature, t_c is the cyclic time, d is the grain size, T_{ref} is the reference temperature, t_{ref} is the reference cyclic time, d_{ref} is the reference grain size, and A and m are constants. The derivation of this unified creep-fatigue formulation is based on the concept of fatigue capacity, which numerically shows the process of gradual consumption of full fatigue capacity by creep effect. Particularly, the relationships between different variables in this unified formulation can be explained by physical meaning. This is a remarkable characteristic for this new formulation, which results in several significant advantages on the creep-fatigue description. Specifically, the unified creep-fatigue equation was well validated at multiple temperatures and cyclic times for multiple materials [25-27], such as 63Sn37Pb, 96.5Sn3.5Ag, stainless steel 316 and Inconel 718, thus the unified characteristic is presented. In addition, this unified formulation can be restored to the Coffin-Manson equation at pure-fatigue condition and can be reorganized to the Manson-Haferd parameter [28] at pure-creep condition, thus the integrated characteristic is included. Furthermore, the coefficients of this unified formulation can be extracted with minimum experimental effort, which provides an effective and efficient method for engineering design. In general, function $c_1(\sigma)$ and constant c_2 are extracted from creep-rupture tests, and the constants C_0, β_0, A and m are derived from creep-fatigue tests. A brief description of the validation on material GP91 casting steel is presented below, based on [25]. Briefly, the pure-creep condition ($\varepsilon_p = 0$) gives the formula of the constant c_2 (Eq.2) through letting T = T_{ref}, and suggests function $c_1(\sigma)$ (Eq.3) through letting t_c = t_{ref}.

$$c_2 = \frac{1}{\log(t_a/t_{ref})} \tag{2}$$

$$c_1(\sigma) = -\frac{c_2}{P_{MH}(\sigma)} \tag{3}$$

Then, creep-fatigue data are applied to obtain the constants of A, m, C_0 and β_0 through minimizing the error (Eq.4) between the predicted creep-fatigue life ($N_{pre,ij}$) and experimental results ($N_{exp,ij}$):

$$error = \sum_{i,j} \left(\log N_{pre,ij} - \log N_{exp,ij}\right)^2 \tag{4}$$

The reference temperature for GP91 casting steel is chosen as 610K, the reference cyclic time is defined as 1s, and the reference grain size is selected as 25μm. The creep-rupture data [29] gives the point of convergence (T_{ref}, $\log t_a$) which is evaluated as (610 K, 18.281), and thus,

$$c_2 = \frac{1}{\log(t_a/t_{ref})} = \frac{1}{\log(10^{18.281}/1)} = 0.0547 \tag{5}$$

And the relationship between stress and the Manson-Hafer parameter (P_{MH}) is given as:

$$-\frac{1}{P_{MH}(\sigma)} = 0.0174 + 2.20 \times 10^{-4}\sigma - 3.2 \times 10^{-7}\sigma^2 \tag{6}$$

Then, substituting Eq.5 and Eq.6 into Eq.3, function $c_1(\sigma)$ is expressed as:

$$c_1(\sigma) = -\frac{c_2}{P_{MH}(\sigma)} = 9.51808 \times 10^{-4} + 1.20344 \times 10^{-5} \cdot f_m \cdot \sigma - 1.75045 \times 10^{-8} \cdot {f_m}^2 \cdot \sigma^2 \tag{7}$$

where f_m is a moderating factor which is introduced to compress the constant stress into an equivalent creep damage under the cyclic situation. The magnitude of f_m is given as 0.6366 for the sinusoidal wave. The empirical data of creep fatigue (T=673K, t_c=5s, d=25μm; T=823K, t_c= 5s, d=25μm; T=873K, t_c=2s, d=35μm) obtained from Ref. [30] give the constants of C_0, β_0, A and m through minimizing the difference between predicted life and experimental life (numerically optimization) (Eq.4). Specifically, C_0 = 0.9532, β_0 = 0.669, A = 0.5588 and m = −0.4053. In addition, the ratios of predicted fatigue life to experimental fatigue life are plotted in Figure 1. This figure shows that all data points fall in a reasonable range (within the upper bound (+25%) and the lower bound (−25%)). This implies that the unified formulation has high accuracy of fatigue-life prediction.

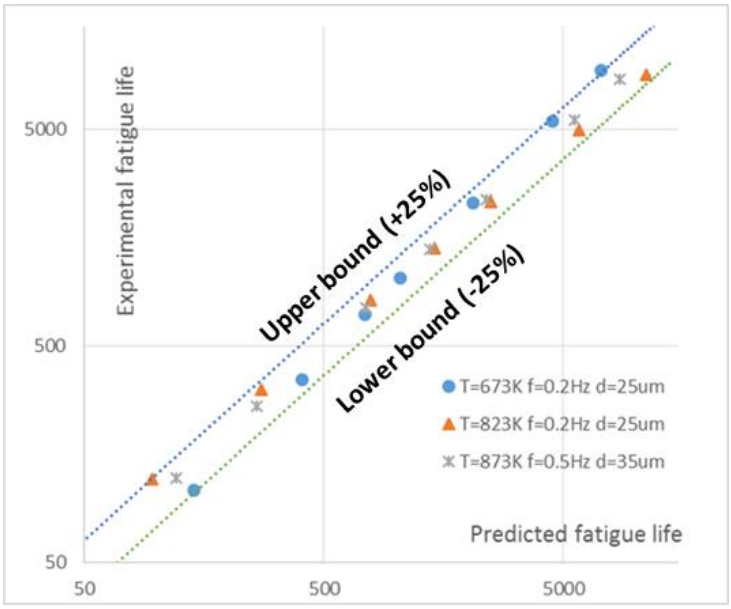

Figure 1 Application of the unified model to predict fatigue life vs. experimental fatigue life for GP91 casting steel, with raw data from physical tests from [29,30].

We also indicated that the unified formulation provides a more economical method of fatigue-life evaluation for engineering application. This was discussed and proved in [31], where the unified formulation was compared with Wong and Mai's equation. Specifically, taking 63Sn37Pb solder as an example, both Wong and Mai's equation and the unified formulation give high accuracy of fatigue-life prediction when all eight groups of creep-fatigue data are imposed. Then, three groups of creep-fatigue data were selected to extract the coefficients of these two formulations. When Wong and Mai's equation with the coefficients obtained at this stage is extended to predict fatigue life at total eight creep-fatigue situations, the average error dramatically worsens. However, only a slight reduction of average error was presented by the unified formulation. This implies that the unified formulation requires less creep-fatigue experiments to extract the coefficients, and thus a more economical method is provided for engineering application.

Overall, the new model presents a good balance between accuracy and economy, which is very important for engineering applications. More information of the advantages presented by the unified formulation is shown in Ref. [31].

3. Influence of Relevant Variables on Creep-Fatigue Behaviour

Creep-fatigue process presents the fatigue behaviour under elevated temperature, where creep effect is active. At the microstructural level, fatigue and creep show different underlying principles. Generally, fatigue effect occurs via cracks through the grains, while creep effect involves the grain boundary cracking [32]. The accumulation of creep-fatigue damage implies that full fatigue capacity is gradually consumed by creep effect, which is macroscopically

influenced by temperature and cyclic time, and is related to grain size in the microstructural level. These relevant variables are accommodated in the unified creep-fatigue equation. We discuss these three main dependencies since they are frequently investigated and presented in the existing creep-fatigue models. Practically, the creep-fatigue behaviour is also influenced by other effects, such as mean stress/strain and applied loading. The effect of mean stress/strain is not included into the unified equation, which is a limitation of this new model and will be considered in future research. In addition, the effect of applied loading (stress and strain) on creep is indirectly incorporated into function $c_1(\sigma)$, where this function is extracted through the relationship between applied loading and the Manson-Haferd parameter. It is generally accepted that the increased loading results in more vulnerable bonds between atoms due to change to inter-atomic spacing. This provides a favourable situation to initiate the atomic movements. In this case, creep damage is intensified with increased loading, and then fatigue capacity is reduced.

The influences of these three main variables (temperature, frequency/cyclic time and grain size) are shown below.

3.1. Temperature Dependency

Temperature has significant influence on creep, but presents negligible effect on pure fatigue [33] where creep is dormant. Normally, creep effect is activated when temperature is higher than 35% of the melting temperature [34], which may be attributed to the behaviour of atomic vibrations [35]. To be specific, atomic vibration is accelerated (also the internal energy is increased) with rising temperature, where favourable conditions to break the bonds between atoms are provided. This threshold temperature is defined as the reference temperature, which is included in the unified formulation (Eq.1). In this case, the discussion of temperature dependency focuses on creep behaviour. Normally, creep mechanisms are divided into Nabarro-Herring creep, Coble creep, grain boundary sliding and dislocation creep [32,36]. Nabarro-Herring creep and Coble creep show a strong dependence on temperature, where diffusional flow of atoms occurs under conditions of relatively high temperature. Grain boundary sliding involves displacements of grains against each other. This is the main mechanism for the creep failure of ceramics at high temperature because of glassy-phase formation at grain boundary, which provides good sliding condition along grain boundary. Therefore, this creep behaviour is not a major contributor to metals and hence is removed from further consideration here. Dislocation creep presents drastic dislocation through the crystal lattice, which results from both line defects and point defects at relatively low temperature. Therefore, high stress is needed and small diffusional flow is involved. This process shows a highly sensitive to the applied stress on material, but not temperature. This is indicated in Ref. [32], wherein a higher stress sensitive exponent is presented compared to the other three creep mechanisms. Based on the brief description of these four creep mechanisms shown above, the diffusion creep (Nabarro-Herring creep and Coble creep), which has strong temperature dependency is used to explain the influence of temperature on creep.

The temperature effect on creep-fatigue is attributed to elevated temperature leading to weaker bonding between atoms at the grain boundary. This is due to better conditions for diffusion.

Then this causes the movements of vacancies [37-39]. This transfer finally results in the overall deformation of the material. Specifically, a vacancy is defined as a point defect in a crystal, where an atom is missing from its original lattice site. During this process, an atom needs to overcome the energy barrier to move from its current site to the nearby vacant site. By this means, the high temperature can provide atoms with enough energy to break their bonds with neighbouring atoms, and then lead to the location transfer (motion) of atoms [40]. This process can be identified as a thermodynamic system with a strong driving force of temperature for diffusion [36]. In addition, diffusion basically is a net movement of atoms from high concentration region to a low concentration region. This reflects the initial driving force for the transfer of atoms. During this process, temperature is an important factor to determine the rate of diffusion, wherein the elevated temperature speeds up the random atom motion, which gives the atom access to a greater physical volume of space, and the new atomic configuration opportunities are provided.

Consequently, the increasing temperature accelerates the process of diffusion (more creep damage occurs), and then reduces the fatigue capacity for the creep-fatigue condition.

3.2. Frequency/Cyclic Time Dependence

Normally, cyclic time does not have significant influence on pure fatigue and at the same order of frequency magnitudes [33]. In our research, the frequency/cyclic time is limited to a range typical for general engineering situations. Thus, the influence of frequency/cyclic time on pure-fatigue life is ignored, and the discussion of frequency/cyclic time effect is based on the creep behaviour.

Creep is normally defined as a time-dependent deformation under a constant loading, which indicates that creep damage is intensified with increasing time. The general influence of frequency/cyclic time on fatigue capacity could be explained through the transient-creep-plus-elastic model shown in Figure 2 [32], where σ is the applied stress. In this model, a high frequency load (which is related to elastic strain rate) primarily causes deformation of spring S_2. This is because of the dynamic resistance effect of dashpot (η_1 (MPa)). Hence the slope of stress-strain curve is S_2 (N/m). However, low frequency loads (events over longer time) cause the deformation of both springs S_1 and S_2, and the dashpot is relatively inconsequential. In this case, the strain (ε (m/m)) may be expressed as:

$$\varepsilon = \frac{\sigma}{S_1} + \frac{\sigma - \eta_1}{S_2} \tag{8}$$

Eq.8 shows that the slope (S_e (N/m)) of stress-strain curve is $S_1S_2/(S_1+S_2)$, which is smaller than S_2. This implies that large time can reduce stiffness, then increase strain and lead to more creep damage.

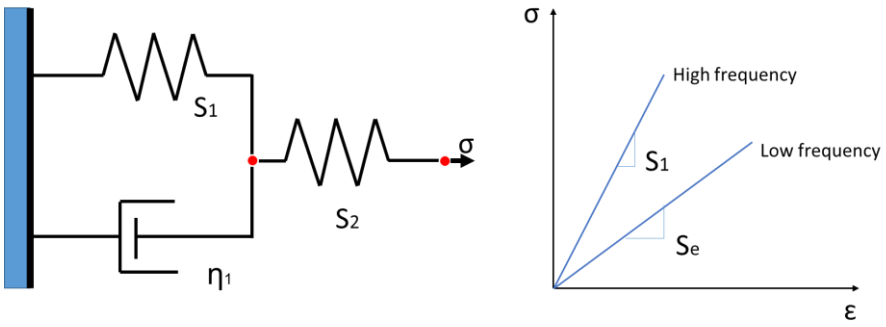

Figure 2 The transient-creep-plus-elastic model. Image adapted from Ref. [33].

Consequently, low frequency (large cyclic time) gives more accumulation of creep under a given temperature and loading. In other words, the longer time leads to more diffusion in microstructure when a material is exposed to high temperature under constant applied loading, and then produces more creep-fatigue damage.

3.3. Grain-Size Dependence

Grain size has significant influence on both fatigue damage and creep damage, but has contrary effects on creep and fatigue. Generally, smaller grain size is more positive for pure-fatigue resistance, while bigger grain size is more beneficial for pure-creep ductility [32]. This phenomenon results from the different failure mechanisms shown by fatigue and creep.

Fatigue failure is caused by the progressive accumulation of plastic deformation under cyclic loading. During fatigue process, cracks initiate at the early stage and then gradually propagate through grain boundary with the increasing number of cycles. It is easy to understand that the propagation of crack needs to penetrate the grain boundary to extend to the next grain, and this may also require a reorientation of the crack growth direction [41,42]. This means that the more grains the crack encounters the slower the progression of fatigue failure, and hence the greater loading (stress or strain) is required to make crack achieve the critical length of failure. In other words, the materials with finer grain size provide better performance of fatigue resistance.

As mentioned above, grain boundary is barrier for the propagation of crack under pure-fatigue condition. However, the grain boundary becomes the source of creep damage at pure-creep condition [36]. Since the stress concentration is intensive in the intersection point among three adjacent grains, the crack growth along grain boundary is promoted in these triple points [43-45]. Consequently the triple point provides an opportunity for further crack propagation under creep. Also relevant to note is that the triple point also contains crystalline defects, where multiple directional opportunities for crack propagation along the grain boundaries are provided. In this way, the finer the grain size, the greater the internal area of grain boundaries and volumetric density of triple points, hence enhanced opportunity for crack propagation under creep. In addition, the influence of grain size on creep also could be explained by the physical mechanism of diffusion creep. Specifically, the atomic diffusion causes the elongation of the grain along the stress axis, which implies finer grain size results in more significant deformation than coarse grain size under a given stress within a same area.

The discussion above shows that the influences of grain size on fatigue and creep are contrary, and thus combined effect between fatigue and creep should be determined by the proportion of fatigue contribution and creep contribution. The research conducted by Hatanaka and Yamada [46], Hattori et al. [47] and Pieraggi and Uginet [48] show that fatigue capacity reduces with increased grain size. This implies that the fatigue effect makes more contribution to creep-fatigue damage than creep effect under the zero-hold-time cyclic loading and relatively short cyclic time. This may be because the total failure time is too short to produce major creep damage in the low-cycle regime. We could image that, for the situation of cyclic loading with hold time or relatively long cyclic time, the contribution of creep effect would increase. Finally, if the creep effect becomes more significant than fatigue effect, the bigger grain size would have more benefits for creep-fatigue behaviour [49].

4. Consistency between the Unified Formulation and Physical Phenomena

Section 3 shows that temperature, time and grain size have significant influences on creep and fatigue behaviours, thus the relationships between them can be ideally derived from the microstructural level. These relationships are well included in the unified equation, wherein the main relationships between different variables show a high consistency with physical mechanisms of fatigue and creep.

4.1. Linear Relationship between Temperature and Strain

The unified creep-fatigue equation can be reorganized to the form:

$$\varepsilon_p = C_0 N^{-\beta_0} - \left[c_1(\sigma)\left(T - T_{ref}\right) + c_2 \log\left(t_c/t_{ref}\right)\right] \cdot \left[A\left(d/d_{ref}\right)^m\right] C_0 N^{-\beta_0} \qquad (9)$$

The first term in Eq.9 shows full fatigue capacity, and the second term reflects the strain caused by creep effect. Significantly, a linear relationship is presented between temperature and creep-related strain (also applied plastic strain ε_p), which is consistent with underlying creep mechanism. According to description of four different creep mechanisms (Nabarro-Herring creep, Coble creep, grain boundary sliding and dislocation creep) in Section 3.1, in the present work, diffusion creep (including Nabarro-Herring creep and Coble creep) is regarded as the main creep mechanism for creep fatigue since it has strong temperature dependency. Therefore, the discussion of temperature-strain relation is built on the mechanism of diffusion. As mentioned in Section 3.1, the process of diffusion is identified as a thermodynamic system. In this case, a piece of crystal containing n atoms is selected, wherein an atom inside is transferred to the surface due to diffusion (Figure 3), and thus a vacancy is formed. Normally, the creep process can be described by Gibbs free energy [50]. This parameter shows the thermodynamic potential to form this vacancy under the situation with a given pressure and a given temperature, is presented by Eq.10.

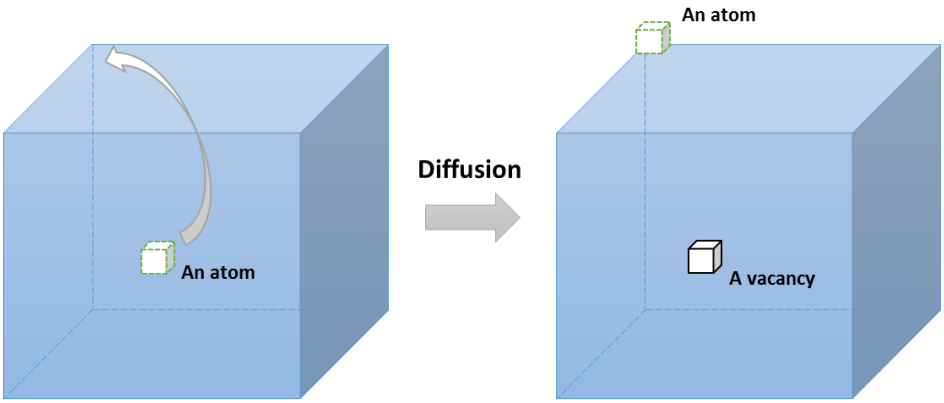

Figure 3 A movement of an atom.

$$\Delta G_f = \Delta E_f + P\Delta V_f - T\Delta S_f \tag{10}$$

where ΔG_f is the Gibbs free energy for formation of a vacancy, ΔE_f is the change in internal energy due to formation of a vacancy, ΔV_f is the volume of a vacancy, ΔS_f is the entropy for formation of a vacancy, P is the pressure and T is the temperature. If n_v vacancies are formed during the process of diffusion, the total change in free energy is presented by Eq.11:

$$\Delta G = n_v \Delta G_f - T\Delta S_c \tag{11}$$

where ΔG is the total change in free energy, and ΔS_c is the configurational entropy (Eq.12) which reflects W different ways of distribution of n_v vacancies among the n sites.

$$\Delta S_c = k \ln W \tag{12}$$

where k is the Boltzmann's constant. Then, the free energy shown by Eq.11 is reorganized as:

$$\Delta G = n_v \Delta G_f - kT \ln C_n^{n_v} = n_v \Delta G_f - kT \ln \left[\frac{n!}{(n-n_v)!\, n_v!}\right] \tag{13}$$

By using Stirling's equation:

$$\ln(x!) = x \ln x - x + O(\ln x) \tag{14}$$

Eq.13 can be simplified and approximated as Eq.15 through assuming $n \ll n_v$:

$$\Delta G \approx n_v \Delta G_f - kTn_v \left(1 + \ln \frac{n}{n_v}\right) \tag{15}$$

This equation shows that the total free energy has a vacancy-number dependency, and thus this free energy varies during the process of transfer. Normally, the minimum value occurs at the two ends of movements, where an equilibrium situation is achieved and is numerically presented through letting $\partial \Delta G / \partial n_v = 0$. Then, this operation gives the equilibrium atomic fraction of vacancies:

$$N_v = \frac{n_v}{n} = exp\left(-\frac{\Delta G_f}{kT}\right) \tag{16}$$

Normally, diffusion is always described by Fick's law [3,37,39]:

$$J = -D\frac{d\varphi}{dx} \tag{17}$$

where J is the diffusion flux which shows the amount of substance flowing across a unit area, D is the diffusion coefficient, x is the position, and φ reflects the concentration of vacancies and is defined as the number of vacancies per unit volume (Eq.18):

$$\varphi = \frac{N_v}{\Omega} \tag{18}$$

where Ω is the atomic volume. Therefore, a proportional relation between diffusion flux and temperature component can be presented:

$$J \propto exp(-1/T) \tag{19}$$

Since creep process indicates that diffusion finally leads to overall deformation, the strain caused by creep effect is proportional to temperature dependency:

$$\varepsilon \propto exp(-1/T) \tag{20}$$

The expression of $exp(1/T)$ can be simplified as a linear dependency when temperature is relatively high enough and within the application range (normally the range of experimental investigation), such as the temperature range from 650 K to 1000 K for the GP91 casting steel [30].

Therefore, we conclude that the underlying physical phenomenon is that diffusion of atoms is based on considerations of free energy and formation of vacancies. The literature shows that this mechanism is represented by an exponential dependency of the form $\varepsilon \propto exp(-1/T)$. We propose that the underlying physical explanation is that the ability of an atom to diffuse is based on the volume of space containing vacancies that it can recruit (hence an exp relationship), and on the rate at which vacancies form within that space. The latter requires activation energy, hence is dependent on temperature to achieve the necessary mobility at the atomic level. The formation of vacancies is therefore retarded at low temperatures, becomes active at intermediate temperatures, and is saturated at sufficient high temperature (all available vacancies have been formed), hence the $exp(-1/T)$ form of the relationship. At sufficiently high temperature the saturation causes this to simplify to a linear relation. This relation is also consistent with the empirical data on the materials of 63Sn37Pb solder [21] and GP91 casting steel [30]. The data on these two materials at the life of 5000 cycles are tabulated in Table 1. Then, the linear relationship between temperature and strain is presented in Figure 4. Results show good quality of linear fitting, with R^2 = 0.9932 for 63Sn37Pb solder and 0.9946 for GP91 casting steel.

Table 1 Data of temperature-strain relation for 63Sn37Pb [21] and GP91 casting steel [30]

Materials	Temperature (K)	Strain	Cyclic Time (s)	Life (Cycles)
63Sn37Pb	233	0.00412	1	5000
	298	0.00364		

	248	0.00332		
	398	0.00307		
GP91 Casting Steel	673	0.00317	20	5000
	823	0.00199		
	873	0.00174		

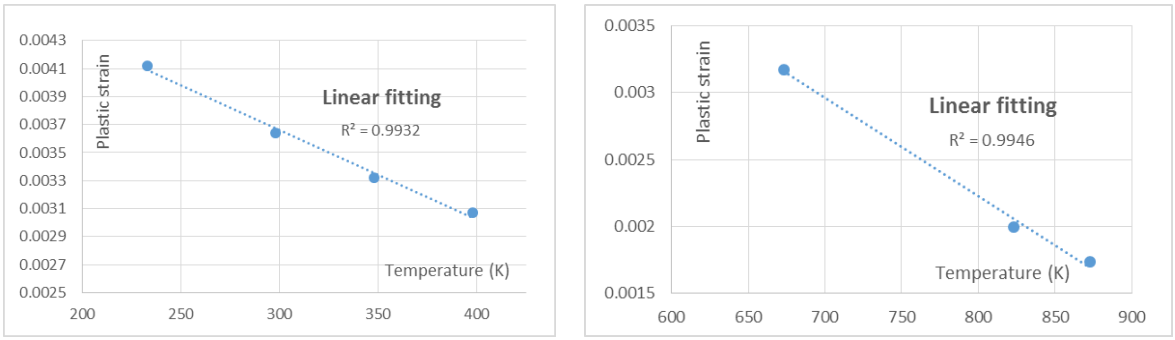

(a) (b)

Figure 4. Curve fitting of temperature vs. strain for experimental data: (a) 63Sn37Pb; (b) GP91 casting steel. Raw data from [21,30] respectively.

Therefore, the creep-related strain is linearly proportional to temperature, and the overall fatigue capacity is reduced by a thermal effect, hence giving rise to the $c_1(\sigma)(T - T_{ref})$ term in the unified formulation.

4.2. Logarithmical Relation between Temperature and Cyclic Time

A logarithmical relation between temperature and cyclic time is presented by the unified creep-fatigue equation, which is consistent with creep mechanism. As shown in Section 4.1, the diffusion behavior gives the logarithmical relationship between temperature and diffusion flux (Eq.19). The definition of "diffusion flux" indicates that this term measures the amount of substance flowing through a cross sectional area during a unit time. In this context, it is a measure of the strain rate, at the microstructural level. Thus, a time dependency is included into this parameter in the form of a rate function. Then, Eq.19 can be presented as:

$$J = \frac{dD_v}{dt} \rightarrow \dot{\varepsilon} \propto exp(-1/T) \tag{21}$$

where D_v reflects the amount of substance following through a unit area. Significantly, Eq.21 gives a logarithmical relation between temperature and cyclic time (unite time), and this is consistent with the relationship shown in the unified creep-fatigue equation.

Theoretically, the temperature and cyclic time effects both decrease the fatigue capacity. In this case, we propose that to a first approximation they are independent of each other rather than

convoluted with each other, hence the overall effect is additive. However, this statement is only reasonable when the creep damage is not specified. If creep is included then temperature can be related to time under one specific damage to show an inversely proportional relation. For example, for one specific creep damage, the effect caused by increasing temperature could be compensated through decreasing cyclic time. Consequently, considering these two situations, the numerical representation of creep effect is given as the sum of the temperature and cyclic time effects, hence of the form: $\left[c_1(\sigma)\left(T - T_{ref}\right) + c_2 \log\left(t_c/t_{ref}\right)\right]$.

The logarithmical relation for cyclic time is also represented by the conventional time-temperature parameter, wherein the time dependence is addressed as rupture time. This is based on the integrated characteristic shown by the unified creep-fatigue model. Specifically, the integrated characteristic shows that the unified creep-fatigue equation can be reorganized to the Manson-Haferd parameter at the pure-creep condition, where a logarithmical temperature-time relation is accommodated. Although this time-temperature parameter was entirely derived from empirical data (no physical basis) [32], it has been successfully validated on different materials, and thus is believed to have ability to describe creep behaviours. In addition, the pure-creep condition could be regarded as the idealization of a creep-fatigue situation with extremely prolonged cyclic time. In this case, it is reasonable for the unified formulation to present creep mechanism in a logarithmical relation between temperature and cyclic time.

In the specific case of cyclic creep, the load fluctuates between tension and compression. The cyclic time is a measure of the duration of time to which the material is exposed to the diffusion flow under tension and compression. Under tensile loading, we propose that the flow is, in practice, limited by dislocation pinning, grain boundaries, and other flow-limiting effects at the microstructural level. This causes the rate of diffusion to be reduced over longer periods, hence the total plastic strain due to this component has the form $c_2 \log\left(t_c/t_{ref}\right)$. This logarithmical relation between plastic strain and cyclic time is also consistent with empirical data on the materials of 63Sn37Pb solder [21] and stainless steel 316 [51]. The creep-fatigue data for the materials at the life of 5000 cycles are tabulated in Table 2, and the curve-fitting results are then presented by Figure 5. The result illustrates a good linear fit between strain and log of cyclic time, which implies a logarithmical relation between cyclic time and plastic strain.

Table 2 Data of cyclic time/strain rate-strain relation for 63Sn37Pb [21] and SS316 [51]

Materials	Cyclic Time (s)	Strain	Temperature (K)	Life (Cycles)
63Sn37Pb	10	0.00344	298	5000
	100	0.00298		
	1000	0.00243		
Materials	Strain rate (%/min)	Strain	Temperature (K)	Life (Cycles)
Stainless Steel 316	0.4	0.00218	973	5000
	4	0.00253		

	40	0.00309		

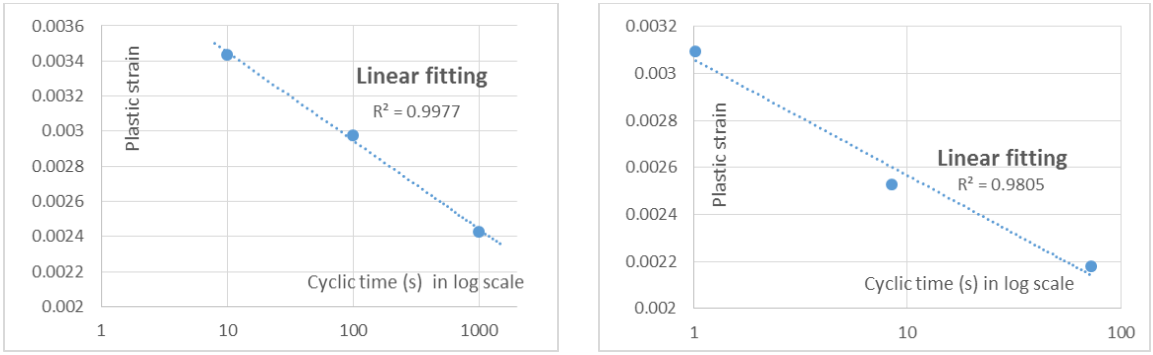

(a) (b)

Figure 5. Curve fitting of log of cyclic time vs. strain for experimental data: (a) 63Sn37Pb; (b) stainless steel 316. Raw data from [21,51] respectively.

When the cycle is reversed, and the load moves into the compression stage, the diffusion is not undone (reversed). This is because changes have occurred at the microstructural level such that it is not the same geometric system as before—the system is inelastic. Consequently, the compression part of the cycle does not completely undo the inelastic strain of the previous stage (during a limited time range imposed for general engineering case). Also, the compression is proposed to undo or at least disturb the flow-limiting effects that arose in the tension stage. Hence the next tension cycle permits further diffusion to occur. We therefore propose that the cyclic time reduces the fatigue capacity per $1 - [c_2 \log(t_c/t_{ref})]$. Although the cycle time provides a limited opportunity for the creep effect to operate, it is still reasonable to assume that the amount of creep that occurs within one part of the cycle follows the logarithmic time-temperature dependency.

Therefore, the diffusion-creep behavior is physically described by the amount of substance (which is logarithmical with temperature) flowing through a specific area during a unit time, thus this gives a logarithmical relation between temperature and time.

4.3. Power-Law Relation between Grain Size and Strain

The derivation of the unified creep-fatigue equation shows that the grain-size component is imposed into creep-related component and is directly extracted from the general creep equation for steady state [32], wherein a power-law relation between creep-related strain and grain size is presented (Eq.9). This relation appears to accurately represent creep behavior.

Generally, diffusion flux for creep behavior is numerically formulated by Fick's equation (Eq.17). A microstructural-level-based discussion shown in Section 4.1 shows that diffusion flux is not only related to the time, but also related to the unit area where substance following through (Eq.22):

$$J = \frac{dD_t}{dA} \propto exp(-1/T) \tag{22}$$

where D_t reflects the amount of substance following during a unit time and A is the area where substance following through. This area can be obtained by the product of number of grains in unit area and average area of grain, wherein the average area has a strong dependency on grain size. Generally, the area of geometry can be numerically related with the key dimension in the form of second power order. In the present work, a complex situation for creep-fatigue condition is presented, wherein creep and fatigue are coupled, and this may cause the intensity of grain-size effect to deviate from the power of two, but the power-law relation should remain. Consequently, based on the general creep mechanism, it is logical that a power-law relation between grain size and strain is presented in the unified formulation.

In addition, bigger grain size is always beneficial for pure creep. This grain-size effect on creep is consistent with the presentation of the unified creep-fatigue equation. According to the validations [25] on the materials of Inconel 718 and GP91 casting steel, the negative exponent to grain size shows the benefit of big grain size on creep resistance.

We propose that the physical explanation for the grain-size dependency is that the diffusion creep phenomenon involves effects at the (irregular) grain boundaries, and to a lesser extent movement within the crystalline structure of the grain. However the latter mechanism becomes stalled once the available dislocations have run their courses. Hence the steady creep loading purges the internal structure of the grain of imperfections. Consequently the larger the grain, the lower the opportunity for diffusion creep to occur. Thus, it is to be expected that plastic strain would be inversely related to grain size, hence m is negative in $\left[A\left(d/d_{ref}\right)^{m}\right]$. For very small grains the effect becomes disproportionately worse, because a small change in grain size results in a large change in the number of grains in the section. This means more grain boundaries and opportunity for creep. A similar change in size for a large grain has a much smaller effect.

We note that m is approximately -0.5 for both materials considered (Inconel 718 and GP91 casting steel). Since creep damage involves crack propagation along a grain boundary, the decreased grain size results in increased opportunity for crack growth within a given area. For example, one square grain is identified to have four sides, hence four crack-growth potentials, then halving or quartering of grain size gives two more or six more potential directions for crack growth respectively for the same total area. Note that the size of one square grain is a reference condition, based on which the grain is halved or quartered. In this case, the grain size of 1 is not specified as 1 μm, but should rather be considered as a mathematical origin for the scaling effect, hence we refer to this as the pseudo grain size. The relationship between pseudo grain size d’ and the number of crack-growth planes is shown in Figure 6. This relationship may be formulated numerically as a power-law relation, with exponent -0.68. In practical situations, the grain boundaries are not flat planes but are instead more irregular. The effect of this is to (a) increase the planar area available, and (b) provide more opportunity for an element of the boundary to be aligned with the preferred crack-growth direction. Hence practical situations are expected to provide greater opportunity for crack growth as the grain size

decreases. The effect of this is to change the exponent closer to zero, e.g., if there were two additional planes at each stage then the exponent becomes -0.523.

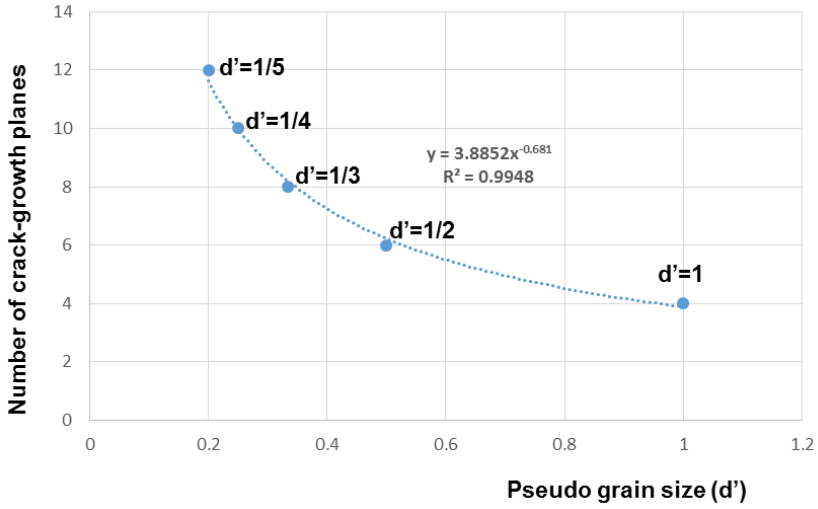

Figure 6 Relationship between pseudo grain size and the number of potential crack-growth planes.

We therefore propose that there are natural reasons for the exponent in the formulation $\left[A\left(d/d_{ref}\right)^{m}\right]$ to be of the order m = -0.681 or larger, and this is compatible with the empirically determined values of m = -0.5411 for Inconel 718 and m = -0.4053 for GP91 casting steel.

4.4. Power-Law Relation between Life and Strain

The derivation of the unified creep-fatigue equation shows an extension of the Coffin-Manson equation. Therefore, the power-law relation shown in the Coffin-Manson equation is accommodated in the unified formulation. It is acceptable that the power-law relation between reversed loading and number of cycles could well present the process of damage accumulation in fatigue perspective.

In the present work, fracture mechanics is presented as an opening model showing direct apart between two crack surfaces, per [52]. Therefore, the stress intensity factor (K) is shown by Eq.23:

$$K = \sigma\sqrt{\pi a/2} \tag{23}$$

where σ is the applied stress and a is the crack length. Crack-growth process shows that plastic deformation occurs around the crack tip due to high stress concentration, where a circular plastic zone ahead of the crack tip is formed (Figure 7). According to the definition of the stress intensity and Eq.23, the stress distribution (σ_{ij}) near the crack tip is:

$$\sigma_{ij} = \sigma\sqrt{\frac{a}{2r}}f(\theta) = \frac{K}{2\pi r}f(\theta) \tag{24}$$

where r and θ are polar coordinates. This equation shows that when r tends towards zero, the stress around the crack tip becomes singular. This implies the existence of a plastic zone, with yield stress (σ_y) presented at the boundary of this zone. Then, through letting $\sigma_{ij} = \sigma_y$ and $f(\theta) = 1$, Eq.25 gives the size of plastic zone [52]:

$$r_y = \frac{1}{2\pi}\left(\frac{K}{\sigma_y}\right)^2 \tag{25}$$

where r_y is the radius of the plastic zone.

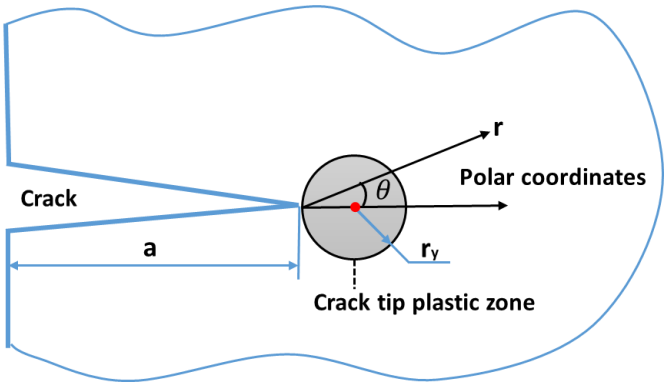

Figure 7 Plastic zone around crack tip.

At the situation with cyclic loading, the stress intensify factor in Eq.25 varies with the change of loading, and then results in expansion or shrinkage of the plastic zone. In this case, the effective stress intensify factor (K_{eff} or ΔK) is introduced and is given as:

$$K_{eff} = K_{max} - K_{min} = \Delta K \tag{26}$$

where ΔK is the difference between maximum (K_{max}) and minimum (K_{min}) stress intensify factors for one cycle. Then, an equivalent radius of the plastic zone ($\overline{r_y}$) can be given by Eq.27:

$$\overline{r_y} = \frac{1}{2\pi}\left(\frac{\Delta K}{\sigma_y}\right)^n \tag{27}$$

This equation shows that the second power order in Eq.25 is reasonably replaced by a general exponent (n) due to the equivalent transformation, which is consistent with FEA result shown by You [53]. Since larger plastic zone gives more crack growth [52], the crack growth in one cycle can be related with ΔK in a power-law relation. This relation (Eq.28) was initially presented by Paris [3] and then demonstrated amounts of empirical data [54,55].

$$\frac{da}{dN} = C(\Delta K)^m \tag{28}$$

where $\frac{da}{dN}$ gives the increased crack length in one cycle, and C and m are constants. According to Eq.23, effective stress intensify factor also can be expressed as:

$$\Delta K = X\Delta\sigma\sqrt{\pi a} \tag{29}$$

where X is a constant and $\Delta\sigma$ is the stress range. Then, introducing Eq.29 into Eq.28 gives:

$$\frac{da}{dN} = C\left(X\Delta\sigma\sqrt{\pi a}\right)^m \tag{30}$$

Applying the integral operation for life gives [56]:

$$N_f = \frac{2\left(a_c^{\frac{2-m}{2}} - a_i^{\frac{2-m}{2}}\right)}{(2-m)C\left(X\Delta\sigma\sqrt{\pi a}\right)^m} \tag{31}$$

where a_c is the critical crack length at which fracture occurs and a_i is the initial crack length at which crack starts to grow under a given stress range. Significantly, this equation shows a typical power-law relation between fatigue life and applied stress range (applied loading), and thus it is also reasonable to relate plastic strain with fatigue life in a power-law relation.

Therefore, the existence and size of the plastic zone at crack tip are the physical basis for the power-law relation for crack growth. It is reasonable to assume that fatigue damage is accumulated at each cycle by the same form. This results in a power-law relation between applied loading and life, hence explaining the form $N^{-\beta_0}$.

4.5. Numerical Presentation of Creep Effect on Fatigue Capacity

The development of the strain-based unified creep-fatigue equation is based on the concept of "fatigue capacity" [26,27]. Briefly, this concept physically indicates that the full fatigue capacity is gradually consumed by the creep effect, and this process is numerically presented by the form of "1-x". This form is accommodated in the unified creep-fatigue formulation (Eq.1).

Equation (9) shown in Section 3.1 indicates that the first term reflects the full fatigue capacity wherein the fatigue behavior under the pure-fatigue condition is presented by the Coffin-Manson equation. In addition, the second term of Eq.9 describes the creep-related effect, where temperature, cyclic time and grain size dependencies are included. This term takes a Coffin-Manson-type formulation, and shows the creep-related damage is accumulated at cyclic loading. The combination of these two terms is numerically presented as the form of "1-x" (Eq.1) and shows the gradual consumption of full fatigue capacity due to creep effect where the residual fatigue capacity is given.

In addition, the reference condition is introduced to show the threshold between pure fatigue and creep fatigue, and creep effect is dormant below the reference condition. At the reference condition, the full fatigue capacity is presented (the second term of Eq.9 equals to zero) in the form of the Coffin-Manson equation. Therefore, the introduction of the reference condition builds a bridge between pure fatigue and creep fatigue. The ability to describe the pure-fatigue condition is proved on the material of GP91 casting steel, where the ratios of predicted fatigue life (obtained by the degenerated form of the unified model) to experimental result (extracted from [30]) fall within the upper bound (+25%) and the lower bound (−25%) (Figure 8). This

implies that the unified formulation provides a good quality prediction of fatigue-life under the pure-fatigue condition, specifically a relatively high correlation between predicted and experimental fatigue life.

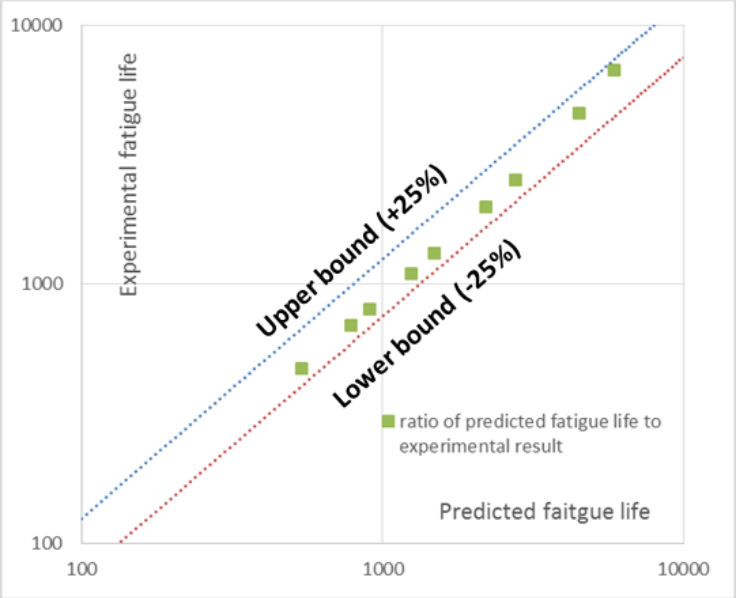

Figure 8 The ratio of predicted fatigue life to experimental result under the pure-fatigue condition, per the unified model, for GP91 casting steel. Raw data from [30].

Consequently, the negative effect of creep on fatigue capacity is numerically formulated as the form of "1-x", and the introduction of the reference condition shows the threshold for the activation of creep effect.

5. Discussion

5.1. Summary

In summary, we propose the following fundamental mechanisms are at work to determine the creep-fatigue behavior of a material; see Figure 9. In this way we propose that the main structural features of the unified creep-fatigue equation are grounded in deeper physical phenomena.

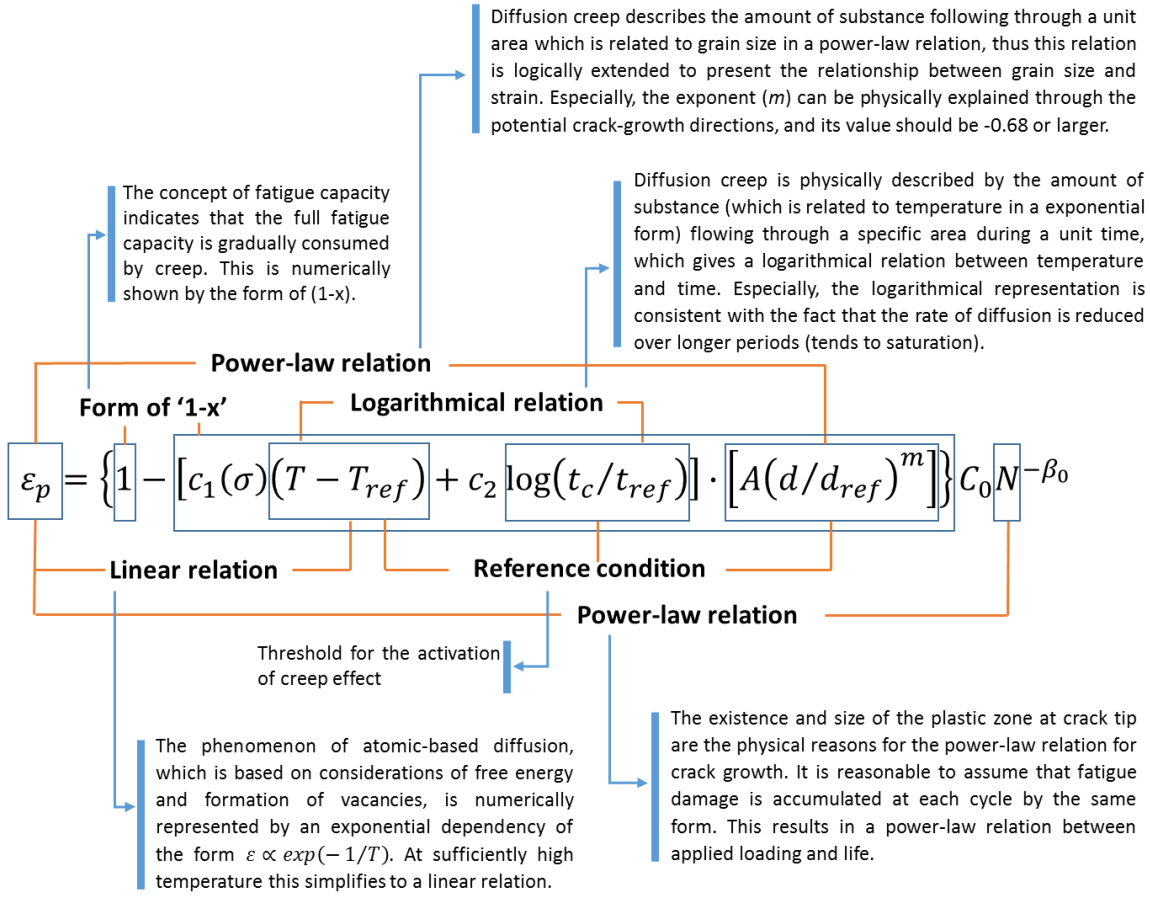

Figure 9 Main relationships and fundamental mechanisms in the unified formulation.

5.2. Limitations and Future Work

The discussion shown above indicates that the relationships between different variables in the unified creep-fatigue formulation are consistent with underlying physical mechanisms, thus this creep-fatigue model has the ability to describe creep-fatigue behaviour numerically and also in terms of physical meaning. Although the relationships between different parameters were derived from underlying physical phenomena, the numerical values of the coefficients still cannot be predicted with precision. In this case, the coefficients need to be extracted through performing creep-fatigue experiments. This is a limitation for this unified formulation, which implies that the coefficients cannot be predicted without any empirical data of fatigue. This model has an opportunity to be further modified/improved to reduce the dependence on fatigue tests, by exploring for more convenient and economical data collection methods.

Generally, reducing the dependence on fatigue test could be conducted through introducing the material-property-related parameters, such as yield strength, into the coefficients. By this means, the coefficients could be directly evaluated through the material properties, and the fatigue test would be eliminated. This work was initially attempted by Manson [57], who proposed a universal slope formulation for the strain-life relation through introducing the parameter of ductility. This provides a possible method to improve this limitation. In addition,

this limitation also could be improved by deeper investigation into physical phenomena of fatigue and creep. For example, the grain-size related coefficients may be related to crystal structure, and the creep-related coefficients may be physically represented through quantitatively investigating the influences of temperature and time on creep-fatigue damage presented by the behaviours of diffusion or thermodynamics.

It is notable that although the new creep-fatigue model is not completely free of the need for empirical data, the method of derivation makes this model fundamentally superior to other existing creep-fatigue models (mentioned in Section 1) because of the good balance between accuracy and economy. The accuracy of fatigue-life prediction has been proved on multiple materials in previous research [25-27]. The good economy of the current model means fewer creep-fatigue data are required to determine the coefficients.

6. Conclusions

Creep-fatigue behavior is normally influenced by temperature, cyclic time and grain size. Generally, the fatigue capacity is gradually consumed by elevated temperature and prolonged cyclic time, and smaller grain size results in better fatigue capacity, but leads to worse creep resistance. These relevant variables are well accommodated in the unified creep-fatigue equation, and the relationships between them are consistent with underlying physical mechanisms of fatigue and creep. Specifically, the creep-related relationships, including linear relation between temperature and strain, logarithmic relation between temperature and cyclic time and power-low relation between grain size and strain, are extracted from diffusion-creep phenomenon. In addition, crack-growth behavior gives a power-law relationship between life and strain. Finally, based on the concept of fatigue capacity, these physical-mechanism-based relationships are numerically constructed in the form of "1-x", and the reference condition is introduced to present the threshold of creep effect.

The original contribution of this work is that the unified creep-fatigue equation is linked to physical phenomena at a microstructural level. Specifically, the influences of different variables (including temperature, cyclic time and grain size) on creep-fatigue behavior were explored, and the numerical relationships shown in this equation were investigated and explained through proposed deeper physical mechanisms of fatigue and creep. A particular contribution is the proposition of a physical explanation of the grain-size exponent (m) via consideration of crack-growth planes.

Author Contributions: The work was conducted by DL and supervised by DP. The investigation of physical-mechanism-based relationships from a microstructural level was conducted by DL. The explanation of how relevant variables influence creep fatigue was conducted by DL and DP. All authors contributed to writing the paper.

Conflicts of Interest: The authors declare no conflict of interest.

References

1. Miner, M.A. Cumulative damage in fatigue. J. Appl. Mech. 1945, 12, 159–164.
2. Palmgren, A. Die lebensdauer von kugellagern. Z. Ver. Dtsch. Ing. 1924, 68, 339–341.
3. Paris, P.; Erdogan, F. A critical analysis of crack propagation laws. J. Basic Eng. 1963, 85, 528–533.
4. Takahashi, Y. Study on creep-fatigue evaluation procedures for high-chromium steels—part i: Test results and life prediction based on measured stress relaxation. Int. J. Press. Vessel. Pip. 2008, 85, 406–422.
5. Takahashi, Y.; Dogan, B.; Gandy, D. Systematic evaluation of creep-fatigue life prediction methods for various alloys. J. Press. Vessel. Technol. 2013, 135, 061204.
6. Payten, W.M.; Dean, D.W.; Snowden, K.U. A strain energy density method for the prediction of creep–fatigue damage in high temperature components. Mater. Sci. Eng. 2010, 527, 1920–1925.
7. Neu, R.; Sehitoglu, H. Thermomechanical fatigue, oxidation, and creep: Part II. Life prediction. Metall. Trans. A 1989, 20, 1769–1783.
8. Ainsworth, R.; Ruggles, M.; Takahashi, Y. Flaw assessment procedure for high-temperature reactor components. J. Press. Vessel. Technol. 1992, 114, 166–170.
9. Cailletaud, G.; Nouailhas, D.; Grattier, J.; Levaillant, C.; Mottot, M.; Tortel, J.; Escavarage, C.; Héliot, J.; Kang, S. A review of creep-fatigue life prediction methods: Identification and extrapolation to long term and low strain cyclic loading. Nucl. Eng. Des. 1984, 83, 267–278.
10. June, W. A continuum damage mechanics model for low-cycle fatigue failure of metals. Eng. Fract. Mech. 1992, 41, 437–441.
11. Chaboche, J.L. Une loi Différentielle D'endommagement de Fatigue avec Cumulation non Linéaire; Office Nationale d'Etudes et de Recherches Aérospatiales: Palaiseau, France, 1974.
12. Metzger, M.; Nieweg, B.; Schweizer, C.; Seifert, T. Lifetime prediction of cast iron materials under combined thermomechanical fatigue and high cycle fatigue loading using a mechanism-based model. Int. J. Fatigue 2013, 53, 58–66.
13. Seifert, T.; Riedel, H. Mechanism-based thermomechanical fatigue life prediction of cast iron. Part I: Models. Int. J. Fatigue 2010, 32, 1358–1367.
14. Charkaluk, E.; Bignonnet, A.; Constantinescu, A.; Dang Van, K. Fatigue design of structures under thermomechanical loadings. Fatigue Fract. Eng. Mater. Struct. 2002, 25, 1199–1206.
15. Constantinescu, A.; Charkaluk, E.; Lederer, G.; Verger, L. A computational approach to thermomechanical fatigue. Int. J. Fatigue 2004, 26, 805–818.
16. Basquin, O. The Exponential Law of Endurance Tests; ASTM International: West Conshohocken, PA, USA, 1910; pp. 625–630.
17. Coffin, L.F., Jr. A Study of the Effects of Cyclic Thermal Stresses on a Ductile Metal; Knolls Atomic Power Lab.: Niskayuna, NY, USA, 1953.
18. Manson, S.S. Behavior of Materials under Conditions of Thermal Stress; Lewis Flight Propulsion Lab.: Cleveland, OH, USA, 1954.
19. Coffin, L. Fatigue at high temperature. In Fatigue at Elevated Temperatures; ASTM International: West Conshohocken, PA, USA, 1973.
20. Solomon, H. Fatigue of 60/40 solder. IEEE Trans. Compon. Hybrids Manuf. Technol. 1986, 9, 423–432.

21. Shi, X.; Pang, H.; Zhou, W.; Wang, Z. Low cycle fatigue analysis of temperature and frequency effects in eutectic solder alloy. Int. J. Fatigue 2000, 22, 217–228.
22. Jing, H.; Zhang, Y.; Xu, L.; Zhang, G.; Han, Y.; Wei, J. Low cycle fatigue behavior of a eutectic 80 au/20 sn solder alloy. Int. J. Fatigue 2015, 75, 100–107.
23. Engelmaier, W. Fatigue life of leadless chip carrier solder joints during power cycling. IEEE Trans. Compon. Hybrids Manuf. Technol. 1983, 232–237.
24. Wong, E.; Mai, Y.-W. A unified equation for creep-fatigue. Int. J. Fatigue 2014, 68, 186–194.
25. Liu, D.; Pons, D. Development of a unified creep-fatigue equation including heat treatment. Fatigue Fract. Eng. Mater. Struct. 2017, doi:10.1111/ffe.12670.
26. Liu, D.; Pons, D.; Wong, E.-H. The unified creep-fatigue equation for stainless steel 316. Metals 2016, 6, 219.
27. Liu, D.; Pons, D.; Wong, E.-H. Creep-integrated fatigue equation for metals. Int. J. Fatigue 2017, 98, 167–175.
28. Manson, S.; Haferd, A. A Linear Time-Temperature Relation for Extrapolation of Creep and Stress-Rupture Data; Lewis Flight Propulsion Lab.: Cleveland, OH, USA, 1953.
29. Tabuchi, M.; Hongo, H.; Li, Y.; Watanabe, T.; Takahashi, Y. Evaluation of microstructures and creep damages in the haz of p91 steel weldment. J. Press. Vessel. Technol. 2009, 131, 021406.
30. Mroziński, S.; Golański, G. Low cycle fatigue of gx12crmovnbn9–1 cast steel at elevated temperature. J. Achiev. Mater. Manuf. Eng. 2011, 49, 7–16.
31. Liu, D.; Pons, D. A unified creep-fatigue equation with application to engineering design. InTechOpen 2017, under review.
32. Dowling, N.E. Mechanical Behavior of Materials: Engineering Methods for Deformation, Fracture, and Fatigue; Pearson Education (US): London, UK, 2012.
33. Shigley, J.E.; Mischke, C.R. Mechanical Engineering Design; McGraw-Hill: New York, NY, USA, 2003.
34. Ashby, M.F.; Shercliff, H.; Cebon, D. Materials: Engineering, Science, Processing and Design; Butterworth-Heinemann: Oxford, UK, 2013.
35. Callister, W.D.; Rethwisch, D.G. Materials Science and Engineering; John Wiley & Sons: New York, NY, USA, 2011.
36. Finnie, I.; Heller, W.R. Creep of Engineering Materials; McGraw-Hill: New York, NY, USA, 1959.
37. Kassner, M.E. Fundamentals of Creep in Metals and Alloys; Elsevier: Amsterdam, The Netherlands, 2015.
38. Poirier, J.-P. Creep of Crystals: High-Temperature Deformation Processes in Metals, Ceramics and Minerals; Cambridge University Press: Cambridge, UK, 1985.
39. Shewmon, P. Diffusion in Solids; Springer: Berlin/Heidelberg, Germany, 2016.
40. Prokoshkina, D.; Esin, V.; Wilde, G.; Divinski, S. Grain boundary width, energy and self-diffusion in nickel: Effect of material purity. Acta Mater. 2013, 61, 5188–5197.
41. Dai, C.; Zhang, B.; Xu, J.; Zhang, G. On size effects on fatigue properties of metal foils at micrometer scales. Mater. Sci. Eng. 2013, 575, 217–222.
42. Hanlon, T.; Kwon, Y.-N.; Suresh, S. Grain size effects on the fatigue response of nanocrystalline metals. Scr. Mater. 2003, 49, 675–680.
43. Cocks, A.; Pontern, A. Mechanics of Creep Brittle Materials 1; Springer Science & Business Media: Berlin, Germany, 1989.
44. Ejaz, N.; Qureshi, I.; Rizvi, S. Creep failure of low pressure turbine blade of an aircraft engine. Eng. Fail. Anal. 2011, 18, 1407–1414.

45. Král, P.; Dvořák, J.; Kvapilová, M.; Svoboda, M.; Sklenička, V. Creep damage of al and al-sc alloy processed by ecap. In Acta Metallurgica Slovaca-Conference, 2013.
46. Hatanaka, K.; Yamada, T. Effect of grain size on low cycle fatigue in low carbon steel. Bull. JSME 1981, 24, 1692–1699.
47. Hattori, H.; Kitagawa, M.; Ohtomo, A. Effect of grain size on high temperature low-cycle fatigue properties of inconel 617. Tetsu To Hagane 1982, 68, 2521–2530.
48. Pieraggi, B.; Uginet, J. Fatigue and Creep Properties in Relation; The Minerals, Metals & Materials Society, Pittsburgh, the United States, 1994.
49. Thébaud, L.; Villechaise, P.; Cormier, J.; Crozet, C.; Devaux, A.; Béchet, D.; Franchet, J.-M.; Organista, A.; Hamon, F. Relationships between microstructural parameters and time-dependent mechanical properties of a new nickel-based superalloy ad730™. Metals 2015, 5, 2236–2251.
50. Fredriksson, H. Solidification and Crystallization Processing in Metals and Alloys; John Wiley & Sons: New York, NY, USA, 2012.
51. Kanazawa, K.; Yoshida, S. Effect of Temperature and Strain Rate on the High Temperature Low-Cycle Fatigue Behavior of Austenitic Stainless Steels; IAEA: Vienna, Austria, 1975.
52. Weertman, J. Fatigue crack propagation theories. In Fatigue and Microstructure; ASM: Metals Park, OH, USA, 1979; pp. 279–206.
53. You, C.; He, B.; Achintha, M.; Reed, P. Numerical modelling of the fatigue crack shape evolution in a shot-peened steam turbine material. Int. J. Fatigue 2017, 104, 120–135.
54. Liang, R.; Ji, Y.; Wang, S.; Liu, S. Effect of microstructure on fracture toughness and fatigue crack growth behavior of ti17 alloy. Metals 2016, 6, 186.
55. Paggi, M. Crack propagation in honeycomb cellular materials: A computational approach. Metals 2012, 2, 65–78.
56. Xiang, Y.; Lu, Z.; Liu, Y. Crack growth-based fatigue life prediction using an equivalent initial flaw model. Part I: Uniaxial loading. Int. J. Fatigue 2010, 32, 341–349.
57. Manson, S. A modified universal slopes equation for estimation of fatigue characteristics of metals. J. Eng. Mater. Technol. 1988, 110, 55.

Paper 8: Conceptual model of crack growth for creep fatigue

Dan Liu * and Dirk John Pons

Department of Mechanical Engineering, University of Canterbury, Christchurch 8140, New Zealand;

*Correspondence: dan.liu@pg.canterbury.ac.nz

Submitted:

Liu, D. and D.J. Pons, Conceptual model of crack growth for creep fatigue, Engineering Fracture Mechanics, 2017.

Abstract

Background – Creep-fatigue damage is generally identified as the combined effect of fatigue and creep. This behaviour is macroscopically described by crack growth, wherein fatigue and creep follow different principles. **Need** – Although the literature contains many studies that explore the crack-growth path, there is a lack of clear models to link these disparate findings and to explain the possible mechanisms at a grain-based level for crack growth from crack initiation, through the steady stage (this is particularly challenging), ending in structural failure. **Method** – Finite element (FE) methods were used to provide a quantitative validation of the grain-size effect and the failure principles for fatigue and creep. Thereafter a conceptual model for the three stages of crack growth was developed by integrating existing crack-growth microstructural observations for fatigue and creep. In particular, the analysis of crack propagation is based on existing mechanisms of plastic blunting and diffusion creep. **Results** - Fatigue and creep effects are treated separately due to the different damage principles. The possible grain-boundary behaviours, such as the mismatch behaviour at grain boundary due to creep deformation, are included. The model illustrates the possible situations for crack propagation at a grain-based level, particularly, the situation when crack encounters grain boundary. **Originality** – The model is consistent with the various creep and fatigue microstructure observations in the literature, but goes further by integrating these together into

a logically consistent framework that describes the overall failure process at the microstructural level.

Keywords: creep fatigue, crack growth, grain boundary, finite element analysis

1. Introduction

Normally, the process of fatigue failure is physically and macroscopically described by crack-growth behaviour. The theory indicates that an engineering structure fails when crack length achieves a critical value, and the total damage is gradually accumulated by the increasing number of cycles. Generally, the process of crack growth under cyclic loading is divided into three phases (Fig.1) [1]: crack initiation, crack propagation and structural fracture. Specifically, the first stage presents a threshold, below which there is no crack growth. The second stage shows a relatively steady state, in which the crack growth rate increases steadily with the increasing number of cycles (this is always described by Paris' Law [2]). The finial stage represents an unstable situation, where the engineering structure fails within a small number of cycles.

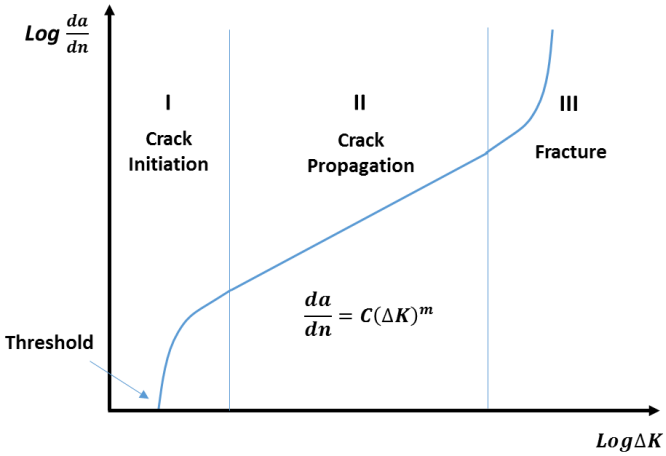

Figure 1 Three stages of crack growth

Significant research effort has been exerted to explore the crack-growth path, through performing fatigue tests and observing the fracture surfaces (fractography). These research efforts mainly focus on the specific features of crack growth for fatigue or creep, such as the creep damage caused by triple points [3-5] and grain-boundary effects for fatigue-crack growth [6, 7]. Hence, the literature contains many disparate findings without an obvious integration into a holistic theory for the crack propagation process.

Although the existing literature [8, 9] indicates three stages of crack growth from initiation to failure, the implications of this for behaviour of the crack at the grain-boundary effect is unclear. The grain boundary is known to play an important role in both fatigue-crack and creep-crack growth, in different ways, hence a grain-boundary effect cannot be ignored. Hence there is a

need to develop a model, qualitative if necessary, to link these details together and to propose a coherent set of mechanisms for the steady stage of crack growth at the grain level. This ideally needs to consider all the loading effects: fatigue, creep, and creep fatigue.

The approach in the present work was to take the known existing principles of fatigue-crack and creep-crack growth. These principles were then used to construct models for finite element analysis (FEA), to produce a grain-based simulation. This was used to verify the grain-size effects on fatigue and creep. The results confirmed that the small grain size is beneficial to fatigue resistance but detrimental to creep, see Section 2.

Next, a conceptual model of the creep-fatigue crack-growth process was developed. This was achieved by imagining the process from the perspective of atoms in orderly grains and at the grain boundaries (where the orderly arrangement between atoms breaks down). The bonds between atoms inside a grain are strong, relative to the bonds between atoms at grain boundaries. We sought to identify a coherent set of mechanisms that would affect the bonds between atoms, for all the loading regimes. This was based on integration of multiple concepts at the microstructural level, such as the plastic blunting process, the mechanisms of dislocation, and the diffusion creep process. These process are extant in the literature, and our contribution is to integrate and apply them to the fine scale to give a new understanding of the interaction between the underlying mechanisms. In addition, a number of new mechanisms for crack growth were also proposed to construct a comprehensive model.

Since the principles of crack growth of fatigue and creep are different (fatigue effect occurs via cracks through the grains while creep effect involves the grain boundary cracking), the fatigue and creep crack-growth behaviours were discussed and illustrated separately. In this conceptual model, three stages of crack growth from crack initiation to structural fracture were included. The second stage of steady crack growth is the primary focus. This is where the majority of the lifetime is consumed. It also presents multiple situations regarding the position of the crack relative to the grain boundary. The result is a proposed theory of the failure mechanisms, and this is represented in the form of a schematic representation, see Section 3.

2. Proposed principles of crack growth

In this paper, the crack-growth behaviours of fatigue and creep are discussed separately because of the different damage principles. Specifically, fatigue-crack growth results from the effect of dislocations, and creep-crack growth is based on diffusion. In this case, the fatigue effect results in crack growth across (through) grains, while creep preferentially follows grain boundaries.

2.1 Established principles in the literature

Crack growth caused by fatigue effect is attributed to plastic deformation at a crack-tip plastic zone, wherein the plastic deformation occurs via dislocations [10]. The simplest form of

dislocation is edge dislocation, see Fig. 2 which represents a simplistic grain unit. Specifically, the dislocation starts from the extra half-plane of atoms (plane I) which is identified as a defect. When a shear stress is applied, and its magnitude is sufficient, the bond between atom A and atom B is cut. Then, the bottom of all planes move to the right, and atom B is bonded with its neighbouring atom (atom C). In this case, a new half-plane of atoms (plane II) is generated. Under the shear stress, this irreversible process is successively and repeatedly presented, with the final result being the creation of a step at the edge of this unit. The process is irreversible because the other atoms in the grain also move into new positions (not shown in the figure) due to other disturbances, hence the atoms do not spontaneously revert to their original positions (plastic deformation). Hence the dislocation is an enduring feature of the grain. It can however be sent in a new direction should the orientation of the shear stress change, as occurs in reversed loading. By this means, the plastic deformation is produced due to the motion of numbers of dislocations. In addition there may be atomic displacement perpendicular to the plane, hence causing a screw dislocation. In practical situations, the behaviours of edge and screw dislocations are mixed, and both contribute to the overall plastic deformation of the grain and ultimately of the macroscopic deformation of the part.

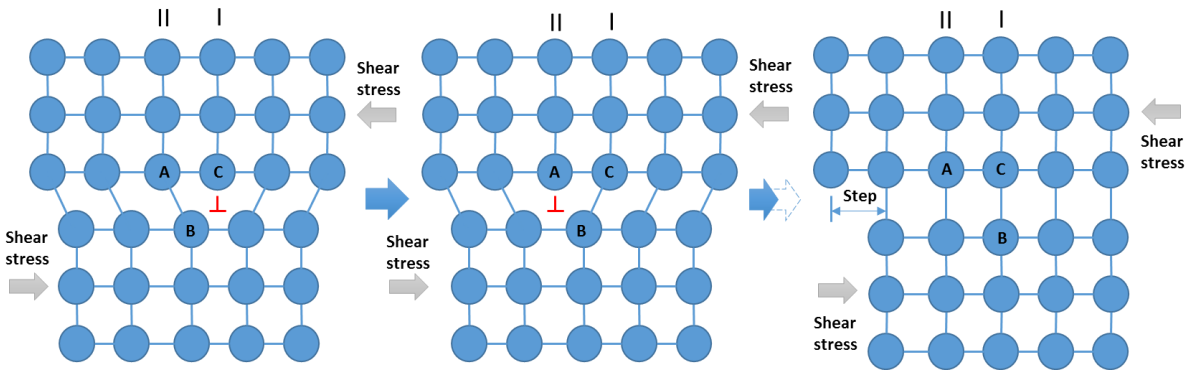

Figure 2 Edge dislocation for fatigue. Adapted from [10]

As mentioned above, the half-plane of atoms is regarded as the source of dislocation. The edge of this half plane is terminated within a grain; hence a large number of dislocations are piled up and then plastic deformation arises for the grain as a whole. This implies that the cracks caused by fatigue are initiated within the grains and then are propagated through the grains, causing the observed transgranular fracture phenomenon.

However, the creep mechanism gives a different crack-growth behaviour, which is crack growth along the grain boundary. In general, crack growth caused by creep is attributed to diffusion behaviour, which is presented as the movements of vacancies [11, 12]. Under the creep situation, a constant applied loading leads to stress concentration at the triple points which are formed by the three adjacent grains (Fig.3). Normally, diffusion is a behaviour of atomic shifts from an area with high stress concentration to an area with low stress concentration. In this case, the atomic movements due to the diffusion mechanism results in the convergence of vacancies at the triple points, which then segregate the triple grain boundaries.

By this means, the micro-crack is initiated at the grain boundary. After the process of micro-crack initiation, the localized stress is highly concentrated at the crack tip, which then recruits more vacancies from the bulk of the grain, and these are diffused to the crack tip along the grain boundary. This leads to further propagation of the creep crack along the grain boundary. High temperature provides more favourable conditions for diffusion behaviour, hence advances the creep crack along grain boundaries. Thus creep failure is strongly temperature dependent.

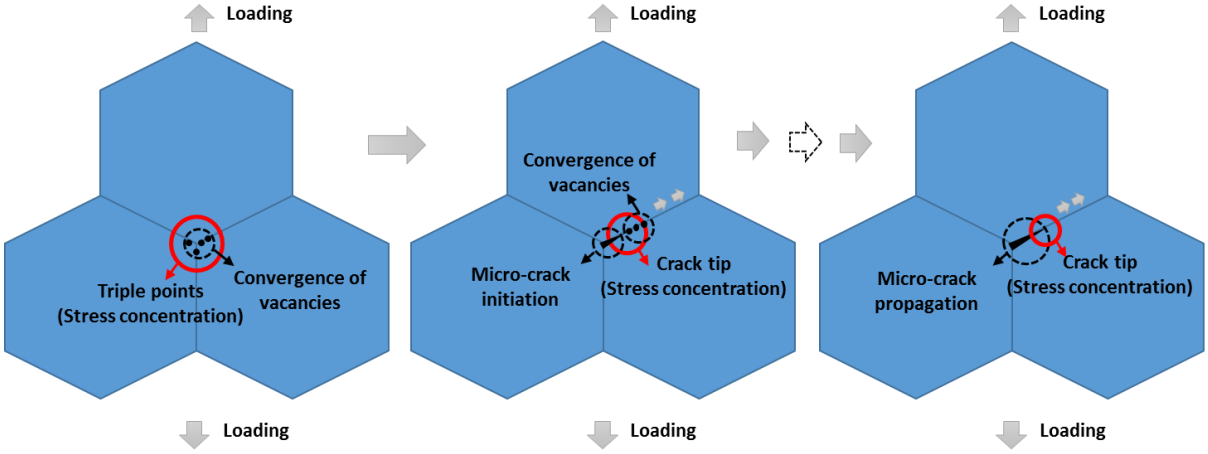

Figure 3 Crack growth by diffusion mechanism

Overall, crack-growth behaviours of fatigue and creep follow the different principles, specifically, fatigue effect occurs via cracks through the grains while the creep effect involves fracture along the grain boundary.

2.2 FEA-based analysis of grain-size effect

As mentioned in section 2.1, fatigue and creep present two different crack-growth behaviours. The theoretical-based discussion has been shown in section 2.1, and this is demonstrated by finite element analysis (FEA) at a grain-based level. This was conducted through investigating the grain-size effects on fatigue and creep damages, and then the numerical results were compared with our general understanding of grain-size effects.

Grain size has significant influences on both fatigue and creep damages, but in opposite ways. Specifically, smaller grain size confers more resistance to pure fatigue, while bigger grain size better resists creep and leads to longer rupture time. This phenomenon results from the different failure mechanisms (crack-growth behaviours) shown by fatigue and creep, specifically, fatigue cracks grow through grains while creep cracks grow along grain boundaries. This was explored by developing FEA models of representative microstructures.

We propose, based on considerations of how the element-based cracks are structured, that the extended finite element method (XFEM) is suitable for modelling fatigue, and the Cohesive Zone Material (CZM) method for creep. This novel proposition is justified below.

The FEA literature shows that XFEM-based and CZM-based methods are used interchangeably for both creep and fatigue loading situations [13, 14]. There is no prior article identifying that

XFEM-based and CZM-based methods may be specific to fatigue and creep behaviours respectively. Our reasoning is that the XFEM crack-growth simulation technique is suitable for simulating fatigue crack propagation because it shows the crack propagating through elements (Fig.13). We believe this is comparable to crack propagation through grains in the pure-fatigue situation. The XFEM crack-growth simulation technique is performed under the 2-D environment (Mechanical APDL in Ansys®) and is restricted to the second region of crack growth (thus based on Paris' Law). Although this approach presents a convenient process because it eliminates the need for re-meshing the crack-tip regions, it ignores large deformation, the crack-tip plasticity effect, and the crack-tip closure effect. However, we accept the possible error may be caused by this condition to perform an easy engineering simulation.

On the other hand, the concept of CZM was developed to model facture along an interface, where the crack growth is simulated through using the traction-separation laws. Specifically, the CZM model presents a gradual separation of surfaces involved in the crack process, and this separation is resisted by cohesive tractions. Comparing with other conventional models (such as LEFM - linear elastic fracture mechanics, and CTOD – crack tip open displacement), the CZM model provides a method to predict the behaviour of uncracked structures, and the size of plastic zone need not be ignored in comparison with the crack zone. In the CZM method, the crack-growth path for FEA is normally constituted through a contact pair, and the crack propagation is simulated by debonding the contact pairs. Obviously, the crack growth is performed along the element boundary (Fig.4), and thus our reasoning is that the CZM model could be used to simulate the crack propagation along the grain boundary, which is a typical pure-creep behaviour.

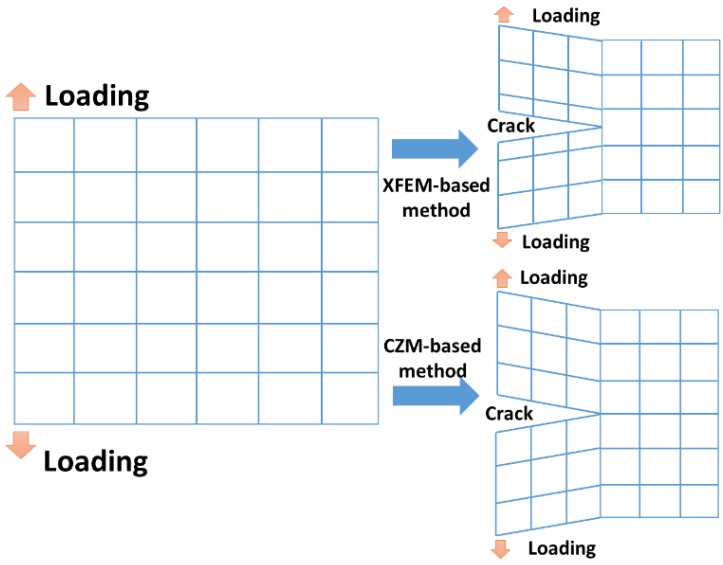

Figure 4 Crack-growth behaviour simulated by XFEM-based and CZM-based methods

Consequently we propose that the grain-size effects can be investigated through XFEM-based method (Mechanical APDL) for pure fatigue, and through CZM-based method (ANSYS WORKBENCH) for pure creep. During the process of simulation, the grain is modelled by an element, and thus the coarse element presents a big grain size and the finer element shows a

small grain size. Compared to coarse element, the finer element was obtained through increasing the number of divisions in the length or width direction, hence relatively smaller sizes were used for the elements, as well as the grains. Then, the geometries with small grain size and big grain size are used to perform simulation under the same applied force (7.5N).

The results obtained through the XFEM-based method for coarse and finer grain sizes under the applied force are shown in Table 1.

Table 1 Simulation results for grain-size effect on fatigue

Condition: fatigue	Applied force [7.5N]		
	Max Strain	Max Pseudo Deformation	Max Pseudo Stress
Small grain size	0.003198	0.091784	417.36
Large grain size	0.005022	0.199358	638.07

Table 1 shows that small grain size benefits the fatigue capacity. Specifically, when the same applied force is applied, the material with small grain size gives smaller damage (strain/deformation) and presents smaller stress than the material with large grain size. This implies that the material with small grain size has better ability against deformation and better stress response against fracture. The results are consistent with the general understanding of grain-size effect on fatigue.

On the other hand, the results obtained through the CZM-based method for coarse and finer grain sizes under the same force are shown in Table 2.

Table 2 Simulation results for grain-size effect on creep

Condition: fatigue	The same applied force [7.5N]		
	Max Strain	Max Deformation	Max Stress
Small grain size	0.0042559	0.9311 mm	745 MPa
Large grain size	0.0029548	0.77826 mm	510 MPa

Table 2 indicates that large grain size benefits the creep capacity, specifically, the material with large grain size gives smaller damage (strain/deformation) and presents smaller stress than the material with small grain size under the same applied force. This implies that the material with large grain size has better ability against deformation and better stress response against fracture. The results are consistent with the general understanding of grain-size effect on creep.

Our proposed explanation is that for small grains the amount of grain boundary is larger relative to the internal area/volume enclosed. The coupling between adjacent elements occurs through the element boundary and the vertices (which correspond to triple points in real grains). The more the (linear) area of element boundaries, and the closer these vertices, the stiffer the structure. Hence for smaller elements (or grains) more of the imposed load is carried by the boundary structure, and correspondingly less stress (or strain) is experienced inside the grain. This idealisation explains the simulation results, which indicate that the smaller elements are more beneficial for trans-element crack-growth behaviour and more negative for crack-growth behaviour along element boundary.

Thus we propose that the element structure in the XFEM and CZM represents a physical phenomenon at the grain boundary. We further propose that the phenomenon arises from different load sharing between the grain boundaries and triple points, vs. the internal bulk of the grain. Hence our suggestion is that the microstructure behaves like a composite material, in having multiple load bearing paths. The scale dependency of these load paths creates the mechanisms that differentiate crack growth of fatigue and creep based on grain size.

Consequently, the grain-size effects obtained from FEA are consistent with the general understanding of the creep and fatigue phenomena. Specifically, the material with smaller grain size gives better fatigue resistance while presenting worse capacity against creep deformation. In particular, this result quantitatively verifies the different principles of fatigue and creep crack-growth behaviours.

In addition, we propose that the XFEM-based method is best suited to analyse fatigue failure and the CZM-based method for creep. Consequently, the FEA-based model applied in this section may give a possible method to evaluate the damages of fatigue and creep.

This section has provided a quantitative validation of the failure principles for fatigue and creep, and proposed a physical explanation for the dependency on grain structures. In the next section we apply these principles to develop a descriptive model of the crack growth process.

3. Model of temporal development of crack-growth for creep fatigue (application of the principles above)

The conceptual model (Figs.6-18) mainly focuses on the second stage of crack growth because the majority of the lifetime is consumed at this stage, and this stage presents a stable process of crack growth. In this conceptual model, the crack-growth behaviours under the tensile partition and compressional partition are discussed separately, and crack-growth behaviours caused by the fatigue effect and creep effect are described separately.

In the present work, we integrate multiple mechanisms, which are proposed in the literature and exist at the microstructural level, to describe crack-growth process. Specifically, it is

proposed that the following major mechanisms operate at the three stages. We note these as premises:

Stage I: Crack initiation

a) That dislocation behaviour [15] is a key mechanism at crack initiation. This effect causes the slip planes to extrude or intrude, which results in stress concentration at the surface and then leads to crack nucleation.
b) That the strain energy release rate [16, 17] determines the crack-growth rate . This mechanism underpins the unstable stage after the threshold of crack initiation. In this stage, increased energy accelerates the increase of crack-growth rate at the beginning phase, which is then retarded due to reduced energy and finally achieves a stable state.
c) That shear effects [8, 9] provide opportunistic directions for crack growth. This mechanism is that the direction oriented at 45^{o} gives a more favourable condition for crack growth at the initial phase of stage I.

Stage II: Crack propagation

d) That the plastic blunting process [18-21] has asymmetrical effects in the tensile and compressive loading cycles. This mechanism describes crack-growth behaviour in one loading cycle. The tensile loading blunts the crack tip, and the new crack surface is created due to a shearing effect. Then, when the loading is reversed, the surface created under tensile loading remains (crack extension) because of a crushing effect.
e) That the crack tip plastic zone [22-24] enhances crack growth. This mechanism involves a highly localized stress around the crack tip. This, on the one hand, results in plastic deformation (crack opening) at the crack tip; on the other hand, gives a more favourable situation for diffusion.
f) That diffusion creep [11, 12] provides a mechanism that leads to grain elongation and then further crack opening. In addition, since atoms diffuse from a high to a low concentration region, more vacancies are generated and converged at the crack tip where highly localized stress is presented, which provides a more favourable situation for creep damage.
g) That existing precipitates [25] cause fatigue resistance. The mechanism is mainly that precipitates are the obstacle to dislocation, hence restrain the process of crack propagation.
h) That crack deflection (change of direction) [26] preferentially occurs at the grain boundary. This is determined by the twist angle and the tile angle.
i) That triple-points [3-5] provide a mechanism for significant stress concentration, which provides a more favourable stress field for creep damage.
j) That a region with high density of micro-cracks is particular weak and supports crack branching activities [27].
k) That the slip bands within grains [28] may cause the crack to re-direct within grains.

Stage III: Structural failure

l) That the plastic energy [9] available exceeds the need for producing the new crack surface. The excess energy is applied to form voids, and thus further worsens creep-fatigue resistance.

The challenge is showing how these multiple premises are integrated together at the microstructural level. There are no models in the literature that provide such integration. To solve this problem, we make the following new propositions of mechanisms that operate at the microstructural level during crack growth:

A. That **energy dynamics** explain the crack initiation and the unstable phase after this, and is based on a liberation of energy due to coalescence of strain. In general, when the internal energy stored in the structure due to cyclic loading arrives at a critical value, the barrier to initiate the crack is overwhelmed. After this, the released energy is gradually consumed to produce new crack surfaces in an accelerated crack growth rate.
B. That **grain-mismatch** occurs due to grain elongation under the tensile loading, resulting in relative movement between two neighbouring grains. Then the shear stress along the grain boundary is increased and a weaker region along the grain boundary is created. This results in a mismatch band at the grain boundary. This widens the crack body and enhances its growth.
C. That **bonding crushing effects** exist at the finer scale. During the process of compression, the atomic bonds, which are distorted and rearranged in the tensile phase, may be further damaged and become potential failure sites for next loading cycle. This process is irreversible since the atoms cannot return to their original position under the compressional loading.
D. That a **crack net** is caused by the aggregation of micro-cracks. This crack net probes a larger volume of material for weaknesses, and then promotes the main crack.
E. That **irregular configuration of the grain boundary** causes stress/strain pile up at the grain boundary, and then results in large driving force for extending crack tip into the neighbouring grain.

Furthermore, it is proposed that these mechanisms are integrated by the following assumptions:

F. That the **primary mechanism** for failure in the creep-fatigue loading regime is crack growth by mechanisms of crack blunting (including shearing and crushing), hence fatigue effects.
G. That the **supporting mechanisms** that augment the extent of damage are grain elongation and diffusion, hence creep effects.

The application of these premises and propositions is detailed below.

3.1 Stage I: Crack initiation

The first stage (stage I) is that of crack initiation. We summarise the crack initiation mechanics as follows. Fundamentally, crack initiation is caused by stress concentration, where two situations are presented. A typical situation is that the crack starts at a surface defect such as a machining mark. This provides a highly localized stress concentration, hence a pre-existing

micro-crack [1]. By this means, a crack is initiated at this specific point, and then the localized plastic strain caused by the ductile micro-tearing events provides opportunity for further propagation.

Second, for the situation with perfect surfaces (defect-free), dislocations play an important role [15] for the initiation of a fatigue crack [29] (Figure 1.9 therein), [30] (Figure 1 therein). During this process, loading cycles cause dislocations to pile up at the microstructural level. These dislocations are in the crystal lattice at the nanoscale. Under loading they align and coalesce to produce thicker slip planes through the crystal and eventually slip bands at the macrostructural level [31]. Under cyclic loading there is more relative movement between the bands so the effect becomes more pronounced – the bands displace further. We suggest this is due to irreversibility caused by the localised hardening effects of the dislocations. In the area of persistent slip bands, the slip planes extrude or intrude to the surface of the object, see Fig.5. This gives tiny steps in the surface, where the stress concentration then results in crack nucleation.

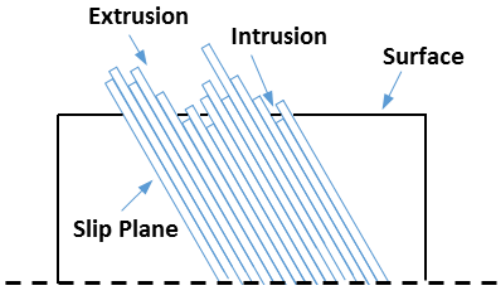

Figure 5 Crack initiation due to dislocation

In the stage I (crack-initiation stage), a stress-intensity threshold exists below which there is no crack growth. We attribute this to the cracks being too short to result in a meaningful stress concentration effect (which is primarily an effect of proportional geometry). Also, if there are many superficial defects - which is usually the case - then the material does not have a geometrically exact boundary at the nanoscale, and hence the stress avoids this region: the many small defects effectively decrease the stiffness of the superficial layer, and hence this layer is to some extent unloaded.

After the threshold stress intensity is exceeded, there is a regime of high acceleration of crack-growth rate. Then, following this high acceleration regime, a transition to a slower acceleration of crack-growth rate is presented.

On the one hand, this process is attributed to the concept of strain energy release rate which describes the energy consumed to create per unit of new crack surface. This implies that the more strain energy is released, the more new crack surfaces are produced. Normally, the strain energy release rate could be numerically related to the M-integral [16, 17]. The relationship between the number of cycles and M-integral was investigated by Margaritis [32] (Figure 7 therein), where M-integral increases with the increasing number of cycles at the early phase, then it decreases over the peak, and finally it reaches a constant situation. This trend is consistent with observation of the initiation stage shown in Fig.1. Specifically, after the

threshold, increased energy (released strain energy) accelerates the increase of crack-growth rate at the beginning phase, then reduced energy retards the acceleration of the crack-growth rate, and finally a steadily increased crack-growth rate is achieved under the situation with constant energy (this is viewed as the crack-propagation stage).

We suggest that the underlying energy dynamics are based on a rapid liberation of energy due to coalescence of strain. Specifically, the internal energy, which is stored in the structure in the form of the irreversible formation of dislocations that increase in number due to cyclic loading. Then, when this energy arrives at a critical value, the vacancies in the dislocations coalesce and form a crack – hence barrier to initiate the crack is broken through. This qualitative leap from perfection to imperfection requires internal energy. This process is accomplished during a short time period by releasing large amounts of energy. After this, the released energy is consumed to produce new crack surfaces in a high acceleration of crack-growth rate, and the whole system is forced into an unsteady condition. Naturally, the need to re-balance this system gradually reduces the amount of released energy (caused by applied loading) until a balanced condition is reached. During this process, the high acceleration of crack-growth rate is gradually retarded, and then this acceleration reaches stabilization (the whole system is re-balanced). The growth of the crack causes further large scale deformation of the grain as a whole, which causes more dislocations to occur within the grain, and repeats the cycle.

An alternative explanation is that the unstable behaviour of crack growth in stage I is due to shear mechanisms [8, 9]. Generally, a crack is propagated through two different methods: the plastic deformation around the crack tip and the shear-stress effect at the planes oriented at 45^{o}. At the initial phase of crack growth, a small plastic zone and a small stress field are presented around the crack tip because of the small magnitude of stress intensity. In this case, the mechanism of plastic deformation around the crack tip may not be significant enough to become the driving force for crack growth. Instead the shear stress at the planes oriented at 45^{o} provides a more favourable condition for crack growth. This is because the shear stress at these planes and the relative movements between these planes under cyclic loading provide more vulnerable areas for crack growth. In this case, a crack grows along the planes oriented at 45^{o} with a minimum of effort, hence a high acceleration of crack-growth rate is given. As the stress intensifies, the shear-stress effect is gradually suppressed by the plastic-deformation mechanism hence the acceleration of crack-growth rate is reduced. This is because, during this process, the direction of the crack growth gradually deviates from the surface of the planes oriented at 45^{o}, and then the behaviour of penetrating the grain boundary results in the deceleration of crack-growth rate. Finally, crack-growth behaviour is stably caused by the crack-tip plastic zone, and a steady situation is achieved (stage II is initiated).

We suggest that both mechanisms apply, and complement each other. We summarise the crack initiation mechanics as follows, see Fig.6. Crack nucleation starts at the surface due to highly localized stress concentration. In the case of smooth surfaces, it is attributed to the presence of persistent slip bands (extrusion and intrusion). Stage I (that stage of crack initiation) has a threshold value, below which no crack growth occurs. Once a crack is initiated, it grows quickly at the early phase, then the acceleration of crack-growth rate is reduced, and the crack-growth

behaviour finally becomes steady (see next section). This process is proposed to be underpinned by the above mechanisms of strain energy release and shear stress.

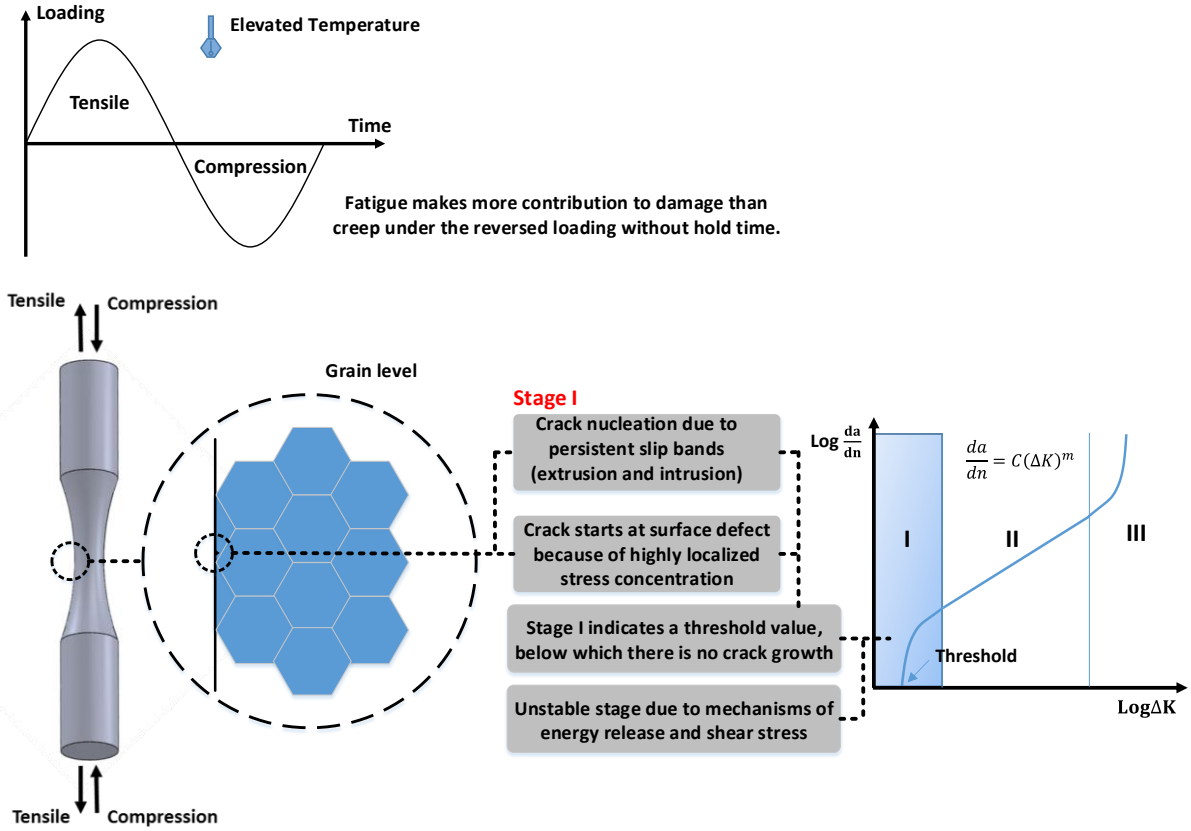

Figure 6 Stage I: Crack initiation

3.2 Stage II: Crack propagation

Numerical representation

The second stage (stage II) shown in Fig.1 presents the behaviour of crack propagation, wherein the crack growth experiences a relatively steady process. This stage is numerically presented by Paris' Law (Eq.1) [2], which shows a power-law relationship between the crack growth rate and the range of the stress intensity factor during the fatigue cycle:

$$\frac{da}{dn} = C(\Delta K)^m \tag{1}$$

where $\frac{da}{dn}$ is the crack growth rate, ΔK is the effective stress intensify factor which is identified as the difference between maximum and minimum stress intensify factors for one cycle, and C and m are constants.

Explanation for plastic blunting of crack

The crack-growth process of creep fatigue is mainly discussed under the second stage of crack growth, and this discussion is based on the idea of the plastic blunting process (illustrated in Fig.7 based on one cycle loading) [18-21].

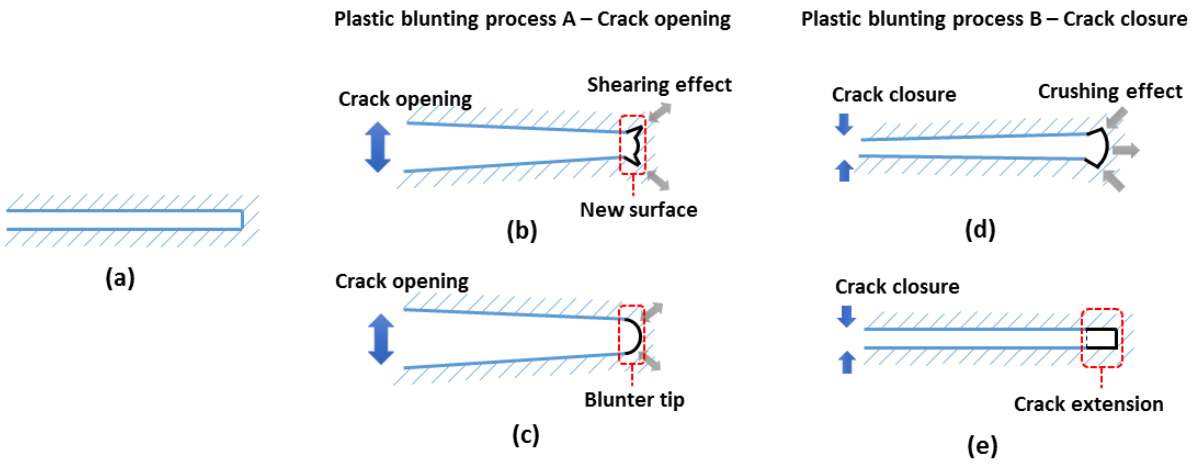

Figure 7 Plastic blunting process

At the beginning of loading cycle, the crack tip is sharp (Fig.7a). Then, the applied tensile stress leads to crack opening, and the stress concentration at crack tip causes the slip along planes at 45° (Fig.7b). This leads to the gradual increase of crack-tip area, and finally the crack tip widens to its maximum plastic deformation (Fig.7c) due to the plastic shear effect. At the same time, the crack tip becomes blunt and grows longer because a new crack surface is created.

When the loading is changed to compressional situation, the crack is closed, and the slip at the crack tip is reversed (Fig.7d). Finally, the crack surfaces are crushed together, and the new crack surface created under tensile loading remains (Fig.7e) (crack extension). Consequently, the sub-cracks promoted by each loading cycle are accumulated, and the structure fails as the total damage achieves a critical value.

The idea of plastic blunting process was integrated with a general understanding of creep mechanism to show crack-growth behaviour of creep fatigue. The process of crack propagation (Fig.8-Fig.17) is described (in a grain-based level) by three typical situations: (1) crack tip within a grain (section 3.2.1); (2) crack tip at the grain boundary (section 3.2.2 (1)) or at the triple point (section 3.2.2 (2)); and (3) crack tip through grain boundary (section 3.2.3).

In the present work, fatigue is identified as crack growth by overloaded local atomic bonds, and creep is regarded as the flow of atoms relative to each other with transfer of bonding to new partners.

3.2.1 Crack tip within a grain

Model for crack growth in the tensile regime

Under tensile loading (Fig.8), the fatigue component follows the idea of the plastic blunting process. In this process (1A in Fig.8), tensile stress leads to crack opening, and shear behaviour is presented at the crack tip. Then, by the plastic shear effect, the new surface is created; meanwhile, the crack tip widens and becomes blunt (the blunting behaviour was illustrated by Figure 12 in Ref [33] and Figure 32 in Ref [34], where a stretch region is presented). Diffusion creep is identified as the main creep mechanism for creep-fatigue damage in the present work.

It is generally believed that diffusion creep leads to grain elongation, which then results in a further opportunity for crack opening (1B in Fig.8).

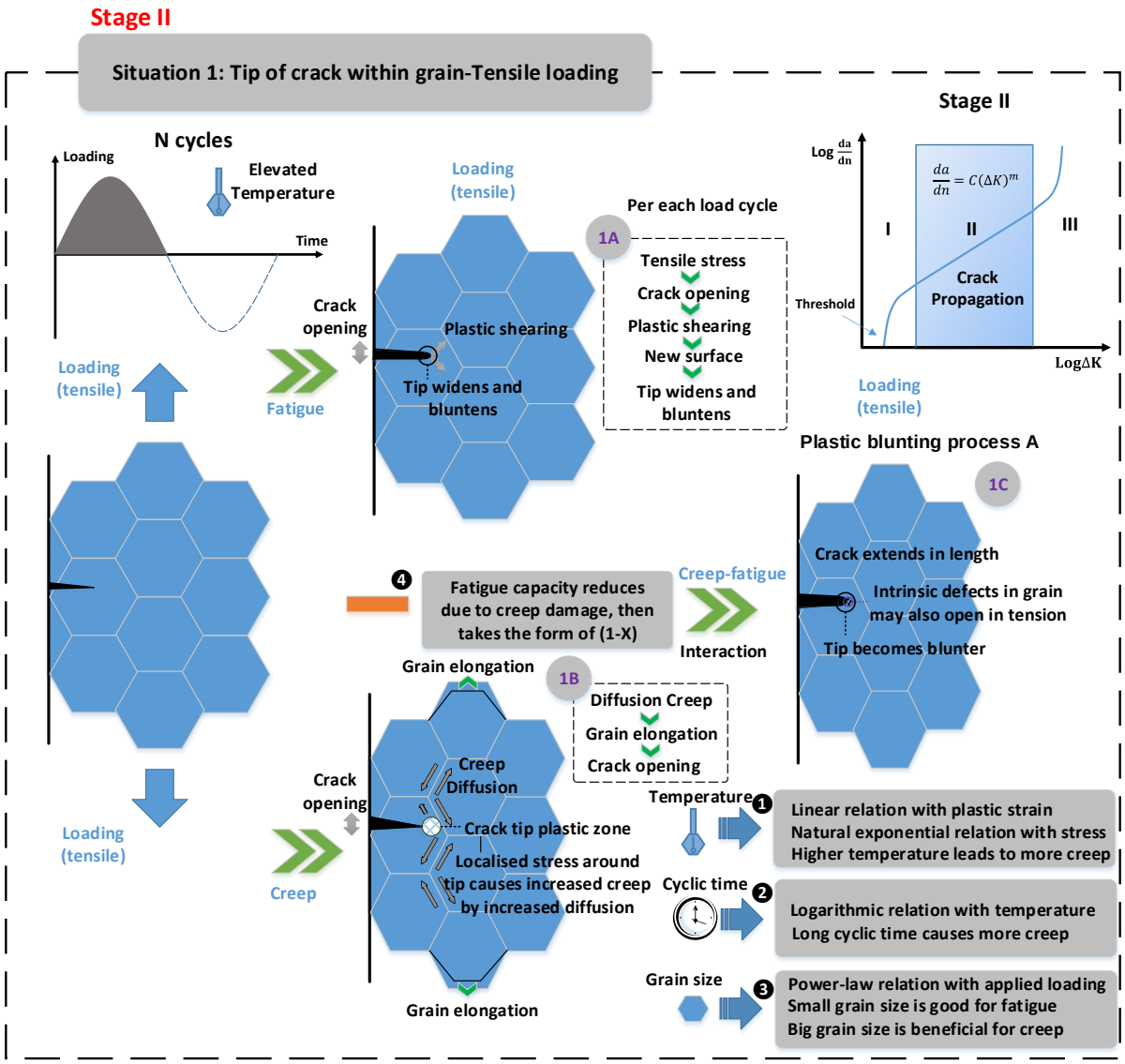

Figure 8 Crack tip within a grain-Tensile loading

In addition, diffusion creep has a dependency on applied loading, and larger loading produces more creep damage. Specifically, the idea of a crack tip plastic zone [22-24] indicates that the localized stress is highly significant around the crack tip, and gradually decreases in the direction of crack growth (Fig.9). This is consistent with the numerical representation (Eq.2) of stress distribution around the crack tip:

$$\sigma_{ij} = \sigma\sqrt{\frac{a}{2r}}f(\theta) = \frac{K}{2\pi r}f(\theta) \tag{2}$$

where σ_{ij} is the stress distribution, a is the crack length, K is the stress intensity factor, and r and θ are polar coordinates. Higher localized stress around crack tip causes more creep damage due to increased diffusion, and thus contributes to crack opening. Specifically, atoms normally

diffuse from a region of high concentration to a region of low concentration. In this case, more vacancies are generated and converged at the crack tip, and then a more favourable situation for creep damage is presented.

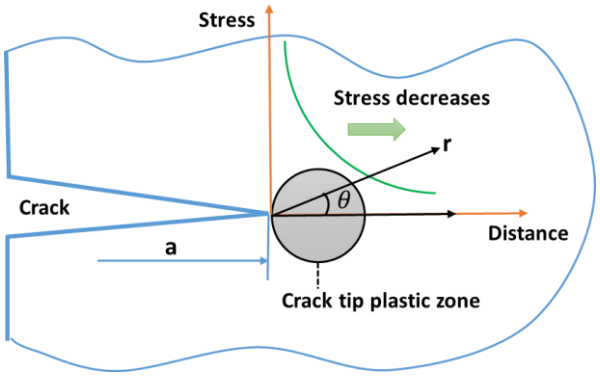

Figure 9 Stress around crack tip

Consequently, the crack tip surface caused by the fatigue effect is further extended and becomes blunter due to the creep effect (1C in Fig.8), which implies the combined effects of fatigue and creep. A defected-related state, such as intrinsic defects, around the crack tip may also promote crack growth (negative to fatigue resistance), where the weakest zone of atomic bonds is represented. An example of presenting a defected-related effect is shown in Figure 32 from [34], where the crack is promoted due to void coalescence and the bridges between voids are sheared off. In addition, precipitates may also be considered as a defected-related effect, but which are normally beneficial to fatigue resistance. On the one hand, this benefit results from the obstacle to further dislocation [25], whereby the precipitates restrain the process of crack propagation. On the other hand, this benefit could also be explained by the fatigue-softening behaviour [35]. Generally, softening behaviour is caused by disordering the stacking sequence of precipitates due to reversed loading, whereby the crack encounters a tougher situation to penetrate this area. In addition, the fatigue-softening behaviour can also be attributed to the reduced area intercepted by the dislocation of the slip planes due to the gradual consumption of precipitates under the reversed loading (the precipitates are cut into smaller sizes under reversed loading, and thus are dissolved).

Normally, creep effect has strong dependencies on temperature, cyclic time and grain size. The influences of these factors on creep-fatigue behaviour was discussed in our previous research [36-38], and a unified creep-fatigue equation was proposed:

$$\varepsilon_p = C_0 c(\sigma, T, t_c, d) N^{-\beta_0} \tag{3-1}$$

with

$$\begin{aligned} c(\sigma, T, t_c, d) &= 1 - \left[c_1(\sigma)\left(T - T_{ref}\right) + c_2 \log\left(t_c/t_{ref}\right)\right] \cdot \left[A\left(d/d_{ref}\right)^m\right] \\ T - T_{ref} &= \begin{cases} T - T_{ref} & for \quad T > T_{ref} \\ 0 & for \quad T \le T_{ref} \end{cases} \\ t_c/t_{ref} &= \begin{cases} t_c/t_{ref} & for \quad t_c > t_{ref} \\ 1 & for \quad t_c \le t_{ref} \end{cases} \end{aligned} \tag{3-2}$$

where ε_p is the plastic strain, C_0 is the fatigue ductility coefficient, β_0 is the fatigue ductility exponent, N is the creep-fatigue life, σ is the stress, T is the temperature, t_c is the cyclic time, d is the grain size, T_{ref} is the reference temperature, t_{ref} is the reference cyclic time, d_{ref} is the reference grain size, and A and m are constants. This equation numerically presents the influences of temperature, cyclic time and grain size on creep fatigue, and the relationships between these parameters can be explained by the underlying physical mechanisms [1, 39]. Generally, a higher temperature leads to more creep damage, and a linear relation between temperature and applied loading is presented in Eq.3 (❶ in Fig.8). In addition, a longer cycle time gives more creep damage, and a logarithmic relation between cyclic time and temperature is presented in Eq.3 (❷ in Fig.8). Furthermore, a small grain size is positive for fatigue while big grain size is beneficial for creep resistance, and a power-law relationship between grain size and applied loading is presented in Eq.3 (❸ in Fig.8). Consequently, the negative creep effect caused by elevated temperature, or prolonged cyclic time, or smaller grain size gives weaker atomic bonds, then this results in adversely affected material. The concept of 'fatigue capacity' indicates that the total fatigue capacity is gradually consumed by creep effect. This process is numerically presented in the unified creep-fatigue equation by taking the form of '1-X' (❹ in Fig.8).

Model for crack growth in the compressional regime

Under compressional loading, crack closure is presented based on the idea of plastic blunting process, see Fig.10. In this process, crack surface, especially the tip zone, is crushed together. Since the crushing process is inelastic and irreversible, the new crack surface created under tensile loading remains (1E in Fig.10). This implies that compressional loading also contributes to crack growth.

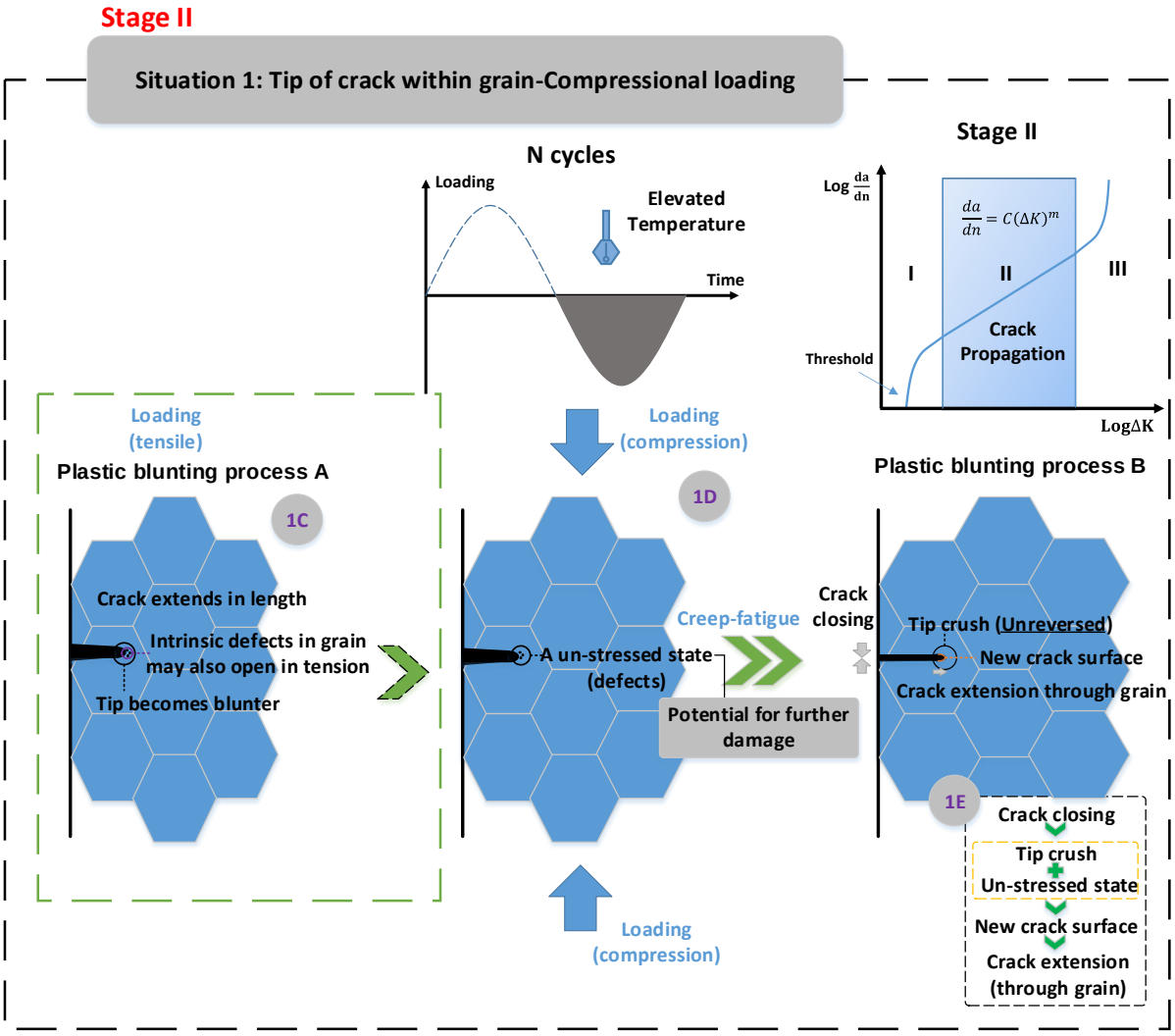

Figure 10 Crack tip within a grain-Compressional loading

This phenomenon may be explained by the observation of the crack tip opening displacements [40, 41] under compressional loading, where the crack is not entirely closed in this loading regime due to the plastic effect (this is illustrated by Figure 3 of Ref [40]).

In addition, the contribution of compressional loading may also be explained by the behaviour of atomic bonds. Specifically, creep fatigue does its damage in the tensile phase by changing the landscape of atom arrangements and hence the bond vulnerability (which implies the bonds are extended and become weaker). During the process of compression, because of the crushing effect, some of these partly broken bonds may be further damaged and become potential failure sites for the next loading cycle, while others may be totally damaged and then lead to crack extension. This is significantly not a reversible process since the atoms cannot return to their original positions after one tension-compression cycle. Furthermore, the defect-related state around the crack tip may further propagate cracks due to the crushing effect. Specifically, the crushing effect causes the crack tip to be squeezed, and then the tip is possibly extruded towards the zone with the weak atomic bonds. In this case, the crack is further extended (1D in Fig.10) by cutting these vulnerable bonds with the assistance of the crushing effect. Consequently, the sub-crack under one loading cycle is formed, which makes a contribution to the final fracture.

After N cycles, the accumulated crack arrives the grain boundary or it encounters the triple point. This reaches the following situation.

3.2.2 Crack tip at grain boundary or triple point

(1) Crack tip at grain boundary

Model for crack growth in the tensile regime

Under tensile stress (Fig.11), the fatigue component experiences the same process shown in 'situation 1-1A', wherein the new crack surface is created due to the plastic shearing effect. Then, this causes the crack tip to widen and become blunt. For the creep component (2B-1 in Fig.11), diffusion creep results in grain elongation along the stress direction. On the one hand, this gives crack opening, which has been discussed in section 3.2.1; on the other hand, shear stress, which results from grain elongation, leads to elongation of the grain boundary, which then causes the crack tip to widen; meanwhile, a mismatch band appears [42, 43]. Specifically, the grain boundary presents a zone of irregular atomic bonds, and thus the bonds at the grain boundary present an anisotropic behaviour. Therefore, the relative movement of points caused by grain elongation at the grain boundary may present different results, the extension or break of atomic bonds. This gives a zone of material where bonds are partly weakened, and provides a potential for further damage. Consequently, creep intensifies the plastic blunting process caused by the fatigue effect, and a blunter crack tip arises.

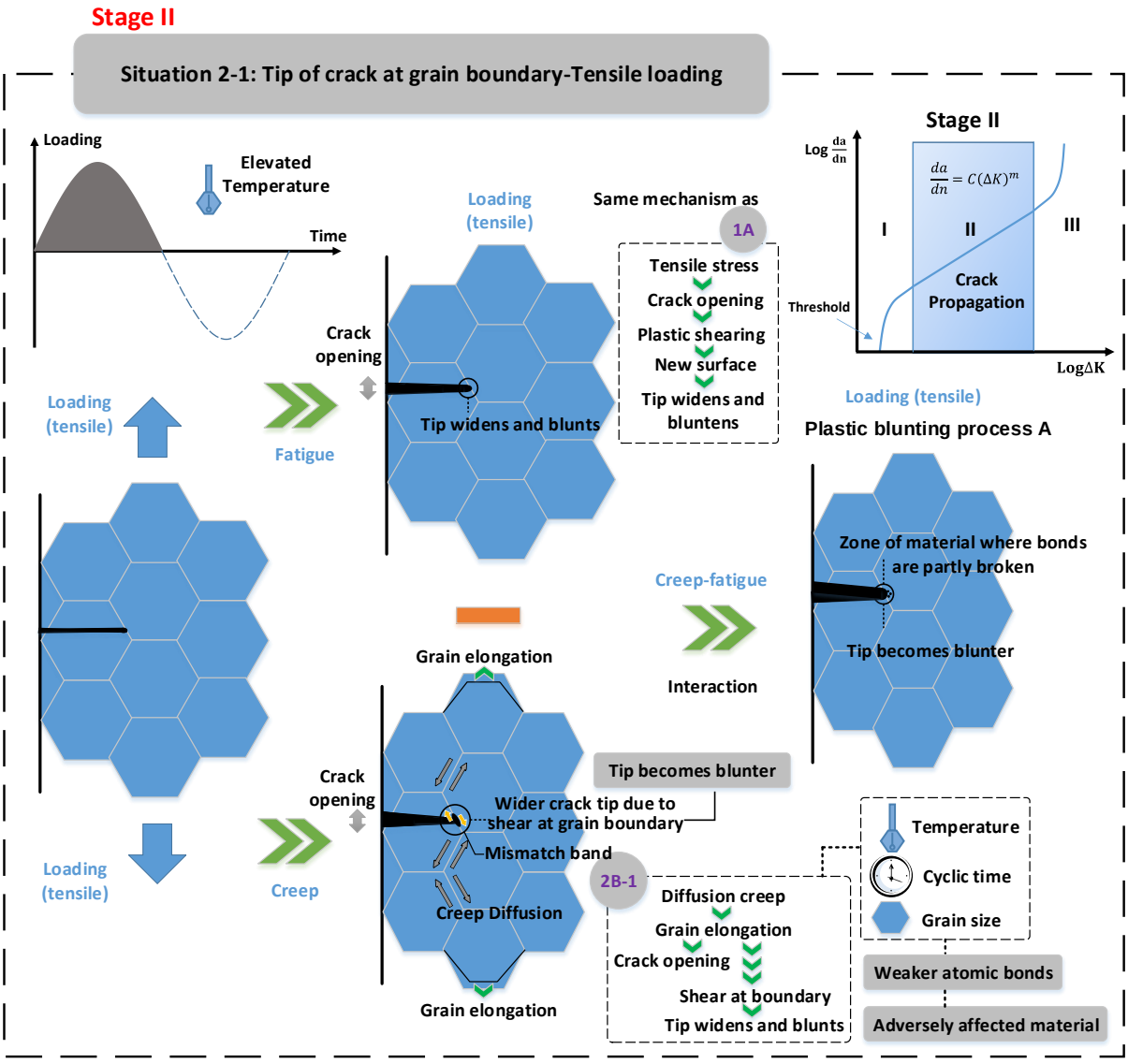

Figure 11 Crack tip at grain boundary-Tensile loading

Model for crack growth in the compressional regime

Under the situation with compressional loading (Fig.12), the same creep-fatigue process shown in ‘situation 1- 1E’ is presented, where reversed loading crushes the material ahead of the crack, even across the grain boundary. As a result, the new crack surface caused by the tensile loading remains by the tip-crush effect, and the crack is further extended across the grain boundary.

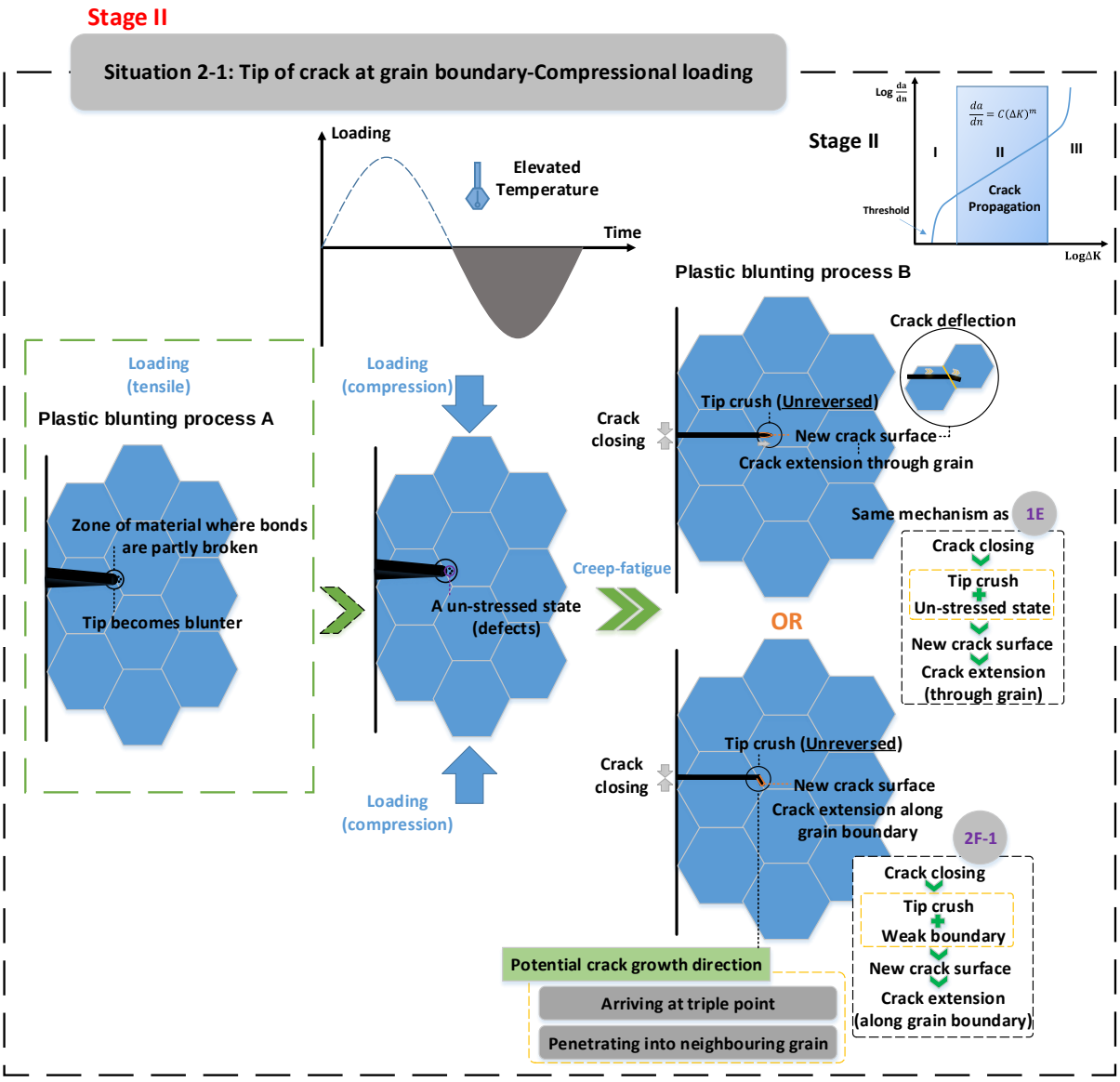

Figure 12 Crack tip at grain boundary-Compressional loading

In particular, the crack path may be deflected (this behaviour is illustrated by Figure 12 of Ref [44]) at the boundary. Specifically, crack deflection at the grain boundary is generally determined by the twist angle *(a)* between two slip planes on the grain boundary and the tilt angle *(b)* between the intersection lines of two slip planes on the cross section [26]. This behaviour is illustrated by Fig.13, where the crack path is redirected at the grain boundary of the sample surface.

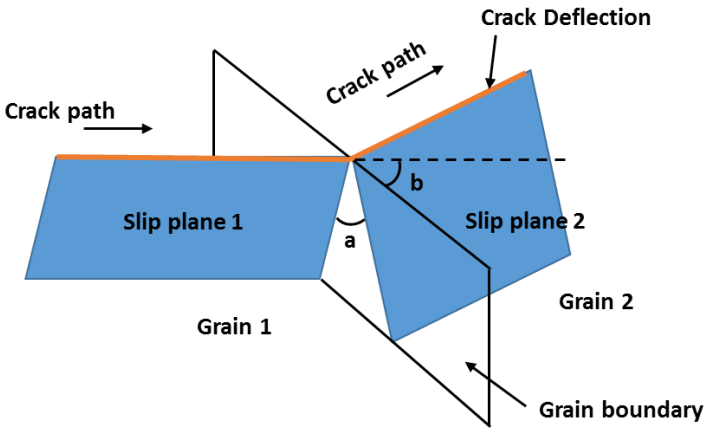

Figure 13 Crack deflection

Alternatively, the tip-crush effect during the process of crack closure may lead to crack growth along the grain boundary. Specifically, grain band sliding, which occurs during crack opening, may result in a weaker region along the grain boundary. This then provides a more likely direction for crack propagation than the direction passing through the grain boundary. After this, the crack may arrive at a triple point or may penetrate into the neighbouring grain (deviated progression along the grain boundary). These two situations will be discussed in the next section.

(2) Crack tip at triple point

Model for crack growth in the tensile regime

The triple point, which is defined as the connection point among three adjacent grains, provides a different crack-growth mechanism for fatigue and creep. Specifically, fatigue effect under tensile stress (Fig.14) presents the same process shown in 'situation 1-1A', where a blunt tip is presented at the triple point according to the idea of plastic blunting process. Comparing with the situation shown in section 3.2.2 (1), creep presents a different behaviour at the triple point. On the one hand, diffusion creep gives grain elongation along the direction of tensile stress, and then this leads to crack opening (2B-2 in Fig.14); on the other hand, the triple point presents a significant stress concentration [3-5], which provides an effective stress field for crack growth along the grain boundary (2B-2 in Fig.14). In this situation, multiple opportunities arise for crack propagation along the grain boundary. Generally, the weakest microstructural zone may finally determine the direction of crack growth. Specifically, the weakest zone shows an intensified state, which is normally caused by defects. These include vacancies which are beneficial to diffusion creep [45, 46], and micro-cracks which aggravate the concentration of stress and hence provide favourable conditions for diffusion. These defect-related effects may also change the direction of crack growth. In addition, according to the idea of the crack tip plastic zone (shown in Fig.9), the stress concentration is presented at the crack tip, where a strong high-stress field is provided hence more creep damage is produced. This implies that this area/direction may have more potential for crack growth. As a result, with the combined effect of fatigue and creep, a blunter crack tip is presented. The crack grows opportunistically

in the direction where the grain boundaries are most vulnerable (for propagation into the grain see below).

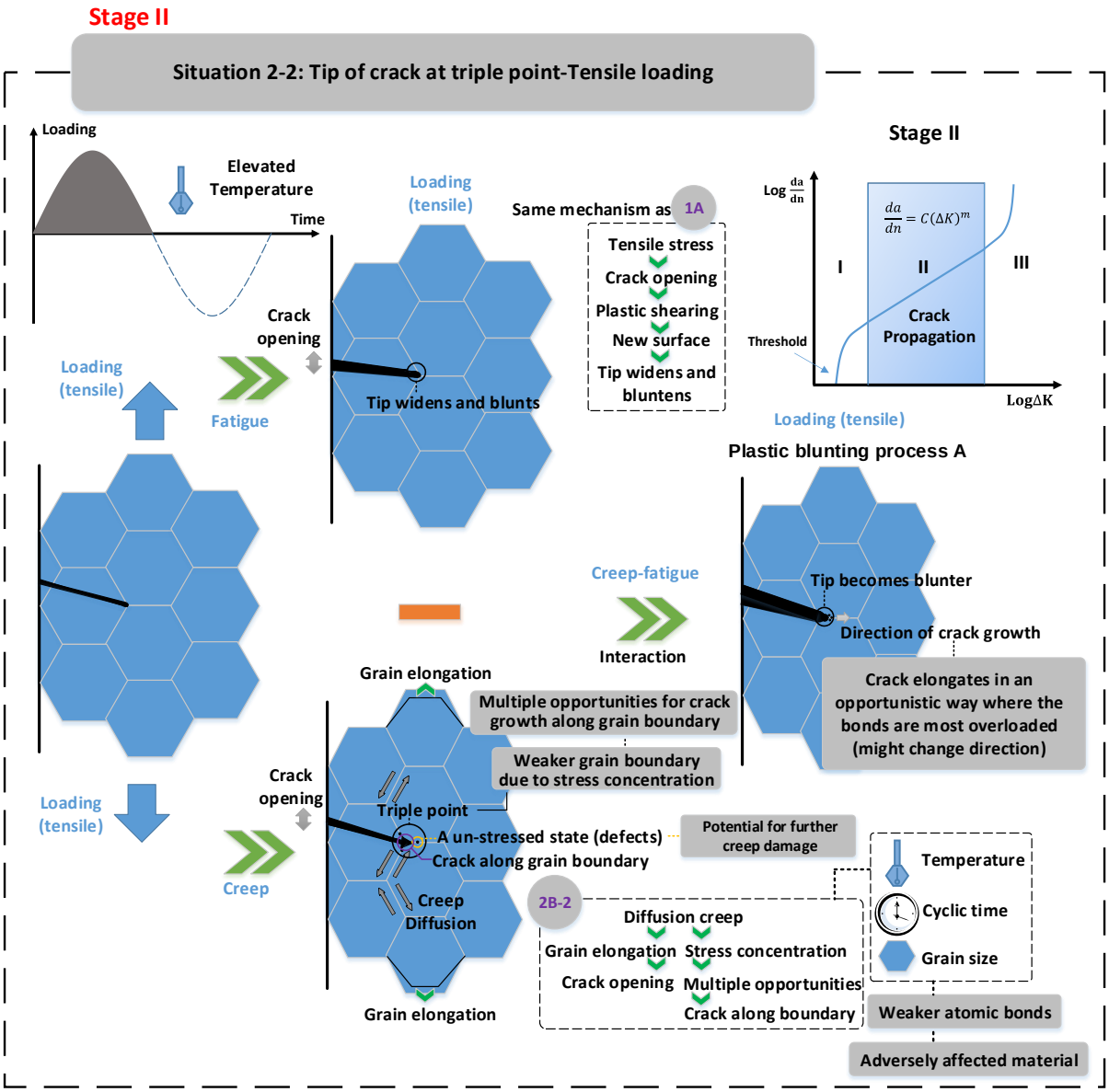

Figure 14 Crack tip at triple point-Tensile loading

Model for crack growth in the compressional regime

Under compressional loading (Fig.15), according to the idea of plastic blunting process, the crushing effect maintains the new crack surface created under the tensile situation, and thus the crack is extended along the grain boundary (2E-2 in Fig.15).

Crack growth at next cycle or next few cycles may have two possible paths (2F-2 in Fig.15). Specifically, on the one hand, a crack may grow traverse (or along) the grain boundary, where weakest atomic bonds are presented. This may be attributed to stress concentration at the grain boundary since the existence of the stress gradient results in the convergence of vacancies [11, 12], and in particular, the vacancies at the grain boundary give a favourable condition for

diffusion creep [45, 46]. In this case, the crack along the grain boundary gradually accumulates, and then reaches the next triple point, where the opportunity for re-direction is provided.

On the other hand, the crack may be deflected away from the grain boundary. This behaviour is illustrated by Figure 3 of Ref [42] and Figure 7 of Ref [43]. This phenomenon may result from defects, such as vacancies in the grain or on its boundary and micro-cracks in the vicinity of the crack. These provide locations for re-direction of crack growth. Specifically, vacancies provides better conditions for diffusion creep, which has been discussed in the previous sections. In addition, the aggregation of micro-cracks, which are attached to the main crack, also contributes to crack deflection at the grain boundary. This phenomenon is identified as branching activities, and is illustrated by Figure 10 of Ref [27] and Figure 13 of Ref [47]. In this situation, a crack-based tree is constructed at the microstructural level, where the main crack is the trunk of this tree and micro-cracks form the branches. The weakest area normally appears at the region with the high density of the micro-cracks, and plays an important role in crack propagation. This is because the aggregation of micro-cracks weaves a crack net which offers multiple sites for shear strain under tensile loading. The shear stress at the inter-atomic level for any one crack is not decreased by having more micro-cracks. Consequently the crack net probes a larger volume of material for weaknesses than a single crack could do on its own. This promotes the main crack to automatically grow in a direction most favourable to increasing the total strain (hence most injurious to the integrity of the part).

In addition, the deviated progression may also be caused by the stress concentration at the grain boundary due to irregular configuration thereof. Specifically, this grain-boundary condition results in stress/strain pileup at the boundary (weak boundary condition is presented) and then leads to larger driving force for extending crack tip into the neighbouring grain, whereby the barrier of the grain boundary is overcome. This is consistent with the general understanding that cracks always propagate towards the direction which requires the minimum energy (stress).

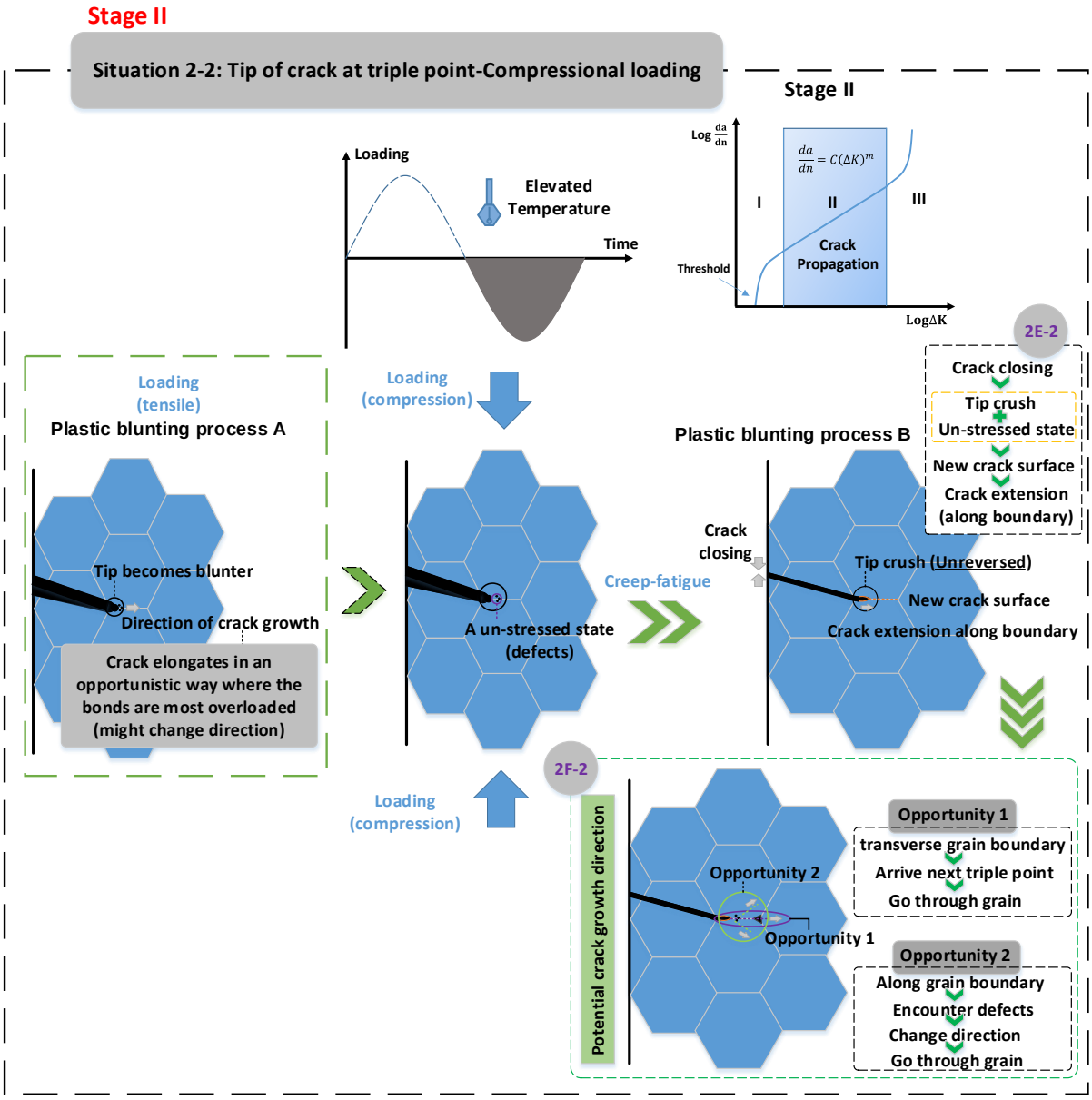

Figure 15 Crack tip at triple point-Compressional loading

These two situations reflect the fact that fatigue makes more contribution than creep in the present case (cyclic loading without hold time). Specifically, the first option implies that the tensile stress, which is perpendicular to grain boundary, provides a tearing stress to peel off the surface at the grain boundary. This is a significant fatigue behaviour, where the bonds at the grain boundary are further overloaded and then broken due to the previous damage caused by creep. In addition, the surface of grain boundary is normally not ideally smooth; the geometric anisotropy or defects at the grain boundary may cause that plastic strain to pile up at one specific point, which means that less stress is needed at this point to break the barrier and penetrate the grain boundary, thereby providing for re-direction for crack growth [48]. This transgranular behaviour (which is consistent with the principle of fatigue-crack growth) is illustrated by Figure 4 of Ref [49].

After this process, crack goes through the grain boundary, and the crack tip is extended to the next grain, which is the third situation and examined below.

3.2.3 Crack tip through grain boundary

Model for crack growth in the tensile regime

Under tensile loading (Fig.16), the fatigue component experiences the same process shown in situation 1-1A (Fig.8), where the new crack surface is produced due to plastic shearing effect, and then the crack tip widens and becomes blunt. For the creep partition (3B in Fig.16), on the one hand, diffusion creep gives grain elongation, which leads to crack opening due to configurational effect of the grain. On the other hand, the extension of the grain boundary caused by grain elongation gives a relative movement between two neighbouring grains, which generates shear stress along the grain boundary. In this case, a mismatch band at the grain boundary is generated due to the distortion of the existing crack under shearing conditions. This band may be further intensified due to pre-existing damage caused by the grain-boundary effect (shown in section 3.2.2 (1), situation 2-1). As a result, this mismatch band widens the crack body and further promotes the crack opening. Finally, the combination of fatigue and creep gives a blunter crack tip.

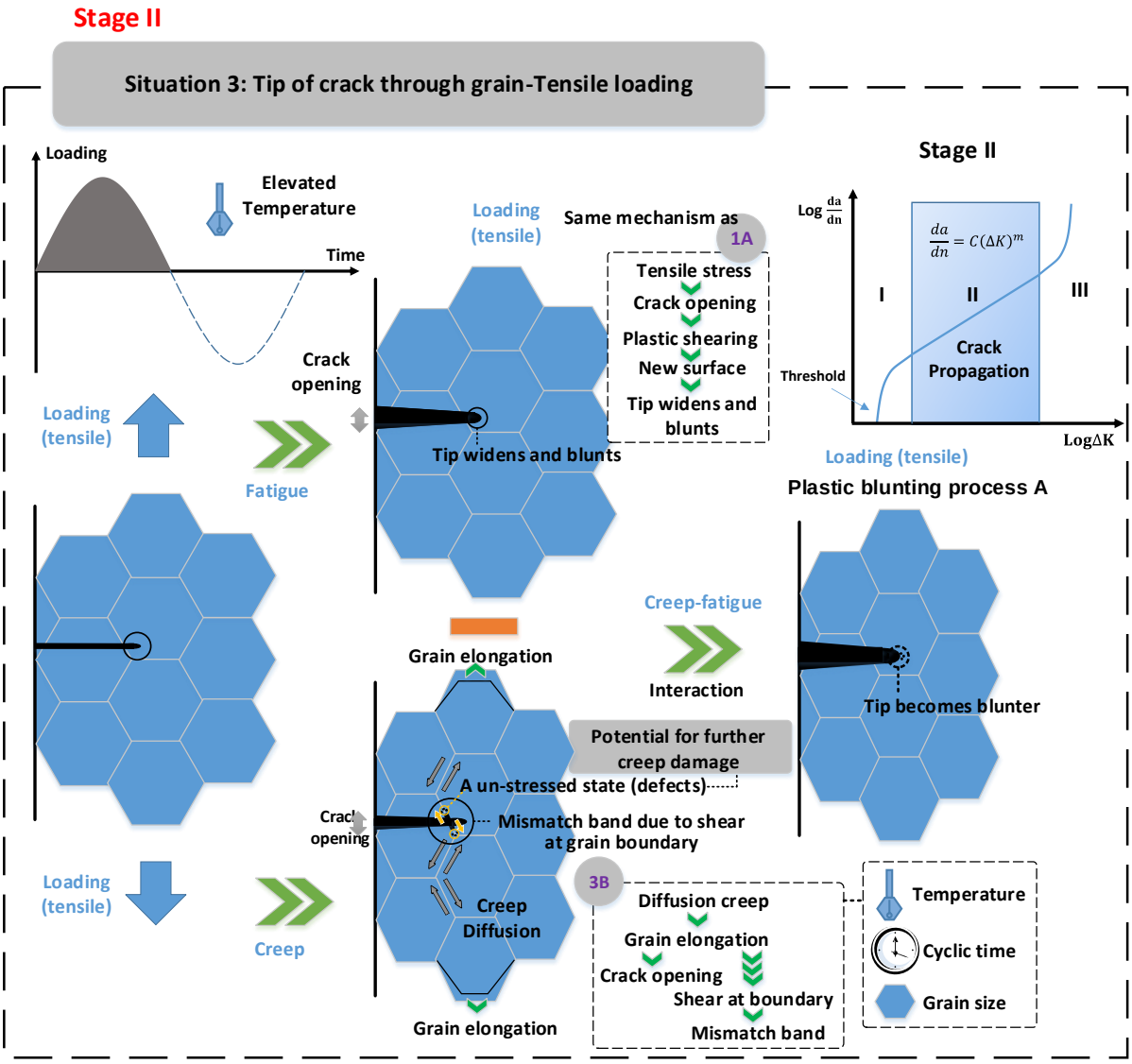

Figure 16 Crack tip through grain boundary-Tensile loading

Model for crack growth in the compressional regime

Under compressional loading (Fig.17), the crack-closure process maintains the new crack surface created under tensile loading. Meanwhile, the fatigue crack is extended during the process of crushing, and this is enhanced by any nearby defects in the material.

It is notable that the slip band may result in a re-direction of the crack within grains, following the slip bands inside the grain. We propose this is caused by the relative movements between slip planes under cyclic loading, which gives a better condition for crack growth along the slip planes. Microstructurally, at the surfaces of the slip bands, the atomic bonds are distorted and elongated under the reversed loading. Thus, these bonds become vulnerable, and then the weakest region (the surfaces of the slip bands) is formed. In this case, at these surfaces, the atomic bonds require the least effort to cut, which then results in crack propagation along the slip bands. The slip band activities are illustrated in Figure 11 of Ref [28], wherein the crack behaviour of re-direction within a grain is presented.

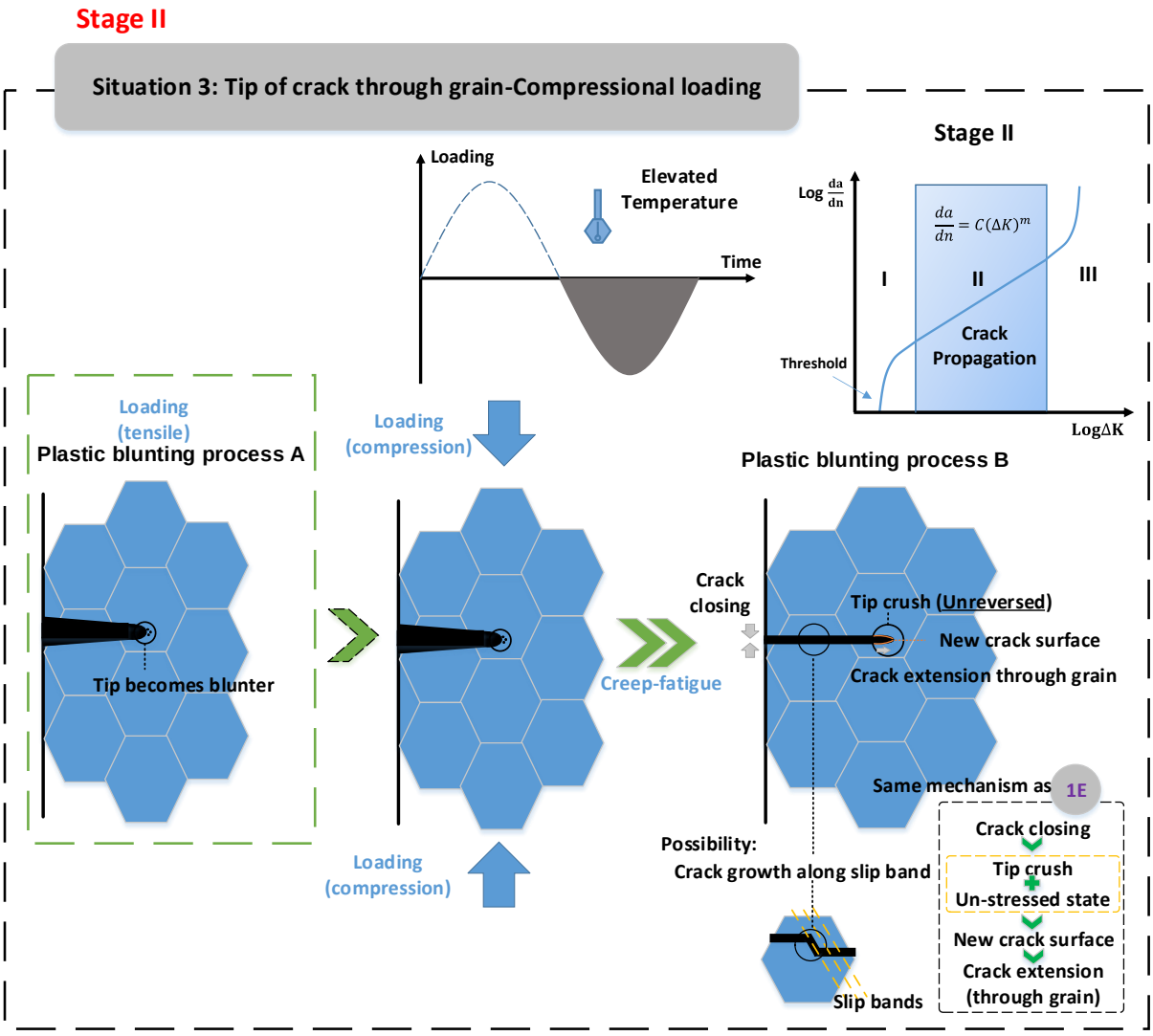

Figure 17 Crack tip through grain boundary-Compressional loading

3.3 Stage III: Structural failure

The final stage shown in Fig.18 illustrates the fracture of an engineering structure:

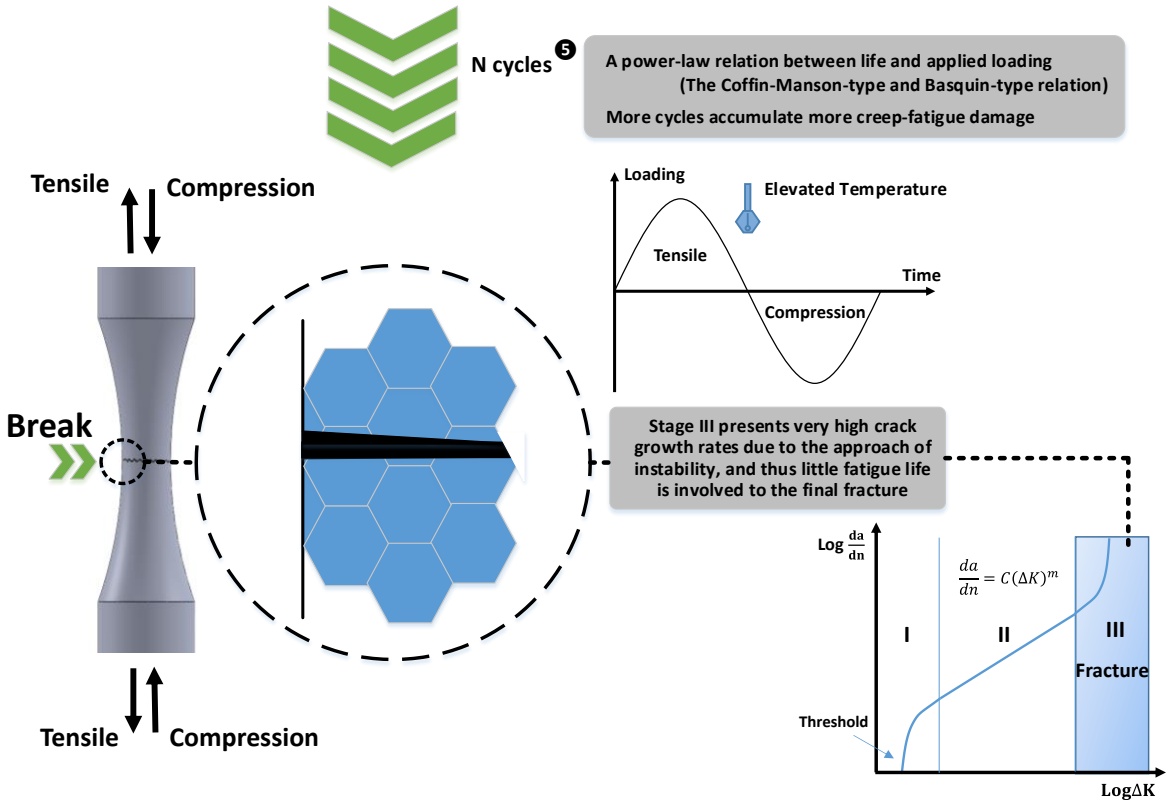

Figure 18 Structural failure

In this stage, crack growth rate rapidly increases, and part-separation commences when the total crack length reaches a critical value (final facture). This stage represents an unstable state, where the equilibrium shown in the second stage of crack growth is broken due to intensified accumulation of damage and reduction of remaining cross sectional area. This is attributed to a high stress field at the crack tip due to high stress intensity [9], hence the plastic zone becomes large compared to the crack size. Under this stress state, the plastic energy available exceeds that needed for producing the new crack surface. In this case, on the one hand, a part of the plastic energy is applied to create new crack surface; one the other hand, the rest of plastic energy is applied to form voids [9] (see Figure 4.11 therein). Then, under the applied stress, these voids are further expanded and then coalesced by internal necking [50]. This phenomenon worsens the creep-fatigue resistance, and then leads to rapid growth of the crack. Therefore, in this stage, a small contribution of loading cycles leads to big creep-fatigue damage, which then results in failure.

During the process of crack growth, the creep-fatigue damage gradually accumulates with the increasing number of cycles, and this process is presented in a power-law relation (❺ in Fig.18). This is also accommodated in the unified creep-fatigue equation (Eq.3), where a power-law relationship between life and applied loading is shown. As discussed in section 3.2.1, the idea of crack tip plastic zone implies that the stress concentration around the crack tip plays an important role in crack growth. Specifically, the more stress is concentrated, the larger the plastic zone, and then the more the crack is promoted. Therefore, we assume that the crack growth is a geometry-related behaviour, and the crack growth rate (crack growth in one cycle) may be related to the size of the plastic zone. Normally, the area of a zone can be presented as

a second-order-power relation with a certain dimension, such as radius for circle and the length of a side for square. In this case, since the stress amplitude is directly related to size of the plastic zone, we believe that the applied loading can be related to the crack growth rate in a power-law form. In addition, this relation is also consistent with the idea of damage accumulation shown in Fig.19. In the first stage, the original steady state (a perfect body) is suddenly broken due to the large amount of accumulated energy, which implies at this stage a small amount of damage is produced with a large number of loading cycles (stage I in Fig.19). Then, after the process of re-balancing, the damage accumulation gives a relatively steady state, where the rate of accumulation stably increases (stage II in Fig.19). Finally, when the totally damage arrives at or close to a critical value, the load bearing capacity collapse in a short time. This stage implies that much damage is produced within a small number of loading cycles (stage III in Fig.19).

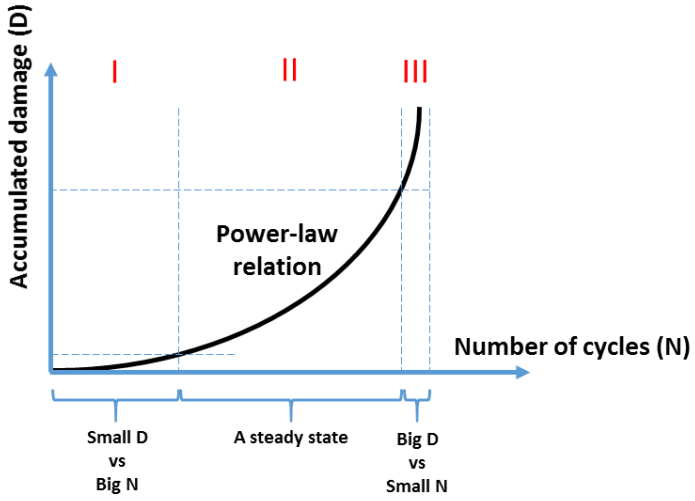

Figure 19 Damage accumulation

4. Discussion

4.1 Outcomes

We have shown, by use of finite element methods (XFEM-based and CZM-based), that the effect of grain size on crack growth is quantitatively validated. In general, the results given by this method can be explained by the principle of FEA. Specifically, the more area of element boundaries in one specific internal area/volume, and the closer the vertices formed by adjacent elements, and the stiffer structure. Therefore, for smaller elements (grains), more imposed loading is carried by the boundaries, while less loading is experienced inside the element. This is consistent with the crack growth of fatigue and creep, where the smaller grain size is more beneficial for the transcrystalline crack-growth behaviour (fatigue), while results in worse situation for crack growth along grain boundaries (creep). Thus, we conclude that the FEA-based method provides the quantitative validation of the failure principles for fatigue and creep.

In addition, a conceptual graphical-based model for creep fatigue was proposed. In this conceptual model, we proposed that different crack growth mechanisms are active for different stages in the temporal evolution of the crack (stages I to III), different parts of the tension-compression cycle, and for different regions within the microstructure (grain boundary, triple point, inside the grain). In general, the temporal evolution of the crack is mainly based on the mechanisms of the plastic blunting process, stress-concentration state and diffusion-creep behaviour. The illustration of crack-growth process is presented by three different stages:

Stage I: Crack initiation

In the first stage (the crack initial stage), a threshold is presented, below which no significant crack is detected. The existence of this threshold can be attributed by the effect of stress concentration. For the surface with defects (such as a machining mark), the stress concentration is caused by the pre-existing micro-cracks. For the defect-free surface, the behaviours of extrusion and intrusion between slip plans give some tiny steps in the surface, which then results in the stress concentration.

Stage II: Crack propagation

In the second stage (the steady stage of crack growth), the crack-growth behaviours under tensile loading and compressional loading were discussed separately. The primary differentiating factor between the tension-compression cycles can be explained by the plastic blunting process. Specifically, the tensile loading creates the new crack surface due to the shearing effect around crack-tip area, and then the crushing effect results in crack extension (by remaining the new surface created by the tensile loading) under the compressional loading. Regarding the microstructure, the plastic blunting process implies that the damage produced within one tension-compression cycle is not a reversed process since the atoms cannot return to their original positions after one cycle.

In addition, the crack-growth behaviours of fatigue and creep were also illustrated separately. Specifically, the fatigue component was generally presented by the plastic blunting process shown above, and the creep component was explained by the mechanism of diffusion creep. On the one hand, stress concentration at the crack tip provides a favourable condition for diffusion to form voids due to the stress-gradient effect, and then the void coalescence by shearing of the bridges between voids results in crack growth. On the other hand, diffusion creep gives grain elongation under tensile loading, which then further opens the crack created by fatigue effect. In addition, grain elongation also gives the shear stress at the grain boundaries between two adjacent grains, which probably results in the mismatch behaviour for the crack due to weak atomic bonds at the boundaries, then the crack widens.

Furthermore, the crack-growth behaviour regarding to the grain-boundary effect was discussed, and this effect plays more important role in creep-crack growth than fatigue behaviour. In this case, due to the shear stress between two adjacent grains caused by grain elongation, the grain-boundary effect results in blunter crack tip or wider crack body (mismatch). In particular, this effect can be presented by a special situation, the triple-point effect. In the triple points, the highly stress concentration provides better condition for diffusion.

Stage III: Structural failure

In the final stage (the structural failure), the fracture occurs within small loading cycles. This can be attributed to the high stress field at the crack tip. Specifically, under this stress state, the plastic energy exceeds the needs for producing the new crack surface. In this case, a part of energy is applied to create the new surface, and the rest of energy is applied to form voids which further promote crack growth by internal necking.

Original contributions

The original contribution of the present work is the proposal of a conceptual model for the multiple crack propagation mechanisms at a grain-based level. In particular, the plastic blunting process was introduced to describe fatigue-crack growth, the mechanism of diffusion was included to present creep-crack growth, and the grain-boundary effect is proposed to describe the possible phenomena when a crack encounters a grain boundary. In addition, based on the general understanding of crack-growth behaviours for fatigue and creep, a FEA-based method was proposed, which offers a quantitative validation on the grain-size effect and the failure principles for fatigue and creep. Overall, while the ideas of crack growth are well known, the literature does not provide a comprehensive explanation of the process from initiation to failure. The novel contribution of the above model is therefore the integration of multiple mechanisms at the microstructural level, inclusion of the grain boundary effect, and coverage of the stages from initiation to failure.

We have proposed a number of new mechanisms for crack growth (propositions A-G in section 3). Using these it has been possible to construct a comprehensive model of the crack growth process at the microstructural level. This model is also consistent with the existing concepts in the literature (premises a-l in section 3). Of itself this does not prove that these propositions are true, but it does show that these concepts are useful in better understanding the creep-fatigue mechanisms.

The analysis presented here does not completely include all possible loading situations, though is believe to be broadly representative.

4.2 Limitations

As mentioned in the section 2.2, the schematic representation of creep-fatigue crack growth is based on the assumption that fatigue damage makes more contribution to failure than creep damage. In this case, the crack mainly grows through the grains. The creep behaviour is regarded as an assistant effect. This may not be true of all situations, especially not at higher temperatures or longer cyclic time where creep begins to dominate.

In addition, there are potential limitations to the FEA-based methods proposed in section 2.2 to numerically demonstrate the grain-size effects on fatigue and creep. The applications of XFEM-based and CZM-based methods are based on the general understanding of crack-growth principles. There is no literature that indicates that the XFEM-based method is special for fatigue and CZM-based method for creep.

4.3 Implications for further research

The graphical-based crack-growth model proposed in this paper is a conceptual model. Some of the fatigue and creep behaviours have been well demonstrated and explained in previous research, such as stress distribution at the crack tip for fatigue and the stress concentration at the triple point for creep. However, there are still some behaviours which are difficult to be validated through experiments, such as the situation with the crack tip at the grain boundary. Our conceptual model has offered an explanation of these behaviours, but this work is conjectural. It would be valuable to test the validity of this at the microstructural level. To achieve this, it would be necessary to combine fractography and fatigue tests. However, it is difficult and complex to empirically examine and investigate the phenomena at the grain boundary since it will be difficult to dynamically capture those moments when the crack tip arrives at the grain boundary. A new experimental method may also need to be developed.

In addition, section 2.2 presents a possible FEA-based model to investigate the grain-size effects on fatigue and creep, which may be further extended to evaluate fatigue and creep damage. Specifically, fatigue damage is evaluated through the XFEM-based method and creep damage is evaluated by the CZM-based method. The evaluation of these two components are conducted respectively, and then the combined effect (creep-fatigue damage) may be ideally calculated by a modified linear damage rule:

$$D = A\sum_{i}\frac{n_i}{N_i} + B\sum_{i}\frac{t_i}{t_{R(i)}} \tag{4}$$

where D is the total damage, $\sum_i \frac{n_i}{N_i}$ is the pure-fatigue damage, $\sum_i \frac{t_i}{t_{R(i)}}$ is the creep damage, n_i is the number of constant amplitude cycles under the ith strain/stress range, N_i is the number of cycles to fatigue failure under the ith strain/stress range, t_i is the duration of creep under the applied stress σ_i at temperature T_i, $t_{R(i)}$ is the creep-rupture time under the applied stress σ_i at temperature T_i, and A and B are constants which reflect the weight of the contribution of fatigue and creep. Generally, the total damage is accumulated by fatigue damage, creep damage, and the damage caused by interaction between fatigue and creep. The modified linear damage rule (Eq.4) eliminates the interaction component because of the unknown method for calculation, thus introduces two factors (A and B) to modify the contributions of creep and fatigue damage. These two coefficients could be obtained from experiments, and the total damage to failure identified as 1. It is notable that based on the discussion shown in section 4.2, the accuracy of FEA-based methods proposed in this paper still needs to be further discussed and validated, hence opens an opportunity for future research.

5. Conclusions

Based on the general understanding of crack-growth behaviour, a conceptual model has been proposed, and represented graphically, wherein fatigue and creep effects are treated separately due to the different damage principles. This conceptual model illustrates the process of damage

accumulation from crack initiation to crack propagation then to structural failure. In particular, the analysis of crack propagation is mainly based on existing mechanisms of plastic blunting and diffusion creep. The possible grain-boundary behaviours, such as the mismatch behaviour at grain boundary due to creep deformation, are included. This model is consistent with the various creep and fatigue microstructure observations in the literature, but goes further by integrating these premises and our proposed propositions together into a logically consistent framework that describes the overall failure process.

In addition, the crack-growth behaviour may be extended to a FEA-based model, wherein the crack growth across grains (fatigue behaviour) is simulated through the XFEM-based method and the crack growth along grain boundary (creep behaviour) is simulated through the CZM-based method. This FEA-based model effectively demonstrates the grain-size effects on fatigue and creep, and supports the proposed crack-growth mechanisms.

Conflict of interests: The authors declare no conflict of interest. The research was conducted without personal financial benefit from any funding body, and no such body influenced the execution of the work.

Contribution statement: Both authors conceptualised the overall model, DL worked out the details and produced the graphical model, DL devised and conducted the finite element analyses, both authors contributed to writing the paper.

References

1. Dowling, N.E., Mechanical behavior of materials: engineering methods for deformation, fracture, and fatigue. 2012, London, UK: Prentice. 954.
2. Paris, P. and F. Erdogan, A critical analysis of crack propagation laws. Journal of Basic Engineering, 1963. 85(4): p. 528-533.
3. Cocks, A. and A. Pontern, Mechanics of creep brittle materials 1. 1989, Berlin/Heidelberg, Germany: Springer Science & Business Media. 310.
4. Ejaz, N., I. Qureshi, and S. Rizvi, Creep failure of low pressure turbine blade of an aircraft engine. Engineering Failure Analysis, 2011. 18(6): p. 1407-1414.
5. Král, P., et al. Creep damage of Al and Al-Sc alloy processed by ECAP. in Acta Metallurgica Slovaca-Conference. 2013.
6. Dai, C., et al., On size effects on fatigue properties of metal foils at micrometer scales. Materials Science and Engineering: A, 2013. 575: p. 217-222.
7. Hanlon, T., Y.-N. Kwon, and S. Suresh, Grain size effects on the fatigue response of nanocrystalline metals. Scripta Materialia, 2003. 49(7): p. 675-680.
8. Miller, K., Materials science perspective of metal fatigue resistance. Materials science and technology, 1993. 9(6): p. 453-462.

9. Rodopoulos, C.A., Fatigue Damage Map as a Virtual Tool for Fatigue Damage Tolerance, in Virtual Testing and Predictive Modeling. 2009, Springer: Berlin/Heidelberg, Germany. p. 73-104.
10. Callister, W.D. and D.G. Rethwisch, Materials science and engineering. Vol. 5. 2011, New Jersey, USA: John Wiley & Sons NY.
11. Liu, C., et al., Creep crack growth behaviour of Alloy 718. Superalloys, 1991. 178(625): p. 537-548.
12. Sadananda, K., A theoretical model for creep crack growth. Metallurgical and Materials Transactions A, 1978. 9(5): p. 635-641.
13. De Moura, M. and J. Gonçalves, Cohesive zone model for high-cycle fatigue of adhesively bonded joints under mode I loading. International Journal of Solids and Structures, 2014. 51(5): p. 1123-1131.
14. Meng, Q. and Z. Wang, Extended finite element method for power-law creep crack growth. Engineering Fracture Mechanics, 2014. 127: p. 148-160.
15. Laird, C., Mechanisms and theories of fatigue. Fatigue and microstructure, 1979: p. 149-203.
16. Banks-Sills, L., Y. Motola, and L. Shemesh, The M-integral for calculating intensity factors of an impermeable crack in a piezoelectric material. Engineering Fracture Mechanics, 2008. 75(5): p. 901-925.
17. Warzynek, P., B. Carter, and L. Banks-Sills, The M-integral for computing stress intensity factors in generally anisotropic materials. 2005, National Aeronautics and Space Administration: Washington, D.C., USA.
18. Chowdhury, P. and H. Sehitoglu, Mechanisms of fatigue crack growth–a critical digest of theoretical developments. Fatigue & Fracture of Engineering Materials & Structures, 2016. 39(6): p. 652-674.
19. Laird, C., The influence of metallurgical structure on the mechanisms of fatigue crack propagation, in Fatigue crack propagation. 1967, ASTM International: Pennsylvania, USA.
20. Laird, C. and R. de La Veaux, Additional evidence for the plastic blunting process of fatigue crack propagation. Metallurgical and Materials Transactions A, 1977. 8(4): p. 657-664.
21. Peralta, P., S.-H. Choi, and J. Gee, Experimental quantification of the plastic blunting process for stage II fatigue crack growth in one-phase metallic materials. International Journal of Plasticity, 2007. 23(10): p. 1763-1795.
22. Shi, K., et al., A prediction model for fatigue crack growth using effective cyclic plastic zone and low cycle fatigue properties. Engineering Fracture Mechanics, 2016. 158: p. 209-219.
23. Wang, G., The plasticity aspect of fatigue crack growth. Engineering fracture mechanics, 1993. 46(6): p. 909-930.
24. Weertman, J., Fatigue crack propagation theories, in Fatigue and microstructure. 1979, American Society for Metals: Ohio, USA. p. 279-206.
25. Ham, R. and T. Broom, The mechanism of fatigue softening. Philosophical Magazine, 1962. 7(73): p. 95-103.
26. Zhai, T., et al., The grain boundary geometry for optimum resistance to growth of short fatigue cracks in high strength Al-alloys. International journal of fatigue, 2005. 27(10): p. 1202-1209.
27. Kinloch, A., et al., Aligning graphene nanoplatelets with an external electric field to improve multifunctional properties of epoxy nanocomposites. 2015: p. 607-618.
28. Villechaise, P., et al. Mechanical behaviour and damage processes of Udimet 720Li: influence of localized plasticity at grain boundaries. in 12th International Symposium on Superalloys. 2012. Champion, Pennsylvania.
29. Claude Bathias, A.P., Fatigue of Materials and Structures: Fundamentals. 2013, New Jersey, USA: John Wiley & Sons. 512.

30. Sangid, M.D., The physics of fatigue crack initiation. International journal of fatigue, 2013. 57: p. 58-72.
31. Wang, Z., I. Beyerlein, and R. LeSar, Slip band formation and mobile dislocation density generation in high rate deformation of single fcc crystals. Philosophical Magazine, 2008. 88(9): p. 1321-1343.
32. Margaritis, G. and J. Botsis, Energy evaluations during crack initiation. Engineering fracture mechanics, 1991. 40(6): p. 1123-1134.
33. Lach, R., et al., Crack toughness behavior of binary poly (styrene-butadiene) block copolymer blends. Journal of materials science, 2004. 39(4): p. 1283-1295.
34. Zerbst, U., C. Klinger, and R. Clegg, Fracture mechanics as a tool in failure analysis—Prospects and limitations. Engineering Failure Analysis, 2015. 55: p. 376-410.
35. Fournier, D. and A. Pineau, Low cycle fatigue behavior of Inconel 718 at 298 K and 823 K. Metallurgical and Materials Transactions A, 1977. 8(7): p. 1095-1105.
36. Liu, D. and D. Pons, Development of a unified creep-fatigue equation including heat treatment. Fatigue & Fracture of Engineering Materials & Structures, 2017: p. 1-13.
37. Liu, D., D. Pons, and E.-h. Wong, The Unified Creep-Fatigue Equation for Stainless Steel 316. Metals, 2016. 6(9): p. 219.
38. Liu, D., D. Pons, and E.-h. Wong, Creep-Integrated Fatigue Equation for Metals. International Journal of Fatigue, 2017. 98: p. 167-175.
39. Evans, R.W. and B. Wilshire, Introduction to creep. 1993, Michigan, USA: The Institute of Materials, University of Michiganb. 115.
40. Pippan, R. and W. Grosinger, Fatigue crack closure: from LCF to small scale yielding. International Journal of Fatigue, 2013. 46: p. 41-48.
41. Prasad, K., et al., A comparative assessment of crack closure mechanisms in Timetal 834 near α titanium alloy under isothermal and thermomechanical fatigue loading. Journal of Alloys and Compounds, 2016. 688: p. 8-11.
42. Guo, Y., et al., Measurements of stress fields near a grain boundary: Exploring blocked arrays of dislocations in 3D. Acta Materialia, 2015. 96: p. 229-236.
43. McMurtrey, M., et al., Strain localization at dislocation channel–grain boundary intersections in irradiated stainless steel. International Journal of Plasticity, 2014. 56: p. 219-231.
44. Pineau, A., Crossing grain boundaries in metals by slip bands, cleavage and fatigue cracks. Philosophical Transactions of the Royal Society A, 2015. 373(2038): p. 20140131.
45. Kassner, M.E., Fundamentals of creep in metals and alloys. 2015, Oxford, UK: Butterworth-Heinemann. 337.
46. Kumar, Y., et al., Study of creep crack growth in a modified 9Cr–1Mo steel weld metal and heat affected zone. Materials Science and Engineering: A, 2016. 655: p. 300-309.
47. Pretty, C.J., M.T. Whitaker, and S.J. Williams, Thermo-Mechanical Fatigue Crack Growth of RR1000. Materials, 2017. 10(1): p. 34.
48. Kacher, J., et al., Dislocation interactions with grain boundaries. Current Opinion in Solid State and Materials Science, 2014. 18(4): p. 227-243.
49. Benz, J.K. and R.N. Wright, Fatigue and Creep Crack Propagation Behaviour of Alloy 617 in the Annealed and Aged Conditions. 2013, Idaho National Laboratory (INL): Idaho, USA.
50. Scheyvaerts, F., T. Pardoen, and P. Onck, A new model for void coalescence by internal necking. International Journal of Damage Mechanics, 2010. 19(1): p. 95-126.

Appendix B

Appendix B: Matlab script

The numerical optimization shown in Section 6.1.1 is conducted by Matlab-based method. The programming code and its explanation are shown below:

**** Step 1: defining constants and matrixes****

*** Creating a 56-by-1 matrix of zeros to store the empirical data of life (56 groups of data)***

```
life = zeros(56,1);
```

*** Matrix of creepfatigue(i,j) includes all empirical data and is imported into Matlab***

*** Loop control statement is applied to import the experimental results of fatigue life into matrix of life(i,j) based on the Coffin-Manson equation***

```
for i=1:56, life(i,1)= (creepfatigue(i,7)/creepfatigue(i,5))^(-1/creepfatigue(i,6));
end
```

*** Defining constants of T_{ref}, t_{ref}, c_2 and f_m ***

```
Tref = 160;
tref = 1;
c2 = 0.1215;
f = 0.6366;
```

*** Creating a 56-by-1 matrix of zeros to store the values of creep function $c(\sigma, T, t_c)$ ***

```
coef1=zeros(56,1);
```

*** Loop control statement gives the values of creep function $c(\sigma, T, t_c)$ under multiple situations***

** $c_1(\sigma) = 9.9586 \times 10^{-4} + 1.01122 \times 10^{-4} \cdot f_m \cdot \sigma + 8.09657 \times 10^{-7} \cdot {f_m}^2 \cdot \sigma^2$**

for i=1:56, coef1(i,1)=1- (creepfatigue(i,2)-Tref) *(0.00099586+0.000101122* f * (creepfatigue(i,9) * creepfatigue(i,7) ^ creepfatigue(i,10))/2+0.000000809657 * (f * (creepfatigue(i,9) * creepfatigue(i,7) ^ creepfatigue(i,10))/2)^2) -c2 * log10(creepfatigue(i,4)/tref);

end

** *Creating a 56-by-1 matrix of zeros to store the errors between predicted fatigue life and experimental fatigue life for multiple situations***

error1 = zeros(56,1);

** *Creating a matrix to store total error***

e =10000*ones(length(c0)*length(b0)+1,1);

**** Step 2: Defining the possible range of variables****

** *Defining the number of incrementing steps***

N = 1000;

** *Defining the possible range of constants C_0 and β_0***

** *Generating row vector c0 of 1000 points linearly spaced between 0.01 and 10***

** *Generating row vector b0 of 1000 points linearly spaced between 0.01 and 1***

c0=linspace(0.01,10,N);

b0=linspace(0.01,1,N);

**** Step 3: Conducting numerical computing to get the desired values which satisfy the constraint condition****

** *Starting a stopwatch timer to calculate the time of operation***

tic

k=1;

** *Loop control statement to give the minimum error***

for i = 1:length(c0)

for j = 1:length(b0)

** *Calculating error for each condition (56 different conditions)***

** *Total error: $\delta_t = \sum\left(\log N_{pre,ij} - \log N_{exp,ij}\right)^2$***

```
        for g=1:56
            error1(g,1)=(log10((creepfatigue(g,7)/(coef1(g,1)*c0(i)))^(-1/b0(j)))-
log10(life(g,1)))^2;
        end
```

*** All errors at 56 different conditions are added to get the total error and which are then imported into the matrix of e(i,1)***

```
            e(k+1,1)=sum(error1);
```

*** All total errors are compared, and then the minimum one is given***

*** The position 'i' for row vector c0 and the position 'j' for row vector b0 where the values of C_0 and β_0 give the minimum error are recorded, and presented by r and s respectively***

```
            if e(k+1,1)<=e(1,1)
                e(1,1)=e(k+1,1);
                r=i;
                s=j;
            end
            k=k+1;
        end
    end
```

*** Stopping a stopwatch timer***

```
    toc
```

**** Step 4: Printing the results****

*** Printing the minimum error***

```
    error_min = sprintf('%0.8f',min(e))]
```

*** Printing the values of C_0 and β_0***

```
    C0 = sprintf('%0.8f', c0(r))
    b0 = sprintf('%0.8f', b0(s))
```

Finally, the results are returned as:

```
    error_min=0.18486234
```

C0=7.90

b0=0.8256

Appendix C

Appendix C: XFEM-based crack-growth simulation method

C.1 Introduction of XFEM-based method

XFEM (the extended finite element method)-based crack-growth simulation technique provides an engineering approach for simulating fatigue crack propagation. This method shows the crack propagates through elements (Fig.C.1) and thus can be used to perform the behaviour of crack propagation through grains (the pure-fatigue situation). The XFEM-based crack-growth simulation technique is performed under the 2-D environment (Mechanical APDL in Ansys®) and is restricted to the second region of crack growth (thus based on Paris's Law). Although this approach presents a convenient process because it eliminates the need for re-meshing the crack-tip regions, it ignores large deformation, the crack-tip plasticity effect, and the crack-tip closure effect. However, we accept the possible error may be caused by this condition to perform an easy engineering simulation.

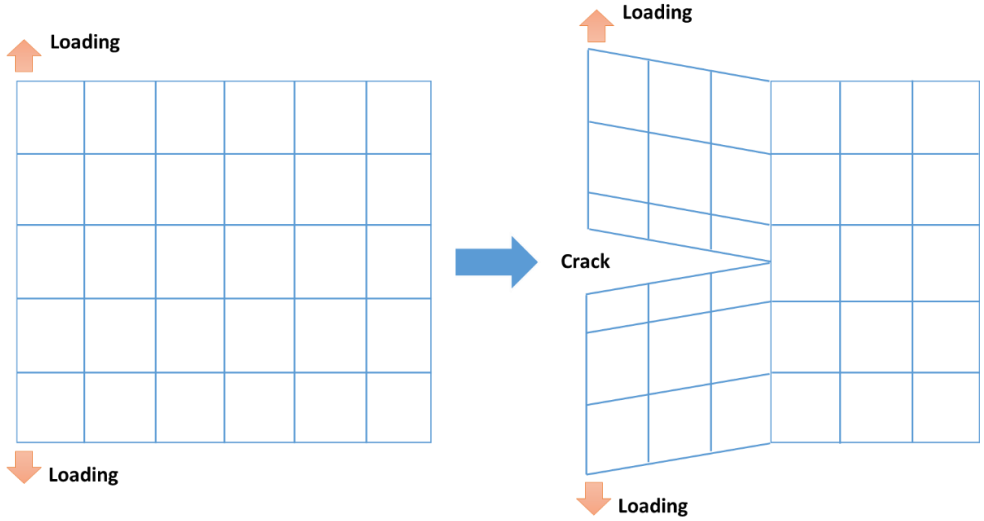

Figure C.1 Crack growth by XFEM-based crack-growth simulation technique

The simulation is conducted by ANSYS APDL, and the general process of this approach is normally divided into six steps:

▪ Step1: Defining an initial crack

Only PLANE182 element can be applied. The initial crack should fully cut elements, and the number of elements could be more than one. The material behaviour only can be defined as linear elastic isotropic. In this step, the command of XFENRICH is used to define crack-propagation-related parameters, and the command of XFDATA is used to define the location of the crack.

▪ Step 2: Specifying the fatigue crack-growth law

Paris' Law is specified in this step to perform crack growth at the second regime, and the commands of TB and TBDATA are involved.

▪ Step 3: Setting up the solution procedure

The fatigue crack-growth simulation is conducted by static analysis procedure, and a life-cycle method is applied. In this step, the command of ANTYPE is used to define analysis procedure, the commands of TIME and DELTIM are used to define load step, and the command of CGROW is used to define the fatigue-related parameter.

▪ Step 4: Evaluating the fracture parameters

The fracture parameters refer to the stress-intensity factors (SIFs), which reflect the stress state around the tip of a crack. The command of CINT is applied to evaluate the fracture parameters.

▪ Step 5: Setting crack-growth calculation parameters

The crack-growth calculation is processed after the solution has converged. In this step, the command of CGROW is used to define crack-growth information, including crack-calculation ID, crack-growth method (XFEM) and fracture criterion.

▪ Step 6: Calculating the fatigue crack growth

In the present work, the fatigue crack-growth calculation is based on the life-cycle (LC) method. The command of CGROW is introduced to specify LC method, maximum crack growth increment and stress ratio.

An example to show crack-growth behaviour at fatigue situation through applying XFEM-based crack-growth simulation technique is shown in the next section.

C.2 Example for applying XFEM-based method

XFEM-based crack-growth simulation technique is applied to simulate the behaviour of crack growth across elements. This provides a FEA method to simulate crack growth for fatigue situation, where the elements are modelled as grains. Based on the description shown above,

an example is given. The simulation is processed by using ANSYS MECHANICAL APDL 17.0, and the commands are shown as follows:

```
/prep7
! Model dimensions
H=5
W=100
! Applied loading
DIS=1
! Material properties
E=2e5
NU=0.3
RO=7.8
PI=ACOS(-1)
! Paris' Law constants
C=2.29e-13
M=3

! Element type
et,1,182
keyopt,1,3,2

! Material behaviour
mp,ex,1,E
mp,nuxy,1,NU
mp,dens,1,RO

! Specification of fatigue crack-growth law
tb,cgcr,2,,,PARIS
tbdata,1,C,M

! Defining keypoints
k,1,0,-H/2
k,2,W,-H/2
k,3,W,H/2
k,4,0,H/2

! Defining area
a,1,2,3,4

! Setting meshing size
xnume=99
ynume=9
lsel,s,line,,1,3,2
LESIZE,all,,,xnume,,,,1
lsel,s,line,,2,4,2
LESIZE,all,,,ynume,,,,1

! Meshing area
type,1
mat,1
MSHKEY,1
amesh,1

! Elements for XFENRICH command
esel,s,cent,y,-2.5,2.5
esel,r,cent,x,0,90
cm,testcmp,elem
allsel

! Defining enrichment identification
xfenrich,ENRICH1,testcmp,,SING,1.5,0.01

! Specification of initial crack
yc = 0.0
xc = 100/99
esel,s,cent,x,0,xc
esel,r,cent,y,-0.001,0.001
cm, cenelem, elem
nelem = 1000
iel = 0
```

```
Phi = 0.0
Psi = 0.0
*do, i, 1, nelem, 1
 iel = elnext(iel)
 *if, iel, ne, 0, then
  *do, j, 1, 4, 1
    nd = nelem(iel,j)
    Phi = ny(nd) - yc
    Psi = nx(nd) - xc
    xfdata, ENRICH1, LSM, iel, nd, Phi, Psi
  *enddo
 *endif
*enddo

xflist

! Crack-tip element
esel,s,elem,,397
cm, crktipelem, elem
allsel,all

! Applying loading
nsel,s,loc,y,-2.5
nsel,r,loc,x,0
d,all,uy,-DIS
nsel,s,loc,y,2.5
nsel,r,loc,x,0
d,all,uy,DIS
allsel

nsel,s,loc,x,100
kbc,1

solve
finish
```

```
nsel,r,loc,y,-5/ynume/2*1.05,5/ynume/2*1.05
d,all,all,0
allsel
finish

! Solution module
/solu

! Defining solution parameters
antype,0
time,1
deltim,0.1,0.1,0.1
outres,all,all

! CINT calculations
CINT,NEW,1
CINT,TYPE,SIFS
CINT,CXFE,crktipelem
CINT,NCON,8
CINT,NORM,0,2

! CGROW calculations
cgrow,new,1
cgrow,cid,1
cgrow,method,xfem
cgrow,fcoption,mtab,2

! Fatigue-related data
CGROW,FCG,METH,LC
CGROW,FCG,DAMX,0.1
CGROW,FCG,SRAT,-1
```

For XFEM-based crack-growth simulation technique, the geometry (Fig.C.1) is built as one solid body, and the crack-growth path is determined by the definition of the initial crack. A displacement is imposed at one end of the body, and a fixed support is applied at the other end (Fig.C.2). The parameters involved in this simulation are shown in Table C.1.

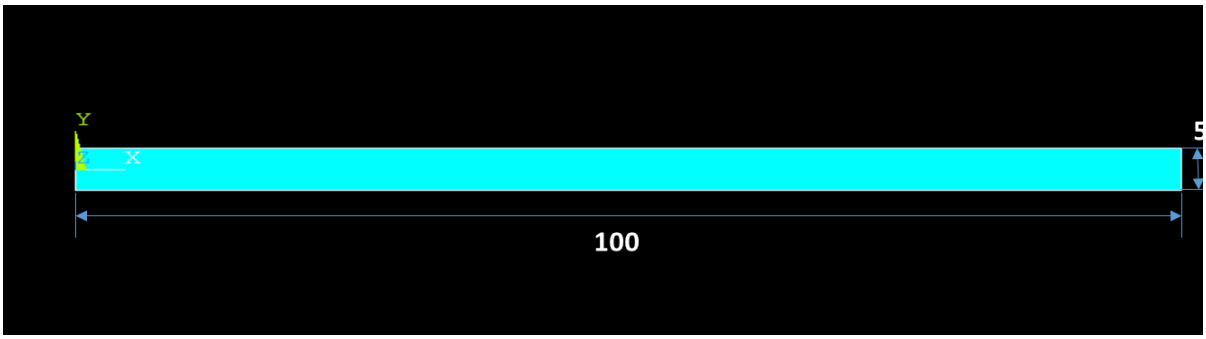

Figure C.1 Geometry

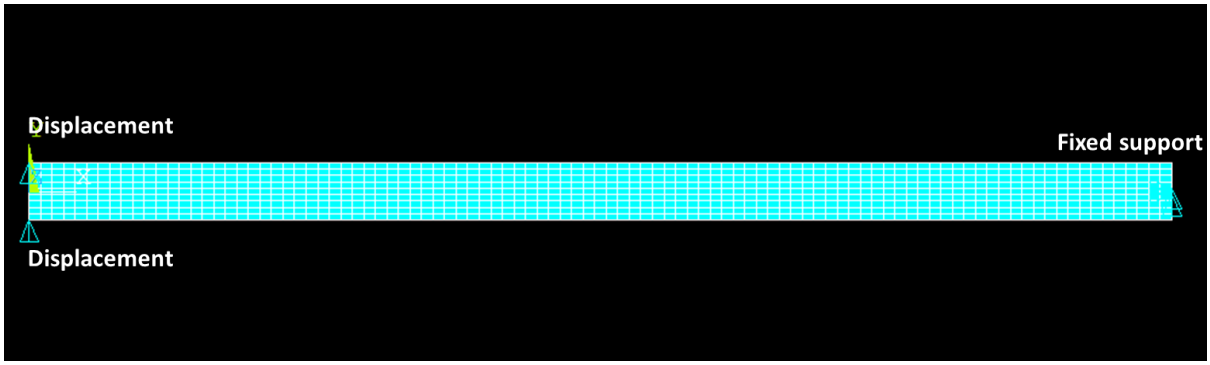

Figure C.2 Applied loading

Table C.1 Parameters for simulation

Material properties			Coefficients for Paris' Law		Loading
Young's Modulus (MPa)	Poisson's ratio	Density (kg/m^3)	C $(\frac{mm}{kg}/(MPa\sqrt{mm})^m)$	m	Displacement (mm)
2E5	0.3	7850	2.29E-13	3	1

The results are shown by the deformation distribution (Fig.C.3), stress distribution (Fig.C.4) and strain distribution (Fig.C.5). The results show the process of crack growth, where the crack-growth path cross through elements (modelled as grains). In addition, the results also suggest that the maximum stress and strain occur around the tip of the crack (Fig.C.6).

It is notable that the stress obtained in Mechanical APDL cannot reflect the real value because the Mechanical APDL does not have the concept of 'Units'. The result shows an enlarged value of stress, and the scale could be obtained through comparing the displacement which is imposed for simulation and the displacement shown in the plot. However, the strain obtained by

simulation may show the real value, since strain represents a proportion where the scale is counteracted.

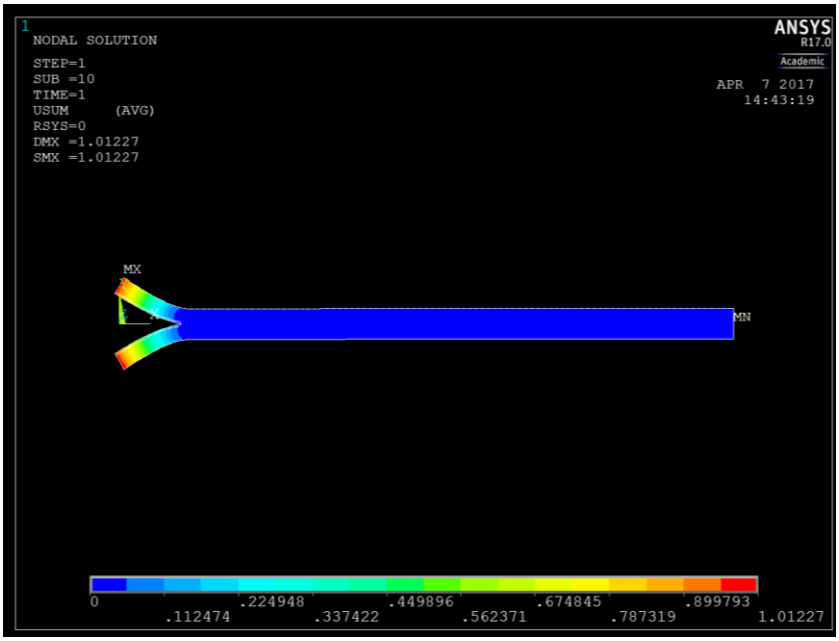

Figure C.3 Deformation distribution

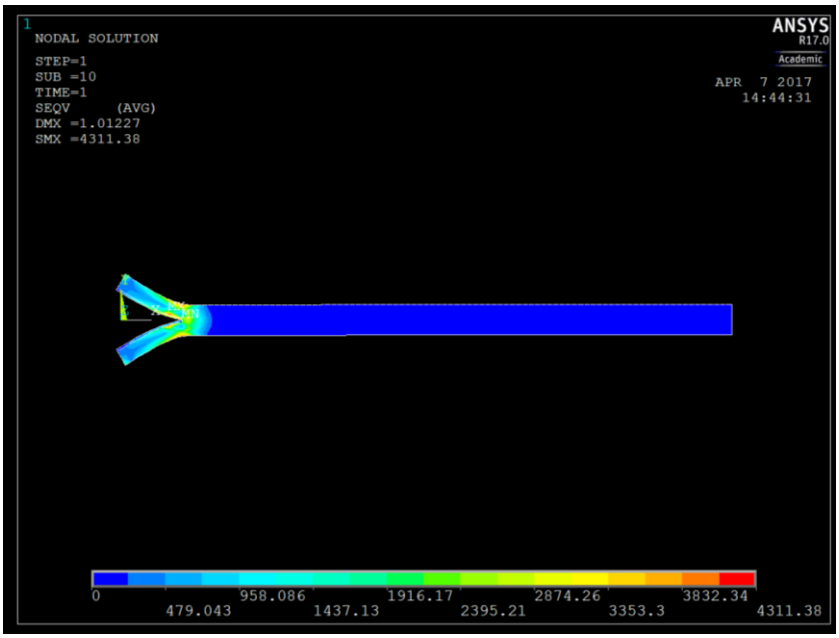

Figure C.4 Stress distribution

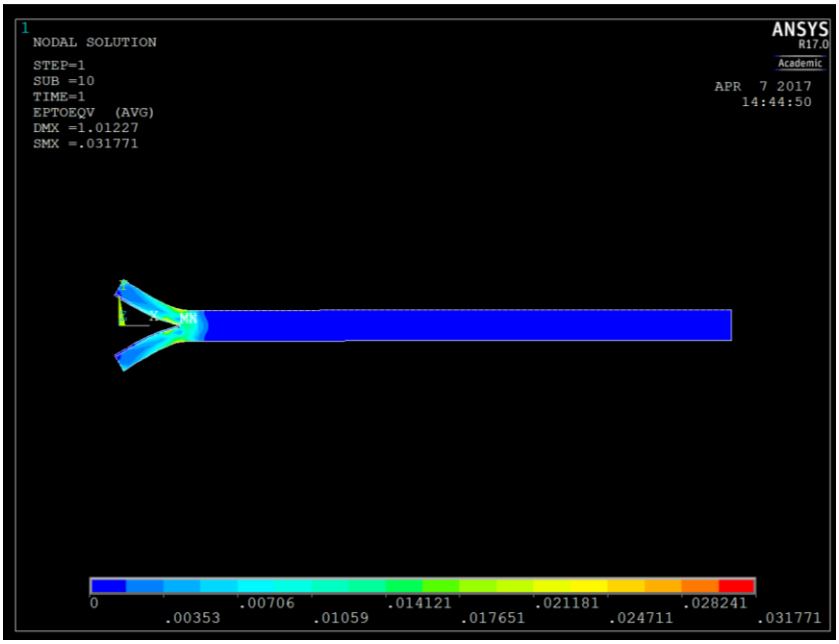

Figure C.5 Strain distribution

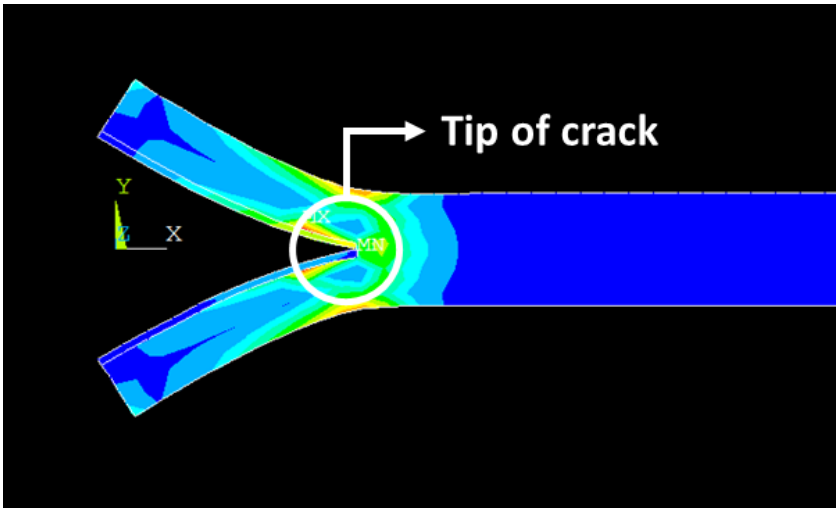

Figure C.6 Maximum situation around tip of crack

Appendix D

Appendix D: CZM-based crack-growth simulation method

D.1 Introduction of CZM-based method

The concept of CZM was developed to model facture along an interface, where the crack growth is simulated through using the traction-separation laws. Specifically, the CZM model presents a gradual separation of surfaces involved in the crack process, and this separation is resisted by cohesive tractions. Comparing with other conventional models (such as LEFM - linear elastic fracture mechanics, and CTOD – crack tip open displacement), the CZM model provides a method to predict the behaviour of uncracked structures, and the size of plastic zone need not be ignored in comparison with the crack zone. In the CZM method, the crack-growth path for FEA is normally constituted through a contact pair, and the crack propagation is simulated by debonding the contact pairs. Obviously, the crack growth is performed along the element boundary (Fig.D.1), and thus the CZM method could be used to simulate the crack propagation along the grain boundary, which is a typical pure-creep behaviour.

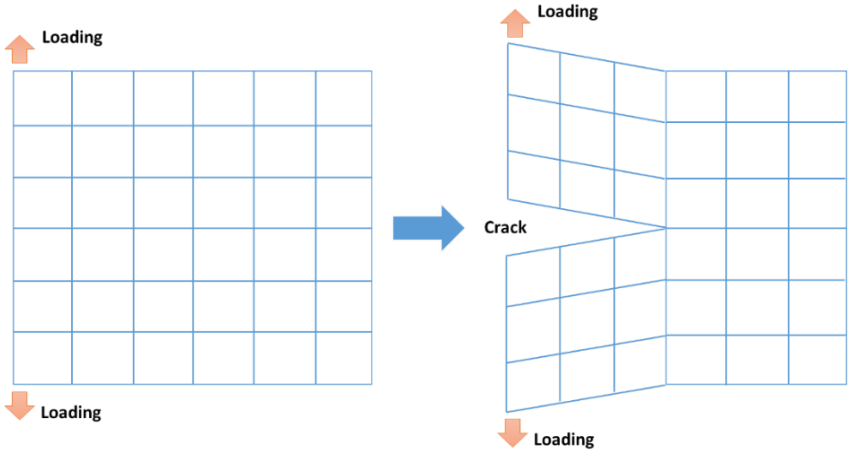

Figure D.1 Crack growth by CZM model

This simulation is conducted by ANSYS WORKBENCH, and the general process of this approach is generally divided into four main steps:

▪ Step 1: Defining material properties for cohesive zone

The material parameter of the cohesive zone is imposed to perform the crack-growth behaviour, which is defined through the property of 'Fracture-Energies based Debonding'.

▪ Step 2: Setting contact pair

The crack-growth simulation is conducted by static analysis procedure. The sub-geometries are built separately and then are combined through geometrical constraint. According to the method of CZM model, the crack-growth path is modelled through the contact pair whose type is defined as bonded.

▪ Step 3: Setting debonding parameters

The debonding parameters are specified through inserting 'Fracture' component, wherein the material properties of the cohesive zone and contact region are inputted in 'Contact Debonding'.

▪ Step 4: Calculating the fatigue crack growth

In this step, the load step is set up, and then the simulation is run. The results give the total deformation, the strain distribution, and the stress distribution.

An example to show crack-growth behaviour in a creep situation by applying CZM-based method is shown in the next section.

D.2 Example for applying CZM-based method

CZM-based model is applied to simulate crack growth along an interface. This provides a FEA method to simulate crack growth for creep situation (crack growth along grain boundary), where elements are modelled as grains. Based on the description shown above, an example is given. The simulation is conducted by applying ANSYS WORKBENCH 17.0 under the analysis of 'Static Structural'. The process of simulation is shown as follows:

D.2.1 Geometry

The sub-geometries are built separately as the name of 'body-1' and 'body-2', and then they are combined through geometrical constraint. The geometry is shown in Fig.D.2.

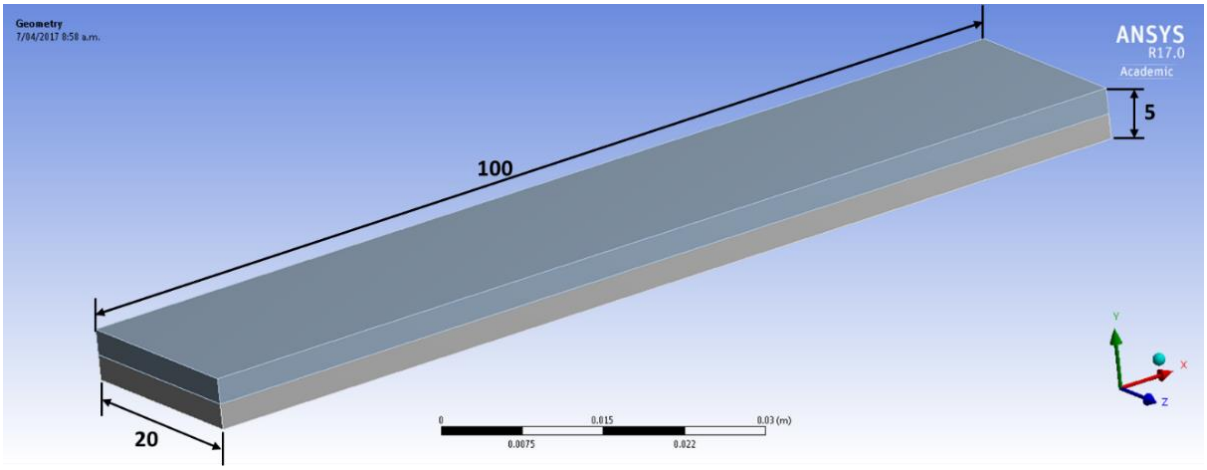

Figure D.2 Geometry

D.2.2 Defining material property

The engineering data of 'Structural Steel' are chosen as the material properties of the body. In the CZM-based method, the crack growth is performed through the debonding behaviour between two combined sub-geometries. Therefore, the property of the cohesive zone is defined through 'Fracture-Energies based Debonding', and the parameters of this property are shown in Table D.1.

Table D.1 The property of 'Fracture-Energies based Debonding'

Parameters	Value
Maximum Normal Contact Stress (Pa)	1.7E6
Critical Fracture Energy for Normal Separation (Jm^-2)	280
Maximum Equivalent Tangential Contact Stress (Pa)	1E-30
Critical Fracture Energy for Tangential Slip (Jm^-2)	1E-30
Artificial Damping Coefficient (s)	1E-8

D.2.3 Contact pairs

The contact pair (Fig.D.3) is identified as the contact surface between two sub-geometries, and the type of contact is defined as 'bonded'.

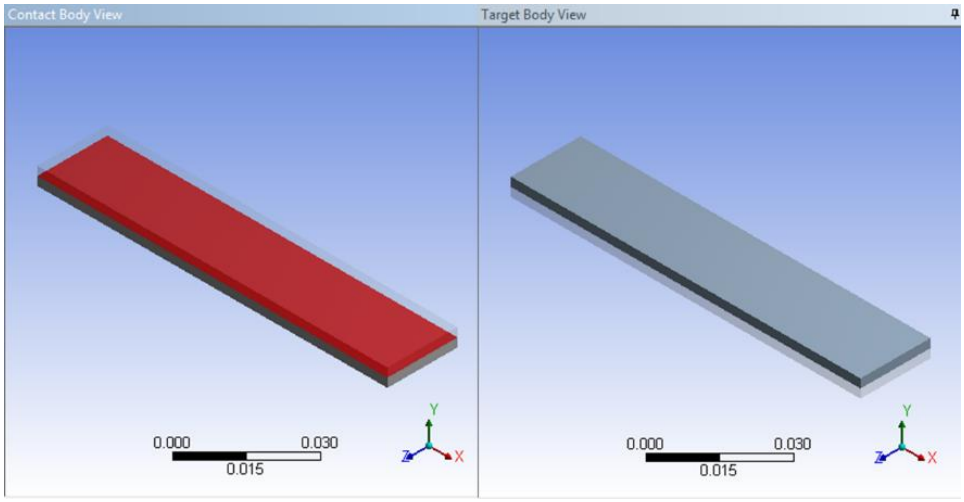

Figure D.3 Contact pairs

D.2.4 Fracture parameter

The ‘Fracture’ component is inserted, under which the ‘Contact Debonding’ is involved to determine the fracture parameter. Then the fracture-related material property defined in the engineering data is imported, and the contact region is identified.

D.2.5 Loading

The displacement (1mm) is imposed at one end of the geometry to process crack growth, and a fixed support is given at the other end of the geometry. This is shown in Fig.D.4.

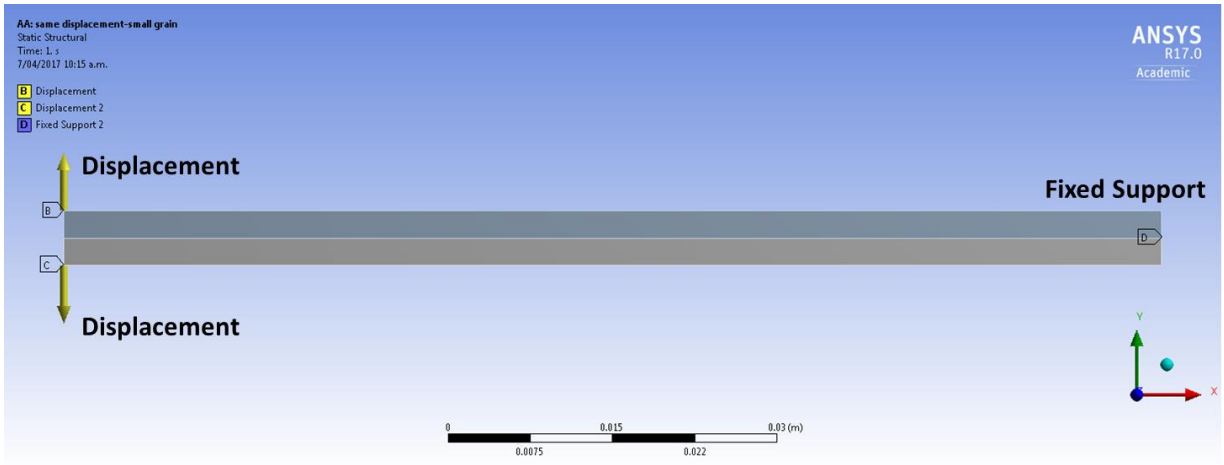

Figure D.4 Applied loading

D.2.6 Results

The results are shown by the deformation distribution (Fig.D.5), stress distribution (Fig.D.6) and strain distribution (Fig.D.7). The results show the process of crack growth, where the crack

propagates along the element boundaries (modelled as grain boundaries). In addition, the results also suggest that the maximum stress and strain occur around the tip of crack (Fig.D.8).

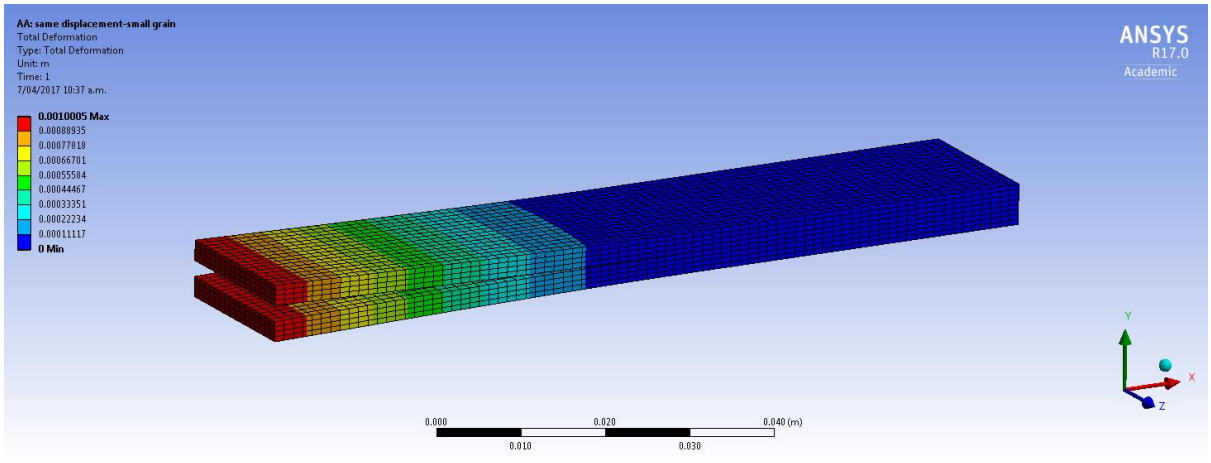

Figure D.5 Deformation distribution

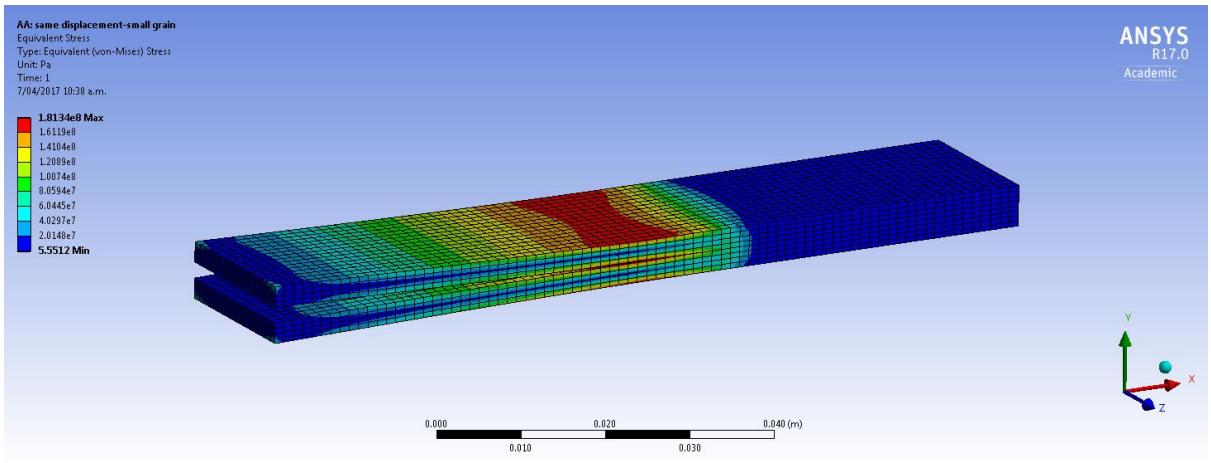

Figure D.6 Stress distribution

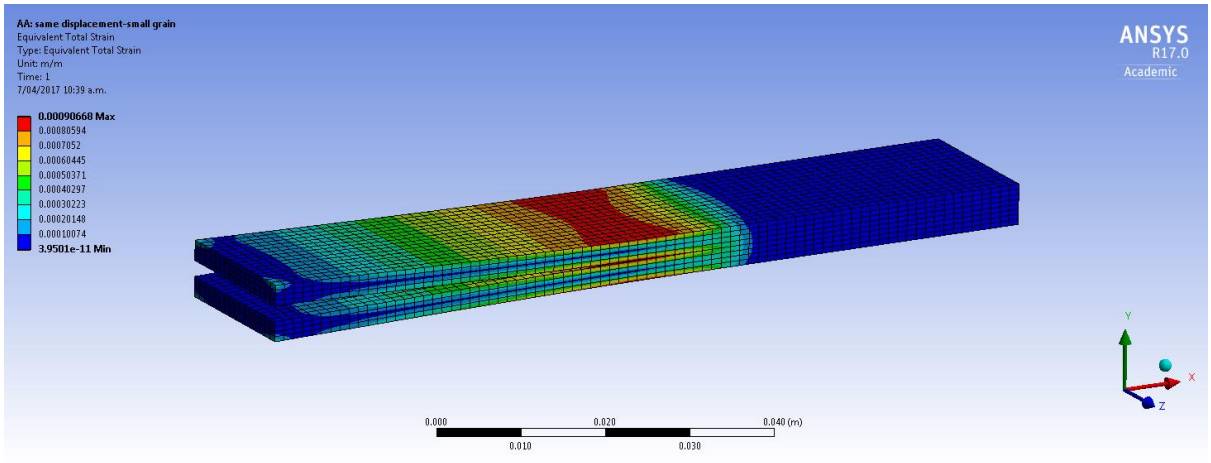

Figure D.7 Strain distribution

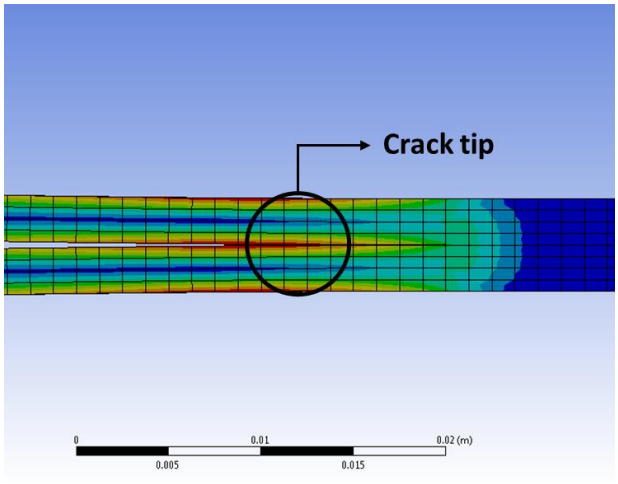

Figure D.8 Maximum situation around tip of crack